SLAC-198
(T/E)

PROCEEDINGS OF

SUMMER INSTITUTE ON PARTICLE PHYSICS

August 2-13, 1976

WEAK INTERACTIONS AT HIGH ENERGY AND THE PRODUCTION OF NEW PARTICLES

Program Directors

David W. G. S. Leith

and

Frederick J. Gilman

Ed. by Martha C. Zipf

Sponsored by Stanford University, National Science Foundation, and Stanford Linear Accelerator Center under contract with the Energy Research and Development Administration
Contract AT(04-3)-515

November 1976

Printed in the United States of America. Available from National Technical Information Service, U.S. Department of Commerce, 5285 Port Royal Road, Springfield, Va. 22161
Prices: Printed copy $12.50; Microfiche $3.00

PREFACE

These proceedings cover both the summer school and the topical conference parts of the fourth SLAC Summer Institute on Particle Physics. The Institute was held from August 2 to 13, 1976 and attended by 253 participants from 13 countries. This year the Summer School consisted of seven concentrated days of lectures, discussion periods, and seminars of a pedagogic character. These were designed at the post-doctoral level to bring those attending up to the active research frontier in the area of "Weak Interactions at High Energy and the Production of New Particles," the central theme of the Summer Institute. There followed a three-day Topical Conference, which more than ever lived up to the word topical, with the latest discoveries, especially the likely candidates for charmed mesons and baryons found just weeks before the conference, resulting in much excitement and standing-room-only sessions in the SLAC auditorium.

The success of this year's Institute is again due in large part to Martha C. Zipf, the coordinator and editor of these proceedings. Our thanks also go to Susan Baumgart who handled the daily arrangements, conference meals, and the many minor problems in a manner which helped continue the friendly and positive atmosphere of previous Summer Institutes.

David W. G. S. Leith and Frederick J. Gilman

Program Directors

Table of Contents

PART I. Lectures on Weak Interactions at High Energy and the Production of New Particles

A. High Energy Weak Interactions — page

JAMES D. BJORKEN
"Weak-Interaction Theory and Neutral Currents" 1

STANLEY G. WOJCICKI
"Weak Interactions at High Energy" 43

B. Production of New Particles in Hadron, Photon, and e^+e^- Collisions

GARY J. FELDMAN
"ψ Spectroscopy" 81
"A New Lepton?" 127

J. D. JACKSON
"Lectures on the New Particles" 147

DAVID HITLIN
"New Particle Production" 203

PART II. Seminars

H. PIERRE NOYES
"A Democritean Approach to Elementary Particle Physics". . . . 239

M. WEINSTEIN
"All Coupling Constant Methods for Studying Cutoff Field Theories" 261

PART III. Topical Conference

H. H. WILLIAMS
"Observation of Neutrino and Antineutrino Elastic Scattering from Protons". 295

C. Y. PANG
"Recent Results from Counter-Spark Chamber Neutrino Experiment at BNL". 313

PAUL MUSSET
"Recent Results in μe Events and Neutral Current in Gargamelle" 327

W. F. FRY
"Characteristics of $\mu^-e^+K^o$ Events Produced by a Neutrino Beam" 337

F. A. NEZRICK
"Search for New Particles Produced in $\bar{\nu}_\mu$ Nucleon Interactions in the 15-foot Bubble Chamber" 347

PART III. Topical Conference (continued) page

L. STUTTE
"Dimuon Production in High Energy Neutrino and Antineutrino Interactions" 367

GERSON GOLDHABER
"Study of Charmed Mesons at SPEAR" 379

D. I. MEYER
"Limits on Charmed Particle Production in Hadron Collisions" 401

P. SCHMÜSER
"New Particle Production from DASP at DORIS" 411

H. MEYER
"Recent Pluto Results from DORIS" 427

GEORGE H. TRILLING
"Study of Intermediate States Produced by Radiative Decays of ψ' " 437

A. J. S. SMITH
"Production of Muons in Hadron-Nucleus Collisions" 449

SHELDON L. GLASHOW
"Convergences" 473

A. DE RUJULA
"The *Ups* and *Downs* of *Strange Charm*" 483

List of Participants 485

WEAK-INTERACTION THEORY AND NEUTRAL CURRENTS*

J. D. Bjorken

Stanford Linear Accelerator Center
Stanford University, Stanford, California 94305

I. EFFECTIVE LAGRANGIANS FOR CHARGED AND NEUTRAL CURRENT PROCESSES

After over thirty years of research on the structure of the interaction responsible for β-decay, we have reached the point where an impressively simple and successful phenomenological theory well represents a wealth of data on decays of nucleons, nuclei, and strange particles, as well as data on neutrino interactions with energies from 1 to 50 GeV. All this can be summarized in an effective Lagrangian density, to be used in lowest order, as follows

$$\mathscr{L}_{\text{eff}} = \frac{G}{\sqrt{2}} \mathscr{J}_\lambda(x) \mathscr{J}^\lambda(x)^\dagger \tag{1.1}$$

Here

$$\begin{aligned} \mathscr{J}_\lambda(x) = {} & \bar{e}\gamma_\lambda(1-\gamma_5)\nu_e + \bar{\mu}\gamma_\lambda(1-\gamma_5)\nu_\mu \\ & + \sum_{i=1}^{3} \left(\bar{d}_i \cos\theta_c + \bar{s}_i \sin\theta_c\right)\gamma_\lambda(1-\gamma_5)u_i \\ & \left\{ + \sum_{i=1}^{3} \left(\bar{s}_i \cos\theta_c - \bar{d}_i \sin\theta_c\right)\gamma_\lambda(1-\gamma_5)c_i \right\}^{??} + ?? \end{aligned} \tag{1.2}$$

$G = 1.02 \cdot 10^{-5}\ M_p^{-2}$ is the Fermi constant. θ_c is the Cabibbo mixing angle ($\sin^2\theta_c \cong 0.055$), while u_i, d_i, s_i are the fields of fractionally charged colored quarks. The last term in curly brackets is the conjectured (but not fully established) charm current involving a fourth quark c_i, about which we shall elaborate later.

*Work supported by the Energy Research and Development Administration.

Again and again this model, as described by Eq. (1.1), has successfully survived experimental tests. This is not to say it is beyond challenge. It is well beyond the scope of these lectures to review the status of the phenomenological theory. However, before leaving it, we do wish to mention recent developments which bear on the question of its validity:

1. In a recent LBL experiment,[1] the polarization of the muon emitted in $K_L \to \mu\pi\nu_\mu$ has been measured, and agrees with the phenomenological theory (supplemented with the PCAC hypothesis). This mitigates a long-standing and vexing discrepancy existing from earlier measurements.[2]

2. Recent experiments on β-transitions in light nuclei[3] have indicated a need for additional anomalous-moment coupling and/or second-class currents[4] of opposite G-parity from that given in Eq. (1.2) in the effective Lagrangian. Such currents are difficult to incorporate in the theoretical structures we discuss in these lectures. It is clearly of great importance to clarify this issue.

3. How to interpret the success of the $\Delta I = 1/2$ rule in $\Delta S=1$ nonleptonic decays remains an ambiguous issue. There is still room for fresh ideas and unconventional interpretations in this area.

4. While there is some experimental evidence for existence of "diagonal" charged-current couplings (e.g., $\bar{\nu}_e\gamma_\lambda(1-\gamma_5)e$ $\bar{e}\gamma^\lambda(1-\gamma_5)\nu_e$ or $\sum_{i,j=1}^{3} \bar{u}_i\gamma_\lambda(1-\gamma_5)d_i\ \bar{d}_j\gamma^\lambda(1-\gamma_5)u_j$), it is more qualitative than quantitative. A strict current-current structure as written in Eq. (1.1) is far from experimentally established.

5. The algebraic properties of the currents, i.e., their commutation relations among each other (e.g., SU(3) ⊗ SU(3) or chiral SU(6) ⊗ SU(6)) suggest the identification of quark fields made in Eq. (1.1). However it may be a little too strong a conclusion to infer the presence of quark-fields from those algebraic properties alone. In particular there is no evidence from the weak interaction phenomenology for the color degree of freedom.

With the discovery of neutral-current phenomena a few years ago and their apparent connection with weak interactions in general, we now face a situation similar to that encountered in the early days ($t \lesssim 1957$) of β-decay: we now must determine the nature of the effective Lagrangian governing neutral-current phenomena. The processes which have been observed include

$$\begin{aligned} &\nu_\mu + N \to \nu_\mu + \text{hadrons} \\ &\bar{\nu}_\mu + N \to \bar{\nu}_\mu + \text{hadrons} \\ &\bar{\nu}_\mu + e^- \to \bar{\nu}_\mu + e^- \\ &\bar{\nu}_e + e^- \to \bar{\nu}_e + e^- \end{aligned} \tag{1.3}$$

A fairly general candidate effective Lagrangian for these reactions is

$$\begin{aligned} \mathcal{L}_{\text{eff}} = \frac{G}{\sqrt{2}} \bar{\nu}_\mu \gamma^\lambda (1-\gamma_5) \nu_\mu \Big[& \epsilon_L(e)\, \bar{e} \gamma_\lambda (1-\gamma_5) e \\ & + \epsilon_R(e)\, \bar{e} \gamma_\lambda (1+\gamma_5) e \\ & + (e \to \mu) \\ & + \epsilon_L(u) \sum_{i=1}^{3} \bar{u}_i \gamma_\lambda (1-\gamma_5) u_i \\ & + \epsilon_R(u) \sum_{i=1}^{3} \bar{u}_i \gamma_\lambda (1+\gamma_5) u_i \\ & + (u \to d) \\ & + (u \to s) \\ & + (u \to c) \\ & + \cdots \Big] \\ + \frac{G}{\sqrt{2}} \Big[& \epsilon_{LL}(e,u)\, \bar{e} \gamma^\lambda (1-\gamma_5) e \sum_{i=1}^{3} \bar{u}_i \gamma_\lambda (1-\gamma_5) u_i \\ & + \epsilon_{RL}(e,u)\, \bar{e} \gamma^\lambda (1+\gamma_5) e \sum_{i=1}^{3} \bar{u}_i \gamma_\lambda (1-\gamma_5) u_i \\ & + \cdots \Big] \end{aligned} \tag{1.4}$$

The most vital assumption made here is that the neutrino emitted in ν-induced neutral current processes is the same type as the incident neutrino. This comment is meant to include helicity: at present there is no evidence at all that a right-handed ν_μ (or left-handed $\bar{\nu}_\mu$) exists as a physical particle. If neutral currents proceed according to

$$\nu_{\mu L} + N \to \nu_{\mu R} + \text{hadrons} \tag{1.5}$$

this would imply existence of a heretofore unknown degree of freedom, and concomitant scalar, pseudoscalar, or tensor neutral-current couplings.[5] There does exist some evidence against pure scalar or pseudoscalar couplings.[6] In any case we here assume they are absent.

Also possible are the reactions

$$\begin{aligned} &\nu_\mu + N \to L^o + \text{hadrons} \\ &\bar{\nu}_\mu + e^- \to \bar{L}^o + e^- \end{aligned} \tag{1.6}$$

with L^o some new neutral lepton. Existence of $\bar{\nu}_\mu$-e neutral current processes at GeV energies argues that the mass of L^o must be small,[7] under 50 MeV (because $\sqrt{s} < 100$ MeV).

There are many coupling constants in Eq. (1.4) to be determined. But this is the basic problem. There are two main routes that may be followed in trying to solve it. They in fact were identified in 1957 for charged-current processes, after the discovery of parity violation provided the impetus needed to straighten out the mess present in that field at that time. One option was simply to measure many, many processes directly and reduce the couplings to a unique form purely from experiment. This program has not been fulfilled to this day, despite its supremely logical nature. (For example, even for muon-decay the couplings have not been uniquely determined.[8]) The other approach was to guess the answer. The masters[9,10] spake: "Let there be V-A."

And there was V-A. A simple working hypothesis, tested over and over again, has by now become a phenomenological theory.

It is too early to know which path will be the most successful with regard to neutral currents, although we do have a good working hypothesis. Again the masters[10,11] spake: "Let there be SU(2) ⊗ U(1)." And thus far the SU(2) ⊗ U(1) gauge theory has done very well. In these lectures we shall travel some distance down both paths—sometimes the straightforward, cautious phenomenological path, and sometimes the hypothetical path of the specific SU(2) ⊗ U(1) gauge theory. In a situation (as at present) of relatively little data and relatively many phenomenological parameters, the latter path is the most powerful and useful (as long as it survives). However whenever possible the former path is to be preferred: it is safer.[12] I was surprised to find how far it is possible to proceed down the phenomenological path. In particular it may turn out that elastic $\nu_\mu p$ and $\bar{\nu}_\mu p$ scattering will play a pivotal role in disentangling the various couplings.

But before embarking upon specifics, we again warn the reader that already in Eq. (1.4) there contain untested implicit assumptions, which if wrong would greatly influence our present conception of neutral-current phenomena. These include:

1. The identity of the outgoing neutrino, a question we have already addressed.

2. Nonexistence of off-diagonal neutral current reactions, e.g., charm changing neutral current processes, such as $\nu_\mu + u_i \to \nu_\mu + c_i$. While the absence of $\Delta S=1$ neutral currents and the motivation for charm (GIM mechanism, discussed in Section II) suggests their absence, this is not an inevitability and should be tested.

3. Correctness of the 4-fermion nonderivative coupling structure of Eq. (1.4). This can be tested by observation of the E_ν and Q^2 dependence of neutral current processes.

4. Use of the color-singlet fractionally charged quark structure. One might be able to build a Pati-Salam-like scheme,[13] with broken color degrees of freedom, which might look quite different from Eq. (1.4).

II. HIGHER ORDERS OF THE WEAK INTERACTION

A. High Energy Cutoffs. The charged-current effective Lagrangian rivals the Lagrangian of quantum electrodynamics in predictive power. Given a weak process, short—usually straightforward—calculations (supplemented with the PCAC hypothesis) leads to results in good agreement with experiment. However, it has been known for a long time[14] that such a phenomenological theory is at best only a provisional description valid at low energy. As soon as one considers higher orders in the Fermi coupling, or equivalently weak processes at energies $\sqrt{s} \gtrsim G^{-1/2} \sim 300$ GeV, the phenomenological theory does not make sense. This can be seen best by looking at pure leptonic scattering processes,[15] for example, $e^- + \nu_\mu \to \nu_e + \mu^-$. Neglecting lepton mass, one helicity-amplitude evidently controls this process. And the total helicity is zero because e^- and ν_μ are both left-handed and have equal and opposite momenta. Because the point Fermi interaction allows no orbital angular momentum the cross section is nonvanishing only in the $J=0$ partial wave. Compute the invariant amplitude $\mathcal{M}$ in the forward direction ($\vec{p}_e = \vec{p}_{\nu_e} = -\vec{p}_\mu = -\vec{p}_{\nu_\mu}$) and in the center-of-mass frame:

$$\mathcal{M} = \frac{G}{\sqrt{2}} \left(\bar{u}_{\nu_e} \gamma_\lambda (1-\gamma_5) u_e\right) \left(\bar{u}_\mu \gamma^\lambda (1-\gamma_5) u_{\nu_\mu}\right)$$

$$= \frac{G}{\sqrt{2}} \left(\frac{2(p_e)_\lambda}{E_e}\right) \cdot \left(\frac{2(p_\mu)^\lambda}{E_e}\right)$$

$$= \frac{4G}{\sqrt{2}} \frac{p_e \cdot p_\mu}{E_e E_\mu} = \frac{8G}{\sqrt{2}} \qquad (2.1)$$

(We normalize $u^\dagger u = 1$, not to m/E in order to avoid awkwardness in handling massless fermion states.) This amplitude should (but does not) fall with

energy in order not to violate unitarity ($\mathcal{M} \lesssim \text{const}/s$). The problem is better seen by computing the differential cross section (from an unpolarized incident electron):

$$d\sigma = \left(\tfrac{1}{2}\right)\left(\tfrac{1}{2}\right) |\mathcal{M}|^2 \frac{d^3p_{\nu_e}}{(2\pi)^3} \frac{d^3p_{\mu}}{(2\pi)^3} (2\pi)^4 \delta^4\left(p_e + p_{\nu_\mu} - p_{\nu_e} - p_\mu\right)$$

$$= |\mathcal{M}|^2 \frac{s\,d\Omega}{128\pi^2} \qquad (2.2)$$

($\tfrac{1}{2}$: e^- spin average; $\tfrac{1}{2}$: flux factor = 2c)

or

$$\frac{d\sigma}{d\Omega} = \frac{G^2 s}{4\pi^2} \qquad (2.3)$$

and

$$\sigma_{tot} = \frac{G^2 s}{\pi} \qquad (2.4)$$

Thus instead of $\sigma_{tot} \sim s^{-1}$, we have $\sigma_{tot} \sim s^{+1}$. Something must happen before 300 GeV in the center-of-mass. We now discuss possible fixes for this situation:

1. Simple unitarization: If rescattering corrections are included in a manner parallel to what might be done in strong interactions (Bethe-Salpeter equation, K-matrix approximation, N/D method, etc.), the amplitude would be damped at energies $\sqrt{s} \sim G^{-1/2} \sim 300$ GeV. This puts an effective cutoff $\Lambda \sim 300$ GeV. By dimensional analysis, higher order effects would occur as

$$\mathcal{M} \sim G + \mathcal{O}(G^2\Lambda^2) + \ldots = G\left[1 + \mathcal{O}(G\Lambda^2) + \ldots\right] \qquad (2.5)$$

which is as large as the lower order effects. Just this much leads to some qualitative predictions (or at least expectations):

a) Neutral currents (as generated by second order loops $\nu_\mu e^- \to \mu^- \nu_e \to \nu_\mu e^-$) should be of the same order of magnitude as charged currents.

b) There is no a priori need to incorporate electromagnetic currents into the scheme.

c) The neutral currents induced by known charged currents acting in higher orders would be expected to be pure V-A.

d) The effective Lagrangian describing the lepton-lepton scattering matrix would contain derivative coupling terms, e.g.,

$$\mathcal{L}^{(2)} \sim G^2\left[\bar{l}\gamma_\lambda \frac{\partial}{\partial x^\sigma}(1-\gamma_5)l'\right]\left[\bar{l}''\gamma^\lambda \frac{\partial}{\partial x_\sigma}(1-\gamma_5)l'''\right] \qquad (2.6)$$

which would become significant at very high energies.[16]

e) Similar neutral current and derivative coupling terms would be expected to be generated in the effective Lagrangian for lepton-hadron interactions, provided the short distance behavior of such interactions parallels that of lepton-lepton interactions (as evidenced by the existence of scaling behavior in deep-inelastic processes). This would, if followed straightforwardly, imply a term[16]

$$\mathcal{L}' \sim G\left[\left(\bar{d}\cos\theta_c + \bar{s}\sin\theta_c\right)\gamma_\lambda(1-\gamma_5)\left(d\cos\theta_c + s\sin\theta_c\right)\right]\bar{u}\gamma^\lambda(1-\gamma_5)u \qquad (2.7)$$

leading to $\Delta S=1$ neutral current processes such as $K_L \to \mu^+\mu^-$, $K^+ \to \pi^+\mu^+\mu^-$, etc.

2. Simple charged intermediate boson exchange; strong W-W couplings. With an intermediate W exchanged between the lepton pairs (Fig. 1a) the amplitude in Eq. (2.1) is multiplied by a factor $m_W^2\left(m_W^2 + t\right)^{-1}$. This factor, in addition to damping the amplitude, distributes it into many partial waves so as to postpone any unitarity crisis to unobservably (i.e., exponentially) high energy. However, without any other restriction it turns out that pair-production processes (Fig. 1b) such as $e^+e^- \to W^+W^-$, with at least one W having helicity zero (longitudinal polarization) in the cms, again violates unitarity in the J=1 wave at $\sqrt{s} \gtrsim G^{-1/2}$. (We shall see this in detail later on.) The simplest panacea (which does not reduce to the previous case) involves supposing that W-W scattering becomes strong[17] but that W couplings to leptons and quarks remain weak

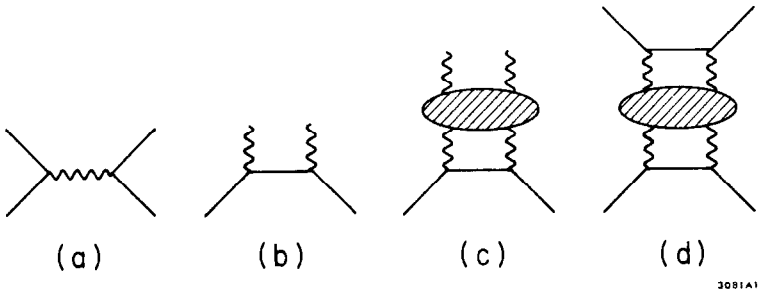

Fig. 1. (a) Weak lepton-lepton scattering via intermediate-boson exchange. (b) Pair production of intermediate bosons by leptons. (c) Intermediate boson rescattering. (d) Lepton-lepton scattering in higher order. The divergence in the loop integration (or in the dispersion integral over $\sigma(\ell\bar{\ell} \to W\overline{W})$) is damped out by the strong W-W rescattering.

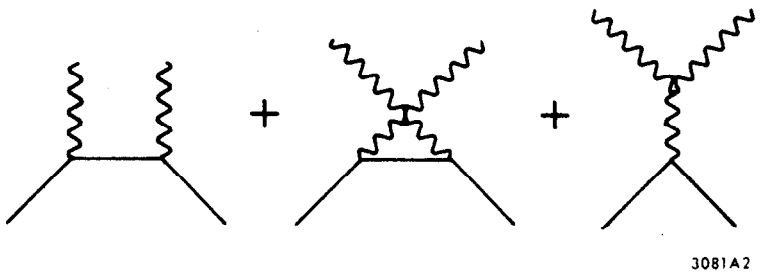

Fig. 2. Amplitudes for $e^+e^- \to W^+W^-$ in a gauge theory. Couplings are arranged so that the sum of these diagrams have a smooth high-energy behavior.

(Fig. 1c). If Λ is the energy for which W-W scattering phase-shifts become of order unity, this will generate higher-order neutral current effects according to Fig. 1d:

$$\mathcal{M}^{(2)} \sim G(G\Lambda^2) \tag{2.8}$$

just as in the previous case. (We again will see this in some detail later on.) With Λ unknown, it is hard to estimate the size of such induced neutral current effects.[18] However it is a safe bet that $\Lambda \gtrsim m_W$. Note also that in this option there could be many W-W resonances of various spins, the W's could like on Regge trajectories, there could be a strong interaction W bootstrap, etc.

3. Simple W-exchange, but cancellations between diagrams to keep the high-energy amplitude growth small (Gauge theories). Under suitable circumstances, it is possible to arrange the couplings of the set of intermediate bosons to fermions (quarks and leptons) and to each other such as to effect cancellations between the individual diagrams[19] shown in Fig. 2. A necessary and sufficient condition that this occur is that the couplings be those of some nonabelian gauge theory. These gauge theories are an elegant starting point for a weak (or for that matter, strong) interaction theory. They are generalizations of quantum electrodynamics introduced long ago by Yang and Mills[20] and designed to handle systems with internal degrees of freedom. It is not our intention to describe this basic starting point in detail. A feeling for it can perhaps be ascertained by the following parallelism:

	Quantum Electrodynamics	Nonabelian Gauge Theories
a)	Electromagnetic potential A_μ	Gauge potentials $B_\mu^{(a)}$, one for each generator T^a in the group algebra: $\left[T^a, T^b\right] = \sum_c f^{abc} T^c$

b)	Electromagnetic coupling e	Gauge coupling g
c)	Electromagnetic field	Gauge fields
	$F_{\mu\nu} = \partial_\mu A_\nu - \partial_\nu A_\mu$	$G^{(a)}_{\mu\nu} = \partial_\mu B^{(a)}_\nu - \partial_\nu B^{(a)}_\mu + g\sum_{bc} f^{abc} B^{(b)}_\mu B^{(c)}_\nu$
d)	Free Lagrangian density	
	$-\frac{1}{4} F_{\mu\nu} F^{\mu\nu}$ + gauge terms	$-\frac{1}{4}\sum_a G^{(a)}_{\mu\nu} G^{(a)\mu\nu}$ + gauge terms
e)	Gauge invariant substitution	
	$i\frac{\partial}{\partial x^\mu} \to i\frac{\partial}{\partial x^\mu} - eA_\mu$	$i\frac{\partial}{\partial x^\mu} \to i\frac{\partial}{\partial x^\mu} - g\sum_a t_a B^{(a)}_\mu$ where the t_a are an appropriate matrix representation (of the generators T_a) for the multiplet on which the derivative operator acts.
f)	Symmetry under local gauge transformations	
	$\psi(x) \to e^{i\Lambda(x)}\psi(x)$	$\psi_r(x) \to \left[e^{it_a\Lambda^a(x)}\right]_{rs}\psi_s(x) \equiv U_{rs}(x)\psi_s(x)$
	$eA_\mu(x) \to eA_\mu(x) + \frac{\partial\Lambda}{\partial x^\mu}$	$gt^a \cdot B^{(a)}_\mu \to U^{-1} gt^{(a)} \cdot B^{(a)}_\mu U - U^{-1}\frac{\partial U}{\partial x^\mu}$

One salient feature to notice is that gauge potentials couple trilinearly (and quartically) to each other as a consequence of the nonlinearity in the definition (c) of $G_{\mu\nu}$. That is, unlike electrodynamics, the gauge fields themselves carry quantum numbers and therefore must couple to themselves (just as the gravitational field carries energy and momentum and therefore couples to itself). This allows for couplings as needed in Fig. 2c. However, we shall go no further in this direction, it being sufficient for our purposes to point out the distinguished pedigree of this class of theory.

More significant perhaps is the inevitable unification of weak and electromagnetic interaction coming from this approach. The amplitude in Fig. 2c for electromagnetic production of W^+W^- by e^+e^-, taken by itself, violates unitarity. It must be cancelled by diagrams involving the weak couplings g. Furthermore, invoking only the charged-current weak coupling of e^- to ν_e is not enough: it is present for only negative-helicity e^-; the electromagnetic amplitude for annihilation of a positive-helicity e^- with the (negative-helicity) e^+ into W^+W^- is unaffected. There are two basic options open at this point. The first is to introduce at least one neutral lepton E^o (or, more extravagantly, a doubly charged $E^{\pm\pm}$) coupled (at least in part) via a V+A interaction to e^- (and W^+). The other basic option is to introduce at least one neutral intermediate Z^o, with at least some V+A coupling, to the e^-e^+ system. We repeat: the gauge-theory solution requires

a) either a neutral heavy lepton E^o (with coupling not pure V-A)

b) or a doubly charged $E^{\pm\pm}$ (with coupling not pure V-A)

c) or a neutral intermediate boson Z^o (with coupling to e^+e^- not pure (V-A)

d) or some combination of the above (including more than one of any kind)

e) and the coupling constant g of W's and Z's to fermions of the same order of magnitude as the electromagnetic coupling e.

Again, as in the previous scheme, neutral currents are generated. Indeed they typically appear in lowest order, although it is possible to concoct,[21] with the help of heavy leptons, a scheme with no extra Z^o's. (However, such a scheme is artificial and even in trouble with experiment.[22]) All this will be treated in detail in Section III.[23]

B. The Motivation for Charm. The charm concept was introduced originally[24,25] both on aesthetic considerations (lepton-hadron parallelism) as well as on an attempt to get closer to the 3 in the then newly-established eightfold way: SU(3). It attained real operational significance only in 1970 when Glashow, Iliopoulos, and Maiani[26] showed its usefulness in alleviating the problems of strangeness-changing neutral currents and higher orders of weak interactions.

We saw that all options treated above require at some level the presence of a neutral-current coupling and that this in turn suggested strongly the existence of semileptonic $|\Delta S=1|$ neutral current couplings as in Eq. (2.7). In addition, given leptonic neutral currents parametrized phenomenologically as

$$\mathscr{L}_{\text{eff}} = \frac{G}{\sqrt{2}} (G\Lambda^2) \left[\bar{e}\gamma_\lambda(1-\gamma_5)e\right]\left[\bar{e}\gamma^\lambda(1-\gamma_5)e\right] \tag{2.9}$$

we would a priori expect similar nonleptonic terms of the same order of magnitude

$$\mathscr{L}_{\text{eff}} \sim \frac{G}{\sqrt{2}} (G\Lambda^2) \left[\bar{d}_c\gamma_\lambda(1-\gamma_5)d_c\right]\left[\bar{d}_c\gamma^\lambda(1-\gamma_5)d_c\right] \tag{2.10}$$

with

$$d_c = d\cos\theta_c + s\sin\theta_c \tag{2.11}$$

Eq. (2.10) contains a $\Delta S=2$ piece

$$\mathscr{L}_{\text{eff}}^{\Delta S=2} = \frac{2G}{\sqrt{2}} (G\Lambda^2) \cos^2\theta_c \sin^2\theta_c \left[\bar{d}\gamma_\lambda(1-\gamma_5)s\right]\left[\bar{d}\gamma^\lambda(1-\gamma_5)s\right] + \text{h.c.} \tag{2.12}$$

which has matrix elements between K and $\bar{K}$ and contributes to the K_L-K_S mass difference. Estimates of this[27,28,29] lead to the limit

$$\Lambda \lesssim 4 \text{ GeV} \tag{2.13}$$

a remarkably low value. This is where charm enters. Given a fourth charmed quark c coupled with a V-A coupling to the combination

$$s_c = s\cos\theta_c - d\sin\theta_c \tag{2.14}$$

as well as a modest amount of permutation symmetry in their couplings, it is possible to show that anywhere[30] one has a neutral-current coupling

$$\bar{d}_c\Gamma_\lambda d_c \tag{2.15}$$

one should generalize it to

$$\bar{d}_c\Gamma_\lambda d_c + \bar{s}_c\Gamma_\lambda s_c \equiv \bar{d}\Gamma_\lambda d + \bar{s}\Gamma_\lambda s \tag{2.16}$$

That is, the Cabibbo strangeness mixing can be rotated away, and with it $\Delta S\neq 0$ neutral-current effects. This is only true in the limit of vanishing quark masses. In order to remain compatible with the K_L-K_S mass difference limit, the charmed-quark mass necessarily had to be less than a few GeV.

This simple and elegant solution to the problem is the GIM mechanism. We emphasize that it is more general than and logically independent of the gauge-theory option of high energy behavior for weak interactions. It was in fact constructed before the flourishing in 1972 of the renormalizable gauge theories.[31]

C. The Higgs Sector. The introduction of gauge-theory couplings is necessary but not sufficient for curing the singular high energy behavior of weak scattering amplitudes. Production of three intermediate bosons in lepton-lepton collisions (Fig. 3) again causes difficulty.[32] Without any cancellations, the cross section would behave as

$$g^6 \frac{s^2}{m_W^6} \sim G(Gs)^2 \tag{2.17}$$

Cancellations do occur after introduction of the quartic coupling between W's in Fig. 3c but they are not complete: there is a residual piece to the J=1 amplitude which gives rise to a cross section of order

$$g^6 \frac{s}{m_W^2} \sim G^2 m_W^2 (Gs) \tag{2.18}$$

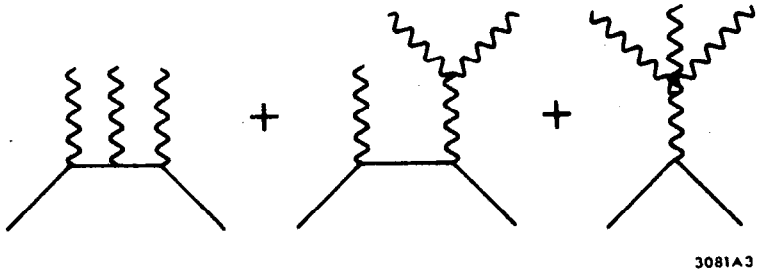

Fig. 3. Typical amplitudes for the production of three gauge bosons in e^+e^- collisions.

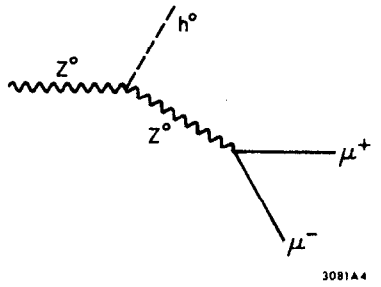

Fig. 4. Diagram for the decay $Z^o \to h^o\mu^+\mu^-$, where h^o is a neutral J=0 Higgs-boson.

To fix up this situation without reverting to a previous case involving large phase-shifts, it is necessary to introduce J=0 particles coupled principally to the gauge bosons W. Such particles, the so-called Higgs particles,[33,34] also play a role in the more fundamental field-theoretical approach. Just as in quantum electrodynamics, the pristine nonabelian gauge bosons are massless. To generate mass, the J=0 Higgs fields ϕ_r are introduced into the Lagrangian in such a way as to undergo spontaneous breakdown, i.e., the ground state contains a superfluid condensate of some of these J=0 bosons such that $<0|\phi_r(x)|0> \neq 0$. This generates a mass term for gauge bosons. There is a solid-state analogy in the Ginsburg-Landau model[35] for superconductivity:

Gauge Theory	Ginzburg-Landau
Higgs particle Lagrangian density	Free energy density
$\mathscr{L} = \frac{1}{2}\left\|\left(i\partial_\mu - g t_a B_\mu^{(a)}\right)\phi\right\|^2 - V(\phi) + \ldots$	$\mathscr{F} = \phi^+ \frac{(\vec{p} - e\vec{A})^2}{2m}\phi + V(\phi) + \ldots$
After spontaneous breakdown	
$\mathscr{L} \to \frac{g^2}{2}\left\|t_a B_\mu^{(a)} <\phi>\right\|^2$	$\mathscr{F} \to \frac{e^2}{2m}\|<\phi>\|^2 \vec{A}^2 + \ldots$
Boson mass term	Meissner effect
$\mu^2 \sim g^2 \|<\phi>\|^2$	$\mathscr{F} = \frac{1}{2m} e^2 <\phi>^2 + \frac{1}{2}(E^2 + B^2)$
	$\Rightarrow \vec{A}(x) = \vec{\epsilon}\, e^{-\lambda x}$
	London penetration depth
	$\lambda \sim \left[\frac{e^2 \|<\phi>\|^2}{m}\right]^{1/2}$
	= "effective photon mass"

Again we digress. The main point is that the exchange of a J=0 boson (coupled in the way appropriate to the spontaneously broken gauge theory) does restore acceptable high energy behavior to this order. Studies to all orders[23] have

shown that this continues to be true, with one qualification. Diagrams containing a fermion loop with three external boson lines may, because of the superficial linear divergence, produce additional problems: this is the triangle anomaly.[36] Discussion of this subtle issue is also beyond the scope of these lectures;[37] it suffices to say that the problem can only be disposed of by again appealing to algebraic cancellation.[38] The trouble in such loop diagrams is independent of fermion mass, and the amplitude, summed over all left-handed fermions which can be inserted in the loop, is multiplied by a factor

$$\mathrm{Tr}\ t_a\left\{t_b, t_c\right\}$$

where the fermion coupling to the gauge-boson in question is

$$\mathscr{L}' = g\bar{\psi}\gamma^{\lambda}(1-\gamma_5)\ t_a\psi B_{\lambda}^{(a)}$$

(Without loss of generality we include only left-handed fermions (and ipso facto right-handed antifermions) in the loop. All fermion degrees of freedom can be included just by redefinitions using CP transformations.) The condition

$$\mathrm{Tr}\ t_a\left\{t_b, t_c\right\} = 0 \tag{2.19}$$

then removes any problems with triangle diagrams, and renders the theory a weak-coupling theory at all practical energies; i.e., it is renormalizable.[39]

Renormalizability (including the above condition, Eq. (2.19)) is widely used as a criterion for a successful gauge theory. If consistently followed, we would be forced to abandon general relativity.[40] A much more persuasive reason for consideration of gauge theories is the underlying gauge principle, which links the gauge theories to electrodynamics at a much deeper level.

However, it is not clear what level we reach when we enter this gauge theory scheme of high energy behavior. We have seen that the sector (of Hilbert space) containing the J=0 Higgs particles appears to be unavoidable. The renormalizability requirement, as we saw, demands them. And if renormalizability is abandoned then some other set of particles (fermions in option 1 in Section IIA above, bosons in option 2) interact strongly at some energy. They may be expected to dynamically generate new J=0 resonances. In any model I know, something like the Higgs sector seems to be present, and on a mass scale $\lesssim$ 300 GeV. The full theory, including the Higgs sector, can be a weak-coupling theory provided the masses of Higgs particles are small compared to 300 GeV, perhaps $\lesssim m_W$ or even less. (This seems to be preferred by Weinberg.[41]) However, this option leads to ugly-duckling, cumbersome Lagrangians with a host of rather ad hoc degrees of freedom. Thus, I believe even the gauge theories do not really solve the problem of high energy behavior in a self-contained way; they instead move it into a more inaccessible region, the Higgs sector.

Is there hope of finding real Higgs bosons experimentally? It appears to be very difficult.[42] The coupling of Higgs bosons to fermions is proportional to fermion mass: the Yukawa coupling to a fermion of mass m_f is typically

$$\mathscr{H}' \sim e\frac{m_f}{m_W}\bar{\psi}\psi\phi \tag{2.20}$$

The Higgs bosons are coupled more substantially to gauge bosons. There is a quadratic coupling similar to the $A^2\phi^2$ seagull in scalar electrodynamics. In addition there is a trilinear $B_\mu B^\mu\phi$ coupling proportional to $e\,m_W$. One hope for entering the Higgs sector is to resonantly produce some neutral Z^0 in e^+e^- collisions, and look for the Higgs boson h in the decay $Z^0 \to he^+e^-$ or $Z^0 \to h\mu^+\mu^-$ (Fig. 4). There are other ideas as well,[43] but they are also futuristic and difficult. More thought on these general issues might well be fruitful.

III. THE SU(2) ⊗ U(1) MODEL

A. Introductory Generalities. We now turn to construction of the simplest and most successful gauge theory model. It consists of no extra fermions (other than a charmed quark), one charged intermediate boson $W^{\pm}$, and one (massive) neutral boson Z^0. As a prelude to its construction we consider the general case in order to exhibit how the gauge theory algebra arises. Let

$$L_i = \begin{pmatrix} e^- \\ \nu_e \\ \cdot \\ \cdot \\ \cdot \end{pmatrix} \tag{3.1}$$

be a column vector for the fermions in some internal symmetry space and the coupling to a set of gauge bosons $B_\mu^{(a)}$ given by

$$\mathcal{H}' = \left[L_f^\dagger g_{fi}^{(a)} L_i\right] \bar{u}_f \gamma^\lambda (1-\gamma_5)\, u_i B_\lambda^{(a)} \tag{3.2}$$

Similarly, for the coupling of gauge bosons a, b, c with polarizations $\epsilon^{(a)}$, $\epsilon^{(b)}$, $\epsilon^{(c)}$ to each other, write[44] (with the momentum conventions in Fig. 5)

$$\mathcal{H}' = f^{ab,c}\left[\epsilon^{(a)}\cdot\epsilon^{(b)}\right]\left[\epsilon^{(c)}\cdot(p_a - p_b)\right] + \text{cyclic permutations of a, b, c} \tag{3.3}$$

Hence

$$f^{ab,c} = -f^{ba,c} \tag{3.4}$$

as follows from Bose symmetry. With these conventions we may write down amplitudes (in the limit of vanishing fermion mass) for the processes $\ell\bar{\ell} \to WW$ corresponding to Fig. 2 and again to Fig. 6 where momentum labels and indices have been carefully included. The amplitude for Fig. 6a is

$$\mathcal{M}^{(1)} = \bar{u}_f \not{\epsilon}^{(a)} \frac{(\not{p}_i + \not{k}^{(b)})}{(p_i + k^{(b)})^2} \not{\epsilon}^{(b)} \left(\frac{1-\gamma_5}{2}\right) u_i \left[L_f^\dagger g_{fn}^{(a)} g_{ni}^{(b)} L_i\right] \tag{3.5}$$

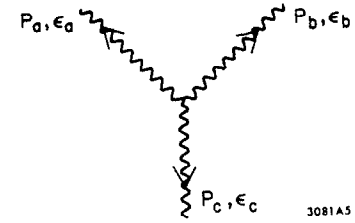

Fig. 5. Trilinear coupling of gauge bosons to each other.

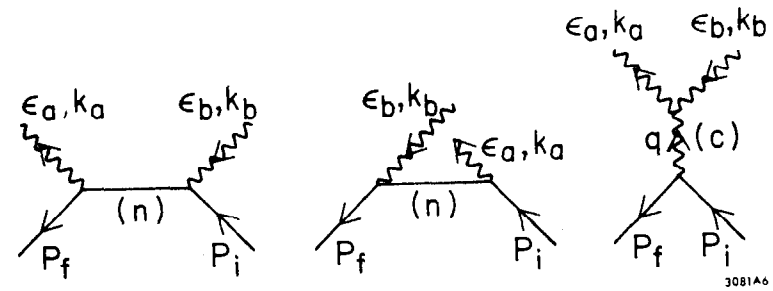

Fig. 6. General amplitudes for the process $\ell\bar{\ell} \to WW$.

Similarly for Fig. 6b, the amplitude is

$$\mathcal{M}^{(2)} = \bar{u}_f \not{\epsilon}^{(b)} \frac{(\not{p}_f - \not{k}^{(b)})}{(p_f - k^{(b)})^2} \not{\epsilon}^{(a)} \left(\frac{1-\gamma_5}{2}\right) u_i \left[L_f^\dagger g_{fn}^{(b)} g_{ni}^{(a)} L_i\right] \tag{3.6}$$

For the intermediate propagator in Fig. 6c we use

$$D_{\mu\nu} = \frac{\left(-g_{\mu\nu} + m^{-2} q_\mu q_\nu\right)}{q^2 - m^2} \tag{3.7}$$

Because of current-conservation at the bottom vertex, the $q^\mu q^\nu$ term can be dropped. This leaves

$$\mathcal{M}^{(3)} = \frac{-\bar{u}_f \gamma^\lambda \left(\frac{1-\gamma_5}{2}\right) u_i \left[L_f^\dagger g_{fi}^{(c)} L_i\right]}{q^2 - m_c^2} \begin{cases} f^{ab,c}\, \epsilon^{(a)} \cdot \epsilon^{(b)} (k^{(a)} + k^{(b)})_\lambda \\ + f^{bc,a}\, \epsilon_\lambda^{(b)}\, \epsilon^{(a)} \cdot (-k^{(b)} + q) \\ + f^{ca,b}\, \epsilon_\lambda^{(a)}\, \epsilon^{(b)} \cdot (-q - k^{(a)}) \end{cases} \tag{3.8}$$

with

$$q = p_i - p_f = k^{(a)} - k^{(b)} \tag{3.9}$$

Why do these amplitudes misbehave at high energy, when they differ from the form of the amplitudes for $e^+e^- \to \gamma\gamma$ (which does not) only by algebraic factors? The crucial difference is the form of the polarization vector ϵ_μ for a massive longitudinally polarized gauge boson. If the boson has four-momentum $k_\lambda = (k_0, 0, 0, |\vec{k}|)$, and mass m, then the polarization vector is

$$\epsilon^\lambda = \frac{1}{m}(|\vec{k}|, 0, 0, -k_0) \tag{3.10}$$

in order that $\epsilon \cdot k = 0$ and $\epsilon^2 = -1$. Thus ϵ^λ is O(k/m), not unity at high energy and, without special cancellation, leads to the singular behavior. Actually the singular part of ϵ^λ is proportional to k^λ:

$$\begin{aligned} \epsilon^\lambda &= \frac{k^\lambda}{m} + \frac{1}{m}(|\vec{k}| - k_0, 0, 0, k_0 - |\vec{k}|) \\ &= \frac{k^\lambda}{m} - \frac{m}{|\vec{k}| + k_0}(1, 0, 0, -1) = \frac{k^\lambda}{m} + O\left(\frac{m}{k}\right) \end{aligned} \tag{3.11}$$

It therefore suffices that $\mathcal{M}$ vanish upon setting one of the boson polarization vectors equal to k_λ/m. Let that vector be $\epsilon^{(b)}$. We get for the first two terms

$$\begin{aligned} \mathcal{M}^{(1)} &\to \frac{1}{m} \bar{u}_f \not{\epsilon}^{(a)} \left(\frac{1-\gamma_5}{2}\right) u_i \left[L_f^\dagger g_{fn}^{(a)} g_{ni}^{(b)} L_i\right] \\ \mathcal{M}^{(2)} &\to \frac{-1}{m} \bar{u}_f \not{\epsilon}^{(a)} \left(\frac{1-\gamma_5}{2}\right) u_i \left[L_f^\dagger g_{fn}^{(b)} g_{ni}^{(a)} L_i\right] \end{aligned} \tag{3.12}$$

A little more algebra, using $\epsilon^{(r)} \cdot k^{(r)} = 0$ and momentum conservation yields

$$\mathcal{M}^{(3)} \to \frac{-1}{m} \frac{L_f^\dagger g_{fi}^{(c)} L_i}{\left(m_a^2 + m_b^2 - 2k_a \cdot k_b - m_c^2\right)} \begin{cases} 2\epsilon^{(a)} \cdot k^{(b)}\, \bar{u}_f \not{k}^{(b)} \left(\frac{1-\gamma_5}{2}\right) u_i \left(-f^{bc,a} + f^{ab,c}\right) \\ + f^{ca,b} \left(-2k^{(a)} \cdot k^{(b)} + m_b^2\right) \bar{u}_f \not{\epsilon}^{(a)} \left(\frac{1-\gamma_5}{2}\right) u_i \end{cases} \tag{3.13}$$

This leads to two conditions. The first is

$$f^{bc,a} = f^{ab,c} = -f^{ba,c} \tag{3.14}$$

That is, we can remove the comma: f^{abc} must be fully antisymmetric. Then as $k^{(a)} \cdot k^{(b)} \to \infty$

$$\mathcal{M}^{(3)} \to \frac{-1}{m} \bar{u}_f \not{\epsilon}^{(c)} \left(\frac{1-\gamma_5}{2}\right) u_i f^{cab} \left[L_f^\dagger g_{fi}^{(c)} L_i\right] \tag{3.15}$$

Putting together Eqs. (3.12) and (3.15) and demanding the cancellation gives

$$L_f \left\{ g_{fn}^{(a)} g_{ni}^{(b)} - g_{fn}^{(b)} g_{ni}^{(a)} - f^{abc} g_{fi}^{(c)} \right\} L_i = 0 \tag{3.16}$$

or in matrix language

$$\left[g^{(a)}, g^{(b)}\right] = f^{abc} g^{(c)} \tag{3.17}$$

This is the defining relation for a Lie algebra, and the gauge-coupling constants (up to a factor) are the structure constants for the algebra.

The condition Eq. (3.14), when applied to the coupling of γ to any charged W, turns into a restriction on its magnetic moment[45]: the gyromagnetic ratio

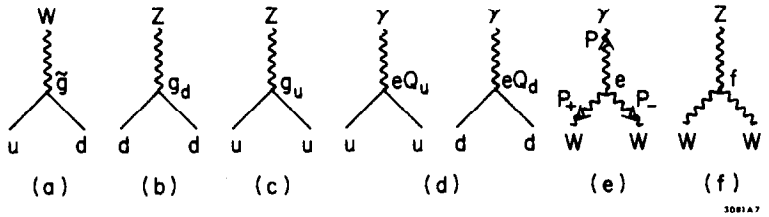

Fig. 7. Yukawa couplings of W to fermions and each other in the SU(2) ⊗ U(1) model.

must be 2 (just like the electron gyromagnetic ratio in the absence of radiative corrections).

B. The SU(2) ⊗ U(1) Model in Detail. We now apply this technique to generate by construction all the couplings needed for the Weinberg-Salam SU(2) ⊗ U(1) model. We assume the only gauge bosons are $W^{\pm}$, Z^0 (and photon), and consider $W^{\pm}$ couplings to u and d quarks. We shall endow these quarks with charge $Q_u=2/3$ and $Q_d=-1/3$ but keep the notation general in order to be able to apply the results to leptons as well. Again we neglect fermion masses, a good approximation at high energies. For the Yukawa couplings illustrated in Fig. 7, we write for the vertices

$$V_{(a)} = \tilde{g}\,\bar{d}\not{\ell}\left(\frac{1-\gamma_5}{2}\right)u \qquad W \longleftarrow u\bar{d}$$

$$V_{(b)} = g_d\,\bar{d}\not{\ell}\left(\frac{1-\gamma_5}{2}\right)d \qquad Z^0 \longleftarrow d\bar{d}$$

$$V_{(c)} = g_u\,\bar{u}\not{\ell}\left(\frac{1-\gamma_5}{2}\right)u \qquad Z^0 \longleftarrow u\bar{u}$$

$$V_{(d)} = eQ_u\left\{\bar{u}\not{\ell}\left(\frac{1-\gamma_5}{2}\right)u + \bar{u}\not{\ell}\left(\frac{1+\gamma_5}{2}\right)u\right\} \qquad \gamma \longleftarrow u\bar{u} \qquad (3.18)$$

$$+ eQ_d\left\{\bar{d}\not{\ell}\left(\frac{1-\gamma_5}{2}\right)d + \bar{d}\not{\ell}\left(\frac{1+\gamma_5}{2}\right)d\right\} \qquad \gamma \longleftarrow d\bar{d}$$

$$V_{(e)} = e\left[(\epsilon^-\cdot\epsilon^+)\,\epsilon\cdot(p_- - p_+) + (\epsilon^+\cdot\epsilon)\,\epsilon^-\cdot(p_+ - p) + (\epsilon\cdot\epsilon^-)\,\epsilon^+\cdot(p - p_-)\right]$$

$$V_{(f)} = f\left[(\epsilon^-\cdot\epsilon^+)\,\epsilon\cdot(p_- - p_+) + \epsilon^+\cdot\epsilon\;\epsilon^-\cdot(p_+ - p) + (\epsilon\cdot\epsilon^-)\,\epsilon^+\cdot(p - p_-)\right]$$

Now we can again write out the diagrams as we did in the general case. We consider only the left-handed helicity amplitudes first; the others can be handled independently later. The overall factor depending on the spinors, polarization vectors, γ-matrices, and the like should be evident and we will not write it explicitly. Instead we consider, for each diagram in Fig. 8 (note how many of them have potential physical significance!), the relationship among the coupling

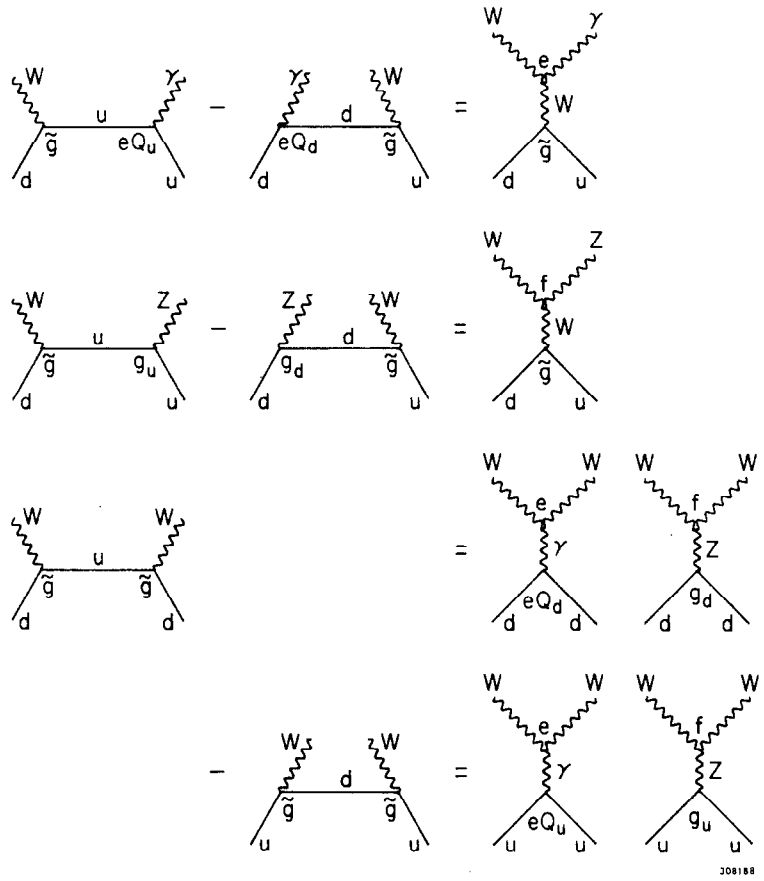

Fig. 8. Diagrams for fermion-antifermion annihilation into two gauge-bosons in the SU(2) ⊗ U(1) model.

constants, as expressed in an excessively succinct way by Eq. (3.17). They are

$$\begin{aligned} \tilde{g}(eQ_u) - (eQ_d)\tilde{g} &= e\tilde{g} \\ \tilde{g}\, g_u - g_d \tilde{g} &= f\tilde{g} \\ \tilde{g}^2 - 0 &= -\left[e^2 Q_d + f g_d\right] \\ 0 - \tilde{g}^2 &= -\left[e^2 Q_u + f g_u\right] \end{aligned} \tag{3.19}$$

Subtracting the last two equations yields the relation

$$2\tilde{g}^2 = e^2 + f^2 = g^2 \tag{3.20}$$

g is the intrinsic SU(2) gauge coupling constant connecting W^+ and W^- to W_0, which is a mixture of A and Z. Indeed letting

$$\begin{aligned} e &= g \sin\theta_W \\ f &= g \cos\theta_W \end{aligned} \tag{3.21}$$

we see that

$$W_0 = A \sin\theta_W + Z \cos\theta_W \tag{3.22}$$

couples with full strength to $W^{\pm}$, while

$$B = A \cos\theta_W - Z \sin\theta_W \tag{3.23}$$

decouples from $W^{\pm}$. The angle θ_W is the Weinberg angle, the most important parameter of the model.

Solving for the couplings gives

$$\begin{aligned} g_u &= \frac{g^2}{2f} - \frac{e^2}{f} Q_u = \frac{g}{\cos\theta_W}\left[\frac{1}{2} - Q_u \sin^2\theta_W\right] \\ g_d &= -\frac{g^2}{2f} - \frac{e^2}{f} Q_d = \frac{g}{\cos\theta_W}\left[-\frac{1}{2} - Q_d \sin^2\theta_W\right] \end{aligned} \tag{3.24}$$

We may now repeat these calculations for the right-handed amplitudes. In this case there is no coupling of W to the $(u, d)_R$ doublet. If there is no other heavy quark coupled to u or d and W, with right-handed coupling, then all the terms on the

left-hand sides of Eqs. (3.19) vanish, and the solutions for the appropriate right-handed couplings g_u^R and g_d^R of u and d to Z are evidently

$$g_u^R = -\frac{e^2}{f} Q_u = \frac{g}{\cos\theta_W}\left[0 - Q_u \sin^2\theta_W\right]$$
$$g_d^R = -\frac{e^2}{f} Q_d = \frac{g}{\cos\theta_W}\left[0 - Q_d \sin^2\theta_W\right] \qquad (3.25)$$

This has the same structure as Eq. (3.24). While we refrain from a proof, it should come as no surprise that for any constituent its coupling to the Z is likewise

$$g_q = \frac{e}{\sin\theta_W \cos\theta_W}\left[T_3 - Q \sin^2\theta_W\right]_q \qquad (3.26)$$

where T_3 is the third component of the weak isospin of the constituent q. The conventional assignment of weak isospin is

$$\text{Doublets} \qquad \begin{pmatrix} T_3 = \frac{1}{2} \\ T_3 = -\frac{1}{2} \end{pmatrix} : \begin{pmatrix} \nu_e \\ e^- \end{pmatrix}_L \quad \begin{pmatrix} \nu_\mu \\ \mu^- \end{pmatrix}_L \quad \begin{pmatrix} u \\ d_c \end{pmatrix}_L \quad \begin{pmatrix} c \\ s_c \end{pmatrix}_L \qquad (3.27)$$

$$\text{Singlets} \qquad e_R^- \quad \mu_R^- \qquad u_R \quad d_R \quad s_R \quad c_R \qquad (3.28)$$

The singlet assignments should, however, be considered tentative. Heavy leptons[46,47] or heavy quarks with new flavors might exist and provide "weak-isospin" partners for the purported singlets. It is one of the fascinating features of the *SU(2) ⊗ U(1) model that within that model the measurement of neutral-current* processes is able to provide information regarding unseen, heavy fermion degrees of freedom which possess charged-current couplings to the observed fermion degrees of freedom.

With all the couplings determined in terms of the Weinberg angle, the mass of the $W^\pm$ can be estimated. Look, for example at muon decay:

$$\mathcal{L}_{\text{eff}} = -\frac{G}{\sqrt{2}}\left[\bar{\nu}_\mu \gamma_\lambda (1-\gamma_5)\mu\right]\left[\bar{e}\gamma^\lambda(1-\gamma_5)\nu_e\right]$$
$$\cong -\frac{\tilde{g}^2}{m_W^2}\left[\bar{\nu}_\mu \gamma_\lambda \left(\frac{1-\gamma_5}{2}\right)\mu\right]\left[\bar{e}\gamma^\lambda\left(\frac{1-\gamma_5}{2}\right)\nu_e\right] \qquad (3.29)$$

Therefore, using Eqs. (3.20) and (3.21),

$$\frac{g^2}{m_W^2} = \frac{4G}{\sqrt{2}} = \frac{g^2}{2m_W^2} = \frac{e^2}{2m_W^2 \sin^2\theta_W} \qquad (3.30)$$

or

$$m_W^2 = \left(\frac{2\pi\alpha\sqrt{2}}{G}\right)\cdot\frac{1}{4\sin^2\theta_W} = \left(\frac{74.6\ \text{GeV}}{2\sin\theta_W}\right)^2 \qquad (3.31)$$

The mass of the Z^0, in general, is not determined without further assumption. A conservative approach is to consider the model a two-parameter theory and fit data to it in that manner. However, what is commonly done is to assume a mass formula relating the Z-mass to the W-mass (and θ_W). This mass relation occurs in the simplest model of spontaneous breakdown involving a minimum number of Higgs bosons.[10] It can also be obtained by the following general picture[48]: *In the beginning we suppose that we have an SU(2) triplet* (W^+, W^-, W^0) degenerate in mass and a singlet B^0 with possibly different mass. Then an additional term mixing B_0 and W^0 is included. The crucial point is that in the absence of the B-W mixing the $W^\pm$ and W^0 are assumed to be degenerate. This means the mass-term in the effective hamiltonian must be

$$\mathcal{H}' = m_W^2\left(W^+W^- + \frac{1}{2}W_0^2\right) + \frac{1}{2}\mu_1^2 B^2 + \mu_2^2 B W_0 \qquad (3.32)$$

Into this we may insert Eqs. (3.22) and (3.23) expressing B_0 and W^0 in terms of A and Z. We then demand the coefficient of A^2 as well as the term mixing A with Z be zero, because A and Z are mass eigenstates and the photon is massless.

This gives two equations, which can be solved for μ_1^2 and μ_2^2. Given μ_1^2 and μ_2^2, one may then further solve for m_Z. One obtains, after a short amount of algebra

$$m_Z = \frac{m_W}{\cos\theta_W} \tag{3.33}$$

It is evident that this is the right answer, because the resultant H'_{mass} is

$$\begin{aligned}\mathcal{H}'_{mass} &= m_W^2 W^+W^- + \tfrac{1}{2}m_Z^2 Z_0^2 \\ &= m_W^2\left[W^+W^- + \tfrac{1}{2}\cdot\frac{1}{\cos^2\theta_W}\left(\cos\theta_W W_0 - \sin\theta_W B\right)^2\right]\end{aligned} \tag{3.34}$$

which clearly satisfies (uniquely) the hypotheses we made.

Knowledge of the mass of the Z allows us to reconstruct the form of the neutral-current effective Lagrangian. From Eq. (3.26) we have (dropping an overall minus sign)

$$\mathcal{L}_{eff} = \frac{e^2}{m_Z^2\sin^2\theta_W\cos^2\theta_W}\left[\bar\psi_1\gamma_\lambda\left(\frac{1\pm\gamma_5}{2}\right)\psi_1\right]\left[\bar\psi_2\gamma^\lambda\left(\frac{1\pm\gamma_5}{2}\right)\psi_2\right]\left(T_3-Q\sin^2\theta_W\right)_1 \left(T_3-Q\sin^2\theta_W\right)_2 \tag{3.35}$$

But using Eq. (3.33) for the Z-mass and Eq. (3.30) relating the W-mass to the Fermi coupling G gives the neat result

$$\mathcal{L}_{eff} = \frac{G}{\sqrt{2}}\bar\psi_1\gamma_\lambda(1\pm\gamma_5)\psi_1\cdot\bar\psi_2\gamma^\lambda\left(\frac{1\pm\gamma_5}{2}\right)\psi_2\cdot 2\left(T_3-Q\sin^2\theta_W\right)_1\left(T_3-Q\sin^2\theta_W\right)_2 \tag{3.36}$$

The neutral current structure is the <u>same</u> as the charged-current one, with only the extra coefficient

$$\epsilon = 2\left(T_3-Q\sin^2\theta_W\right)_1\left(T_3-Q\sin^2\theta_W\right)_2 \tag{3.37}$$

to normalize the strength for any given choice of fermions and their helicities. For ν-induced neutral currents (the only processes for which there in fact exists positive evidence!), we have

$$2\left(T_3-Q\sin^2\theta_W\right)_{\nu_\mu \text{ or } \nu_e} = 1 \tag{3.38}$$

and the amplitude strength relative to the charged current strength is simply

$$\boxed{\epsilon = T_3-Q\sin^2\theta_W} \tag{3.39}$$

If one only remembers this one result, that is sufficient to reconstruct predictions for ν-induced processes in the SU(2) ⊗ U(1) model.

With an additional assumption, even the final parameter in this model, θ_W, can also be estimated <u>theoretically</u>, as shown by Georgi, Quinn, and Weinberg.[49] The assumption is that the SU(2) ⊗ U(1) model is only a small portion of the full weak-interaction theory, and that there is a <u>simple</u> group G within which SU(2) ⊗ U(1) resides as a subgroup. Such a situation is natural[50] in a truly unified weak-electromagnetic theory, for then there is only one independent coupling constant (instead of the two coupling constants of SU(2) ⊗ U(1)).

The main consequence of this embedding of SU(2) ⊗ U(1) into G is a large proliferation of the gauge-bosons in the model; one assumes[50] that all the remaining bosons have masses large compared with the $W^\pm$ and Z^0 and contribute negligibly to present-day phenomenology. This is not an especially disagreeable possibility; there exists a hierarchy of masses in the fermion sector ($m_e \ll m_\mu \ll m_U$; $m_{u,d} \ll m_s \ll m_c$) which is not at all understood. A similar such hierarchy in the intermediate-boson sector may bear some relationship. But in any case, assuming such an embedding, the result of Georgi, Quinn, and Weinberg is the following: Let $\mathcal{R}$ be the basis of some fermion representation of the group G; i.e., $\mathcal{R}$ is some multiplet of fermions appropriate to the group G. It therefore can be decomposed according to the SU(2) ⊗ U(1) subgroup. Then the GQW

result is

$$\sin^2 \theta_W = \frac{\sum_{i \text{ in } \mathscr{R}} T_{3i}^2}{\sum_{i \text{ in } \mathscr{R}} Q_i^2} \tag{3.40}$$

where the sum goes over all chiral (two-component) degrees of freedom in the multiplet $\mathscr{R}$, T_{3i} is third component of weak isospin of the ith fermion, and Q_i is its charge.

The proof of Eq. (3.40) is short. We note first that W^O and B, gauge bosons appropriate to $SU(2) \otimes U(1)$, are also gauge-bosons of G. The coupling of W_0 to fermion i is proportional to T_{3i}. The coupling of B is a weak isosinglet; call its coupling to the ith fermion T_{0i}. Because W_0 and B are both gauge particles for the group G, we must have, for any representation of G

$$\sum_{i \text{ in } \mathscr{R}} T_{3i}^2 = \sum_{i \text{ in } \mathscr{R}} T_{0i}^2 \tag{3.41}$$

because a symmetry operation U of the group G can transform W_0 into B; U however transforms $\mathscr{R}$ into itself. (Another way to see this is to look at the W_0 and B propagators; the vacuum polarization insertions (in the symmetry limit) in Fig. 9 must be the same. But they are proportional to the quantities in Eq. (3.41).)

Completion of the proof is now simple algebra. The photon is a gauge particle for G; furthermore it lies in the $SU(2) \otimes U(1)$ subgroup (by construction; see the previous sections). Therefore the charge Q_i must be a linear combination of T_{3i} and T_{0i}; indeed from Eqs. (3.22) and (3.23), it is clear that

$$A^\lambda = W_0^\lambda \sin \theta_W + B^\lambda \cos \theta_W \tag{3.42}$$

and necessarily

$$Q_i = (\text{const}) \left[T_{3i} \sin \theta_W + T_{0i} \cos \theta_W \right] \tag{3.43}$$

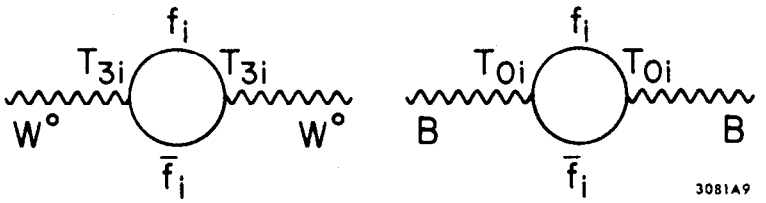

Fig. 9. Vacuum polarization insertions in gauge boson W_0 and B propagators. Note that they are proportional to T_{3i}^2 and T_{0i}^2 respectively.

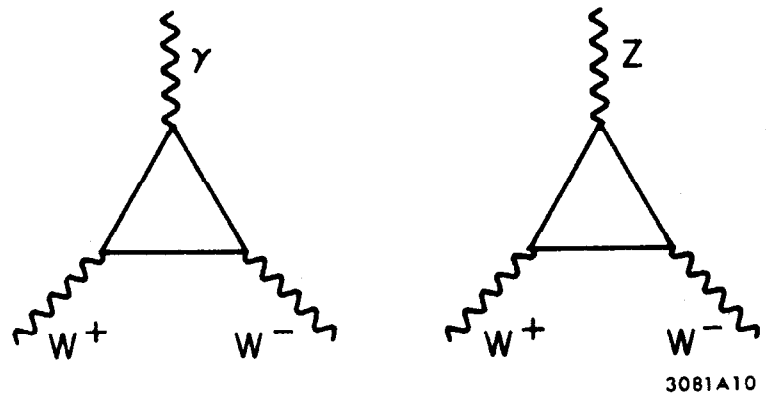

Fig. 10. Triangle diagrams in $SU(2) \otimes U(1)$ model.

Finally, in order to have $\Delta Q_i = \pm 1$ for members of weak isospin multiplets, we need the constant to be $(\sin\theta_W)^{-1}$; i.e.,

$$Q_i = T_{3i} + \cot\theta_W\, T_{0i} \tag{3.44}$$

Now we square Eq. (3.44), and sum over members i in the multiplet $\mathscr{R}$ of G. The cross term vanishes

$$\sum_i T_{3i}\, T_{0i} = 0 \tag{3.45}$$

when summed over any weak-isospin submultiplet. We obtain

$$\sum_{i\ \text{in}\ \mathscr{R}} Q_i^2 = \sum_{i\ \text{in}\ \mathscr{R}} T_{3i}^2 + \cot^2\theta_W \sum_{i\ \text{in}\ \mathscr{R}} T_{0i}^2 \tag{3.46}$$

and upon utilizing Eq. (3.41), we obtain the main result, Eq. (3.40).

It is fun to estimate $\sin^2\theta_W$ using the known fermions. We take 3 or 4 examples:

1. <u>All leptons form a basis $\mathscr{R}$ for a representation of the group G.</u> Then

$$\sin^2\theta_W = \frac{\left(\frac{1}{2}\right)^2_{e_L^-} + \left(\frac{1}{2}\right)^2_{\mu_L^-} + \left(\frac{1}{2}\right)^2_{\nu_\mu} + \left(\frac{1}{2}\right)^2_{\nu_e} + ?}{(1)_{e_L^-} + (1)_{e_R^-} + (1)_{\mu_L^-} + (1)_{\mu_R^-} + ?} = \frac{1+?}{4+?} = .25 + ? \tag{3.47}$$

where the ? signifies the contribution of unknown degrees of freedom we have omitted.

2. <u>All quarks separately form a basis for a representation $\mathscr{R}$ of G.</u> Then

$$\sin^2\theta_W = \frac{3\cdot\left\{\left(\frac{1}{2}\right)^2_{u_L} + \left(\frac{1}{2}\right)^2_{d_L} + \left(\frac{1}{2}\right)^2_{s_L} + \left(\frac{1}{2}\right)^2_{c_L} + ?\right\}}{3\cdot 2\cdot\left\{\left(\frac{2}{3}\right)^2_{u} + \left(\frac{1}{3}\right)^2_{d} + \left(\frac{1}{3}\right)^2_{s} + \left(\frac{2}{3}\right)^2_{c} + ?\right\}} = \frac{3+?}{\frac{20}{3}+?} = .45 + ? \tag{3.48}$$

Consistency demands that these two values be <u>the same</u>. This requires either proliferation of fermion degrees of freedom or else combining both lepton and hadron degrees of freedom in <u>all</u> representations of G. Elegant examples of this concept have been given by Georgi and Glashow,[51] and by Gursey and Sikivie.[52,53] Combination of <u>all</u> fermion degrees of freedom—quarks and leptons—leads to the estimate

$$\sin^2\theta_W = \frac{\left(\frac{1}{2}\right)^2\{4 + 3.4 + ?\}}{2\cdot\left\{2 + 3\cdot\frac{10}{9} + ?\right\}} = \frac{4+?}{\frac{32}{3}+?} = .375 + ? \tag{3.49}$$

Such fully unified models require intermediate bosons of fractional charge and baryon number (leptoquarks) and in at least many cases tend to destabilize the proton via reactions such as $q+q \to \bar{q}+\ell$. This requires such leptoquark gauge-bosons to be extremely massive, typically with mass $\gtrsim 10^{15}$ GeV.

A panacea which is considerably less grand in scope is to increase the leptonic estimate of $\sin^2\theta_W$ by presuming the existence of massive neutral heavy leptons E^o and M^o coupled via right-handed currents to e^- and μ^- respectively. This leads to the estimate

$$\sin^2\theta_W = \frac{\frac{1}{4}\cdot(8 + ?)}{2\cdot(2 + ?)} = .50 + ? \tag{3.50}$$

which is more in line with the estimate from the quarks. However both values, as we shall see, are in rather marginal agreement with the data, which prefers a value of $\sin^2\theta_W$ somewhat smaller. Nevertheless, all these estimates are not all that far from the data, and may be taken as another argument in favor of gauge theories, and in particular the $SU(2)\otimes U(1)$ model, as a correct description of weak-interaction phenomena.

Before closing this section, we should mention the question of triangle anomalies in the $SU(2)\otimes U(1)$ model. The only triangle diagrams involve $W^+W^-Z^o$ and $W^+W^-\gamma$. We see that upon summing over <u>all</u> fermions, the condition for cancellation of the $W^+W^-\gamma$ triangle-anomaly is, from Eq. (2.19)

$$\sum_{\text{left-handed fermions } i} \langle i\,|\{T^+, T^-\}Q\,|i\rangle = 0 \tag{3.51}$$

There is no new information that comes from the W^+W^-Z triangle couplings, because automatically

$$\sum_i \langle i | \left[T_+, T_- \right] T_3 | i \rangle = 0 \tag{3.52}$$

With the assignment of the standard model, Eq. (2.19), this means we should have

$$\sum_{\substack{\text{(all fermions i in} \\ \text{left-handed weak} \\ \text{doublets)}}} Q_i = 0 = -1+0-1+0+3\left(\frac{2}{3}-\frac{1}{3}-\frac{1}{3}+\frac{2}{3}\right) \tag{3.53}$$

$$e \quad \nu_e \quad \mu \quad \nu_\mu \quad u \quad d \quad s \quad c$$

which actually works! Such a condition is widely considered a boon, and a positive indication of the relevance of $SU(2) \otimes U(1)$, charm, and nothing else as a correct model of nature. However, the only basis for demanding anomaly-cancellation is renormalizability, and in a rather high order of perturbation theory at that. As mentioned before this may not be a safe criterion to demand of a physical theory.

IV. INTERMEDIATE BOSONS IN GENERAL

The apparent current-current structure of charged-current weak interactions—and perhaps of neutral-current reactions as well—strongly suggests the intermediate boson hypothesis, even in the absence of some underlying gauge theory. However, the hypothesis of an underlying gauge theory is more predictive. We saw that in the $SU(2) \otimes U(1)$ model the masses of $W^\pm$ and Z^0 are determined rather well, m_W typically in the range 50–75 GeV, and m_{Z^0} in the range 75–85 GeV.

It turns out that such estimates can be generalized beyond the $SU(2) \otimes U(1)$ model.[54] The main assumption needed for such a generalization is, as in the preceding discussion, that the underlying gauge group G be simple, i.e., have only one coupling constant. Another is that the low-energy effective weak Lagrangian is of current-current form and built from tricolored fractionally charged quarks. With a few more relatively innocuous assumptions, it is possible to construct upper and lower bounds for the masses of W and upper bounds for the mass of the Z. Here the W and Z are defined as the <u>least massive</u> charged and neutral gauge-bosons in the theory (apart from the photon) which couple the known fermions. Before stating these bounds define

$\mathscr{R}$ = basis for some fermion representation of G, as before.

$R_0 = \sum_{i \text{ in} \mathscr{R}} Q_i^2$ (as in the usual definition of R for $e^+e^- \to$ hadrons)

(4-component fermions summed).

M = number of independent terms in $\mathscr{J}_\lambda^\dagger \mathscr{J}^\lambda$ coupling in the effective charged-current Lagrangian.

B_f = branching ratio of W into fermion pair f (assuming $m_W >> m_f$ for all f in $\mathscr{R}$).

Then the result is

$$\text{I:} \quad 75 \text{ GeV} \sqrt{B_{e\bar{\nu}_e} R_0} \leq m_W \leq 75 \text{ GeV} \sqrt{\frac{R_0}{M}} \tag{4.2}$$

A less restrictive result, which can be obtained without assuming the current-current structure of the effective Lagrangian, but only that the effective Lagrangian for semileptonic processes is of the usual form, is

$$\text{II:} \quad m_W \leq 75 \text{ GeV} \left(\frac{4}{3}\right)^{1/4} \sqrt{\frac{R_0}{M'}} \tag{4.3}$$

where

$$M' = \begin{cases} \geq 3 & \text{if only u, d, s quarks are accepted as members of } \mathscr{L}_{\text{eff}}. \\ \geq 6 & \text{if u, d, s, c quarks, along with the GIM coupling, are accepted.} \end{cases} \tag{4.4}$$

Examples of what these formulae mean are given in Table I for various choices of the representation $\mathscr{R}$.

Table I: General Bounds on m_W (in GeV).

Representation R	Lower Bound I	Upper Bound I	Upper Bound II (fewer assumptions)
$e^-, \nu_e, \mu^-, \nu_\mu, \ldots$?	$\geq 75 \pm ?$	$\leq 75 \pm ?$	--
$u_i, d_i, s_i, \ldots$? (color)	$\geq 61 \pm ?$	$\leq 61 \pm ?$	--
$u_i, d_i, s_i, c_i, \ldots$? (GIM, color)	$\geq 56 \pm ?$	$\leq 56 \pm ?$	--
$e^-, \nu_e, \mu^-, \nu_\mu, \ldots$? $u_i, d_i, s_i, \ldots$? (color)	$\geq 67 \pm ?$	$\leq 67 \pm ?$	$\leq 68 \pm ?$
$e^-, \nu_e, \mu^-, \nu_\mu, \ldots$? $u_i, d_i, s_i, c_i, \ldots$? (GIM, color)	$\geq 61 \pm ?$	$\leq 61 \pm ?$	$\leq 71 \pm ?$
$e^-, \nu_e, \mu^-, \nu_\mu, E^0, M^0, \ldots$? (E^0, M^0, coupled to e^-, μ^- with right-handed currents)	$\geq 53 \pm ?$	$\leq 53 \pm ?$	--

The method for deriving these bounds is to first embed G in an SU(N) group (with N = numbers of 2-component fermion degrees of freedom in the multiplet $\mathscr{R}$), and then to use straightforward Schwartz inequality methods. One sees that the results are very similar (not surprisingly) to those obtained within the $SU(2) \otimes U(1)$ scheme.

The bounds on the Z^0 mass, regrettably, are less restrictive. Defining

$$R = \left.\frac{\sigma_{tot}(\nu N \to \nu \text{ hadrons})}{\sigma_{tot}(\nu N \to \mu^- \text{hadrons})}\right|_{E_\nu \text{ large}}, \begin{pmatrix}\text{but below new-}\\ \text{flavor thresholds}\end{pmatrix}$$

$$\bar{R} = \left.\frac{\sigma_{tot}(\bar{\nu} N \to \bar{\nu} \text{ hadrons})}{\sigma_{tot}(\bar{\nu} N \to \mu^+ \text{hadrons})}\right|_{E_\nu \text{ large}} \tag{4.5}$$

$$R_{cc} = \left.\frac{\sigma_{tot}(\bar{\nu} N \to \mu^+ \text{hadrons})}{\sigma_{tot}(\nu N \to \mu^- \text{hadrons})}\right|_{E_\nu \text{ large}}$$

we find, under the previous assumptions

$$m_{Z^0} \leq (75 \text{ GeV}) R_0^{1/2} \left[\frac{2\left(1-R_{cc}^2\right)}{M'\left(R-\bar{R}R_{cc}^2\right)}\right]^{1/4} \tag{4.6}$$

This turns out to be a rather poor restriction in comparison to what is obtained within the $SU(2) \otimes U(1)$ model. Competitive bounds are obtained with the strong assumption that only one Z^0 mediates the observed neutral-current phenomena. Then

$$\text{IV:} \qquad m_{Z^0} \leq (75 \text{ GeV}) R_0^{1/2} \left[\frac{(1+R_{cc})}{4M'(R+R_{cc}\bar{R})}\right]^{1/4} \tag{4.7}$$

If in addition ν_μ-ν_e universality is presumed, one can gain an additional improvement of a factor $\sqrt[4]{2}$:

$$\text{V:} \qquad m_{Z^0} \leq (75 \text{ GeV}) R_0^{1/2} \left[\frac{1+R_{cc}}{8M'(R+R_{cc}\bar{R})}\right]^{1/4} \tag{4.8}$$

Finally, with all assumptions but the last one, a direct estimate (via the technique used to obtain lower bounds for m_W) gives

$$\text{VI:} \qquad m_Z \approx (75 \text{ GeV}) R_0^{1/2} \left[\frac{B_{\nu_\mu \bar{\nu}_\mu} B_{had}(1+R_{cc})}{M'(R+R_{cc}\bar{R})}\right]^{1/4} \tag{4.9}$$

We summarize these bounds and estimates in Table II.

Table II: Bounds and Estimates of m_{Z^0} (in GeV).

Representation	Upper Bound III (general)	Upper Bound IV (only one Z^0 for observed phenomena)	Upper Bound IV (as in IV, plus ν_μ-ν_e universality)	Estimate VI[a] (as in IV)
$e^-, \nu_e, \mu^-, \nu_\mu, \ldots$				
$u_i, d_i, s_i, \ldots$ (color)	$\leq 189 \pm ?$	$\leq 107 \pm ?$	$\leq 90 \pm ?$	--
$e^-, \nu_e, \mu^-, \nu_\mu, \ldots$				
$u_i, d_i, s_i, c_i, \ldots$ (GIM, color)	$\leq 184 \pm ?$	$\leq 104 \pm ?$	$\leq 88 \pm ?$	$69 \pm ?$

[a] We use $B_{\nu_\mu \bar{\nu}_\mu} = 8\%$, $B_{had} = 75\%$, in accord with the simplest of guesses using only statistical weights.

Can the W and Z actually be produced in any foreseeable future? There is considerable reason to believe that, if these estimates are correct, the answer is yes. In hadron-hadron collisions, the Drell-Yan mechanism[55,56] appears thus far to provide a good description of the electromagnetic production of massive dilepton pairs. This mechanism is a parton model process in which pointlike quarks and antiquarks annihilate into the lepton pairs. It is beyond the scope of these lectures (however, cf. the lectures of D. Hitlin; these proceedings) to describe this. Suffice it to say that, if the process $q+\bar{q} \to \ell^+ + \ell^-$ can be observed, so also can the resonant processes $q+\bar{q} \to W$ or $q+\bar{q} \to Z^0$. One only needs the width for $W \to q+\bar{q}$ or $Z \to q+\bar{q}$ to calculate the cross sections,[57] which turn out to be in the range $10^{-33} - 10^{-35}$ cm^2 and accessible to future pp storage rings.

It is a straightforward, model independent, calculation to estimate the width of the W as a function of its mass. The simplest of Feynman-diagram calculations gives

$$\Gamma(W^- \to e^- \bar{\nu}_e) = \frac{G m_W^3}{6\pi\sqrt{2}} \tag{4.10}$$

with a branching ratio (assuming u, d, s, c, color, and GIM charm) of

$$B_{e\bar{\nu}_e}^{-1} = \underset{e\bar{\nu}_e}{1} + \underset{(\mu\bar{\nu}_\mu)}{1} + \underset{(u\bar{d})}{3} + \underset{(c\bar{s})}{3} + ? \geq 8 \tag{4.11}$$

or

$$B_{e\bar{\nu}_e} \leq 12.5\% \tag{4.12}$$

Staying within the $SU(2) \otimes U(1)$ scheme and taking the experimental (as well as theoretical!) limits on $\sin^2\theta_W$, to be discussed in Section V,

$$.25 \lesssim \sin^2\theta_W \lesssim .50 \tag{4.13}$$

leads to

$$\begin{aligned} m_W &= 64 \pm 11 \text{ GeV} \\ m_Z &= 80 \pm 6 \text{ GeV} \end{aligned} \tag{4.14}$$

and

$$\Gamma(W^- \to e^- \bar{\nu}_e) \sim 115 \text{ MeV} \tag{4.15}$$

Thus

$$\Gamma(W \to \text{all}) \gtrsim 900 \text{ MeV} \tag{4.16}$$

The W is rather broad!

For the Z we estimate, in the $SU(2) \otimes U(1)$ scheme

$$\frac{\Gamma(Z \to \nu_\mu \bar{\nu}_\mu)}{\Gamma(W^- \to e^- \bar{\nu}_e)} = \left(\frac{m_Z}{m_W}\right) \frac{\left(\frac{1}{2} \cdot \frac{e}{\sin\theta_W \cos\theta_W}\right)^2}{\left(\frac{e}{\sqrt{2}\sin\theta_W}\right)^2} = \frac{1}{2}\left(\frac{m_Z}{m_W}\right)^3 \tag{4.17}$$

The ratio (m_Z/m_W) comes from dimensional analysis; evidently

$$\Gamma = m \times (\text{factors } 2, \pi, \text{ etc. from phase-space}) \times (\text{coupling constants}) \quad (4.18)$$

The coupling constant of Z to $\nu_\mu \bar{\nu}_\mu$ is the second factor in the numerator, obtained from Eq. (3.26), while the W coupling to $e\bar{\nu}_e$ in the denominator is found in Eq. (3.30). Finally we have used the mass formula relating m_Z and m_W; Eq. (3.33).

This yields the estimate (using $m_W = 65$ GeV, $m_Z = 80$ GeV)

$$\Gamma(Z \to \nu_\mu \bar{\nu}_\mu) \sim 110 \text{ MeV} \quad (4.19)$$

Then, remembering that Z-couplings are proportional to $(T_3 - Q\sin^2\theta_W)$, all other partial widths are immediately written down:

$$\frac{\Gamma(Z \to \mu^+\mu^-)}{\Gamma(Z \to \nu_\mu \bar{\nu}_\mu)} = \frac{\left(-\frac{1}{2} + \sin^2\theta_W\right)^2_{LH} + \left(\sin^2\theta_W\right)^2_{RH}}{\left(\frac{1}{2}\right)^2} = 1 - 4\sin^2\theta_W + 8\sin^4\theta_W \quad (4.20)$$

$$\frac{\Gamma(Z \to u\bar{u})}{\Gamma(Z \to \nu_\mu \bar{\nu}_\mu)} = \frac{3\left\{\left(\frac{1}{2} - \frac{2}{3}\sin^2\theta_W\right)_{LH} + \left(\frac{2}{3}\sin^2\theta_W\right)^2_{RH}\right\}}{\left(\frac{1}{2}\right)^2} = 3 - 8\sin^2\theta_W + \frac{32}{3}\sin^4\theta_W \quad (4.21)$$

(Notice the factor 3 for color; it must be there if one includes it in describing R in $e^+e^- \to$ hadrons.) Finally

$$\frac{\Gamma(Z \to d\bar{d})}{\Gamma(Z \to \nu_\mu \bar{\nu}_\mu)} = \frac{3\left\{\left(-\frac{1}{2} + \frac{1}{3}\sin^2\theta_W\right)^2 + \frac{1}{9}\sin^4\theta_W\right\}}{\left(\frac{1}{2}\right)^2} = 3 - 4\sin^2\theta_W + \frac{8}{3}\sin^4\theta_W \quad (4.22)$$

For $\sin^2\theta_W = 0.36$, one calculates

$$\frac{\Gamma(Z \to \mu^+\mu^-)}{\Gamma(Z \to \nu_\mu \bar{\nu}_\mu)} = 0.6 \qquad \frac{\Gamma(Z \to u\bar{u})}{\Gamma(Z \to \nu_\mu \bar{\nu}_\mu)} = 1.5 \qquad \frac{\Gamma(Z \to d\bar{d})}{\Gamma(Z \to \nu_\mu \bar{\nu}_\mu)} = 1.9 \quad (4.23)$$

and therefore, using GIM, color, and charm:

$$\frac{\Gamma_{tot}}{\Gamma(Z \to \nu_\mu \bar{\nu}_\mu)} \geq \underset{(\nu_e)}{1} + \underset{(\nu_\mu)}{1} + \underset{(e)}{0.6} + \underset{(\mu)}{0.6} + \underset{(u)}{1.5} + \underset{(c)}{1.5} + \underset{(d)}{1.9} + \underset{(s)}{1.9} = 10.0 \quad (4.24)$$

or

$$\Gamma^{Z^0}_{tot} \approx 1.1 \text{ GeV}$$
$$B_{Z \to e^+e^-} \lesssim 0.06 \quad (4.25)$$

In addition to W and Z production in strong interactions, resonant production of Z^0 in e^+e^- colliding beams would clearly be an extraordinary powerful and clean way[58] of studying all objects of moderate mass coupled to Z^0. To get an idea of what is involved, we need only look at the peak cross section, as follows from the Breit-Wigner formula:

$$\sigma_{BW}(e^+e^- \to Z^0) = \frac{12\pi\,\Gamma(Z \to e^+e^-)\,\Gamma(Z \to f)}{\left(s - m_Z^2\right)^2 + m_Z^2\,\Gamma^2_{tot}} \quad (4.26)$$

At the resonance peak, this means

$$\sigma_{peak}(e^+e^- \to Z^0) = \frac{12\pi}{m_Z^2} B_{e^+e^-} B_f \quad (4.27)$$

Notice, for $m_Z \sim 80$ GeV and $\Gamma_Z \gtrsim 1$ GeV, the finite machine-resolution ($\ll 1\%$) does not lower significantly the peak cross section (unlike the case of resonant production of the ψ). Taking the $SU(2) \otimes U(1)$ estimates

$$B_{e^+e^-} \sim 6\%$$
$$B_f \sim 1 - B_{\nu_e \bar{\nu}_e} - B_{\nu_\mu \bar{\nu}_\mu} \approx 80\% \quad (4.28)$$
$$m_Z \sim 80 \text{ GeV}$$

along with a luminosity $\mathscr{L} \sim 10^{32}$ cm^{-2} sec^{-1} (a typical futuristic estimate for such rings) this gives

$$\text{Rate of Z-production} \sim 10 \text{ Z's/sec} \quad . \quad (4.29)$$

With such a yield of pure Z's, one should think hard about rare decay-modes of the Z^0. One that comes to mind is the decay $Z^0 \to W^+ e^- \bar{\nu}_e$. However, with SU(2)⊗U(1) parameters, a crude estimate gives a discouraging number ($B(We\nu_e) \lesssim 10^{-6}$). More interesting is the decay $Z^0 \to h^0 \mu^+ \mu^-$, with h_0 the Higgs boson in the simple SU(2)⊗U(1) model. A straightforward calculation (slightly beyond the scope of these lectures), optimistically assuming that a single Higgs boson is responsible for the Z mass, gives

$$\frac{1}{\Gamma(Z \to \mu\mu)} \frac{d\Gamma}{dx} = \frac{\alpha}{4 \sin^2\theta_W \cos^2\theta_W} \frac{\left[1 - x + \frac{x^2}{12} + \frac{2}{3}\frac{m_h^2}{m_Z^2}\right]\left(x^2 - \frac{4m_h^2}{m_Z^2}\right)^{1/2}}{\left(x - \frac{m_h^2}{m_Z^2}\right)^2} \tag{4.30}$$

where

$$x = \frac{2E_{higgs}}{m_Z} \tag{4.31}$$

and the kinematic limits are

$$\frac{2m_h}{m_Z} \leq x \leq 1 + \frac{m_h^2}{m_Z^2} \tag{4.32}$$

Rough numerical integration provides the yield shown in Fig. 11. We see that for $m_h \lesssim 40$ GeV, the branching ratio relative to μ pairs $B(Z \to h^0 \mu^+ \mu^-)/B(Z^0 \to \mu^+ \mu^-)$, is $\gtrsim 3 \times 10^{-5}$. Recalling that a 6% $\mu^+\mu^-$ branching ratio still means ~0.6 $Z^0 \to \mu^+\mu^-$ events/second, this leaves a tolerable production of Higgs bosons. The signature evidently is very good; one looks at a peak in the mass recoiling against an energetic acoplanar dilepton pair. We must, however, point out that this estimate, as is any estimate which directly involves the Higgs sector, is very unreliable: the theoretical status is very poorly understood.[42] Indeed there is no certainty that $m_h \lesssim 40$ GeV; Higgs bosons could be ten times more massive.[59] And there could well be several.

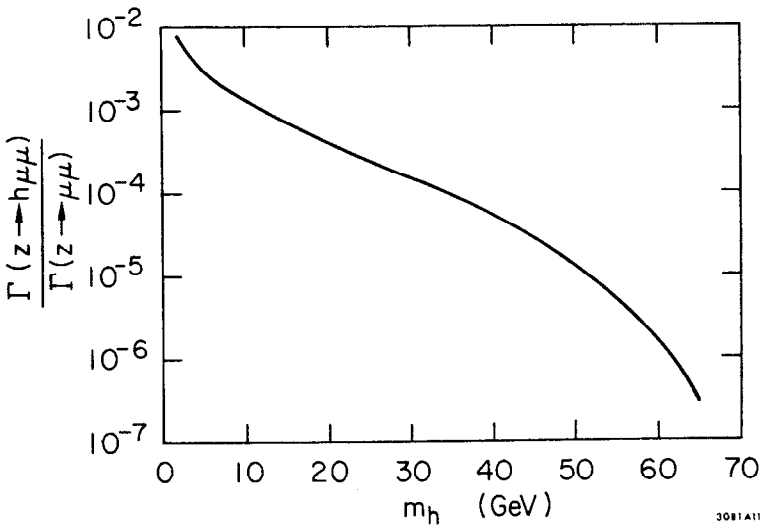

Fig. 11. Estimated branching ratio of $Z \to h^0\mu^+\mu^-$ relative to $Z^0 \to \mu^+\mu^-$. We have taken $\sin^2\theta_W = 1/3$.

On the other hand, if $m_h < \frac{1}{2} m_Z$, the decay $Z^o \to h^o h^o$ has a very large branching ratio, nearly competitive with $Z^o \to \mu^+ \mu^-$. Observability of this process depends upon the dominant decay modes of h^o, an uncertain matter indeed.

V. SOME NEUTRAL CURRENT PHENOMENOLOGY

Thus far, we have only laid the groundwork for describing the observations on charged and neutral-current phenomena. We now discuss some of the relevant experimental information. Regrettably, there is not the time to discuss even all the neutral-current data which bears on the issues. We sacrifice any extensive discussion of resonance and/or single pion production, i.e., reactions such as

$$\begin{aligned} \nu p &\to \nu \Delta^+ \\ \nu n &\to \nu p \pi^- \\ \nu p &\to \nu p \pi^+ \pi^- \end{aligned} \tag{5.1}$$

This is not to be interpreted that these reactions are not of interest; on the contrary it should be possible to learn a great deal, especially isospin-structure of the neutral current couplings, by such studies. An excellent and most authoritative introduction to the subject can be found in the lectures of Adler[60] at the 1975 Hawaii Summer School. We shall instead concentrate on what might be learned from existing deep-inelastic data, from the new data on elastic νp and $\bar{\nu} p$ scattering, and from the experiments on parity-violation in atomic physics which are now in progress.

We shall approach the phenomenology from two points of view:

1. Can we determine the neutral-current couplings (as defined in the effective Lagrangian in Eq. (1.4)) in a model independent way?

2. Is the $SU(2) \otimes U(1)$ gauge theory model (or variants thereof) in accord with the data??

A. Leptonic Neutral Currents. There are three channels for which there exists some data:

$$\begin{aligned} \bar{\nu}_\mu e^- &\to \bar{\nu}_\mu e^- \\ \nu_\mu e^- &\to \nu_\mu e^- \\ \bar{\nu}_e e^- &\to \bar{\nu}_e e^- \end{aligned} \tag{5.2}$$

The first two have been studied in the CERN PS neutrino beam, both in the heavy liquid bubble chamber Gargamelle,[61] and in a counter experiment (Aachen-Padua) behind it.[62] The Gargamelle data consist of three $\bar{\nu}_\mu e^-$ events and no $\nu_\mu e^-$ events above background, from which come the estimates

$$\begin{aligned} \sigma_{\bar{\nu}_\mu e^-} &= \left(.11 \,{}^{+.21}_{-.09}\right) \times 10^{-41} \, E_\nu \, \text{cm}^2 \, \text{GeV}^{-1} \\ \sigma_{\nu_\mu e^-} &< .26 \times 10^{-41} \, E_\nu \, \text{cm}^2 \, \text{GeV}^{-1} \; (90\% \text{ conf.}) \end{aligned} \tag{5.3}$$

The Aachen-Padua group, on the other hand, find a considerably larger yield, and quote[63]

$$\begin{aligned} \sigma_{\bar{\nu}_\mu e^-} &= (.54 \pm .17) \times 10^{-41} \, E_\nu \, \text{cm}^2 \, \text{GeV}^{-1} \\ \sigma_{\nu_\mu e^-} &= (.24 \pm .12) \times 10^{-41} \, E_\nu \, \text{cm}^2 \, \text{GeV}^{-1} \end{aligned} \tag{5.4}$$

The theoretical cross section for $\nu_\mu e^-$ scattering is easily derived from the effective Lagrangian written down in Section I; Eq. (1.4). It is (at high energy)

$$\sigma_{\nu_\mu e^-} = \frac{2G^2 m_e E_\nu}{\pi} \left\{ |\epsilon_L(e)|^2 + \frac{1}{3} |\epsilon_R(e)|^2 \right\} \tag{5.5}$$

while

$$\sigma_{\bar{\nu}_\mu e^-} = \frac{2G^2 m_e E_\nu}{\pi} \left\{ \frac{1}{3} |\epsilon_L(e)|^2 + |\epsilon_R(e)|^2 \right\} \tag{5.6}$$

Putting in the numbers gives the estimates

$$|\epsilon_L(e)|^2 + \frac{1}{3}|\epsilon_R(e)|^2 = \begin{cases} \leq .15 \text{ (90\% conf.) GGM} \\ .31 \pm .10 \text{ AP} \end{cases}$$
$$|\epsilon_R(e)|^2 + \frac{1}{3}|\epsilon_L(e)|^2 = \begin{cases} .06^{+.12}_{-.05} \text{ GGM} \\ .14 \pm .07 \text{ AP} \end{cases} \qquad (5.7)$$

The SU(2)⊗U(1) model, from the rule in Eq. (3.39) that (for neutrino-induced reactions) $\epsilon = T_3 - Q \sin^2\theta_W$, gives

$$\epsilon_L(e) = -\frac{1}{2} + \sin^2\theta_W$$
$$\epsilon_R(e) = \sin^2\theta_W \qquad (5.8)$$

provided e_R^- is a weak singlet; if it is a weak doublet (i.e., e_R^- is coupled via $W^\pm$ to a heavy lepton E^0) evidently $\epsilon_R(e) = \epsilon_L(e)$. The present limits, as quoted by Gargamelle, give rise to the allowed regions in Fig. 12. Clearly these measurements are not yet good enough to draw much of any quantitative conclusions. However knowledge of the very existence of the neutral current reaction $\bar{\nu}_\mu e^- \to \bar{\nu}_\mu e^-$ is, of course, of very great importance.

Data on the reaction $\bar{\nu}_e e^- \to \bar{\nu}_e e^-$ at low energy (using reactor $\bar{\nu}_e$'s of a few MeV energy) has recently been reported.[64] The ordinary diagonal charged-current coupling is expected to contribute here as well as any additional neutral current coupling. Adding this to Eq. (1.4), along with a Fierz transformation, gives

$$\mathscr{L}_{\text{eff}} = \frac{G}{\sqrt{2}} \bar{\nu}_e \gamma_\lambda (1-\gamma_5) \nu_e \left[(1 + \epsilon_L(e))\, \bar{e}\gamma^\lambda(1-\gamma_5)e + \epsilon_R(e)\, \bar{e}\gamma^\lambda(1+\gamma_5)e \right] \qquad (5.9)$$

with again a differential cross section of a form as in Eq. (5.6); when $E \gg m_e$

$$\sigma_{\bar{\nu}_e e^-} = \frac{2G^2 m_e E}{\pi} \left\{ |\epsilon_R(e)|^2 + \frac{1}{3}|1 + \epsilon_L(e)|^2 \right\} \qquad (5.10)$$

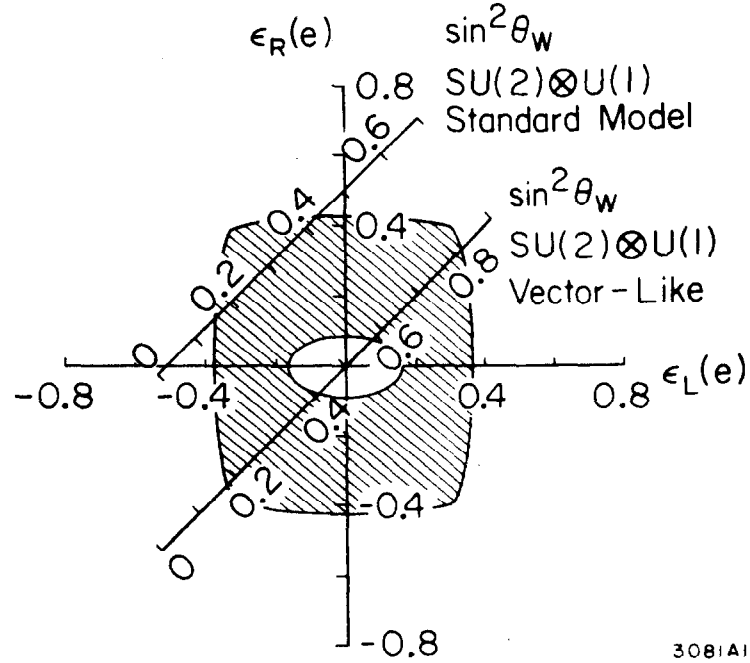

Fig. 12. Allowed values of the coupling constants $\epsilon_L(e)$ and $\epsilon_R(e)$ governing the processes $\nu_\mu e^- \to \nu_\mu e^-$ and $\bar{\nu}_\mu e^- \to \bar{\nu}_\mu e^-$. We have used the limits as quoted by Gargamelle.

Because the detection efficiency is dependent upon positron energy, the one-standard deviation limits on the coupling constants are actually quoted. These are reproduced in Fig. 13, along with the SU(2)⊗U(1) predictions, for both the weak-singlet and weak-doublet options for e_R^-. Consistency exists for both options over a considerable range of $\sin^2\theta_W$, as well as for the pure charged-current coupling corresponding to $\epsilon_L(e) = \epsilon_R(e) = 0$.

In general, it is clear that, while the existence of these processes appear to be established and to have a reasonable magnitude, it is difficult to draw decisive quantitative conclusions.

B. Deep-Inelastic Neutral Currents. There exist three measurements of the processes $\nu N \to \nu$ hadrons and $\bar{\nu} N \to \bar{\nu}$ hadrons at relatively large energies,[65,66,67] where the scaling concepts used in charged-current deep-inelastic scattering are found to be of use. In interpreting these measurements, we shall make a few simplifying assumptions (which should not introduce errors of much more than 10% or so). We shall first of all adopt the naive quark-parton model description of the cross section. This is probably not too terrible an assumption, inasmuch as this description reproduces charged-current data, and much of the neutral-current phenomena are isospin (and SU(3) rotations) of the charged current phenomena. Secondly we shall neglect any contribution of strange quark-partons (or strange antipartons), as well as any new currents involving charmed quarks or other new flavors. The neglect of new charged currents, as well as neutral currents, is especially dangerous when considering $\bar{\nu}$-induced processes. The experimentalists measure the ratio of the $\bar{\nu}N$ neutral current cross section to the $\bar{\nu}N$ charged-current cross section. If there is anomalous behavior in the $\bar{\nu}N$ charged-current process (cf., the lectures of S. Wojcicki, these Proceedings), this will reflect itself in the numbers quoted for the neutral-current measurements. However most of the neutral-current data is for

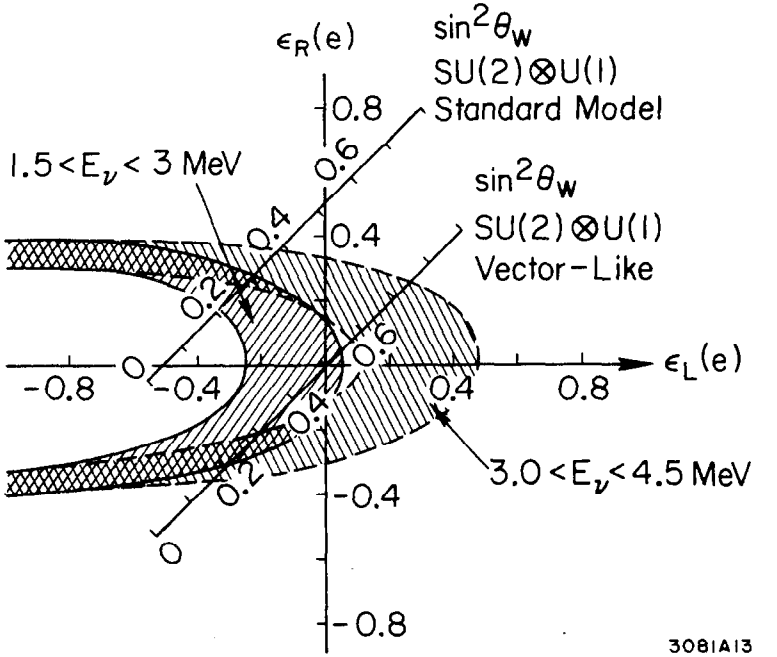

Fig. 13. Allowed values of the coupling constants $\epsilon_L(e)$ and $\epsilon_R(e)$ as determined from $\bar{\nu}_e e^-$ scattering.

$E_{\bar{\nu}} \lesssim 50$ GeV, while the anomalous behavior is probably only large for $E_{\bar{\nu}} \gtrsim 50$ GeV.

We now turn to the expressions for the cross sections for charged and neutral current processes. Using the simple parton model calculations,[68] one obtains for the charged-current process $\nu p \to \mu^- \text{hadrons}$

$$\sigma_{cc}^{\nu p} = \frac{2G^2 M E_\nu}{\pi}\left\{\int_0^1 dx\left[d(x) + \tfrac{1}{3}\bar{u}(x)\right]\right\} \tag{5.11}$$

where

$$\frac{d(x)}{x} = \frac{dN_d}{dx} = \text{number of down quarks in an energetic proton possessing fraction x (in dx) of the proton total momentum} \tag{5.12}$$

with similar definitions for $u(x)$, $\bar{u}(x)$, and $\bar{d}(x)$. The experiments we shall discuss are on complex nuclei, and using charge symmetry, i.e.,

$$\begin{aligned} u(x)_{\text{proton}} &= d(x)_{\text{neutron}} \\ \bar{u}(x)_{\text{proton}} &= \bar{d}(x)_{\text{neutron}} \end{aligned} \tag{5.12}$$

we write for the cross section <u>per nucleon</u> N

$$\sigma_{cc}^{\nu N} = \frac{2G^2 M E_\nu}{\pi}\int_0^1 dx\left[q(x) + \tfrac{1}{3}\bar{q}(x)\right] \tag{5.13}$$

with

$$\begin{aligned} q(x) &= \tfrac{1}{2}\left[u(x) + d(x)\right] \\ \bar{q}(x) &= \tfrac{1}{2}\left[\bar{u}(x) + \bar{d}(x)\right] \end{aligned} \tag{5.14}$$

Likewise

$$\sigma_{cc}^{\bar{\nu}N} = \frac{2G^2 M E_\nu}{\pi}\int_0^1 dx\left[\tfrac{1}{3}q(x) + \bar{q}(x)\right] \tag{5.15}$$

Using the effective Lagrangian, Eq. (1.4) we can immediately write down the corresponding neutrino cross section on a proton:

$$\sigma_{NC}^{\nu p} = \frac{2G^2 M E_\nu}{\pi}\left\{|\epsilon_L(u)|^2\int_0^1 dx\left[u(x) + \tfrac{1}{3}\bar{u}(x)\right] + |\epsilon_R(u)|^2\int_0^1 dx\left[\tfrac{1}{3}u(x) + \bar{u}(x)\right]\right.$$
$$\left. + |\epsilon_L(d)|^2\int_0^1 dx\left[d(x) + \tfrac{1}{3}\bar{d}(x)\right] + |\epsilon_R(d)|^2\int_0^1 dx\left[\tfrac{1}{3}d(x) + \bar{d}(x)\right]\right\} \tag{5.16}$$

On an average nucleon N, this is

$$\sigma_{NC}^{\nu N} = \frac{2G^2 M E_\nu}{\pi}\left\{\left[|\epsilon_L(u)|^2 + |\epsilon_L(d)|^2\right]\int_0^1 dx\left[q(x) + \tfrac{1}{3}\bar{q}(x)\right]\right.$$
$$\left. + \left[|\epsilon_R(u)|^2 + |\epsilon_R(d)|^2\right]\int_0^1 dx\left[\tfrac{1}{3}q(x) + \bar{q}(x)\right]\right\} \tag{5.17}$$

and for antineutrinos

$$\sigma_{NC}^{\bar{\nu}N} = \frac{2G^2 M E_\nu}{\pi}\left\{\left[|\epsilon_L(u)|^2 + |\epsilon_L(d)|^2\right]\int_0^1 dx\left[\tfrac{1}{3}q(x) + \bar{q}(x)\right]\right.$$
$$\left. + \left[|\epsilon_R(u)|^2 + |\epsilon_R(d)|^2\right]\int_0^1 dx\left[q(x) + \tfrac{1}{3}\bar{q}(x)\right]\right\} \tag{5.18}$$

Define again the ratios R, $\bar{R}$, R_{cc} already introduced in Eq. (4.5). The experimental values quoted for these quantities are

		Gargamelle	HPWF	CITF
$R = \frac{\sigma_{Nc}^{\nu N}}{\sigma_{cc}^{\nu N}}$	=	$.25 \pm .04$	$.29 \pm .04$	$.24 \pm .04$
$\bar{R} = \frac{\sigma_{Nc}^{\bar{\nu}N}}{\sigma_{cc}^{\bar{\nu}N}}$	=	$.39 \pm .06$	$.39 \pm .10$	$.35 \pm .11$
$R_{cc} = \frac{\sigma_{cc}^{\bar{\nu}N}}{\sigma_{cc}^{\nu N}}$	=	$.38 \pm .02$		

(5.19)

Inasmuch as

$$R_{cc} = \frac{\int_0^1 dx\left[\frac{1}{3}q(x) + \bar{q}(x)\right]}{\int_0^1 dx\left[q(x) + \frac{1}{3}\bar{q}(x)\right]} \tag{5.20}$$

we find from Eqs. (5.17) and (5.18) that

$$\begin{aligned} R &= |\epsilon_L(u)|^2 + |\epsilon_L(d)|^2 + R_{cc}\left\{|\epsilon_R(u)|^2 + |\epsilon_R(d)|^2\right\} \\ \bar{R} &= |\epsilon_L(u)|^2 + |\epsilon_L(d)|^2 + R_{cc}^{-1}\left\{|\epsilon_R(u)|^2 + |\epsilon_R(d)|^2\right\} \end{aligned} \tag{5.21}$$

These can be solved for the basic couplings

$$\begin{aligned} |\epsilon_L(u)|^2 + |\epsilon_L(d)|^2 &= \frac{R_{cc}^{-1}R - R_{cc}\bar{R}}{R_{cc}^{-1} - R_{cc}} \\ |\epsilon_R(u)|^2 + |\epsilon_R(d)|^2 &= \frac{\bar{R} - R}{R_{cc}^{-1} - R_{cc}} \end{aligned} \tag{5.22}$$

Putting in the numbers gives

$$\begin{aligned} |\epsilon_L|^2 &\equiv |\epsilon_L(u)|^2 + |\epsilon_L(d)|^2 = .26 \pm .04 \\ |\epsilon_R|^2 &\equiv |\epsilon_R(u)|^2 + |\epsilon_R(d)|^2 = .06 \pm .05 \end{aligned} \tag{5.23}$$

The error-assignments here are not to be taken seriously, especially for the value of $|\epsilon_R|^2$. It would be best for the experimental groups to directly quote their estimate of these quantities. Especially important is to firmly establish that $|\epsilon_R(u)|^2 + |\epsilon_R(d)|^2 \neq 0$. It is my understanding that in fact there is evidence both from Gargamelle and CITF that, at a level approaching two standard deviations, a pure left-handed (V-A) neutral-current coupling is ruled out. In the case of the CITF experiment, this is exhibited in Fig. 14. The quantities g_L^2 and g_R^2 in that plot are defined by the expression

$$d\sigma_{Nc}^{\nu N}/dy = \left[g_L + g_R(1-y)^2\right]\frac{G^2 ME}{\pi} \tag{5.24}$$

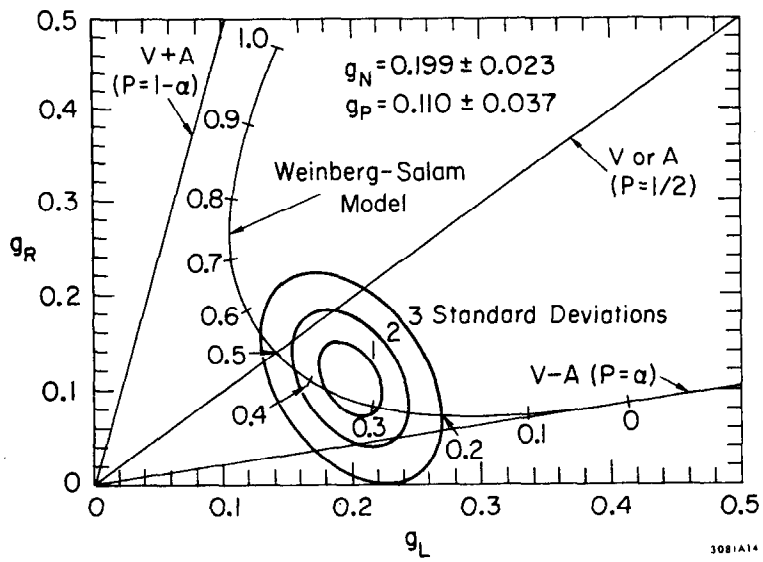

Fig. 14. Range of left and right helicity coupling allowed by the CITF neutral-current data. See text for definitions of g_L and g_R.

with

$$y = \frac{E_{hadron}}{E_\nu} = \frac{\nu}{E_\nu} \qquad 0 \leq y \leq 1 \tag{5.25}$$

Hence

$$g_L \sim |\epsilon_L|^2 + \frac{\int_0^1 dx\, \bar{q}(x)}{\int_0^1 dx\, q(x)} |\epsilon_R|^2$$

$$g_R \sim |\epsilon_R|^2 + \frac{\int_0^1 dx\, \bar{q}(x)}{\int_0^1 dx\, q(x)} |\epsilon_L|^2 \tag{5.26}$$

The antiquark content is best determined by studies of the charged-current y-distributions, and is conventionally parametrized by the quantity

$$B = \frac{\int_0^1 dx\, [q(x) - \bar{q}(x)]}{\int_0^1 dx\, [q(x) + \bar{q}(x)]} \tag{5.27}$$

Estimates of B, in the appropriate energy range, vary from ~0.7 to ~0.95, giving an antiquark content varying from

$$.16 \gtrsim \frac{\int_0^1 \bar{q}(x)\, dx}{\int_0^1 q(x)\, dx} \gtrsim .05 \tag{5.28}$$

(See the lectures of S. Wojcicki, these Proceedings; in particular Fig. 28, for more details.)

What is theoretically expected for ϵ_L and ϵ_R? In the SU(2)⊗U(1) model, the values are easily calculated from Eq. (3.39), which states that $\epsilon(q) = \left(T_3 - Q\sin^2\theta_W\right)_q$. Evidently u_L and d_L form a weak doublet (we here ignore effects of Cabibbo mixing); however one must decide upon the assignments of u_R and d_R. Without introducing new quarks of charge greater than unity, this leaves four basic variants to consider[69]:

1. u_R and d_R weak singlets: this is the standard model.

2. d_R is singlet and $(u\ b)_R$ a doublet; b is a heavy "bottom" quark of charge -1/3. This model (with $m_b \sim 4$ GeV) gives a good account of the anomalous behavior of $\bar{\nu}$-induced charged current processes at high energy.[70] It has been discussed by several authors,[70,71] including Gursey and Sikivie[72] who embed it into a fully unified theory based on the exceptional group E7. We shall see that this model is consistent with most neutral-current data.

3. u_R a singlet and $(t\ d)_R$ a doublet involving a new heavy "top" quark. This model fares poorly when compared with experiment, as we shall see.

4. $(u\ b)_R$ and $(t\ d)_R$ both weak doublets. This leads to a parity-conserving vector neutral current,[73] which is in considerable disagreement with experiment. In particular the HPWF group has tested this hypothesis against their data[74] and claim it is ruled out by at least 3 standard deviations. Models based upon this scheme have been quite popular.

The coupling constants for the schemes are given below. In all variants

$$\epsilon_L(u) = \frac{1}{2} - \frac{2}{3}\sin^2\theta_W \tag{5.29}$$

$$\epsilon_L(d) = -\frac{1}{2} + \frac{1}{3}\sin^2\theta_W \tag{5.30}$$

For the right-handed currents we have

$$
\begin{array}{lll}
\text{Standard model} & \epsilon_R(u) = -\frac{2}{3}\sin^2\theta_W & \epsilon_R(d) = \frac{1}{3}\sin^2\theta_W \\
(u\ b)_R & \epsilon_R(u) = \frac{1}{2}-\frac{2}{3}\sin^2\theta_W & \epsilon_R(d) = \frac{1}{3}\sin^2\theta_W \\
(t\ d)_R & \epsilon_R(u) = -\frac{2}{3}\sin^2\theta_W & \epsilon_R(d) = -\frac{1}{2}+\frac{1}{3}\sin^2\theta_W \\
\text{Vector-like} & \epsilon_R(u) = \frac{1}{2}-\frac{2}{3}\sin^2\theta_W & \epsilon_R(d) = -\frac{1}{2}+\frac{1}{3}\sin^2\theta_W
\end{array}
\qquad (5.31)
$$

These are plotted in Fig. 16. We see that the vector model and $(t\ d)_R$ models do not agree well with the data. It should also be kept in mind that we have assumed the mass formula, Eq. (3.33) relating m_W and m_Z. Changing m_Z by a factor 2 changes $|\epsilon_L|^2$ and $|\epsilon_R|^2$ by a factor 16. We see therefore that the standard model not only agrees remarkably well with the data, but that no other choice of m_Z than that given by the mass-formula would give agreement. This is also true of the vector-like, and to some extent, of the $(t\ d)_R$ models but not of the $(u\ b)_R$ model which could accommodate a change in m_Z, provided it were accompanied by a change in $\sin^2\theta_W$.

As an additional complication, it is also possible to introduce mixing of u_R and d_R with additional heavy quarks which have a different weak isospin. This will evidently allow predictions which interpolate between the cases we have discussed.

C. Elastic Neutrino-Proton Scattering. Two experiments[75,76] have recently been performed at Brookhaven in which the elastic scattering processes $\nu_\mu p \to \nu_\mu p$ and $\bar\nu_\mu p \to \bar\nu_\mu p$ have been observed. These experiments are especially useful in determining the isospin-structure of the neutral-current couplings. The formalism for describing this process as well as a comparison with data has been discussed in several recent theoretical papers.[77,78,79] Usually this is done in the context of models. Here we shall first approach it from the general point of view of finding additional restrictions on the couplings $\epsilon_{L(R)}(u)$ and $\epsilon_{L(R)}(d)$. We write the effective Lagrangian in terms of vector and axial coupling:

$$
\mathscr{L}_{\text{eff}} = \frac{G}{\sqrt{2}}\left[\begin{array}{l}\left\{\epsilon_L(u)+\epsilon_R(u)\right\}\bar u\gamma_\lambda u + \left\{\epsilon_R(u)-\epsilon_L(u)\right\}\bar u\gamma_5\gamma_\lambda u \\ +\left\{\epsilon_L(d)+\epsilon_R(d)\right\}\bar d\gamma_\lambda d + \left\{\epsilon_R(d)-\epsilon_L(d)\right\}\bar d\gamma_5\gamma_\lambda d\end{array}\right]\bar\nu_\mu\gamma^\lambda(1-\gamma_5)\nu_\mu \qquad (5.32)
$$

We again ignore all contributions of the strange quark current, even for this elastic process. When matrix-elements of $\mathscr{L}_{\text{eff}}$ are taken between proton states, we shall have to deal with amplitudes $\langle p|\bar u\gamma^\lambda u|p\rangle$ and $\langle p|\bar d\gamma^\lambda d|p\rangle$, which in turn are related to the electromagnetic form factors of the proton and neutron. Specifically[80]

$$
\langle p|\tfrac{2}{3}\bar u\gamma_\lambda u - \tfrac{1}{3}\bar d\gamma_\lambda d|p\rangle = \bar u(p')\left[\gamma_\lambda F_{1p}(q^2) - \frac{\kappa_p}{4M}[\gamma_\lambda, q']F_{2p}(q^2)\right]u(p) \qquad (5.33)
$$

and from charge symmetry

$$
\langle p|\tfrac{2}{3}\bar d\gamma_\lambda d - \tfrac{1}{3}\bar u\gamma_\lambda u|p\rangle = \bar u(p')\left[\gamma_\lambda F_{1n}(q^2) - \frac{\kappa_n}{4M}[\gamma_\lambda, q']F_{2n}(q^2)\right]u(p) \qquad (5.34)
$$

with $p' = p+q$ and $\kappa_p = 1.79$, $\kappa_n = 1.91$ the anomalous magnetic moments. The Dirac form factors are normalized to unity (or zero) at $q^2=0$. For the axial form factors, we know the I=1 portion from β-decay and from analyses of the quasi-elastic processes $\nu_\mu + n \to \mu^- + p$:

$$
\langle p|\bar u\gamma_5\gamma_\lambda u - \bar d\gamma_5\gamma_\lambda d|p\rangle = 1.24\,\bar u(p')\gamma_5\gamma_\lambda u(p)\,F_A(q^2)^{I=1} \qquad (5.35)
$$

Note there is only one form factor; there can be no induced pseudoscalar piece that contributes (because of the conserved ν-currents).

For the I=0 axial form factor, there is considerable uncertainty.[81] In this discussion we shall use what we consider a "best guess". We choose the ratio of isoscalar and isovector axial matrix elements to be the same as the ratio of the isoscalar and isovector magnetic contributions (proportional to the total moments of proton and neutron, i.e., to $G_M \sim F_1+\kappa F_2$). The reasoning is that

this choice is in accord with static SU(6), the naive quark model, and the improvements given by the Melosh transformation.[82] This is equivalent to the statement that the F/D ratio for axial form factors (as measured in hyperon β-decay processes) is the same as the F/D ratio for magnetic moments. The theoretical justification, such as it is, is that in the static limit, both the axial current and the magnetic moment operator reduces to $\vec{\sigma}\lambda_i$ (with λ_i the SU(3) matrices); hence all matrix elements are proportional.

There is some additional experimental justification for this choice. An old sum rule[83] relates the (intrinsic) asymmetry A in deep-inelastic scattering of longitudinally polarized electrons by longitudinally polarized protons to a matrix element of I=0 and I=1 axial-vector currents between protons at $q^2=0$:

$$\bar{u}\gamma_5\gamma_\lambda u \int_1^\infty \frac{d\omega}{\omega}\left[\nu W_2(\omega)\right]\cdot A = \langle p|\tfrac{4}{9}\bar{u}\gamma_5\gamma_\lambda u + \tfrac{1}{9}\bar{d}\gamma_5\gamma_\lambda d|p\rangle$$
$$= \tfrac{1}{6}(1.24)\,\bar{u}\gamma_5\gamma_\lambda u + \tfrac{5}{18}\langle p|\bar{u}\gamma_5\gamma_\lambda u + \bar{d}\gamma_5\gamma_\lambda d|p\rangle \qquad (5.36)$$

With the SU(6) prediction of +0.6 for the isoscalar-to-isovector mixture, it turns out that the isoscalar contribution should approximately equal the isovector (with the same sign). The weighted asymmetry should be approximately zero for the neutron[84] while for the proton

$$\int_0^1 \frac{d\omega}{\omega}\cdot\nu W_2\cdot A \cong \tfrac{1}{3}\left|\frac{g_A}{g_V}\right| \sim \tfrac{1}{3}(1.24) \qquad (5.37)$$

Recent data[85] show a large asymmetry of the correct sign, and my own rough estimate of the sum gives a value between ~0.5 and ~1.0 of the right-hand side of Eq. (5.37). This would imply a value of the isoscalar form factor (at $q^2=0$) somewhere between zero and the SU(6) prediction which we use. In any case what we do use for the isoscalar axial form factor is explicitly

$$\langle p|\bar{u}\gamma_5\gamma_\lambda u + \bar{d}\gamma_5\gamma_\lambda d|p\rangle = (1.24)\cdot\frac{3(1+\kappa_p+\kappa_n)}{(1+\kappa_p-\kappa_n)}\,\bar{u}\gamma_5\gamma_\lambda u\, F_A(q^2) \qquad (5.38)$$

Here we blindly assume the same q^2 dependence for I=0 and I=1 axial form factors. The justification this time (a not very good one) is only that this works for the magnetic form factors reasonably well.

At this point, one has all the ingredients for estimating the cross sections. The matrix elements needed are given in Eqs. (5.33), (5.34), (5.35) and (5.38) and can be inserted into the matrix element of $\mathscr{L}_{eff}$ in Eq. (5.32), taken between proton states. The resultant amplitude is then squared, spin-sums taken, and phase-space calculated. As in elastic electron-proton scattering, there is great advantage in utilizing the Sachs form factors[80]

$$G_E = F_1 + \frac{\kappa Q^2}{4M^2}F_2 \qquad G_M = \frac{F_1+\kappa F_2}{1+\kappa} \qquad (5.39)$$

and, in accord with experiment,[86] approximating them with the dipole form

$$G_{Ep} = G_{Mp} = G_{Mn} \cong \left(1+\frac{Q^2}{m_V^2}\right)^{-2}$$
$$m_V^2 = .71\ \text{GeV}^2 \qquad (5.40)$$

(Note the Drell definition $Q^2=-q^2>0$ is used here.)

Likewise the axial form factor is conventionally written

$$G_A(q^2) = F_A(q^2) = \left(1+\frac{Q^2}{m_A^2}\right)^{-2} \qquad (5.41)$$

with typically $m_A^2 \sim 0.9\ \text{GeV}^2$ from experiment although values from 0.7 to $1.2\ \text{GeV}^2$ might be entertained.[87] When all this is put together one finds the

differential cross section:

$$\frac{d\sigma^{\nu,\bar{\nu}}_{p}}{dQ^2} = \frac{G^2}{2\pi}\left[\left(\epsilon_V^1+3\epsilon_V^0\right)^2\left(1+\frac{Q^2}{m_V^2}\right)^{-4}\left[(1+\tau)^{-1}\left(1-\tau\frac{M}{E}\right)^2-\tau\frac{M^2}{E^2}\right]\right.$$
$$+\left(4.7\,\epsilon_V^1+2.6\epsilon_V^0\right)^2\left(1+\frac{Q^2}{m_V^2}\right)^{-4}\left[\frac{\tau}{1+\tau}\left(1-\tau\frac{M}{E}\right)^2+\frac{\tau^2M^2}{E^2}\right]$$
$$+(1.24)^2\left(\epsilon_A^1+0.55\epsilon_A^0\right)^2\left(1+\frac{Q^2}{m_A^2}\right)^{-4}\left[\left(1-\tau\frac{M}{E}\right)^2+\tau(1+\tau)\frac{M^2}{E^2}\right]$$
$$\left.\pm(1.24)\left(4.7\epsilon_V^1+2.6\epsilon_V^0\right)\left(\epsilon_A^1+.55\epsilon_A^0\right)\left(1+\frac{Q^2}{m_V^2}\right)^{-2}\left(1+\frac{Q^2}{m_A^2}\right)^{-2}4\tau\frac{M}{E}\left(1-\tau\frac{M}{E}\right)\right] \tag{5.42}$$

with

$$\tau = Q^2/4M^2 \tag{5.43}$$

and, in a hopefully obvious notation,

$$\begin{aligned}
\epsilon_V^1 &= \tfrac{1}{2}\left[\epsilon_L(u)+\epsilon_R(u)-\epsilon_L(d)-\epsilon_R(d)\right]\\
\epsilon_V^0 &= \tfrac{1}{2}\left[\epsilon_L(u)+\epsilon_R(u)+\epsilon_L(d)+\epsilon_R(d)\right]\\
\epsilon_A^1 &= \tfrac{1}{2}\left[\epsilon_L(u)-\epsilon_R(u)-\epsilon_L(d)+\epsilon_R(d)\right]\\
\epsilon_A^0 &= \tfrac{1}{2}\left[\epsilon_L(u)-\epsilon_R(u)+\epsilon_L(d)-\epsilon_R(d)\right]
\end{aligned} \tag{5.44}$$

The various contributions should be fairly recognizable. The first line is the contribution proportional to the electric coupling G_E^2, the second line to the magnetic coupling G_M^2, and the third to G_A^2. The only V-A interference occurs between the (spin-dependent) magnetic and axial form factors. To go from νp to $\bar{\nu}p$ scattering just involves changing the sign of the V-A interference term. To go from νp to νn elastic scattering, it is only necessary to change the sign of ϵ_V^1 and ϵ_A^1. If one wishes to test the dependence of this cross section on the magnitude of the isoscalar axial-vector form factor, one simply multiplies ϵ_A^0 by an appropriate scale factor η (with, probably, $0 \lesssim \eta \lesssim 1$ according to the rough indications from polarized electroproduction). In order to get an idea of the sensitivity of the BNL data to the four ϵ-parameters, we first average over the neutrino spectrum

$$\left\langle\frac{M}{E}\right\rangle_\nu \approx .5 \qquad \left\langle\frac{M^2}{E^2}\right\rangle_\nu \approx .4 \tag{5.45}$$

and then average the kinematical factors dependent on τ over the range $0.3\ \mathrm{GeV}^2 < Q^2 < 0.9\ \mathrm{GeV}^2$, using $m_V^2 = m_A^2 = 0.71\ \mathrm{GeV}^2$ for simplicity. This gives $\langle\tau\rangle \cong 0.13$ and a cross section dependence

$$\sigma \sim 0.8\gamma_E^2 + 2\gamma_M^2 + 1.4\gamma_A^2 \pm 1.4\gamma_M\gamma_A$$

with

$$\begin{aligned}
\gamma_E &= \epsilon_V^1+3\epsilon_V^0\\
\gamma_M &= \epsilon_V^1+.55\epsilon_V^0\\
\gamma_A &= \epsilon_A^1+.55\epsilon_A^0
\end{aligned} \tag{5.46}$$

The experimental piece of information we shall use is the small ratio of $\sigma_{\bar{p}p}$ to $\sigma_{\nu p}$ reported by the HPW experiment:

$$\frac{\sigma_{\bar{p}p}}{\sigma_{\nu p}} = 0.4 \pm 0.2 \tag{5.47}$$

This requires a large interference term; in particular

$$\frac{2.8\gamma_M\gamma_A}{0.8\gamma_E^2+2\gamma_M^2+1.4\gamma_A^2+1.4\gamma_M\gamma_A} \gtrsim 0.6 \pm 0.2 \tag{5.48}$$

The ratio above is maximized when $\gamma_M \approx \gamma_A$; $\gamma_E = 0$, giving the value ~ 0.58. Large excursions away from this value are not tolerable, and without belaboring the point here with numerical examples, the result is that

i) $|\gamma_M - \gamma_A|$ cannot be too large

ii) $\gamma_M+\gamma_A$ is large and is rather well determined from σ_{tot}

iii) γ_E cannot dominate the total cross section.

These results are not sensitive to the choice of m_A^2. Upon noticing that (from Eqs. (5.46) and (5.44))

$$\gamma_M+\gamma_A = 1.55\ \epsilon_L(u) - 0.45\epsilon_L(d) = 1.55\left[\epsilon_L(u) - 0.3\epsilon_L(d)\right]$$
$$\gamma_M-\gamma_A = 1.55\ \epsilon_R(u) - 0.45\epsilon_R(d) = 1.55\left[\epsilon_R(u) - 0.3\epsilon_R(d)\right] \qquad (5.49)$$

we see that it is simply $\epsilon_L(u) - 0.3\epsilon_L(d)$ which is required to be as large as possible in order to maximize the interference term.

We may visualize this better by looking at ϵ_L space and ϵ_R space as shown in Fig. 15. The regions allowed (at the one-standard deviation level) by the deep-inelastic data are shown shaded, along with predictions of various $SU(2)\otimes U(1)$ models. A crude estimate of the limits on $\epsilon_L(u) - 0.3\epsilon_L(d)$ from the line of arguments given above is shown as the shaded band on the right. However, it is clearly better to simply search all values of ϵ's in the allowed regions and ask how acceptable the fit to the elastic scattering data is. A somewhat cursory search reveals that the only region in ϵ_L space in which there is a large ratio of νp to $\bar{\nu}p$ scattering is the lower right quadrant $\epsilon_L(u) > 0$, $\epsilon_L(d) < 0$. There is a little restriction on $\epsilon_R(u)$ and $\epsilon_R(d)$, in general, although there is considerable correlation between allowed values of $\vec{\epsilon}_R$ with the precise value of $\vec{\epsilon}_L$. However these lectures are an inappropriate place to perform a serious analysis of the allowed values of the couplings. Suffice it to say that the values of $\epsilon_L(u)$ and $\epsilon_L(d)$ are constrained to lie fairly near that predicted by $SU(2)\otimes U(1)$ models, and that more accurate data is needed to meaningfully restrict further the right-handed couplings.

Several serious analyses have been performed to see how the data compares with popular $SU(2)\otimes U(1)$ models. We exhibit selections from the work of Albright, Quigg, Schrock, and Smith,[78] which compares the observed differential

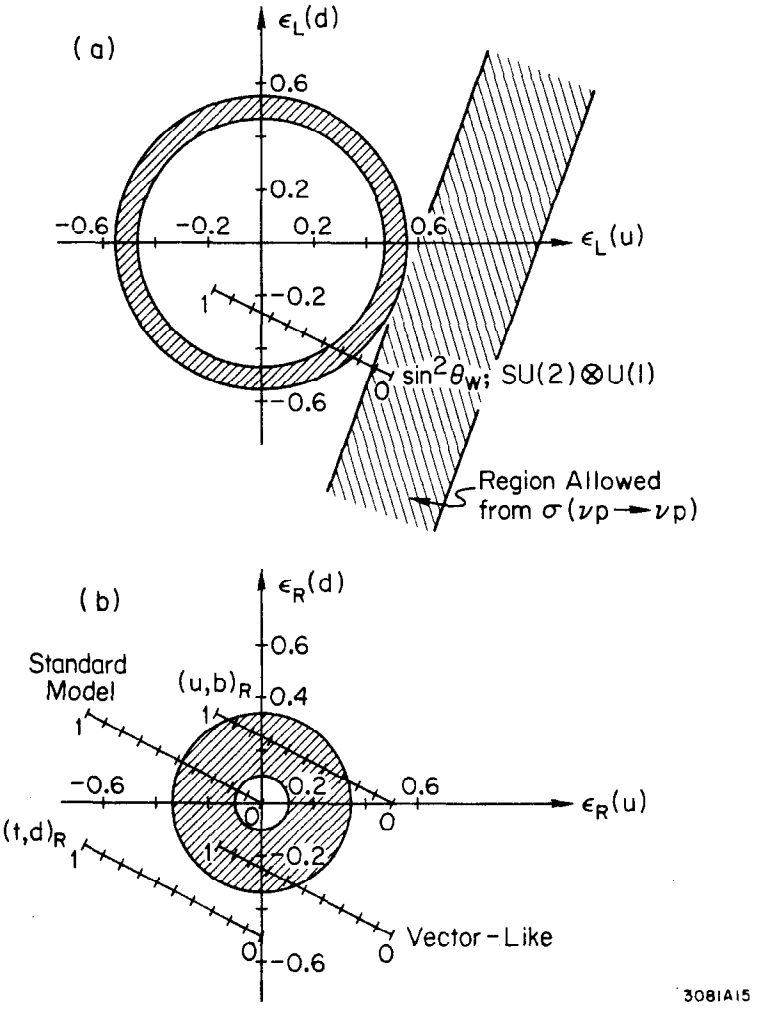

Fig. 15. Allowed regions (a) in $\epsilon_L(u)$-$\epsilon_L(d)$ space, and (b) in $\epsilon_R(u)$-$\epsilon_R(d)$ space from the deep-inelastic neutral-current data. The shaded panel on the right is the allowed region (at ~1 standard deviation) coming from the νp and $\bar{\nu}p$ elastic scattering measurements. Predictions of various $SU(2)\otimes U(1)$ models are given as a function of $\sin^2\theta_W$.

cross sections of HPW[76] with their calculations. These are shown in Figs. 16-18. Evidently vector-like theories (for which there is no interference term and therefore $d\sigma_{\bar{\nu}p}/dQ^2 = d\sigma_{\nu p}/dQ^2$) have difficulty with experiment. Even the dependence on Q^2 is poor. The standard $SU(2) \otimes U(1)$ model, as well as the $(u, b)_R$ variant, are acceptable fits to the data, given the uncertainties in choice of $G_A(Q^2)$ and the limited statistics of the $\bar{\nu}p$ measurement as well as the difficulty inherent in measuring such a process.

The cross section for νp elastic scattering has been determined by both the HPW and CIR experiments. The number quoted is the ratio of the neutral current elastic to the quasi-elastic process $\nu_\mu n \to \mu^- p$. They quote (see also the reports of H. Williams and of W. Y. Lee in these Proceedings)

$$\frac{\sigma_{\nu p \to \nu p}}{\sigma_{\nu n \to \mu^- p}} = \begin{cases} .23 \pm .09 & \text{CIR} \\ .17 \pm .05 & \text{HPW} \end{cases} \qquad (5.50)$$

(These are cut over ranges of Q^2 and/or θ_p; see the reports of H. Williams and W. Lee for the details.)

The theoretical expectation is somewhat lower, but not seriously so, as shown in Fig. 19. The model-independent analysis we gave suggests it may not be completely simple to find (within the assumption of a local V-A effective Lagrangian), any choice compatible with deep-inelastic data, a small value of $\sigma^{el}_{\bar{\nu}p}/\sigma^{el}_{\nu p}$, and a value as large as above. This underlines my belief that as the elastic scattering data becomes more accurate, it will become a powerful tool is disentangling the possible neutral current couplings in a largely model-independent way.

D. Resonance Production. Careful study of the production of single-pion and double pion production by the neutral current should reveal additional information on its isospin structure. Regrettably there was not the time (nor did I have the energy) to review the subject in these lectures in detail. In addition to

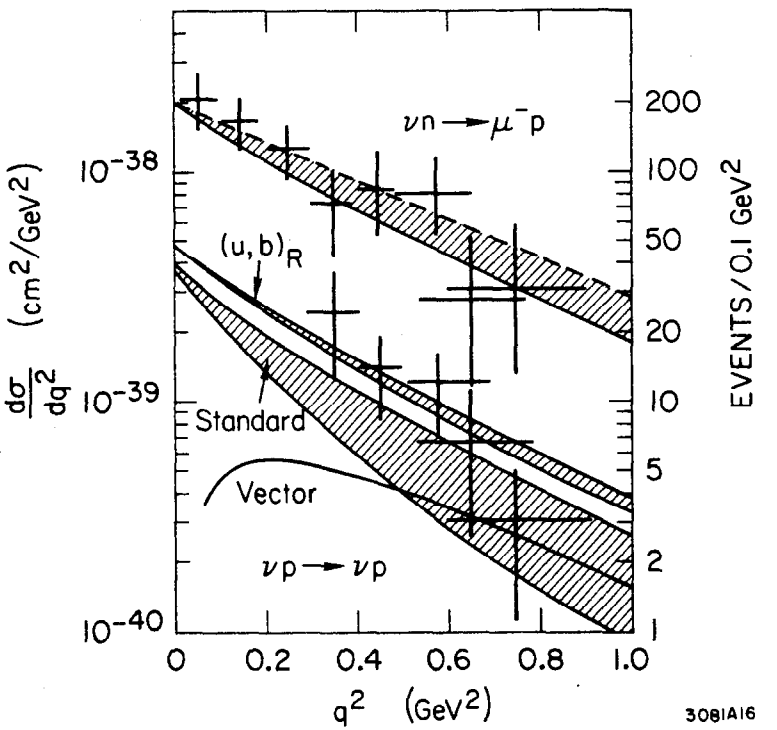

Fig. 16. Data of HPW for νp elastic scattering, along with the calculations of Albright et al. for various models and choices of m_A.

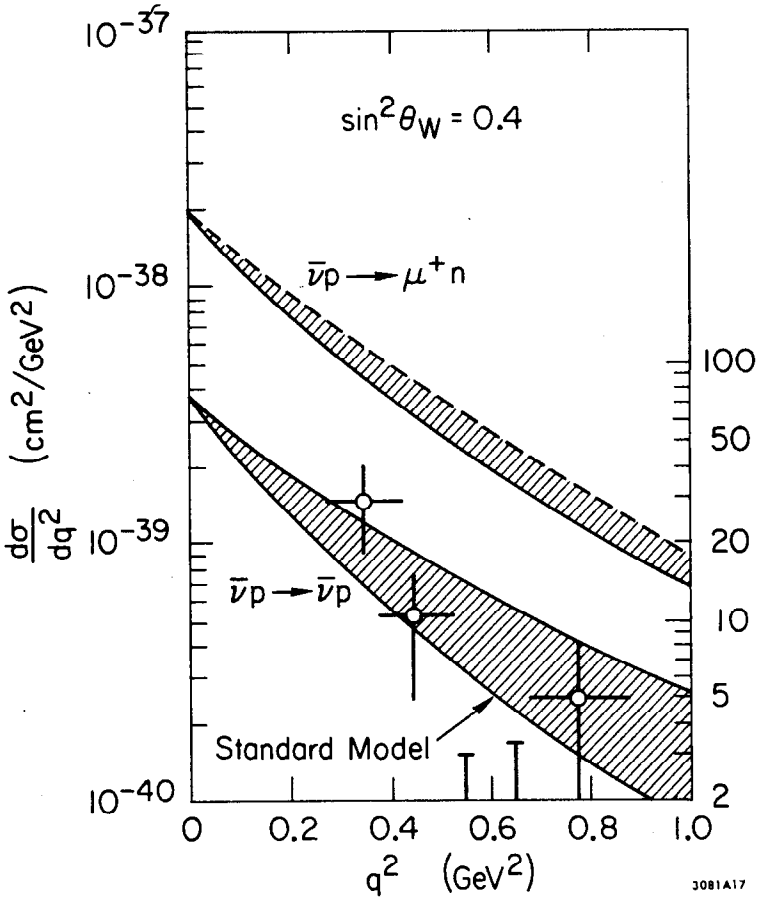

Fig. 17. Data of HPW for $\bar{\nu}p$ elastic scattering, along with the calculations of Albright et al. for the standard model and various choices of m_A.

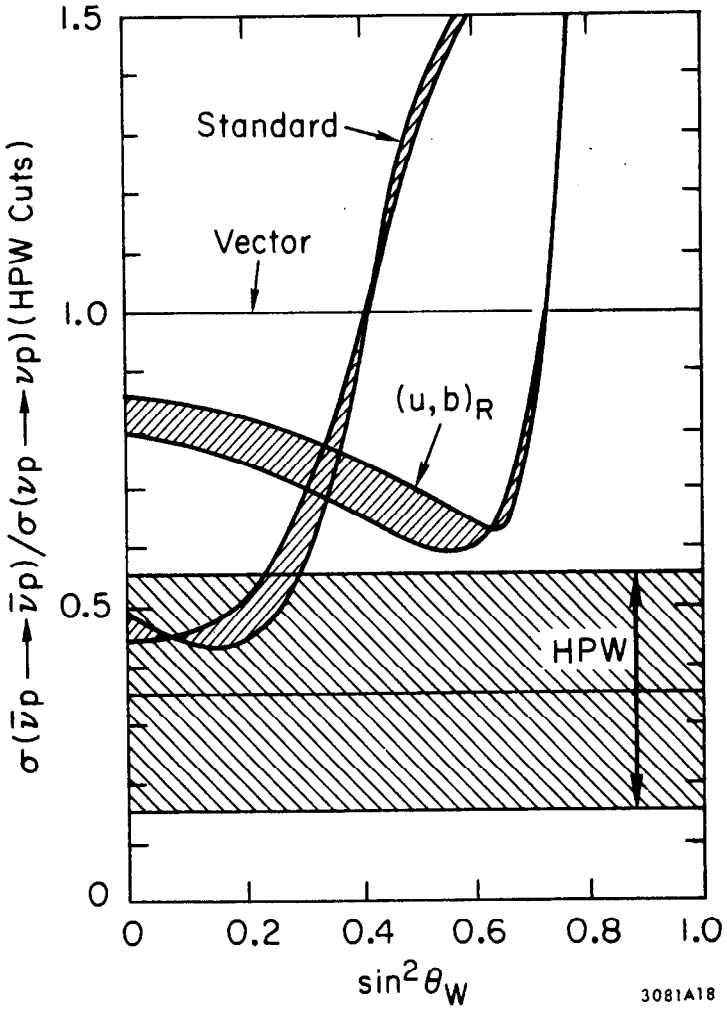

Fig. 18. Ratio of $\sigma_{\bar{p}p}$ to $\sigma_{\nu p}$ as calculated by Albright et al. compared with the HPW measurement.

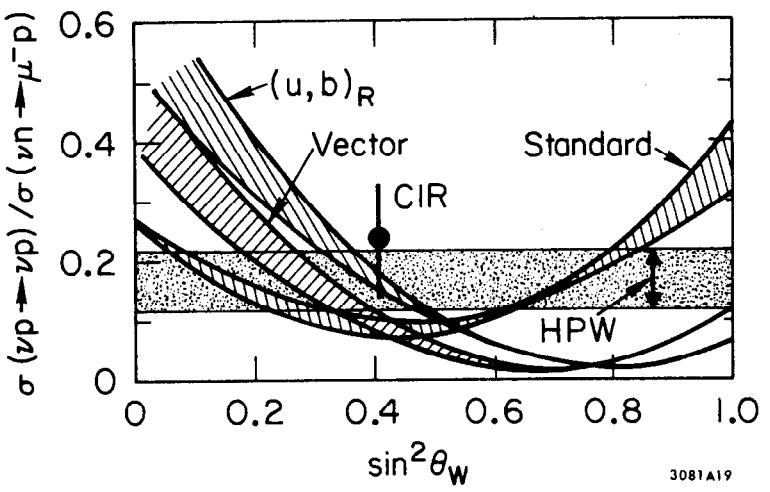

Fig. 19. Expected ratio of $\sigma(\nu p \to \nu p)/\sigma(\nu n \to \mu^- p)$ as calculated by Albright et al. compared with the HPW and CIR measurements.

a considerable body of data, a large amount of very careful and thorough work has been done by Stephen Adler and his collaborators on the theory.[88] We reiterate that Adler's lectures at the Hawaii Summer School last year serve as an excellent introduction to the subject. We note here only a few salient features from the experiments:

1. Δ production: The CIR counter experiment at BNL, while observing a clear Δ peak in charged-current processes, do not have any clear evidence for a Δ peak in the neutral-current process[89] $\nu p \to \nu p \pi^0$. Absence of this peak would be quite disquieting, given the indication of a large isovector left-handed neutral current from the elastic neutrino scattering. It is not easy to see how this would lead to a small Δ-production cross section by the neutral current.

2. Evidence for isovector neutral current: The Gargamelle experiment[90] has measured the π^0/π^- ratio for single pion production by the neutral current (in heavy liquid). Were the neutral current pure isoscalar this ratio should be unity, whereas it is found to be 1.8 ± 0.4 for ν incident and 2.5 ± 0.6 for $\bar{\nu}$ incident (after background corrections). (For pure isovector they expect a value of 2.6.)

3. Evidence for isoscalar-vector interference: In an exposure of the BNL seven-foot bubble chamber filled with D_2, double-pion production by incident neutrinos has been observed.[91] The measurement of the n/p ratio is

$$\frac{\sigma(\nu n \to \nu n \pi^+ \pi^-)}{\sigma(\nu p \to \nu p \pi^+ \pi^-)} = .49 \pm .19 \qquad (5.51)$$

It should be unity if the neutral current is either pure isovector or isoscalar. This follows from the fact that the two amplitudes are equal by charge symmetry (up to an overall sign) if the neutral current has definite properties under isospin rotations (either I=1 or I=0 but not both). In addition, at Argonne National Laboratory a deuterium exposure of the 12-foot chamber to neutrinos[92] yielded

events of the single-pion production processes

$$\nu n \to \nu p \pi^-$$
$$\nu p \to \nu n \pi^+ \qquad (5.52)$$

The rates for these processes are in reasonable agreement with the calculations of Adler et al. using the $SU(2) \otimes U(1)$ model, but the π^- and π^+ momentum spectra, which should be similar if isovector amplitudes dominate (as expected in this region) look rather different, again indicating some isoscalar interference.

E. Parity Violation in Atomic Physics. The presence of a parity-violating neutral current coupling the electron to hadrons, as exists in the standard $SU(2) \otimes U(1)$ model, can give rise to observable effects in atomic radiative transitions. Three experiments which are in progress were reported[93] recently at the International Conference on Atomic Physics held at the University of California at Berkeley. Two experiments, both involving the same radiative transition in Bi, have reached a sensitivity which has impact on the neutral current models which we have been discussing.

The relevant effective Lagrangian is constructed from Eq. (1.4). Before writing it all out, we note that since the experiments attempt to detect a parity-violating effect, only the axial electron current × vector hadron current (or vice versa) need to be considered. Furthermore, only the time component of the vector hadron current gives a contribution which is coherent over the A nucleons in the bismuth (Z=83, N=126). (This is one reason a heavy nucleus is used; another is the large value of $|\psi(0)|^2$.) Thus we need only keep the time-component of the electron-axial current multiplied with the time component of the hadron vector current. Noticing that

$$\bar{e}(x)\gamma_0\gamma_5 e(x) \approx -i\, e^+(x)\left[\frac{\sigma\cdot\vec{\nabla}}{2m_e} - \frac{\sigma\cdot\overleftarrow{\nabla}}{2m_e}\right]e(x) \qquad (5.53)$$

we obtain (up to a difficult overall minus-sign, which we do not here attempt to trace) the effective Hamiltonian density

$$H'_{PV} = (-)^{?}\frac{iG}{2\sqrt{2}\,m_e} e^+(x)\left[\sigma\cdot\vec{\nabla} - \sigma\cdot\overleftarrow{\nabla}\right]e(x)\begin{bmatrix}(2Z+N)\epsilon(e,u)_{A,V}\\ +(Z+2N)\epsilon(e,d)_{A,V}\end{bmatrix} \qquad (5.54)$$

with

$$\epsilon_{A,V}(e,u) = \epsilon_{RL}(e,u) + \epsilon_{RR}(e,u) - \epsilon_{LL}(e,u) - \epsilon_{LR}(e,u)$$
$$\epsilon_{A,V}(e,d) = \epsilon_{RL}(e,d) + \epsilon_{RR}(e,d) - \epsilon_{LL}(e,d) - \epsilon_{LR}(e,d) \qquad (5.55)$$

$$? = 0 \text{ or } 1$$

There is little reason at this stage to try to hold to the general case; there isn't enough information to warrant such generality. Within an $SU(2) \otimes U(1)$ picture we may reduce the couplings further. For example, using the $\left(T_3 - Q\sin^2\theta_W\right)$ rule of Eq. (3.37)

$$\epsilon_{RL}(e,u) = 2\left(T_3 + \sin^2\theta_W\right)_e\left(\frac{1}{2} - \frac{2}{3}\sin^2\theta_W\right)$$
$$\epsilon_{LL}(e,u) = 2\left(-\frac{1}{2} + \sin^2\theta_W\right)_e\left(\frac{1}{2} - \frac{2}{3}\sin^2\theta_W\right) \qquad (5.56)$$

Only the difference of terms as above occur in Eq. (5.55) for H'_{PV}, because only the axial electron current contributes. Thus if, as in the standard model, e^-_R is a weak isosinglet we get

$$\epsilon_{RL}(e,u) - \epsilon_{LL}(e,u) = \epsilon_L(u) = \left(T_3 - Q\sin^2\theta_W\right)_u$$
$$= \frac{1}{2} - \frac{2}{3}\sin^2\theta_W \qquad (5.57)$$

On the other hand, if e^-_R is a member of a weak isodoublet $(E^0, e^-)_R$, the electron current is vector-like, the terms in Eq. (5.56) for H' cancel pairwise, and H'_{PV} vanishes. A sufficient condition for the absence of a parity-violating effect in this atomic transition is a vector-like electron theory. If this is the case, there

is of course little more to say theoretically. We hereafter restrict our attention to the standard SU(2) ⊗ U(1) model for leptons, which gives, according to Eqs. (5.55) and (5.57)

$$\epsilon(e,u)_{A,V} = \epsilon_L(u) + \epsilon_R(u)$$
$$\epsilon(e,d)_{A,V} = \epsilon_L(d) + \epsilon_R(d) \qquad (5.58)$$

with $\epsilon_L(u)$ and $\epsilon_L(d)$ defined in the previous discussion of neutrino processes. This gives,[94] finally

$$H'_{PV} = -\frac{iG}{4\sqrt{2}\,m_e} e^+(x)(\vec{\sigma}\cdot\vec{\nabla} - \vec{\sigma}\cdot\vec{\nabla})\, e(x)\Big|_{x=0} Q_W(Z,N) \qquad (5.59)$$

with the coupling-strength Q defined by

$$Q_W(Z,N) = 2(2Z+N)[\epsilon_L(u)+\epsilon_R(u)] + 2(Z+2N)[\epsilon_L(d)+\epsilon_R(d)] \qquad (5.60)$$

For the four SU(2) ⊗ U(1) variants we discussed before, we may evaluate the coupling strength

Standard model	$Q_W = Z(1-4\sin^2\theta_W) - N$
$(u\ b)_R$	$Q_W = Z(3-4\sin^2\theta_W)$
$(t\ d)_R$	$Q_W = -3N - 4Z\sin^2\theta_W$
Vector-like	$Q_W = 2Z(1-2\sin^2\theta_W) - 2N$

(5.61)

These are plotted in Fig. 20. In general an effect at least as large as the standard model is anticipated.[95]

The relevant transition is an M1 transition between $^2D_{3/2}$ and $^4S_{3/2}$ levels in the $(6p)^3$ shell. One looks for an E1 admixture caused by mixing of the atomic $(6p)^3$ wave functions with $(6p)^2$ ns states. The atomic physics calculations[96] are considered reliable at least to a factor two, although it is also said that not nearly enough theoretical work has yet been done. Any E1 mixing with M1 leads to a preference of one circular polarization over the other in the radiative decay.

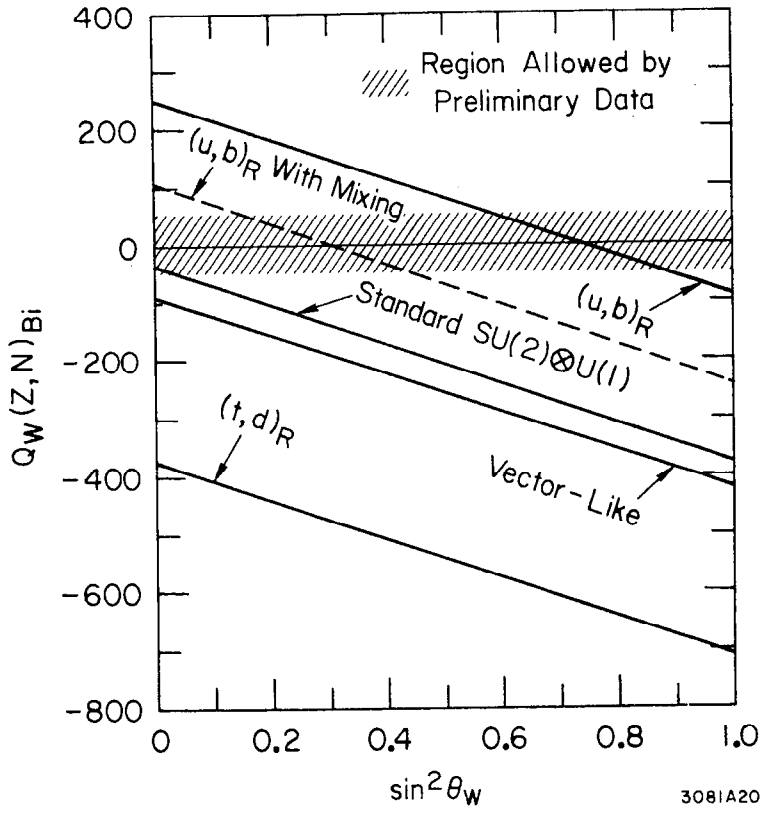

Fig. 20. Values of Q(Z, N), the effective nuclear charge, in the hamiltonian for parity-violating electron-nucleus couplings for various models. The shaded area is the region allowed by experiment. The dashed line is an SU(2) ⊗ U(1) model with mixing between c_R and u_R. See Eq. (5.65) and the adjacent words.

This in turn means that the resonant absorption of left and right circularly polarized light will differ slightly. Rather than measure the absorption, the experimentalists[97] prefer to observe the difference in the anomalous dispersion by utilizing the Faraday effect. Linearly polarized laser light (modulated by a standard Faraday cell) is passed through bismuth vapor, thereafter through a crossed polariod, and then detected. One then searches for a rotation of the polarization vector by the Bi vapor in addition to that provided by the Faraday-cell modulator. Using the standard $SU(2)\otimes U(1)$ model as a prototype, the calculations predict a rotation of the polarization vector of about 3.5×10^{-7} radians/absorption length. Both experimental groups (University of Washington, Seattle and Oxford University) set an upper limit of 1×10^{-7} for any parity violating effect,[93] with residual effects observed at a level 2 or 3 times lower. However these residual effects may be attributable to systematic errors which are not yet understood. At present these experiments pose a serious challenge to the correctness of the $SU(2)\otimes U(1)$ scheme.

It is probably a little too soon to draw far-reaching conclusions from these experiments, which are still not complete. Nevertheless, if we accept uncritically the result, what does it mean? As we saw in Fig. 20, none of the four basic $SU(2)\otimes U(1)$ options survive. However, it is possible in the $(u\ b)_R$ option to, for example, mix the u quark with some other weak isosinglet with charge 2/3, for example, the charmed c-quark. If we do this, the only change in the neutral current coupling which involves nonstrange quarks is as follows:

$$\mathscr{L}_{\text{eff}} \to \frac{G}{\sqrt{2}}\,\bar{\nu}_\mu\gamma_\lambda(1-\gamma_5)\,\nu_\mu\left\{\begin{array}{l}\bar{u}'\gamma^\lambda(1+\gamma_5)\,u'\left(\frac{1}{2}-\frac{2}{3}\sin^2\theta_W\right)\\ +\,c'\gamma^\lambda(1+\gamma_5)\,c'\left(-\frac{2}{3}\sin^2\theta_W\right)\end{array}\right. \tag{5.62}$$

with

$$\begin{aligned} u' &= u\cos\alpha + c\sin\alpha\\ c' &= -u\sin\alpha + c\cos\alpha\end{aligned} \tag{5.63}$$

This implies

$$\epsilon_R(u) \to \frac{1}{2}\cos^2\alpha - \frac{2}{3}\sin^2\theta_W \tag{5.64}$$

and consequently

$$Q_W(Z,N) = Z\left(1+2\cos^2\alpha-4\sin^2\theta_W\right)+N(\cos^2\alpha-1) \tag{5.65}$$

This clearly is an interpolation (cf., Eq. (5.61)) between the standard model ($\cos\alpha=0$) and the $(u\ b)_R$ option ($\cos\alpha=1$), each of which do reasonably well in accounting for other neutral-current and charged-current phenomena. Inasmuch as these models predict atomic parity-violating effects of opposite sign, it is possible to choose the mixing angle such that $Q_W(Z,N)=0$. A choice of $\alpha\sim45^\circ$ does quite well; this is plotted in Fig. 20 as the dashed line.

Such a mixed neutral-current coupling has other implications, the most direct being the existence of charm-changing neutral current processes, e.g., $D^+\to\pi^+e^+e^-$; $D^0\to e^+e^-$, etc. The nonleptonic effective Lagrangian could also contain terms with $\Delta C=1$, $\Delta S=0$ leading to hadronic final states not containing strange particles as well as $\Delta C=2$, $\Delta S=0$ which induces D-$\bar{D}$ mixing.

We have already discussed another alternative compatible with the atomic physics results which is to assign e_R^- to a weak isodoublet $(E^0e^-)_R$. In this case the parity-violating atomic effect vanishes. This choice changes the predicted cross section for $\bar{\nu}_e e^-\to\bar{\nu}_e e^-$ scattering, but the revised value is compatible with the data, as we have already discussed. The predicted cross section for $\bar{\nu}_\mu e^-$ scattering is lowered, but the data are sufficiently sparse that this does not yet pose an insurmountable problem (unless the Aachen-Padua numbers are accepted).

A third alternative is to abandon $SU(2)\otimes U(1)$ and posit a pure isovector neutral-current coupling.[99] If one does this, assumes single-Z^0 exchange, and assumes the axial coupling of Z^0 to the electron has the same strength as the

axial coupling of Z^0 to ν_μ, one finds the result (for bismuth)

$$Q_W(Z,N) = (Z-N)\left[\epsilon_L(u) + \epsilon_R(u)\right] = -43\left[\epsilon_L(u) + \epsilon_R(u)\right] \qquad (5.66)$$

compared with the experimental limit of $|Q_W| \lesssim 50$. Given the limits on $\epsilon_L(u)$ and $\epsilon_R(u)$ from the deep-inelastic data (Eq. (5.29)), there is evidently no problem with experiment.

Finally, one might ask what might be said in a model-independent way. It is not too much. Assuming that the electron neutral current coupling is related to the ν_μ neutral current coupling by the previous assumptions of single-Z^0 and equal axial couplings of Z^0 to e and ν_μ, it is easy to see that given any choice of $\epsilon_R(u)$ and $\epsilon_R(d)$ compatible with deep inelastic data, it is possible to find a very small range of values of $\epsilon_L(u)$ and $\epsilon_L(d)$ in the vicinity of the pure isovector point $\epsilon_L(u) = -\epsilon_L(d) \sim 0.35$ such that $|Q_W| < 50$. Varying over all possibilities for $\vec{\epsilon}_R$, the estimated bound on a left-handed isoscalar coupling is not very strong.

$$|\epsilon_L(u) + \epsilon_L(d)| \lesssim 0.4 \qquad (5.67)$$

This is to be compared with

$$|\epsilon_L(u) - \epsilon_L(d)| \sim 0.7 \qquad (5.68)$$

VI. CONCLUSIONS

Given the rapid experimental progress taking place in this field at the present time, it is probably the wrong time to try to draw any firm conclusions. But certainly the $SU(2) \otimes U(1)$ model has survived the first round of reasonably quantitative neutral-current experiments remarkably well. At present, only the atomic-physics experiment provides a serious challenge to its validity.

If the $SU(2) \otimes U(1)$ model can be trusted for a basis of weak interaction phenomenology (and that is a big if), then we can use the neutral current information to help limit the nature of new flavor degrees of freedom, i.e., hadronic constituents beyond the charmed quark. Here this field appears to be as yet tied to the phenomenology: new quarks are added as required by the data, without any underlying Grand Scheme. Even the question of the necessity of more than four quarks remains open.

This is not to say that there are not candidates for Grand Schemes—only that as yet the evidence does not clearly point to any particular one. The Grand Principle[100] of the vector-like models, based on the idea that all constituents be weak isodoublets, appears to be in trouble with experiment. Another Grand Scheme[72] is that of Gursey and collaborators. It is a superunified theory based on the exceptional group E7. It does not have trouble with experiment as yet (it essentially belongs to the $(u\ b)_R$ option), and has nice esthetic features: a natural place for the color degrees of freedom, in particular. But the E7 representations are big; predicted are two new charged heavy leptons, five (4-component) neutral leptons, 35 weak-electromagnetic gauge bosons, and 133 leptoquarks, presumably of very high mass ($\gtrsim 10^{15}$ GeV). Leptoquark masses are necessarily large in order to protect the stability of the proton. Even if such a scheme is true, we have a long way to go to find out.

Among these conclusions, there is one that is unassailable: since the emergence of the existence of neutral currents from the Gargamelle data a few years ago, the field has made truly remarkable progress. The impact of neutral currents on physics has been similar to the impact of the θ-τ parity violation puzzle on β-decay: revolutionary progress has been made in many fields on many different energy scales. In the case of the neutral currents, we have seen that important information is coming from experiments using photon beams of energy 10^{-10} GeV, reactor neutrino beams of energy $\sim 10^{-3}$ GeV, BNL and ANL neutrino beams of energy $\sim$1 GeV, as well as the higher energy CERN and FNAL beams of energy 5-100 GeV. It is a good reminder of the unity of physics: progress comes from experimentation across a broad front, not only from the cutting edge of the very highest energies.

REFERENCES

1. G. Shen (Ph.D. thesis), preprint LBL-4275.
2. See for example B. Stech, Journal de Physique, Collogue C1, suppl. 10 34, C1 (1973).
3. F. Calaprice, S. Freedman, W. Mead, and H. Vantine, Phys. Rev. Lett. 35, 1566 (1975) and references therein.
4. S. Weinberg, Phys. Rev. 112, 1375 (1958).
5. E. Fischbach, J. Gruenwald, S. Rosen, and B. Kayser, Phys. Rev. Lett. 37, 582 (1976); also B. Kayser, G. Garvey, E. Fischbach, and S. Rosen, Phys. Lett. B 52, 385 (1974).
6. F. Sciulli, in Particles and Fields, 1975, ed. H. Lubatti and P. Mockett (University of Washington, Seattle, Washington, 1975), p. 76.
7. I am indebted to L. Sehgal for this observation.
8. See for example E. Commins, Weak Interactions (McGraw Hill, New York, 1973). Also S. Derenzo, Phys. Rev. 181, 1854 (1969).
9. R. P. Feynman and M. Gell-Mann, Phys. Rev. 109, 193 (1958); E.G.C. Sudarshan and R. E. Marshak, Phys. Rev. 109, 1860 (1958).
10. S. Weinberg, Phys. Rev. Lett. 19, 1264 (1967).
11. A. Salam, in Elementary Particle Theory, ed. N. Svartholm (Almquist and Wiksell, Stockholm, 1969), p. 367.
12. Such a phenomenological approach has been advocated by P. Hung and J. J. Sakurai, preprint CERN-TH-2171 (1976).
13. J. Pati and A. Salam, Phys. D 8, 1240 (1973).
14. T. D. Lee and C. N. Yang, Phys. Rev. Lett. 4, 307 (1960).
15. A thorough discussion is given by B. L. Ioffe, L. B. Okun, and A. Rudik, Zk. Eksperim. Teor. Fiz. 47, 1905 (1964) [Soviet Phys. JETP Lett. 20, 1281 (1965)].
16. See for example T. Appelquist and J. Bjorken, Phys. Rev. D 4, 3726 (1971).
17. G. Feinberg, Phys. Rev. B 134, 1295 (1964).
18. A review of such approaches and experimental limits on Δ is given by B. L. Ioffe and E. Shabalin, Yadernaya Fiz. 6, 828 (1968) [Sov. J. Nucl. Phys. 6, 603 (1968)].
19. S. Weinberg, Phys. Rev. Lett. 27, 1688 (1971). A. Vainstein and I. Khriplovitch, Sov. J. Nucl. Phys. 13, 111 (1971).
20. C. N. Yang and R. Mills, Phys. Rev. 96, 191 (1954).
21. H. Georgi and S. Glashow, Phys. Rev. Lett. 28, 1495 (1972).
22. For example, see B. Barish, Proceedings of the 1975 International Symposium on Lepton and Photon Interactions at High Energies (Stanford University, Stanford, California, 1975).
23. The most extensive study of this approach to gauge theories has been carried out by J. Cornwall, D. Levin, and G. Tiktopoulos, Phys. Rev. D 10, 1145 (1974).
24. B. J. Bjørkén and S. Glashow, Phys. Lett. 11, 255 (1964).
25. Y. Hara, Phys. Rev. B 134, 701 (1964).
26. S. Glashow, J. Iliopoulos, and L. Maiani, Phys. Rev. D 2, 1285 (1970).
27. R. Mohapatra, J. Rao, and M. Marshak, Phys. Rev. Lett. 20, 1081 (1968); P. Olesen, University of Rochester report (unpublished).
28. T. Appelquist, J. Bjorken, and M. Chanowitz, Phys. Rev. D 7, 2225 (1973).
29. G. Preparata, Phys. Letters B 40, 253 (1972).
30. This approach is discussed in Ref. 28. It depends strongly on the assumption of lepton-hadron universality of all weak couplings. This is not satisfied in unified gauge theories because the strength of electromagnetic coupling is not universal. However, lepton-hadron universality of neutral current couplings is still consistent with the data.
31. The application of this idea to gauge theories was suggested by S. Weinberg, Ref. 19.
32. A. Vainstein and I. Khriplovitch, Ref. 19. D. Boulware, Ann. Phys. 56, 140 (1970). L. Faddeev, Theor. and Math. Phys. 1, 1 (1970).
33. P. Higgs, Phys. Lett. 12, 132 (1964).
34. T. Kibble, Phys. Rev. Lett. 13, 585 (1964).
35. V. Ginzburg and L. D. Landau, Zh. Eksp. Teor. Fiz. 20, 1064 (1950). For an introduction, see for example, C. Kuper, An Introduction to the Theory of Superconductivity (Clarendon Press, Oxford, 1968).
36. A study of the role of triangle anomalies in spontaneously broken gauge theories is given by C. Bouchiat, J. Iliopoulos, and P. Meyer, Phys. Lett. B 38, 519 (1972) and by D. Gross and R. Jackiw, Phys. Rev. D 6, 477 (1972).
37. For a comprehensive discussion, see S. Adler, Lectures on Elementary Particles and Quantum Field Theory, ed. S. Deser, M. Grisaru, and H. Pendleton (MIT Press, Cambridge, Massachusetts, 1970).

38. For example, see H. Georgi and S. Glashow, Phys. Rev. D 6, 429 (1972).

39. Proof of the renormalizability of spontaneously broken gauge theories is due to G. 't Hooft, Nucl. Phys. B 33, 173 (1971); B 35, 167 (1971). The importance of this work and its impact on weak interaction theory cannot be overestimated.

40. For a discussion of the nonrenormalizability of general relativity in the presence of external sources, see for example, S. Deser and P. van Nieuwenhuizen, Phys. Rev. Lett. 32, 245 (1974).

41. S. Weinberg, "Gauge Theory of CP Violation," Harvard preprint, footnote 5.

42. A recent critique and study is given by J. Ellis, M. K. Gailliard, and D. Nanopoulos, Nucl. Phys. B 106, 292 (1976).

43. For example, B. L. Ioffe and L. B. Okun (private communication) suggest $e^+e^- \to h^0Z^0$.

44. We ignore possible higher-order polynomials of the momenta in the couplings; this only worsens the problem of high-energy behavior.

45. S. Weinberg, Ref. 19.

46. Y. S. Tsai, Phys. Rev. D 4, 2821 (1971).

47. J. Bjorken and C. H. Llewellyn Smith, Phys. Rev. D 7, 887 (1973).

48. While I know no reference for this argument, I believe it is a well-known one.

49. H. Georgi, H. Quinn, and S. Weinberg, Phys. Rev. Lett. 33, 451 (1974).

50. S. Weinberg, Phys. Rev. D 5, 1962 (1972).

51. H. Georgi and S. Glashow, Phys. Rev. Lett. 32, 438 (1974).

52. F. Gursey and P. Sikivie, Phys. Rev. Lett. 36, 775 (1976).

53. See also Ref. 49 for an elaboration of the implications of such a scheme.

54. J. Bjorken, SLAC preprint SLAC-PUB-1841.

55. S. Drell and T.-M. Yan, Phys. Rev. Lett. 25, 316 (1970); Ann. Phys. (N.Y.) 66, 578 (1971).

56. cf. the lectures of D. Hitlin and the contribution of L. Lederman, these proceedings.

57. This general connection (via the CVC hypothesis) is due to Y. Yamaguchi, Nuovo Cimento 43, 193 (1966).

58. The feasibility of reaching such energies has been discussed by B. Richter, SLAC preprint SLAC-PUB-1738.

59. On the other hand S. Weinberg (Phys. Rev. Lett. 36, 294 (1976)) argues that radiative corrections alone (arising from emission and reabsorption of virtual W's and Z's) provide a lower bound to m_{h^0} of a few GeV. See also E. Gildener and S. Weinberg (to be published).

60. S. Adler, in Proceedings of the Sixth Hawaii Topical Conference, ed. P. Dobson et al. (University of Hawaii Press, Honolulu, Hawaii, 1975).

61. P. Musset, report to 18th International Conference on High Energy Physics, Tbilisi, USSR (1976).

62. H. Faissner, report to 18th International Conference on High Energy Physics, Tbilisi, USSR (1976).

63. For a recent summary of neutral current data, see the report of B. Lee at the Aachen Neutrino Conference, preprint FERMILAB-Conf-76/61-THY.

64. F. Reines, H. Gurr, and H. Sobel, Phys. Rev. Lett. 37, 315 (1976).

65. P. Musset, report to 18th International Conference on High Energy Physics, Tbilisi, USSR (1976).

66. A. Benvenuti et al., Proceedings of the Conference on Particles with New Quantum Numbers, University of Wisconsin, Madison, 1976; also A. Benvenuti et al., Phys. Rev. Lett. 37, 1039 (1976).

67. L. Stutte, as in Ref. 66; also D. Buchholz, report to the Aachen Neutrino Conference, 1976.

68. For example, C. H. Llewellyn Smith, Phys. Reports C 3, 263 (1972). A nice recent review is given by L. Sehgal, "Phenomenology of Neutrino Reactions," Argonne National Laboratory report ANL-HEP-PR-75-45.

69. There are countless theoretical studies of these options. A partial list is contained in Refs. 70-73. We apologize to those contributors not cited here.

70. M. Barnett, Phys. Rev. Lett. 34, 41 (1975); Phys. Rev. D 11, 326 (1975); D 13, 671 (1976). See also V. Barger and D. Nanopoulos, Phys. Lett. B 63, 168 (1976).

71. Y. Achiman, K. Koller, and T. Walsh, Phys. Lett. B 59, 261 (1975).

72. F. Gursey and P. Sikivie, Phys. Rev. Lett. 36, 775 (1976).

73. H. Fritsch, M. Gell-Mann, and P. Minkowski, Phys. Lett. B 59, 256 (1975). A. DeRujula, H. Georgi, and S. Glashow, Phys. Rev. D 12, 3589 (1975). S. Pakvasa, W. Simmons, and S. Tuan, Phys. Rev. Lett. 35, 702 (1975). F. Wilczek, A. Zee, R. Kingsley, and S. Treiman, Phys. Rev. D 12, 2768 (1975).

74. A. Benvenuti et al., Phys. Rev. Lett. 37, 1039 (1976).

75. W. Lee et al., Phys. Rev. Lett 37, 186 (1976).

76. D. Cline et al., Phys. Rev. Lett. 37, 252 (1976); 37, 648 (1976).

77. M. Barnett, Harvard preprint (1976).

78. C. Albright, C. Quigg, R. Schrock, and J. Smith, Phys. Rev. D 14, 1780 (1976).

79. D. Sidhu, BNL reports 21468 and 21511 (1976).
V. Barger and D. Nanopoulos, University of Wisconsin preprint COO-562.

80. Our conventions are those of J. Bjorken and S. Drell, Relativistic Quantum Mechanics (McGraw Hill, New York, 1964).

81. Compare, e.g., the discussions in Refs. 77 and 78.

82. See, for example, A. Hey, Acta Physica Polonica B 6, 831 (1975) for a discussion and references.

83. J. Bjorken, Phys. Rev. D 1, 1376 (1970).

84. This is discussed by F. Gilman, Proceedings of the 1973 SLAC Summer Institute on Particle Physics, Vol. 2, p. 71; SLAC-167.

85. M. Alguard et al., Phys. Rev. Lett. 37, 1261 (1976).

86. A review is given by M. Gourdin, Phys. Reports 11, 29 (1974).

87. For a review, see D. H. Perkins, Proceedings of the 1975 International Conference on Lepton and Photon Interactions at High Energies, Stanford, California (1975).

88. S. Adler, Phys. Rev. D 12, 2644 (1975); S. Adler, R. Dashen, J. Healy, I. Karliner, J. Lieberman, Y. J. Ng, and H. S. Tsao, Phys. Rev. D 12, 1322 (1975) and references cited therein.

89. W. Y. Lee, these Proceedings.

90. B. Coremans et al., Phys. Lett. B 61, 207 (1976); also private communication from D. Perkins.

91. M. Murtagh and M. Derrick, private communication.

92. M. Derrick, remarks at Wisconsin Conference, cf. Ref. 66 and private communication.

93. Reports of C. Bouchiat, E. Fortson, and P. Sandars to the Fifth International Conference on Atomic Physics, Berkeley, California, 1976.

94. C. Bouchiat and M. Bouchiat, Phys. Lett. B 48, 111 (1974).

95. This has been emphasized by J. Bernabeau and C. Jarlskog, preprint CERN-TH-2206 (1976).

96. Several have been carried out. See for example, E. Henley and L. Wilets, Phys. Rev. (to be published); M. Brinicombe, C. Loving, and P. Sandars, Oxford University preprint (to be published); I. B. Khriplovitch, Pisma Zh. Eksp. Teor. Fiz. 20, 686 (1974) [JETP Lett. 20, 315 (1974)]. Khriplovitch argues that core polarization and other many-body effects may reduce the number quoted by the other authors by a factor $\lesssim 2$, but there is no general agreement on this point.

97. Earlier limits and a description of the technique of the Seattle experiment are found in D. Soreide et al., Phys. Rev. Lett. 36, 352 (1976).

98. This option has been discussed by many of the authors in Ref. 73.

99. For example, S. Adler and S. F. Tuan, Phys. Rev. D 11, 129 (1975).

100. For example, see Fritsch and Minkowski, Ref. 73.

WEAK INTERACTIONS AT HIGH ENERGIES

Stanley G. Wojcicki

Stanford University
Stanford, California 94305

I. INTRODUCTION

These lectures shall attempt to review the experimental status of high energy weak interactions with a special emphasis on its relation to the physics of "new" particles. In reviewing a field that is moving as rapidly as the high energy neutrino physics today, there is always a difficult choice to be made as to the material to be included. On one hand one can limit oneself to the well established results at the expense of excluding the most recent and hence probably the most interesting data; on the other, one can try to be as all inclusive as possible and thus take the risk of including the results that may already be discredited at the time of publication of the review. I have opted for the latter course and shall try to include all of the data that I am aware of that has been presented publicly, either orally or in written form. It shall fall on the reader to judge the data critically in areas where there is a discrepancy if that discrepancy will not have been resolved already by the time this review appears in print.

I shall commence these lectures with a brief description of the experimental techniques used in high energy neutrino physics with an emphasis on the advantages and limitations of each method. Subsequently, by way of a theoretical introduction, I would like to review the status of the neutrino physics 2 years ago from the point of view of its excellent agreement with the naive quark model. Then, in the main body of these lectures, I would like to discuss the various aspects of the experimental data and see how these results compare with the predictions of the "new orthodoxy" - i.e. the four quark model. Finally, I would like to end by pointing out some of the discrepancies between the theoretical predictions and the experimental data and comment as to what even newer physics these results might be pointing to.

These lectures shall be limited to the charged current aspect of the neutrino interactions, with the main emphasis on the experimental data. The neutral current data and the deeper theoretical questions are discussed in the parallel lectures by Bjorken.

II. EXPERIMENTAL OVERVIEW

a) Beams. All of the high energy neutrino beams used up to this time have utilized the neutrinos originating predominantly from π or K decay. The basic features of all the neutrino beams are illustrated in Fig. 1 where we show schematically the present Fermilab and BNL neutrino setups. The sequential elements of a neutrino beam are:

1. proton beam striking a target and making secondary hadrons.
2. a focusing and/or momentum selecting element(s).
3. drift space, to allow hadrons to decay.
4. a shield to stop all hadrons and range out muons.
5. neutrino detectors.

The most important difference between various neutrino setups resides in points 1, 2 and 5, i.e. incident proton energy, focusing element, and the detector. The length of the drift space and the shield are generally comparable and scale with the energy. The unique feature of all the neutrino setups, illustrated in Fig. 1b, is the ability to stack several detectors one behind the other with only a slight loss of solid angle for the more distant detectors.

A very serious limitation in interpreting the results of a large number of neutrino experiments is the ill defined momentum of the neutrino beam. Accordingly, a great deal of ingenuity has gone into the designs and construction of focusing and momentum selecting elements with the goal of either containing the largest possible number of neutrinos or

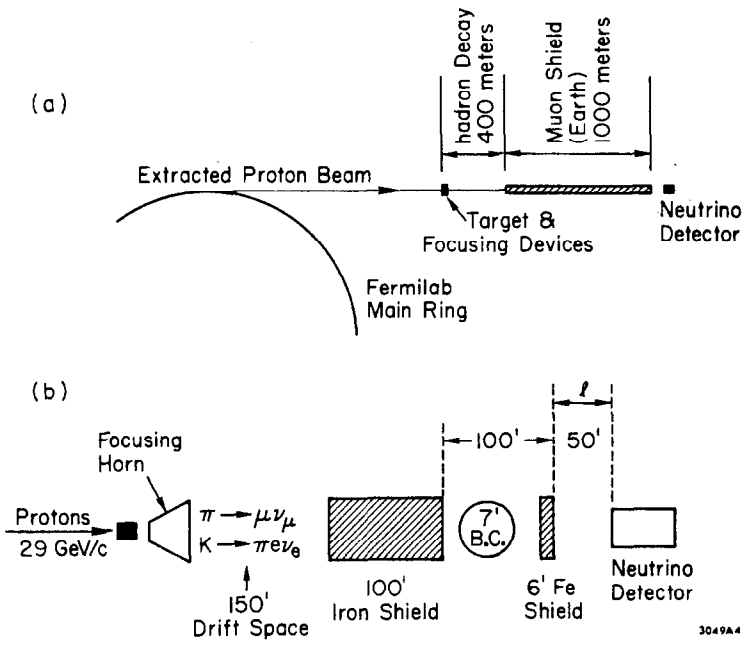

Fig. 1 A schematic drawing of the Fermilab (a) and the BNL (b) neutrino setups.

purifying and better defining the accepted neutrino flux.

The basic "facts of life" that determine these schemes are the following:

1. the typical transverse momentum of hadrons produced in the hadronic collisions is of the order of 300 MeV/c. This should be compared with 30 MeV/c and 236 MeV/c as the maximum possible p_T that a neutrino can obtain from π and K decay respectively. Thus the hadronic transverse momentum tends to dominate the divergence of the neutrino beam and by focusing the hadrons into a parallel beam one can increase the flux considerably.
2. the present size of the detectors subtends a solid angle at the hadron target comparable to the angular divergence of the highest energy neutrinos. Thus focusing buys relatively little extra flux at high energies and becomes significantly more important for lower energy neutrinos.
3. Because of small $m_\pi - m_\mu$ mass difference the maximum laboratory momentum of a neutrino from π decay is only about 40% of the initial pion momentum. In contrast, a K meson can transfer almost all of its momentum to its daughter neutrino. Thus the highest energy neutrinos come only from K decay. Coupled with the increase of K^+/K^- production ratio as a function of increasing secondary energy, this means that $N_\nu/N_{\bar{\nu}}$ ratio will also increase towards the high end of the neutrino momentum spectrum.

In light of these considerations we can now consider various focusing schemes used in neutrino beams.

1. bare target, or absence of any focusing or momentum selecting elements. It is clearly the simplest scheme, but the price paid is low intensity, lack of distinction between ν's and $\bar{\nu}$'s, and lack of any momentum selection.

2. horn beam. This scheme utilizes a focusing element around the target to focus the hadrons of one sign into a parallel beam. The advantages are maximum possible neutrino (antineutrino) flux and good rejection of the antineutrinos (neutrinos). The disadvantages are short spill (this may actually be an advantage for some experiments, where the desire to gate out the cosmic rays is the most important consideration) and the difficulty in calculating and/or measuring the neutrino flux. The rejection of hadrons of the unwanted sign deteriorates as the energy of the secondaries increases because these particles tend to come out at relatively low angles. This becomes a serious limitation for the study of high energy $\bar{\nu}$ interactions. Accordingly a commonly used variation is a double horn system with a plug down the middle to absorb hadrons produced very close to 0°. This eliminates most of the unwanted ν contamination at the expense of part of high energy $\bar{\nu}$ flux.

3. quadrupole beam. Here the focusing element becomes a quadrupole system set generally to optimize transmission of a relatively high energy hadron beam. This enhances the high energy neutrinos, suppresses the low energy ones, and results in a relatively flat spectrum. The advantages are possibility of a long spill, relative enhancement of higher energy portion of the spectrum, and a relatively good understanding of the neutrino energy spectrum. The disadvantages are lower flux and lack of neutrino/antineutrino selection. The fluxes from all of these schemes are illustrated in Fig. 2, taken from Al Mann's 1976 Coral Gables talk.[1)]

4. dichromatic beam. Here the beam elements consist of both dipoles and quadrupoles so that the beam entering the decay drift space consists of hadrons with a finite momentum bite and a unique sign. There can be several variations on this idea.

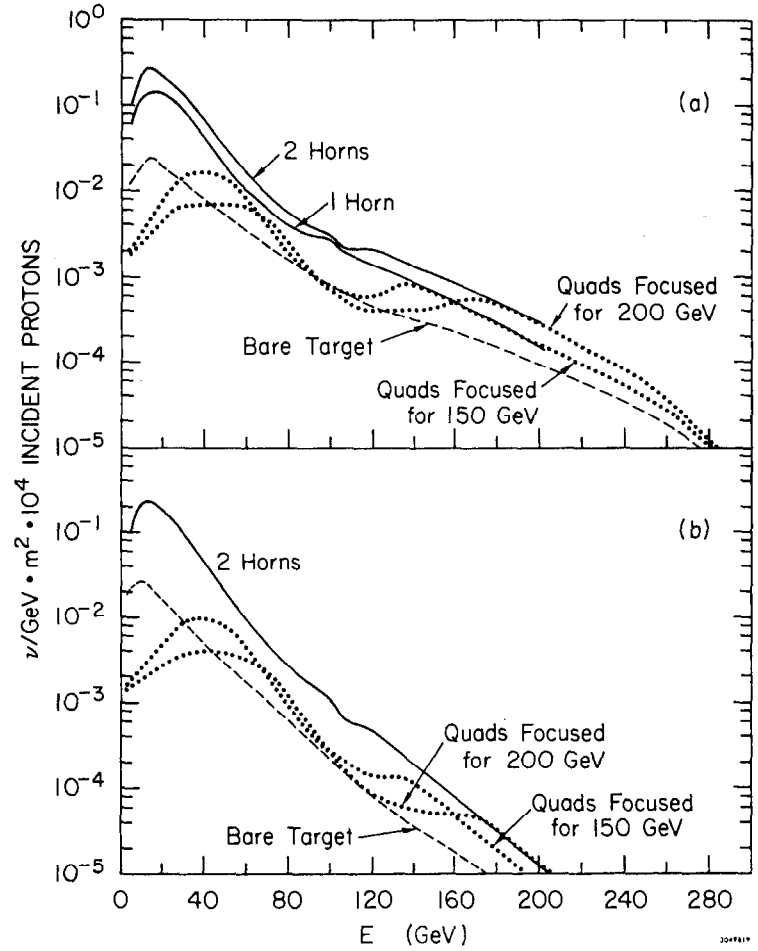

Fig. 2 Calculated neutrino (a) and antineutrino (b) energy spectra for 400 GeV protons.

In the simplest scheme, one utilizes the fact that most of the neutrinos originating from K decay come out at much larger angles than those from π decay.[2] Thus a detector of relatively small transverse dimensions will intercept only a small fraction of K neutrinos, or more specifically if positioned at 0°, only the very high energy ones. Hence the spectrum of neutrinos will consist of two discrete bunches, the low energy ones from π decay and the high energy ones from K decay.

A variation of this scheme consists of displacing the detector away from 0°, thus missing the majority of π neutrinos and selecting only the K neutrinos of energy slightly below the peak energy.[3] One thus obtains a relatively pure monochromatic neutrino beam. Another variation is making the detector large enough so that a sizable fraction of K neutrinos is intercepted.[4] The radial position of the interaction is now directly related to the neutrino energy, and one thus has energy information independent of the calorimetry. The basics variations on this dichromatic scheme can be easily seen in Fig. 3, illustrating the K and π decay kinematics.

Clearly the dichromatic beam scheme yields the cleanest neutrino beam. The price that one has to pay, however, is the significant reduction in flux resulting from the finite momentum bite.

b) Detectors. In discussing the detectors used in the neutrino experiments it is convenient to divide them into two categories: the electronic detectors and the bubble chambers. We commence with a brief discussion of the electronic detectors. The typical neutrino apparatus performs the combined functions of a target, hadron detector, and muon spectrometer. The different setups can be classified according to how the various parts of the detector are arranged.

1. separate function detector. Here the target-hadron detector part of the apparatus comes first and is subsequently followed by a magnetic system to analyze the muons. Such a system has

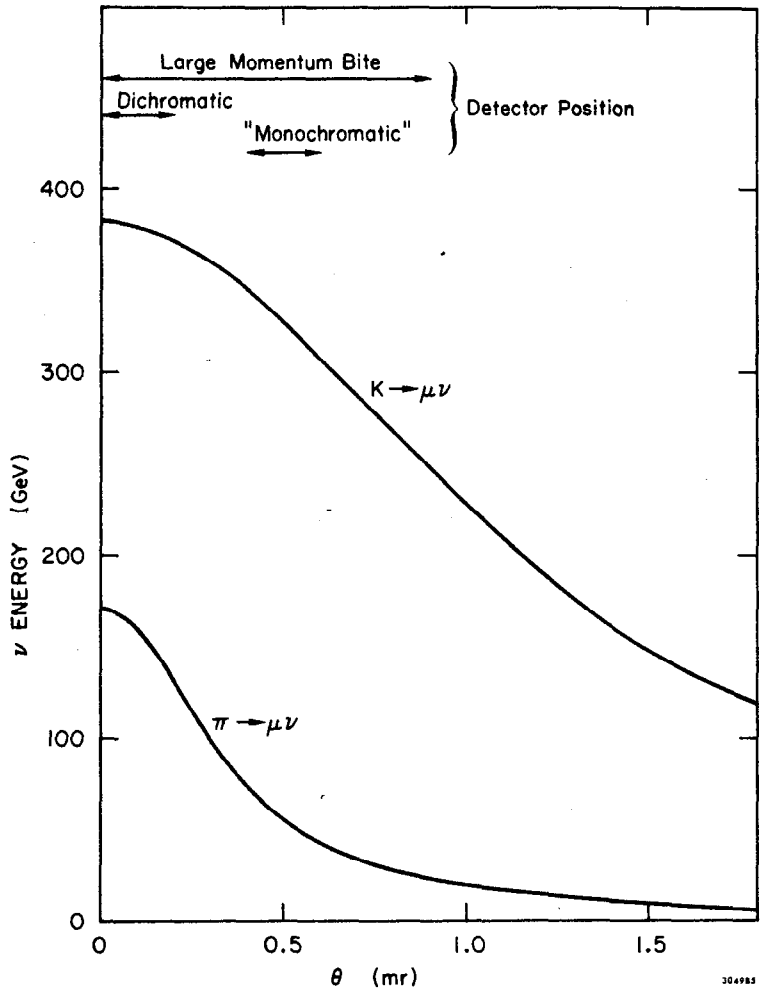

Fig. 3 K and π decay kinematics.

a relatively high flexibility from the point of view of changes in the target part but a relatively poor acceptance, especially for wide angle muons. The Harvard-Penn-Wisconsin-Fermilab (HPWF) setup and the old Cal-Tech-Fermilab setup (E21) fall into this category.

2. combined function detector. The target, hadron detector, and the muon spectrometer are all interleaved together. The system has very high acceptance for muons, but loses some flexibility. The new setup at CERN SPS exemplifies this kind of approach.
3. mixed detector. A separate target-detector is subsequently followed by a combined function detector. The new Cal Tech setup at Fermilab falls into this category.
4. non magnetic detectors. There are also used special purpose detectors without any magnetic field. These have been used for specific experiments at relatively low energies where the large acceptance is more important than magnetic analysis. The 2 setups to measure elastic ν scattering at BNL exemplify this category.

As with all classifications, these should not be considered very rigid, but rather as exemplifying the different ways of arranging the separate parts of the apparatus. Thus, for example, placing a hydrogen target in front of the CERN SPS detector would turn it into a mixed detector in our nomenclature.

The bubble chamber systems can be classified into two categories: cryogenic and warm chambers. The cryogenic chambers use hydrogen, deuterium, or neon as the fill or some combination of these ingredients. The obvious advantage of hydrogen or deuterium is the simplicity of the target; the obvious disadvantages: low target mass, long absorption length ($\sim$8 m for H_2) and long radiation length ($\sim$9 m for H_2). These last two

factors make the lepton identification very difficult and make complimentary electronic detectors highly desirable.

The warm bubble chambers, of which the European Gargamelle is the most famous example, generally use an organic fill with higher density and shorter radiation length than even the neon filled chambers. In that sense they are highly complimentary to the hydrogen chambers, emphasizing good lepton identification with the simultaneous introduction of a complicated target.

c) Energy Measurement. The measurement of the total energy (hadronic, leptonic, and electromagnetic) in neutrino interactions is an important problem as it is crucial both to the cross section and scaling variable measurements. Thus it is worthwhile to briefly point out here the advantages and shortcomings of different beams and/or detectors.

The dichromatic beam, at least in principle, is the ideal instrument to measure the total neutrino energy, as a crude calorimetry measurement of the total hadronic energy in the detector will allow one to separate π and K neutrino interactions. Then, if the momentum bite of the beam is small enough, and the beam clean enough, the energy of the neutrino is defined quite well.

In wide band and quadrupole beams one must rely exclusively on the calorimeter and muon spectrometer to measure the total energy. The typical accuracy here is about $\pm 10\%$. Of course this technique will only give a lower limit if some secondary neutrinos are given off in the interaction.

The "heavy fill" bubble chambers can in principle use visual calorimetry to measure total energy with some correction for the escaping neutrals. The light fill bubble chambers, where most of the neutrals (n, K^o, γ) escape detection, generally measure total energy present in charged particles and then, using an empirical formula, scale this to the total energy.

d) Lepton Identification. The electron identification is easy only in "high" Z bubble chambers. More specifically, a medium Z fill, like 80% H_2 and 20% Ne, makes the electron identification possible at about 50% efficiency level in the 15' B.C., but the identification requires rather careful scanning. The techniques used here rely on visible bremstrahlung, $e^{\pm}$ materialization, trident production, and delta rays, as unique signatures of the $e^{\pm}$. The electron identification in a much heavier fill, like freon in Gargamelle, is quite straightforward, almost 100% efficient, and completely unambiguous. The relative merits of various fills in identifying electrons and muons are illustrated in Table I.

TABLE I

The absorption and radiation lengths for various bubble chamber fills.

	Absorption Length	Radiation Length
Hydrogen	790 cm	890 cm
Deuterium	342 cm	764 cm
"Light" neon-hydrogen (21% Ne)	230 cm	110 cm
Neon	75 cm	24 cm
Propane (C_3H_8)	176 cm	111 cm
Freon (CF_3Br)	73.5 cm	11 cm

There have been efforts to identify electrons in electronic detectors,[5] and they have met with some measure of success. On the other hand the basic incompatibility of the large target mass necessary for neutrino experiments and low graininess required for good electron identification and measurement make these experiments extremely difficult.

On the other hand the electronic detectors find the muon identification considerably easier, with penetration through some 1 kg/cm^2 of material a relatively clean signature. Of course this technique becomes much more difficult for lower energy ($P_\mu < 1.5$ GeV/c) muons, since they tend to range out before hadrons can be cleanly eliminated.

In general, even for heavier fills, the absorption length in bubble chambers is comparable to the potential pathlength in the detector and

thus "bare" bubble chambers suffer in their ability to detect muons. The external muon identifier (EMI) around the 15' chamber[6] remedies this difficulty by essentially extending the sensitive volume beyond the bubble chamber (see Fig. 4). It consists of a layer of proportional chambers preceded by several absorption lengths of zinc. Requiring a correlation between the B.C. track and a hit in PWC's provides a powerful rejection against hadrons. The main shortcoming of the EMI at the present time is its limited solid angle.

The bubble chamber experiments have been quite successful in using kinematics to identify the muon. Here one relies on the fact that muons tend to have high energy and high Q^2. Comparison with EMI results indicates that on the average one can do quite well in identifying muons by this technique, but of course the method in ineffective for muons in kinematically suppressed regions.

e) Strange Particle Identification. This facet of experimental detection, very important in the context of new particle production, has been almost an exclusive preserve of the bubble chambers. Heavy fill bubble chambers have some difficulty separating Λ's from K^o's. The $K^{\pm}$'s so far have been identified solely in bubble chambers either by their decays or by stopping. Because of very strong bias toward low energy K's, and the very low efficiency, charged K identification has not been used so far in any systematic way.

f) Summary of Existing Detectors. It appears worthwhile to end this purely experimental section with a table summarizing the vital statistics of the existing neutrino setups. This list will soon be enlarged by the new CERN-SPS detectors and the new Cal-Tech-Fermilab-Northwestern detector.

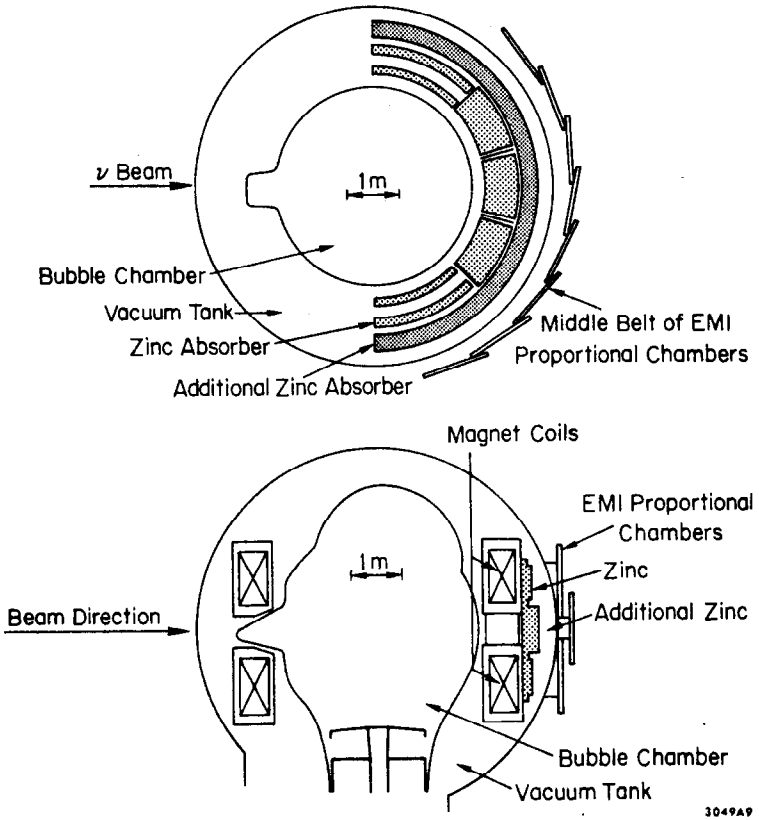

Fig. 4 The External Muon Identifier for the 15' Fermilab bubble chamber.

TABLE II

Experimental neutrino setups.

Group	Detector	Size/Fid.Size	Laboratory	Proton Energy
	HBC	7'	BNL	30 GeV
	HBC	12'	Argonne	12 GeV
	HBC	15'	Fermilab	400 GeV
	GGM	12'/3m^3	CERN	25 GeV
HPWF	Liquid Sc.	60 tons	Fermilab	400 GeV
CITF	Fe	170 tons	Fermilab	400 GeV
USSR	Fe	96/34 tons	Serbukhov	70 GeV
CIR	Al	26/8 tons	BNL	30 GeV
HPW	Liquid Sc.	33 tons	BNL	30 GeV

III. NEUTRINO PHYSICS AND THE NAIVE QUARK MODEL

We would like to start the discussion of the status of neutrino physics by summarizing the predictions of the naive quark model and show its excellent agreement with what was known 3 years ago. Very briefly the essential features of the simple quark model are the following.

The neutron and proton are each composed of three quarks, namely 2d + u and 2u + d respectively. The up (u) quark carries a charge of + 2/3, the down (d) quark a charge of -1/3. In addition, there may be a sea of quark-antiquark pairs whose presence would be exhibited mainly at low values of Feynman x. The quarks are point constituents without any form factors and thus lepton nucleon scattering can be treated in terms of superposition of fundamental current - quark interactions. All the weak interactions occur via V-A couplings and thus only the left handed quarks (or right handed sea antiquarks) participate in the reaction. Finally, since the same quarks also are responsible for the deep inelastic e-p scattering, the structure functions, i.e. "momentum" distributions of the quarks in the nucleons, as derived from e-N scattering can be carried over directly to the neutrino interactions.

This simple picture leads right away to several quantitative predictions. Thus, since the fundamental charged current neutrino reaction can occur only on the down quark, i.e.

$$\nu\, d \to u\, \mu^-$$

the νn to νp cross section ratio should be 2 to 1, a simple consequence of the relative number of the down quarks in the two nucleons. More refined analysis,[7] incorporating the actual structure functions and the sea quarks, yield predicted ratios of between 1.57 and 2.05 in fair agreement with the experimental numbers of

1.48 ± 0.17	7' BC experiment at BNL[8]
$1.4 \pm .3$	12' BC experiment at Argonne[9]
2.1 ± 0.3	Gargamelle experiment[10]

Another simple prediction is the agreement of neutrino derived structure functions with those obtained from the ep scattering. This agreement was first seen in the Gargamelle data[11] and is illustrated in Fig. 5. One should emphasize here that the agreement of the absolute normalization constitutes an experimental verification of the mean square charge of the quark in the nucleus being 5/18 as predicted by the quark model. This is because the coupling of the electromagnetic current to the quark is proportional to the electric charge squared, a factor which is absent in the weak current coupling. Alternatively we can look on the size of the neutrino cross section as constituting a measurement of the mean square charge of the quark.

The relative size of the neutrino and antineutrino cross sections also follows directly from the quark model, it being the consequence of the V-A nature of the coupling. If we look at the neutrino quark scattering in the center of mass both 0 and 180° scattering are allowed by the required helicity and the conservation of angular momentum.

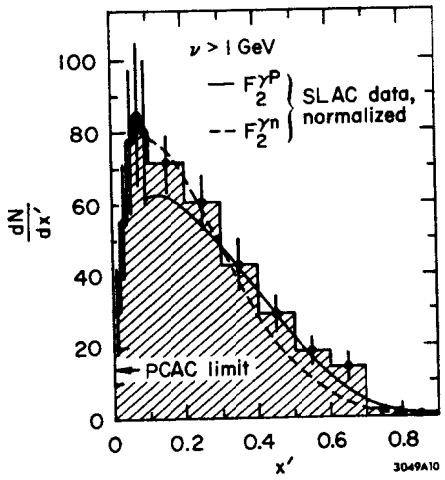

Fig. 5 Comparison of the Gargamelle neutrino data with the structure function obtained from SLAC ep and ed data. Because of low energies the Bloom-Gilman variable x^1 is used rather than x.

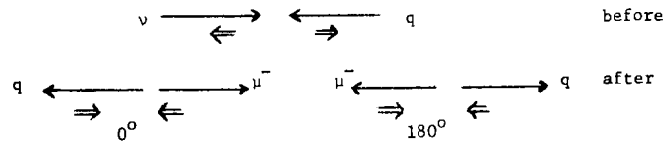

However, for antineutrino quark scattering 180° scattering is forbidden by angular momentum conservation, since it is impossible to both conserve

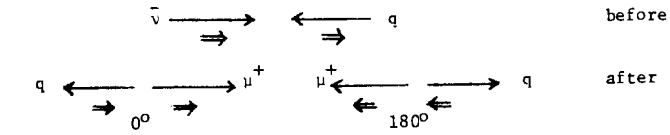

the angular momentum and maintain the proper helicity of the two scattering particles. More quantitatively, in terms of the scaling variable $y \equiv \frac{E_h}{E_\nu}$, the neutrino distribution will be flat and the antineutrino one will follow $(1-y)^2$, giving the required zero at y = 1 i.e. 180° scattering in the center of mass system. Integrating we obtain the predicted ratio

$$\frac{\sigma_{\bar{\nu}}^{TOT}}{\sigma_{\nu}^{TOT}} = 1/3$$

to be compared with the original experimental results of

	0.38 ± 0.04	1-10 GeV	GGM	12)
	0.40 ± 0.11	38 GeV	CIT-F	13)
	0.23 ± 0.11	110 GeV	CIT-F	13)
and	0.34 ± 0.03	10-30 GeV	HPWF	14).

Similarly the original "low energy" (i.e. $E_{\nu,\bar{\nu}} \lesssim 30$ GeV) data appeared to reproduce the predicted dσ/dy distributions for both the ν and $\bar{\nu}$ scattering.

Finally, the total cross section for ν and $\bar{\nu}$ interactions should follow a linear behavior with E, a consequence of point nature of the neutrino quark scattering. The agreement with the data as of two years ago was indeed excellent as can be seen in Fig. 6.

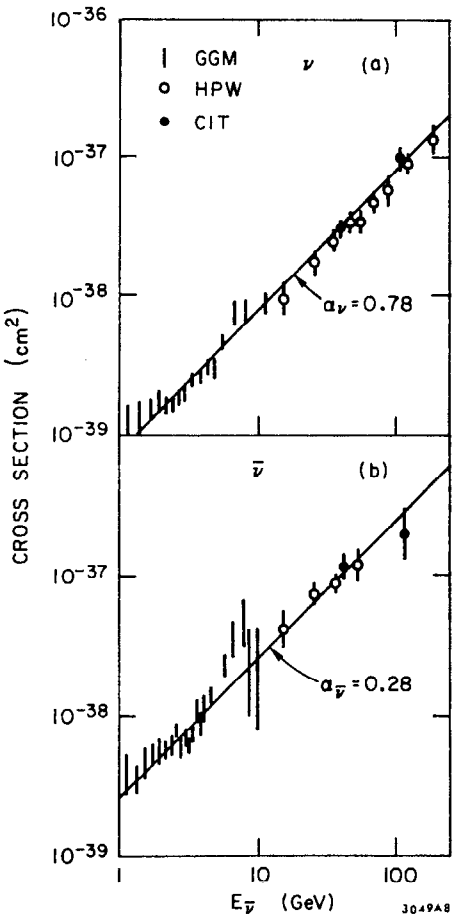

Fig. 6 Early measurements of total ν and $\bar{\nu}$ cross sections as a function of energy (from 1974 London Conference).

In summary, even though the detailed predictions of the model were not tested rigorously, the low energy neutrino data appeared to be in very good agreement with the predictions of the simplest quark model.

IV. 4 QUARK MODEL PREDICTIONS

We consider next the ramifications of the 4 quark model on the neutrino physics. In this picture the hadronic current becomes

$$J_\mu^{cm} = \bar{u}\,\gamma_\mu\,(1-\gamma_5)\,d_c + \bar{c}\,\gamma_\mu(1-\gamma_5)\,s_c$$

where $\quad d_c = d\cos\theta_c + s\sin\theta_c$

$$s_c = -d\sin\theta_c + s\cos\theta_c$$

and the s and c are the strange and charmed quark respectively and θ_c is the Cabibbo angle.

We must remember now that the Cabibbo angle is small, i.e. $\sin^2\theta_c \approx 0.05$ and that the number of s and c quarks and antiquarks in the nucleons is supposed to be small, since their only source is the sea of quark-antiquark pairs that should be important only at low x. It is for these two reasons that the naive 2 quark model can be expected to give good results even if the 4 quark picture represents the "ultimate truth". This is especially true at low energies where the charmed quark production is negligible or even below threshold.

We may now consider specific mechanisms that can lead to charmed particle production in neutrino interactions.

a) $\nu\, d \to \mu^- c$. This process would be suppressed by $\sin^2\theta_c$ with respect to other charged current reactions. Furthermore, the equivalent process involving the valence quarks does not exist for the $\bar{\nu}$'s.

b) $\nu\, s \to \mu^- c$

$\bar{\nu}\, \bar{s} \to \mu^+ \bar{c}$

This process must proceed off sea quarks. Thus it should be dominant at low x and the general level should be ∿5-10% (i.e. fraction of sea

quarks indicated by low energy neutrino experiments).

c) $\nu\bar{c} \rightarrow \mu^- s$ c quark is "liberated"

$\bar{\nu}c \rightarrow \mu^+ \bar{s}$ $\bar{c}$ quark is "liberated"

This process should be suppressed even more than (b) as the $c\bar{c}$ sea is expected to be even smaller than the $s\bar{s}$ sea due to the higher mass of the charmed quark.

d) Diffractive Production of F^*. F^* is expected to have the same quantum numbers as the weak current and thus the weak current could transform directly[15] in the presence of a nucleon into F^*. However, because of observed low production of ρ mesons in the neutrino interactions, which can also proceed via this mechanism, this process is expected to be relatively unimportant.

We can now turn to the question of the signatures of the charmed particle production in neutrino interactions.

a) Bumps in the Hadronic States. These would have to have specific features in order to be associated with charm particles:

Narrow - i.e. consistent with resolution, since the charmed ground states would decay via weak interactions.

Massive - the mass would be expected to be around 2 GeV.

Strange - the predominent decay modes could be expected to involve strange particle decay.

Exotic - the charge and strangeness quantum numbers of the parent state would be expected to have opposite sign.

This is certainly a classical way to look for new short lived particles. For several reasons, however, it is difficult as far as charmed particles are concerned. Firstly, at the present time it is accessible only to the bubble chambers and thus the numbers of events are rather limited. Secondly, the many expected decay modes require large statistics to obtain a meaningful signal. Finally, one expects large multiplicity because of high mass, and this makes the detection of neutral particles very important. Low Z chambers have good resolution but poor detection probability; the high Z chambers have much better detection efficiency but much worse resolution.

The present statistics of bubble chambers are too limited to offer any substantial contribution here, but one can expect significant increase in the data in the next few years.

b) Di-lepton Production. The charmed particle production can give rise to dilepton production via the mechanism

$$\nu + N \rightarrow \mu^- + C + \text{hadrons}$$
$$\hookrightarrow \ell^+ + \nu + \text{hadrons}$$

where C is some charmed meson or baryon. This mechanism would yield dileptons of opposite sign because of the $\Delta Q/\Delta C$ rule which is operative here both in the production and the decay processes. Some additional features associated with this process which would lend further credence to charmed particle production interpretation are associated strange particle production, asymmetry between μ^- and μ^+, i.e. mostly $P_{\mu^-} > P_{\mu^+}$, and relatively high P_T of μ^+.

c) $\Delta Q/\Delta S$ Violation. There is by now very good evidence from low energy weak decay processes that $\Delta Q/\Delta S$ rule holds down to the level of a percent or so in amplitude. The combined production and decay process of a charmed particle in neutrino interactions is expected to yield $\Delta Q = -\Delta S$ since the production process would have $\Delta Q = +1$ and $\Delta C = +1$ and the decay process $\Delta C = -1$ and $\Delta S = -1$. Thus observation of a reaction with $\Delta Q = -\Delta S$ would be strong evidence for charmed particle production. Unfortunately, to be convincing, any purported evidence for $\Delta Q = -\Delta S$ must be able to exclude associated production, i.e. other missing strange particles. These could be charged K's misidentified as π's or escaping K_L^o's. Thus this technique must demonstrate the absence of missing K's either on

a statistical basis, necessitating good statistics, or on an individual basis by means of a highly constrained fit. The latter situation would strongly favor low energy where, however, the charm production is expected to be smaller. It is doubtful that any other detector besides bubble chambers would be able to demonstrate $\Delta Q/\Delta S$ rule violation.

d) Strange Particle Excess. From the production mechanisms discussed above, and the fact that charmed particles should decay predominantly into strange particles, we can anticipate one or two strange particles in the final state for every charm event. Thus one might expect a rise in strange particle yield well above charm production threshold.

e) Anomalies in Scaling Variables. Charm production would represent an onset of new phenomena and thus would imply that there is a relevent mass scale of the order of few GeV. Thus we would expect a change in scaling variable behavior when we pass the charm threshold. Most specifically, for kinematical reasons, the effects of new particles soon after threshold would exhibit themselves as enhancements at low x, high y, and high W.

In conclusion, one should point out that at least some of these manifestations, e.g. dilepton production and scaling variable anomalies, are not specific to the charm model, but would apply equally well to any new particle production with new quantum number. What distinguishes the charmed particle model from other possibilities is the specific nature of its predictions. It not only makes additional predictions regarding strange particle excess, but it also sets at least approximately the level at which charmed particle production may be expected. This level is relatively small due both to the smallness of the Cabibbo angle and the fact that the sea contribution, as measured by the initial neutrino experiments, is relatively small (i.e. at the 5-10% level).

V. EXPERIMENTAL STATUS OF DILEPTONS

a) Experimental picture of μe Events. The initial μe events produced by neutrinos were observed in the Gargamelle exposure at CERN[16]. Because of the very short radiation length, the electron identification is unambiguous as can be seen from one of the events displayed in Fig. 7. The main background comes from asymmetric $e^{\pm}$ pairs, resulting either from Dalitz or external conversion of γ rays. On the basis of analysis of 44.5 K charged current events with visible energy greater than 1 GeV one can reach several conclusions.[17]

1. $\mu^- e^+ V^o$ events are seen. 3 clear examples have been observed, in two of which the V^o is ambiguous in its interpretation between K^o and Λ. In the third event the V^o is definitely a Λ. In addition a fourth event has a neutron star and 2 external $e^{\pm}$ conversions but no V^o. Thus it is a strong candidate for a $\Lambda \to n\pi^o$ decay. The expected $\mu^- e^+ V^o$ background is less than 0.1 event.
2. $\mu^- e^+$ events without a V^o have also been seen.
3. there is a strong correlation between the observation of a $\mu^- e^+$ event and presence of a V^o. If they were uncorrelated, one would expect 256 (rather than 16 observed) $\mu^- e^+$ events based on 3 seen $\mu^- e^+ V^o$ events.
4. there were no $\mu^+ e^- V^o$ events seen in $\bar{\nu}$ events (in a sample about 1/5 as big).
5. the authors do not quote a rate for this process but an estimate can be obtained from previously published upper limit on charmed particle production (Fig. 8) based on a sample of 6.1K charged current events and 1 observed $\mu^- e^+ V^o$ event. Assuming the same neutrino spectrum, we get for production cross section by neutrinos above 3 GeV

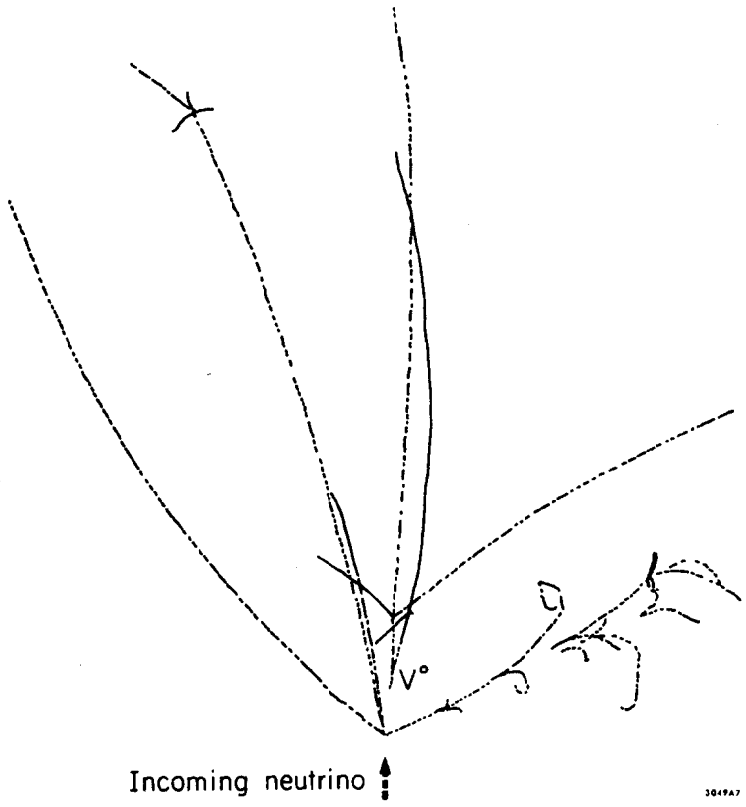

Fig. 7 An example of one of the 3 μeV° events seen in the Gargamelle.

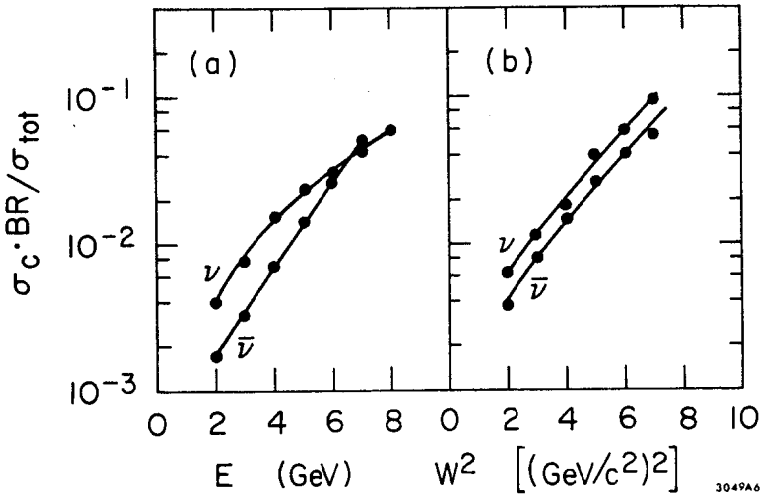

Fig. 8 The initially published Gargamelle upper limits for charmed particle production followed by its decay into a μeV°.

$$\frac{\sigma_c \cdot BR}{\sigma_{TOT}} = 8\times10^{-3} \times \frac{1}{2.3} \times \frac{6.1}{44.5} \times 3 \approx 1.5\times10^{-3}.$$

The results on the μe search of the Gargamelle Collaboration are summarized in Table III.

TABLE III

Observed and expected (from background sources) numbers of μe events.

Event Type	Numbers of Events	
	Observed	Expected
$\mu^- e^+ V^o$ + anything	$3^{(\pm)}$	$\sim 9 \times 10^{-2(\pm)}$
$\mu^- e^+$ + anything	16	5 ± 3
$\mu^- e^-$ + anything	23	25.6 ± 8.0
$e^- V^o$ + anything	5	2.5 ± 0.8
e^+ + anything	6	5.4 ± 1.6

(±) These numbers refer to the full experiment (44500 CC events above 1 GeV) whilst the remaining numbers refer to the 1975 run (34100 CC events above 1 GeV).

The Columbia-BNL group has tried to extract information on μe production from their experiment designed to study neutrino nucleon elastic scattering using an array consisting of Al spark chambers and scintillators.[18] The muon identification is straightforward, but the electron identification is very difficult, the main backgrounds being γ ray conversions near the interaction vertex and ν_e interactions (about 1% of events.) The μe events are isolated by requiring the first spark of the "electron" track to be close to the vertex and a reasonable length of straight track before shower initiation.

The authors claim observation of 7 events, of which at least 4 they believe to be genuine $\mu^- e^+$ events. They quote the rate for observed events

$$\frac{\mu e}{ALL} \approx 3\times10^{-4}$$

On the other hand, one must remember that the cuts are very severe, so that if the analysis is correct the actual rate must be considerably higher.

Recently the Wisconsin-Berkeley-CERN-Hawaii group[19] presented the first results from the exposure of Fermilab 15' bubble chamber filled with a light Ne-H_2 mixture to a wide band horn focused neutrino beam. The 20% Ne mixture shortens the radiation length to 110 cm and thus allows one to identify approximately 50% of the electrons above 800 MeV by looking for accompanying tridents, conversion pairs, or sudden changes in curvature (bremstrahlung). By following the identical procedure on converted γ rays the actual conversion efficiency has been measured to be 48 ± 7% and essentially flat for electrons above 800 MeV. The collaboration draws several conclusions based on a scan of some 5000 ν interactions with the total observed energy above 5 GeV.

1. 15 $\mu^- e^+$ events have been observed.
2. There is a strong correlation between those events and the presence of a strange particle. More specifically, one sees in association 7 K^o's, 2Λ's, and 2 V's ambiguous between K^o and Λ. Furthermore 2 K^+'s are identified unambiguously. This should be compared with 16% of all charged current events at this energy being associated with a V^o. [20]
3. The observed number of K^o's, after correcting for neutral and K^o_L decays yields the average number of K^o's/event $\langle N_{K^o}\rangle = 2.0 \pm 0.6$.
4. There is a strong asymmetry between μ^- and e^+, with
$$\frac{\langle P_{\mu^-}\rangle}{\langle P_{e^+}\rangle} = 6.6$$
5. There is no evidence for any apparent production threshold, with a possible hint of cross section dropping somewhat below 20 GeV.
6. The production rate depends on the specific model assumed for charmed particle production and decay, since the experiment is sensitive only to electrons above 800 MeV. Taking

Barger's and Phillip's model[21] of $D \to K e\nu$ decay, one obtains

$$\frac{e^+\mu^-}{ALL} \approx (1 \pm 0.3) \times 10^{-2}$$

The same fill of the bubble chamber was also exposed to the wide band horn $\bar{\nu}$ beam by the FNAL-IHEP-ITEP-Michigan collaboration.[22] Out of a total of 644 events with energy greater than 10 GeV they find one rather poor candidate, with $E_{\bar{\nu}}$ = 36 GeV, where a background of 0.4 ± 0.2 events is expected. The upper limits on the total new particle production rate times the branching ratio into $\mu e(V^o)$ are given as the function of energy in the accompanying table.

TABLE IV

Upper limits on e production by antineutrinos.

$E_{\bar{\nu}}$ *)	μ^+ Events	$\sigma(\mu^+e^-)/\sigma(\mu^+s)$	$\sigma(\mu^+e^-\nu^o)/\sigma(\mu^+x)$
>10 GeV	644	$\leq$ 1.0%	$\leq$ 0.6%
>20 GeV	366	$\leq$ 1.7%	$\leq$ 1.0%
>30 GeV	191	$\leq$ 3.2%	$\leq$ 1.9%
>40 GeV	88	$\leq$ 4.1%	$\leq$ 4.1%

*) An average correction for neutral energy loss has been applied.

b. Review of the $\mu^+\mu^-$ Situation. The first 2 $\mu^+\mu^-$ events produced in neutrino interactions have been observed by the HPWF group some 3 years ago and reported at the London conference.[23] Since that time the group has considerably extended this investigation[24] by greatly increasing the statistics, studying the phenomenon with several different beams, and doing a more detailed analysis of all the relevant variables. The muons are required to penetrate through sufficient steel so as to unambiguously eliminate the possibility of hadron punchthrough. This does, however, set a lower limit on the detectable muon momentum of 4 GeV/c.

The main conclusions reached by the HPWF group are the following.

1. the events definitely do not come from π and/or K decay and thus must represent new physics. The basic justification for this statement comes from the fact that the production ratio in light (liquid scintillator) and heavy (iron) target are the same. Those two targets differ in their mean density by a factor of 3.54. To take into account the slightly different detection efficiencies for the two targets a Monte Carlo calculation was performed yielding the result that π-K decay process can be excluded as the sole source of $\mu^+\mu^-$ events at the 4σ level. These results are presented graphically in Fig. 9.
2. The visible energy is high but the ratio of $\mu^+\mu^-$ events to all the charged current events is constant above about 40 GeV. More specifically one obtains

$$\frac{\mu^+\mu^-}{\mu^-} = (0.8\pm0.3)\times10^{-2} \text{ at } \bar{E}_\nu = 100 \text{ GeV based on 51 } \mu^+\mu^- \text{ events}$$

and $$\frac{\mu^+\mu^-}{\mu^-} = (0.9\pm0.3)\times10^{-2} \text{ at } \bar{E}_\nu = 55 \text{ GeV based on 14 } \mu^+\mu^- \text{ events}$$

The large neutrino energy responsible for these events is illustrated in Fig. 10 where for comparison we also plot the energies of the first 7 μ^-e^+ events observed in the 15" B.C. and the calculated ν spectrum for the conditions under which these $\mu^+\mu^-$ data were taken. One should be very careful, however, about drawing any conclusions about threshold from these data since there is a strong bias against detection of lower energy neutrino events. Without a specific production and decay model it is impossible to estimate the actual magnitude of this bias. Furthermore, one must remember that the μ^-e^+ events have quite different biases and were taken in a horn beam that strongly emphasizes lower energy neutrinos (c.f. Fig. 2a).

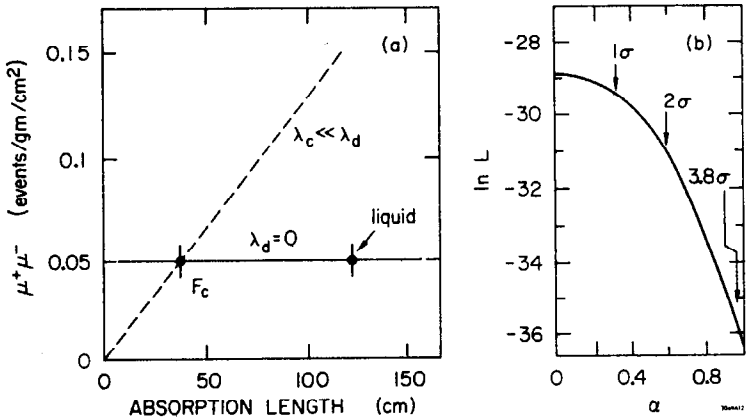

Fig. 9 a) the number of $\mu^+\mu^-$ events g cm^2 as a function of the absorption length. b) results of the likelihood analysis of the fraction α of events that arise from π or K decays.

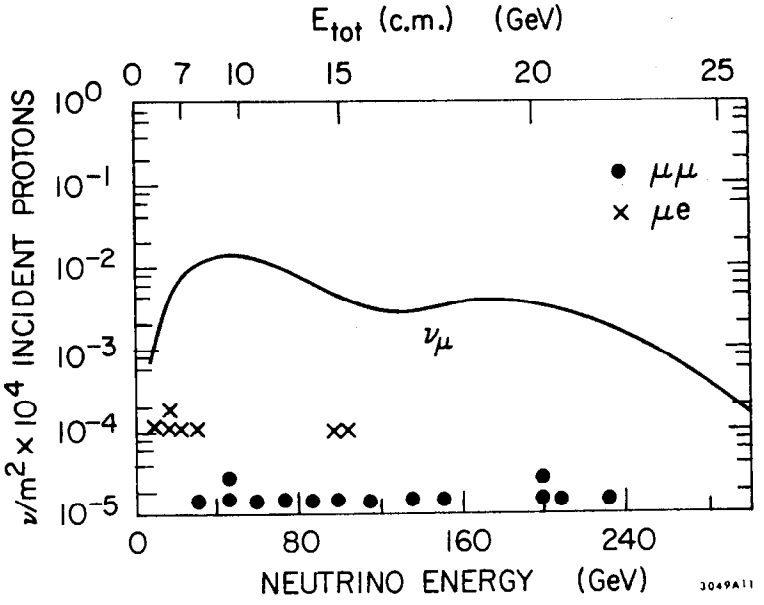

Fig. 10 Total energy distribution of the $\mu^+\mu^-$ events and of the μ^-e^+ events.

3. there is a strong asymmetry between μ^- and μ^+ with ratio for all events being

$$\frac{\langle p_- \rangle}{\langle p_+ \rangle} = 3.7 \pm 0.65.$$

Some fraction of these events are most likely caused by the antineutrinos since the data were taken in a quadrupole focused beam. Thus if one makes the assumption that the higher energy muon carries the lepton number of the incoming neutrino, then one can remove the 9 events with $P_- < P_+$ on the assumption that these are produced by $\bar{\nu}$.

One then obtains for the ratio

$$\frac{\langle P_- \rangle}{\langle P_+ \rangle} = 6.1 \pm 0.8$$

The support for the validity of this assumption is provided by the independent run[25] with a double horn $\bar{\nu}$ beam which yielded 5 $\mu^+\mu^-$ events, 4 of which had $P_+ > P_-$. This is quite significant since $\bar{\nu}/\nu$ ratio in that beam is of the order of 10. For the $\bar{\nu}$ horn run one obtains the rate ratio of

$$\frac{\mu^+\mu^-}{\mu^+} = (2 \pm 1) \times 10^{-2}$$

i.e. consistent with the ν data.

4. The projected transverse momentum distribution of the "wrong" sign muon is considerably higher than that of the typical hadron. The transverse momentum is defined as being out of the plane defined by the neutrino and the right sign muon. Furthermore the distribution appears to cut off around 1 GeV/c. The definition of the transverse momentum and its actual distribution (on a semi-log scale) are illustrated in Fig. 11.

Soon after the initial observation of the $\mu^+\mu^-$ events by the HPWF group, these results were corroborated by an independent experiment of

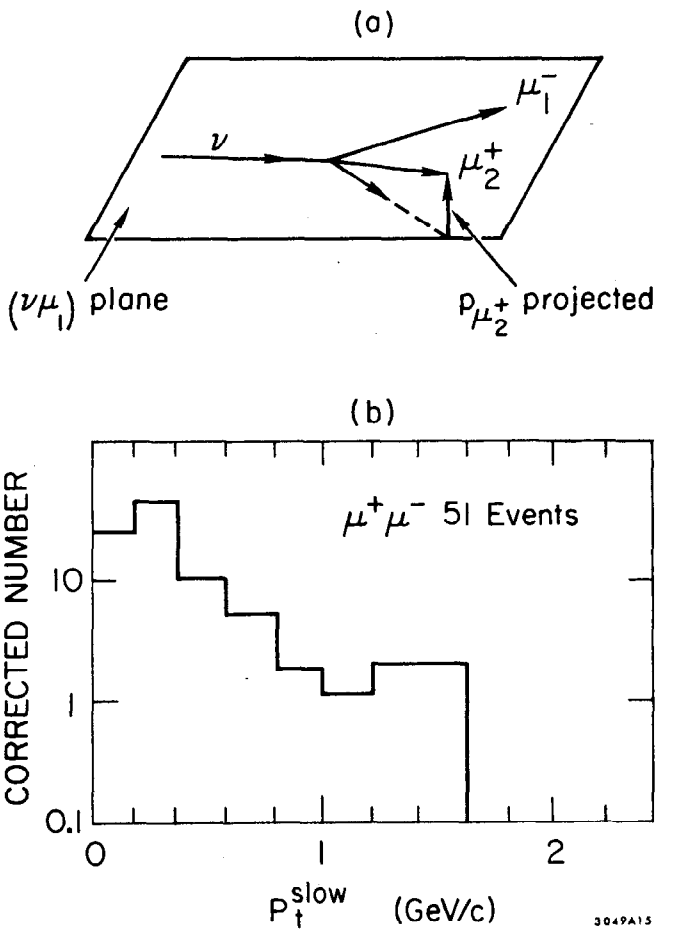

Fig. 11 a) Definition of the transverse momentum variable.
b) Distribution of the events in the transverse momentum variable.

the Cal Tech-Fermilab group.[26] Here the muon identification was obtained by the requirement of penetration through 2m of Fe, or effective cut on the muon momentum of 3 GeV. The fundamental limitation of this experiment was the small solid angle subtended by the 5' diameter magnet at the end of the apparatus. Thus in a large number of dimuon events either one or both of the muons could not have their charge identified. The overall experimental situation is summarized in Table V.

TABLE V

Number of single and double muon events.

Beam	1μ	2μ	"Right Sign" Identified	Both Charges Identified
ν	2313	19	8	4
$\bar{\nu}$	446	2	2	0

One can again draw several conclusions from the data, supporting those of the HPWF group.

1. There seems to be an excess of observed 2μ events beyond the number expected from π or K decay as illustrated in Fig. 12.
2. All of the events where both momenta are measured satisfy $P_{\mu^-} > P_{\mu^+}$ and give
$$\frac{\langle P_{\mu^-} \rangle}{\langle P_{\mu^+} \rangle} = 3.6$$
3. As seen from Fig. 13, the ratio of 2μ to single μ events appears to increase with energy; more specifically it appears to be considerably higher for the ν's originating from K decay ($\bar{E}_\mu \gtrsim 150$ GeV) than for those from the π decay ($\bar{E}_\nu \gtrsim 50$ GeV). Again one must ask how much of this effect is due to experimental bias as opposed to any threshold phenomena. The answer to that question must await better data but several remarks can be appropriately made here. The $P_\mu > 3$ GeV cut is already a severe detection limitation at low energy but one should emphasize that for most

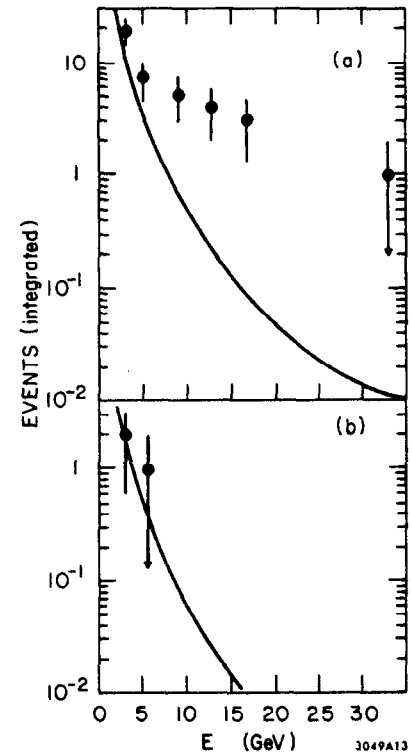

Fig. 12 Number of dimuon events with $E_{\mu^+} > E$ from neutrino (a) and antineutrino (b) running. The curves represents the Monte Carlo calculation of the number of μ's arising from π or K decay.

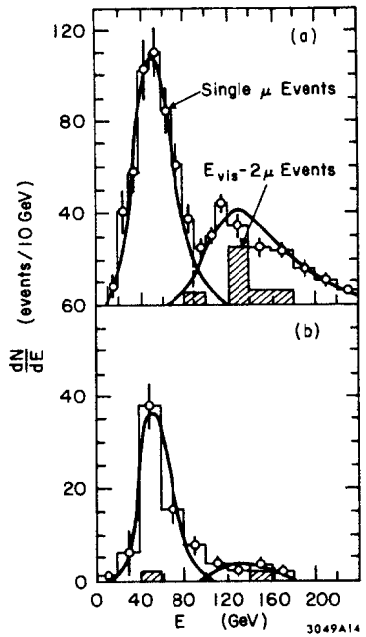

Fig. 13 Total energy distribution of single μ and 2μ events having the "right sign" muon through the spectrometer for the ν (a) and $\bar{\nu}$ (b) runs.

configurations the effective cut is even higher. This is due to the fact that for typical P_T's of the second muon ($\langle P_T^+ \rangle$ = 1.2 GeV/c for the 4 events with both μ's through the magnet) the probability at low incident energies that the muon will leak out through the side of the apparatus before it has a chance to penetrate 2 m of iron is quite high. This will increase the P_μ cutoff to somewhere around 6 GeV/c for the CITF geometry, strongly suppressing the probability of observing and identifying dimuon events at the lower energies.

We end the discussion of the $\mu^+\mu^-$ data by summarizing the results from Serpukhov.[27] The groups there performed 3 runs: 2 with different ν spectra and one with a $\bar{\nu}$ beam. The spectra for these three runs are illustrated in Fig. 14. As can be seen ν run 2 has the high energy end of ν spectrum enhanced compared to run 1. By defining a muon as a particle penetrating 0.48 m of Fe one can obtain a preliminary ratio of 2μ/μ events for the three runs. These results are indicated in Table VI and show a significant rise of this ratio when the high energy part of the spectrum is enhanced.

TABLE VI

Number of single and double muon events in Serpukhov experiment.

Run	Beam	No. of Protons	# 1μ	# 2μ	$R = \frac{2\mu}{\mu}$
1	ν	9.4×10^{16}	11830	91	$.77 \times 10^{-2}$
2	ν	13.6×10^{16}	8270	173	2.09×10^{-2}
3	$\bar{\nu}$	15.5×10^{16}	3600	19	$.53 \times 10^{-2}$

The majority of the "2μ" events, however, correspond to the events where the other muon is either a π or K decay product or a hadron punch-through. Accordingly, for each run a Monte Carlo calculation was performed to calculate the expected number of "2μ" events due to such

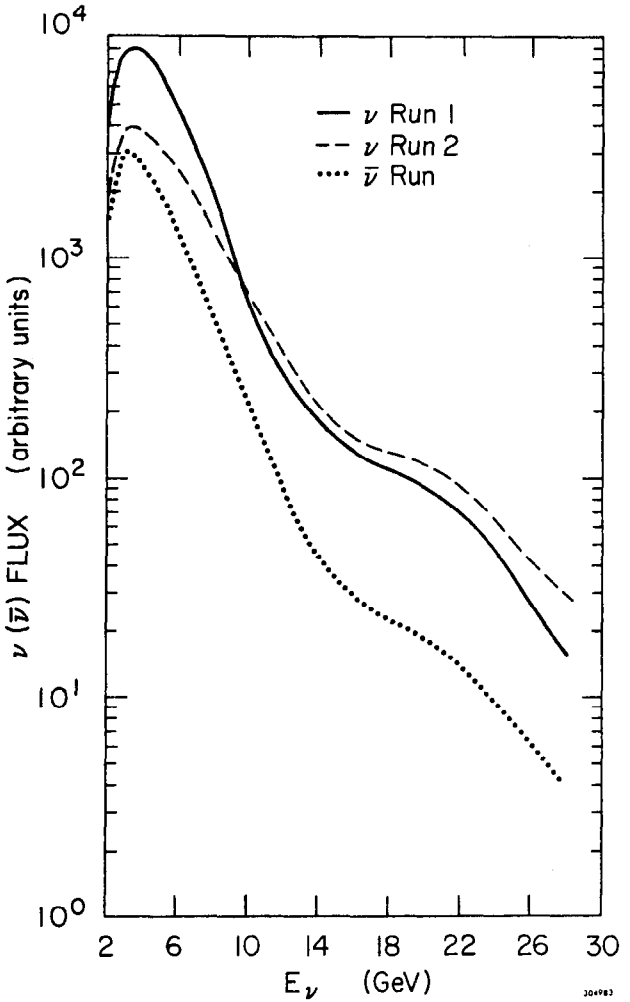

Fig. 14 The ν and $\bar{\nu}$ spectra for the three Serpukhov runs.

conventional mechanisms as a function of the definition of the muon. The variable parameter in defining the muon was the amount of Fe that was required for the muon to penetrate. The results of this calculation, as well as the experimental data, are displayed in Fig. 15. A significant deviation is seen for run 2 for the muons above a certain energy, which the authors interpret as the evidence for dimuon production by neutrinos involving a new mechanism.

It is difficult to quote an absolute rate but the authors claim that their results are consistent with

$$\frac{\mu^+\mu^-}{\mu} \approx 10^{-2}$$

for neutrino energies above 10 GeV.

c. Interpretation of the Dilepton Data. Before discussing the comparison of the dilepton data with the charm picture one should briefly dispose of some of the other possible mechanisms that could have generated dilepton events (see Fig. 16).

1. neutral current + $V^o \to \mu^+\mu^-$. This process would give dimuons with unique (or a set of unique) mass values and could not (in the context of conventional ideas) give μe events. The observed continuum of the $M_{\mu\mu}$ spectrum and the presence of μe events excludes this hypothesis.

2. $\nu\mu \to \nu\mu$ scattering. This process is very interesting in its own right and as such has been calculated extensively.[28] The observed rate is far too large to account for the observed events and some of the theoretical distributions differ greatly from the observed ones. Specifically, these 4-fermion interaction events should be quasielastic, i.e. display a low total hadronic energy and give $M_{\mu\mu}$ mass peaked near 2_μ masses. Both of the experimental distributions deviate markedly from these predictions.

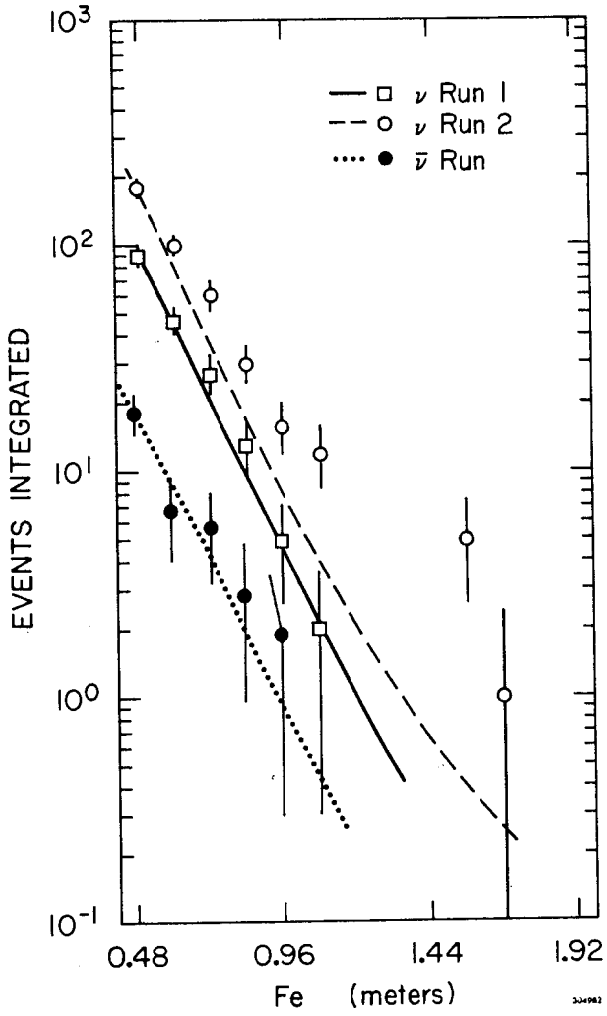

Fig. 15 Comparison of the observed number of "dimuon" events with the number calculated from π and K decay and hadron punchthrough.

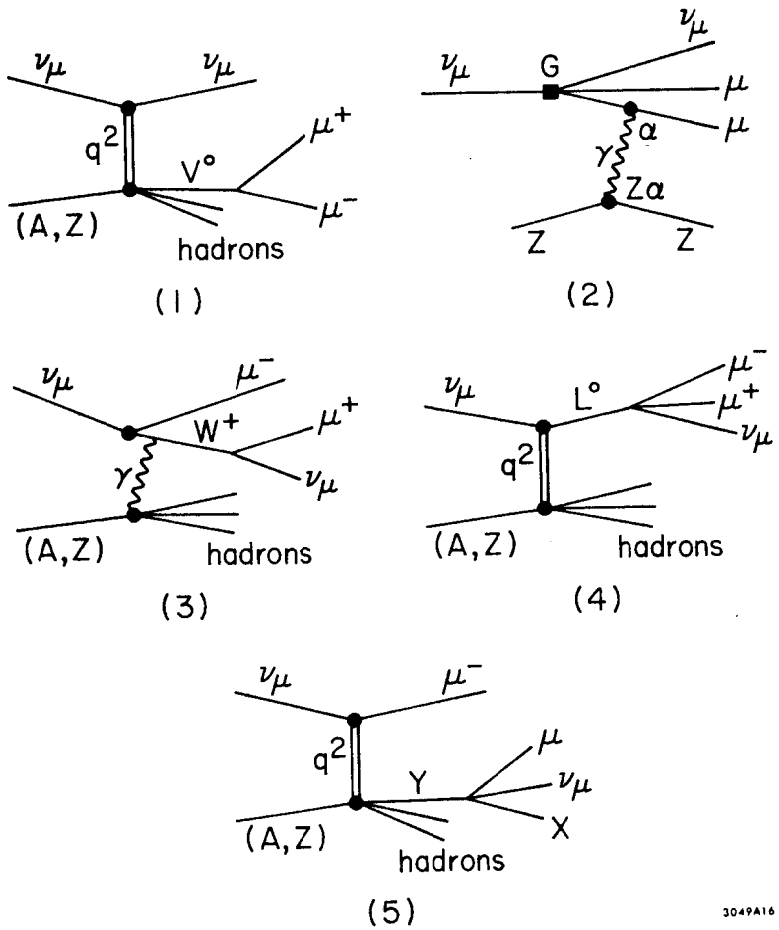

Fig. 16 The possible mechanisms for the dimuon production.

3. W boson production. If the W boson is responsible for the observed dilepton events, then its mass would be in the vicinity of 5 GeV. This would have two important repercussions, both of which are in disagreement with the data. The transverse momentum of μ^+ would be about a factor of 2 wider than the observed one and one would see important propagator effects in the total cross section, none of which are seen. In addition one would expect $P_{\mu^+} > P_{\mu^-}$ contrary to the experiment.

4. neutral heavy lepton production. This has been an interesting theoretical possibility and has been studied rather extensively. There are now, however, several strong arguments against this possibility. Firstly, in heavy lepton decay both muons would be produced locally and thus $M_{\mu\mu}$ spectrum should be independent of the energy of the incident neutrino. The opposite appears to be true, the mass spectrum becoming wider with increasing neutrino energy.

Even more important is the argument put forth by Pais and Treiman[29] which shows that on very general grounds the ratio R defined by

$$R = \frac{<P_{\mu^-}>}{<P_{\mu^+}>}$$

must satisfy the condition $\frac{1}{2} < R < 2$ if we limit ourselves to V, A couplings. In full generality the condition becomes $(9-4\sqrt{2})/7 \leq R \leq (9+4\sqrt{2})/7$. As discussed above, this prediction is in strong disagreement with the data and thus appears to exclude the heavy lepton hypothesis. The experimentally observed ratio R may conceivably need some correction due to contamination by μ's from π or K decays and possible confusion as to the ν or $\bar{\nu}$ source of the event but it is highly unlikely that these numbers could be brought anywhere close to the Pais Treiman limit.

5. new hadron production. This then brings us to the most likely interpretation of these events namely a production of a hadron with new quantum numbers, which subsequently decays leptonically (or semileptonically). It remains to ask the question whether the data are self consistent and whether they agree with the several predictions of the charm (GIM) model.[30]

Association with strange particles - One might expect that at low energies, i.e. in Gargamelle exposure, the charmed particles would be produced off valence quarks, and thus unaccompanied by strange particles. At these low energies we would expect prevalence of charmed baryons and only one strange particle in the final state. At higher energies e.g. 15' exposure at Fermilab, production off sea quarks might become more important resulting in 2 strange particles in the final state. Certainly, the correlation with strange particles appears to be well established experimentally in both experiments; there may be even indications of too high a kaon yield at higher energies if one assumes that $\bar{N}_{K^0} = \bar{N}_{K^+}$. However, the statistics are too limited on this point to say that the GIM model is violated here.

Spectra - We can compare here with a specific model of Barger and Phillips that assumes a charmed meson mass of 2.3 GeV and a decay into a Kev final state without any hadronic form factor. The agreement of the HPWF data with these predictions is quite good, as can be seen from Fig. 17.

Rate - What we observe is a product of charmed particle production rate times its semileptonic branching ratio, i.e.

$$\frac{\sigma_{charm}}{\sigma_{Ch\ Curr}} \cdot \frac{B_{charm \rightarrow \ell\nu\ hadrons}}{CHARM \rightarrow all}$$

where the branching ratio is an average over the several possible

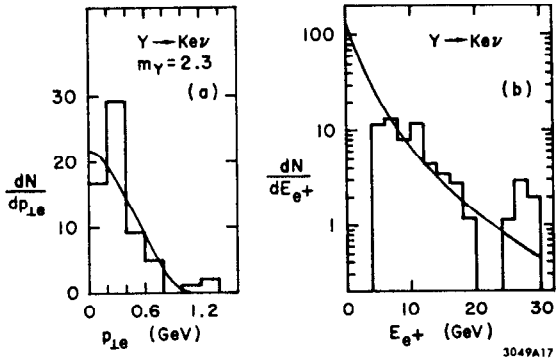

Fig. 17 Comparison of the predicted transverse momentum distribution (a) and the laboratory momentum distribution (b) of the electron from D decay with the observed μ^- distributions from the HPWF experiment.

charmed particle ground states weighed by their production cross section. According to the basic ideas discussed above we would expect:

$$\frac{\sigma_{charm}}{\sigma_{c.c.}} \approx 10\%$$

Furthermore, a reasonable guess[31] for the leptonic branching ratio is also about 10%, giving a product of 1%. In comparing with the data one must keep in mind that the dimuon data needs an appreciable correction because of the muon energy cutoff. In the Barger-Phillips model, that correction factor is about 3. Thus we conclude that there exists a fair agreement, with a discrepancy of maybe a factor of 2 or 3 between μe and μμ data, the μμ data being slightly high.

Threshold - for the process

$$\nu_\mu N \to C \mu^-$$

the threshold is P_ν = 2.5 GeV/c if one takes M_c = 2.25 GeV. The fact that all three GGM events occur above 3 GeV is consistent with this picture.

M_{Ke} and $M_{\Lambda e}$ spectra - if both the electron and the strange particle originate from the decay of one particle then the effective mass of this di-particle system must be less than the mass of the parent. The fact that the mass of this system is below 2 GeV for all the measurable observed events indicates that here too the agreement with the GIM model is quite good.

d) Dileptons of Same Sign. The HPWF group have also reported observation of 7 $\mu^-\mu^-$ and 3 $\mu^+\mu^+$ events. The natural question here is again whether these events represent a new phenomenon or come from an uninteresting source like a secondary π or K decay. The fact that 7 out of 10 events (see Table VII below) came from the iron hadron filter and only 3 are produced in much lighter liquid scintillator appears to argue against

TABLE VII

Parameters of the $\mu^-\mu^-$ and $\mu^+\mu^+$ Events

Target	E_H (GeV)	P_1 (GeV/c)	P_2 (GeV/c)	θ_{12} (mr)	P_{t1} (GeV/c)	P_{t2} (GeV/c)
Filter		53.3	11.5	111	.58	.16
Filter		30.6	14.0	67	.6	.6
Filter		57.9	38.8	89	.34	.14
Filter		25.2	12.8	81	.09	.36
Calorimeter	123	51.7	6.1	65	1.9	.38
Filter		14.1	5.5	300	4.0	1.1
Calorimeter	22	19.9	4.2	295	2.7	.33
Calorimeter**	22	8.8	4.8	68	.36	.13
Filter**		17.5	9.1	255	.17	.37
Filter**		28.5	2.4	125	.05	.33

** $\mu^+\mu^+$

the decay hypothesis. On the other hand both the momentum distribution and the P_T distribution of the lower energy muon appear lower than in the case of $\mu^+\mu^-$ events, indicating that the π-K decay may not be an insignificant source. Finally one must remember that the HPWF Monte Carlo analysis of the $\mu^+\mu^-$ events indicated that within one standard deviation about 25% of them could be due to π or K decay, a fraction that corresponds to a total number that is higher than the observed number of $\mu^{\pm\pm}$ events.

Nevertheless, it is interesting to speculate about the possible origin of these events if they do not come from π or K decay. An obvious possibility would be the associated production of the same new particles that are responsible for $\mu^+\mu^-$ events. This would be very exciting, as it would point to a relatively high cross section for new particle production in hadronic interactions. Of course, only time and better statistics will resolve this question.

VI. $\Delta S/\Delta Q$ and STRANGE PARTICLE PRODUCTION

As mentioned previously, charm production should exhibit itself as an increase in strange particle production, due both to the high probability of producing strange particles in association with charm, as well as due to the supposed preference of charm decay into strange particles.

The Table VIII below gives the fractions of all charged current events which have at least one strange particle associated with them, for different average energies of the neutrino beam. As can be seen there does

TABLE VIII

Fraction of charged current events with 1 or more strange particles.

Chamber	Fill	Beam	$\overline{E_\nu, \bar{\nu}}$	Fraction	Reference
12'	H,D	ν	2 GeV	7 ± 4%	32
GGM	Freon	ν	> 1 GeV	8 ± 2%	33
7'	H,D	ν	> 4 GeV	8 ± 3%	8
15'	H	$\bar{\nu}$	23 GeV	18 ± 7%	20
25'	H	ν	38 GeV	16 ± 3%	34

indeed appear to be a rise with the energy. The question remains, however to what extent that effect can be ascribed to purely kinematical effects like the simple increase in multiplicity in energy. The measurement charged prong multiplicity[35] increases from an average value of 3.84 for $15 < E_\nu < 30$ GeV to 5.25 for $E_\nu > 50$ GeV. This increase thus appears to be too slow to account for the whole effect and the rise in the strange particle yield probably does have a dynamical explanation.

We turn next to the question of $\Delta Q/\Delta S$ violation as evidence for charmed particle production. The evidence against $\Delta Q = -\Delta S$ comes from the absence of several decay modes, namely

a) in K^o, $\bar{K}^o$ system $\bar{K}^o \not\to e^+$ and $K^o \not\to e^-$

b) absence of $\Sigma^+ \to n\, \ell^+\nu$ mode

c) absence of $K^+ \to \pi^+\pi^+ e\nu$ mode.

The data is good enough to exclude the $\Delta Q/\Delta S$ amplitude at the level of 1% or so in amplitude. Thus evidence for its violation in ν interactions would be a strong evidence for charm production. This rule would appear to be violated if the charmed particle production proceeded off a valence quark, resulting in $\Delta S=0$ and $\Delta Q=\Delta C=1$ in the production process. If subsequently the charm particle decayed via strange particle mode, the decay would obey $\Delta C=\Delta S=-1$, resulting in the overall $\Delta Q=-\Delta S$. This process might be expected to dominate close to threshold since the charm production off the quark-antiquark sea is expected to become more important at higher energies.

The now famous BNL event, illustrated in Fig. 18, is very likely one of the first examples of production and decay of a charmed particle.[36] The observed event fits the interpretation

$$\nu p \to \mu^- \Lambda \pi^+ \pi^+ \pi^+ \pi^-$$

and is reported to have only a 3×10^{-5} probability for other interpretations. The total sample of charged current events out of which this event was found included 335 events, 14% of which had $E_\nu > 4$ GeV, and 1.5% $E_\nu > 20$ GeV.

If one interprets the event as

$$\nu p \to \mu^- C^{++}, \quad C^{++} \to \Lambda \pi^+ \pi^+ \pi^+ \pi^-$$

then the mass of the charmed baryon C turns out to be 2426 ± 12 MeV.

Corroborative evidence for this process was looked for[20] at Fermilab in the 15' bubble chamber filled with liquid hydrogen. Because of higher energy the probability of missing π^0's is very high and thus one can only make the argument on a statistical basis. In the total exposure 17 single Λ events were found and 3 events with both a Λ and a K^0_s. If one assumes K^0_s, K^+ production equality then the calculated number of $\Delta Q=-\Delta S$ events turns out to be $17-5.3\times3=0.8$. Thus at a 90% confidence level one can put

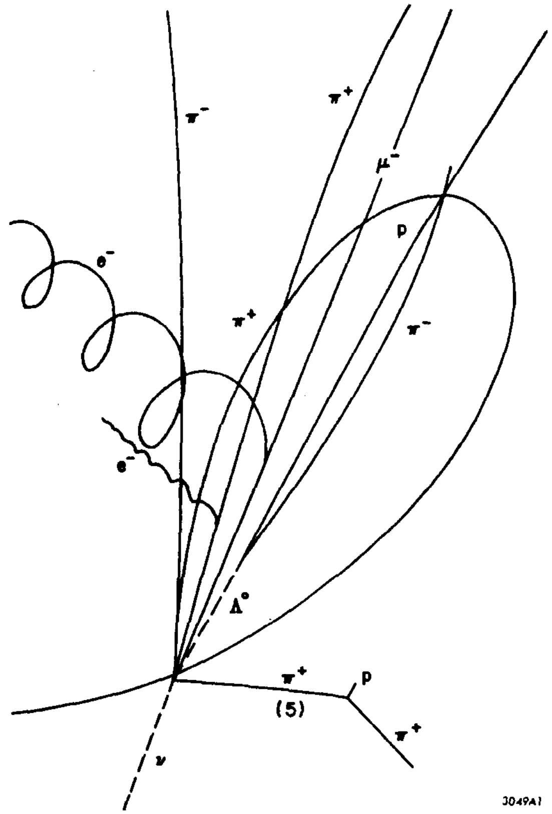

Fig. 18 The BNL event appearing to violate $\Delta Q = \Delta S$ rule.

the limit on the $\Delta Q=-\Delta S$ process at less than 3.6% of all charged current events for neutrino energies above 10 GeV.

The search for $\Delta Q=-\Delta S$ is equally difficult in Gargamelle exposure because of the much worse measuring accuracy and a complicated target, which make kinematical fitting impossible. In that exposure out of 1450 charged current events with hadronic mass W satisfying $W > M_K + M_\Lambda$, 28 single Λ events were found with a detection probability of $52 \pm 4\%$. All of them, however, are consistent with having another strange particle.[33)]

VII. SCALING VARIABLE DISTRIBUTIONS

We start our discussion here with a very brief review of the standard formulas used in discussing neutrino interactions. The scaling variables x and y are defined by

$$x = -q^2/2\nu \text{ and } y = \nu/m_p E_\nu$$

where ν is the measure of inelasticity defined by $\nu = m_p(E_\nu - E_\mu)$.
The 2 dimensional scattering formula then becomes

$$\frac{d^2\sigma^{\nu,\bar{\nu}}}{dx\,dy} = \frac{G^2 m_p E_\nu}{\pi}\left[F_2(x)(1-y) + 2x F_1(x)\frac{y^2}{2} \mp x F_3 y\left(1-\frac{y}{2}\right)\right]$$

$$= \frac{G^2 m_p E_\nu}{\pi} F_2(x)\left[(1-y+\frac{y^2}{2})(R+L) \mp y\left(1-\frac{y}{2}\right)(L-R)\right]$$

with $R = \sigma_R/(\sigma_R + \sigma_L + 2\sigma_s)$ and $L = \sigma_L/(\sigma_R + \sigma_L + 2\sigma_s)$

and the - sign in the original expression corresponding to the ν scattering and the + sign to antineutrino scattering. The σ_R, σ_L, σ_s are the cross sections for the right handed, left handed, and scalar scattering. The F's are scaling functions related to the quark antiquark distributions in the nucleon. The F_1 and F_2 can be obtained from the deep inelastic electron scattering, but F_3, representing V,A interference must be obtained from the difference between neutrino and antineutrino scattering.

It is conventional to define quark, antiquark distributions $q(x)$, $\bar{q}(x)$ by

$$q(x),\ \bar{q}(x) = \frac{1}{2} F_2(x) \mp x F_3(x)$$

and a function B(x) that is related to quark, antiquark asymmetry in the nucleon

$$B(x) = \frac{q(x) - \bar{q}(x)}{q(x) + \bar{q}(x)} = -\frac{xF_3(x)}{F_2(x)}$$

Finally, if the nucleon constituents (quarks) have spin 1/2, we have the Callan Gross relation $F_2(x) = 2x F_1(x)$.

In terms of this nomenclature we can rewrite the equation for the differential distribution as

$$\frac{d^2\sigma^\nu}{dxdy} = \frac{G^2 m_p E_\nu}{\pi}\left[q(x) + \bar{q}(x)(1-y)^2\right]$$

and a similar relation for $\sigma^{\bar{\nu}}$, with $q(x)$ and $\bar{q}(x)$ interchanged.
Alternatively we can write

$$\frac{d^2\sigma^{\nu,\bar{\nu}}}{dxdy} = \frac{G^2 m_p E_\nu}{\pi}\int F_2(x)\,dx\left[(1-y+\frac{y^2}{2}) \pm By\left(1-\frac{y}{2}\right)\right]$$

Now, in the quark model we can turn proton into a neutron by merely interchanging the down and up quarks. Since the neutrinos can interact only with the down quarks and antineutrinos with the up quarks, this statement leads to the conclusion that $F_i^{\nu p} = F_i^{\bar{\nu} n}$. Finally, since an isoscalar target (a good approximation for most nuclei) is composed of an equal number of neutrons and protons, we must have $F_i^{\nu} = F_i^{\bar{\nu}}$, a statement known as charge asymmetry. This right away leads us to the prediction that

$$\left.\frac{d\sigma^\nu}{dy}\right|_{y=o} = \left.\frac{d\sigma^{\bar{\nu}}}{dy}\right|_{y=o}$$

provided only that charge asymmetry holds, i.e. $F_2^{\nu}(x) = F_2^{\bar{\nu}}(x)$.

We can also see easily from the above formulas two other predictions based only on the validity of scaling. Clearly the integral over the functions of x and y is independent of energy if scaling holds and thus

the total cross section must increase linearly with energy. Secondly, as E_ν increases the range of ν also increases linearly and since $x = Q^2/2\nu$ that must imply that $\langle Q^2 \rangle$ must also increase linearly with energy.

We would like to discuss next the restrictions placed by the kinematics on the scaling variables in new particle production. It is convenient to discuss the threshold behavior in terms of the portion of the q^2,ν plot (Fig. 19) that will be first populated just after the threshold is passed. We start off with the standard expression for momentum transfer squared, q^2

$$q^2 = (E_H - m_p)^2 - p_H^2 \quad ; \; E_H \text{ and } p_H \text{ are energy and momentum of the total hadronic system.}$$

$$= W^2 - 2E_H m_p + m_p^2$$

$$= W^2 - m_p^2 - 2\, m_p\, (E_h - m_p)$$

$$= W^2 - m_p^2 - 2\nu$$

For elastic scattering $W^2 = m_p^2$, i.e. $q^2 = -2\nu$ or $x=1$

For inelastic scattering $W > m_p$ and thus $x < 1$. Thus inelastic scattering populates the q^2, 2ν plot below the 45° line along which are concentrated all the elastic events.

We consider the behavior immediately above threshold for new particle production. If we neglect the lepton mass, then

$$(E_{th} + m_p)^2 - P_{TH}^2 = W^2$$

and

$$E_{th} = (W^2 - m_p^2)/2\, m_p$$

At threshold, all of the energy will go into the hadronic system (in the approximation of zero lepton mass). Thus

$$E_H = E_{th} = E_\nu \quad \text{i.e. } y = 1$$

Furthermore

$$q^2 = W^2 - m_p^2 - 2\nu$$

$$= 2\, m_p\, E_{th} - 2\nu$$

$$= 2\, m_p\, E_{th} - 2 m_p E_\nu = 0$$

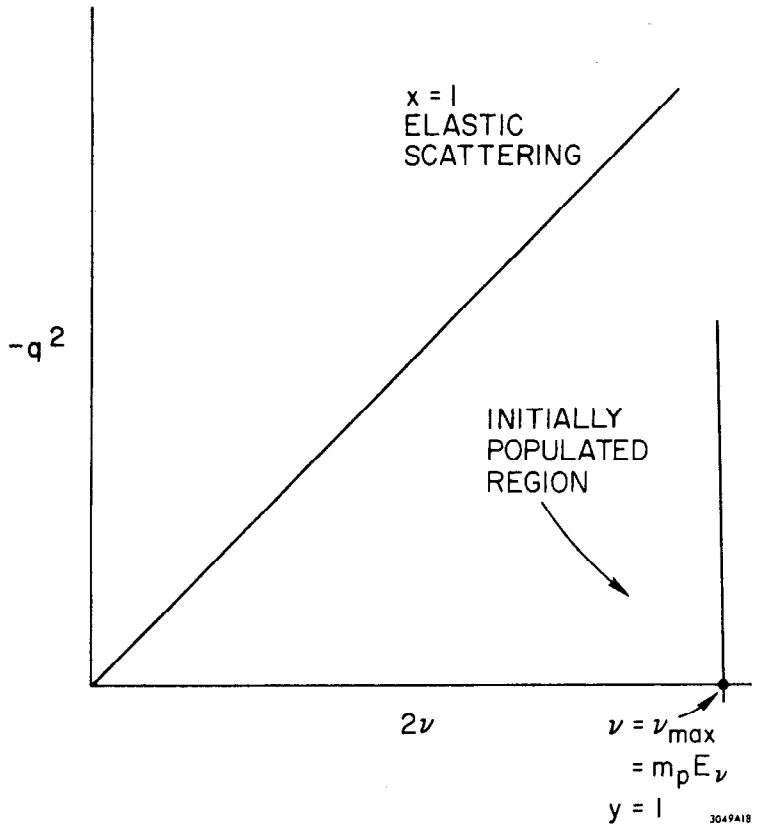

Fig. 19 q^2, ν plot for inelastic scattering.

Thus the events will first come in at the lower right hand corner, i.e. $x = 0$, $y = 1$. As we increase the energy, i.e. E_ν, the total hadronic energy E_H will also increase. Therefore, above threshold

$$1 \geq y \geq E_{th}/E_\nu$$

Consider now x behavior above threshold

$$x = -q^2/2\nu$$

$$2\nu x = -q^2 = 2\nu - (W^2 - m_p^2)$$

$$\leq 2\nu - 2m_p E_{th}$$

$$x \leq 1 - \frac{m_p E_{th}}{\nu} \leq 1 - m_p \frac{E_{th}}{m_p y E_\nu} \leq 1 - \frac{E_{th}}{yE_\nu}$$

And thus the values of x will be limited to

$$0 \leq x \leq 1 - E_{th}/yE_\nu$$

For completeness we derive also the expression for W, i.e. the total effective mass of the hadronic system.

$$y(1-x) = \frac{E_H}{E_\nu} \frac{W^2 - m_p^2}{2\nu}$$

$$= \frac{E_H}{E_\nu} \frac{W^2 - m_p^2}{2m_p E_H} = \frac{W^2 - m_p^2}{2m_p E_\nu}$$

$$W^2 = m_p^2 + 2m_p y\,(1-x)\,E_\nu$$

Thus the new particle production will tend to populate the kinematical region of high W, high y, and low x. Thus any new threshold phenomena can be seen much easier in the $\bar{\nu}$ interactions because the "old" physics suppresses the y≈1 region through the $(1-y)^2$ factor in the expression for the differential cross section.

We can illustrate in Fig. 20 the expected y behavior of both ν and $\bar{\nu}$ processes right above threshold for the new particle production and in the asymptotic region. It remains to ask about the expected magnitude of

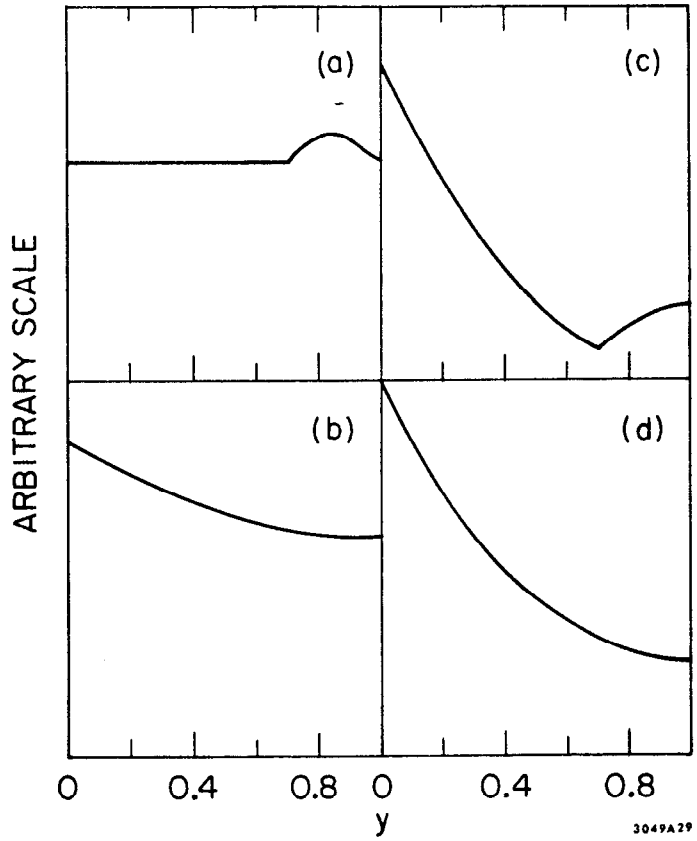

Fig. 20 Expected y distribution for ν (e,b) and $\bar{\nu}$ (c,d) right above threshold for new particle production (a,c) and in the asymptatic region (b,d). The curves are meant to be only qualitative.

these effects. The answer here clearly depends on the specific model of the new particle production;[37] the charm picture predicts that these effects cannot be large because:

1. $\sin^2\theta_c$ is small($\sim$0.05) and thus production off valence quarks is suppressed.
2. the $q\bar{q}$ sea is small($\sim$5-10% according to the analysis of low energy interactions) and thus production from the s or $\bar{s}$ quarks is also small. This statement assumes scaling, i.e. ability to extrapolate to high energies the low energy results on q(x) and $\bar{q}(x)$ distributions.

We turn now to the discussion of the data, starting with a review of the bubble chamber experiments. Compared to the electronic experiments, these have in common relatively low statistics, and a lower average neutrino energy since all of the exposures have been done with the horn beam.

The Fermilab-Michigan group has analyzed[38] some 450 charged current events representing neutrino interactions in the hydrogen filled 15' bubble chamber. The data, displayed in Fig. 21, is in good agreement with scaling predictions with some small excess of events near low x. A natural interpretation for this phenomenon, if high statistics will indeed uphold its validity, is the scaling violation already seen in inelastic lepton scattering, both in electron scattering data at SLAC and more recently in muon scattering at Fermilab. In brief, the violation exhibits itself as an increase in $F_2(x)$ at low x as we go to higher q^2 and can be understood theoretically in terms of gluon bremstrahlung models.

There have been two exposures of the horn $\bar{\nu}$ beam in the 15' chamber, one in a pure hydrogen fill, the other in a light neon-hydrogen mixture. The Argonne-Carnegie Mellon[39] collaboration has studied 106 events in hydrogen with a mean neutrino energy of 23 GeV (see Fig.22). The y distribution is consistent with $(1-y)^2$ form predicted by the simple quark model and the x

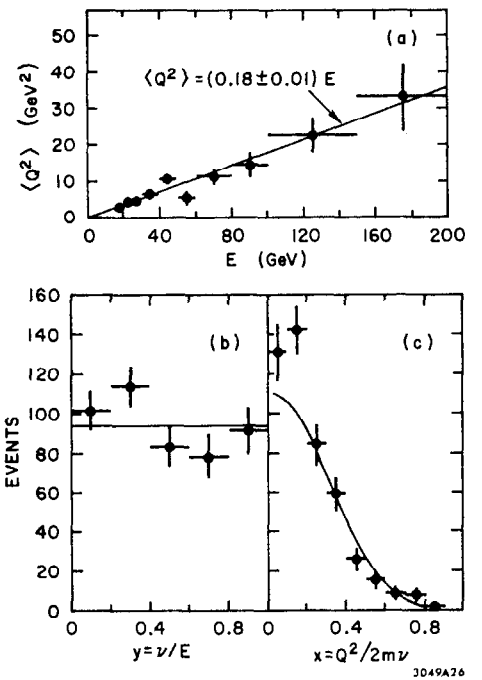

Fig. 21 Results of the Fermilab-Michigan neutrino experiment.
a) average value of q^2 plotted as a function of energy
b) y distribution for the events in the 15-200 GeV region
c) x distribution for the events in the 15-200 GeV region.

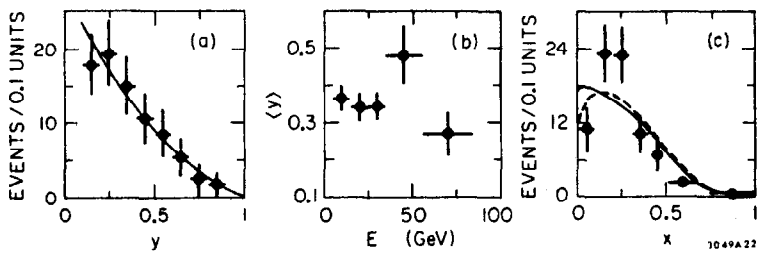

Fig. 22 Results of the Argonne-Carnegie Mellon $\bar{\nu}$ experiment a) y distribution, b) <y> as a function of E, and c) x distribution.

distribution agrees with the scaling function derived from lepton production data. It should be emphasized however that the data is heavily dominated by the low energy antineutrinos.

The Fermilab-ITEP-IHEP-Michigan groups have reported[40] on 493 charged current antineutrino interaction with energies between 10 and 200 GeV in the light neon mixture. Their y distribution shown in Fig. 23 is consistent with the $(1-y)^2$ form plus a small constant term that is consistent with the amount of the antiquark component derived from the low energy data. The x distribution shown in Fig. 24 is consistent with the $F_2^{ed}(x)$ obtained at SLAC except for some enhancement at low x. The authors argue that this behavior would be expected in the region where the antiquark contribution is large (i.e. low x) because of a relatively higher cross section of the antineutrinos on antiquarks. Whereas the quark and antiquark components contribute equally to inelastic lepton scattering, the antiquarks are enhanced in antineutrino scattering by a factor of 3 resulting from the difference in y distributions.

The two electronic experiments providing information on the scaling variable distributions are those of the HPWF and CITF collaborations. The original indications for onset of new phenomena came from the HPWF group[41] who reported significant deviations from the $(1-y)^2$ distribution for the antineutrinos above 30 GeV with $x < 0.1$. These data are displayed in Fig. 25. In addition, if one normalizes the data by assuming equal cross sections at $y=0$ for $x < 0.1$, then the data for $x < 0.1$ gives a cross section higher by about a factor of 3 than the $\bar{\nu}$ cross section, implying a breakdown of charge symmetry.

The more recent data[42] strengthens the evidence for deviation from $(1-y)^2$ for higher energy $\bar{\nu}$ data, but there no longer appears to be strong evidence for a qualitatively different behavior below and above x=0.1. The authors analyze all the data with $x < 0.6$ and fit the y distributions

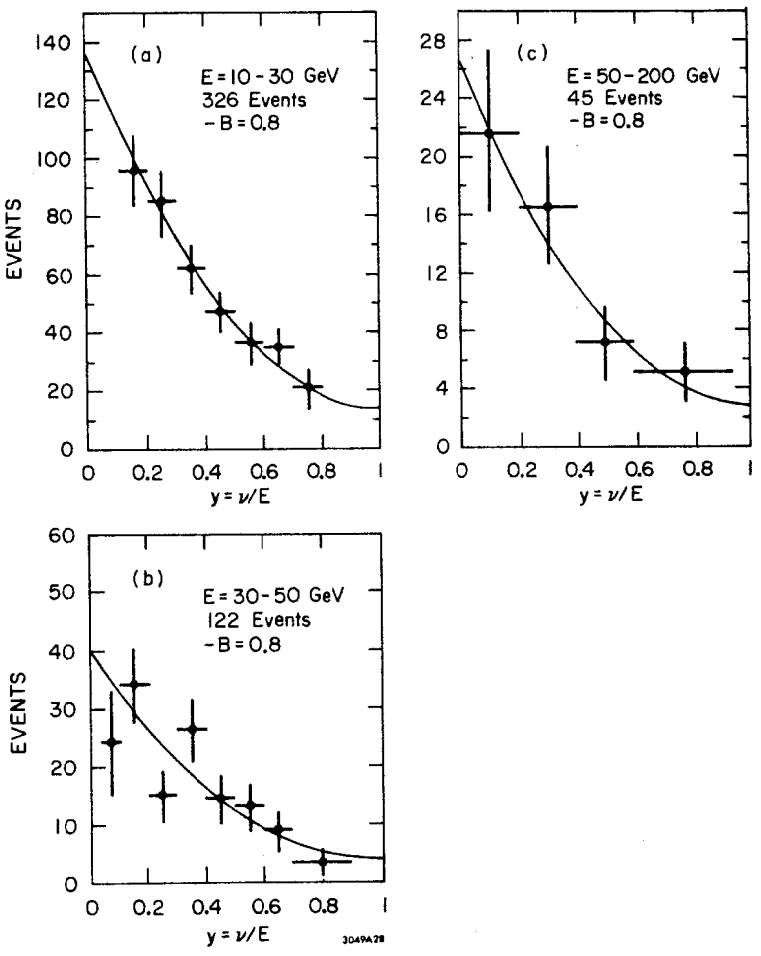

Fig. 23 y distribution for 3 different energy intervals for the Fermilab-ITEP-IHEP-Michigan experiment.

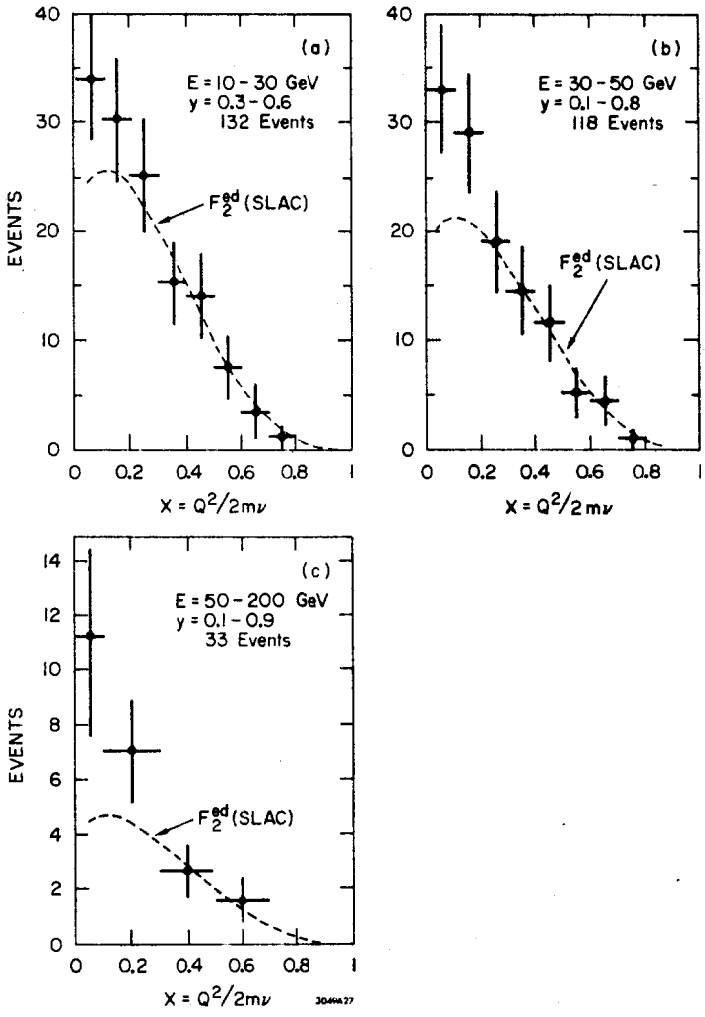

Fig. 24 x distribution for 3 different energy intervals for the Fermilab-ITEP-IHEP-Michigan experiment.

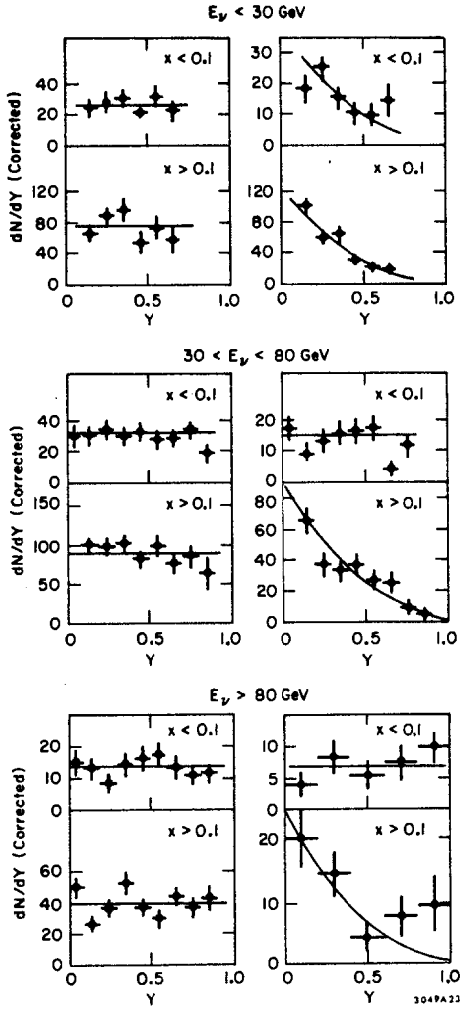

Fig. 25 y distributions for different energies from the HPWF experiment. The ν data is plotted on the left, the $\bar{\nu}$ data on the right.

in the regions where the efficiency for detection is quite high. This imposes a cut in y_{max} on the data that increases with the increasing energy. As can be seen from Fig. 26, the low energy data ($E_{\bar{\nu}}$ < 30 GeV) is consistent with $(1-y)^2$ but a significant isotropic term appears above 70 GeV.

The data have been analyzed as a function of the incident energy in terms of the average y value both for the neutrinos and antineutrinos, and then compared with the predictions expected for two different values of B. The prediction changes as a function of energy because of different acceptance for high y events as a function of energy. We can see from Fig. 27 that the neutrino data is rather insensitive to the B value but the antineutrino data appears to demand a decreasing value of B as a function of energy. Within these statistics at any one energy both the ν and $\bar{\nu}$ data can be fitted by the same value of B, indicating consistency at this level with the charge symmetry hypothesis.

The CITF group has recently presented[43] the analysis of their 1974 data in terms of the x and y variables. Here also there is no external normalization since the data were taken with the fast (1 msec) spill. The qualitative conclusions are similar to those of the HPWF group, i.e. a flattening of the $\bar{\nu}$ y distribution at higher energies. More specifically, the fits to B yield $0.64\ ^{+0.22}_{-0.26}$ for the neutrinos from π decay ($\bar{E}_\nu$ = 52 GeV) and $0.36\ ^{+0.30}_{-0.36}$ for the ν and $\bar{\nu}$ from K decay ($\bar{E}_\nu$=146 GeV). If one normalizes the data at y=0 for x > 0.1 so that $\frac{d\sigma_\nu}{dy}_{y=0} = \frac{d\sigma_{\bar{\nu}}}{dy}_{y=0}$ in that region then one obtains good agreement with charge symmetry hypothesis for x<0.1. It should be emphasized, however, that there is no idependent verification that this hypothesis is valid.

In general one can make the following conclusions:

1. The isotropic term in $\bar{\nu}$ y distributions appears to increase with energy. This is illustrated in Fig. 28 taken from Nezrick's Aachen talk. The statistics however are quite poor and the effect relies mainly on the two high energy points.

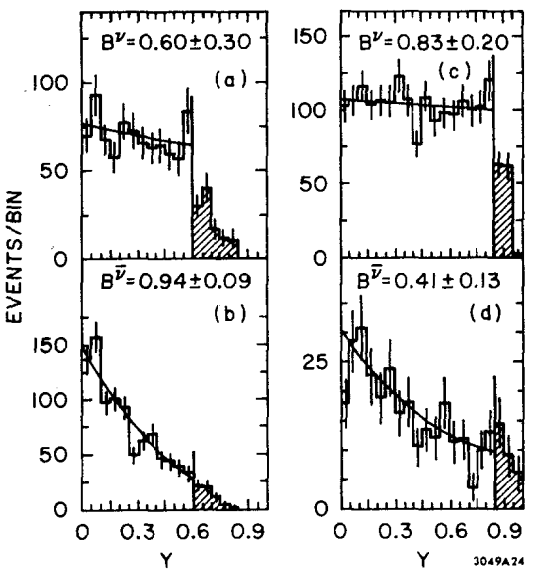

Fig. 26 The y distributions for $10 < E_{\nu,\bar{\nu}} < 30$ GeV - a) for ν and b) for $\bar{\nu}$ and for $E_{\nu,\bar{\nu}} > 70$ GeV a) for ν and d) for $\bar{\nu}$. The cross hatched areas represent the data not used in the fit where the detection efficiency is incomplete.

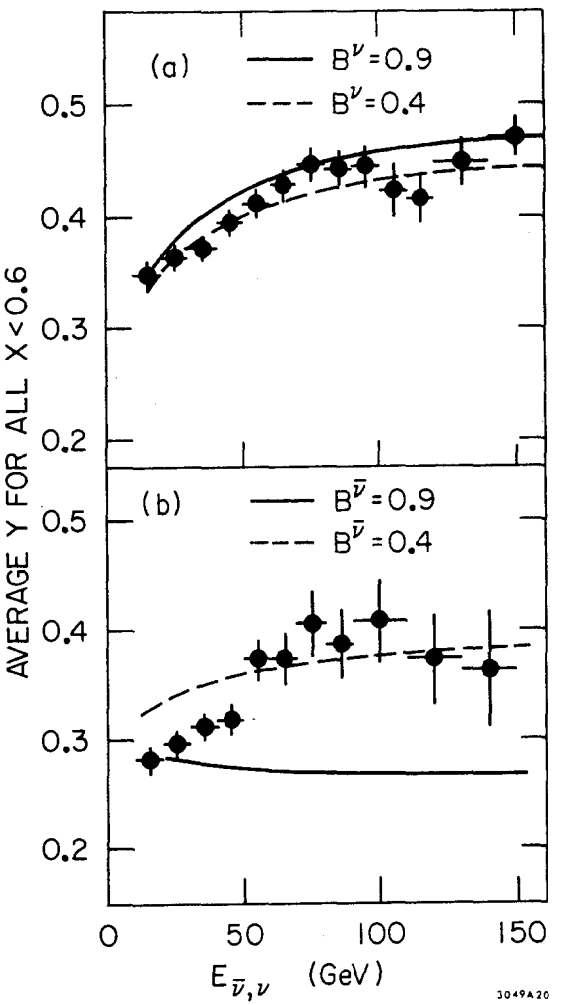

Fig. 27 Average value of y as a function of energy for the neutrino (a) and antineutrino (b) data. The expected behavior for B_{ν} = 0.4 is B_{ν} = 0.9 is also shown.

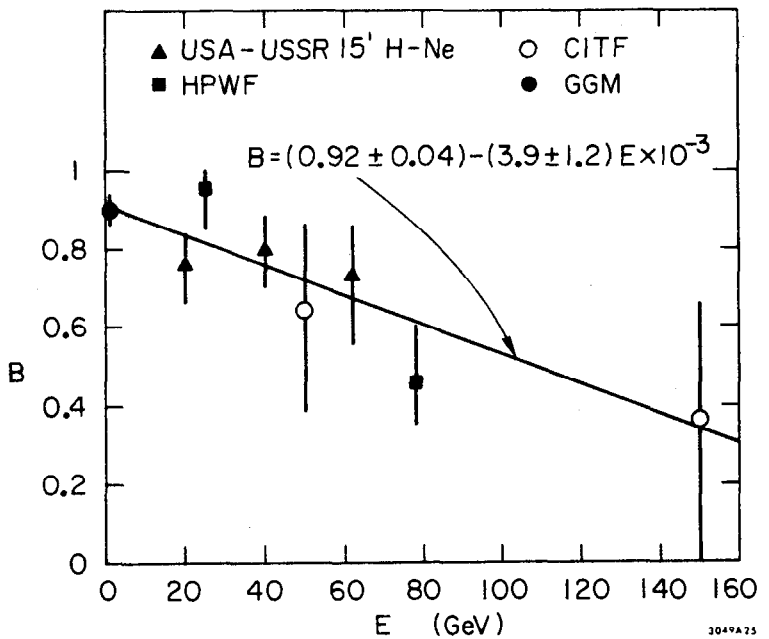

Fig. 28 A compilation of the fits to the B parameter as a function of energy.

2. There is some evidence for excess of events at low x, when compared with $F_2(x)$ obtained from ed scattering. This is probably consistent with the recent data from lepton scattering.
3. There appears to be no compelling evidence for charge symmetry violation.

VIII. σ_{TOTAL} AND THE RATIO $\sigma_c(\bar{\nu})/\sigma_c(\nu)$

The question that has not been answered by the data discussed above is whether the flattening of the y distribution (so called y anomaly) represents an excess of events at high y as charge symmetry would demand or a depletion of events at low y or overall redistribution in y, both of which would imply violation of charge symmetry. The answer to that question can only come from a measurement of total ν and $\bar{\nu}$ cross sections or at least their ratio, a traditionally difficult measurement in neutrino physics.

To date, there is only one measurement of cross sections that relies on absolute flux measurement.[13] Even though rather weak statistically (it relies only on 11 $\bar{\nu}$ events at the higher energy) it appears to be consistent with no rise in the $\sigma_c(\bar{\nu})/\sigma_c(\nu)$ ratio. Specifically it yields for that ratio

$$0.40 \pm 0.11 \text{ at } 38 \text{ GeV}$$

$$\text{and} \quad 0.23 \pm 0.11 \text{ at } 107 \text{ GeV}$$

Insofar as the detection apparatus does not see all the events because of the limited size of the magnet, one has to assume a distribution for $\frac{d\sigma}{dy}$ in order to make a correction. Assuming the form

$$\frac{d\sigma}{dy} = \alpha + (1-y)^2$$

the CITF group uses $\alpha = 0.17^{+0.3}_{-0.15}$ to calculate the total cross section from the observed events. Since $B = 1-2\alpha$, the value of α used may be low in light of the more recent results. Too low a value of α would tend to

reduce the calculated $\sigma_c(\bar{\nu})/\sigma_c(\nu)$ ratio.

If one interprets the recent CITF results[43] on y distribution in the framework of charge symmetry validity at y=0 then one obtains the following numbers for the cross section ratios

$$0.52 \begin{smallmatrix}+.15\\-.11\end{smallmatrix} \quad \text{at} \quad 50 \text{ GeV}$$

$$\text{and} \quad 0.69 \begin{smallmatrix}+.31\\-.19\end{smallmatrix} \quad \text{at} \quad 150 \text{ GeV}$$

i.e. an apparent disagreement with the older result at the high energy.

The original measurement of the cross section ratio by the HPWF group[14] relied on a quadrupole focused beam and a calculation of the relative ν and $\bar{\nu}$ yield based on the yield measurements of charged π's and K's. That result indicated no statistically significant departure from the ratio of 1/3 up to an energy of 70 GeV.

More recently much more extensive measurements have been made[44] utilizing both a quadrupole focused beam and a horn focused beam. Three independent methods were used to calculate the ν and $\bar{\nu}$ flux:

1. for quadrupole beam data only, one can calculate the ν, $\bar{\nu}$ fluxes from the measured yields of π^+, π^-, K^+, K^- and the focusing properties of the quadrupole system. This is essentially the same method as used in the oirginal measurement.
2. For all the data, one calculates the flux assuming the equality and energy independence of quasielastic and N^* cross sections for neutrinos and antineutrinos. This method is used here up to 60 GeV as the statistics are said to be too limited above this energy.
3. using the arguments put forth by Sakurai,[45] one assumes the equality of $\frac{d\sigma}{dW^2}$ for low values of W for the neutrinos and antineutrinos. The range of values of W used is varied to check the self consistency of the method.

The three sets of measurements are displayed in Fig. 29 and they appear to yield a consistent answer, namely that the ratio of cross sections rises as the energy increases and reaches a value around 0.6 at 100 GeV.

IX. OVERALL SUMMARY

We would like to end these lectures with an overall comparison of the data with the predictions of the charm model, and specifically point out which are the questions that might present most severe difficulties for the GIM model.

We might first address ourselves to the comparison of the dilepton data and the y anomaly, and ask whether they both could be two different manifestations of the same phenomena, i.e. the production and decay of a charmed particle. It is our feeling that the dilepton data appears quite consistent with the charm picture, except possibly for too high a rate of $\mu^+\mu^-$ events vis a vis μ^-e^+ events. The two crucial questions regarding the dilepton events are their energy dependence and the average number of strange particles associated with each event. Hopefully both of these questions will be resolved in the near future hy higher statistics experiments, like the Columbia-BNL exposure in a heavy neon filled 15' bubble chamber.

Is the y anomaly real and is it related to the dilepton events? The experimental evidence for the y anomaly is mounting but at the same time the evidence increases for lack of the anomaly at lower energies, energies where the dilepton production appears already to be high. The HPWF group argues that both the dimuon events and the y anomaly come in around 40 GeV, but the μe data and the recent Serbukhov results, as well as strong experimental biases against detection of 2μ events, argue, to me at least, against this hypothesis.

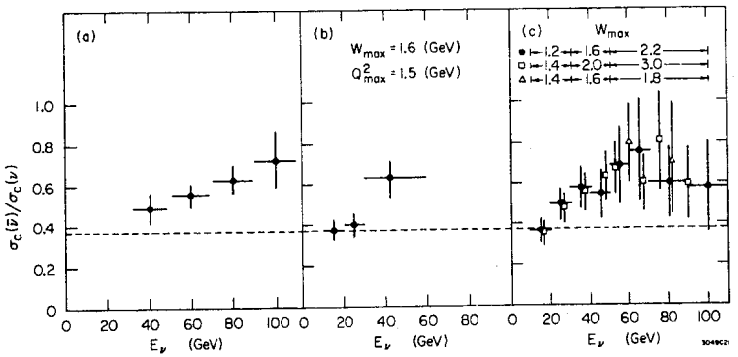

Fig. 29 $\sigma^{cc}_{\nu\bar{\nu}}/\sigma^{cc}_{\nu}$ measurements by the HPWF group as a function of energy. The three different techniques for flux determination are discussed in the text.

Furthermore, the size of the y anomaly and the accompanying rise in $\bar{\nu}$ cross section, if confirmed by further experiments, appear difficult to understand in the framework of the GIM picture, since the charm contribution here is not expected to be very big. It is tempting to speculate here about these phenomena being evidence for additional quark production. A variety of models can be constructed[46] which can explain the data very well if one assumes the production of a heavy quark with a mass in the 3-4 GeV range. To obtain the large y anomaly, one would have to invoke right handed coupling for the new quark.

Another approach to the explanation of the y anomaly and the rising cross section ratio assumes a scaling violation at high energy, or more specifically an increase in the $q-\bar{q}$ sea at high energy.[47] To me, at least, this kind of picture appears rather unattractive and ad hoc.

In summary, we can say that in spite of the spectacular success of the GIM model in predicting the observed phenomena in e^+e^- annihilations some doubt still remains whether the GIM picture describes the whole story in neutrino interactions. The possibility of "something else" is very real and only further data will help to resolve this question.

REFERENCES

1. A. K. Mann, New Vistas in Neutrino Physics, Paper presented at the Orbis Scientiae 1976. University of Miami, Coral Gables, Florida, January, 1976.

2. For a more detailed discussion of dichromatic beams see F. Sciulli et al., Fermilab proposal E-21.

3. This scheme was used by the Cal Tech-Fermilab group in their Fermilab experiment E-262. See also proposal E-320.

4. This is the arrangement of the detector at the CERN SPS.

5. See for example L. Mo et al., Fermilab proposal E-253; also W. Lee et al., paper submitted to the 1976 Aachen Neutrino Conference.

6. R. J. Cence et al., The External Muon Identifier for the Fermilab 15-ft Bubble Chamber. LBL-4816; also submitted to Nucl. Instr. and Methods.

7. A DeRujula et al., RMP 46, 391 (1974); V. Berger and R. Phillips, Nucl. Ph. B73, 269 (1974). R. McElhaney and S. F. Tuan, Nucl. Ph. B72, 487(1974).

8. N. P. Samios, 1975 Symposium on Lepton and Photon Interactions of High Energies, Stanford, California.

9. S. J. Barish et al., ANL-HEP-PR 75-36.

10. M. Haguenauer, La Physique des Neutrino a Haute Energie, p.327, CNRS, Paris 1975.

11. G. Myatt and D. H. Perkins, Phys. Lett. 34B, 542 (1971).

12. Gargamelle collaboration, paper presented at the 1976 Tbilisi Conference.

13. B. C. Barish et al., Phys. Rev. Lett. 35, 1316 (1975).

14. A. Benvenuti et al., Phys. Rev. Lett. 32, 125 (1974).

15. For a more detailed discussion of this process see L. N. Chang et al., Phys. Rev. Lett. 35, 1252 (1975).

16. J. Blietschau et al., Phys. Lett. 60B, 207 (1976).

17. Gargamelle Collaboration, Observation of Muon-neutrino Reactions Producing a Positron and a Strange Particle, CERN/EP/PHYS 76-31.

18. W. Lee et al., a paper submitted to the June, 1976, Aachen conference.

19. J. von Krogh et al., Phys. Rev. Lett. 36, 710 (1976) and the mini-rapporteur talk by M. L. Stevenson at the 1976 Tbilisi conference, CERN/EP/PHYS 76-38.

20. J. P. Berge et al., Phys. Rev. Lett. 36, 127 (1976).

21. V. Barger and R.J.N. Phillips, Phys. Rev. Lett. 36, 1226 (1976).

22. J. P. Berge et al., Search for μe Events in Antineutrino-Nucleon Interactions, a paper submitted to the Aachen Neutrino Conference (1976).

23. C. Rubbia (HPWF collaboration), XVII International Conference on High Energy Physics, London 1974, p. IV-118.

24. A Benvenuti et al., Phys. Rev. Lett. 34, 419 (1975); A. Benvenuti et al., Phys. Rev. Lett. 35, 1199 (1975) and 35, 1203 (1975).

25. A. Benvenuti et al., Phys. Rev. Lett. 35, 1249 (1975).

26. B. C. Barish et al., Phys. Rev. Lett. 36, 939 (1976).

27. A. E. Asratyan et al., Further Search for Muonic Pairs in the neutrino and Antineutrino Beams at the IHEP 70 GeV Accelerator, paper submitted to the 1976 Aachen Conference on Neutrino Physics.

28. W. Czyz, G. C. Sheppey and J. D. Walecka, Nuovo Cimento 24, 404 (1964).

29. A. Pais and S. B. Treiman, Phys. Rev. Lett. 35, 1206 (1975).

30. S. L. Glashow, J. Iliopoulos, L. Maiani, Phys. Rev. D2, 1285 (1970).

31. M. K. Gaillard, B. W. Lee and J. L. Rosner, Rev. Mod. Phys. 47, 277 (1975).

32. S. J. Barish et al., Phys. Rev. Lett. 33, 1446 (1974).

33. H. Deden et al., Phys. Lett. 58B, 361 (1975).

34. M. Derrick et al., Phys. Rev. Lett. 36, 936 (1976).

35. J. W. Chapman et al., Phys. Rev. Lett. 36, 124 (1976).

36. E. G. Cazzoli et al., Phys. Rev. Lett. 34, 1125 (1975).

37. For an extensive discussion of various models, see A. De Rujula et al., Rev. of Mod. Ph. 46, 391 (1974).

38. J. P. Berge et al., Phys. Rev. Lett. 36, 639 (1976).

39. M. Derrick et al., Phys. Rev. Lett. 36, 936 (1976).

40. F. Nezrick, Scaling Variable Distributions for Antineutrino-Nucleon Scattering in the 15-ft Bubble Chamber at Fermilab, Fermilab-Conf.-76/68-EXP. Paper presented at the 1976 Neutrino Conference in Aachen.

41. B. Aubert et al., Phys. Rev. Lett. 33, 984 (1974).

42. A. Benvenuti et al., Phys. Rev. Lett. 36, 1478 (1976).

43. B. C. Barish et al., Charged Current Differential Distributions in the Caltech-Fermilab ν-Experiment, CALT 68-560, paper presented at the 1976 Neutrino Conference in Aachen.

44. A Benvenuti et al., Phys. Rev. Lett. 37, 189 (1976).

45. J. J. Sakurai, UCLA preprint UCLA/73/TEP/79, 1973.

46. see for example R. M. Barnett, Phys. Rev. Lett. 36, 1163 (1976).

47. see for example S. S. Gershtein and V. N. Folomeshkin, Charge Asymmetry in Neutrino Experiments above the Charmed Particle Production Threshold, paper presented to the 1976 Tbilisi Conference.

ψ SPECTROSCOPY

Gary J. Feldman

Stanford Linear Accelerator Center
Stanford University, Stanford, California

CONTENTS

I. Introduction
II. The e^+e^- spectrum
  A. The s-channel resonances
  B. Limits on other narrow states
  C. The continuum
III. Detectors
IV. Widths of the ψ and ψ'
V. Spin, parity, and charge conjugation of the ψ and ψ'
VI. Hadronic decays of the ψ
  A. Table of results
  B. Techniques
  C. Isospin and G parity
  D. SU(3)
  E. Tests of Zweig's rule
  F. Radiative decays
  G. Is anything missing?
VII. Hadronic decays of the ψ'
  A. Table of results
  B. ψ' → ψ decays
  C. Second order electromagnetic decays
  D. Direct decays to hadrons
  E. ψ' → γχ decays
    1. χ decays to hadrons
    2. χ decays to γψ
    3. Monochromatic photons
  F. Is anything missing?
VIII. χ states
  A. Masses and branching ratios
  B. Spins and parities
  C. Comparisons to theoretical models
IX. The X(2800)
X. Summary

I. Introduction

These first two lectures will cover the properties of the various members of the ψ family, the bound states of a charmed quark and a charmed anti-quark. The recent identification of charmed mesons in e^+e^- annihilation[1-4] has effectively removed other explanations of the origin of the ψ particles as viable alternatives. Accordingly, whenever it is convenient to do so in these lectures, we will freely assume that members of the ψ family are states of charmonium.

As an introduction, we will investigate what can be learned by studying the e^+e^- spectrum, that is, the total cross section for e^+e^- annihilation into hadronic final states as a function of energy. Then after a brief description of a few detectors, we will start on the main topic of these lectures, the properties of the ψ's and χ's as determined from their production and decay.

II. The e^+e^- spectrum

II.A. The s-channel resonances

Figure 1 shows the ratio, R, of the total cross section for hadron production to the total cross section for μ pair production as a function of center-of-mass energy. The data come from Novosibirsk,[5-8] Orsay,[9-15] Frascati,[16-20] CEA,[21,22] and SPEAR.[23-27] The most obvious features of this spectrum are a series of resonances. We can understand these resonances as bound states of quark-antiquark pairs. For each type of quark, we can form an s-wave state with quark spins parallel. Such states will have the quantum numbers of a photon and can be produced as s-channel resonances in e^+e^- annihilations as illustrated in Fig. 2.

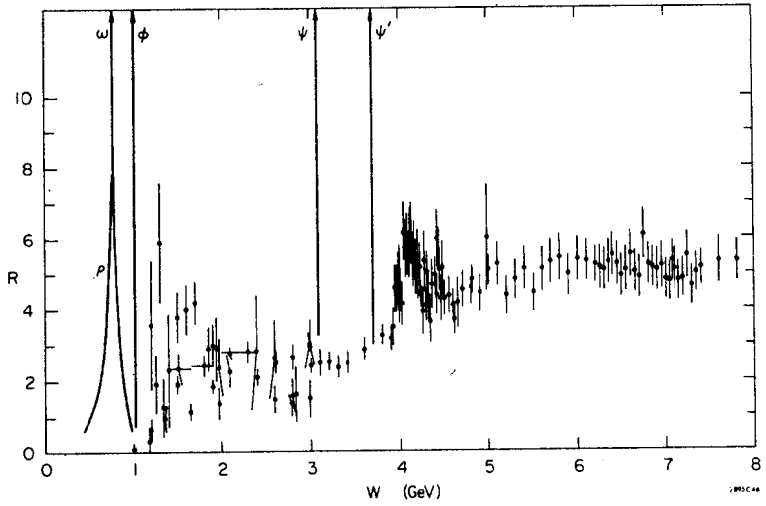

FIG. 1. Ratio, R, of the total cross section for hadron production to the total cross section for μ pair production as a function of center-of-mass energy.

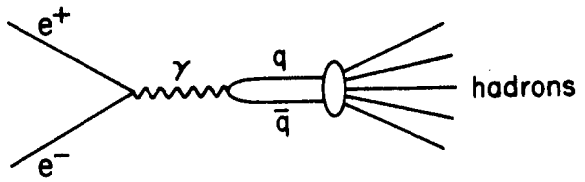

FIG. 2. Production of s-channel resonances in e^+e^- annihilation.

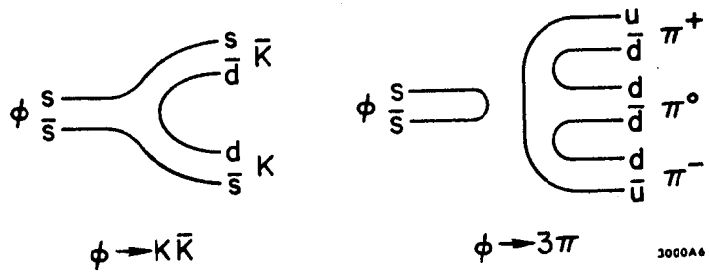

FIG. 3. Quark diagrams illustrating Zweig's rule in φ decays.

Table I lists the narrow s-channel resonances, their quark composition and their Q values, where, in this case, the Q value is the maximum kinetic energy released in the decay of the resonance to the lowest mass state which contains the constituent quarks of the resonance.

TABLE I. Quark content of vector mesons. Q value is the kinematic energy released in the decay to the lowest lying mesons containing the constituent quarks.

Meson	Quark content	Q value (MeV)
ρ	$\frac{1}{\sqrt{2}}(u\bar{u} - d\bar{d})$	491
ω	$\frac{1}{\sqrt{2}}(u\bar{u} + d\bar{d})$	369
ϕ	$s\bar{s}$	32
ψ	$c\bar{c}$	-635
ψ'	$c\bar{c}$	-46
$\psi''(4.03)$	$c\bar{c}$	300

The ϕ meson has a small Q value for decaying into two K mesons; nevertheless, this is its dominant decay mode. The suppression of the three pion mode was explained phenomenologically a decade ago by the Okubo-Zweig-Iizuka rule[28-30] (which we'll call the Zweig rule for short). The rule is illustrated in Fig. 3. Quark diagrams which are disconnected are suppressed relative to diagrams which are not. A disconnected diagram is one in which one or more particles can be isolated by drawing a line which does not cross any quark lines. The Zweig rule will be a key concept in understanding much of the ψ spectroscopy. It will be covered in detail in Dave Jackson's lectures.[31]

When we come to the ψ we find a new phenomenon in nature -- a resonance with only Zweig suppressed decays. Nature has given us an even greater gift in the ψ' -- a radially excited state with only Zweig suppressed decays. If the ψ' had been 100 MeV/c^2 higher in mass, the rich spectroscopy of the χ states, the $C = +1$ intermediate states, would not have been experimentally accessible to us.

It is not until we get to the second radial excitations in the 4 GeV region that we find charmonium states whose decays are not Zweig suppressed, that is, states which can decay to charmed particles. The e^+e^- spectrum for this region is shown in Fig. 4.[26] This region is quite complicated and is not well understood. There are probably several resonances and many thresholds for charmed meson production conspiring to create the complex structure seen in Fig. 4. There appears to be an isolated resonance at 4414 MeV/c^2, shown in more detail in Fig. 5, but we do not yet understand very much about it.

II.B. Limits on other narrow states.

From the first four types of quarks we have learned that we can expect at least one narrow vector meson in the e^+e^- spectrum for each type of quark. The question then immediately arises: Are there more types of quarks in the energy range accessible to SPEAR?

Before we look at the data on limits on narrow states, we should ask what we would expect for a new quark. While there is no rigorous way to specify this, it is worth noting that there seems to be a regularity in the first four vector mesons.[32] The leptonic width of the

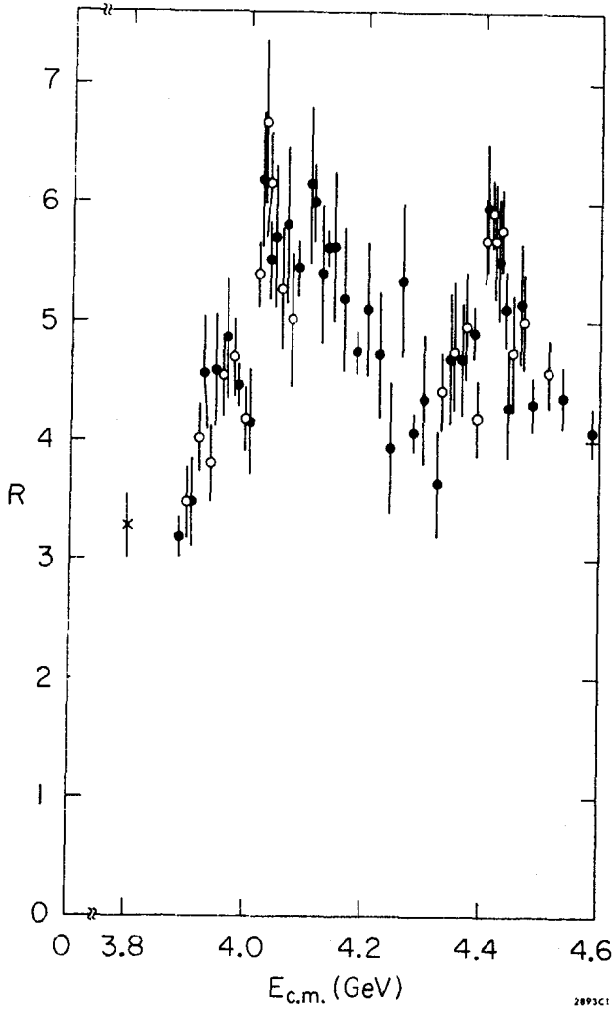

FIG. 4. R as a function of center-of-mass energy in the region 3.9 to 4.6 GeV. Open and closed circles represent data taken at different times.

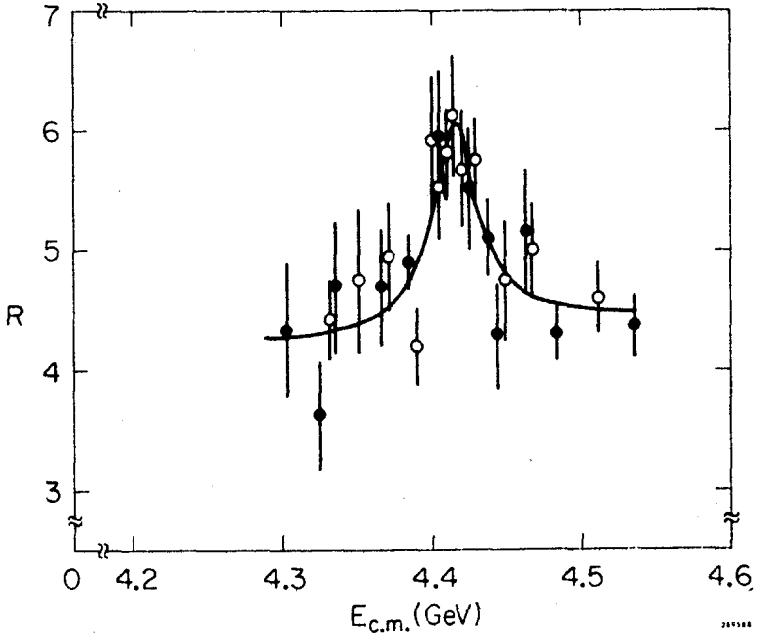

FIG. 5. R as a function of center-of-mass energy in the vicinity of the $\psi(4414)$. The curve is the fit to the $\psi(4414)$ line shape.

mesons divided by a unitary symmetry factor, which is equivalent to the square of the constituent charge, is almost constant:

$$\frac{\Gamma(\rho \to e^+e^-)}{1/2} \qquad \frac{\Gamma(\omega \to e^+e^-)}{1/18} \qquad \frac{\Gamma(\phi \to e^+e^-)}{1/9} \qquad \frac{\Gamma(\psi \to e^+e^-)}{4/9}$$

$$= 13.0 \pm 1.8 \ : \ 13.7 \pm 1.4 \ : \ 12.1 \pm 1.3 \ : \ 11.3 \pm 0.8 \quad (1)$$

This relationship holds to about 20% and so one might expect it to hold approximately for the next quark also. Thus we expect leptonic widths of 4.8 or 1.2 KeV depending on whether the quark charge is 2/3 or 1/3. The leptonic width is a convenient quantity to consider since, as we will derive in Sec. IV, it is proportional to the total integrated cross section for the production of the vector meson,

$$\Gamma_{ee} = \frac{m^2}{6\pi^2} \int \sigma_{tot} \, dE. \qquad (2)$$

The way one searches for narrow vector mesons is to increase the storage ring energy a few MeV at a time and measure the cross section at each energy. The first search of this type was rather crude -- a few hadronic events a point (Fig. 6).[33] However, it proved that the technique worked since the ψ' was discovered by it.[34] More recently, the region between 5.7 and 7.4 GeV was studied in much greater detail,[35] partially in response to reports of possible new resonances around 6 GeV found in hadronic interactions.[36,37] Part of these data are displayed in Fig. 7. The data for $6.4 < E_{cm} < 7.0$ were taken quite recently and have not been fully analyzed yet.

Limits on Γ_{ee} of possible narrow resonances are summarized in

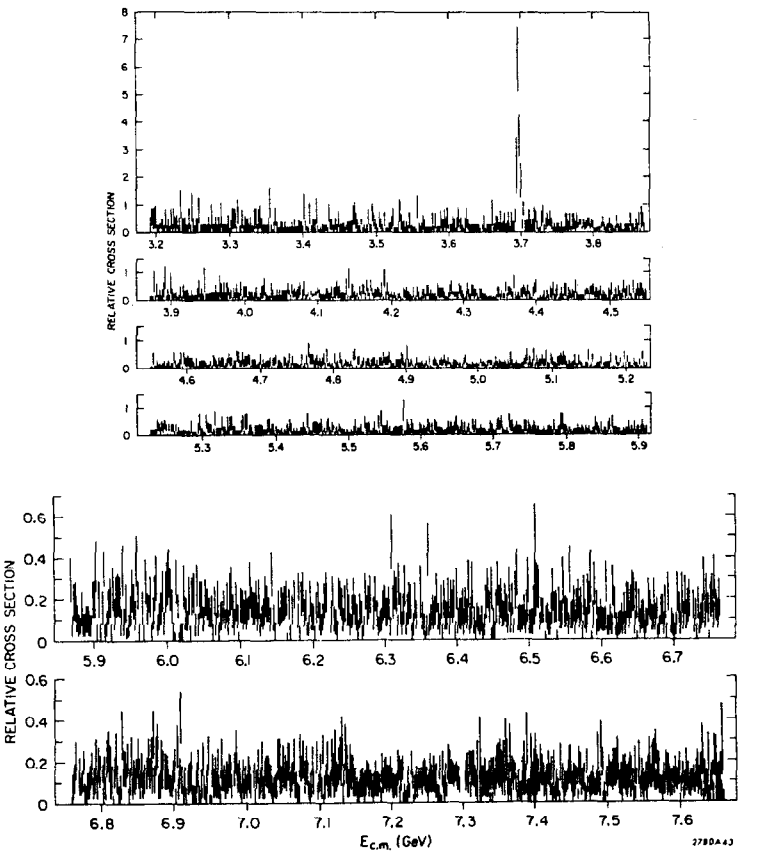

FIG. 6. Fine scan cross section (1 unit ≈ 100 nb) as a function of center-of-mass energy.

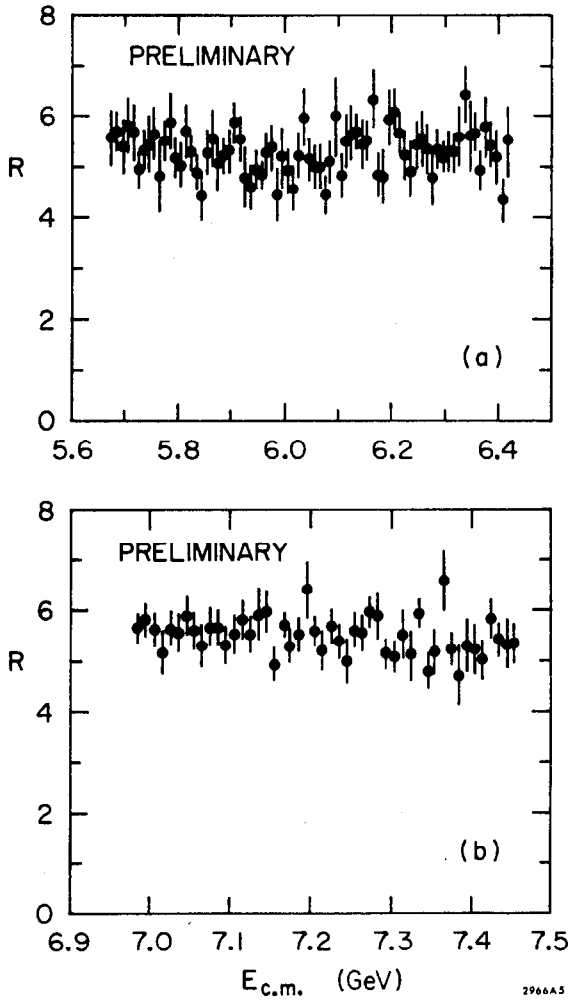

FIG. 7. Preliminary fine scan R as a function of center-of-mass energy plotted in 10 MeV bins.

Table II. From the considerations we just discussed, it is unlikely that a bound state of a charge 2/3 quark exists below 7.6 GeV. However, it is quite possible that a bound state of a charge 1/3 quark could exist in the mass range 4.9 to 5.7 GeV, and we just missed it in the coarse scan. We plan to study this region in detail in the coming year.

TABLE II. Limits on narrow resonances.

E_{cm}	Γ_{ee}(eV)(90% c.l.)
3.2 - 4.9	600 [a]
4.9 - 5.7	1100
5.7 - 6.4	150
6.4 - 7.0	∿100-200 [b]
7.0 - 7.4	70

a. The region between 3.2 and 4.5 GeV has been well studied, but not systematically.

b. Preliminary estimate based on on-line results.

II.C. The continuum

The total e^+e^- annihilation cross section in the continuum is one of the basic measurements of physics. In the parton picture, the ratio, R, of the total cross section to the μ pair production cross section measures the sum of charges squared of the fundamental fermions. (Conventionally the electron and muon are excluded from this sum since experimentally they are easy to separate out in the total cross section.)

Measurements of R from SPEAR are shown in Fig. 8.[27] As an ex-

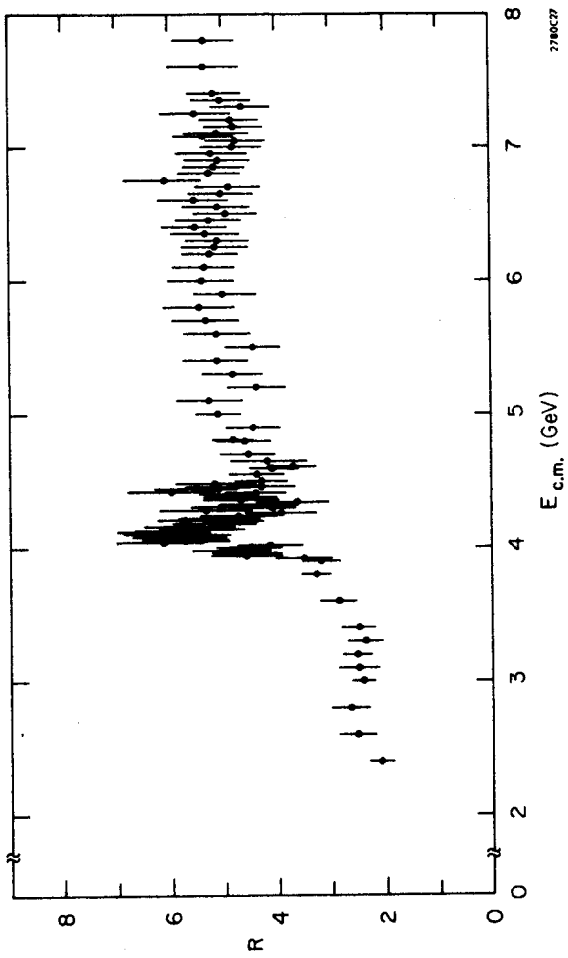

FIG. 8. SPEAR measurements of R as a function of center-of-mass energy.

ercise, let's take these results seriously and follow them to their logical conclusion. There are two plateaus in R, the region below 3.5 GeV and the region above 5 GeV. In these two regions we observe values of R about 2.5 and 5.2. But from the standard three-color quark model we expect values of 2 and 3 1/3. There are two sources of error. First, there is a 15% systematic uncertainty in the experiment, and second, the theory may have corrections at non-asymptotic energies.[38] We will assume, without any justification, that these errors are energy independent and use a combined experimental-theoretical fudge factor of 1.25 to make the lower plateau agree with experiment. Now we expect R to be 4.1 in the higher plateau from the quark model, leaving a difference of 1.1 units between the measurements and the fudged theory.

We need another fundamental fermion to resolve this discrepancy. A charge 1/3 quark will only contribute 1/3 to R, which is not enough. Therefore, we need either a charge 2/3 quark which will contribute 1 1/3 (1 2/3 after applying the fudge factor) or a new lepton which will contribute one unit.

The lepton is preferred for a number of reasons. First, if there is a new quark, t, then there should be a narrow $t\bar{t}$ bound state in the 4-5 GeV region with a leptonic width of 4 to 5 KeV, but limits presented in the previous section clearly exclude this. This difficulty, however, can be avoided if the $t\bar{t}$ state has some mixture of $c\bar{c}$ and is broad.

Second, in order to retain lepton-hadron symmetry, if we have any additional fermions, we need both leptons and quarks. In the two cases we have so far the lepton is lighter than the corresponding quarks.

Third, (and this is probably the only convincing reason), we have

direct experimental evidence for a new lepton. This will be the topic of the third lecture.

III. Detectors

Before we get down to the main business of these lectures, the properties of the ψ family, it is worthwhile spending a few minutes describing two general detectors which provide most of the data which we will discuss.

The SLAC-LBL magnetic detector[39,40] at SPEAR is a general purpose, large solid angle, charged particle detector. It is shown in a telescoped view in Fig. 9a and in more detail in a side view in Fig. 9b. The detector has a solenoidal coil which produces a magnetic field parallel to the incident beams. A set of cylindrical spark chambers measures trajectories of charged particles over about 70% of the full solid angle. Two cylindrical arrays of 48 trigger counters and 24 lead-scintillator sandwich shower counters detect charged particles and γ-rays over about 65% of the solid angle. The trigger for an event is two or more charged particles which each fire a trigger and shower counter. Separation of π's, K's, and p's is accomplished by time-of-flight measurements in the trigger counters. π-K separation is possible to momenta of about 700 MeV/c and K-p separation is possible to momenta of about 1 GeV/c. Electrons can be identified as particles which cause large pulse heights in the shower counters and muons can be identified as particles which penetrate the flux return and fire the muon spark chambers. Additional muon detection is provided by barite-loaded concrete absorbers above the main detector.

The DASP detector[41,42] at DORIS, shown in Fig. 10, is in several ways

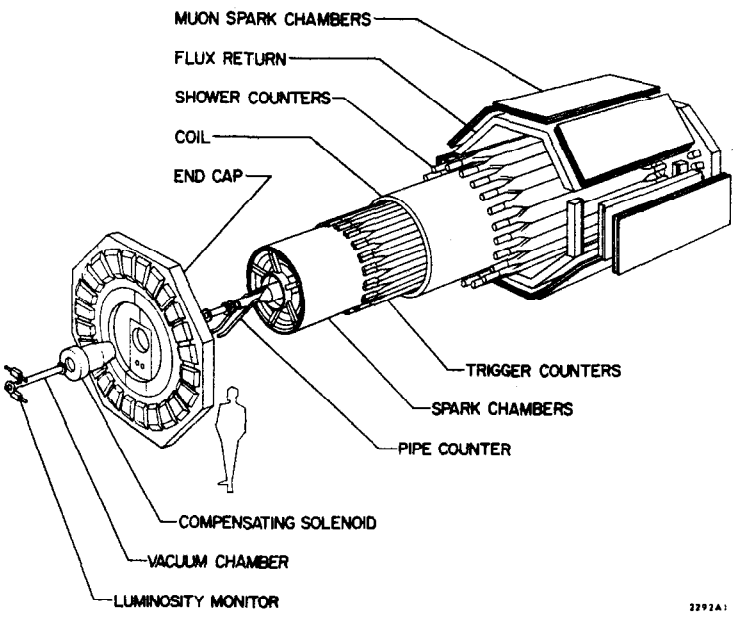

FIG. 9a. Telescoped view of the SLAC-LBL magnetic detector at SPEAR.

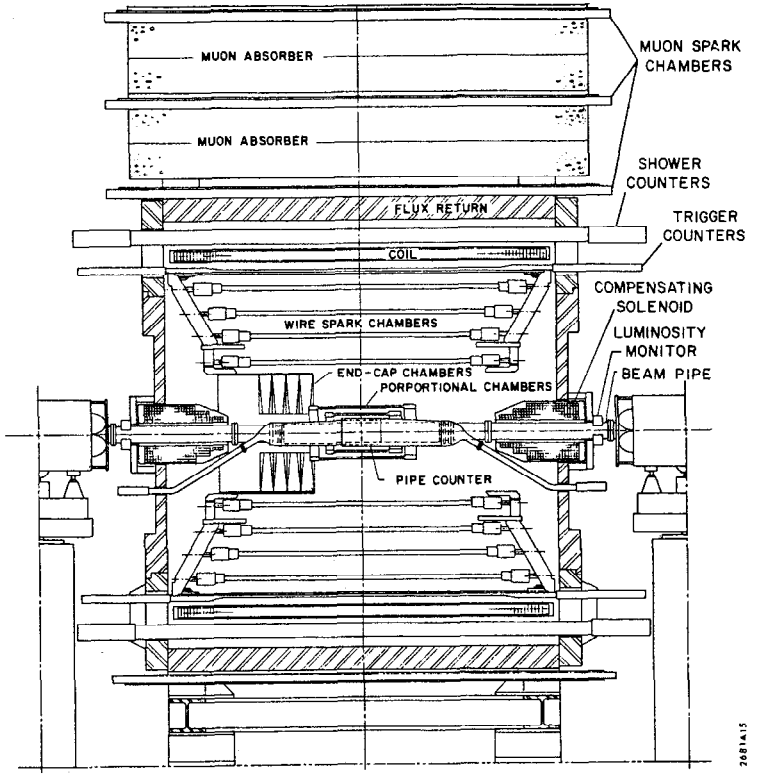

FIG. 9b. Side view cross section of the SLAC-LBL magnetic detector at SPEAR.

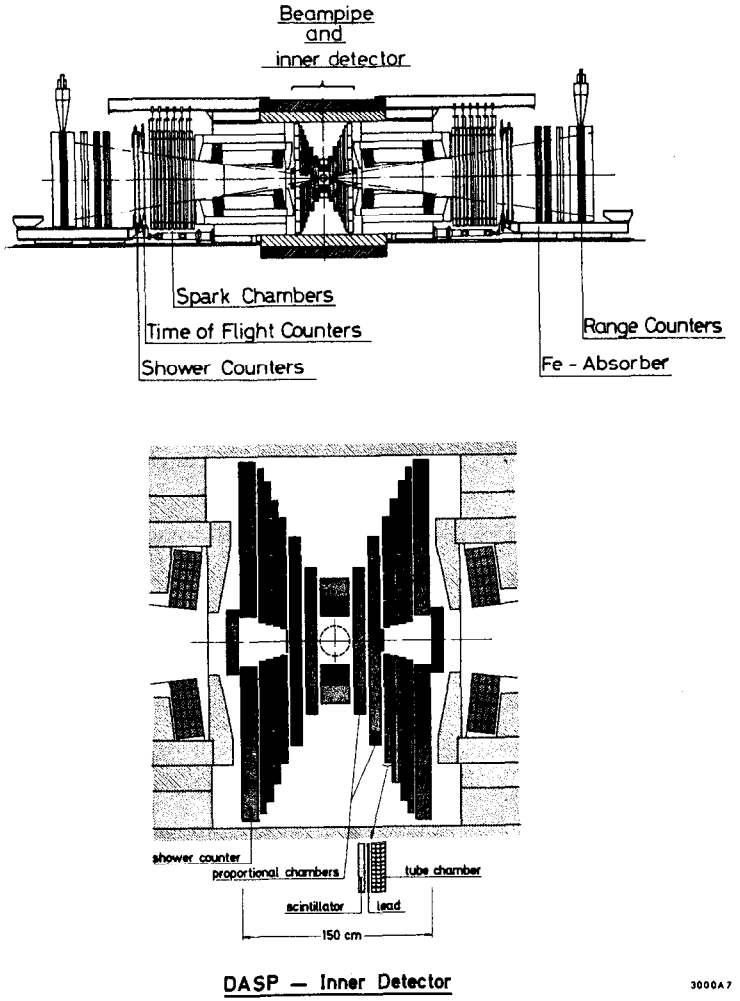

FIG. 10. DASP detector at DORIS.

complementary to the SLAC-LBL detector. It consists of two parts: two magnetic spectrometers on either side of the interaction region covering about 10% of the solid angle and a non-magnetic inner detector covering about 70% of the solid angle.

The magnetic spectrometers have better momentum resolution than the SLAC-LBL detector and much better time-of-flight resolution due to a 5 m flight path. Pions can be separated from kaons up to 1.5 GeV/c and kaons from protons up to 3 GeV/c.

The inner detector is well suited for photon direction and energy measurements. It is composed of an eight radiation length thick lead-scintillator shower counter preceded by four units, each of which contains a scintillation counter hodoscope, 5mm of lead, and two to three layers of proportional tubes. The direction of a shower is determined to about $\pm 2^{\circ}$. The efficiency of the detector is 50% for 50 MeV photons rising to about 90% for 100 MeV photons.

IV. Widths of the ψ and ψ'

Figures 11 and 12 show the measured cross sections for hadron production, μ pair production, and e pair production (or scattering) in the vicinity of the ψ and ψ'.[24,25] These are only apparent cross sections because in both cases the true widths of the resonances are considerably smaller than the experimental resolution.

In cases such as this the true widths must be determined by a "trick". Here the trick is that we measure ψe^+e^- coupling two different ways. As can be seen from Fig. 13, $e^+e^- \to \psi \to$ anything is proportional to this coupling, while $e^+e^- \to \psi \to e^+e^-$ is proportional to the square.

The formalism is fairly simple. For any state f, the resonant

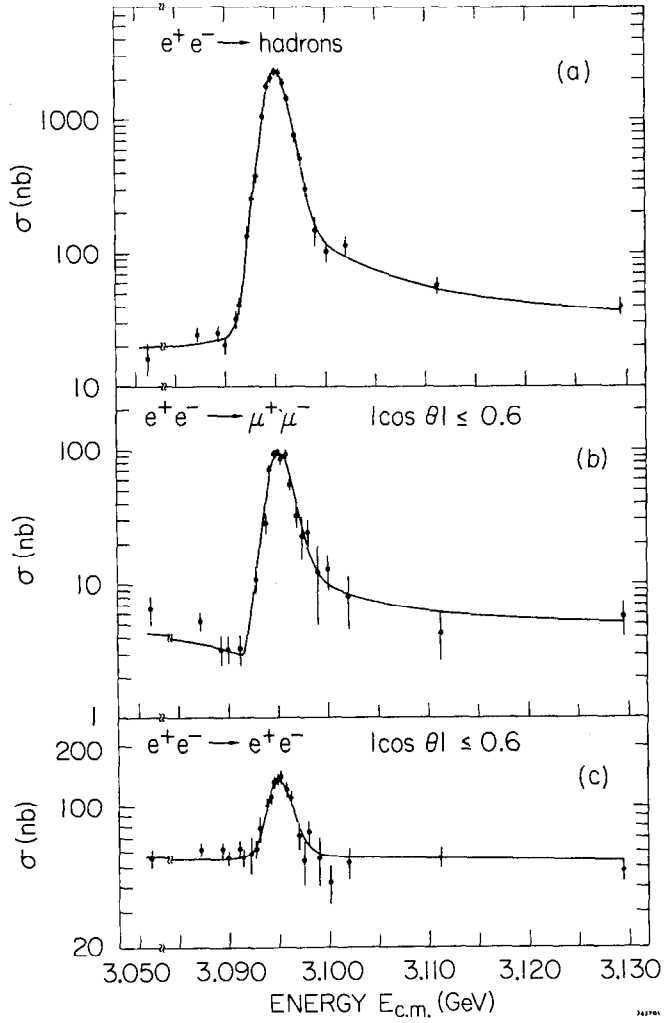

FIG. 11. Cross sections for a) hadron production, b) μ pair production, and c) e pair production and scattering in the vicinity of the $\psi(3095)$.

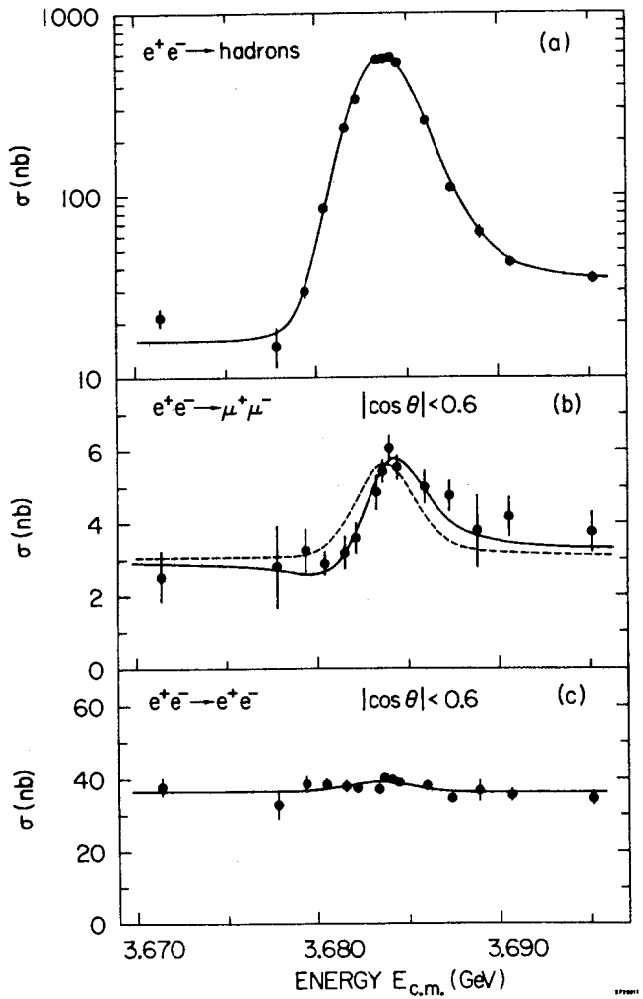

FIG. 12. Cross sections for a) hadron production, b) μ pair production, and c) e pair production and scattering in the vicinity of the ψ'(3684).

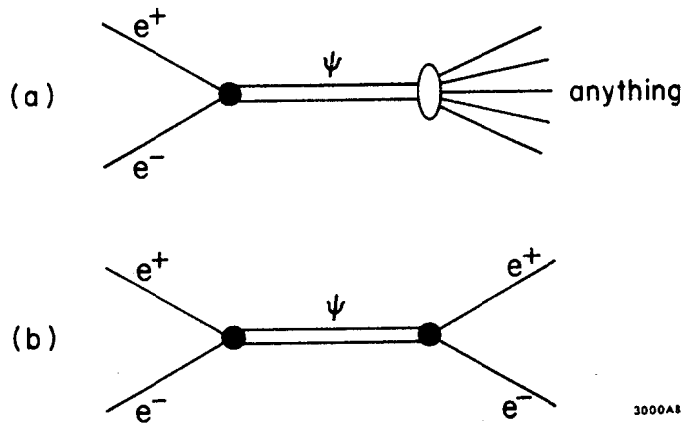

FIG. 13. Diagrams for a) $e^+e^- \to \psi \to$ anything and b) $e^+e^- \to \psi \to e^+e^-$.

cross section will be given by

$$\sigma_{\psi,f} = \frac{\pi(2J+1)}{m^2} \frac{\Gamma_{ee}\Gamma_f}{(E-m)^2 + \Gamma^2/4} , \tag{3}$$

where m is the mass of the ψ, J is its spin, Γ_f is the partial decay width to the state f, and Γ is the total decay width.

Integrating Eq. (3) and using J = 1 (which we will establish in a few minutes), we obtain

$$\Sigma_{\psi,f} \equiv \int \sigma_{\psi,f}\, dE = \frac{6\pi^2}{m^2} \frac{\Gamma_{ee}\Gamma_f}{\Gamma} . \tag{4}$$

We can now use Eq. (4) to obtain all the widths. In particular,

$$\Gamma_{ee} = \frac{m^2}{6\pi^2} \Sigma_{\psi,all} \tag{5}$$

and

$$\Gamma = \frac{\Sigma_{\psi,all}}{\Sigma_{\psi,ee}} \Gamma_{ee} . \tag{6}$$

For simplicity we have ignored radiative effects and interference between ψ decays and the direct channel $e^+e^- \to f$. These effects can be included in a straightforward way.

The widths determined by the SLAC-LBL collaboration for the ψ,ψ', and higher resonances are given in Table III.[24-26] (The world averages for the ψ and ψ', which are only slightly different, will be given later in a complete list of decay modes.) Note that although we don't know how many resonances are in the 4.1 GeV region or their locations and widths, we can still determine that the branching fractions to electron pairs are of order 10^{-5} since they are only proportional to the peak cross sections.

TABLE III. Widths of the ψ particles. SLAC-LBL values.[24-26]

	$\psi(3095)$	$\psi'(3684)$	"4.1 region"	$\psi'''(4414)$
Γ(MeV)	0.069 ± 0.015	0.228 ± 0.056	$\sim$ 200	33 ± 10
Γ_{ee}(KeV)	4.8 ± 0.6	2.1 ± 0.3	$\sim$ 2	0.44 ± 0.14
$B_{ee} = \frac{\Gamma_{ee}}{\Gamma}$	0.069 ± 0.009	0.0093 ± 0.0016	$\sim 10^{-5}$	$(1.3 \pm 0.3) \times 10^{-5}$

V. Spin, parity, and charge conjugation of the ψ and ψ'

If the ψ particles are states of charmonium, they should be produced in e^+e^- annihilations by coupling to the photon, in which case they would have the same quantum numbers, $J^{PC} = 1^{--}$. This would not have to be the case, however, if they coupled directly to leptons, so an experimental check is clearly important.

We can determine the quantum numbers directly by observing the interference between the leptonic decays of the ψ particles,

$$e^+e^- \to \psi \to e^+e^- \tag{7}$$

and

$$e^+e^- \to \psi \to \mu^+\mu^- \tag{8}$$

and the direct production of lepton pairs,

$$e^+e^- \to e^+e^- \tag{9}$$

and

$$e^+e^- \to \mu^+\mu^- . \tag{10}$$

The amplitude for reaction (10) is

$$A(e^+e^- \to \mu^+\mu^-) = \left(\frac{3\pi}{E^2}\right)^{1/2} \left(-\frac{2\alpha}{3}\right) , \tag{11}$$

and the amplitude for reaction (8) is

$$A(e^+e^- \to \psi \to \mu^+\mu^-) = \left(\frac{(2J+1)\pi}{E^2}\right)^{\frac{1}{2}} \frac{\Gamma_{ee}}{m - E - i\Gamma/2} \quad . \qquad (12)$$

If the ψ particles have the quantum numbers of the photon, the cross section will have the form

$$\frac{d\sigma}{d\theta} = \frac{9\pi}{8E^2}(1 + \cos^2\theta) \left| -\frac{2\alpha}{3} + \frac{\Gamma_{ee}}{m - E - i\Gamma/2} \right|^2 . \qquad (13)$$

The sum of the amplitudes which go into Eq. (13) is shown graphically in Fig. 14. As the resonance proceeds around the diagram, it is clear that there will be destructive interference below the resonant energy.

The ratio of muon pairs to electron pairs as a function of energy is shown for the ψ and the ψ' in Fig. 15. This ratio is used because it is least sensitive to normalization effects and because the electron pairs are expected to have a small constructive interference below the resonance (due to interference with the spacelike diagram). The data are inconsistent with no interference by 2.7 standard deviations in the ψ region and by 4.9 standard deviations in the ψ' region. This is sufficient to confirm that the quantum numbers of both the ψ and ψ' are those of the photon, $J^{PC} = 1^{--}$.

VI. Hadronic decays of the ψ

VI.A. Table of results

Table IV contains a compendium of the world measurements of ψ decays. The cutoff date for inclusion of data in this table (and other tables in these lectures) was July 26, 1976, although in a few important cases, new data presented during the topical conference have been included.

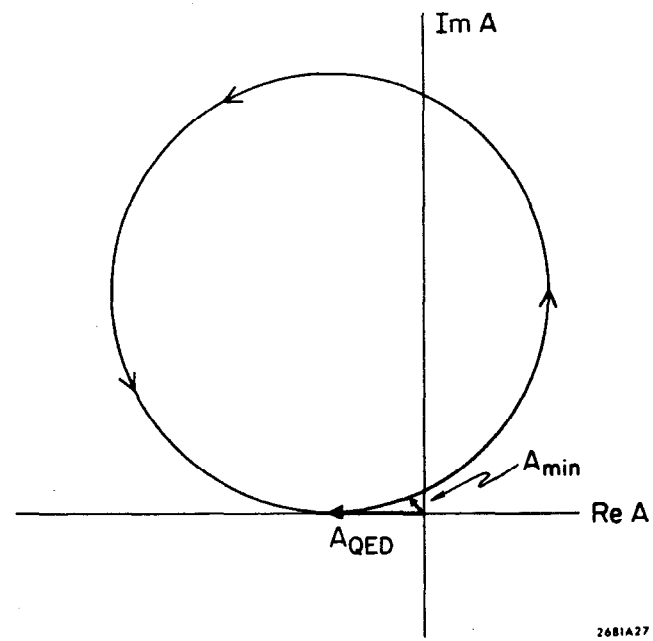

FIG. 14. Amplitude for μ pair production in the vicinity of a vector meson. A_{QED} is the amplitude for μ pair production far below and far above the resonant energy.

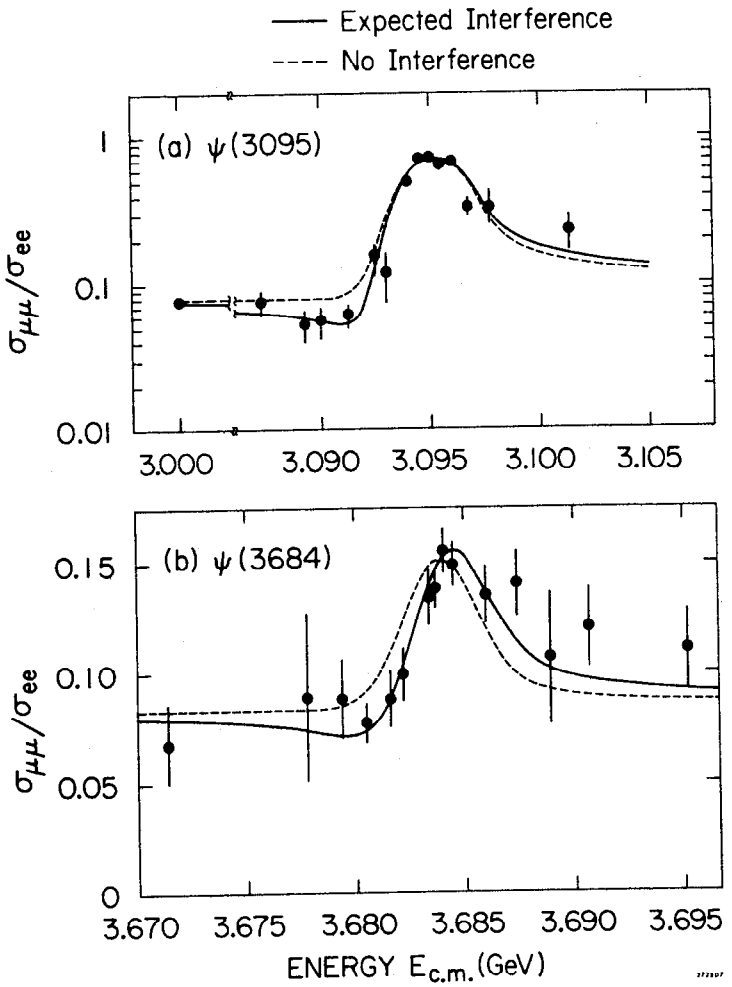

FIG. 15. The ratio of μ pair yield to e pair yield in the vicinity of a) the ψ(3095) and b) the ψ(3684) for $|\cos\theta| \leq 0.6$.

TABLE IV. Decay modes of ψ (3095)

General modes include resonant contributions, e.g. $K^+K^-\pi^+\pi^-$ includes a contribution from $\phi\pi^+\pi^-$. The branching fraction always refers to the mode plus its charge conjugate state and unless qualified to the sum of all possible charge states, e.g. $\rho\pi = \Sigma(\rho^+\pi^- + \rho^0\pi^0 + \rho^-\pi^+)$. Upper limits are at the 90% confidence level. References not used in determining a branching fraction are listed in parentheses.

Mode	Fraction (%)	Ref.	Footnotes
e^+e^-	7.3 ± 0.5	24,42-48	a
$\mu^+\mu^-$	7.4 ± 0.5		
$\pi^+\pi^-$	0.01 ± 0.007	49,(50,51)	b
$\pi^+\pi^-\pi^0$	1.6 ± 0.6	52	c
$2\pi^+ 2\pi^-$	0.4 ± 0.1	52	d
$2\pi^+ 2\pi^- \pi^0$	4.0 ± 1.0	52	
$3\pi^+ 3\pi^-$	0.4 ± 0.2	52	d
$3\pi^+ 3\pi^- \pi^0$	2.9 ± 0.7	52	
$4\pi^+ 4\pi^- \pi^0$	0.9 ± 0.3	52	
$\rho\pi$	1.25 ± 0.2	49,52	e
$A_2^+ \pi^-$	<0.43	49	f
$\omega\pi\pi$	1.0 ± 0.3	53,(52)	g
$\rho\pi\pi\pi$	1.8 ± 0.45	52	g
ρA_2	0.9 ± 0.6	53	g
$\omega 2\pi^+ 2\pi^-$	0.85 ± 0.34	53	
K^+K^-	<0.015	49,51	h,i
$K_S K_L$	<0.008	54	h,j
$K^+K^-\pi^+\pi^-$	0.72 ± 0.23	53,(55)	
$2K^+ 2K^-$	0.07 ± 0.03	53	
$K^+K^- 2\pi^+ 2\pi^-$	0.3 ± 0.1	55	

TABLE IV continued

Mode	Fraction (%)	Ref.	Footnotes
K^+K^{-*}	0.34 ± 0.06	49,53,(54)	k
$K^o \bar{K}^{o*}$	0.27 ± 0.06	53,(54)	k
$K^+ K^{-**}$	<0.15	53,(49,54)	h,k
$K^o \bar{K}^{o**}$	<0.20	53,(54)	h,k
$K^{o*} \bar{K}^{o*}$	<0.5	53,(54)	h,k
$K^{o*} \bar{K}^{o**}$	0.67 ± 0.26	53,(54)	k
$K^{o**} \bar{K}^{o**}$	<0.29	53,(55)	h,k
$\phi \pi \pi$	0.21 ± 0.09	53,(55)	g
$\omega K^+ K^-$	0.03 ± 0.02	53	
$\phi K^+ K^-$	0.09 ± 0.04	53	
$\phi \eta$	0.07 ± 0.04	53	
$\phi \eta'$	0.05 ± 0.04	53	l
$\phi f'$	0.08 ± 0.05	53	
$p \bar{p}$	0.22 ± 0.02	47,49,56	m
$p \bar{n} \pi^-$	0.38 ± 0.08	57,(55)	
$p \bar{p} \pi^o$	0.10 ± 0.02	57,(55)	
$p \bar{p} \eta$	0.19 ± 0.04	56	
$p \bar{p} \pi^+ \pi^-$	0.41 ± 0.08	57	
$p \bar{p} \pi^+ \pi^- \pi^o$	0.11 ± 0.04	57	
$p \bar{p} \omega$	0.05 ± 0.01	57	
$\Lambda \bar{\Lambda}$	0.16 ± 0.08	55	m
$\Lambda \bar{\Sigma}$	<0.04	58	f
$\Xi^- \bar{\Xi}^-$	∿0.04	59	n
$\gamma \gamma$	<0.03	50,(41,46)	o
$\gamma \pi^o$	<0.016	65,(41,60)	
$\gamma \eta$	0.10 ± 0.02	65,(61)	
$\gamma \eta'$	0.24 ± 0.06	65,66,(50,61-63)	
γ X(2800)	<3.0	67	
γ X(2800)→3γ	∿0.015	50,62,(61)	p
γ X(2800)→$\gamma p\bar{p}$	<0.004	56	

a. From a simultaneous fit to measurements on leptonic and total widths. The fit value for the total width is 69 ± 7 KeV.

b. Based on 2 observed events with a calculated background of 0.24 events. This decay is isospin violating and thus presumably proceeds via a second-order electromagnetic interaction. With this assumption, $|F_\pi(q^2 = m_\psi^2)|^2 = (5.6 \pm 4.0) \times 10^{-3}$.

c. Mainly $\pi\rho$.

d. Proceeds via a second-order electromagnetic interaction. The total hadronic decay fraction via this type of interaction is (17 ± 3)%. (Ref. 24).

e. $\Gamma(\rho^o\pi^o)/ (\rho^+\pi^-) + \Gamma(\rho^+\pi^-) = 0.59 \pm 0.17$. (Ref. 52).

f. Forbidden by isospin.

g. Isospin invariance used to calculate modes with more than one neutral.

h. Forbidden by SU(3).

i. Implies $|F_{K^\pm}(q^2 = m_\psi^2)|^2 < 8.6 \times 10^{-3}$

j. Implies $|F_{K^o}(q^2 = m_\psi^2)|^2 < 4.3 \times 10^{-3}$.

k. $K^* \equiv K^*(892)$ and $K^{**} \equiv K^*(1420)$.

l. Based on 2 events observed in $K^+K^-\pi^+\pi^-$ + (η missing).

m. Angular distribution of $1 + \cos^2\theta$ assumed. This is in agreement with measurements of the $\psi \to p\bar{p}$ mode.

n. Four events observed.

o. Forbidden for a spin 1 particle.

p. The existence of this state needs confirmation.

VI.B. Techniques

We will not have time to discuss all of the results presented in Table IV, much less discuss the data on which they are based. However, it is worthwhile to spend a few minutes examining some examples, so that one obtains a feeling for the quality and limitations of the data.

With a few important exceptions, the shower counters in the SPEAR magnetic detector do not have sufficient position or energy resolution to be useful for photon measurements. Thus, most of the hadronic final state analysis from this device uses techniques familiar in bubble chamber physics. If there are no neutral particles in the event and all the charged particles are detected, the event is over constrained and a four-constraint (4-C) fit is possible. If there is only one neutral particle, a 1-C fit is possible. An example of the latter is shown in Fig. 16, $\psi \to \pi^+\pi^-\pi^+\pi^-\pi^o$, the largest of the ψ hadronic decay modes. The missing mass squared of the missing neutral is plotted and a prominent peak is seen at the π^o mass squared. This decay can then be isolated with about 20% background. After isolating this decay, we can investigate it further by plotting the invariant mass of each $\pi^+\pi^-\pi^o$ combination (Fig. 17). A strong peak appears at the ω mass and we can isolate $\psi \to \omega\pi^+\pi^-$ also with about 20% background. In Sec. VI.E., we will go one step further and examine the $\pi^+\pi^-$ mass spectrum in the $\omega\pi^+\pi^-$ final state as part of our study of Zweig's rule.

The decay $\psi \to K\bar{K}^*$ offers a good example of different techniques studying the same reaction. In the SPEAR magnetic detector one of the ways this decay has been studied is to search for final states containing $K^o_S K^+\pi^-$, where the K^o_S decays to $\pi^+\pi^-$. This is a 4-C situation and kine-

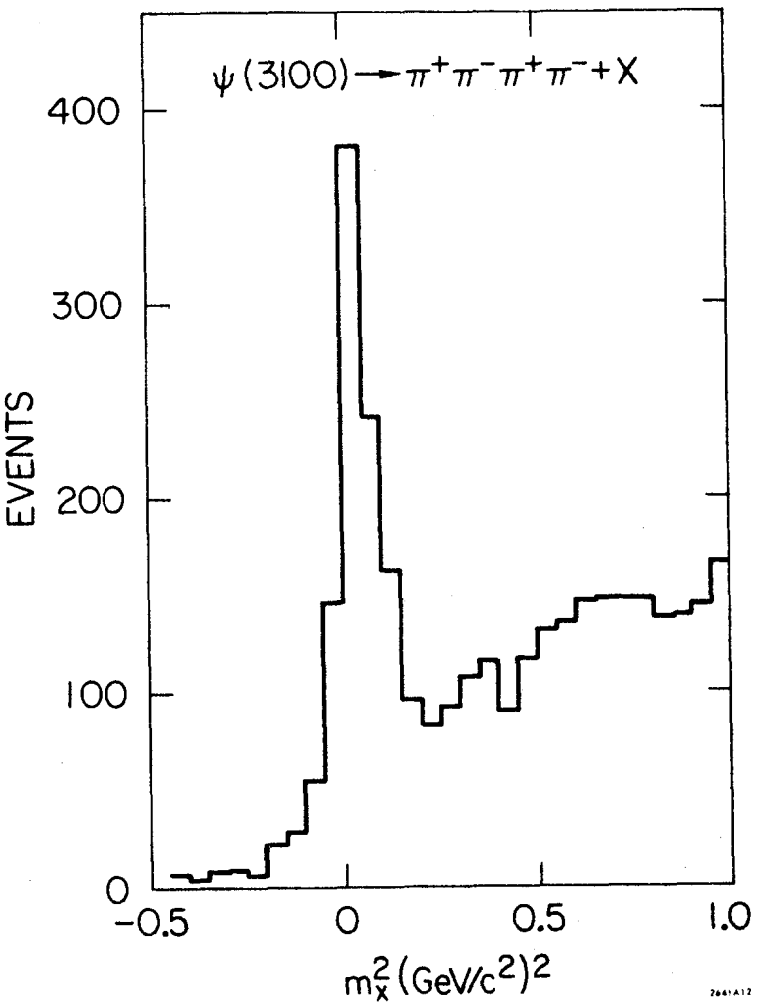

FIG. 16. The invariant mass squared recoiling against four charged pions in ψ decays.

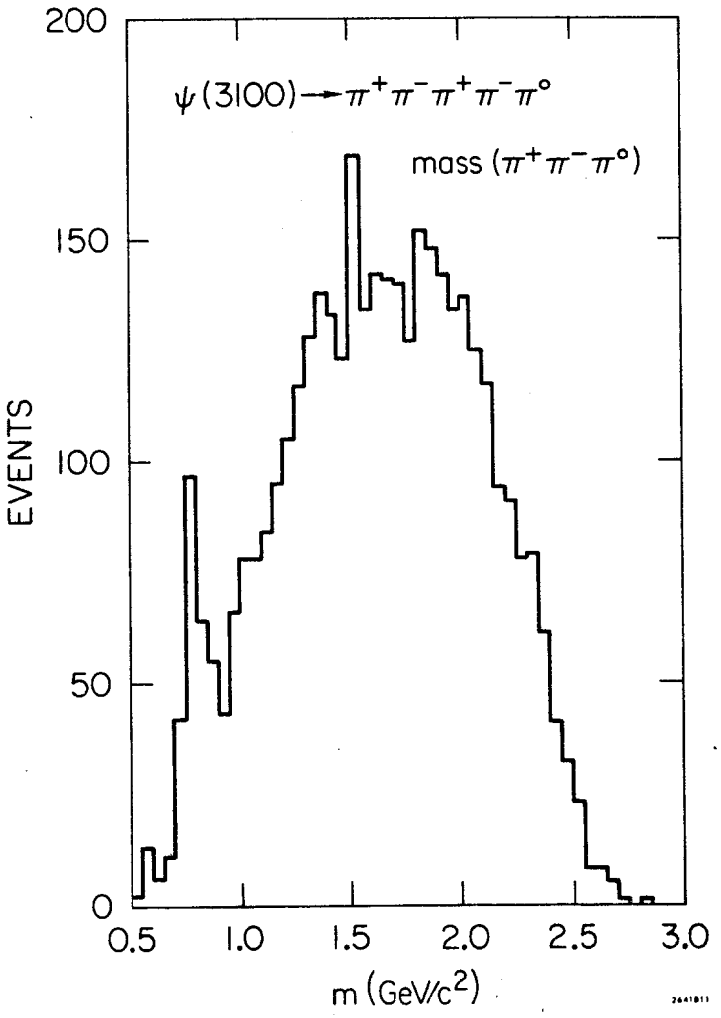

FIG. 17. The invariant mass of $\pi^+\pi^-\pi^0$ combinations from the decay $\psi \to 2\pi^+2\pi^-\pi^0$.

matics alone is sufficient to identify the final state. The Dalitz plot shown in Fig. 18 clearly displays both the charged and neutral $K\bar{K}^*$ modes.[53]

In the DASP spectrometer at DORIS, the charged mode of this decay was measured by detecting the charged K with good momentum and time-of-flight resolution and observing the K^* in the recoil mass spectrum (Fig. 19).[49] The two experiments obtained consistent results. This decay will be important in Sec. VI.D, where we study the SU(3) properties of the ψ.

VI.C. Isospin and G parity

We can determine the G parity of the ψ by observing whether it decays into even or odd numbers of pions. It turns out that the ψ decays into both even and odd numbers of pions -- a violation of I spin. However, this violation occurs in precisely the way we expect it to occur, and in the way it is required to occur, if the ψ couples to a photon.

Consider the three diagrams in Fig. 20. Figure 20(a) shows the direct decay of the ψ into hadrons, (b) shows the decay of the ψ into hadrons via an intermediate photon, and (c) shows the decay into μ pairs. In (b), the nature of the final state, except for a phase factor, must be the same as the non-resonant final state produced in e^+e^- annihilation at the same energy. This state need not conserve isospin and may be quite different from the state produced by (a). Furthermore, we know what contribution (b) must make because the ratio between (b) and (c) must be the same as it would be if the ψ were not in the diagram, about 2.5. Thus, from the data in Table IV, we deduce that if the ψ couples to a photon (a) contributes 68% to the width of the ψ, (b) contributes 18%, and the leptonic modes contribute 14%.

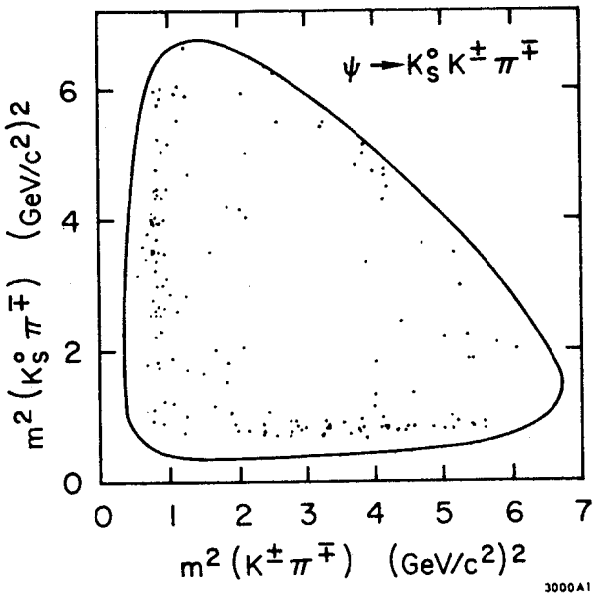

FIG. 18. Dalitz plot for $\psi \to K^0_S K^\pm \pi^\mp$.

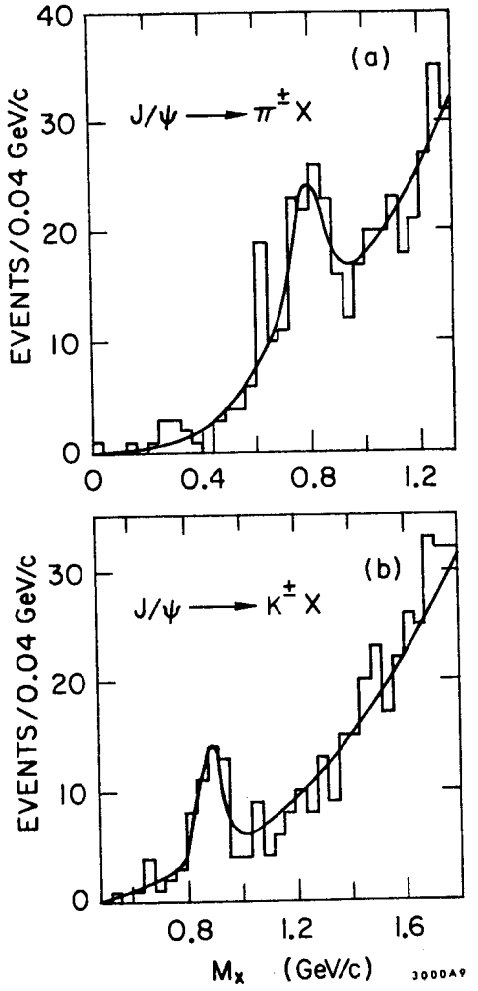

FIG. 19. Missing mass spectrum recoiling against single a) pions and b) kaons in ψ decays as measured by DASP.

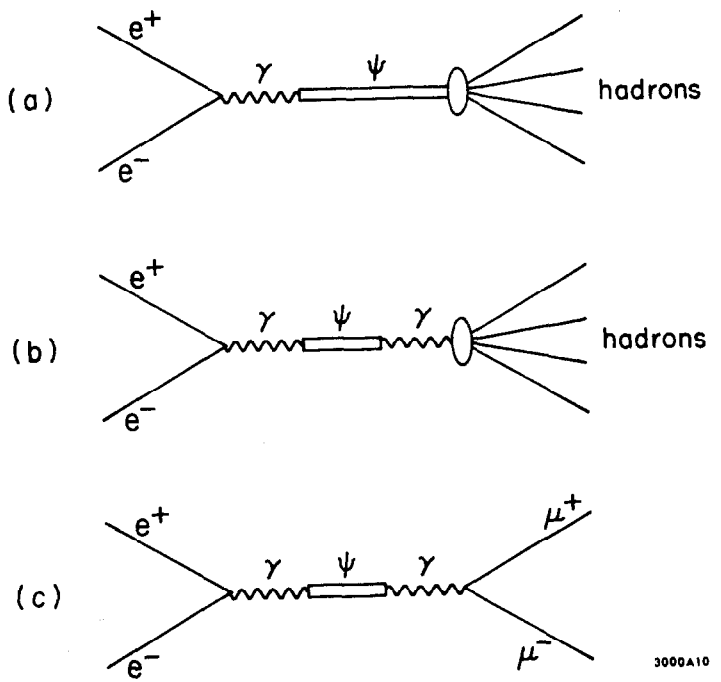

FIG. 20. Diagrams for a) direct ψ decays to hadrons, b) ψ decays to hadrons via an intermediate photon, and c) ψ decay to μ pairs.

To test this hypothesis we want to compare the ratio of all pion final state cross sections to μ pair cross sections on-and off-resonance. we compute the ratio α, defined

$$\alpha = \frac{\sigma_{n\pi}^{\psi}}{\sigma_{\mu\mu}^{\psi}} \Big/ \frac{\sigma_{n}^{3.0}}{\sigma_{\mu\mu}^{3.0}} \quad , \tag{14}$$

where data at 3.0 GeV are used as the off-resonance sample. Values of α for three to seven pion production are shown in Fig. 21.[52] The results are consistent with all of the even number of pion production (G even, I odd) coming from the intermediate photon decay, Fig. 20b. Most of the odd pion production comes from the direct ψ decay, Fig. 20a, and the ψ appears to decay directly into a pure $I^G = (\text{even})^-$ state.

It is relatively easy to show that I = 0. We will give just one argument here. Figure 22 shows the Dalitz plot for $\psi \to 3\pi$. This channel is clearly dominated by $\psi \to \rho\pi$, which implies that either I = 0 or I = 2. If I = 0, then $\Gamma_{\rho^0\pi^0} = \Gamma_{\rho^0\pi^0}$, whereas for I = 2, $\Gamma_{\rho^0\pi^0} = 4\Gamma_{\rho^+\pi^-}$. The data indicate that $\Gamma_{\rho^0\pi^0} = (1.18 \pm 0.34)\Gamma_{\rho^+\pi^-}$, strongly favoring I = 0. These properties, the coupling to photon pairs via a photon, the conservation of isospin in direct decays, and I = 0, are just the properties we expect of a state of charmonium.

VI.D. SU(3)

If the ψ is a state of charmonium, then we expect it to behave as a singlet with respect to the approximate SU(3) symmetry of the three lighter quarks. For each SU(3) multiplet there is a generalized charge conjugation, $\mathscr{C}$, which is equal to C of the I = 0 part of the multiplet. If the ψ is an SU(3) singlet, then it cannot decay into two mesons with the same $\mathscr{C}$.[68]

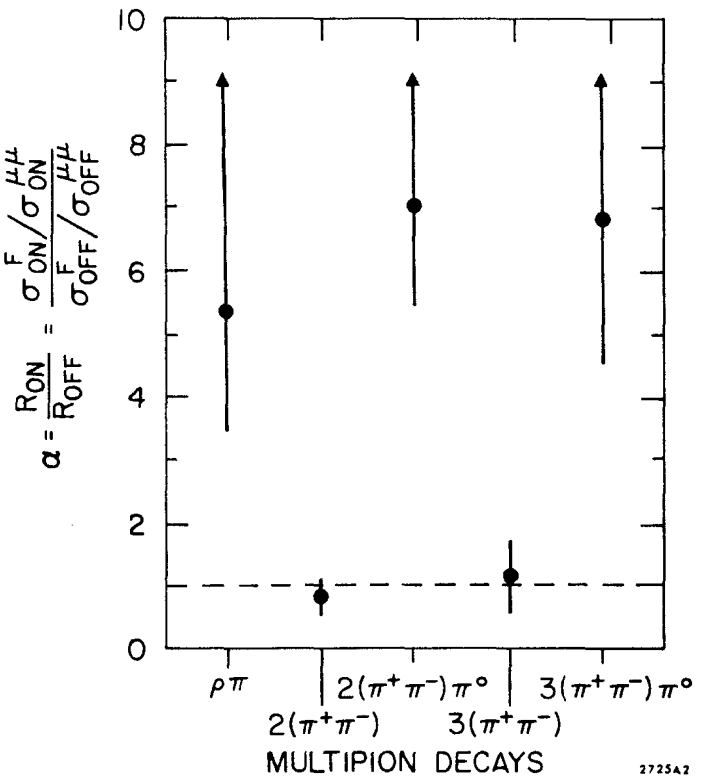

FIG. 21. α (defined in Eq. 14) versus number of pions in ψ decays.

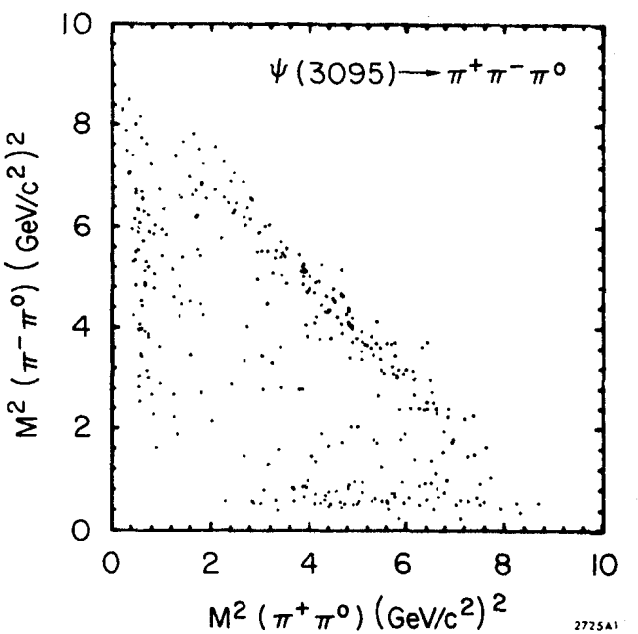

FIG. 22. Dalitz plot for $\psi \rightarrow \pi^+\pi^-\pi^o$.

If we consider the well established pseudoscalar (P), vector (V), and tensor (T) meson multiplets, then decays to PP, PT, VV, and TT meson pairs are forbidden, while decays to PV and VT pairs are allowed. Examining Table IV for decays involving K, $K^*(890)$, and $K^{**}(1420)$, we find that in each case the allowed modes are observed and the forbidden modes are not. In particular note that

$$\frac{\Gamma(K\bar{K}^*)}{\Gamma(K\bar{K})} > 30 \qquad (15)$$

and

$$\frac{\Gamma(p\bar{p})}{\Gamma(k\bar{k})} > 25 \quad . \qquad (16)$$

It is not true in general that heavy particles do not decay into two pseudoscalars. Shortly we will see that the X(3415) decays into both $\pi^+\pi^-$ and K^+K^- with branching fractions of about 1%.

For the two allowed modes, PV and VT, we can proceed one step further and ask whether the branching fractions to individual channels are in accord with SU(3) symmetry. In the PV case, per channel,

$$\Gamma(\pi\rho) \ : \ \Gamma(K\bar{K}^*) \ : \ \Gamma(\eta\phi) \qquad (17a)$$

should be

$$1.0 \ : \ 1.0 \ : \ 0.48 \ . \qquad (17b)$$

Correcting for phase space (17b) becomes

$$1.0 \ : \ 0.84 \ : \ 0.36 \ . \qquad (17c)$$

The data from Table IV are

$$0.42 \pm 0.07 \ : \ 0.15 \pm 0.03 \ : \ 0.07 \pm 0.04 \ . \qquad (17d)$$

Dividing by the predicted ratios (17c), we obtain

$$0.42 \pm 0.07 \ : \ 0.18 \pm 0.04 \ : \ 0.19 \pm 0.11 \ . \qquad (17e)$$

Thus $\Gamma(\rho\pi)$ is about a factor of two larger than expected from $\Gamma(K\bar{K}^*)$.

For the VT decays, we expect, per channel

$$\Gamma(\rho A_2) \ : \ \Gamma(K^*\bar{K}^{**}) \ : \ \Gamma(\phi f') \qquad (18a)$$

to be

$$1.0 \ : \ 1.0 \ : \ 1.0 \ . \qquad (18b)$$

Correcting for s-wave phase space (18b) becomes

$$1.0 \ : \ 0.90 \ : \ 0.78 \ . \qquad (18c)$$

The data are

$$0.30 \pm 0.10 \ : \ 0.34 \pm 0.13 \ : \ 0.08 \pm 0.05 \ . \qquad (18d)$$

Dividing by the predictions, (18c), we obtain

$$0.30 \pm 0.10 \ : \ 0.38 \pm 0.14 \ : \ 0.10 \pm 0.06 \ . \qquad (18e)$$

In this case there is good agreement between ρA_2 and $K^*\bar{K}^{**}$. $\phi f'$ is low, but its predicted rate is sensitive to the assumption of s-wave phase space.

Thus, in general, the ψ does appear to behave as an SU(3) singlet. Allowed decays are observed and forbidden ones are not. Decay rates are roughly correct, but the discrepancy between $\pi\rho$ and $K\bar{K}^*$ indicates some SU(3) breaking.

Although we have not yet discussed their decays, this is probably the best place to make a few remarks on the SU(3) properties of other members of the ψ family. The only evidence we have for the ψ' is that the decay to $p\bar{p}$ has been observed and is at least four times larger than the decay to $K\bar{K}$, which has not been seen. This indicates some inhibition of the $K\bar{K}$ mode.

There are several predictions for the ψ states under the assumption that they are SU(3) singlets. These are listed in Table V.

Although the errors are large, there is no apparent deviation from the SU(3) predictions.

TABLE V. SU(3) tests for the χ states.

State	Modes	Expected ratio	Observed ratio
χ(3415)	$\frac{\pi^+\pi^-}{K^+K^-}$	1	1.0 ± 0.4
χ(3415)	$\frac{K^{*o}K^-\pi^+ + c.c.}{\rho^o\pi^+\pi^-}$	$\frac{4}{3}$	1.4 ± 0.8
χ(3510)	$\frac{K^{*o}K^- + c.c.}{\rho^o\pi^+\pi^-}$	$\frac{4}{3}$	1.2 ± 1.2
χ(3550)	$\frac{K^{*o}K^-\pi^+ + c.c.}{\rho^o\pi^+\pi^-}$	$\frac{4}{3}$	1.1 ± 0.9

VI.E. Tests of Zweig's rule

As we noted previously, the ψ is narrow because all of its decays are suppressed by Zweig's rule. The decays $\psi \to \omega\pi\pi$ and $\psi \to \phi\pi\pi$ allow the examination of this phenominological rule further since the $\phi\pi\pi$ decay is doubly suppressed, as illustrated in Fig. 23a and 23b.

From Table IV

$$\frac{\Gamma(\phi\pi\pi)}{\Gamma(\omega\pi\pi)} = 0.21 \pm 0.11 \qquad (19)$$

which gives an overall suppression factor of about five. However, this overall factor is quite misleading. To understand the dynamics better, we want to study the ratio in Eq. 19 as a function of ππ mass, which is plotted in Fig. 24. Above 1100 MeV/c^2, there is only one observed $\phi\pi\pi$ event and the suppression factor is of order 70. But below 1100 MeV/c^2, there does not appear to be any suppression.

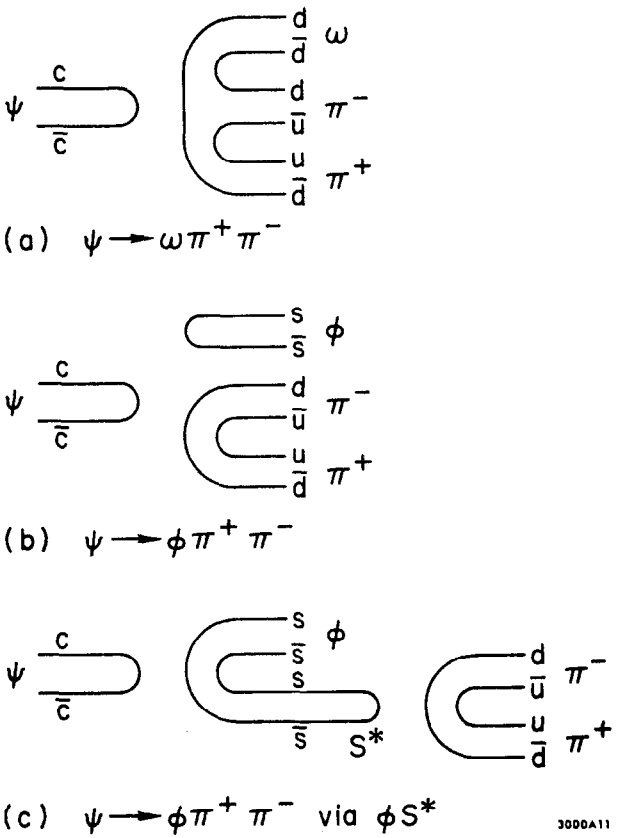

FIG. 23. Quark diagrams illustrating a) $\psi \to \omega\pi^+\pi^-$, b) $\psi \to \phi\pi^+\pi^-$, c) $\psi \to \phi S^* \to \phi\pi^+\pi^-$.

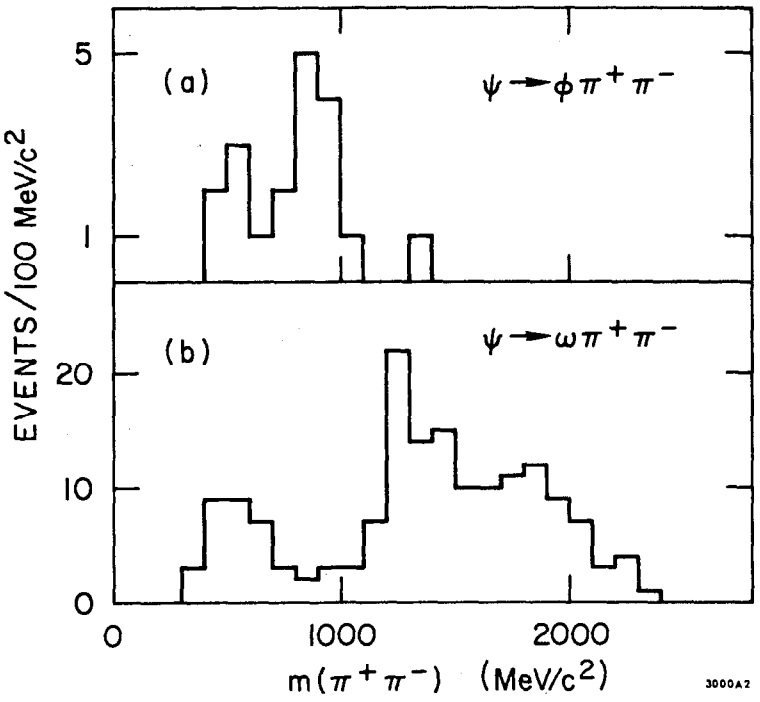

FIG. 24. Invariant mass of $\pi^+\pi^-$ in a) $\psi \rightarrow \phi\pi^+\pi^-$ and b) $\psi \rightarrow \omega\pi^+\pi^-$.

One way this could occur is shown in Fig. 23c.[69] Two pair of $s\bar{s}$ quarks could be formed with only single Zweig suppression. One pair forms a ϕ, the other a $s\bar{s}$ state near or below threshold for K pairs, for example the $S^*(993)$. Because of either phase space or kinematics, this state will be forced to decay into pions rather than kaons.

VI.F. Radiative decays

With the addition of some new data from DORIS presented at this conference,[65,66] we are now in a position to draw some interesting conclusions from ψ radiative decays. From Table IV, we note that $\psi \rightarrow \gamma\pi^0$ has not been observed and the upper limit on the branching fraction is quite small, $< 1.6 \times 10^{-4}$. $\psi \rightarrow \gamma\eta$ and $\psi \rightarrow \gamma\eta$ are seen with branching fractions $(1.0 \pm 0.2) \times 10^{-3}$ and $(2.4 \pm 0.6) \times 10^{-3}$.

Three processes which could account for these decays are shown in Fig. 25. In Fig. 25a the photon is emitted from the light quarks. The SU(3) coupling here is a singlet going to a pair of octets. From SU(3) we would expect $\gamma\pi^0$ to be three times $\gamma\eta$. This clearly cannot be an important mechanism since the $\gamma\pi^0$ branching fraction is very small.

The second mechanism (Fig. 25b) is for the photon to be emitted from the charmed quark pair. This SU(3) coupling must be a singlet going to a pair of singlets. This diagram should be completely dominated by $\gamma\eta'$ since the η' is almost a pure SU(3) singlet, while the η is almost pure octet. If this diagram is to account for all of the radiative decays, it is hard to understand why the η to η' ratio is so large.

This brings us to an interesting suggestion.[70,71] If there is a

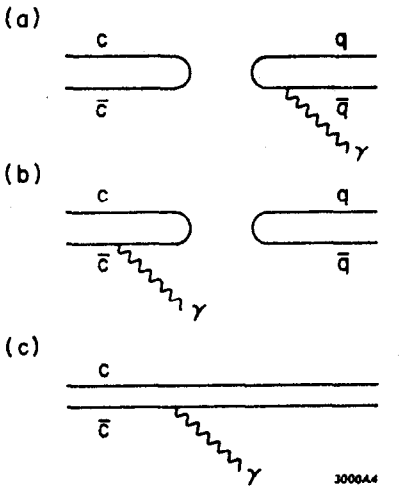

FIG. 25. Quark diagrams illustrating three mechanisms for $\psi \to \gamma\pi^0$, $\psi \to \gamma\eta$, and $\psi \to \gamma\eta'$ decays.

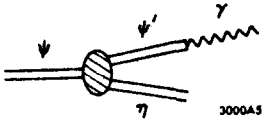

FIG. 26. Diagram for caluclating $\psi \to \gamma\eta$ from $\psi' \to \psi\eta$ using vector meson dominance.

small amount of $c\bar{c}$ mixing in the η and η' (there can be no mixing in the π^0 by isospin conservation), then the radiative decays can occur without Zweig suppression, as shown in Fig. 25c. The data on radiative decays give support to this suggestion. In Sec. VII.B additional support will come from the $\psi' \to \psi\eta$ decay.

An interesting sidelight is that part of Figs. 25b and 25c can be calculated by applying vector dominance to the decay $\psi' \to \psi\eta$, as shown in Fig. 26. This calculation gives a value which is an order of magnitude too large.[68] This should at least caution us that the use of vector dominance at the ψ mass is dangerous.

VI.G. Is anything missing?

With all of the data that have now been collected on ψ decays, it is interesting to ask whether we can account for all of the ψ decays in a reasonable way. This is attempted in Table VI.[72]

TABLE VI. Estimates of ψ decay modes. The quality of the estimate is indicated by the number of question marks following the estimate. No question mark means that the branching fraction is measured or can be derived from measurements listed in Table IV with the aid of isospin conservation. One question mark means that the branching fraction can be estimated from measurements and statistical arguments. Two question marks means a guess based on similar decays. And three question marks means that there is not enough information to even make an intelligent guess.

mode	branching fraction (%)	quality
lepton pairs	14.7	
second order electromagnetic	17.0	
3π	1.6	
5π	6.0	
7π	6.2	?
9π	2.2	?
$\geq 11\pi$	0.7	??
	16.7	
$K\bar{K}\ \pi$	0.6	
$K\bar{K}\ 2\pi$	3.1	?
$K\bar{K}\ 3\pi$	4.5	??
$K\bar{K}\ 4\pi$	2.7	?
$K\bar{K}\ n\pi,\ n \geq 5$	2.0	??
	12.9	
$2K\ 2\bar{K}$	0.3	?
$2K\ 2\bar{K}\ n\pi,\ n \geq 1$	0.7	??
	1.0	
$N\bar{N}$	0.4	
$N\bar{N}\ \pi$	0.6	
$N\bar{N}\ \eta$	0.4	
$N\bar{N}\ 2\pi$	1.7	?
$N\bar{N}\ 3\pi$	0.5	?
	3.6	
$\Lambda\bar{\Lambda}x$, $\Sigma\bar{\Sigma}x$, etc.	1.8	??
$\gamma\eta$, $\gamma\eta'$	0.3	
$\gamma x(2800)$	2.0	???
η + anything	20-30	
TOTAL	90-100	???

The decays to lepton pairs and all pion states and the decays which proceed via a second-order electromagnetic interaction (Fig. 20b) are fairly well measured. The decays involving kaons and nucleons are less certain, but can be reasonably estimated. There is certainly some double counting between the second-order e.m. decays and those involving kaons and nucleons, which we are ignoring. These decays added together account for about 70% of the total. We have not yet considered decays involving η's, about which we have no experimental information. However, based on the fraction of events involving kaons, it does not seem unreasonable that 20 to 30% of the decays should have η's in them.

Thus, although we have explicitly measured only a small fraction of hadronic decays, there is no compelling argument that there is a large component of the decays which we do not understand. However, such a situation is also not excluded by the data.

VII. Hadronic decays of the ψ'.

VII.A. Table of results

There are four classes of ψ' decays which we will discuss: a) $\psi' \to \psi$ decays, b) second-order electromagnetic decays, c) direct decays to ordinary hadrons and d) radiative decays to intermediate states (χ states). Table VII contains a compendium of world measurements of these decays.

TABLE VII. Decay Modes of $\psi'(3684)$.
(See heading for Table IV.)

Mode	Fraction (%)	Ref.	Footnotes
$e^+ e^-$	0.93 ± 0.16	25	a
$\mu^+ \mu^-$	0.93 ± 0.16	25,(73)	a
$\psi \pi^+ \pi^-$	33.0 ± 2.6		
$\psi \pi^o \pi^o$	16.2 ± 2.8	50,61,73,75-77	b
$\psi \eta$	4.1 ± 0.7		
$\psi \gamma + \psi \pi^o$	< 0.15	76	c
$\pi^+ \pi^-$	< 0.005	51,(49)	d
$2\pi^+ 2\pi^-$	0.08 ± 0.02	78	e
$2\pi^+ 2\pi^- \pi^o$	0.35 ± 0.15	55	
$\rho^o \pi^o$	< 0.1	55	
$K^+ K^-$	< 0.005	51,(49)	f
$K^+ K^- \pi^+ \pi^-$	0.14 ± 0.04	78	
$p \bar{p}$	0.023 ± 0.007	79,(49)	g
$\Lambda \bar{\Lambda}$	< 0.04	59	
$\Xi^- \bar{\Xi}^-$	∿ 0.02	59	h
$\gamma \gamma$	< 0.5	80,(61)	i
$\gamma \pi^o$	< 0.7	80,(61)	
$\gamma \eta$	< 0.13	61,(80)	
$\gamma \eta'$	< 0.11	66,(61)	
γ x(2800)	< 1.1	81,(67)	
γ x(2800) → 3γ	< 0.037	61	
$\gamma \chi(3415)$	10. ± 4.	67	j
	7.5 ± 2.6	81	
$\gamma \chi(3510)$	9. ± 3.	67	k
$\gamma \chi(3550)$	8. ± 3.	67	k
$\gamma \chi(3455) \rightarrow \gamma\gamma\psi$	0.8 ± 0.4	81	l

a. $\Gamma(ee) = \Gamma(\mu\mu)$ was assumed. Without this assumption, $\Gamma(\mu\mu)/\Gamma(ee) = 0.89 \pm 0.16$ (Ref. 74). The total decay width was determined to be 228 ± 56 KeV. (Ref. 25).

Table VII continued footnotes

b. From a simultaneous fit to measurements of $\psi' \rightarrow \psi$ + anything, $\psi' \rightarrow \psi$ + neutrals, $\psi' \rightarrow \psi\pi^+\pi^-$, $\psi' \rightarrow \psi\pi^o\pi^o$, $\psi' \rightarrow \psi\eta$, and $\psi' \rightarrow \gamma\chi \rightarrow \gamma\gamma\psi$.

c. $\psi\gamma$ forbidden by C and $\psi\pi^o$ forbidden by isospin.

d. Forbidden by isospin.

e. Proceeds by second-order electromagnetic interaction. The total hadronic decay fraction via this type of interaction is (2.9 ± 0.4)% (Ref. 25).

f. Forbidden by SU(3).

g. Angular distribution of $1 + \cos^2\theta$ assumed. This is in agreement with measurements of the $\psi \rightarrow p\bar{p}$ decay.

h. Two events observed.

i. Forbidden for a spin 1 particle.

j. Angular distribution of $1 + \cos^2\theta$ assumed in agreement with spin 0 assignment and experimental measurements (Ref. 56).

k. Angular distribution assumed to be isotropic.

l. The existence of this state needs confirmation.

VII.B. $\psi' \to \psi$ decays

The ψ' decays over half the time into the ψ. These decays have now been measured at both SPEAR[73,75-77] and DORIS[50,61] with consistent results from both laboratories.

The total $\psi' \to \psi$ branching fraction can be determined by simply observing the μ pair decay of inclusive ψ's. Figure 27 shows the invariant mass distribution of the two highest momentum oppositely charged particles in each ψ' decay. (The particles are assumed to be μ's and electrons have been eliminated.)

The dominent $\psi' \to \psi$ decay, $\psi' \to \psi\pi^+\pi^-$ is visible in two different ways. Figure 28a shows the missing mass recoiling against all combinations of $\pi^+\pi^-$. Figure 28b shows the same distribution for events which satisfy a 4-C fit to $\psi' \to \mu^+\mu^-\pi^+\pi^-$.

The decay $\psi' \to \psi\eta$ is seen best in the mode in which $\eta \to \pi^+\pi^-\pi^0$ or $\pi^+\pi^-\gamma$. We search for events in which two μ's at the ψ mass and two π's are visible, but in which there is missing energy and momentum. The mass squared recoiling against the two μ's, Fig. 29 shows that all these events are consistent with the $\psi\eta$ decay mode.

Finally, the $\psi' \to \psi\pi^0\pi^0$ decay has been measured directly at DORIS[50] and indirectly at SPEAR by subtracting all other $\psi' \to \psi$ modes (including $\psi' \to \gamma\chi \to \gamma\gamma\psi$ which will be discussed in Sec. VI.E) from $\psi' \to \psi$ + anything.

There are three important conclusions to be drawn from the measurements of $\psi' \to \psi$ decays. First, the ψ' and ψ are closely related. There is much more phase space for $\psi' \to \omega\pi\pi$ than for $\psi' \to \psi\pi\pi$, yet the branching fraction for the latter decay is more than two orders of magnitude larger than that for the former.

Second, as expected for a state of charmonium, isospin is conserved

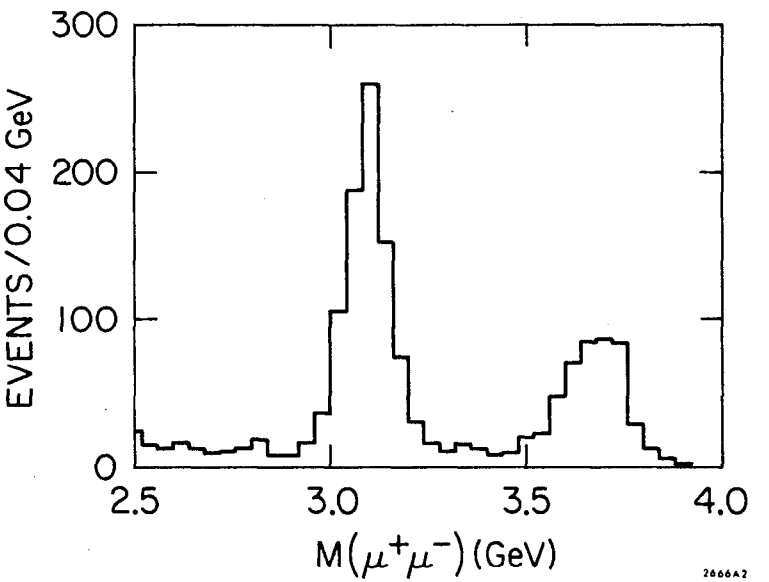

FIG. 27. $\mu^+\mu^-$ invariant mass for the highest momentum oppositely charged particle pair from each ψ' decay. Electron pairs are excluded.

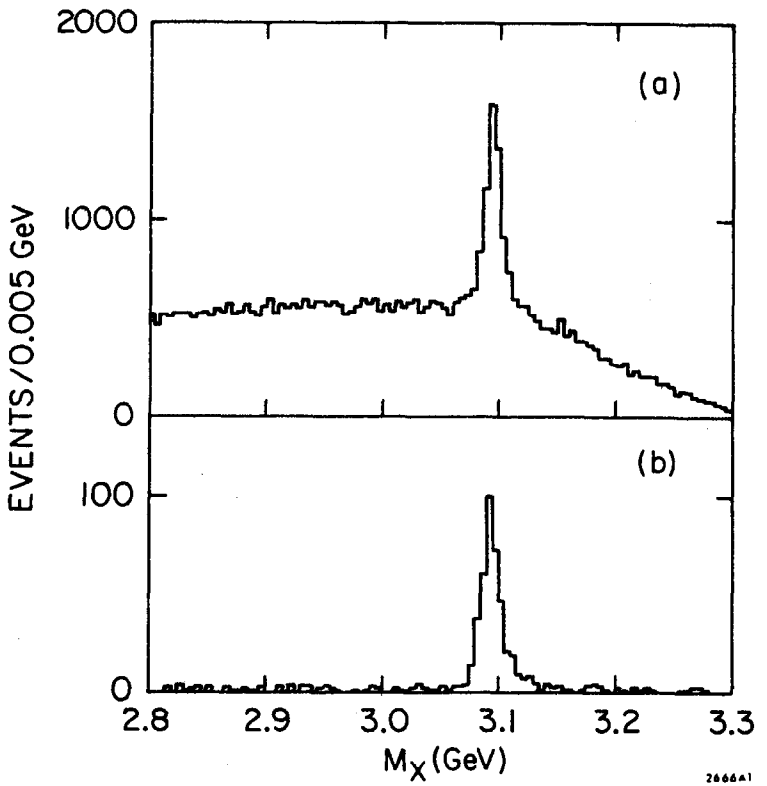

FIG. 28. Missing mass recoiling against pairs of oppositely charged particles a) in all ψ decays, and b) ψ decays with four charged particles conserving energy and momentum.

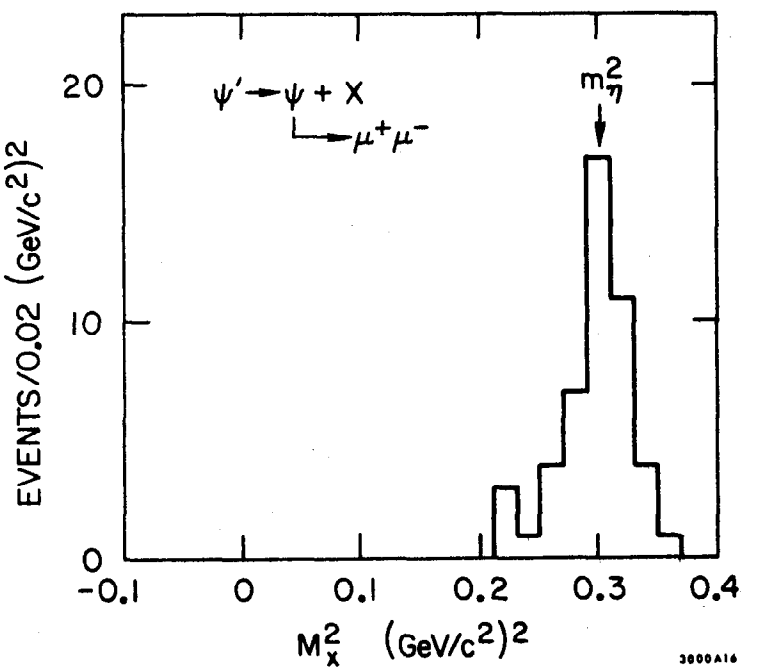

FIG. 29. Missing mass squared recoiling against the ψ in events in which the ψ and two charged pions are detected, but which are not consistent with the decay $\psi' \rightarrow \psi\pi^+\pi^-$.

in the decay and is equal to zero. This can be seen from the ratio of the $\psi\pi^0\pi^0$ mode to the $\psi\pi^+\pi^-$ mode which is equal to 0.49 ± 0.09. Correcting for phase space, we expect this ratio to be 0.52 for I = 0, 0 for I = 1, and 2.1 for I = 2. Additional evidence for isospin conservation comes from the observation of $\psi' \to \psi\eta$ but not $\psi' \to \psi\pi^0$. The latter decay is not observed at the level of 3% of the former and it is inhibited only by isospin.

The third conclusion has to do with the only real surprise in the $\psi' \to \psi$ decays, the size of $\psi' \to \psi\eta$. This decay is quite large -- it is about a 4% branching fraction -- even though it has everything working against it:

1) There is little phase space; the Q value is only 40 MeV.
2) This is a P-wave decay, so there is an angular momentum barrier.
3) The decay is SU(3) forbidden in the limit that the η is pure octet.

We have already discussed a way out of these difficulties. If there is some $c\bar{c}$ mixing in the η, $\psi' \to \psi\eta$ is no longer Zweig suppressed and its large branching fraction can easily be understood.

VII.C. *Second order electromagnetic decays*

The arguments of Sec. VI.C. which were applied to the ψ apply equally well to the ψ'. The branching fractions to e^+e^- and to $\mu^+\mu^-$ are each about 1%. Therefore the branching fraction for hadrons produced via an intermediate photon (Fig. 20b) should be about 3% since the non-resonant value of R in the vicinity of the ψ' is about 3.

VII.D. Direct decays to hadrons

Few direct decays of the ψ' to ordinary hadrons have been observed and only two modes, $p\bar{p}$ and $K^+K^-\pi^+\pi^-$, have been measured well. This is partially because the direct decays are usually masked by a large background of $\psi' \to \psi\pi\pi$ decays and partially because not enough effort has been expended on finding these decays. Both the $p\bar{p}$ and $K^+K^-\pi^+\pi^-$ modes were measured in the process of working on χ decays.

Nevertheless, these two modes give us a considerable amount of information on direct ψ' decays. Table VIII shows a comparison of ψ and ψ' decays to these two modes and to lepton pairs. For all three decays the ratio of the ψ' to ψ partial widths is equal within errors. This can be understood if

$$\Gamma(\text{hadrons}) \propto |\Psi(0)|^2 , \qquad (20)$$

where $\Psi(0)$ is the wave function at the origin.[38] A heuristic argument for Eq. 20 is that the charm quarks are heavy and so the interaction is fairly local.

If we assume the validity of Eq. 20, then the branching fraction for ψ' direct decay to ordinary hadrons is about 9%.

TABLE VIII. Comparison of direct ψ and ψ' decays.

mode	Γ_ψ(KeV)	$\Gamma_{\psi'}$(KeV)	$\Gamma_{\psi'}/\Gamma_\psi$
e^+e^-	5.0 ± 0.3	2.1 ± 0.3	0.42 ± 0.07
$p\bar{p}$	0.15 ± 0.01	0.05 ± 0.02	0.33 ± 0.11
$K^+K^-\pi^+\pi^-$	0.50 ± 0.16	0.32 ± 0.09	0.64 ± 0.27

VII.E. $\psi' \to \gamma\chi$ decays

If we consider the ψ the triplet S ground state of charmonium and the ψ' a radially excited state of the ψ, other states should exist which could be reached by radiative transitions from the ψ'.[82-85] The expected scheme

is shown in Fig. 30. There are three triplet P states and two singlet S states. The states above the ψ could decay radiatively to the ψ or could decay directly to ordinary hadrons. As we will discover in the following sections, the P states are well established. There are also candidates for the two pseudoscalar S states, but they are in need of further experimental confirmation.

We will use χ, a name suggested over a decade ago by Bjorken and Glashow for states of charmonium,[86] as a generic name for all these new C-even states. The name P_C was originally suggested by the DASP collaboration[87] for the state we now identify as the $\chi(3510)$; this name is also common in the literature.

The $\psi' \to \gamma\chi$ decays have been detected by three techniques: 1) by detecting the hadronic decay of the χ's, 2) by detecting the ψ and one or both of the cascade photons in $\psi' \to \gamma\chi \to \gamma\gamma\psi$, and 3) by detecting monochromatic photons. We will now discuss each of these techniques in turn.

VII.E.1. χ decays to hadrons

As an example of this technique we will go through the steps used in isolating the $\chi \to 2\pi^+2\pi^-$ decays. The search begins in Fig. 31, which contains scatter plots of missing mass squared (m_x^2) versus missing momentum (p_x) for four-prong events from ψ and ψ' decays.[88] In the ψ case (Fig. 31b) a dense band of events exists near $m_x^2 = 0$ extending across the entire p_x range. These events correspond to the five-pion decay of the ψ. The ψ' decays shown in Fig. 31a after subtraction of $\psi' \to \psi\pi^+\pi^-$ decays appear quite different. The band is absent, but instead there is a cluster of events in the p_x region between 100 and 300 MeV/c.

To investigate this further, we select the events in this region ($100 < p_x < 300$ MeV/c) and plot the projection of these data on the m_x^2

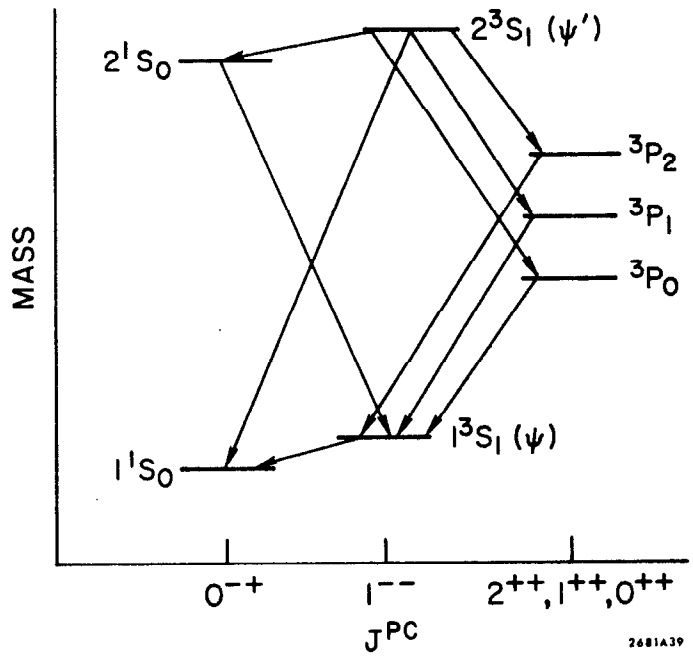

FIG. 30. States and radiative transitions expected from bound fermion-antifermion system.

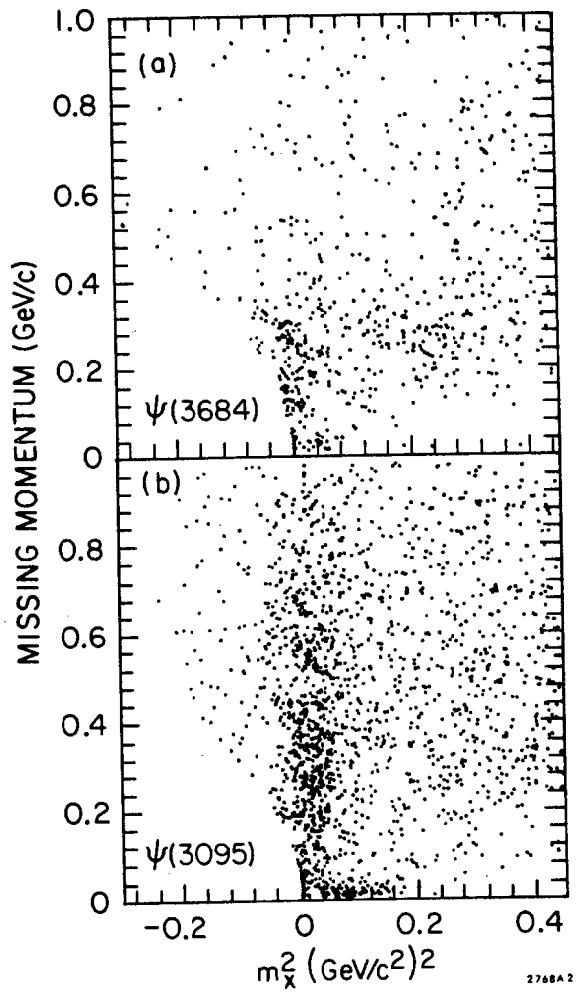

FIG. 31. Scatter plots of missing momentum versus missing mass squared for four prong events in a) ψ' decays and b) ψ decays.

axis. The results are shown in Fig. 32 for the ψ' and ψ. In the case of the ψ (Fig. 32b) the m_x^2 distribution is consistent with a missing π^o, but inconsistent with a missing γ. In the ψ' decays (Fig. 32a) the exact opposite is true -- the missing neutral is consistent with being a γ and is not consistent with being a π^o. Thus, we have the exceptional circumstance that in this p_x range we are observing a $4\pi\gamma$ final state.

We now select those events near $m_x^2 = 0$ ($-0.03 < m_x^2 < 0.03$ GeV/c^2), make a one-constraint fit, and plot the resulting 4π mass in Fig. 33a. Events with masses above 3.60 GeV/c^2 are consistent with the second order electromagnetic decay $\psi' \to 4\pi$. There are three other clear peaks at masses of about 3415, 3500, and 3550 MeV/c^2 each of which we identify with a new χ state.[78,79]

Figures 33b, 33c, and 33d show the mass plots for χ decays to $K^+K^-\pi^+\pi^-$, $3\pi^+3\pi^-$, and $\pi^+\pi^-$ or K^+K^-, all obtained by similar techniques. The same three states are found in these plots, but not as clearly in all cases. In the $K^+K^-\pi^+\pi^-$ mode the $\chi(3510)$ is weak. In the $3\pi^+3\pi^-$ mode the $\chi(3510)$ and $\chi(3550)$ are not resolved. In the $\pi^+\bar{\pi}$ or K^+K^- mode, the $\chi(3415)$ is quite clear and there are eleven events in the vicinity of the $\chi(3550)$ with an estimated background of only two or three events. There are only two events in the vicinity of the $\chi(3510)$ and these are consistent with backgrounds. These decays into two pseudoscalars will be important when we consider the spin assignments of the χ states in Sec. VIII.B.

VII.E.2. χ decays to $\gamma\psi$

Two methods have been used to detect the $\psi' \to \gamma\chi \to \gamma\gamma\psi$ cascade. In both methods the ψ is observed in its muon pair decay, so that we have a final state corresponding to $\psi' \to \gamma\gamma\mu^+\mu^-$.

In the first method, which has been used in the SPEAR magnetic de-

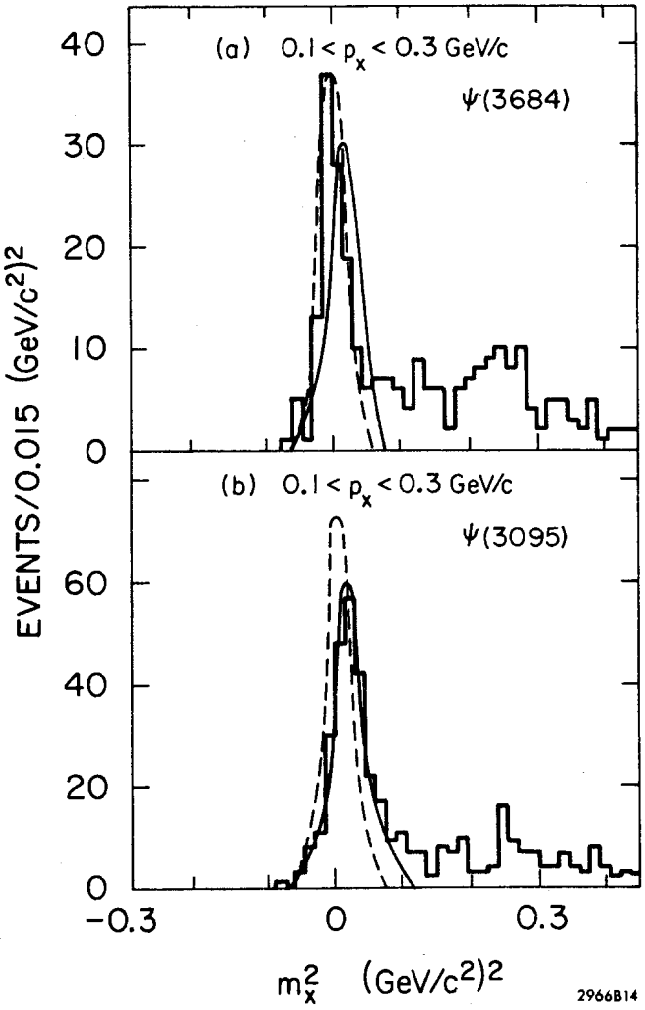

FIG. 32. Missing mass squared for four prong events with missing momentum in the range 100 to 300 MeV/c for a) ψ' decays and b) ψ decays. The solid and dashed lines give the predicted resolution functions for a missing π^0 and γ, respectively.

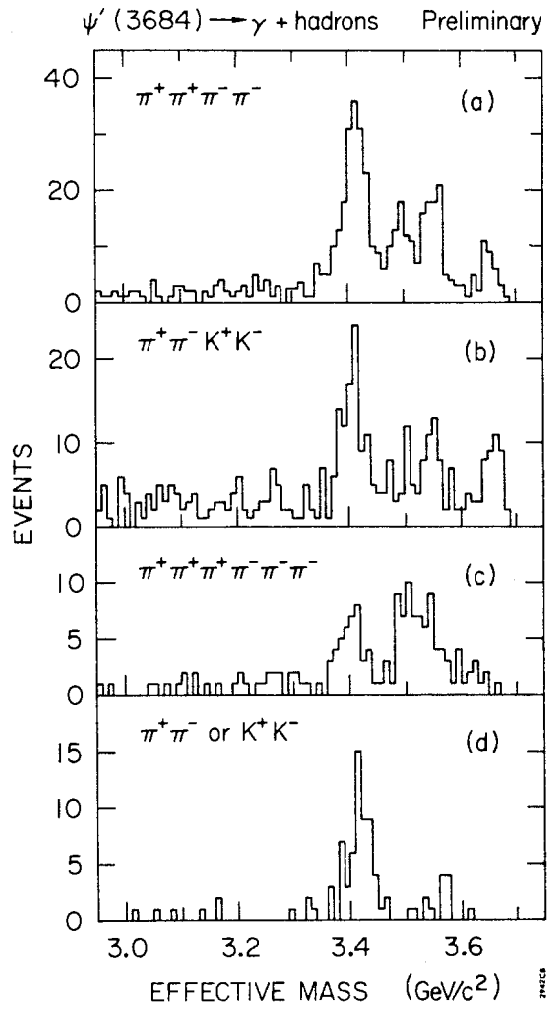

FIG. 33. Invariant χ mass distributions for ψ' → γχ for a) $2\pi^+2\pi^-$ b) $\pi^+\pi^-K^+K^-$ c) $3\pi^+3\pi^-$, and d) the sum of $\pi^+\pi^-$ and K^+K^-.

tector, we detect $\mu^+\mu^-$ and observe a conversion of one of the photons in the 0.052 radiation lengths of material surrounding the beam pipe.[90] A 1-C fit is then performed to the event. A computer reconstruction of this type of event is shown in Fig. 34.

In the second method, which has been used both at SPEAR[90] and at DORIS,[61] both photons are detected in shower counters and the angle measurements are used to give a 2-C fit. In the SPEAR magnetic detector, the azimuthal angle is determined by which shower counter is hit and the polar angle is determined by the relative pulse height at the two ends of the counter. This second method provides worse resolution, but much higher statistics than the first method. It will be useful in Sec. VIII.B where we discuss the angular distributions.

Whichever method is used, there are two solutions for each event since we do not know a priori which photon was emitted first. This two-fold ambiguity can be resolved by observing the widths of the reconstructed χ masses since the first photon will be monochromatic, while the second is Doppler shifted by the motion of the χ.

Figure 35 shows the $\gamma\psi$ masses obtained by the first method at SPEAR.[81] There are four clusters of events. The $\chi(3510)$ and $\chi(3550)$ are clearly visible and the two-fold ambiguity is resolved in favor of the higher mass states in agreement with the observation of χ's from their hadronic decays. There is a single event consistent with coming from the $\chi(3415)$.

The new element in Fig. 35 is the cluster of four events at 3454 MeV/c^2. Since the expected background in all of Fig. 35 is only one event, it seems unlikely that this cluster is due to background. Nevertheless, these four events are the only evidence for this possible state; it clearly is on shaky experimental ground and badly needs confirmation. We will tentatively

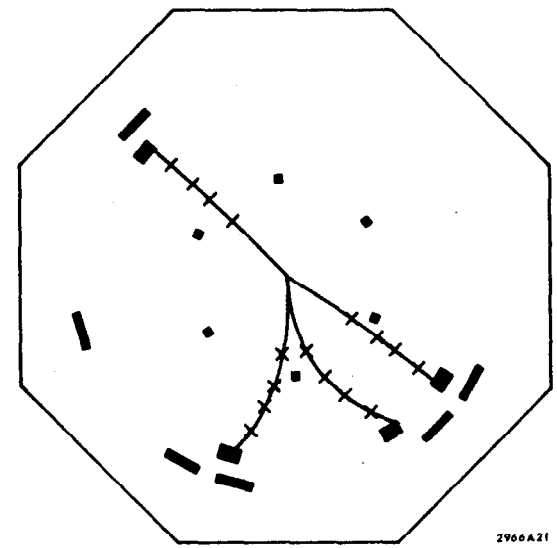

FIG. 34. Computer reconstruction of a $\psi' \to \gamma\chi \to \gamma\gamma\psi \to \gamma\gamma\mu\mu \to \gamma e^+e^-\mu^+\mu^-$ cascade. The short boxes respresent trigger counters and the long boxes represent shower counters. The unconverted γ is detected by the isolated shower counter on the left.

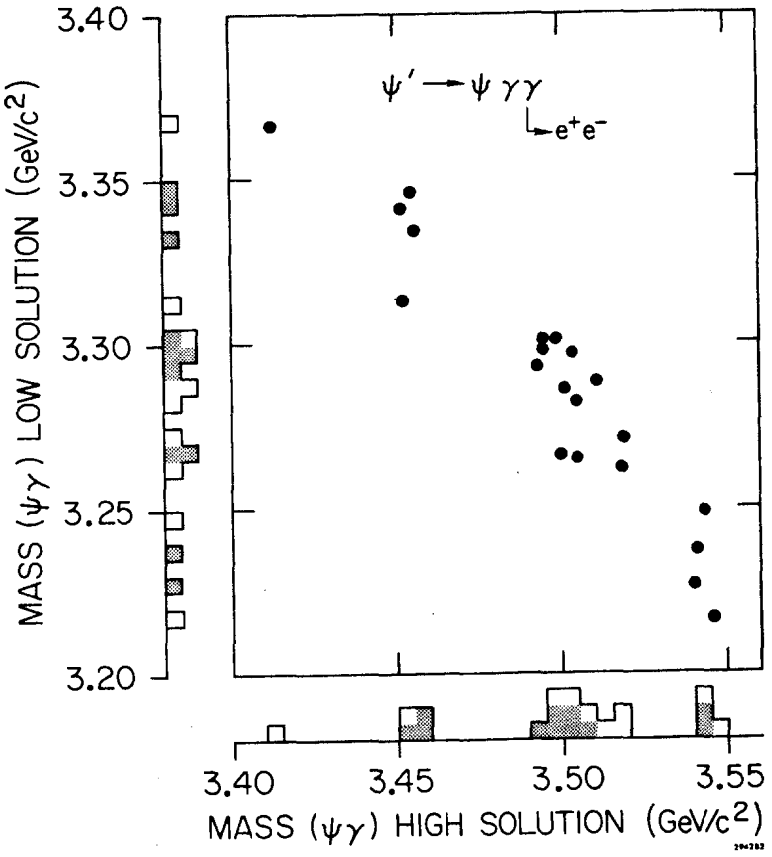

FIG. 35. Scatter plot of the two solutions for the mass of χ states in $\psi' \to \gamma\chi \to \gamma\gamma\psi$ events.

dub it the χ(3455) and discuss it, but the reader is forewarned of its weak status.

The latest data from DORIS[91] show the same pattern as Fig. 35, but with fewer events and worse resolution. There are five events at the χ(3510), one event each consistent with coming from the χ(3415) and χ(3550), and one event ambiguous between the χ(3510) and the χ(3455).

VII.E.3. Monochromatic photons

In order to measure the branching ratios for $\psi' \to \gamma\chi$, it is necessary to detect the monochromatic photons. Two measurements of this type have now been performed. The first comes from the magnetic detector at SPEAR.[81] Photons were detected by observing conversions in the material around the beam pipe. For low energy photons, the rms energy resolution is about 2% for this technique. Photon energy spectra from ψ and ψ' decays are shown in Fig. 36. A peak is seen in the ψ' spectrum at 261 MeV, corresponding to the χ(3415). The branching fraction for $\psi' \to \gamma\chi(3415)$ from these data is 0.075 ± 0.026. The other χ states correspond to lower photon energies and are not visible because of rapidly falling acceptance in this region.

A special experiment was conducted at SPEAR to search for monochromatic photons by a collaboration from Maryland, Pavia, Princeton, San Diego, SLAC, and Stanford (MPPSDSS).[67] A sketch of the apparatus is shown in Fig. 37. Arrays of large NaI crystals were used to detect the photons with about 5% rms energy resolution. The data from ψ and ψ' decays are shown in Fig. 38. There are no significant peaks in the ψ spectrum, but four clear peaks are apparent in the ψ' spectrum. The first three correspond to the χ(3550), χ(3510) and χ(3415), and the last is from the Doppler broadened photon in the $\chi(3510) \to \gamma\psi$ decay. The branching ratios for $\psi' \to \gamma\chi$ are 0.10 ± 0.04, 0.09 ± 0.03, and 0.08 ± 0.03 for the χ(3415), χ(3510), and χ(3550), respectively. The branching fraction for $\psi' \to \gamma\chi(3415)$ determined by these

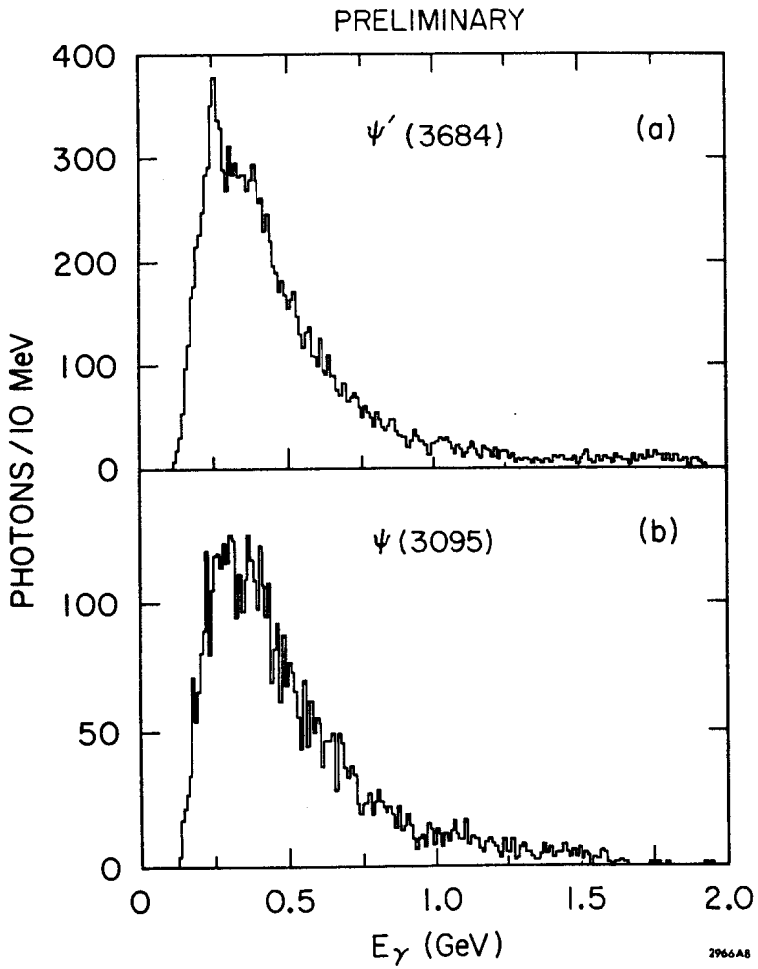

FIG. 36. Inclusive photon energy distributions for a) ψ decays and b) ψ' decays.

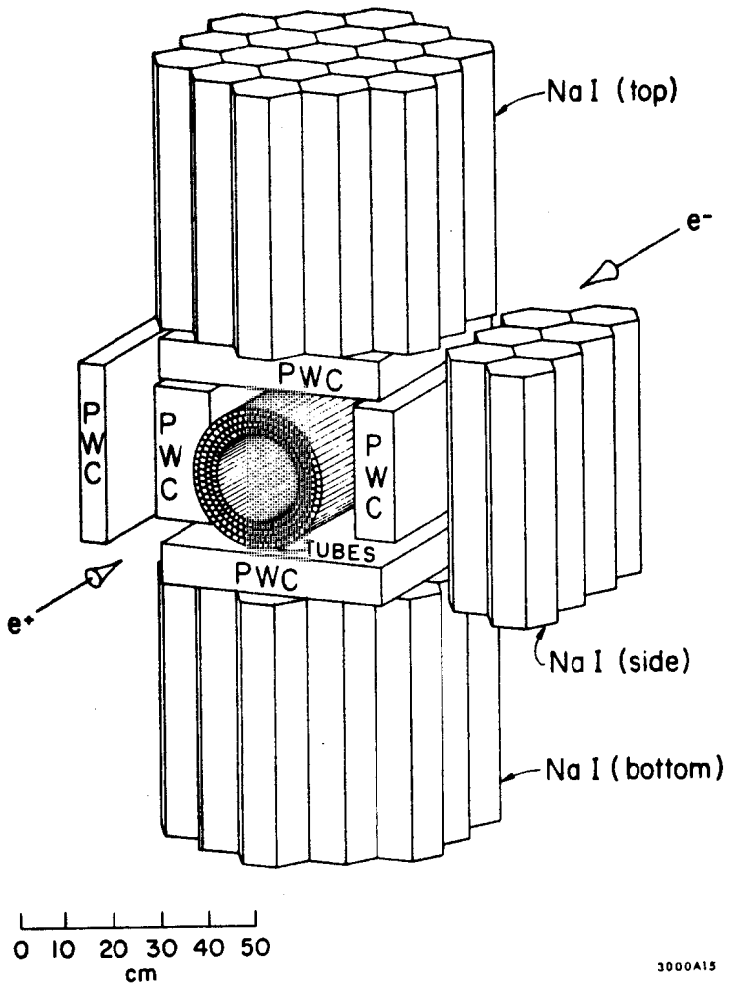

FIG 37. MPPSDSS experiment detector.

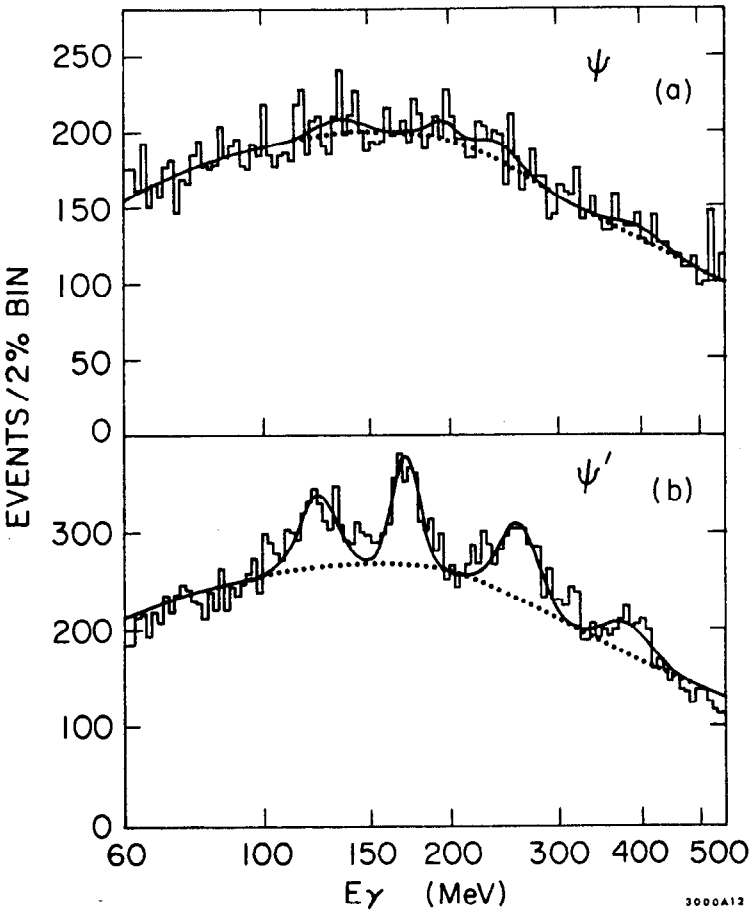

FIG. 38. Inclusive photon energy distributions for a) ψ decays and b) ψ' decays measured by the MPPSDSS experiment.

two experiments agree within errors. For the remainder of this lecture, we use the MPPSDSS branching fractions so that we have a consistent set of values.

VII.F. Is anything missing?

A little over a year ago, before the χ states and direct ψ' decays were found, there was a large fraction of ψ' decays that could not be accounted for.[74] It is now interesting to ask whether the situation has been rectified. The accounting is given in Table IX. There is much less guess work here than was necessary for the ψ (Table VI). We can account for (95 ± 12)% of the ψ' decays. There is still room for new decay modes but they are no longer mandated by the data.

TABLE IX. Summary of ψ' decay modes.

mode	branching fraction (%)
lepton pairs	1.9 ± 0.3
hadrons via second-order e.m. interaction	2.9 ± 0.4
direct decays to ordinary hadrons	9 ± 5
$\psi\pi\pi$, $\psi\eta$	53.3 ± 4.4
$\gamma\chi$	28 ± 10
TOTAL	95 ± 12

χ states

VIII.A. Masses and branching ratios

Table X lists the mass determinations of the χ states. The average values are 3414 ± 4, 3454 ± 7, 3508 ± 4, and 3552 ± 6 MeV/c^2.

Tables XI, XII, and XIII give a compendium of χ branching ratios.

TABLE X. Mass Determinations of the χ States

Masses are referenced to $m_{\psi'} = 3684$ MeV/c^2. See footnote b.

State	Mass (MeV/c^2)	ψ' Decay Mode	Ref.	footnotes
$\chi(3415)$	3415 ± 10	γ + hadrons	78	
	3413 ± 5	monochromatic γ	81	
	3413 ± 10	$\gamma\gamma\psi$	81	a
	3418 ± 7	monochromatic γ	67	
	3412 ± 8	$\gamma\gamma\psi$	61	a,b
average	3414 ± 4			
$\chi(3455)$	3454 ± 7	$\gamma\gamma\psi$	81	c
$\chi(3510)$ or P_c	3500 ± 10	γ + hadrons	78	
	3504 ± 7	$\gamma\gamma\psi$	81	
	3512 ± 7	monochromatic γ	67	
	3512 ± 7	$\gamma\gamma\psi$	61	b
average	3508 ± 4			
$\chi(3550)$	3550 ± 10	γ + hadrons	78	
	3543 ± 7	$\gamma\gamma\psi$	81	
	3561 ± 7	monochromatic γ	67	
average	3552 ± 6			d

a. A total of three events have been observed in $\chi(3415) \to \gamma\psi$, two at DESY and one at SLAC.

b. DESY mass assignments have been increased by 4 MeV/c^2 to correct for the difference in ψ' mass measurements between SLAC and DESY.

c. The existence of this state needs confirmation.

d. Error increased by 30% due to high χ^2.

TABLE XI. Decay Modes of the $\chi(3415)$

The branching fraction for $\psi' \to \gamma\chi(3415)$ is assumed to be 0.10 (Ref. 67). All the values and errors in this Table will scale inversely with this value. See heading for Table IV.

Mode	Fraction (%)	Ref.	footnote
$\gamma\psi$	5. ± 3.	61,81	a
$\pi^+\pi^-$	0.7 ± 0.2	78,(61,88)	
K^+K^-	0.7 ± 0.2	78,(61,88)	
$2\pi^+ 2\pi^-$	3.2 ± 0.6	78,(88)	
$K^+K^-\pi^+\pi^-$	2.7 ± 0.7	78,(88)	
$3\pi^+ 3\pi^-$	1.4 ± 0.5	78,(88)	
$\rho^o\pi^+\pi^-$	1.2 ± 0.4	78	
$K^{o*} K^+ \pi^+$	1.7 ± 0.8	78	
$\gamma\gamma$	< 0.013	61	

a. A total of three events have been observed in $\chi(3415) \to \gamma\psi$, two at DESY and one at SLAC.

TABLE XII. Decay Modes of the $\chi(3510)$ or P_c

The branching fraction for $\psi' \to \gamma\chi(3510)$ is assumed to be 0.09 (Ref. 67). All the values and errors in this Table will scale inversely with this value. See heading for Table IV.

Mode	Fraction (%)	Ref.	footnotes
$\gamma\psi$	30. ± 8.	61,81(87)	
$\pi^+\pi^-$ and K^+K^-	< 0.17	78,(61)	a
$2\pi^+ 2\pi^-$	1.2 ± 0.5	78,(88)	
$K^+K^-\pi^+\pi^-$	0.7 ± 0.3	78,(88)	
$3\pi^+ 3\pi^-$	$\sim$ 1.4	78,(88)	b
$\rho^o\pi^+\pi^-$	0.29 ± 0.24	78	
$K^{o*} K^- \pi^+$	0.35 ± 0.21	78	
$\gamma\gamma$	< 0.015	61	c

a. Forbidden for a $J^{PC} = 1^{++}$ state

b. $\chi(2510) \to 3\pi^+ 3\pi^-$ and $\chi(3550) \to 3\pi^+ 3\pi^-$ are not resolved experimentally. The total combined branching fraction for these two states is $\psi' \to \gamma\chi \to \gamma 3\pi^+ 3\pi^- = (2.5 \pm 0.8) \times 10^{-3}$.

c. Forbidden for a spin 1 particle.

TABLE XIII. Decay Modes of the $\chi(3550)$

The branching fraction for the $\psi' \to \gamma\chi(3550)$ is assumed to be 0.08 (Ref. 67). All the values and errors in this Table will scale inversely with this value. See heading in Table IV.

Mode	Fraction (%)	Ref.	footnote
$\gamma\psi$	12.5 ± 7.5	81	
$\pi^+\pi^-$ and K^+K^-	0.29 ± 0.15	78	
$2\pi^+ 2\pi^-$	2.0 ± 0.5	78,(88)	
$K^+K^-\pi^+\pi^-$	1.8 ± 0.5	78,(88)	
$3\pi^+ 3\pi^-$	$\sim$ 1.6	78,(88)	a
$\rho^o\pi^+\pi^-$	0.62 ± 0.36	78	
$K^{o*} K^- \pi^+$	0.66 ± 0.36	78	

a. $\chi(3510) \to 3\pi^+ 3\pi^-$ and $\chi(3550) \to 3\pi^+ 3\pi^-$ are not resolved experimentally. The total combined branching fraction for these two states is $\psi' \to \gamma\chi \to \gamma 3\pi^+ 3\pi^- = (2.5 \pm 0.8) \times 10^{-3}$.

VIII.B. Spins and parities

Although we have not explicitly determined the spin of any of the χ states, we now have enough information to give an experimentally preferred assignment under the mild, but powerful, assumption that we are dealing with the low lying states of a fermion-antifermion system.

We will assume that the possible spin-parity states are those shown in Fig. 30, 0^-, 0^+, 1^+, and 2^+. We will then go through a series of arguments which will exlcude certain spin-parity assignments for certain states. At the end, if we make the additional assumption that each of the the four spin states should be assigned to one of the four χ states, we obtain a unique solution.

The first piece of evidence for spin assignments comes from χ decays to two pseudoscalars, $\pi^+\pi^-$ or K^+K^-. The possible J^{PC} states for two pseudoscalars are 0^{++}, 1^{++}, 2^{++}, etc. The χ states have **even** C since they are reached by radiative transitions from the ψ'. Therefore any χ state which decays to $\pi^+\pi^-$ or K^+K^- must have $J^P = 0^+$, 2^+, etc. In Fig. 33, there is overwhelming evidence that the χ(3415) decays to $\pi^+\pi^-$ or K^+K^- and there is strong evidence for the χ(3550) decay to $\pi^+\pi^-$ or K^+K^-.

The other technique which can be used to determine χ spins is a study of angular distributions of the photons. The most information comes from the $\psi' \to \gamma\chi \to \gamma\gamma\psi \to \gamma\gamma\mu\mu$ cascade.[92-94] There are five independent angles as illustrated in Fig. 39. For spin 0, the distribution is unique,

$$W(\theta, \phi, \Theta, \theta', \phi') \propto (1 + \cos^2\Theta)(1 + \cos^2\Theta') \ . \qquad (21)$$

For other spins, the distributions are quite complex and depend on which multipoles are excited. A study has been made at SPEAR of these distributions for the χ(3510) using the second method of detecting cascade events

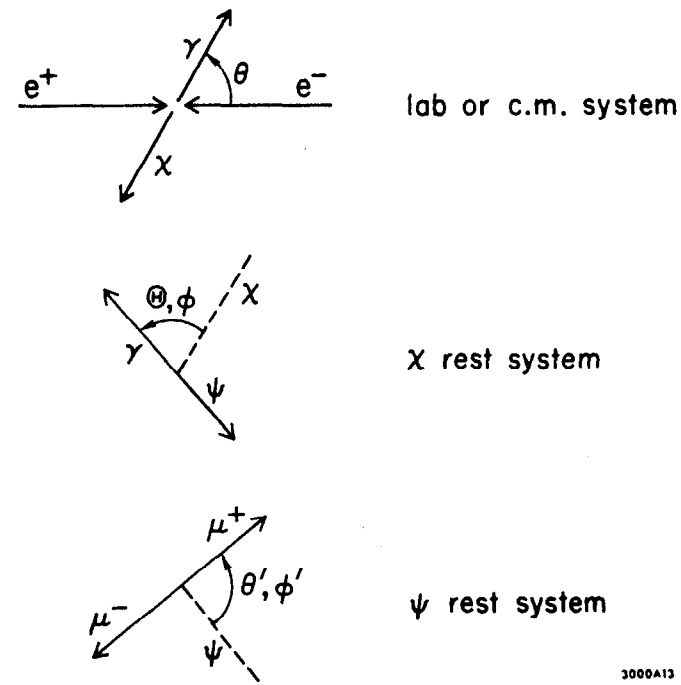

FIG. 39. Definition of angles for the cascade decay $\psi' \to \gamma\chi \to \gamma\gamma\psi \to \gamma\gamma\mu^+\mu^-$.

discussed in Sec. VII.E.2.[77] Preliminary results indicate that the observed distributions completely exclude spin 0. Work is now in progress to determine whether spin 1 or 2 is favored and which multipoles are involved in the decay.

The DESY-Heidelberg collaboration has also concluded that the $\chi(3510)$ spin is not zero by just studying the θ distribution.

The angular distribution of the photon in the production of the $\chi(3415)$ and the $\chi(3550)$ has been studied in $\chi \to 4\pi$ and $\chi \to K^+K^-\pi^+\pi^-$ decays.[78] Figure 40 shows the θ distributions when χ's are detected in these modes. The angular distribution must be of the form

$$W(\theta) \propto 1 + \alpha \cos^2\theta \,, \tag{22}$$

and from Eq. 21 $\alpha = 1$ for spin 0. Fits for α to the data of Fig. 40 give

$$\alpha = 0.21 \,^{+\,0.39}_{-\,0.31} \text{ for } \chi(3550), \tag{23a}$$

$$\alpha = 0.25 \,^{+\,0.56}_{-\,0.38} \text{ for } \chi(3510) \,, \tag{23b}$$

and

$$\alpha = 1.37 \,^{+\,0.51}_{-\,0.41} \text{ for } \chi(3415) \,, \tag{23c}$$

Thus, the X(3415) is consistent with spin 0, but the X(3550) is inconsistent with spin 0 to about two standard deviations.

All of these arguments are summarized in Table XIV. A number of conclusions can be drawn: Without any assumptions, none of the three well established states, X(3415), X(3510), or X(3550), can be a pseudoscalar. Also if the X(3550) has a spin below 4, its spin-parity must be 2^+. If we assume that the four candidate spin states each correspond to

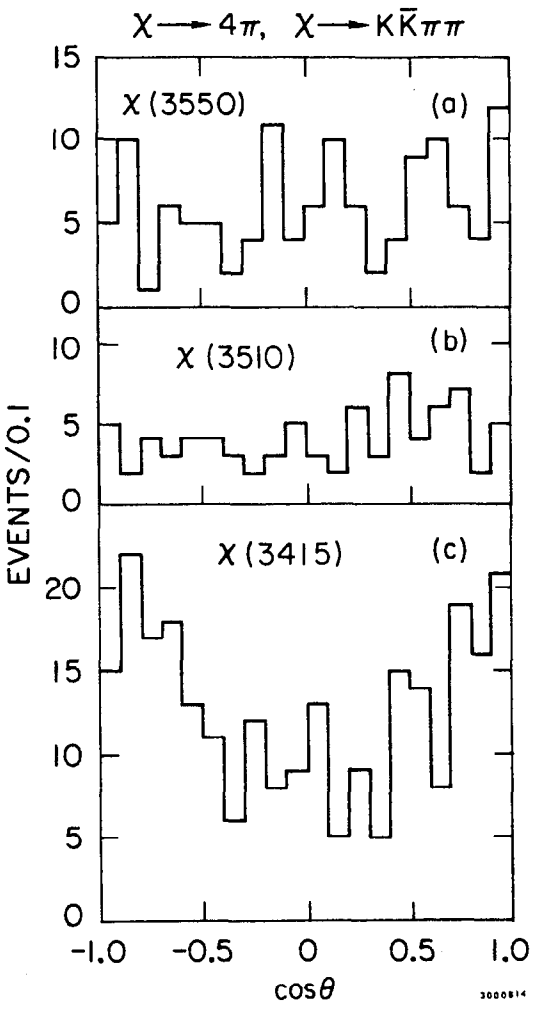

FIG. 40. Distribution of cos ϕ for $\psi' \to \gamma\chi$, $\chi \to 2\pi^+2\pi^-$ or $K^+K^-\pi^+\pi^-$.

one of the four χ states, there is a unique assignment:

State	J^P
χ(3550)	2^+
χ(3510)	1^+
χ(3445)	0^-
χ(3415)	0^+ .

Note that the χ(3455) has been assigned to be a pseudoscalar, not because we know anything about it, but because that was the only slot left. There are other possibilities. Jaffe suggested that this state could be an exotic[96] and Harari suggested that it could be a singlet D state, $J^{PC} = 2^{-+}$.[97]

TABLE XIV. Spin assignments of the X states. The preferred assignments depend on assumptions discussed in the text.

State/J^P	0^-	0^+	1^+	2^+
χ(3550)	excluded by $\chi \to \pi^+\pi^-$ or K^+K^- and by angular distribution in $\psi' \to \gamma\chi \to \gamma$ hadrons	excluded by angular distribution in $\psi' \to \gamma\chi \to \gamma$ hadrons	excluded by $\chi \to \pi^+\pi^-$ or K^+K^-	preferred
χ(3510)	excluded by angular distribution in $\psi' \to \gamma\chi \to \gamma\gamma\psi$	excluded by angular distribution in $\psi' \to \gamma\chi \to \gamma\gamma\psi$	preferred	
χ(3455)	preferred			
χ(3415)	excluded by $\chi' \to \pi^+\pi^-$ or K^+K^-	preferred	excluded by $\chi \to \pi^+\pi^-$ or K^+K^-	

VIII.C. Comparisons to theoretical models.

The data on P states appear to be in reasonable agreement with most charmonium models. First, the order of the states is correct. In all models the 2^+ state should be heaviest and the 0^+ state should be lightest. Second, the ratio of $\psi' \to \gamma\chi$ partial widths is in agreement with simplest assumption: that they should be proportional to the phase space factor for dipole transitions. We expect:

$$\Gamma(\psi' \to \chi(3550)) : \Gamma(\psi' \to \chi(3510)) : \Gamma(\psi' \to \chi(3415)$$
$$= 5k^3 : 3k^3 : k^3$$
$$= 1.0 : 1.4 : 1.6 , \qquad (24a)$$

where k is the available momentum and the coefficients are spin factors. With large errors the observed values are:

$$1.0 : 1.1 : 1.25 . \qquad (24b)$$

The χ(3510) has a larger branching fraction to γψ than either the χ(3415) or χ(3550), presumably due to a suppression of χ(3510) → hadrons. This behavior was expected for 1^+ P state in models in which C-even states decays to hadrons via two massless vector gluons.[98] Since a spin 1 particle cannot decay into two massless vector particles, these decays are suppressed.

The assignment of the χ(3455) as the η_c' appears to be in strong disagreement with models where it decays via two vector gluons. Chanowitz and Gilman[99] point out that from $\psi' \to \gamma\eta_c$ has the same matrix element as $\eta_c' \to \gamma\psi$. Accounting for phase space,

$$\Gamma(\chi(3455) \to \gamma\psi) \approx \tfrac{1}{4}\Gamma(\psi' \to \gamma\eta_c) , \qquad (25)$$

from which we can conservatively deduce

$$\Gamma(\chi(3455) \to \text{all}) < 5 \text{ KeV} \quad , \tag{26}$$

whereas one expects a width of several MeV in these models.

IX. The X(2800)

Two experiments at DORIS have reported evidence for a state at about 2800 MeV/c^2 which is detected in the sequence $\psi \to \gamma X \to \gamma\gamma\gamma$.[61,62] Only the photon angles are measured and a 1-C fit is performed. Backgrounds are $\psi \to \gamma\eta$, $\psi \to \gamma\eta'$, and radiative (non-resonant) two photon production.

The original data were not completely conclusive, so additional data were collected at DORIS. Peter Schmuser will report the new DASP results in the topical conference,[65] so we will not cover the details here.

Unfortunately, the new DASP results are still not completely conclusive. There is a slightly over three standard deviation signal, but this level of significance is generally not considered sufficient to establish a new particle. New results from the DESY-Heidelberg group are not available yet; these results may help to clarify the situation.

No experiment at SPEAR has been sensitive to the three photon mode. Originally, it was reported that $\psi \to \gamma\chi \to \gamma p\bar{p}$ with a branching fraction of about 2×10^{-4}, based on the observation of two events.[61] This result was later withdrawn, but in the meantime a search was made for the $\gamma p\bar{p}$ decay mode in the SPEAR magnetic detector. The background is $\psi \to p\bar{p}\pi^0$ since a π^0 and photon will not be completely separable by missing mass. The data are shown in Fig. 41. There is no sign of the X(2800) and an upper limit on the branching fraction for $\psi \to \gamma X \to \gamma p\bar{p}$ can be set at 4×10^{-5}. Searches for X(2800) decays into other hadronic modes have all been unsuccessful, but none of the limits are small enough to be conclusive.

The status of the X(2800) and the X(3455) are quite similar. We

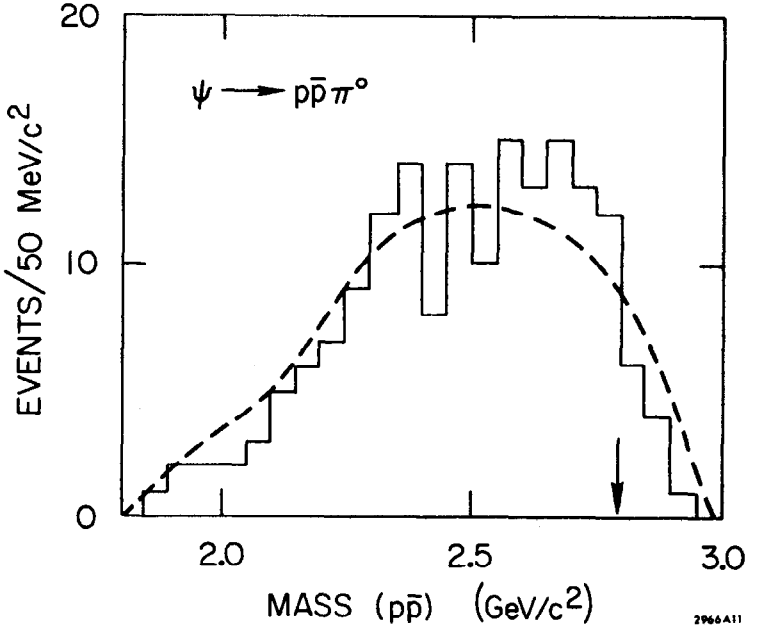

FIG. 41. Invariant mass of $p\bar{p}$ in $\psi \to p\bar{p}\pi^0$ or $p\bar{p}\gamma$ decays.

have enough evidence to take these states seriously, but not enough to establish them. Confirmation of both is badly needed.

X. Summary

In less than two years after the discovery of the ψ, we have learned a a great deal about it and its relatives. In some cases we understand a state of charmonium better than its analogue in light quarks. An attempt to summarize as much of this information as possible on one page is made in Fig. 42.

As we look to future work in this field it is clear that a great deal of it should and will go into understanding the structure of the charmonium states in the 4 GeV region and into studying the spectroscopy of charmed particles. There is, however, more work that should be done on ψ and ψ' decays. Below is a list in no particular order. Some of these items can be worked on now, others will have to await better detectors.

1) The status of the 0^- states is clearly the outstanding question. The masses and transition widths to these states are crucial parameters for charmonium calculations.

2) Although we now have a preferred set of X spin assignments, it is important to determine the spins directly without imposing assumptions on the possible values.

3) There is still a missing P state, the singlet 1^{+-} state. The best way of finding it may be in the $\chi(3550) \to \gamma\, 1^{+-}$ decay.

4) The direct ψ' decays to ordinary hadrons needs much more study. Much more can be done with just the present data.

5) The suggestions that there is $c\bar{c}$ mixing with the lighter quarks in the pseudoscalar states should be followed up. We have seen evidence

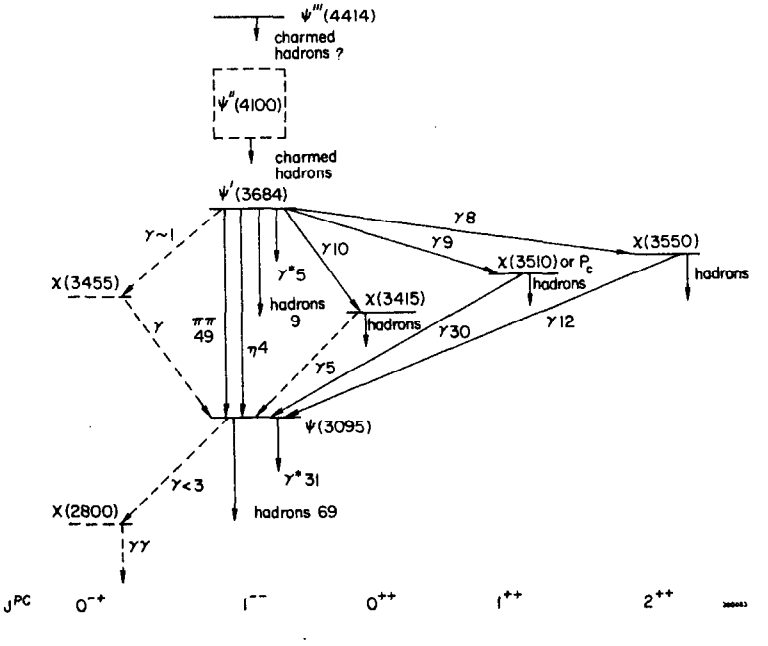

FIG. 42. Summary of observed charmonium states and transitions. Uncertain states and transitions are indicated by dashed lines. Numbers indicate branching fractions in per cent.

for it in radiative ψ decays and in the rate of $\psi' \to \psi\eta$. Inclusive and exclusive state studies of η and η' production in ψ decays would be useful for the further study of this possible mixing.

6) Finally there is a great deal of bread and butter physics to be done. We can imagine mega- and multimega-event runs with powerful second generation detectors. Systematic measurements of all ψ and ψ' decay modes from these data could have three separate objectives:

a) To study the dynamics of charmonium annihilation.

b) To study ordinary hadron spectroscopy from a new perspective. In Sec. IV.D, we saw that ψ decays to PV and VT mesons were allowed and that all channels were populated approximately equally. The scalar (S) and axial vector (A^+, A^-) multiplets of ordinary mesons are not well understood yet. By studying the allowed VS, VA^+, and PA^- ψ decays we may gain new insight into them. Note that the possible ϕS^* decay discussed in Sec. IV.E is a VS type decay; by SU(3) all the others should be present too.

c) And finally, to look for surprises which may provide the germ of the next level of understanding.

REFERENCES

1. G. Goldhaber et al., Phys. Rev. Lett. 37, 255(1976).
2. I. Peruzzi et al., Phys. Rev. Lett. 37, 569(1976).
3. D. Hitlin, these proceedings.
4. G. Goldhaber, these proceedings.
5. V.L. Auslander et al., Phys. Lett. B25, 433(1967).
6. V.L. Auslander et al., Sov. J. Nucl. Phys. 9, 114(1969).
7. V.E. Balakin et al., Phys. Lett. B34, 328(1971).
8. L.M. Kurdadze et al., Phys. Lett. B42, 515(1972).
9. J.-E. Augustin et al., Phys. Lett. B28, 508(1969).
10. J.-E. Augustin et al., Phys. Lett. B28, 513(1969).
11. J.-E. Augustin et al., Phys. Lett. B28, 517(1969).
12. J.C. Bizot et al., Phys. Lett. B32, 916(1970).
13. D. Benakas et al., Phys. Lett. B39, 289(1972).
14. G. Cosme et al., Phys. Lett. B40, 685(1972).
15. D. Benakas et al., Phys. Lett. B42, 507(1972).
16. B. Bartoli et al., Phys. Rev. D6, 2374(1972).
17. C. Bacci et al., Phys. Lett. B44, 533(1973).
18. M. Grilli et al., Nuovo Cimento 13A, 593(1973).
19. F. Ceradini et al., Phys. Lett. B47, 80(1973).
20. M. Bernardini et al., Phys. Lett. B51, 200(1974).
21. A. Litke et al., Phys. Rev. Lett. 30, 1189(1973).
22. G. Tarnospolsky et al., Phys. Rev. Lett. 32, 432(1974).
23. J.-E. Augustin et al., Phys. Rev. Lett. 34, 764(1975).
24. A.M. Boyarski et al., Phys. Rev. Lett. 34, 1357(1975).
25. V. Lüth et al., Phys. Rev. Lett. 35, 1124(1975).
26. J. Siegrist et al., Phys. Rev. Lett. 36, 700(1976).

27. R.F. Schwitters in Proceedings of the 1975 International Symposium on Lepton and Photon Interactions at High Energies (Stanford University, 1975). p. 5.
28. S. Okubo, Phys. Lett. 5, 165(1963).
29. G. Zweig, unpublished work (1964).
30. J. Iizuka, Suppl. Prog. Theor. Phys. 37-38, 21(1966).
31. J.D. Jackson, these proceedings.
32. D.R. Yennie, Phys. Rev. Lett. 34, 239(1975).
33. A.M. Boyarski et al., Phys. Rev. Lett 34, 762(1975).
34. G.S. Abrams et al., Phys. Rev. Lett. 33, 1453(1974).
35. H.L. Lynch, SLAC report number SLAC-PUB-1750, (1976).
36. D.C. Hom et al., Phys. Rev. Lett. 36, 1236(1976).
37. D. Eartly, G. Giacomelli, and K. Pretzl, Phys. Rev. Lett. 36, 1355(1976).
38. T. Appelquist and H.D. Politzer, Phys. Rev. Lett. 34, 43(1975).
39. J.-E. Augustin et al., Phys. Rev. Lett. 34 233(1975).
40. G.J. Feldman and M.L. Perl, Phys. Rep. 19C 233(1975), Appendix A.
41. W. Braunschweig et al., Phys. Lett. 53B, 393(1974).
42. W. Braunschweig et al., Phys. Lett. 56B, 491(1975).
43. R. Baldini-Celio et al., Phys. Lett. 58B, 471(1975).
44. B. Esposito et al., Lett. Nuovo Cimento 14, 73(1975).
45. C. Bemporad in Proceedings of the 1975 International Symposium on Lepton and Photon Interactions at High Energies (Stanford University, 1975), p. 113.
46. R.L. Ford et al., Phys. Rev. Lett. 34, 604(1975).
47. L. Criegee et al., DESY report 75/32 (1975).
48. A.D. Lieberman in Proceedings of the 1975 International Symposium on Lepton and Photon Interactions at High Energies (Stanford University, 1975), p. 55
49. W. Brauschweig et al., Phys. Lett. 63B, 487(1976).
50. G. Wolf, Proceedings of the International Meeting on Storage Ring Physics., Flaine, France, Feb. 22-28, 1976 (to be published).
51. G.J. Feldman, internal SLAC-LBL memorandum (quoted in ref. 50).
52. B. Jean-Marie et al., Phys. Rev. Lett. 36, 291(1976).
53. F. Vannucci, internal SLAC-LBL memorandum.
54. F. Vannucci et al., SLAC report SLAC-PUB-1724 (1976).
55. G.S. Abrams in Proceedings of the 1975 International Symposium on Lepton and Photon Interactions at High Energies (Stanford University, 1975) p. 25.
56. G. Goldhaber, LBL report number LBL-4884 (1976).
57. I. Peruzzi and M. Piccolo, and S.M. Alam, SLAC-LBL internal memoranda.
58. G. Goldhaber, LBL report number LBL-4224 (1975).
59. G. Goldhaber, SLAC-LBL internal memorandum.
60. C. Bacci et al., Lett. Nuovo Cimento 12, 269(1975).
61. B. Wiik in Proceedings of the 1975 International Symposium of Lepton and Photon Interactions at High Energies (Stanford University, 1975), p. 69.
62. J. Heintze in Proceedings of the 1975 International Symposium on Lepton and Photon Interactions at High Energies (Stanford University, 1975), p. 97.
63. R. Baldini-Celio, Phys. Lett. 58B, 475(1975).
65. P. Schmuser, these proceedings.
66. W. Bartel et al., DESY report number 76/40 (1976).

67. D.H. Badtke et al., paper submitted to the XVIII International Conference on High Energy Physics, Tbilisi, USSR, July 15-21, 1976; D.E. Lyon and J.G. Smith, private communications.
68. F.J. Gilman, SLAC report SLAC-PUB-1600 (1975).
69. This mechanism was first suggested to us by F.J. Gilman.
70. R.N. Cahn and M.S. Chanowitz, Phys. Lett. 59B, 277(1976).
71. H. Harari, Phys. Lett. 60B, 172(1976).
72. I am grateful to F.J. Gilman for pointing out several calculational errors in the original table.
73. E. Hilger et al., Phys. Rev. Lett. 35, 625(1975).
74. V. Lüth, SLAC report SLAC-PUB-1599 (1975).
75. G.S. Abrams, et al., Phys. Rev. Lett. 34, 1181(1975).
76. W. Tanenbaum et al., Phys. Rev. Lett. 36, 402(1976).
77. W. Tanenbaum, SLAC-LBL internal memorandum and private communication.
78. F.M. Pierre, LBL report number LBL-5324.
79. C.J. Feldman, SLAC-LBL internal memorandum.
80. E.B. Hughes et al., Phys. Rev. Lett. 36, 76(1976).
81. J.S. Whitaker et al., SLAC report SLAC-PUB-1817 (1976).
82. C.G. Callan et al., Phys. Rev. Lett 34, 52(1975).
83. T. Appelquist et al., Phys. Rev. Lett. 34, 365(1975).
84. E. Eichten et al., Phys. Rev. Lett. 34, 369(1975).
85. B.J. Harrington et al., Phys. Rev. Lett. 34, 706(1975).
86. J.D. Bjorken and S.L. Glashow, Phys. Lett. 11, 255(1964).
87. W. Braunschweig et al., Phys. Lett. 57B, 407(1975).
88. G.J. Feldman et al., Phys. Rev. Lett. 35 821(1975).
89. G.H. Trilling, these proceedings.
90. W. Tanenbaum et al., Phys. Rev. Lett. 35, 1323(1975).
91. S. Orito, Invited talk at the New Physics Meeting, Rutherford Laboratory, Chilton, Didcot, England, February 18-20, 1976.
92. G. Karl, S. Meshkov, J.L. Rosner, Phys. Rev. D13, 1203(1976).
93. L.S. Brown and R.N. Cahn, Phys. Rev. D13, 1195(1976).
94. P.K. Kabir and A.J.G. Hey, Phys. Rev. D13, 3161(1976).
95. H. Rieseberg, Invited talk at the 2nd International Conference at Vanderbilt University on New Results in High Energy Physics, Nashville, Tennessee, March 1-3, 1976.
96. R.L. Jaffe, comments during the discussion period.
97. H. Harari, CERN report Th.2222-CERN (1976).
98. R. Barbieri, R. Gatto, and E. Remiddi, Phys. Lett. 61B, 465(1976).
99. M.S. Chanowitz and F.J. Gilman, Phys. Lett. 63B, 178(1976).

A NEW LEPTON?

Gary J. Feldman

Stanford Linear Accelerator Center
Stanford University, Stanford, California

CONTENTS

I. Introduction

II. Existence of anomalous eμ events

- A. Original data
- B. Muon tower data
- C. Other experiments

III. Hypotheses for the origin of the anomalous eμ events

IV. Properties of the anomalous eμ events

- A. Colinearity angle distribution
- B. Momentum spectrum
- C. Are there missing hadrons?
- D. Conclusion

V. Consistency checks to the hypotheses of a new lepton

- A. Point-like energy dependence
- B. Total e^+e^- annihilation cross section
- C. Leptonic branching fraction
- D. Anomalous ee and μμ events
- E. Anomalous μ-hadron events
- F. Inclusive anomalous two-prong μ events

VI. Summary

I. Introduction

In this third lecture we will review the data and arguments which are leading us to the conclusion that a new charged lepton exists in the mass range 1.6 to 2.0 GeV/c^2. We will first discuss the evidence for the existence of anomalous eμ events. Next we will consider the properties of these events and conclude that the only simple hypothesis compatible with all the data is that these events come from the decay of pairs of new leptons. Accepting this as a working hypothesis we will then investigate six predictions of this hypothesis.

The nature of the material in this lecture will force us to concentrate on experimental details to a much greater extent than in the first two lectures. For this reason it is worthwhile to review the properties of the SLAC-LBL magnetic detector at SPEAR.[1,2] Figure 1 shows a side view of the detector. The trigger for an event is two or more charged particles each of which fires a trigger and shower counter. These counters subtend about 65% of the solid angle. Charge particles are detected and momentum analyzed by the cylindrical spark chambers over about 70% of the solid angle.

Electrons are identified solely by the presence of a large pulse height in the shower counters. The criterion that was applied for most of the analysis was that the pulse height be greater than that of a 500 MeV electron. As we will see, hadrons will be misidentified as electrons roughly 20% of the time.

The shower counters are also useful for the detection of photons. The detection efficiency for photons is 50% at 100 MeV and rises to over 90% at 250 MeV.

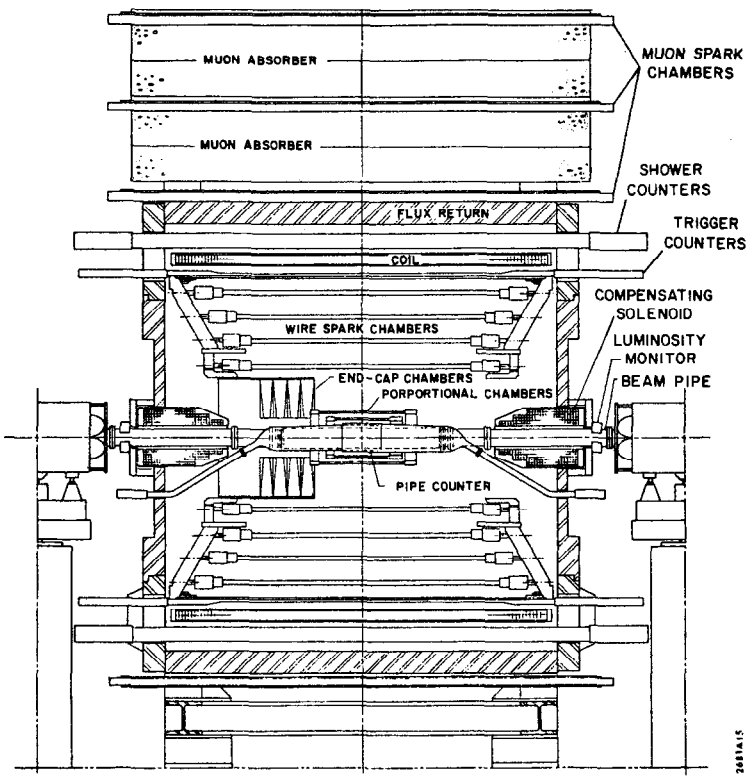

FIG. 1. Side view cross section of the SLAC-LBL magnetic detector at SPEAR

Muons are identified by penetrating the coil, shower counters, and the 20 cm iron flux return and by being detected in a muon spark chamber. Since this material only corresponds to about 1.7 hadronic interaction lengths, there is roughly a 20% probability that a hadron will be misidentified as a muon. Starting in January 1975, additional muon detectors were added above the main detector. These detectors, called the muon tower, consist of two 222 gm/cm^2 thick barite-loaded concrete slabs each followed by spark chambers. The muon tower subtends only 9% of the total solid angle, but provides much smaller hadron misidentification.

II. Existence of anomalous $e\mu$ events

II.A. Original data

The anomalous signal is an electron, a muon and no other charged or neutral particles detected in the detector. We have now observed about 180 of these events with an estimated background of about 45 events.

To illustrate how these events are found and the nature of the backgrounds, it is pedagogically easiest to consider the original data in which the signal was discovered.[3] One reason for this is that the muon spark chambers covered the full azimuthal angle for these data (Fig. 2, SPEAR I), while for later data the side chambers were moved to the muon tower (Fig. 2, SPEAR II). These modifications do not change the basic analysis, but make it slightly more complicated.

The motivation for searching for this signal was in fact to look for a new sequential lepton,

$$e^+e^- \to L^+L^- \begin{cases} \to e^- \bar{\nu}_e \nu_L \\ \to \mu^+ \nu_\mu \bar{\nu}_L \end{cases} . \qquad (1)$$

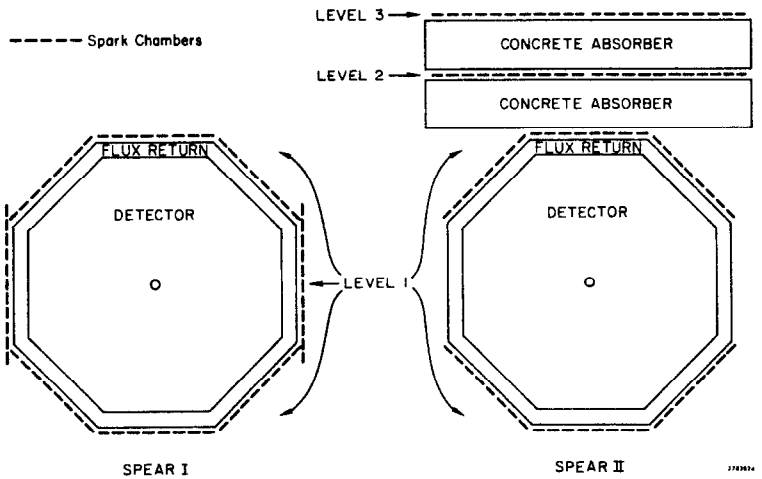

FIG. 2. Configuration of the magnetic detector muon identification system for SPEAR I and SPEAR II.

To find such events the following criteria were used:

1) two and only two charged tracks,
2) the two prongs acoplanar with the incident beams by at least 20° (to help eliminate backgrounds from radiative lepton pairs),
3) both momenta over 650 MeV/c (to reduce misidentification of hadrons as leptons),
4) no extra shower counters firing (since there should be no photons in the event), and
5) the two prongs should be oppositely charged.

Table I contains the events satisfying criteria 1 through 3 for a sample of events taken at E_{cm} = 4.8 GeV. The events are categorized by the identification of the prongs, whether they have the same or opposite charge, and by the number of detected photons. The 24 $e\mu$ events with no associated photons are the events that we wish to investigate to see if they could come from well known sources. One possible source is the two-virtual-photon process $e^+ + e^- \rightarrow e^+ + e^- + \mu^+ + \mu^-$. Calculations indicate that this source is negligible, and the absence of $e\mu$ events with charge 2 confirms this point since the number of charge 2 $e\mu$ events should equal the number of charge 0 $e\mu$ events from this source.

We determine the background from hadron misidentification or decay by using three-or-more-prong events and assuming that every particle called an e or a μ by the detector either was a misidentified hadron or came from the decay of a hadron. We use $P_{h \rightarrow l}$ to designate the sum of the probabilities for misidentification or decay causing a hadron h to be called a lepton l. Since the P's are momentum dependent we use all the

TABLE I. Distribution of 513 two-prong events, obtained in the SPEAR I configuration at $E_{c.m.} = 4.8$ GeV, which meet the criteria listed in the text. Events are classified according to the number N_γ of photons detected, the total charge, and the nature of the particles. All particles not identified as e or μ are called h for hadron.

	N_γ	0	1	>1	0	1	>1
Particles		Total charge = 0			Total charge = ±2		
ee		40	111	55	0	1	0
eμ		24	8	8	0	0	3
μμ		16	15	6	0	0	0
eh		20	21	32	2	3	3
μh		17	14	31	4	0	5
hh		14	10	30	10	4	6

eh, μh, and hh events in column 1 of Table 1 to determine a "hadron" momentum spectrum, and weight the P's accordingly. We obtain the momentum-averaged probabilities $P_{h \to e} = 0.183 \pm 0.007$ and $P_{h \to \mu} = 0.198 \pm 0.007$. Collinear ee and μμ events are used to determine $P_{e \to h} = 0.056 \pm 0.02$, $P_{e \to \mu} = 0.011 \pm 0.01$, $P_{\mu \to h} = 0.08 \pm 0.02$, $P_{\mu \to e} < 0.01$.

Using these probabilities and assuming that all eh and μh events in Table I result from particle misidentifications or particle decays, we calculate the corrected number of events for column 1 of Table I in Table II. The total eμ background is then 4.6 ± 1.2 events. The statistical probability of such a number yielding the 24 signature eμ events is very small. The same analysis applied to columns 2 and 3 of Table I yields 5.6 ± 1.5 eμ background events for column 2 and 8.6 ± 2.0 eμ background events for column 3, both consistent with the observed number of eμ events.

II.B. Muon tower data

We now have sufficient data analyzed by the above methods (about 180 events with about 45 background) that a statistical fluctuation is completely out of the question. The only valid question is whether the background has been calculated correctly.

For this reason it is worthwhile to look at a subset of the data in which the backgrounds due to misidentifications will be smaller. This is possible using data from the muon tower. We will refer to muons being identified at three levels (see Fig. 2). Level 1 corresponds to particles which penetrate the shower counters, the coil, and the flux return. The original data were analyzed exclusively at this level. Level

TABLE II. Corrections to data from column 1 of Table I.

Particles	events	from ee	from μμ	from hh	corrected events
ee	40		0	1.5 ± 0.3	44.3 ± 6.9
eμ	24	1.0 ± 1.0	< 0.3	3.3 ± 0.6	19.7 ± 5.3
μμ	16	0		1.8 ± 0.3	17.0 ± 4.5
eh	18	4.7 ± 1.7	0	10.2 ± 1.8	3.1 ± 5.7
μh	15	0	2.8 ± 0.7	11.0 ± 10	1.2 ± 5.4
hh	13	0.1 ± 0.1	0		40.7 ± 6.4

2 or 3 correspnds to particles which penetrate level 1 and one or two of the concrete slabs.

We take all SPEAR II data with $E_{c.m.}$ ranging from 3.9 to 7.8 GeV and require that

a) two and only two oppositely charged tracks be visible in the detector, and no photons be visible in the shower counters.

b) both momenta be over 650 MeV/c,

c) one particle be a muon candidate at level 2 or 3 and the other particle be a muon candidate at level 1,

d) the two particles be acoplanar by at least 20°,

e) the square of the missing mass recoiling against the two particles be greater than 1.5 $(GeV/c^2)^2$.

A muon candidate is defined as a particle which has sufficient momentum and is heading in the right direction to be seen in a muon spark chamber if it were a muon. The last two requirements are included to reduce the number of radiative e^+e^- and $\mu^+\mu^-$ pairs.

A total of 109 events satisfied these criteria. Fifteen were identified as e^+e^-, 18 events were identified as $\mu^+\mu^-$, and the other 76 events were identified as other combinations of e's, μ's, and hadrons, including 13 events which appear to be an eμ pair with the μ identified at level 2 or 3.

We now want to calculate the number of eμ events which would be expected to occur from misidentifications of known processes. We determine the probability that an electron is identified as a muon or vice versa by studying collinear lepton pairs. The probability that an electron gives a small pulse height in a shower counter and also gives a signal at levels 1 and 2 in the muon tower is less than 2×10^{-3}. And the probability

that a muon both gives a large pulse height in the shower counter and fails to fire a muon chamber is less than 3×10^{-3}. The probability for a hadron to be identified as an electron is the same as in Sec. II.A, about 0.18. The probability for a hadron to be misidentified as a muon in the tower was calculated with the aid of the Oak Ridge High Energy Nucleon-meson Transport Code HETC.[4] For the momenta involved in this case it averages 0.033.

We take the number of ee and μμ events detected as the number of true ee and μμ events and make the conservative assumption that the other 76 events come from multihadronic events in which all but two charged hadrons were undetected. The arithmetic is summarized in Table III. The expected number of background events in the 13 eμ events is 0.53. The statistical probability of backgrounds accounting for all 13 events is completely negligible.

Figure 3 shows a computer reconstruction of an eμ event in the muon tower. The event occurred in $E_{c.m.} = 6.6$ GeV. The positively charged particle heading into the muon tower is clearly identified as a muon. It has a momentum of 1.6 GeV/c. The other particle has a negative charge and a momentum of 1.0 GeV/c and is identified as an electron by the large pulse height (113 units) in the shower counter. On the average, a 1.0 GeV electron typically gives a pulse height of 100 in a shower counter.

II.C. Other experiments

The DASP collaboration has announced "one extremely clean" eμ event with no additional detected charged or neutral particles.[5] At the Topical Conference, Hinrich Meyer will report on 6 eμ events from the Pluto experiment.[6]

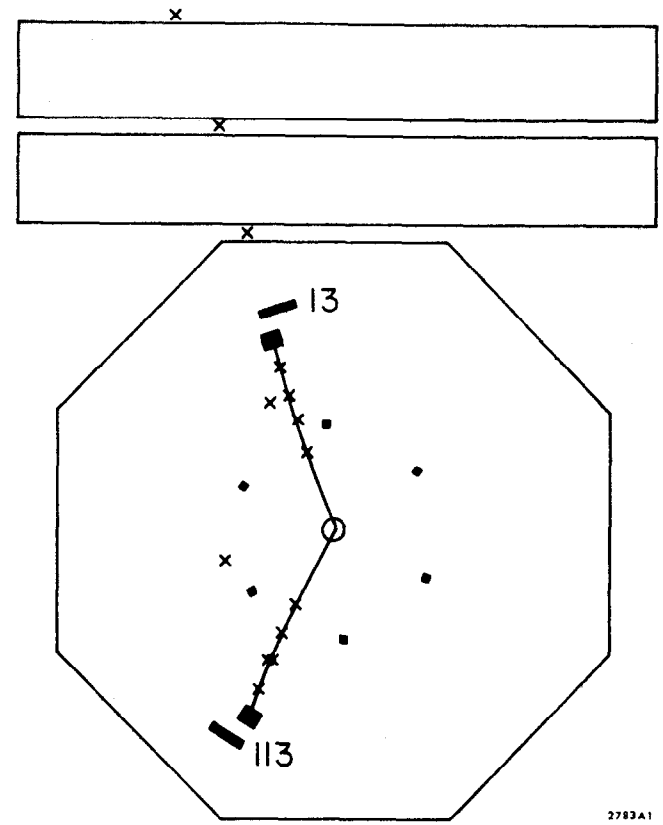

FIG. 3. Computer reconstruction of an eμ event. The numbers indicate shower counter pulse heights.

TABLE III

Calculation of expected backgrounds from misidentifications to the 13 eμ events observed in the muon tower.

mode	events	misidentification probability	expected background
ee	15	0.002	0.03
μμ	18	0.003	0.05
hh	76	0.18 × 0.033	0.45
total	109		0.53

Given all these data, we take the existence of the anomalous eμ signal to be established. We now address ourselves to the question What is it?

III. Hypotheses for the origin of the anomalous eμ events

We can imagine several hypothetical new processes which could account for these events. One possibility is the process which motivated the search in the first place, the leptonic decays of a new sequential lepton

$$e^+e^- \to L^+L^- \quad \begin{cases} \to e^- \bar{\nu}_e \nu_L \\ \to \mu^+ \nu_\mu \bar{\nu}_L \end{cases} \qquad (1)$$

A second possibility is that these events result from the two-body leptonic decay of a charged (and presumably vector) meson,

$$e^+e^- \to V^+V^- \quad \begin{cases} \to e^- \bar{\nu}_e \\ \to \mu^+ \nu_\mu \end{cases} \qquad (2)$$

And a third possibility is that these events arise from semileptonic decays of new mesons, for example

$$e^+e^- \to M^+M^- \quad \begin{cases} \to e^- \bar{\nu}_e K^0 \\ \to \mu^+ \nu_\mu \bar{K}^0 \end{cases} \qquad (3a)$$

or

$$e^+e^- \to M^0\bar{M}^0 \quad \begin{cases} \to e^- \bar{\nu}_e K^0 \\ \to \mu^+ \nu_\mu K^- \end{cases} \qquad (3b)$$

To decide between these hypotheses, we will want to determine

1) whether the decay is two-body or three-body, and

2) whether there are undetected hadrons in the decay.

IV. Properties of the anomalous eμ events[7]

IV.A. Colinearity angle distribution

Evidence that the origin of these events is the decay of a pair of new particles is obtained from the distribution of the angles between the two prongs. Figure 4 shows the distribution of the cosine of the colli-nearity angle for three E_{cm} regions. At low energy the angles are much more uncorrelated than at high energy. This is characteristic of the decay of a pair of fixed mass particles; as the energy increases, the Lorentz transformation forces the decay products back to back. The data in Fig. 4 have been corrected for background events, which do not exhibit this behavior (Fig. 5).

IV.B. Momentum spectrum

From the inclusive momentum spectrum we can obtain information on the number of particles in the decay. To combine data from different

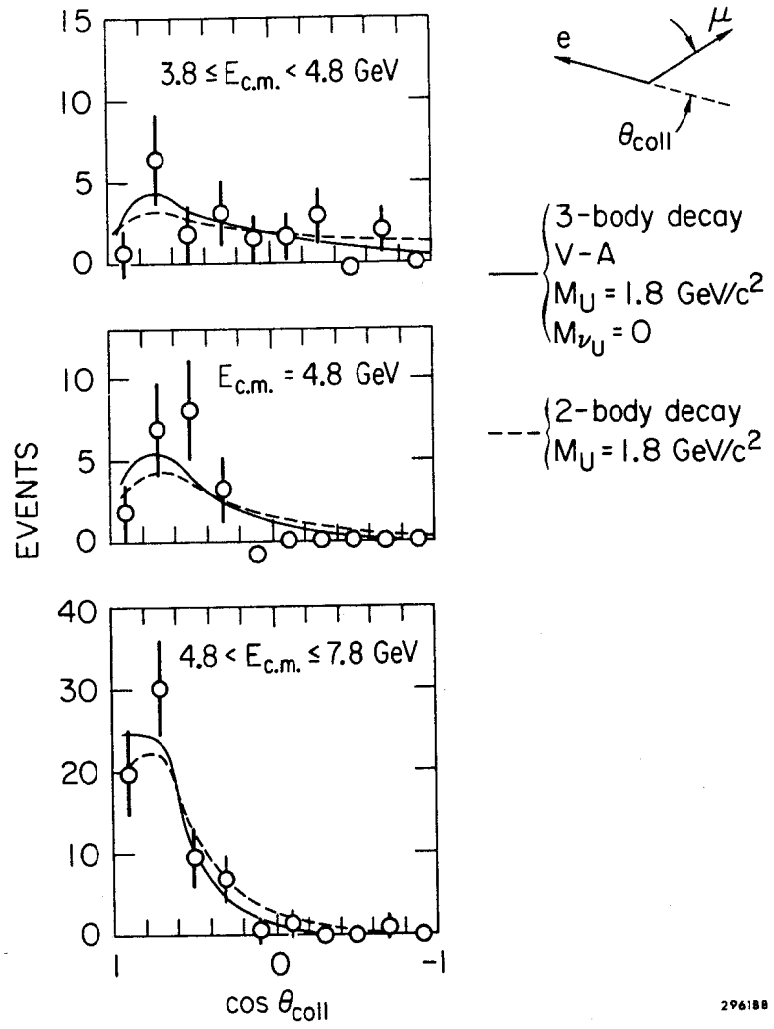

FIG. 4. Cosine of the colinearity angle.

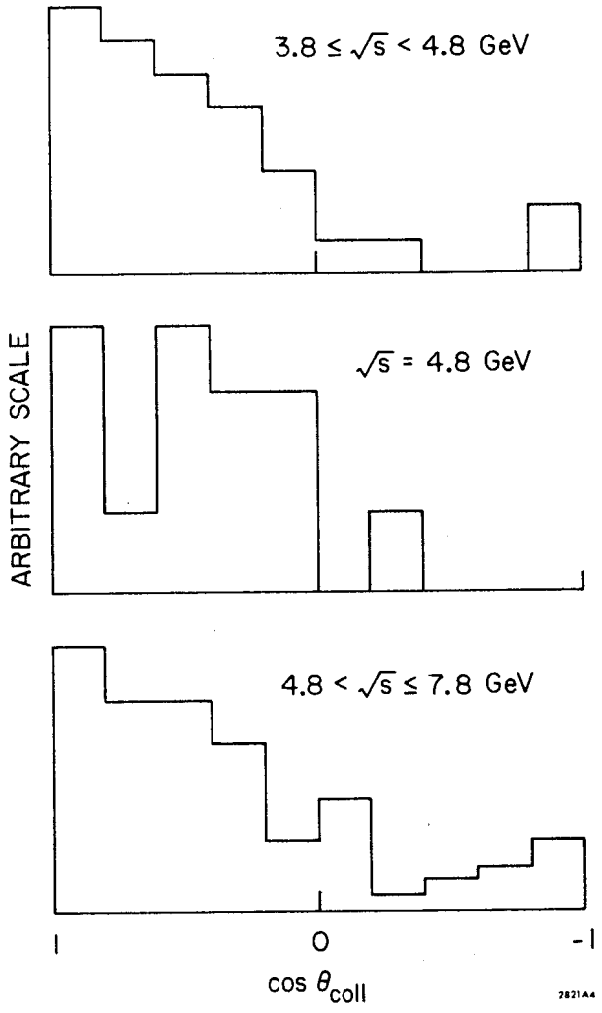

FIG. 5. Cosine of the colinearity angle for background events.

energies we construct the reduced momentum, ρ,

$$\rho = \frac{p - 0.65}{p_{max} - 0.65} \quad , \tag{4}$$

where p is the momentum of each detected particle in GeV/c and p_{max} is the maximum momentum allowed for the decay of 1.8 GeV/c^2 particle into massless particles. (The use of any mass in the range 1.6 to 2.0 GeV/c^2 would not alter these conclusions.) The ρ distribution is given in Fig. 6 for all the data and in Fig. 7 for three energy ranges. Background contamination has been subtracted. The background ρ distribution, shown in Fig.6, is similar to the signal ρ distribution; thus, the background subtraction does not appreciably alter this distribution.

In Figs. 6 and 7, the solid curve is for a heavy lepton with mass 1.8 GeV/c^2 and a V-A coupling. The dashed curve is for a mass 1.8 GeV/c^2 boson with a 2-body decay mode ignoring spin correlations or polarization effects. The dot-dashed curve represents an extreme case of polarization of a 1.8 GeV/c^2 vector meson with a 2-body decay mode, the meson being only in the helicity = 0 state. Values of χ^2 for these hypotheses are shown in Table IV for the three energy ranges. Taking all of the data together, two body decay modes are excluded.

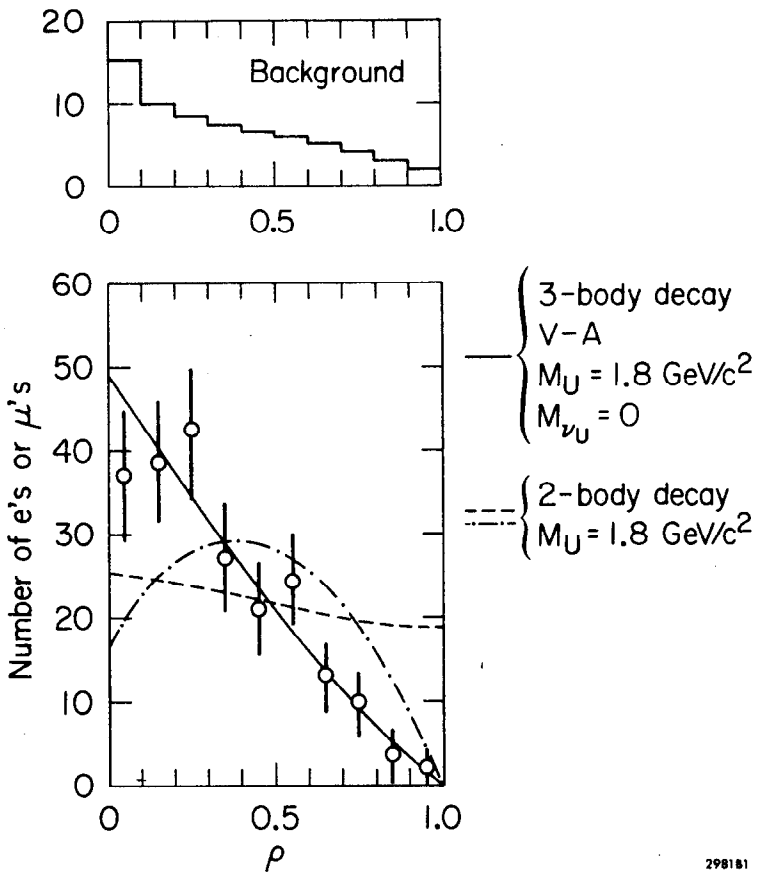

FIG. 6. Reduced momentum (Eq. 4) spectrum.

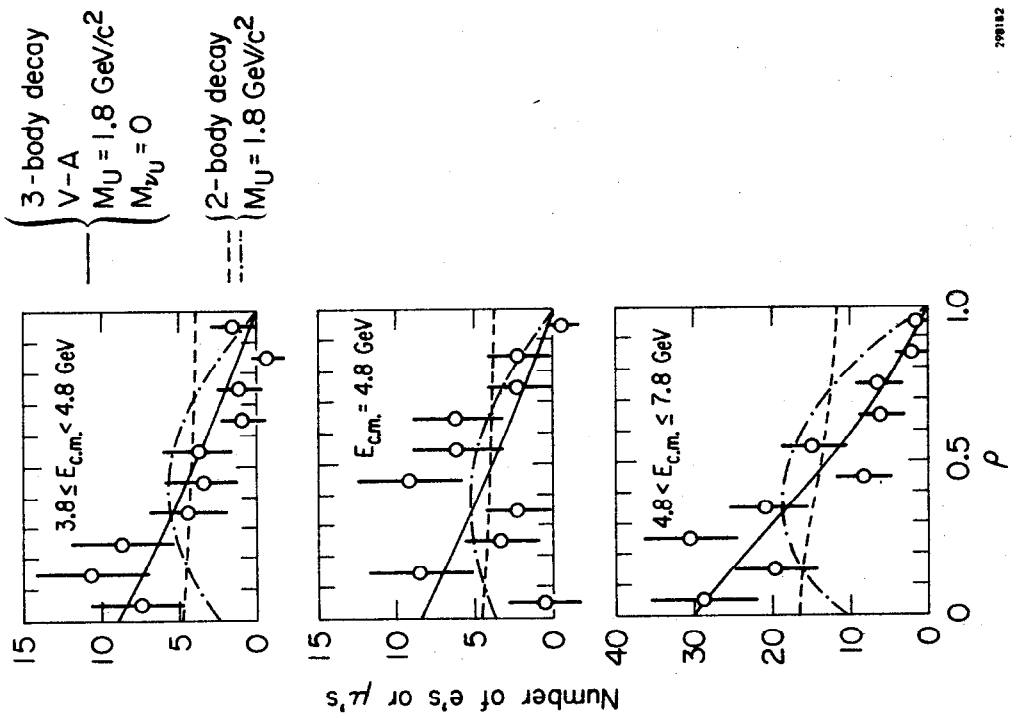

FIG. 7. Reduced momentum spectra for three energy ranges.

TABLE IV

χ^2 tests of ρ distributions. E_{cm} in GeV

	$3.8 < E_{cm} < 4.8$	$E_{cm} = 4.8$	$4.8 < E_{cm} < 7.8$	$3.8 < E_{cm} < 7.8$
Degrees of freedom	4	4	9	9
χ^2 for heavy lepton, M_U = 1.8 GeV/c^2, M_{ν_U} = 0.0 V-A coupling	2.2	9.5	8.6	4.3
χ^2 for boson with 2-body decay M_U = 1.8 GeV/c^2 no spin correlation or polarization	28.3	10.5	98.0	107.4
χ^2 for vector meson with 2-body decay M_U = 1.8 GeV/c^2 each meson only in helicity = 0 state	20.6	3.3	38.1	35.4

II.C. Are there missing hadrons?

We have so far seen evidence that we are observing the decays of a pair of fixed mass particles and that each decays into at least three particles. Are all the missing particles neutrinos or are there some hadrons which escape detection? We will show that most of the time the missing particles can only be neutrinos by systematically eliminating all other possibilities.

The neutron is eliminated as a candidate for one of the undetected particles by the ρ distributions which set an upper limit of 0.7 GeV/c^2 (95% confidence level) on the mass which can be possessed by any of the undetected particles in the three body decay. Figure 8 shows these distributions with curves representing the distributions expected for a 1.8 GeV/c^2 heavy lepton decaying to two massless particles and a heavy neutrino via a V-A coupling. The use of other couplings or of phase space has no effect on this conclusion since a high mass undetected particle limits the maximum value of ρ independent of the coupling.

To determine whether a K_L^o could be one of the undetected particles, we searched for events of the form

$$e^+e^- \rightarrow e^{\pm}\mu^{\mp}K_s^o + \text{missing mass} \qquad (5)$$

where the K_S^o is detected by its decay $K_S^o \rightarrow \pi^+\pi^-$. In a data sample which contained 82 eμ events with no other detected particles,[8] only one example of reaction (5) was observed. Assuming that the decay rate of the new particle into K_L^o is equal to the decay rate into K_S^o, the fraction of decays in reaction (1) containing a K^o is less than 0.09 at the 90% confidence level.

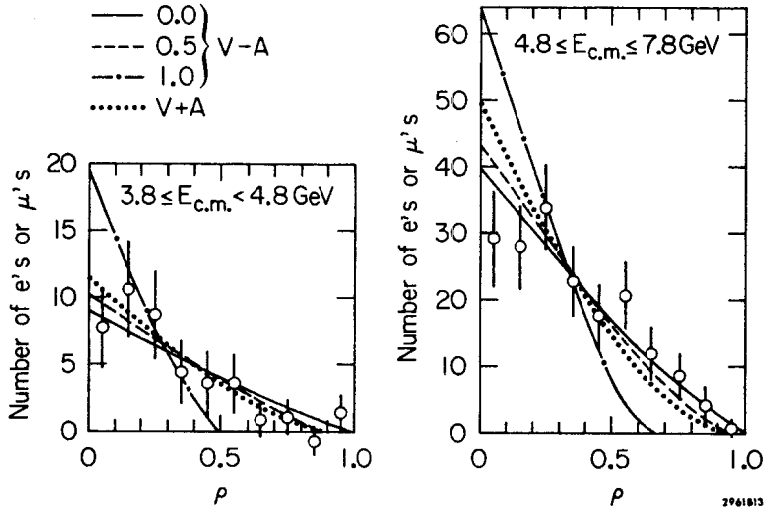

FIG. 8. Reduced momentum spectra with curves showing the effect of a heavy neutrino.

To determine whether the undetected particles could be photons, π^o's, or charged particles which escape detection by passing through uninstrumented sections of the detector, we construct a table, Table V, of all events which contain an oppositely charged electron and muon. Events are categorized by charged multiplicity and whether photons were detected in the shower counters. The data sample is the same as was used for the K^o_S search. The e and μ selection is similar to that used in Sec. II.A except that no coplanarity requirement was imposed in events with three or more charged prongs.

Two estimates of the number of events we expect from misidentifications of hadronic events are included in Table V. The first is an estimate obtained from misidentification probabilities as a function of momentum measured in ψ decays, assuming no anomalous sources of lepton production in these decays. The second is an estimate obtained from three or more prong events in the data set from which the table is constructed. The true number of events caused by hadron misidentifications is probably somewhere between the two limits given in Table V because misidentification probabilities can increase with c.m. energy, particularly for hadrons being misidentified as electrons.

At the present stage of analysis, Table V argues neither for nor against anomalous di-lepton production in topologies other than the two prong, no photon, topology. The sole function of the table is to show that there are an insufficient number of events in the other topologies to explain the anomalous eμ events as events in which additional charged particles or photons are produced, but escape detection.

For example, assume that the anomalous eμ were to be explained as events in which each new particle decayed into a lepton, a π^o, and a

TABLE V

The number of events with an identified oppositely charged electron and muon categorized by total observed charged multiplicity and by whether photons are detected. The numbers in parentheses represent minimal and maximal background estimates and are explained in the text.

charged multiplicity	no photons	> one photon
2	110 (14-28)	109 (51-104)
3	67 (28-58)	198 (94-193)
4	79 (37-76)	338 (180-356)
> 5	101 (56-109)	884 (506-971)

neutrino, but that neither π^o was detected by the shower counters. Since the typical efficiency for detecting at least one photon from a π^o decay is 0.65, there is only a 0.12 probability of $2\pi^o$'s escaping detection. Thus, to explain the 82 anomalous two prong events without photons, we would have to observe 600 two prong events with photons. From Table V, there are only 109 events of this type, and only 58 events after the subtraction of the minimal background.

Similar arguments can be made for any combination of undetected charged and neutral particles. Table VI gives upper limits on the fraction of decays in the anomalous eμ events which could have undetected photons or charged particles of various types, using the minimal background estimates from Table V. Overall, using very conservative estimates of backgrounds, at the 90% confidence level only 39% of the anomalous decays can contain undetected photons or charged particles.

IV.D. Conclusion

We have seen that there is evidence

1) that the anomalous eμ events come from decays of a pair of fixed mass particles,

2) that, most of the time, the missing particles are neutrinos.

Thus, the decays that lead to the anomalous eμ events seem to have the form,

$$U^- \to \ell^- \nu\nu, \qquad (6)$$

the usual signature of a heavy lepton.[9] This is the only simple hypothesis which fits all of the data.

Assuming that the U is a new lepton with V-A coupling, its mass is

TABLE VI

90% confidence level upper limits on the fraction of decays in the anomalous eμ events which can contain an undetected particle or combination of particles. The smaller backgrounds given in Table V have been used. The total is less than the sum of the limits due to the quadratic addition of errors and elimination of double counting between modes.

Undetected particles	90% confidence level
K^o	0.09
π^o or γ	0.18
Charged particle	0.09
Charged particle + π^o or γ	0.11
TOTAL	0.39

in the range 1.6 to 2.0 GeV/c^2 and its leptonic branching ratio is

$$\frac{\Gamma(U^- \to \nu_U e^- \bar{\nu}_e)}{\Gamma(U^- \to \text{all})} = \frac{\Gamma(U^- \to \nu_U \mu^- \bar{\nu}_\mu)}{\Gamma(U^- \to \text{all})} = 0.17 \begin{matrix} + 0.06 \\ - 0.03 \end{matrix} . \qquad (7)$$

V. Consistency checks to the hypotheses of a new lepton

We now have a new lepton as a working hypothesis. The nice thing about this hypothesis is that there are almost no free parameters. We can make a large number of predictions. The verification of any one of them, or even all of them, does not prove the hypothesis, but the hypothesis is destroyed if even one of them is disproved.

For some of the predictions, it will be necessary to know how a heavy lepton decays. These decays are calculable from experimental measurements and rather mild theoretical assumptions. Table VII gives a calculation of the branching fractions along with the inputs to the calculation. The basic formulae are all given by Tsai.[10] Gilman recalculated some of the values.[11] The most uncertain calculation is the decay to the "hadron continuum". This depends on the measurement of R ($\sigma_{tot}/\sigma_{\mu\mu}$) in the region below 1.8 GeV. Unfortunately it is measured poorly in this region, as can be seen from Fig. 9. In calculating the values for Table VII, I set R = 0 for $E_{cm} < 1.2$ GeV and R = 2 for $1.2 < E_{cm} < 1.8$ GeV.

One interesting result of the calculation in Table VII is that 87% of all heavy lepton decays will contain only one charged particle (assuming that 40% of the hadron continuum decays contain one charged particle). Thus most of the heavy lepton pair production events will be two-prong events.

TABLE VII

Calculation of the decays of a 1.8 GeV/c^2 lepton.

	fraction (%)	input
$e\nu\bar{\nu}$	20	measurement of μ decay
$\mu^-\nu\bar{\nu}$	20	measurement of μ decay
$\pi^-\nu$	12	measurement of π decay
$K^-\nu$	1	measurement of K decay
$\rho^-\nu$	23	measurement of $e^+e^- \to \rho^0$ and conserved vector current
$K^{*-}\nu$	1	above plus sum rules on the vector and axial vector currents
$A_1^-\nu$	8	
hadron continuum	15	measurements of $e^+e^- \to$ all, $E_{cm} < 1.8$ GeV[a], conserved vector current, and equal contributions from the vector and axial-vector currents.

a. R = 0, $E_{cm} < 1.2$ GeV and R = 2, $1.2 < E_{cm} < 1.8$ GeV assumed.

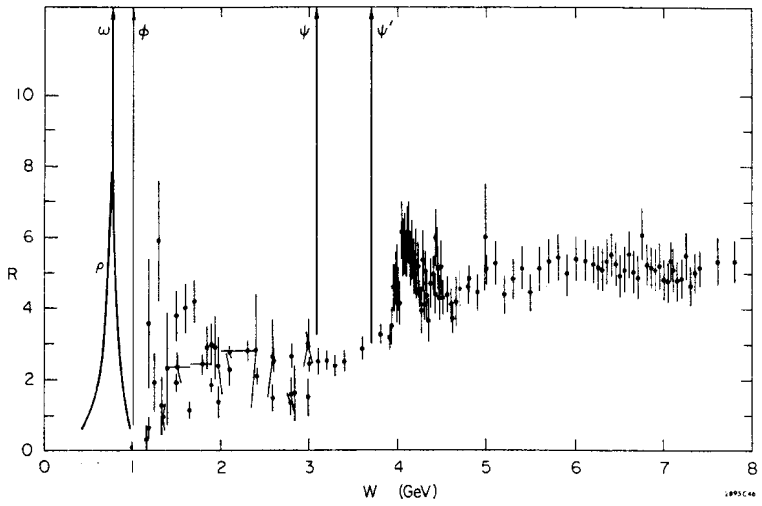

FIG. 9. R as a function of center-of-mass energy.

V.A. Point-like energy dependence

The first consistency check is that we must have a point-like production cross section as a function of E_{cm}. This is implicit in what we mean by a lepton. The observed cross sections are shown in Fig. 10 along with the predicted values for a 1.8 GeV/c^2 lepton. Although the statistical errors are large, the data are consistent with being point-like.

V.B. Total e^+e^- annihilation cross section

R, the ratio between the total e^+e^- annihilation cross section and the μ pair production cross section, measures the sum of squares of charges of the fundamental fermions in the conventional models. Thus if we have a new lepton, we must have room for it in the total cross section. This point was discussed in detail in Sec. II.C of lecture 1. We not only have room for it, but measurements of R seem to require a new fermion.

V.C. Leptonic branching fraction

Based on very general theoretical considerations, Table VII requires about a 20% branching fraction to each leptonic mode. The measured value is $17 \begin{smallmatrix} +6 \\ -3 \end{smallmatrix}$%.

V.D. Anomalous ee and μμ events.

Since we interpret the anomalous eμ events to be the result of independent decays, one containing an e and one containing a μ, we expect half as many anomalous ee and μμ events. These events are harder to measure because there are backgrounds from leptonic processes which are comparable to the anomalous signal. We have subtracted backgrounds from

$$e^+e^- \to \ell^+\ell^-\gamma, ^{12} \quad (8)$$

$$e^+e^- \to \ell^+\ell^-\gamma\gamma, ^{13} \quad (9)$$

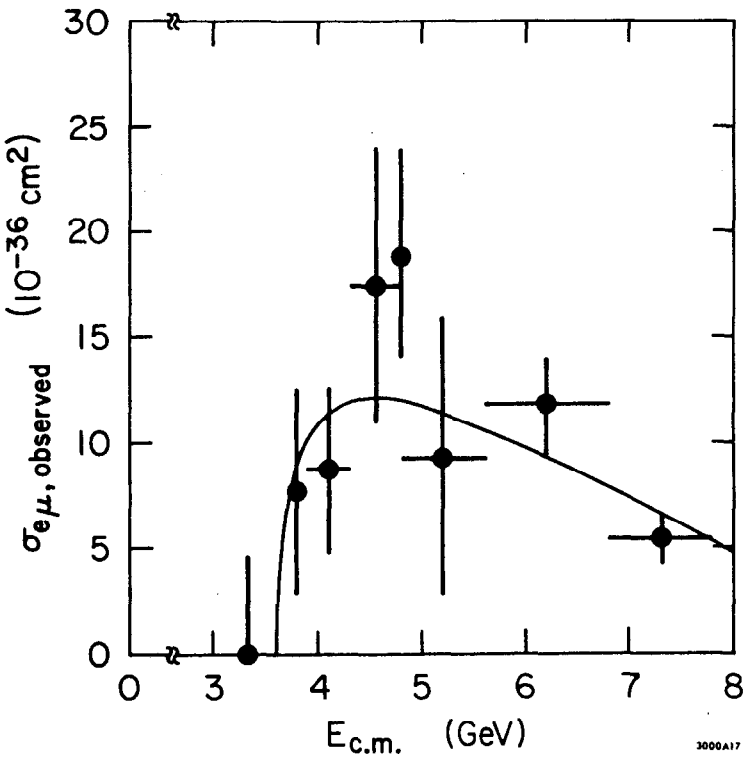

FIG. 10. Observed eμ cross section as a function of center-of-mass energy. The curve represents the expected observed cross section for a 1.8 GeV/c^2 lepton decaying to $\mu\bar{\nu}\nu$ and $e\bar{\nu}\nu$ each with a branching fraction of 0.17 via a V-A interaction.

and

$$e^+e^- \to e^+e^-\ell^+\ell^-,^{14} \tag{10}$$

where ℓ stands for either e or μ. The preliminary results are[15]

$$\frac{\sigma_{ee}}{\sigma_{e\mu}} = 0.39 \pm 0.21 \tag{11}$$

and

$$\frac{\sigma_{\mu\mu}}{\sigma_{e\mu}} = 0.66 \pm 0.16 \ . \tag{12}$$

Within large errors, these results agree with the expected value of 0.5.

V.E. Anomalous μ-hadron events.

From Table VII, we expect to observe two-prong events with one of the particles a μ and the other a hadron. To search for these events we will repeat the analysis given in Sec. II.B, where we looked for eμ events with the μ in the muon tower. To search for μ-hadron events we make two changes in the criteria listed in Sec. II.B:

1) We require the particle not heading toward the muon tower to be identified as a hadron, and
2) we allow photons in the events.

There are 109 events satisfying these criteria. In 16 events the particle going toward the tower is identified as a muon. To conservatively estimate backgrounds we take all 109 events to be hadron-hadron events. Then misidentification of the hadron as a muon will give 3.6 events background. The only other important source of background are μμ events in which a μ is identified as a hadron. There are 24 μμ events which give a background of 1.1 events. Thus the total background is 4.7 events out of 16 events observed. The probability that this could be due to a statistical fluctuation is less than one part in 10^{-4}.

V.F. Inclusive anomalous two-prong μ events[16]

In the previous sections we have seen evidence for anomalous μe, μμ, and μ-hadron events. It is thus obvious that there will be anomalous μ-anything events. Nevertheless, it is useful to study these events as a final consistency check since we will have sufficient statistics to calculate a meaningful cross section.

We take as the initial sample of events all two-prong events, with or without photons, in which one prong is a muon candidate at level two or three of the muon tower. (As in Sec. II.B, a muon candidate is defined as a particle which has sufficient momentum and is heading in the right direction to fire a muon spark chamber if it were a muon.) To simplify the background calculations, events in which both prongs are identified as electrons are eliminated. We then require the two prongs to be acoplanar with the incident beams by at least 20° and for the square of the missing mass recoiling against the two observed prongs to be greater than 1.5 $(GeV/c^2)^2$. Backgrounds from hadron penetration and decay and leptonic backgrounds as discussed in Sec. V.D are then subtracted to obtain the number of anomalous two-prong μ events.

The results for three energy ranges are summarized in Table VIII. (There were negligible data taken in the missing energy range from 4.8 to 5.8 GeV.) The anomalous muon cross section in all three energy ranges is compatible with that expected from the decays of pairs of heavy leptons. The later cross sections listed in Table VIII are for a mass range 1.6 to 2.0 GeV/c^2, a branching fraction into $\mu\nu\bar{\nu}$ of 0.17, and other branching fractions as given in Table VII.

TABLE VIII

Inclusive anomalous muon production in two prong events.

E_{cm} range (GeV)	3.9 to 4.3	4.3 to 4.8	5.8 ± 7.8
Average E_{cm} (GeV)	4.05	4.4	6.9
Integrated luminosity (pb^{-1})	2.44	2.35	16.2
Candidates	181	224	902
Muons	24	29	177
Radiative μ pairs	2.3	2.2	17
$ee\mu\mu$ events	1.4	1.8	29
Hadron penetration or decay	5.0	6.4	28
Anomalous muons	15.3 ± 5.1	18.6 ± 5.7	103 ± 18
Anomalous cross section (pb)	194 ± 71	253 ± 86	212 ± 49
Expected heavy lepton contribution (pb)	252 ± 57	290 ± 197	195 to 218

Two other experiments have made measurements of inclusive anomalous muon production in two-prong events. The Maryland-Princeton-Pavia group reported 13 events with 4 background at 4.8 GeV, corresponding to a cross section of $285 \begin{smallmatrix} + 151 \\ - 113 \end{smallmatrix}$ pb.[16] I calculate that one would expect about 275 pb from heavy lepton decays in that experiment. Unfortunately there was a factor of two error in calculating the background from radiative μ pair production.[17] This will reduce the anomalous cross section to the vicinity of 190 pb, but the errors are sufficiently large that the result is still compatible with that expected from heavy lepton decays.

The PLUTO experiment has searched for anomalous muons in the energy range 4.0 to 4.2 GeV. Preliminary results will be presented by Hinrich Meyer in the Topical Conference.[6] At present this experiment gives only an upper limit, but one that is not incompatible with a heavy lepton in the mass range 1.6 to 2.0 GeV/c^2.

I. Summary

There is strong evidence for anomalous eμ events. The properties of these events indicate that they come from decays of a pair of particles, each of which decays to a charged lepton and two neutrinos. Taking the existence of a new lepton as a working hypothesis, we examined six consistency checks, the point-like energy dependence, the value of the total e^+e^- annihilation cross section, the leptonic branching fraction, anomalous ee and μμ events, anomalous μ-hadron events, and anomalous μ-anything events. In all cases, the present data are compatible with the hypothesis. Thus, the answer to the question which forms the title of this lecture is: We either have a new lepton or a very good imitation.

REFERENCES

1. J.-E. Augustin et al., Phys. Rev. Lett. 34, 233(1975).
2. G.J. Feldman and M.L. Perl, Phys. Rep. 19C, 233(1975).
3. M.L. Perl et al., Phys. Rev. Lett. 35, 1489(1975).
4. Neutron Physics Division, Oak Ridge National Laboratory, ORNL report number CCC-178 (undated).
5. B. Wiik, invited talk at the Conference on Quarks and the New Particles, Irvine, California, December 5-6, 1975.
6. H. Meyer, these proceedings.
7. M.L. Perl et al., Phys. Lett. 63B, 466(1976).
8. The data sample is all events for which a proportional chamber around the beam pipe was operational. This chamber was used in the K^o_s identification.
9. The hypothetical particle responsible for the anomalous eμ events was named U by Martin Perl at this institute a year ago. (Proceedings of Summer Institute on Particle Physics, July 21-31, 1975, SLAC report SLAC-191.) The U stood for "unknown" and it was stated that the name may be changed when the nature of the particle is understood. Recently, at the 1976 Neutrino Conference at Aachen, Perl suggested that if the U is confirmed as a sequential lepton, a suitable name might be τ (for τριτον) since it would be the third charged lepton. (SLAC-PUB-1764).
10. Y.S. Tsai, Phys. Rev. D4, 2821(1971).
11. F.J. Gilman, private communication.
12. F.A. Berends, K.J.F. Gaemers, and R. Gastmans, Nucl. Phys. B57, 381(1973).
13. K.J.F. Gaemers and F.B. Heile, unpublished calculation. The calculation adds a second hard photon in the peaking approximation to the exact α^3 calculation of Ref. 12.

14. G. Grammer, Jr. and T. Kinoshita, Nucl. Phys. B80 461(1974).

15. F.B. Heile, Bull. Am. Phys. Soc. 21, 568(1976).

16. M. Cavalli-Sforza et al., Phys. Rev. Lett 36, 588(1976).

17. D. Coyne, private communication.

LBL-5500

LECTURES ON THE NEW PARTICLES*

J. D. Jackson

Department of Physics and Lawrence Berkeley Laboratory
University of California, Berkeley, California 94720

August 18, 1976

Notes for lectures delivered at the SLAC Summer Institute on Particle Physics, August 2-13, 1976. These notes will appear in the Proceedings of the Summer Institute, to be issued as a SLAC Report.

* Supported in part by the U. S. Energy Research and Development Administration.

Preface and Acknowledgments

The lecture notes represent an attempt to discuss the systematics of the new particles and their spectroscopy in a simple way, understandable to relative beginners in the field and to the experimenters who are so busy making discoveries that they have no time to digest the indigestible theoretical papers that are triggered by each new revelation. The coverage is uneven and far from complete. Part of this is from lack of time and part is from the division of subject matter among the lecturers. The properties of particle production above the charm threshold, for example, are covered in Dave Hitlin's lectures. The phenomenology of the ψ and ψ' decays is contained in Gary Feldman's.

Sophisticates may find the notes pedestrian (if H. Lipkin will permit a borrowing), even naive and overly sold on the simplest version of charmonium. For the first, I make no apology. The lectures were aimed at the student, theorist or experimenter, whom I believe likes to know from whence come some of the theoretical results. For the second, I confess some enthusiasm and a conviction born of the preparation of these lectures, that we are dealing in the ψ particle sector at least with an essentially simple, nearly nonrelativistic, bound system of quark and anti-quark.

The notes were prepared under intense time pressure. As a result, the references are fragmentary and quite incomplete. I apologize to those authors whom I have wronged through oversight. I acknowledge with pleasure the assistance of N. Fleischon, K. Gottfried, K. M. Lane and S. B. Treiman.

Outline

I. Introduction

II. Charm and SU(4)

III. High-powered theoretical ideas

1. Color
2. Asymptotic freedom
3. Quark confinement
4. Adler-Bell-Jackiw anomalies

IV. Zweig's rule

V. Weak decays of charmed mesons

1. General framework
2. Leptonic decays of pseudoscalars
3. Semileptonic decays of pseudoscalars
4. Inclusive semileptonic and hadronic rates
5. Multiparticle hadronic decays
6. Hadronic 2-body decays; generalization of the $\Delta I = 1/2$ rule
7. Exotic final states, D^0-$\bar{D}^0$ mixing, charmed baryon decays

VI. Hadronic masses according to De Rújula, Georgi and Glashow

1. Darwin-Breit-Fermi interaction in QED
2. Effective quark Hamiltonian in color gauge theory
3. Examples of mass splittings within SU(3) multiplets; quark masses

VII. Charmonium

1. Vector meson decay into $\bar{l}l$
2. Hadronic widths of charmonium s-states
3. First orientation on wave functions and matrix elements with a very simple model
4. Radiative transitions
   (a) E1 transitions
   (b) Dipole sum rules: upper and lower bounds on $\Gamma(\chi_J \to \gamma\psi)$, quark charges
   (c) M1 transitions
5. Decay of p-states into gluons or photons
6. Systematics of the energy levels in charmonium

VIII. Conclusion

References

I. Introduction

Since November 1974, the "production of new particles" has meant only one thing to those of us west of the Sierra Nevada and perhaps only two things to those east of them. The phenomenal success of the magnetic detector at SPEAR is widely known and will become better known as Gary Feldman and Dave Hitlin proceed. A rich spectrum of states is being unfolded. At least a dozen totally new hadronic states in the mass range 1.8 GeV to 4.5 GeV have been discovered in the past twenty months. That is not keeping pace with the initial rate of a new state every 10 days, but it is astounding, nevertheless! Some of these states are new, with properties largely unknown, but others, notably the ψ (3095) and ψ' (3684), have been studied in detail. It now seems rather clear, as these lectures and the topical conference will bear out, that the new degree of hadronic freedom responsible for this outburst of unexpected phenomena is charm, precisely in the original sense of Bjorken and Glashow (1964) and Glashow, Iliopoulos and Maiani (1970).

The rich spectrum of states implies a rich and complicated spectroscopy. That is the main subject of these lectures. The vehicle of discussion is a hybrid - part nonrelativistic quantum mechanics as learned from Schiff, a few things from Bjorken and Drell, Vol. 1, plus some concepts that go beyond B.-D., Vol. 2 and even Vol. 3! Thus we need to be at least introduced to asymptotic freedom, quark confinement (infrared slavery), anomalies, etc. For these latter items, you must take the experts' word for them - I have not the expertise, nor the time, to do more than present them briefly.

Since this is a school, I shall attempt to teach, not pontificate. In the time available it is impossible to derive everything, but some calculations will be worked out fairly completely so that the steps, tricks (if any), and the origin of the all important and often confusing factors of 9/2 or -4/3 is clear.

II. Charm and SU(4)

The use of SU(4) in hadronic physics is not new. It was employed nearly 40 years ago by Wigner (who else?) to describe nuclei in the approximation of spin- and isospin-independent forces. The supermultiplets (called Wigner supermultiplets) were then decomposed into sub-multiplets by the symmetry-breaking interactions, as particle physicists have now learned to do.

The relevant event for us was the introduction of SU(3) in the early 60's. Soon theorists began toying with bigger groups - SU(4),.... Motivations varied. Some were just flexing their manipulative muscles. Gell-Mann toyed and passed over to fractionally charged quarks. Bjorken and Glashow (1964) were motivated partly by some meson spectroscopy and partly by lepton-hadronic-fermion symmetry. You have already heard from Bjorken on that aspect. The addition of a fourth quark carrying a new quantum number had immediate consequences for the spectrum of hadronic states. Multiplets with 8 or 9 states in SU(3) were enlarged to 15 or 16 states in SU(4). The additional states were not seen. It was therefore necessary to propose that the mass of the new quark was considerably greater than the masses of the other three. This would

plausibly push the new states sufficiently high in mass to put them into an unexplored part of the mass scale and perhaps give them complex enough decay modes to prevent easy recognition. As you know, the idea of charm and SU(4) lay dormant in the face of the successes of SU(3) until 1970. Then peculiarities of weak interactions (absence of strangeness-changing neutral currents, K_S^o-K_L^o mass difference) were explained in an elegant fashion by Glashow, Iliopoulos and Maiani (1970) using the charmed quark. Bjorken has described the GIM model, augmented by the ideas of unified gauge theories of weak and electromagnetic interactions. We shall make use later of the effective current-current interaction of this model to discuss the weak decays of charmed mesons. For the present, however, we focus on the hadronic properties of the quarks in SU(4) and the states formed from them.

Table 1 shows the conventional spin 1/2, fractional-charged quarks and their hadronic quantum numbers. All the quarks have baryon number $B = 1/3$. The quantum number C (for charm, not for charge-conjugation) is an additive quantum number like hypercharge Y. The Gell-Mann-Nishijima displaced-charge-multiplet formula is

$$Q = I_3 + \frac{1}{2}(B + S + C) \qquad (2.1)$$

and hypercharge and strangeness are connected by $Y = S + B - C$.

Table 1
Quarks and their quantum numbers in SU(4)

Symbol	Q	I_3	C	Y	S
u(p)	2/3	1/2	0	1/3	0
d(n)	-1/3	-1/2	0	1/3	0
s(λ)	-1/3	0	0	-2/3	-1
c(p')	2/3	0	1	-2/3	0

The lowest meson multiplet $q\bar{q}$ can be built up as a matrix array by labelling the rows by the q symbols and the columns by $\bar{q}$ symbols. For example, the vector meson 16-plet appears as follows:

$$V = \begin{array}{c} \\ (\bar{u}) \\ (\bar{d}) \\ (\bar{s}) \\ (\bar{c}) \end{array} \begin{array}{c} \begin{array}{cccc} (u) & (d) & (s) & (c) \end{array} \\ \begin{pmatrix} \frac{1}{\sqrt{2}}(\omega + \rho^o) & \rho^- & K^{*-} & D^{*o} \\ \rho^+ & \frac{1}{\sqrt{2}}(\omega - \rho^o) & \bar{K}^{*o} & D^{*+} \\ K^{*+} & K^{*o} & \phi & F^{*+} \\ \bar{D}^{*o} & D^{*-} & F^{*-} & \psi \end{pmatrix} \end{array} \qquad (2.2)$$

In making this array we have used the nonet (magic mixing) scheme for the familiar neutral SU(3) mesons and have assumed that the ψ is purely $(c\bar{c})$. The designations D^{*o}, D^{*+}, F^{*+}, etc. for the visibly charmed vector mesons is becoming standard (Gaillard, Lee, and Rosner, 1975). The matrix array (2.2) and the corresponding one for the pseudoscalar mesons are useful in writing down SU(4) invariant couplings such as VPP and VVP (See Gasiorowicz, 1966, p. 282).

The lowest baryon multiplets can be constructed as qqq. It turns out that the SU(3) octet of spin 1/2 baryons is enlarged to a 20-plet, while the SU(3) decuplet of spin 3/2 baryons grows to a 20-plet, too. The meson and baryon multiplets are shown in Fig. 1 (taken from Glashow, 1975).

In strong interactions isospin, strangeness and charm are all conserved, while in weak interactions these conservation laws fail to hold in general. In production of charmed hadrons there must be

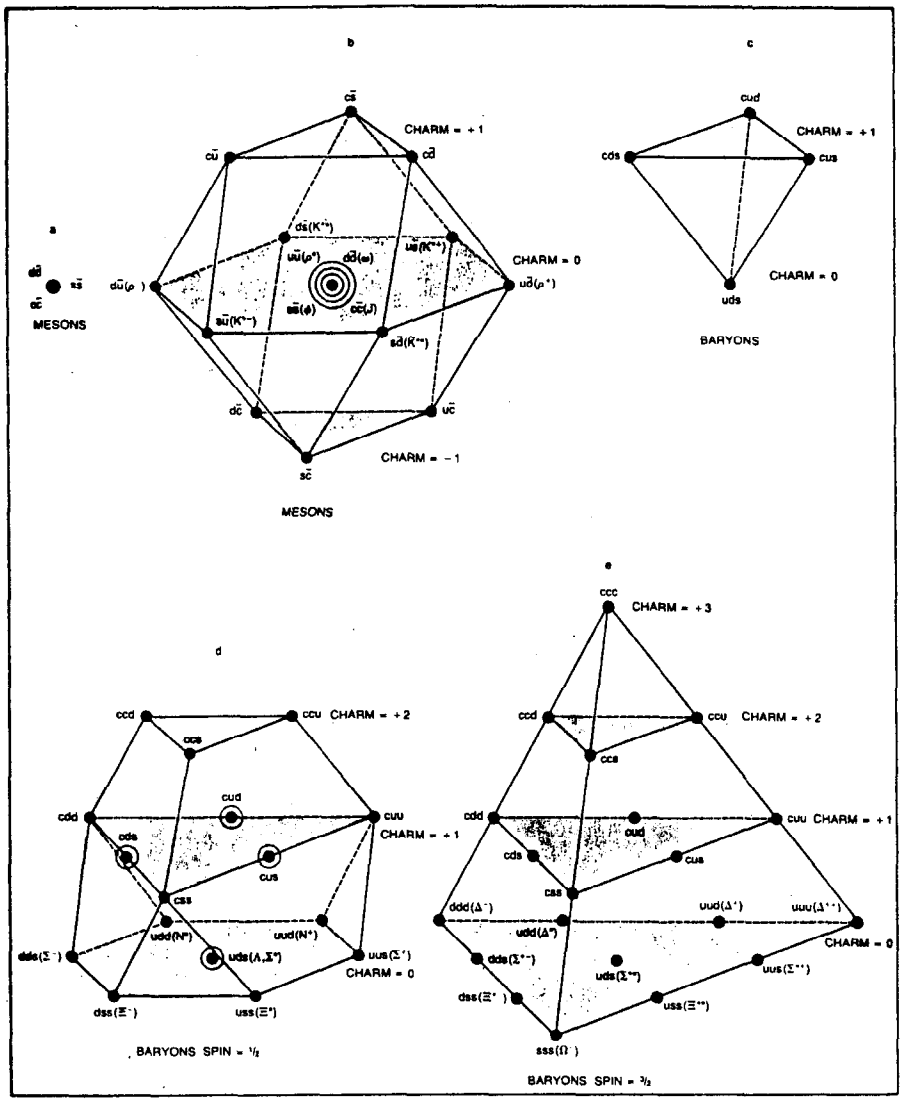

Figure 1 . Supermultiplets of mesons and baryons in SU(4). The familiar SU(3) multiplets (Charm = 0) are seen in the middle layer of the mesons and the bottom layers of the baryons.

associated production then, just as for strange particles. In weak decays, analog of the K^{o}-$\bar{K}^{o}$ mixing occurs for the charmed pair, D^{o}-$\bar{D}^{o}$.

III. High-powered Theoretical Ideas

We now turn to some of the background and dogma that lies beneath and around the ultimately rather simple model with which we interpret the new spectroscopy. There are differences of opinion among theorists as to the importance of any one of the concepts. I shall list them impartially, with only a remark occasionally about doubts or arguments of irrelevance.

1. Color

The concept of color is that there are three times as many quarks as the naive description, that this additional degree of freedom is realized in a SU(3) of color, and that hadronic states occuring in nature are always color-singlets. Color is thus a perfect symmetry. We speak of the color-charm quark model as involving SU(4) ⊗ SU(3), where the first group of transformations is associated with the usual hadronic quantum numbers, called flavors, and the second with color. There are many worlds described by such a theoretical framework. Ours is assumed to be the one that lies in the color-singlet sector of the Hilbert space.

Hadronic interactions are almost color-blind, but the presence of the color dimension can be verified in processes involving electro-

magnetic interactions. What are the reasons for color? There are four main ones:

(i) Spin-statistics for quark models of baryons;

(ii) Rate of $\pi^0 \to \gamma\gamma$;

(iii) Experimental value of R in e^+e^- annihilation;

(iv) Asymptotic freedom needs the non-Abelian aspect provided by colored gluons.

The naive quark model of baryons has the low-lying states made up of (qqq) in relative s-waves. To minimize the kinetic energy, one requires no nodes and so gets a spatially symmetric wave function. The $\Delta^{++}(1232)$, for example, has an obviously totally symmetric isospin and spin wave function. Without color therefore the wave function is totally symmetric, violating the spin-statistics theorem. Color comes to the rescue. The color-SU(3) singlet wave function of three quarks is totally *antisymmetric* (like $\vec{a} \cdot (\vec{b} \times \vec{c})$ *for ordinary vectors* in 3-space). The product wave function, including color, is antisymmetric. Pauli can lie easy. Actually, if this were the only argument for color, Pauli would have said "Dummkopf!". At this stage, color appears to be just an excuse for violating the connection between spin and statistics.

The decay $\pi^0 \to \gamma\gamma$ is a time-honored process that bears on another theoretical concept, anomalies, but here we are concerned with a quantitative argument for color. The first unambiguous calculation of $\pi^0 \to \gamma\gamma$ was done by Steinberger (1949). The process was assumed to proceed via a virtual proton-antiproton loop, as indicated in Fig. 2.

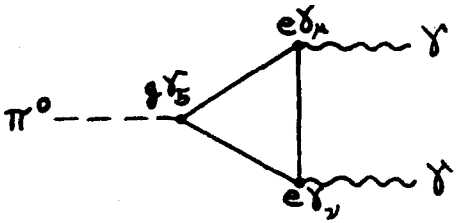

Fig. 2. $\pi^0 \to \gamma\gamma$ via intermediate proton-antiproton loop. A typical triangle graph contributing to the Adler-Bell-Jackiw anomaly.

With pseudoscalar coupling for $\pi\bar{N}N$ and point Dirac couplings with no anomalous magnetic moment for $\gamma\bar{p}p$, Steinberger found

$$\Gamma(\pi^0 \to \gamma\gamma) = \frac{\alpha^2}{16\pi^2}\left(\frac{g^2}{4\pi}\right)\frac{m_\pi^3}{m_N^2} \qquad (3.1)$$

With $g^2/4\pi = 14.6$, this gives 13.8 eV, compared with the experimental value of 7.8 ± 1.0 eV, an amazingly lucky (?) agreement.

The modern approach to $\pi^0 \to \gamma\gamma$ is via current algebra and PCAC (Adler, 1969). This amounts to using the Goldberger-Treiman relation, $g = \sqrt{2}\, f_A(0) m_N / f_\pi$, to eliminate g in favor of the pion decay parameter, $f_\pi \approx 138$ MeV. If we also replace the virtual protons by virtual quarks, including color, the π^0 decay rate becomes

$$\Gamma(\pi^0 \to \gamma\gamma) = \frac{9e_Q^4\alpha^2}{32\pi^3}\,|f_A(0)|^2\left(\frac{m_\pi}{f_\pi}\right)^2 m_\pi \qquad (3.2)$$

With $f_A(0) \approx 1.23$, Eq. (3.2) yields $\Gamma = 10.5\,(9e_Q^4)$ eV. The factor

of $9 = 3^2$ comes from the sum in the amplitude over the three colors of the $\bar{q}q$ intermediate loop. The factor e_Q^4 stands for the square of the average charges squared in the π^0. Thus $e_Q^4 = \left[\frac{1}{2}\left(\frac{2}{3}\right)^2 + \frac{1}{2}\left(-\frac{1}{3}\right)^2\right]^2 = 25/324$, and $\Gamma(\pi^0 \to \gamma\gamma) = 10.5 \times 0.694 = 7.3$ eV. The perfect agreement with experiment is only achieved with the "color" factor of 9. Now one could argue about whether $|f_A(0)|^2$ should be present or not with quark loops, but independently of this factor of $\sim$1.5, there is a clear need for color in order to get quantitative agreement with experiment. Some reader may wonder why we should believe this lowest order result. To go into that would take most of us (certainly me) beyond my depth. Suffice it to say that to the extent the pion mass is small the lowest order calculation can be believed. Incidentally, this quantitative agreement using 9, and not 16 for example, is an argument for SU(3) and not some higher group that would have solved the spin and statistics problem just as well.

The third argument for color is the numerical value of $R = \sigma(e^+e^- \to \text{hadrons})/\sigma_{QED}(e^+e^- \to \mu^+\mu^-)$. As Feldman has discussed, the experimental data on R can be imagined to consist of two plateaus, one at c. m. s. energies from 1.5 to 3.5 GeV and another from 4. to 7. GeV, with resonant structure superposed. The "low" energy plateau has $R \simeq 2.5$, while the high energy plateau is $R \simeq 5.0$. In simple quark-parton models and also fancier asymptotically-free gauge theories, the cross section for $e^+e^- \to$ hadrons is given at high energies by the cross section for $e^+e^- \to q_j\bar{q}_j$, summed over all types of quarks. The $q\bar{q}$ pairs are assumed to turn into hadrons with unit probability.

The ratio R is then

$$R = \sum_j Q_j^2 + \begin{pmatrix}\text{finite energy}\\ \text{corrections}\end{pmatrix} \qquad (3.3)$$

where Q_j is the charge of the jth quark in units of the protonic charge. For quark models without color, the charges given in Table 1 lead to $R = 2/3$ for SU(3) and $R = 10/9$ for SU(4). Both of these values are ridiculously small compared with experiment. With color, the number of quarks of each charge is tripled and the R values become $R(3q \times \text{color}) = 2.0$, $R(4q \times \text{color}) = 10/3$. These are now in crude agreement with observation, the smaller value appropriate to the low energy domain where the charmed quark is not excited and the larger value to the high energy region, above the presumed (and now almost certainly established) charm threshold. Gauge theories (e.g., Appelquist and Politzer, 1975 b) predict that the strong-interaction corrections to (3.3) at finite energies decrease rather slowly, as inverse logarithms of the energy. If we attribute the difference between 2.5 and 2.0 to these corrections, we anticipate a value of R somewhat above the charm threshold to be $R \simeq (2.5/2.0) \times 10/3 \simeq 4.2$. This is 1 unit away from the experimental value, a circumstance viewed as fortunate in the light of the anomalous μ-e events (Perl et al., 1975 and G. Feldman, these lecture notes). The anomalous μ-e events seem more and more like the production and decay of a charged heavy lepton pair. While this process is not part of $e^+e^- \to$ hadrons, it does contribute to the "hadronic" cross section as presently defined in the magnetic detector. With unit charge, the heavy lepton production

will contribute $\Delta R \gtrsim 1$ quite soon above threshold.

The fourth argument for color is a purely theoretical one. Asymptotic freedom needs color, or something like it, for its realization. Since the idea of asymptotic freedom is one of the major underpinnings of our picture of the new hadrons, we turn to that topic now.

2. Asymptotic freedom

Field theory has had a dramatic resurgence in the 1970's. One aspect of this is the unified gauge theories of weak and electromagnetic interactions, proposed in 1967 by Weinberg and by Salam and receiving respectability, i.e. proof of renormalizability, at the hands of 't Hooft and B. W. Lee in 1970. Bjorken has discussed the application of these ideas to high-energy weak interactions in detail. Unification of weak and electromagnetic interactions whetted appetites for a grand unification - strong, e-m, weak, even gravitational. For sometime theorists were unsure of how to include hadrons (quarks). Then Politzer (1973) and independently Gross and Wilczek (1973) showed that there is a class of theories in which the effective coupling constant becomes smaller and smaller as the energy becomes larger and larger. Such theories are called "asymptotically free" field theories (See the review by Politzer, 1974). Perturbation theory then works at high energies.

Just a few technical remarks. In any field theory with interactions there are coupling constants. Before renormalization the Lagrangian involves the bare couplings. The physical coupling constants are only defined by means of the size of some amplitude at some convenient point in the relevant kinematic variables. For example, the physical (renormalized) pion-nucleon coupling constant $g^2/4\pi$ can be defined as the residue of the neutron pole in the $\pi^- p$ forward scattering amplitude. It is not necessary to choose that point, of course. Other definitions can and have been used (The Watson-Lepore definition was in terms of the strength of the one-pion exchange potential between nucleons at zero kinetic energy.). Different energy or distance scale regimes may require different dynamical variables and different effective couplings. This is the essence of the so-called renormalization group attack on physical problems, whether for short-distance or high-energy behavior in particle physics or critical point phenomena in solids and fluids. For each energy domain it is appropriate to define the coupling constant at a mass value in that energy range. Thus we have the concept of a "running" coupling constant, $g^2(s)/4\pi$, that measures the strength of particle emission and absorption at that energy, $\sqrt{s}$.

What was shown by Politzer and Gross and Wilczek was that non-Abelian (Yang-Mills) gauge theories in which fermions (quarks) are coupled to massless gauge vector particles (gluons) have a "running" coupling constant that becomes smaller and smaller, the higher the energy, at least for Euclidean space-time. The color SU(3) gauge group provides the non-Abelian character that is necessary for asymptotic freedom (Coleman and Gross, 1973). In a particular $SU(4) \otimes SU(3)$ theory, the "running" coupling constant turns out to be

$$\bar{\alpha}(s) = \frac{\alpha_s}{1 + \frac{25}{12\pi}\alpha_s \ln(s/M^2)} \qquad (3.4)$$

where α_s is the (strong) coupling constant, defined at $s = M^2$. [In passing we note that it is $\overline{\alpha}(s)$ times some kinematic threshold factors that provides the finite energy corrections to Eq. (3.3) for R.]

With a color gauge theory of gluons interacting with quarks, there is a hope that the high-energy or short-distance behavior of strong interactions can be described relatively simply. Bjorken scaling (with logarithmic violations) and the plateaus in R emerge naturally from this picture. The relatively early scaling in deep inelastic electron scattering implies that "high energies" might be as low as 1 GeV. Thus in hadronic spectroscopy, attempts are made to discuss the ordinary hadrons of masses less than 2 GeV in terms of the same picture that we shall use with more assurance at 3-4 GeV. Some aspects work surprisingly well, others not so well. Since $\overline{\alpha}(s)$ is of order 0.5 at 1 GeV this is as good as might be expected.

3. Quark Confinement

Our talks about quarks and gluons has one seemingly fatal flaw. Quarks have not as yet been observed as particles in their own right, i.e., as asymptotic states. Since individual quarks and gluons carry color quantum numbers and it has been decreed that only color-singlet states occur in nature, one might argue that their absence is inevitable. It is necessary, nevertheless, to have a consistent mechanism for quark confinement. There are several "bag" models designed to do the job. Yang-Mills gauge theories deal with the problem by means of "infrared slavery", the other end of the asymptotic freedom candle. If the coupling becomes weak at high energies, then conversely the coupling tends to be strong at low energies or large distances. If q and $\overline{q}$ are separated, the attractive interaction between them becomes stronger and stronger until it becomes energetically favorable to make $q\overline{q}$ pairs between them. The net result is a chain of $q\overline{q}$ pairs with some typical hadronic spacing between q and $\overline{q}$. The pairs interact with each other, but in a normal "colorless" way. We have a chain of mesons formed, but no free quarks.

The technical problems of handling the infrared divergences in Yang-Mills theories are sufficiently great that there is no general theory of quark confinement. Some general features can nevertheless be deduced from the field-theoretic forms of dual models of hadrons, following Nambu, Koba and Nielson, Mandelstam and others. The duality diagram of Harari and Rosner, shown in Fig. 3a, evolves into a rubber-like sheet that becomes the intersecting world sheets of the hadrons, as indicated in Fig. 3b. The world sheet is then envisioned as the

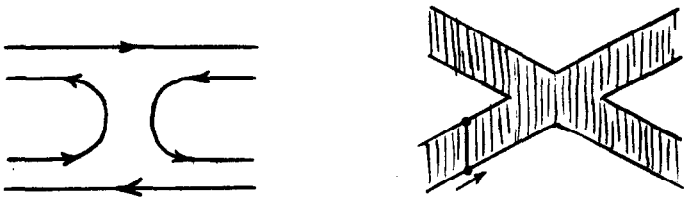

(a) (b)

Fig. 3. (a) Planar Harari-Rosner duality diagram for meson-meson scattering with quark lines shown, (b) Dual model diagram of the world sheets of mesons that scatter, with string and quarks indicated.

time evolution of a hadronic string with quark and anti-quark at the ends. All of this has some mathematics behind it, once some assumption is made about the action integral. The net result is a string-like model of a hadron, with a potential energy between quarks that increases linearly with their separation. In these models, quarks are not seen in the laboratory because infinite energy is needed to achieve infinite separation. Before that can occur, the string breaks with creation of $q\bar{q}$ pairs, as already described.

In the absence of a full-fledged theory, we can plausibly use the ideas of dual models to describe phenomenologically the interaction between quarks at large distances and can hope that the behavior at short distances is described by a color gluon gauge theory with a "running"coupling constant that is small. Much of the remainder of these lectures will explore to what extent this holds true and where.

4. Adler-Bell-Jackiw anomalies

Though they are not really important for us, anomalies do crop up in discussion from time to time and they do motivate theorists who have faith that quantum field theory will provide the ultimate description of nature. Thus we make a few naive comments.

In a spinor electrodynamics with massless fermions, the vector current is obviously conserved, and because of γ_5 invariance, the axial vector current also is formally conserved. Nevertheless, as Adler (1969) showed, triangle graphs like the one in Fig. 2 make the divergence of the axial current nonvanishing. There is thus no Ward identity for the axial current and renormalization is impossible.

In theories with PCAC, the usual proportionality of the divergence of the neutral isospin current and the π^0 field is altered to

$$\partial_\lambda A_3^\lambda = \frac{m_\pi^2 f_\pi}{\sqrt{2}}\,\phi_3 + c\,\frac{e^2}{16\pi^2}\,\tilde{F}_{\mu\nu}F^{\mu\nu} \qquad (3.5)$$

where c is a number of order unity that depends on the details of the theory. This result can be used to explain $\pi^0 \to \gamma\gamma$ (as a failure of PCAC), but unless compensated by other triangle diagrams, leads to renormalization difficulties.

In unified gauge theories, with or without gluons, the situation is generally the same, but more complex. Gross and Jackiw (1972) treat the problem in detail and discuss how to augment a theory possessing anomalies with additional particles in order to cancel the existing ones and get a theory with no anomalies. They show that renormalizability and/or unitarity of the S-matrix is destroyed by anomalies. The motivation of the true believer is therefore strong to make a theory anomaly-free. Crudely speaking, for every multiplet of fermions in the theory present as a left-handed current, there must be a corresponding multiplet present as a right-handed current. This is described by Georgi and Glashow (1972) as a "vector-like" theory. These authors show that, unless the gauge group is "safe" (SU(2), SO(6), and a few more), it is necessary that the coupling of the gauge fields to the fermion multiplets can be written as

$$W_\mu^a\,\bar{\psi}\,\gamma^\mu\,\Gamma^a\,\psi = W_\mu^a\,\bar{\psi}'\,\gamma^\mu\,T^a\,\psi' \qquad (3.6)$$

where on the left the gauge group operators Γ^a can involve 1 and

γ_5 , while on the right the operators T^a are numerical matrices. Only the spinor ψ' may involve γ_5. It is some linear combination of the fermion fields. The right hand side of (3.6) thus appears to be a purely vector coupling.

These few probably confusing remarks about anomalies will, I hope, at least warn the reader that some theorists worry about having their theories clean and anomaly-free. This requirement is one of the arguments for more quarks as soon as there are more leptons. It can be thought of as part of or a generalization of the old desire for lepton-hadronic-fermion symmetry.

IV. Zweig's rule

Zweig's rule, more properly known as the OZI rule (after Okubo, Zweig and Iizuka), forbids any hadronic transition whose duality diagram involves annihilation or creation of any of the hadrons. Said another way, the transition is forbidden if a line not originating "inside" any hadron can be drawn through the diagram without crossing any quark lines. For the ϕ meson, assumed to be made up totally of $\bar{s}s$ quarks, Fig. 4 shows OZI-allowed and OZI-forbidden transitions. Note that in both diagrams there is "pair creation" of quarks, but the quarks go to different hadrons. Only in Fig. 4(b) is there annihilation of the two quarks in the same hadron.

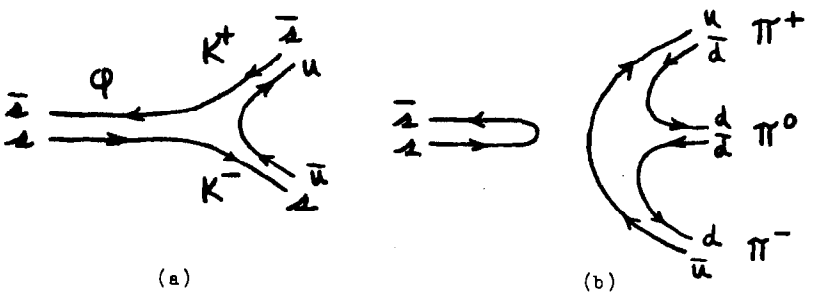

Fig. 4. OZI-allowed (a) and forbidden (b) transitions in ϕ meson decay.

The OZI rule has been invoked for ϕ decay to "explain" the relative suppression of $\phi \to 3\pi$ compared to $\phi \to K\bar{K}$, as indicated above, and also to "explain" the extremely small widths of the ψ and the ψ'. The inhibition for ϕ decay is moderate, perhaps a factor of 50 in the rate, while for the ψ and the ψ' the suppression factor is of the order of 5×10^3.

There are at least three attitudes towards the approximate validity of the OZI rule. One is to accept it as a rigorous (if not understood) selection rule in the limit of perfect SU(3) or SU(4) symmetry. Then its violation can be understood via symmetry breaking, e.g., by small admixtures of $u\bar{u}$ and $d\bar{d}$ quarks in the wave function of the ϕ meson, and analogous admixtures in the wave functions of ψ and ψ'. The tendency for the OZI rule to hold better for the ψ and ψ' than for the ϕ can be understood, qualitatively at least, in a calculation of the eigenstates of the mass matrix of the 16-plet of vector mesons. The relative purity of the ψ follows from the remoteness of its mass eigenvalue from the other vector mesons.

A second, dynamical, approach appeals to dual models and the concept of intermediate pomeron-like states that transmit no quantum numbers. To motivate these we must consider how the pomeron is viewed in duality diagram language. Figure 5 shows some diagrams. At the top are simple planar and nonplanar or twisted diagrams, the second obtained from the first by s-u crossing (if the s-channel is the horizontal direction). The diagram at bottom left is two twisted diagrams fastened together. It is a diagram that arises in higher order and has the significant feature that the quark lines end up in their original configurations after excursions in the t-channel in the intermediate state. The diagram at bottom right is merely a distortion of the one at bottom left, the aim being to enhance the impression of a somewhat complicated object being exchanged in the vertical (t-channel) direction. This is the duality diagram for the pomeron in lowest order. It is called a "cylinder" contribution in the language of the topological expansion of Veneziano. The relative weakness of the pomeron (you thought of it as strong, but you are wrong!) is understood in the Veneziano scheme because in the topological expansion in inverse powers of N^2 (N is equal to the number of quarks) the lowest order corresponds to planar duality diagrams and the cylinder contributions come in higher orders.

Planar

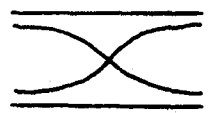

Twisted

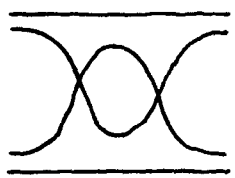

Two Twisted diagrams fastened together

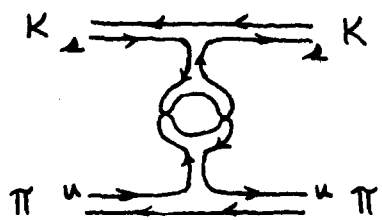

Same as on the left, but distorted in a suggestive manner to show twists

Fig. 5

Although the pomeron trajectory (with its even signature states, 0^{++}, 2^{++}, ...) cannot enter as an intermediate state in ϕ or ψ decay, its first daughter can. Freund and Nambu (1975) proposed a specific model for decays that violate the OZI rule. The diagram of Fig. 6(a) indicates the scheme for $\phi \to \rho\pi$ via the vector state "0".

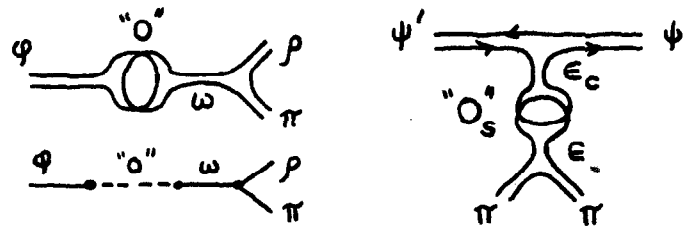

(a) (b)

Fig. 6. OZI rule violation via intermediate states that lie on daughters of the pomeron trajectory.

The vector state "0" is assumed to be a SU(4) singlet that mixes ϕ and ω. From Regge systematics, its mass is expected to be of order $\sqrt{2}$ - $\sqrt{3}$ GeV. Calculations are made using a sequential pole model, as indicated in the lower part of Fig. 6(a). Although this model suffers from the introduction of a family of particles that have not been seen and also some arbitrariness in how to compute numbers, it has some quantitative success (Bolzan et al., 1975).

If we consider the Zweig-forbidden cascade decay, $\psi' \to \psi\pi\pi$, it is necessary to invoke the second daughter trajectory of the pomeron, with its 0^{++} state, as indicated in Fig. 6(b). The pomeron daughter is coupled to the ψ-ψ' system via a $c\bar{c}$ s-wave state ε_c, while the s-wave pion pair couples on the other side via the well-known (and ill-defined) ε. Detailed calculations for this decay and others are given by Chaichain and Hayashi (1976). The model has numerous parameters, while the available data are still fragmentary enough that it is difficult to judge the success of this approach to the violations of the OZI rule.

A somewhat related, but less specific, discussion of the OZI rule and its violation has been given by Chew and Rosenzweig (Chew and Rosenzweig, 1976; Rosenzweig, 1976). They give arguments to show that the S-matrix may be asymptotically planar, in the sense of Veneziano's topological expansion, with non-planar contributions diminishing as t increases. Then the S-matrix elements possess exchange degeneracy and the OZI rule is obeyed. Near $t = 0$ cylinder contributions are important and the OZI rule is violated, trajectories are shifted from their linear behavior away from $t = 0$. A study of the relevant particle states indicates that the cylinder "quenching interval", i.e. the mass squared interval over which a significant decrease in the nonplanar contribution occurs, is larger for the unnatural spin-parity trajectories than for the natural spin-parity ones. This may help to understand the lack of ideal mixing for the π^0, η, η', as compared to the neutral vector mesons. Rosenzweig (1976) has attempted a phenomenological analysis on the basis of these ideas.

Two remarks before leaving S-matrix, duality approaches to the OZI rule. The first is that the Freund-Nambu model, while using duality and the pomeron, is rather orthogonal to the Chew-Rosenzweig mechanism. Freund and Nambu had explicitly to exclude higher mass $J = 1^{--}$ states that would normally appear in dual models - at least one such state would plausibly lie close enough to the ψ to cause a resonant enhancement rather than an inhibition! The second remark is that new thresholds may play an important part in causing drastic departures from the smoothly decreasing strength of the OZI-rule violation as energy increases. Törnqvist (1976) has considered such effects above and below the charm threshold in e^+e^- annihilation. There are not enough data at present to test his predictions, but the idea seems plausible. One should expect widely different OZI inhibition factors for the various resonances (ψ, ψ', ψ'' ...), with a smooth trend visible only in the region well above 4 GeV (assuming there are not other important thresholds too soon after crossing the charm threshold).

Our final remarks about the OZI rule concern asymptotic freedom. Zweig-forbidden decays such as $\phi \to 3\pi$, shown in Fig. 4(b) as a duality diagram, are translated in gauge field theories into a collection of Feynman diagrams like Fig. 7(a). The $s\bar{s}$ bound state annihilates into

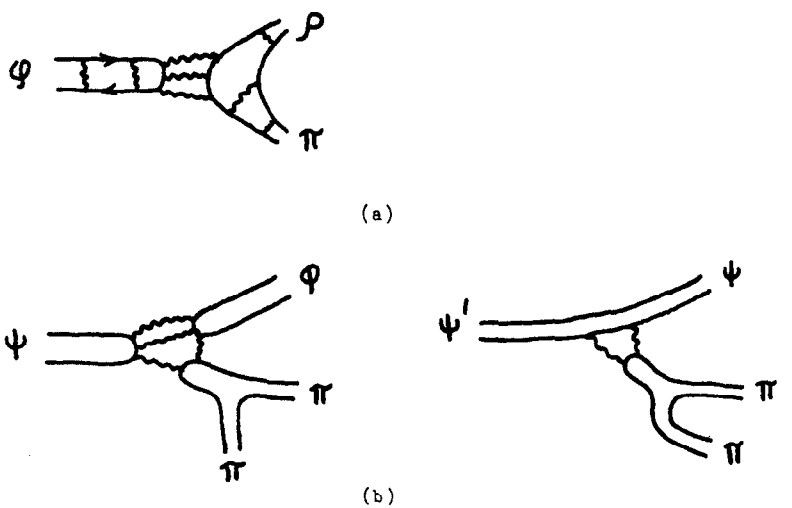

Fig. 7. (a) Feynman diagram describing $\phi \to \rho\pi$.
(b) Two "Feynman" diagrams for Zweig-forbidden ψ decays. Only the OZI-rule violating gluons are shown.

three massless vector gluons (Yang's theorem forbids fewer for a $J = 1$ state) which, because they carry no flavor, materialize into lighter $u\bar{u}$ or $d\bar{d}$ pairs to give a $\rho\pi$ final state. In perturbation theory the rate for a process involving n "hard" gluons, each carrying an average mass squared of s, will be proportional to $\left[\bar{\alpha}(s)\right]^n$. If the "running" coupling constant is small, we thus expect the rate of the Zweig-forbidden decay, $\phi \to \rho\pi$, to be proportional to α_s^3. Given that $\phi \to \rho\pi$ is inhibited, we infer that α_s is small. Then the general concept of asymptotic freedom, or the specific energy dependence of Eq. (3.4), implies that Zweig's rule should get better and better as the mass of the decaying state increases. We shall see in a later section that the experimental numbers for ϕ decay are not that compelling ($\alpha_s \simeq 0.5$), but that for ψ decay things are somewhat more favorable ($\alpha_s \simeq 0.2$). Thus the qualitative features of the violations of the OZI rule are consistent with asymptotic freedom.

There is one cause for concern. In Fig. 7(b) are shown two Zweig-forbidden ψ decays. The left-hand process plausibly involves "hard" enough gluons to give a healthy inhibition, but the cascade decay shown on the right involves relatively "soft" gluon exchange. Asymptotic freedom arguments do not seem to apply. Things may not be too unsatisfactory, however, because the cascade decay $\psi' \to \psi\pi\pi$ is less inhibited than $\psi \to$ hadrons. Comparison of $\psi' \to \psi\pi\pi$ with $\rho' \to \rho\pi\pi$ gives, after correction for the very different phase spaces, an estimate of $\sim$10 MeV for $\psi' \to \psi\pi\pi$ without any inhibition. The observed width of $\sim$0.13 MeV implies an OZI rule inhibition factor of $\sim$75, not very different from that of the ϕ meson and far less than for $\psi \to$ hadrons. This is somewhat comforting, but far from convincing.

The conclusion about Zweig's rule is that at the hand-waving level asymptotic freedom gives an explanation, as does cylinder "quenching" in Veneziano's topological expansion. At the quantitative level there is some phenomenology, but no deep understanding.

V. WEAK DECAYS OF CHARMED MESONS*

1. General Framework

As Bjorken has discussed in detail, the "conventional" model, a Weinberg-Salam theory with left-handed weak isodoublets,

$$\begin{pmatrix} \nu_\mu \\ \mu^- \end{pmatrix}_L , \quad \begin{pmatrix} \nu_e \\ e^- \end{pmatrix}_L , \quad \begin{pmatrix} u \\ d' \end{pmatrix}_L , \quad \begin{pmatrix} c \\ s' \end{pmatrix}_L \tag{5.1}$$

and right-handed weak isosinglets, leads to an effective 4-fermion interaction,

$$H_w = \frac{G}{\sqrt{2}} (J_\ell + J_h) (J_\ell + J_h)^\dagger \tag{5.2}$$

where J_ℓ is the lepton current and J_h is the hadronic (quark) current. Lorentz group and charge structure have been suppressed in (5.2). The symbols d' and s' in (5.1) stand for the Cabibbo-rotated linear combinations of fields. The interaction sorts itself out into lepton-lepton, lepton-hadron, and hadron-hadron pieces involving charged currents and neutral currents. The particle content of the various terms in the current are:

---

*This discussion is very derivative. It is based largely on Gaillard, Lee and Rosner (1975), with some brief remarks about 20-plet enhancement.

Charged leptonic current:

$$J_\ell^C = \bar{\nu}_e e + \bar{\nu}_\mu \mu \qquad (5.3a)$$

Neutral leptonic current:

$$J_\ell^N = \bar{\nu}_e \nu_e + \bar{\nu}_\mu \nu_\mu - \bar{e}e - \bar{\mu}\mu \qquad (5.3b)$$

Charged hadronic current:

$$J_h^C = \cos\theta\,(\bar{u}d + \bar{c}s) + \sin\theta\,(\bar{u}s - \bar{c}d) \qquad (5.3c)$$

Neutral hadronic current:

$$J_h^N = \bar{u}u + \bar{c}c - \bar{d}d - \bar{s}s \qquad (5.3d)$$

Here $\theta \approx 0.23$ radians is the famous Cabibbo angle.

The Lorentz group structure of the currents is not shown in Eqs. (5.3). For the charged currents it is V-A everywhere, e.g., $\bar{\nu}_e\gamma_\mu(1+\gamma_5)e$ in my (old-fashioned) notation and $\bar{\nu}_e\gamma_\mu(1-\gamma_5)e$ in the notation of Bjorken and Drell. For the neutral currents the mixing of the photon and the Z^o in a gauge theory with spontaneous symmetry breaking causes the effective neutral currents involving charged particles to be mixtures of V-A and V. In the Weinberg (1972) theory, for example, the neutral leptonic current has $\gamma_\mu(1+\gamma_5)$ between the neutrino spinors, but $\gamma_\mu(1-4\sin^2\theta_w+\gamma_5)$ between the electron and muon spinors. The angle θ_w is the Weinberg angle, a mixing angle not fixed a priori in the model. For the neutral hadronic current (with only p and n fields, representing proton and neutron), the $\bar{n}n$ term in (5.3d) reads explicitly as $\bar{n}\frac{1}{2}\gamma_\mu(1+\gamma_5)n$ while the $\bar{p}p$ term is $\bar{p}\frac{1}{2}\gamma_\mu(1-4\sin^2\theta_w+\gamma_5)p$. Since Bjorken has discussed these things thoroughly and we will only need the charged current aspects, we abandon further consideration of the neutral currents, except for a final remark that Eq. (5.3d) shows explicitly the GIM mechanism in operation. Without the charmed quark c coupled to the strange quark s, the neutral current would have involved a $(\bar{d}s + \bar{s}d)$ term, a strangeness-changing neutral current. The symmetry of the two weak isodoublets of quarks in (5.1) leads to the strangeness, charm, and isospin-conserving neutral current, (5.3d).

The hadronic selection rules contained in the charm-changing part of the charged current (5.3c) are

(a) Cabibbo-allowed transitions (cos θ in the amplitude):

$$\Delta Q = \Delta C = \Delta S\,,\quad \Delta I = 0 \qquad (5.4)$$

(b) Cabibbo-forbidden transitions (sin θ in the amplitude)

$$\Delta Q = \Delta C\,,\quad \Delta S = 0\,,\quad \Delta I = \tfrac{1}{2}$$

It is perhaps easier just to look at the adjoint of the current itself,

$$J^\dagger \;\alpha\; \cos\theta\,(\bar{s}c) - \sin\theta\,(\bar{d}c) + \ldots \qquad (5.5)$$

Eq. (5.5) shows immediately that semi-leptonic or hadronic decays of charmed mesons should preferentially yield $\bar{K}$ or K mesons according to $D \to \bar{K} + \ldots$ and $\bar{D} \to K + \ldots$

2. Leptonic decays of pseudoscalars

The decay amplitude for $P \to \ell\nu$ is

$$M = \frac{G}{\sqrt{2}} \langle 0 \mid \left(J_h^C \right)_\mu \mid P \rangle (\bar{\ell} \gamma_\mu (1+\gamma_5) \nu) \qquad (5.6)$$

where, for example,

$$\begin{aligned} \langle 0 \mid J_\mu \mid \pi^-(q) \rangle &= i f_\pi \cos\theta \, q_\mu \\ \langle 0 \mid J_\mu \mid K^-(q) \rangle &= i f_K \sin\theta \, q_\mu \\ \langle 0 \mid J_\mu \mid D^-(q) \rangle &= -i f_D \sin\theta \, q_\mu \\ \langle 0 \mid J_\mu \mid F^-(q) \rangle &= i f_F \cos\theta \, q_\mu \end{aligned} \qquad (5.7)$$

The Cabibbo angle structure in (5.7), including relative signs, is determined by comparing the quark structure of each meson from (2.2) with the corresponding term in the current (5.3c). The constants f_π, f_K, f_D, f_F are called the meson decay constants. If SU(4) is not spontaneously broken (or badly broken, except for quark masses), we expect these decay constants to be all approximately equal. The charged pion decay rate is

$$\Gamma(\pi^- \to \mu^- \bar{\nu}_\mu) = \frac{G^2}{8\pi} f_\pi^2 \cos^2\theta \, m_\mu^2 \left(1 - \frac{m_\mu^2}{m_\pi^2} \right)^2 m_\pi \qquad (5.8)$$

The experimental rate of $\Gamma = 3.84 \times 10^7 \text{ sec}^{-1}$ leads to $f_\pi \simeq 0.138$ GeV. For other mesons we merely substitute the appropriate mass and factor from (5.7) to replace $f_\pi \cos\theta$. With a Cabibbo angle of $\theta \simeq 0.23$-0.24 radians (determined from an overall fit to meson and baryon decays), the rate $\Gamma = 5.14 \times 10^7 \text{ sec}^{-1}$ for $K^+ \to \mu^+ \nu_\mu$ gives $|f_K| = 1.15 \, |f_\pi|$, with an uncertainty of about $\pm 3\%$ from the error in the Cabibbo angle.

Since the phase-space factor $(1 - m_\mu^2/m_K^2)^2 = 0.91$ for K decay and will be closer to unity for heavier particles, we can estimate that

$$\Gamma(D^+ \to \mu^+ \nu) \simeq \frac{m_D}{m_K} \Gamma(K^+ \to \mu\nu)$$

and (5.9)

$$\Gamma(F^+ \to \mu^+ \nu) \simeq \frac{m_F}{m_K} \cot^2\theta \, \Gamma(K^+ \to \mu\nu)$$

With $m_D = 1.86$ GeV and $m_F \simeq 2.0$ GeV, we have

$$\begin{aligned} \Gamma(D^+ \to \mu^+ \nu) &\simeq 2 \times 10^8 \text{ sec}^{-1} \\ \Gamma(F^+ \to \mu^+ \nu) &\simeq 3.6 \times 10^9 \text{ sec}^{-1} \end{aligned}$$

Since the overall decay rate is estimated to be of the order of 10^{12} sec^{-1} or greater (see below), these purely leptonic decays should be a negligible contribution.

3. Semileptonic decays of pseudoscalars

The decay $D^+ \to \bar{K}^0 \ell^+ \nu$ is analogous to $K^0 \to \pi^- \ell^+ \nu$. The structure of the current tells us that the D decay has a cos θ factor, while the K decay has sin θ. The hadronic matrix element has two form factors, $f_+(q^2)$ and $f_-(q^2)$. To the extent that we can neglect m_ℓ/m_K or m_ℓ/m_D, only f_+ enters. Assuming a constant form factor,

the rate is (see Jackson, 1962, for example)

$$\Gamma = \frac{G^2|f_+|^2}{768\pi^3} M^5 F(m/M) \qquad (5.10)$$

where M is the mass of the decaying meson, m the mass of the decay hadron, and

$$F(x) = 1 - 8x^2 + 8x^6 - x^8 - 24x^4 \ln x \qquad (5.11)$$

Assuming equal form factors, apart from Cabibbo angle multipliers, the $D_{\ell 3}$ rate is thus estimated to be

$$\Gamma(D^+ \to \bar{K}^0 \ell^+ \nu) \simeq \left(\frac{m_D}{m_K}\right)^5 \frac{F(m_K/m_D)}{F(m_\pi/m_K)} \cot^2\theta \cdot \Gamma(K^0 \to \pi^- \ell^+ \nu) \qquad (5.12)$$

With $m_D = 1.86$ GeV and $\Gamma(K^0 \to \pi^- e^+ \nu) \simeq 7.5 \times 10^6$ sec^{-1}, we find

$$\Gamma(D^+ \to \bar{K}^0 \ell^+ \nu) = \Gamma(D^0 \to K^- \ell^+ \nu) \simeq 1.0 \times 10^{11} \text{ sec}^{-1}.$$

The sum of $D_{\mu 3}$ and D_{e3} rates is then

$$\Gamma(D \to \bar{K}\mu\nu) + \Gamma(D \to \bar{K}e\nu) \simeq 2 \times 10^{11} \text{ sec}^{-1} \qquad (5.13)$$

The Cabibbo-forbidden decay $D^+ \to \pi^0 \mu^+ \nu$ is suppressed by a factor $\tan^2\theta \simeq 0.05$ relative to the rate (5.13).

The strange charmed meson $F^+ = (c\bar{s})$ will transform into $(s\bar{s})$ with strength $\cos\theta$ and $d\bar{s}$ with $\sin\theta$. Thus we expect the dominant semileptonic transitions to be

$$F^+ \to \eta \ell^+ \nu \quad \text{and} \quad F^+ \to \eta' \ell^+ \nu$$

while $F^+ \to K^0 \ell^+ \nu$

should be $\tan^2\theta$ suppressed. Because of SU(3) mixing in η and η' there is some additional uncertainty in the rates. Very roughly, we expect the sum of the rates for $F^+ \to \eta\mu^+\nu$ and $\eta e^+\nu$ to be comparable to (5.13) if the F^+ mass is around 2 GeV.

Because the charmed meson masses are relatively large, the possibility of multi-hadronic semi-leptonic decays needs to be entertained. We can consider successive pion emission within the framework of PCAC. As Gaillard, Lee and Rosner remark, a multipion amplitude vanishes in the soft-pion limit for every pion, basically because the relevant piece $(\bar{c}s)$ of the quark current is an isoscalar and commutes with the isotopic axial charge Q_5^α. Thus semileptonic decays with multiple hadrons may be somewhat suppressed.

4. Inclusive semileptonic and hadronic rates

A naive estimate can be made of the rate for $D \to \ell\nu +$ hadrons or $D \to$ hadrons by imagining the weak decay process to proceed via quasi-free quarks, with the quarks transforming into hadrons subsequently, as indicated schematically in Fig. 8. It is assumed that

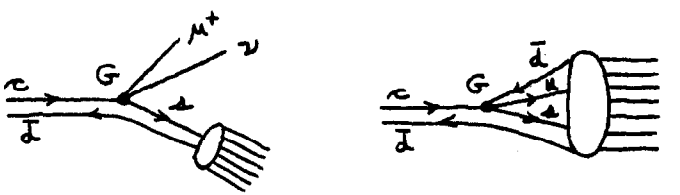

Fig. 8. Schematics of how inclusive decays can be estimated.

the quarks turn into hadrons with unit probability.

For the semi-leptonic inclusive process we can take over the usual beta decay rate formula, or the one for muon decay if we assume that the charmed quark mass is much larger than the mass of the other quarks. The latter rate is

$$\Gamma(\mu \to e\nu\bar{\nu}) = \frac{G^2 m_\mu^5}{192\pi^3} \qquad (5.14)$$

With m_μ replaced by $m_c \approx 1.6$ GeV, we estimate from $\Gamma(\mu \to e\nu\bar{\nu}) = 4.55 \times 10^5$ sec^{-1},

$$\Gamma(D \to \ell\nu + \text{hadrons}) \approx 0.7 \times 10^{12} \text{ sec}^{-1} \qquad (5.15)$$

The hadrons should almost always contain a K meson.

For the inclusive hadronic decay estimate, the relevant interaction is the product of the hadronic current (5.3c) with its adjoint. There is thus a factor $\cos^2\theta$ multiplying the term $(\bar{u}d)(\bar{s}c)$. There is in addition an enhancement factor A responsible for the $\Delta I = \frac{1}{2}$ rule of hadronic decays. We comment on this in a subsequent section. For the present just accept the estimate, $A \sin\theta \approx 1$. The rate for decay of $D \to$ hadrons is thus estimated to be a factor of $\frac{1}{2}(A\cos^2\theta)^2 \approx \frac{1}{2}\operatorname{cosec}^2\theta$ larger than (5.15):

$$\Gamma(D \to \text{hadrons}) \approx 7 \times 10^{12} \text{ sec}^{-1} \qquad (5.16)$$

Without the enhancement factor of $\sim$19, this rate would be 3.5×10^{11} sec^{-1}, about $\frac{1}{2}$ of (5.15). Then a very large fraction of D decays would contain leptons. There are already experiments that probably bear on this. New results from DESY, reported at the Tblisi Conference (and at the SLAC Topical Conference by P. Schmuser and H. Meyer) on the channels $e^\pm X$ and $e^\pm(K_S^0 \to \pi^+\pi^-)X$, where X = hadrons, can plausibly be associated with inclusive semi-leptonic decays of charmed mesons. At 4.1 GeV the cross section for $e^\pm X$ is >1 nb, while for $e^\pm(K_S^0 \to \pi^+\pi^-)X$ is 0.8 nb. At 4.03 GeV, the "new" part of the total cross section is about 15 nb. With a $D\bar{D}$ pair in each event, there is then $\sim$30 nb for inclusive D (or $\bar{D}$) production. Correcting for the unseen $K_S \to \pi^0\pi^0$ and the K_L^0 yields $0.8 \times 1.8 = 1.4$ nb for $e^\pm K^0 X$ decays. The branching ratio for the inclusive semileptonic (e and μ) decay $D \to \ell K^0 X$, (mostly $D^\pm$?) is then 2.8 nb/30 nb $\approx$ 0.1. This is in agreement with (5.15) and (5.16), but is probably an underestimate. (K^0's come preferentially from charged D's if X = 0. There are more D^0 and $\bar{D}^0$ than $D^\pm$ produced at 4.03 GeV.) An actual cross section for $e^\pm X$ and a value for $K^\pm/K_S^0$ in these events will help clarify the situation. Depending on how much the total semi-leptonic branching ratio rises above 0.1, our use of the empirical $\Delta I = \frac{1}{2}$ enhancement factor in D decays will be less or more justified by the facts.

5. Multiparticle hadronic decays

There is no theory for multiparticle hadronic decays of charmed mesons. Gaillard, Lee and Rosner estimate the relative amounts of $K\pi$, $K\pi\pi$, $K\pi\pi\pi$, etc. using a very simple statistical model. They then use the inclusive rate, (5.16), to get very rough estimates of actual rates. We follow their footsteps for a while and then indicate modifications.

If Lorentz-invariant phase space is the controlling factor for $D \to \bar{K} + n\pi$, then

$$\Gamma_n = \frac{\text{constant}}{(\xi f_\pi)^{2n}} F_n \qquad (5.17)$$

where the matrix element has been taken as proportional to $(\xi f_\pi)^{-n}$, as might follow (with $\xi = 1$) from current algebra, and the phase space integral F_n is

$$F_n = \frac{1}{(2\pi)^{3n+3}} \int \frac{d^3k}{2k_o} \prod_{j=1}^{n} \frac{d^3p_j}{2E_j} \, \delta^{(4)}(k + \Sigma p_j - P) \tag{5.18}$$

For massless particles (including the K meson!), the integral can be done in elementary terms, with the result,

$$F_n^{(o)} = \frac{8M^{2n-2}}{(4\pi)^{2n+3} n!(n-1)!} \tag{5.19}$$

where M is the invariant mass of the decaying system. Combining (5.19) and (5.17) we find the GLR result for the ratio of successive rates for D meson decay,

$$\Gamma_{n+1}/\Gamma_n \simeq \left(\frac{m_D}{4\pi\xi f_\pi}\right)^2 \frac{1}{n(n+1)} \tag{5.20}$$

GLR's Table IV is computed from (5.20) with $\xi = 1$. In our Table 2 below we give their estimates for $m_D = 1.86$ GeV, together with those for $\xi = 0.5$. It can be seen that the distribution over the various states is rather sensitive to the n-dependence of the matrix element (the volume of the box, in the thermodynamic model of particle production).

Apart from unknown dynamics, there is a serious failing in the kinematics. The neglect of all masses grossly over-estimates the higher pion multiplicities. A very small step towards correcting this can be made by including at least the K meson mass in the calculation. For the decay of a particle of mass M into a particle of mass m plus n massless particles the invariant phase space integral (5.18) can be written for $n \geq 2$ as

$$F_n = F_n^{(o)} \cdot \left(1 + \frac{m^2}{M^2}\right)^n n(n-1) \int_{x_{min}}^{1} \sqrt{x^2 - x_{min}^2}\,(1-x)^{n-2} dx \tag{5.21}$$

where $x_{min} = 2Mm/(M^2+m^2)$. With $M = 1.86$ GeV and $m = 0.494$ GeV, $x_{min} = 0.50$. Then we find

$$F_2/F_2^{(o)} \simeq 0.62, \qquad F_3/F_3^{(o)} \simeq 0.38.$$

With an asymptotic estimate for higher n values, I find the numbers shown in Table 2 in columns 3 and 5, labelled $m_K \neq 0$. It is clear that the $(Kn\pi)$ states are rather sensitive to assumptions about

TABLE 2

Relative amounts of nonleptonic decays of a charmed pseudoscalar meson of mass 1.86 GeV, according to Eq. (5.20), and with phase space corrected for the nonvanishing K meson mass.

Final states	$\xi = 1.0$		$\xi = 0.5$	
	$m_K=0$	$m_K\neq0$	$m_K=0$	$m_K\neq0$
$\bar{K}\,\pi$	59%	72%	17%	30%
$\bar{K}\,2\pi$	34%	25%	39%	43%
$\bar{K}\,3\pi$	6^+%	3%	30%	20%
$\bar{K}\,4\pi$	1^-%		11%	6%
$\bar{K}\,5\pi$			3%	1%

masses and matrix element.

One thing seems clear. The naive statistical model, specially with mass corrections to the kinematics, does not predict large multiplicities for the dominant decay modes. It will be difficult to stretch its parameters to make $(K3\pi)/(K\pi) \gtrsim 3$, as is indicated by experiment (Goldhaber et al.; 1976). One modification of the model would be a matrix element that was damped strongly for high pion momenta. This would suppress the two-body mode most and could be adjusted to favor large multiplicities. Another possibility is strong resonance formation in the final state, e.g. $D \to K^* \pi\pi$ or even $K^{**}\pi$, although I know of no evidence for it at present.

6. Hadronic two-body decays of charmed mesons; generalization of the $\Delta I = \frac{1}{2}$ rule

Purely hadronic decays of particles are governed by the product of the hadronic current (5.3c) with its adjoint. In all its glory, the product is

$$\begin{aligned} J_h^c J_h^{c\dagger} = & \\ & \cos^2\theta \left[(\bar{u}d)(\bar{d}u) + (\bar{c}s)(\bar{s}c) + (\bar{u}d)(\bar{s}c) + (\bar{d}u)(\bar{c}s)\right] \\ + & \sin^2\theta \left[(\bar{u}s)(\bar{s}u) + (\bar{c}d)(\bar{d}c) - (\bar{u}s)(\bar{d}c) - (\bar{s}u)(\bar{c}d)\right] \\ + & \sin\theta\cos\theta \left[(\bar{u}d)(\bar{s}u) - (\bar{u}d)(\bar{d}c) + (\bar{c}s)(\bar{s}u) - (\bar{c}s)(\bar{d}c)\right] \\ & + \text{h.c.} \end{aligned} \tag{5.22}$$

If we consider ordinary $\Delta S = 1$ decays, the operative term is the first one in the last bracket. The SU(2) transformation properties are evident from the quark content:

$$(\bar{u}d)(\bar{s}u) \sim \pi^- K^+ \sim \sqrt{\tfrac{2}{3}}\ (I = \tfrac{1}{2}) - \tfrac{1}{\sqrt{3}}\ (I = \tfrac{3}{2})$$

Thus the primitive current-current interaction possesses both $\Delta I = \frac{1}{2}$ and $\Delta I = \frac{3}{2}$ terms, contrary to observation. [The $\Delta I = \frac{3}{2}$ amplitude is found to be only $\sim 5\%$ in magnitude relative to the dominant $\Delta I = \frac{1}{2}$.] Some dynamical mechanism is needed to enhance the $\Delta I = \frac{1}{2}$ part relative to the $\Delta I = \frac{3}{2}$ part. In SU(3) terms, since $\Delta I = \frac{1}{2}$ occurs in the $\underline{8}$ resulting from the product of the currents while $\Delta I = \frac{3}{2}$ occurs in the $\underline{27}$, we speak of "octet enhancement" as the necessary dynamic phenomenon. There are various theoretical arguments for octet enhancement. We mention one of them below.

For SU(4) and charm the basic situation is the same. We want the $\Delta I = \frac{1}{2}$ rule for the SU(3) sub-group in our theory, but the enhancement will be a SU(4) thing and will affect charmed particle decays, too. The necessary group theory has been done by a number of people (Altarelli, Cabibbo and Maiani, 1975; Kingsley et al., 1975; Einhorn and Quigg, 1975). The current-current product formerly of two octets, is now

$$\left[\underline{15} \otimes \underline{15}\right]_{SYM} = \underline{1} \oplus \underline{15}_S \oplus \underline{20} \oplus \underline{84}$$

The symmetric $\underline{15}$ does not actually enter this particular model of weak interactions. Only the $\underline{20}$ and $\underline{84}$ are relevant for $\Delta S = 1$ or $\Delta C = 1$ transitions. The SU(3) content of these two SU(4) representations is

	$\Delta C = 0$	$\lvert\Delta C\rvert = 1$
$\underline{20}$	$\underline{8}$	$\underline{6}$, $\overline{\underline{6}}$
$\underline{84}$	$\underline{8}$, $\underline{27}$	$\underline{15}$, $\overline{\underline{15}}$, ...

The observed octet dominance in $\Delta C = 0$ transitions evidently argues for the dominance of the $\underline{20}$ of SU(4) over the $\underline{84}$. This in turn implies a dominance of $\underline{6} + \underline{\bar{6}}$ for the charm-changing transitions. For pseudoscalar meson decays the consequence of $(\underline{6} + \underline{\bar{6}})$ dominance is that the modes involving only two pseudoscalars are all related by one matrix element. Thus, up to phase space correction factors and the neglect of η-η' mixing, we have the striking prediction,

$$\Gamma(D^+ \to \bar{K}^0\pi^+) = \Gamma(D^+ \to \pi^0\pi^+) = 0$$

(I, U, and V-spin afficianados will not be surprised to know that there is a V-spin argument for this.)

and

$$\begin{aligned}
\Gamma(D^0 \to \bar{K}^0\pi^0) &= \Gamma_0 \quad \text{(definition)} \\
\Gamma(D^0 \to K^-\pi^+) &= 2\Gamma_0 \\
\Gamma(D^0 \to K^-K^+) &= 2\tan^2\theta\,\Gamma_0 \\
\Gamma(D^0 \to \pi^-\pi^+) &= 2\tan^2\theta\,\Gamma_0 \\
\Gamma(D^0 \to \bar{K}^0\eta^0) &= \tfrac{1}{3}\Gamma_0 \\
\Gamma(D^+ \to \bar{K}^0K^+) &= 2\tan^2\theta\,\Gamma_0 \\
\Gamma(D^+ \to \eta^0\pi^+) &= \tfrac{4}{3}\tan^2\theta\,\Gamma_0 \\
\Gamma(F^+ \to \bar{K}^0K^+) &= 2\Gamma_0 \\
\Gamma(F^+ \to \eta^0\pi^+) &= \tfrac{4}{3}\Gamma_0
\end{aligned}$$

etcetera.

How plausible is $\underline{20}$ dominance? Opinion is divided. Considerations of the Weinberg-Salam theory and a color gauge symmetry of strong interactions based on the Wilson short-distance expansion show that the singular behavior of the octet part of the product of two currents is greater than that of non-octet parts, but only by a fractional power of $\log(r)$ (Gaillard and Lee, 1974). Whether this enhancement is enough to produce the $\Delta I = \frac{1}{2}$ rule is not clear. See B. W. Lee (1975, 1976) for an expert summary. In any event, it may be dangerous to use the octet enhancement factor $A \approx (\sin\theta)^{-1}$ deduced from $\Delta C = 0$ process, for charmed meson decays. Thus our comment below Eq. (5.16) should be noted again.

7. Odds and ends: Exotic final states, D^0-$\bar{D}^0$ mixing, Charmed baryon decays

As signatures of charmed particle decay, exotic final states are useful to exclude the alternative of just another mesonic of baryonic state. Recall that "exotic" means possessing quantum numbers of isospin and strangeness not allowed by the SU(3) $q\bar{q}$ and qqq model of hadrons. If you found a narrow resonance in the $\pi^+\pi^0$ system at a mass of 494 MeV, for example, and you could by some means establish that the J value was even, you would deduce that the $\pi^+\pi^0$ system had $I = 2$ and hence was exotic. Since no exotic meson has been observed, especially not below 1 GeV, you would rightly conclude that the $\pi^+\pi^0$ state was probably the result of a weak decay. You would have discovered the K^+ meson!

The newly discovered narrow state at 1.88 GeV, seen in $K^\pm\pi^\mp\pi^\mp$, is an example of such an exotic channel (Peruzzi et al., 1976). The nonexotic $K^\pm\pi^+\pi^-$ system shows no peak. While a narrow exotic state is, just on the basis of strong interaction systematics, probably something new and exciting, the systematics of the weak interactions

tells you to expect exotic final states from charmed particle decays. The Cabibbo-allowed decays have $\Delta C = \Delta S$. For the D^+ meson, $C = 1$, $S = 0$. Thus the final state will have $C = 0$, $S = -1$, $Q = +1$. From the Gell-Mann-Nishijima formula (2.1), we find $I_3 = \frac{3}{2}$, exotic.

Gaillard, Lee and Rosner argue that exotic states may be relatively suppressed, but then come to the view that it may only be the effect of the $\underline{20}$-plet enhancement: $K^+ \to \pi^+\pi^0$ is a $\Delta I = \frac{3}{2}$ transition; $D^+ \to \bar{K}^0\pi^+$ is exotic and is forbidden by $\underline{6} + \overline{\underline{6}}$ dominance. The $(\bar{K}n\pi)^+$, etc. final states may not be suppressed at all. Indeed, the relative amount of $K^\pm\pi^\mp\pi^\mp$ seen indicates no great inhibition compared with the D^0 decay modes.

Earlier we eluded to D^0-$\bar{D}^0$ mixing in analogy to the K^0-$\bar{K}^0$ system. The same general arguments apply, but the off-diagonal elements of the mass matrix are of order $\tan^2\theta \approx 0.05$ relative to the diagonal elements. This means that $\Delta\lambda/\lambda \ll 1$, $\Delta m/\lambda \ll 1$ are expected. The effects of the mixing will be small in general; initially formed D^0's will decay dominantly into $S = -1$ final states and so on. The mixing may be detectable nonetheless and may bear on the "wrong-sign" dimuon events at Fermilab (Kingsley et al., 1975; Kingsley, Wilczek and Zee, 1976).

Since charmed baryons have already been seen or are expected momentarily, a few remarks about their weak decays are in order. The Cabibbo-allowed decays will have

$$\Delta C = \Delta S = \Delta Q \quad , \Delta I = 0 \quad \text{(Semi-leptonic)}$$
and
$$\Delta C = \Delta S = -\Delta I_3, \Delta I = 1 \quad \text{(nonleptonic)} \qquad (5.23)$$

The non-strange charmed baryon with $C = 1$, $I = 0$, called C_o by GLR and Λ_c^+ by others, with quark content $c(ud)_{\text{antisym}}$, will decay to a final state with $S = -1$, $I = 1$, $I_3 = 1$ (e.g. $\Lambda\pi^+$) This is not exotic. But the Σ_c^{++}, with $C = 1$, $I = 1$, $I_3 = 1$ and quark content cuu, even if unstable against strong decay will go ultimately to an exotic final state with $Q = I_3 = 2$, $S = -1$, $I \geq 2$. The Brookhaven neutrino event (Cazzoli et al., 1975) has a final state of μ^- and the exotic combination $(\Lambda\,\pi^+\pi^+\pi^+\pi^-)$. The mass of the hadrons is 2.426 GeV. A ready interpretation of the hadronic state, as the authors point out, is Σ_c^{++}. See Chapter VI, Sec. 3, below.

The probability of multiparticle hadronic states can be estimated crudely by the statistical phase space arguments of Section 5, e.g. Eq. (5.17) and (5.21). For decay of a charmed baryon of mass M into an uncharmed baryon of mass m and n massless pions, Eq. (5.21) can be expanded in $(M-m)^2/(M+m)^2$ to give

$$F_n = \frac{4\sqrt{\pi}}{(4\pi)^{2n+3}} \frac{(M+m)}{M^2} \frac{(M-m)^{2n-1}}{(n-1)!\Gamma(n+\frac{1}{2})} \left[1 - \frac{n-1}{2n+1}\left(\frac{M-m}{M+m}\right)^2 - \cdots\right] \qquad (5.24)$$

For typical values of $M \approx 2.26$ GeV and $m = 1.115$ GeV, $(M-m)^2/(M+m)^2 \approx 0.114$. The correction term is less than 6% for all n. Neglecting this correction we find the ratio of successive rates given by

$$\Gamma_{n+1}/\Gamma_n \approx \left(\frac{M-m}{4\pi\xi f_\pi}\right)^2 \frac{1}{n(n+\frac{1}{2})} \qquad (5.25)$$

This is essentially the same as the mesonic formula (5.20), but with (M-m) instead of M. The net effect is to favor low multiplicities, relative to those shown in Table 2. In order to generate appreciable branching ratios for $\Lambda_c^+ \to (\Lambda 3\pi)^+$, for example, the model will need a matrix element that favors even softer pions that statistical.

VI. HADRONIC MASSES ACCORDING TO DE RÚJULA, GEORGI AND GLASHOW

As a warm-up for the detailed discussion of the new spectroscopy of states seen in e^+e^- annihilation, we give a summary of the view of hadronic masses that follows from arguments of asymptotic freedom, quarks, and quark confinement (De Rújula, Georgi and Glashow, 1975, abbreviated as DGG below). The assumptions that go into the scheme are

(1) Essentially non-relativistic dynamics, with v/c or v^2/c^2 corrections, can be used to describe quark motion inside all hadrons, except perhaps the very lighest.

(2) The quark confinement interaction is a long-range potential that is independent of spins and of masses of the quarks.

(3) At short distances the SU(3) symmetric color gluon gauge theory is manifest with small enough coupling constant that the results from the quasi-static limit of QED can be taken over directly. (The question of whether the gluon propagator is proportional to k^{-2}, leading to a 1/r potential in the static limit, or some more complicated function of k^2, is not important for the most part. We comment on this question at the appropriate place below.)

(4) The only symmetry breaking comes from the different masses assigned the quarks of different flavors.

(5) The physical states are color singlets.

1. Darwin-Breit-Fermi interaction in QED

The classical Lagrangian of interaction between charged particles, including velocity-dependent terms to order v^2/c^2, is called the Darwin Lagrangian and is

$$L_{\text{Darwin}} = \frac{1}{2}\sum_i m_i v_i^2 + \frac{1}{8c^2}\sum_i m_i v_i^4 - \sum_{i>j} \frac{Q_i Q_j}{r_{ij}}\left[1 - \frac{1}{2c^2}\left(\vec{v}_i \cdot \vec{v}_j + \vec{v}_i \cdot \hat{r}_{ij}\, \vec{v}_j \cdot \hat{r}_{ij}\right)\right] \tag{6.1}$$

as can be found in any good textbook on electromagnetism. Similarly, the classical interaction energy of two magnetic moments $\vec{\mu}_1$ and $\vec{\mu}_2$ is found to be

$$H_{\text{hfs}}^{(1)} = -\frac{8\pi}{3}\,\vec{\mu}_1 \cdot \vec{\mu}_2\,\delta(\vec{r}) + \frac{1}{r^3}\left[\vec{\mu}_1 \cdot \vec{\mu}_2 - 3\hat{r} \cdot \vec{\mu}_1\, \hat{r} \cdot \vec{\mu}_2\right] \tag{6.2}$$

where $\vec{r} = \vec{r}_1 - \vec{r}_2$ is the relative separation. The second term here is the familiar dipole-dipole interaction that vanishes for particles in a relative s-state. The first term is called the Fermi hyperfine interaction. It was first obtained by a nonrelativistic reduction of the Dirac equation, but is really a classical phenomenon associated with the fact that currents are the source of magnetic moments (See any good textbook, as mentioned above). If the particles possessing the magnetic moments also carry electric charge, the interaction energy is augmented by $-\vec{\mu}_i \cdot \vec{B}_j$ terms, where $\vec{B}_j$ is the magnetic field at the

ith particle caused by the motion of the jth charge. Nonrelativistically this interaction is

$$H^{(2)}_{hfs} = \frac{1}{r^3}\left[\frac{Q_2}{m_2}(\vec{r}\times\vec{p}_2)\cdot\vec{\mu}_1 - \frac{Q_1}{m_1}(\vec{r}\times\vec{p}_1)\cdot\vec{\mu}_2\right] \tag{6.3}$$

With the quantum-mechanical substitution,

$$\vec{\mu}_j = g_j\frac{Q_j\hbar}{2m_jc}\vec{s}_j \tag{6.4}$$

where $\vec{s}_j$ is the jth spin and g_j the jth Landé g-factor, the sum of (6.2) and (6.3), generalized in an obvious way to more than two particles if need be, can be used immediately to treat hyperfine structure in atoms. The Darwin Lagrangian (6.1) also has a quantum-mechanical analog obtained, first by Breit (1929), by replacing the velocities in the last interaction term by Dirac $\vec{\alpha}_j$ matrices (and the kinetic energy terms by a sum of free-particle Dirac energy operators). The Hamiltonian so obtained is called the Breit Hamiltonian. In the subsequent Pauli reduction there are momentum-dependent terms that emerge from (6.1) by the classical substitution, $\vec{v}_j \to \vec{p}_j/m_j$, but also spin-dependent terms that are similar in structure to (6.2) and (6.3). For a two-body system they all are exhibited on p. 193 of Bethe and Salpeter (1957). We do not bother to write them out here because we display the gauge-theoretical expression in Eq. (6.7) below. The Breit Hamiltonian is used to discuss relativistic effects in two (or more) - electron atoms.

2. Effective Quark Hamiltonian in color gauge theory

The Breit-Fermi Hamiltonian can be taken over almost immediately into the color gauge theory by replacing the electromagnetic coupling $\alpha = e^2/4\pi$ by the strong coupling constant α_s. There is only one catch - the substitution is actually

$$\alpha \to \begin{cases} -\frac{4}{3}\,\alpha_s & \text{for } q\bar{q} \\ -\frac{2}{3}\,\alpha_s & \text{for } qqq \end{cases} \tag{6.5}$$

The factors of $-\frac{4}{3}$ and $-\frac{2}{3}$ follow from the SU(3) color gauge group couplings and the requirement of color singlets for hadrons (see Barbieri, 1975).

Since we promised to compute some things, we derive these factors. There are 8 color gluons, labelled by a, b, c,.... The strength of their coupling to quarks of different colors (labelled by i, j, k = 1, 2, 3) is $g\,\lambda^a_{ij}/2$ for quarks, and $-g\,\lambda^a_{ij}/2$ for anti-quarks, where the λ's are the familiar SU(3) matrices. The "wave functions" of a color singlet $q\bar{q}$ system is $\delta_{ij}/\sqrt{3}$, corresponding to $|(q\bar{q})\rangle = \frac{1}{\sqrt{3}}\sum_{i=1}^{3}|q_i\bar{q}_i\rangle$. The corresponding baryon wave function is the totally antisymmetric $\epsilon_{ijk}/\sqrt{6}$. In Figs. 9a and 9b are shown the relevant gluon exchange diagrams.

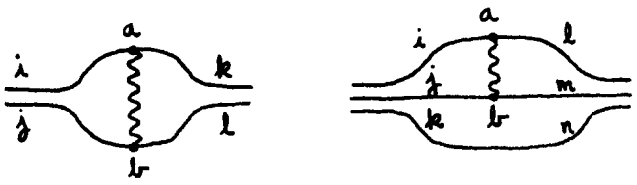

(a) (b)

Fig. 9 Gluon exchange in (a) $q\bar{q}$ system, and (b) qqq system. The constrictions at each end imply the color-singlet requirement.

For the $q\bar{q}$ system the effective coupling is given by

$$g_{\text{eff}}^2 = \sum_{a,b} \sum_{i,j,k,\ell} \frac{1}{\sqrt{3}} \delta_{ij} \left(\frac{g}{2} \lambda^a_{ik} \right) \left(-\frac{g}{2} \lambda^b_{\ell j} \right) \frac{1}{\sqrt{3}} \delta_{k\ell}$$

$$= -\frac{g^2}{12} \sum_{a,b} \sum_{j,\ell} \lambda^a_{j\ell} \lambda^b_{\ell j}$$

$$= -\frac{g^2}{12} \sum_{a,b} \text{Tr}(\lambda^a \lambda^b) = -\frac{g^2}{6} \sum_{a,b} \delta^{ab}$$

$$= -\frac{8}{6} g^2 = -\frac{4}{3} g^2$$

Similarly for the qqq system, we have the effective coupling,

$$g_{\text{eff}}^2 = \sum_{a,b} \sum_{\substack{i,j,k \\ \ell,m,n}} \frac{\epsilon_{ijk}}{\sqrt{6}} \left(\frac{g}{2} \lambda^a_{i\ell} \right) \left(\frac{g}{2} \lambda^b_{jm} \right) \frac{\epsilon_{\ell mn}}{\sqrt{6}} \delta_{kn}$$

$$= \frac{g^2}{24} \sum_{a,b} \sum_{i,j,\ell,m} \lambda^a_{i\ell} \lambda^b_{jm} \sum_{k} \epsilon_{ijk} \epsilon_{\ell mk}$$

Now

$$\sum_k \epsilon_{ijk} \epsilon_{\ell mk} = \delta_{i\ell} \delta_{jm} - \delta_{im} \delta_{j\ell}$$

Thus our coupling becomes

$$g_{\text{eff}}^2 = \frac{g^2}{24} \sum_{a,b} \left\{ \text{Tr}(\lambda^a) \, \text{Tr}(\lambda^b) - \text{Tr}(\lambda^a \lambda^b) \right\}$$

$$= -\frac{2g^2}{3}$$

Now we can write down the quasi-static Hamiltonian for a bound state of quarks with masses m_j and spins $\vec{s}_j$. In the notation of DGG, the Hamiltonian is

$$H = \sum_i \left(m_i + \frac{\vec{p}_i^{\,2}}{2m_i} + \ldots \right) + L(\vec{r}_1, \vec{r}_2, \ldots) + \sum_{i>j} (\alpha Q_i Q_j + k\alpha_s) S_{ij} + \ldots \tag{6.6}$$

The potential L describes the universal quark binding force, $k = -\frac{4}{3}$ for $q\bar{q}$ and $-\frac{2}{3}$ for qqq, and the quasi-static Breit-Fermi-Coulomb potential operator S_{ij} is

$$S_{ij} = \frac{1}{r} - \frac{1}{2m_i m_j}\left[\frac{\vec{p}_i\cdot\vec{p}_j}{r} + \frac{\hat{r}\cdot(\hat{r}\cdot\vec{p}_i)\,\vec{p}_j}{r}\right]$$
$$- \frac{1}{m_i m_j r^3}\left[3(\vec{s}_i\cdot\hat{r})(\vec{s}_j\cdot\hat{r}) - \vec{s}_i\cdot\vec{s}_j + (\vec{r}\times\vec{p}_i)\cdot\vec{s}_j - (\vec{r}\times\vec{p}_j)\cdot\vec{s}_i\right]$$
$$- \frac{8\pi}{3}\frac{\vec{s}_i\cdot\vec{s}_j}{m_i m_j}\delta(\vec{r}) - \frac{\pi}{2}\left(\frac{1}{m_i^2} + \frac{1}{m_j^2}\right)\delta(\vec{r}) \qquad (6.7)$$
$$- \frac{1}{2r^3}\left[\frac{1}{m_i^2}(\vec{r}\times\vec{p}_i)\cdot\vec{s}_i - \frac{1}{m_j^2}(\vec{r}\times\vec{p}_j)\cdot\vec{s}_j\right]$$

Here $\vec{r} = \vec{r}_i - \vec{r}_j$. We see in this rather formidable operator some familiar terms. The first two correspond exactly to the Darwin interaction in Eq. (6.1). The next two are the hyperfine interaction terms, (6.2) and (6.3). The last two are purely quantum-mechanical, arising in the Pauli reduction of the Dirac matrices.

It is useful in discussing the $c\bar{c}$ system to have the effective gauge theory Hamiltonian specialized to its equal-mass, center of momentum frame form for particle and anti-particle:

$$H = \left(2m + \frac{\vec{p}^2}{2\mu} + \ldots\right) + V(r)$$
$$- \left(e_Q^2\,\alpha + \frac{4}{3}\alpha_s\right) S_{12} + \ldots \qquad (6.8a)$$

with

$$S_{12} = \frac{1}{r} + \frac{1}{2m^2}\left[\frac{\vec{p}^2}{r} + \frac{\hat{r}\cdot(\hat{r}\cdot\vec{p})\vec{p}}{r}\right]$$
$$+ \frac{1}{m^2 r^3}\left[\vec{s}_1\cdot\vec{s}_2 - 3(\vec{s}_1\cdot\hat{r})(\vec{s}_2\cdot\hat{r})\right] - \frac{8\pi}{3}\frac{\vec{s}_1\cdot\vec{s}_2}{m^2}\delta(\vec{r})$$
$$- \frac{3}{2m^2 r^3}(\vec{r}\times\vec{p})\cdot(\vec{s}_1+\vec{s}_2) - \frac{\pi}{m^2}\delta(\vec{r}) \qquad (6.8b)$$

With $V = 0$ this is just the positronium Hamiltonian in the quasi-static limit. The terms in (6.8b) after the first correspond to H_2, H_5, H_3 and H_4, respectively, on p. 193 of Bethe and Salpeter.

It seems unrealistic to some people that the quasi-static Coulomb potential should apply at any but the very shortest distances. Because of the many desirable features of the DGG approach, soon to be elucidated, one searches for a relatively bland modification. One plausible, but by no means unique, recipe is to modify the propagator of the exchanged gluon (Schnitzer, 1976a; Pumplin, Repko, and Sato, 1975; Schnitzer, 1975):

$$\frac{g^2\gamma_\mu^{(1)}\gamma_\mu^{(2)}}{k^2} \to \gamma_\mu^{(1)}\gamma_\mu^{(2)}\,v(k^2)$$

where $v(k^2)$ is the Fourier transform of some potential. With the assumption that this potential is the phenomenological universal binding potential $V(r)$, the effective Hamiltonian (6.8) has the following

modification:

$$-\frac{4}{3}\alpha_s S_{12} + \frac{1}{3m^2}\left(\frac{d^2V(r)}{dr^2} - \frac{1}{r}\frac{dV(r)}{dr}\right)\left[\vec{s}_1\cdot\vec{s}_2 - 3(\vec{s}_1\cdot\hat{r})(\vec{s}_2\cdot\hat{r})\right]$$
$$+\frac{2}{3m^2}\vec{s}_1\cdot\vec{s}_2\,\nabla^2V(r)$$
$$+\frac{3}{2m^2}\left(\frac{1}{r}\frac{dV(r)}{dr}\right)(\vec{r}\times\vec{p})\cdot(\vec{s}_1+\vec{s}_2) \qquad (6.9)$$
$$+ \text{spin-independent terms}$$

We discuss the effects of this phenomenological modification of the potential below.

3. Examples of mass splittings within SU(3) multiplets; quark masses

The lowest states of the $q\bar{q}$ and qqq are $\ell = 0$ states of the relative orbital angular momenta of all pairs. The orbital angular momentum and tensor force parts of (6.7),(6.8b) or (6.9) vanish for these states. The only spin-dependent term that survives in S_{ij} is

$$(S_{ij})_{\ell=0} = -\frac{8\pi}{3}\frac{\vec{s}_i\cdot\vec{s}_j}{m_i m_j}\delta(\vec{r}) \qquad (6.10)$$

[If the propagator modification is used, the delta function gets replaced by $\nabla^2_{ij} V_{ij}$].

Consider first the baryon states made with the same set of quarks, e.g., the Λ, Σ, and Σ^* states. Then the masses of the states are

$$M \cong M_o + \xi \sum_{i>j}\frac{\langle\vec{s}_i\cdot\vec{s}_j\rangle}{m_i m_j} \qquad (6.11)$$

where M_o is a constant for all members and ξ is a positive constant determined from the spatial integral of (6.10), weighed with the square of the three-quark totally symmetric coordinate-space wavefunction (assumed independent of quark flavor and spin). The mass differences between Λ, Σ, and Σ^* comes from the different quark masses and the different expectation values, $\langle\vec{s}_i\cdot\vec{s}_j\rangle$. In detail, since there is only one s quark in these baryons,

$$M = M_o + \frac{\xi}{m_1^2}\left[\left\langle \vec{s}_1\cdot\vec{s}_2\right\rangle + \frac{m_1}{m_3}\left\langle(\vec{s}_1+\vec{s}_2)\cdot\vec{s}_3\right\rangle\right] \qquad (6.12)$$

where $m_u = m_d = m_1 = m_s = m_3$, and $\vec{s}_3$ is the spin of the s quark. Consider the Σ^+ and Σ^{*+} states. These are u u s. The identical quarks u u are in an I = 1, S = 1 state. Thus $\left\langle \vec{s}_1\cdot\vec{s}_2\right\rangle = \frac{1}{4}$. For the Σ and Σ^* states we have

$$S^2 = (\vec{s}_1+\vec{s}_2+\vec{s}_3)^2 = \begin{Bmatrix}\frac{3}{4}\\ \\ \frac{15}{4}\end{Bmatrix} \text{ leading to } \left\langle(\vec{s}_1+\vec{s}_2)\cdot\vec{s}_3\right\rangle \begin{Bmatrix}-1\\ \\ +\frac{1}{2}\end{Bmatrix}$$

Therefore

$$M_\Sigma = M_o + \frac{\xi}{m_1^2}\left(\frac{1}{4} - \frac{m_1}{m_3}\right)$$

$$M_{\Sigma^*} = M_o + \frac{\xi}{m_1^2}\left(\frac{1}{4} + \frac{m_1}{2m_3}\right)$$

For the Λ we have u d s, with the u d pair in an I = 0, S = 0 state and $\left\langle \vec{s}_1\cdot\vec{s}_2\right\rangle = -\frac{3}{4}$. Then $\left\langle(\vec{s}_1+\vec{s}_2)\cdot\vec{s}_3\right\rangle = 0$ and the mass is

$$M_\Lambda = M_o + \frac{\xi}{m_1^2}\left(-\frac{3}{4}\right)$$

From the experimental masses of 1.116 GeV (Λ), 1.193 GeV (Σ), and 1.385 GeV (Σ^*), the ratio of the mass of the strange quark to the up or down quark is determined to be

$$\frac{m_3}{m_1} = 1 + \frac{3}{2}\frac{(M_\Sigma - M_\Lambda)}{(M_{\Sigma^*} - M_\Sigma)} = 1.60 \qquad (6.13)$$

In the spirit of the model DGG argue that the quark masses have a realistic meaning, even though quarks are confined. In particular, if the quarks have a normal g-factor of 2, the up/down quark mass can be determined from the relation,

$$m_1 = \frac{M_p}{\mu_p} = \frac{0.938}{2.793} = 0.336 \text{ GeV}$$

From (6.13) we then have

$$m_3 = 0.538 \text{ GeV}$$

It is of some interest to note the difference between the actual mass and the sum of quark masses for various hadrons:

N	-70 MeV
Λ	-94 MeV
Σ	-17 MeV
Ξ	-97 MeV
Δ	226 MeV
Σ^*	175 MeV
Ξ^*	120 MeV
Ω^-	58 MeV
π	-532 MeV
K	-380 MeV
ρ/ω	100 MeV
K^*	18 MeV
ϕ	-56 MeV

There numbers indicate that, except for the lightest mesons, the binding energies are a small fraction of the sum of the quark masses.

This was, of course, one of the motivations of the original "realistic quark" model of Dalitz, Morpurgo and others (Kokkedee, 1969).

DGG discuss the ordinary mesons, electromagnetic properties and mass differences, P-state mesons and baryons, etc. We take time only for mention of some charmed baryons. In this picture, with the discovery of the ψ (3.1), the charmed quark's mass was roughly determined. Thus, guessing at $\sim$200 MeV of binding, we infer

$$m_4 = m_c \simeq 1.65 \text{ GeV}.$$

The lightest charmed baryon Λ_c^+ consists of u d c, i.e., a Λ hyperon with s $\rightarrow$ c. It is a $C = +1$, $S = 0$, $I = 0$ state (The notation Λ_c is perhaps a bit unfortunate; the Λ denotes $I = 0$, not $S = -1$). With another guess of $\sim$70 MeV binding for the baryon, we have

$$M_{\Lambda_c} = 2(.336) + 1.650 - 0.070 = 2.25 \text{ GeV}.$$

(This value has some hindsight in it - it could have been off by several hundred MeV.) The analogs of the Σ and the Σ^*, called Σ_c and Σ_c^* here, have masses that can be estimated relative to the Λ_c by exactly the same considerations as before. Assuming that ξ remains the same as for the lighter baryons, we obtain

$$M_{\Sigma_c} - M_{\Lambda_c} \simeq \left(\frac{m_4 - m_1}{m_4}\right)\left(\frac{m_3}{m_3 - m_1}\right)\left(M_\Sigma - M_\Lambda\right)$$

$$\simeq 2.12\,(.077) = 0.163 \text{ GeV}$$

Similarly, for the charmed analog of the Y_1^* (1385) we find

$$M_{\Sigma_c^*} - M_{\Lambda_c} \simeq \left(\frac{2m_4 + m_1}{2m_4}\right)\left(\frac{m_3}{m_3 - m_1}\right)\left(M_\Sigma - M_\Lambda\right) \simeq 0.226 \text{ GeV}$$

Taking the Λ_c mass at 2.25 GeV, we have Σ_c at 2.41 GeV and Σ_c^* at 2.48 GeV. These states are shown in Fig. 10, with their cascade hadronic decays indicated.

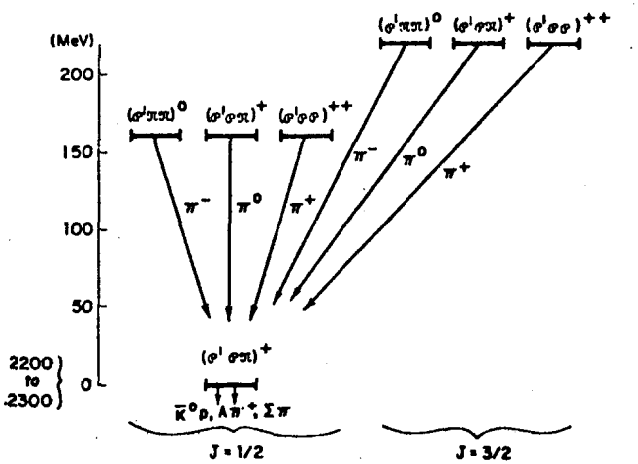

Fig. 10. The expected spectrum of low-lying singly charmed, nonstrange baryons (from De Rújula, Georgi and Glashow, 1975).

The event of Cazzoli et al. (1975) presumably corresponds to

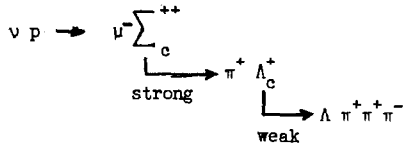

as we have already mentioned. At the topical conference after these lectures, you will presumably hear more about these states.

In the mesonic spectrum the charmed nonstrange pseudoscalar mesons D^0 and D^+ are expected to lie somewhat below $m_1 + m_3 = 1.99$ GeV. The new states at 1.865 GeV (neutral) and 1.876 GeV (charged) are presumably they. The binding energy is thus $\sim$120 MeV. Using this binding value, one expects the strange charmed meson F^+ to have a mass of $m_3 + m_4 - 0.120$ GeV $\simeq$ 2.07 GeV. Similarly, the rather well-established D^{0*} at 2.01 GeV implies the F^{*+} at 2.21 GeV. These last estimates are probably good to within 100 MeV. DGG found rather *different values for the* F, D^*, F^* *using only the* $\psi(3.1)$ *to fix* m_4 and a mass formula that included all the pseudoscalars.

VII. CHARMONIUM

The spectrum of states in the mass range above 3 GeV uncovered by the experiments at SPEAR and at DORIS is presumed to be the energy levels of a charmed quark and antiquark bound system. Using asymptotic freedom ideas, Appelquist and Politzer (1975a, b, and pre-November, 1974 seminars and preprint) expressed the hope that the $\bar{c}c$ system, with massive quarks moving nonrelativistically, would provide a hadronic analog of positronium, with a spectrum of "atomic" states and properties that could be deduced from the color gluon gauge interaction at short distances. They called the system "charmonium" and inferred a number of properties in correspondence with positronium, annihilation into ordinary hadrons being associated with annihilation into two or three gluons with rates taken over from QED, etc. Their qualitative picture has been extremely successful - the existence of narrow states below the charmed meson pair production threshold, the rise in R above that threshold and the existence of structure there, too.

We accept this bound state picture of the ψ, ψ' χ,... states and explore the consequences. Our approach will be strictly empirical at the beginning, with the aim of obtaining a qualitative or semi-quantitative understanding, of seeing whether the whole picture makes sense. At some point we must quote from detailed model calculations in order to test quantitatively the theory against experiment. We begin with what we can learn from the width of a vector meson for decay into e^+e^- or $\mu^+\mu^-$.

1. Vector meson decay into $\bar{\ell}\ell$

In the pre-bound state view of vector mesons with odd charge conjugation, the ideas about ρ-meson dominance of the charged pion form factor led to a description of $V \to e^+e^-$ as indicated in Fig. 11(a). The dominance of the form factor leads to the conclusion that the V-γ coupling is

$$e\, G_V = e\, \frac{m_V^2}{f_V} \qquad (7.1)$$

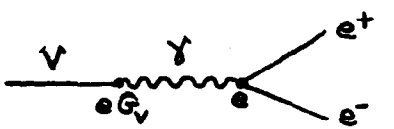

(a)

(b)

Fig. 11. $V \to e^+e^-$. (a) Vector dominance diagram. (b) Bound state annihilation diagram.

For the ρ-meson at least, we expect f_V to be related to $f_{\rho\pi\pi}$ ($f^2_{\rho\pi\pi}/4\pi \simeq 2.5$). For heavier vector mesons the relation to hadronic coupling constants is not so clear. Eq. (7.1) defines f_V. A simple calculation (that we do not perform) yields the decay rate for $V \to e^+e^-$ (and for $\mu^+\mu^-$, if we neglect m_μ^2/m_V^2) :

$$\Gamma(V \to \bar{\ell}\ell) = \frac{1}{3}\alpha^2\left(\frac{4\pi}{f_V^2}\right) m_V \qquad (7.2)$$

From the observed rates for ρ, ω, ϕ, ψ into e^+e^- or $\mu^+\mu^-$ we find $f_V^2/4\pi \simeq 2.5$, 18, 15, and 12, respectively. For the ψ', an excited state, we find $f_V^2/4\pi \simeq 31$. The values of $f_V^2/4\pi$ are plausibly strong interaction in magnitude, but need more assumptions before sense can be made of them. The vector dominance approach is quoted chiefly for completeness and comparison.

The rate of decay can be interpreted alternatively in terms of a bound state picture. The idea is sketched in Fig. 11(b). The dashed vertical lines represent the binding potential in the ladder approximation (Schrödinger equation). The particle and antiparticle come together and annihilate into a virtual photon. The decay rate is thus proportional to $|\psi(0)|^2$, where $\psi(\vec{r})$ is the bound state wave function. The rate of decay into $\bar{\ell}\ell$ can be computed using bound-state methods from the beginning. We follow a simpler path of relating the bound state annihilation for weak binding (just below the $c\bar{c}$ threshold) to the low energy limit of the exothermic $c\bar{c} \to e^+e^-$ cross section.

The Feynman diagram of annihilation of $q\bar{q}$ into e^+e^- is shown in Fig. 12. The quarks have charges $\pm e_Q$ in units of the

Fig. 12

protonic charge and mass m. The electron (or muon) mass is neglected. The square of the center of mass energy is s. We are interested in the limit, $s \to 4m^2 \simeq M^2$, where M is the mass of the decaying vector meson. In everyone's notation (up to i^n), the matrix element is

$$\mathcal{M} = \frac{e_Q e^2}{s}\,\bar{v}(p_2)\,\gamma_\mu u(p_1)\,\bar{v}(k_2)\,\gamma_\mu u(k_1) \qquad (7.3)$$

We shall compute the cross section two ways. The first is the standard technique of traces. For an unpolarized beam incident, we need the average over initial spins and sum over final spins. Thus

$$\frac{1}{4}\sum_{\text{spins}} |\mathcal{M}|^2 = \frac{1}{4}\frac{e_Q^2 e^4}{s^2}\,\mathrm{Tr}\left[(-m-i\gamma\cdot p_2)\gamma_\mu(m-i\gamma\cdot p_1)\gamma_4\gamma_\nu\gamma_4\right] \times \mathrm{Tr}\left[(-i\gamma\cdot k_2)\gamma_\mu(-i\gamma\cdot k_1)\gamma_4\gamma_\nu\gamma_4\right]$$

where the notation is mine, not Bj-D. The traces give the result,

$$\frac{1}{4}\sum_{\text{spins}} |\mathcal{M}|^2 = \frac{4e_Q^2 e^4}{s^2}\sum_{\mu\nu}\left[\tfrac{1}{2}s\,\delta_{\mu\nu} + (p_1)_\mu(p_2)_\nu + (p_2)_\mu(p_1)_\nu\right] \times \left[\tfrac{1}{2}s\,\delta_{\mu\nu} + (k_1)_\mu(k_2)_\nu + (k_2)_\mu(k_1)_\nu\right]$$

(true, even if the lepton masses are not neglected). Omitting a little kinematic algebra, we find the spin-averaged matrix element square to be

$$\frac{1}{4}\sum_{\text{spins}} |\mathcal{M}|^2 = e_Q^2 e^4\left(1 + \beta^2\cos^2\theta + \frac{4m^2}{s}\right)$$

where $\beta = (1 - 4m^2/s)^{\frac{1}{2}}$ is the quark velocity in the c.m.s. and θ is the angle between $\vec{p}_1$ and $\vec{k}_1$ in the c.m.s. The c.m.s. differential cross section is $(k/64\pi^2 sp)$ times (7.3):

$$\frac{d\sigma}{d\Omega} = \frac{\alpha^2 e_Q^2}{4s}\frac{k}{p}\left(1 + \beta^2\cos^2\theta + \frac{4m^2}{s}\right) \qquad (7.4)$$

The total cross section for $q\bar{q} \to e^+e^-$ is thus

$$\sigma = \frac{\pi\alpha^2 e_Q^2}{s}\cdot\frac{k}{p}\left(1 + \frac{1}{3}\beta^2 + \frac{4m^2}{s}\right) \qquad (7.5)$$

The extreme relativistic limit in which we neglect the quark mass m compared to $\sqrt{s}$ yields the cross section,

$$\sigma \to \sigma_{QED} = \frac{4\pi}{3}\frac{e_Q^2\alpha^2}{s} = \frac{86.8\,\text{nb}}{s(\text{GeV}^2)}\cdot e_Q^2 \qquad (7.6)$$

For $e_Q = 1$, this is the standard comparison cross section, usually called σ_{QED} or $\sigma_{\mu\mu}$.

The other limit of $\beta \to 0$ is our concern. Near threshold, the q and $\bar{q}$ move nonrelativistically. Then

$$p \to \frac{m}{2}v_{rel}\ , \quad k \to m, \quad s \to 4m^2$$

where $v_{rel} = |\vec{v}_1 - \vec{v}_2|$ is the relative velocity of q and $\bar{q}$, the quantity of interest in the incident flux. At threshold, the cross section has the well-known v_{rel}^{-1} behavior of exothermic reactions:

$$\sigma\, v_{rel} = \frac{\pi\alpha^2 e_Q^2}{m^2} \qquad (7.7)$$

The quantity $\sigma\, v_{rel}$ is the transition probability for the process with the incident beam normalized to one particle per unit volume at the origin. If we consider a weakly bound $q\bar{q}$ system in its triplet spin state with $\ell = 0$, the transition probability for its annihilation into e^+e^- can be obtained from (7.7) by

(i) multiplying by $|\psi(0)|^2$, where ψ is the spatial wave function calculated with the neglect of the annihilation channel, and

(ii) multiplying by a factor of $\frac{4}{3}$ to account for the fact that in the bound state the spins are always in the triplet state, whereas for the statistical mixture assumed for σ the spins are $\frac{3}{4}$ triplet and $\frac{1}{4}$ singlet.

The annihilation rate for $V \to e^+e^-$ on a bound state picture is

$$\Gamma'(1^{--} \to e^+e^-) = \frac{16\pi}{3} \frac{\alpha^2 e_Q^2}{M^2} |\psi(0)|^2 \qquad (7.8)$$

where M is the mass of the vector meson. Eq. (7.8) is valid provided the binding is weak and the annihilation channel is coupled weakly enough not to disturb significantly the wave functions and energy levels.

With color symmetry, there is an additional factor of $\sqrt{3}$ in the amplitude, coming from the sum of three equal diagrams, one for each color of $q\bar{q}$, and a $1/\sqrt{3}$ present in the color "wave function", as described above. Thus the rate for $V \to e^+e^-$, with colored quarks, is

$$\Gamma(1^{--} \to e^+e^-) = 16\pi \frac{\alpha^2 e_Q^2}{M^2} |\psi(0)|^2 \qquad (7.9)$$

We now apply (7.9) to the vector meson decays into e^+e^-. We need the effective values of e_Q^2:

$$\rho = \frac{1}{\sqrt{2}}(u\bar{u} - d\bar{d}) \longrightarrow e_Q^2 = \left|\frac{1}{\sqrt{2}}\left(\frac{2}{3} + \frac{1}{3}\right)\right|^2 = \frac{1}{2}$$

$$\omega = \frac{1}{\sqrt{2}}(u\bar{u} + d\bar{d}) \longrightarrow e_Q^2 = \left|\frac{1}{\sqrt{2}}\left(\frac{2}{3} - \frac{1}{3}\right)\right|^2 = \frac{1}{18}$$

$$\phi = \lambda\bar{\lambda} \longrightarrow e_Q^2 = \frac{1}{9}$$

$$\psi = c\bar{c} \longrightarrow e_Q^2 = \frac{4}{9}$$

With these charges and the experimental widths, we compute $|\psi(0)|^2$, as shown in Table 3. The values of $|\psi(0)|^2$ are plotted on

Table 3

Vector meson decays into e^+e^-

Meson	M(GeV)	e_Q^2	Γ(keV)	$\lvert\psi(0)\rvert^2$(GeV^3)
ρ	0.770	1/2	6.5 ± 0.8	0.29×10^{-2}
ω	0.783	1/18	0.76±0.17	0.31×10^{-2}
ϕ	1.020	1/9	1.34±0.08	0.47×10^{-2}
ψ	3.095	4/9	4.8 ± 0.6	3.9×10^{-2}
ψ'	3.684	4/9	2.1 ± 0.3	2.4×10^{-2}

log-log graph paper versus mass M and reduced mass $\mu = m_q/2$ in Fig. 13. The solid straight line corresponds to $|\psi(0)|^2 \propto \mu^n$ with $n = 1.89 \pm 0.15$. The steeper dashed line has the same slope, while the one through the ρ/ω and ψ points has slope 1.58. This power law dependence on M or μ can be compared with the dependence found from the Schrödinger equation for various types of potentials:

Potential	$\lvert\psi(0)\rvert^2$
$-e^2/r$	$\sim \mu^3$
r/b^2 (b independent of μ)	$\sim \mu$
$\frac{1}{2} kr^2$ (k independent of μ)	$\sim \mu^{3/4}$
$\frac{1}{2} \mu\omega_o^2 r^2$ (ω_o independent of μ)	$\mu^{3/2}$

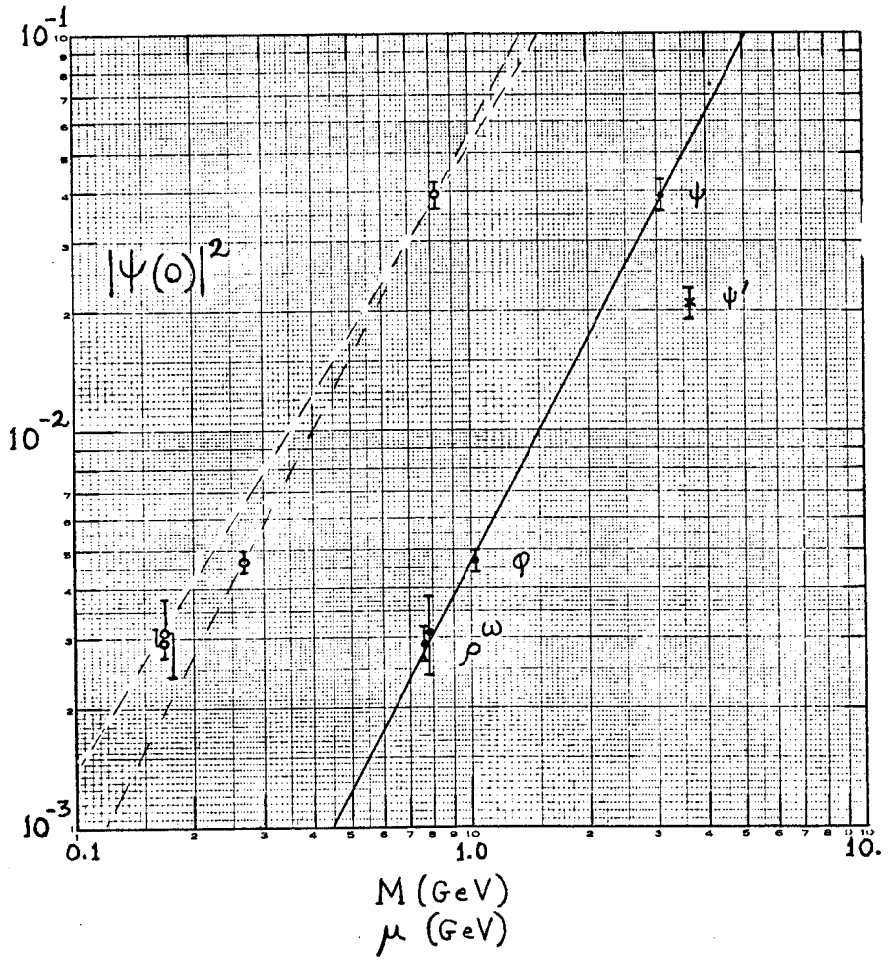

Fig. 13. Log-log plot of $|\psi(0)|^2$ for vector meson states versus mass M (solid-points) and reduced mass μ (open circles). The straight line has a slope 1.89±0.15.

The variation as μ^n, n ≈ 1.6-1.9, is plausible. It also shows that the extreme of a gluon "Coulomb" potential effective over most of the size of the "atom" is not realized. In passing we note that, it can easily be demonstrated for all s-states, ground and excited,

$$|\psi(0)|^2 = 2\mu \left\langle \frac{dV}{dr} \right\rangle \tag{7.10}$$

Thus a linear potential has the same $|\psi(0)|^2$ for all s-waves. The data for the ψ and ψ' show that this equality does not hold, assuming as we all do that the ψ and ψ' are the 1s and 2s states of charmonium.

We now return to the second method of obtaining the decay rate (7.8) or (7.9). This involves a study of the helicity structure of the matrix element (7.3) in the nonrelativistic limit for the quarks. The quark-antiquark factor in $\mathcal{M}$ is

$$\mathcal{M}_\mu(\lambda_2,\lambda_1) = \bar{v}_{\lambda_2}(\vec{p}_2)\gamma_\mu u_{\lambda_1}(\vec{p}_1) \tag{7.11}$$

where λ_i, $\vec{p}_i$ are the helicity and momentum of each particle. The v spinors for the antiparticle are a bit of a nuisance. We therefore use two identities:

$$v_\lambda(\vec{p}) = (-1)^{\lambda-\frac{1}{2}}\gamma_5 u_{-\lambda}(\vec{p})$$

$$u_\lambda(\vec{p}) = \gamma_4 u_{-\lambda}(-\vec{p})$$

to transform the v spinor. The second one is just a convenience

in the c.m.s., where $\vec{p}_2 = -\vec{p}_1 = -\vec{p}$. In the c.m.s., we have

$$\vec{\mathcal{M}}(\lambda_2, \lambda_1) = i(-1)^{\lambda_2 - \frac{1}{2}} \bar{u}_{\lambda_2}(\vec{p})\vec{\sigma}\, u_{\lambda_1}(\vec{p}) . \qquad (7.12)$$

Note that now the spinors have a common momentum; only the helicity labels are distinct. The time component $\mathcal{M}_o$ is proportional to $(\bar{u}\gamma_5 u)$ and so vanishes like p^2/m^2 as $p \to 0$. The nonrelativistic limit of (7.12) is

$$\vec{\mathcal{M}}(\lambda_2,\lambda_1) \to 2mi(-1)^{\lambda_2 - \frac{1}{2}} \langle \lambda_2 | \vec{\sigma} | \lambda_1 \rangle \qquad (7.13)$$

where the 2×2 Pauli spin operator acts on Pauli spinors.

The full matrix element (7.3) then has the limit,

$$\mathcal{M} \to i(-1)^{\lambda_2 - \frac{1}{2}} \frac{e_Q e^2}{M} \langle \lambda_2 | \vec{\sigma} | \lambda_1 \rangle \cdot \bar{v}(k_2)\vec{\gamma} u(k_1) \qquad (7.14)$$

The triplet nature of the initial state is manifest by the presence of $\vec{\sigma}$. We have a choice now of how to proceed. One way, if you have a little black book, is to read off the helicity amplitudes for the e^+e^- and make a list of helicity amplitudes. Another way is to choose the initial helicities to have some particular values, e.g., $\lambda_1 = \lambda_2 = \frac{1}{2}$ (we imagine a polarized beam on a polarized target). Then $\langle \lambda_2 | \vec{\sigma} | \lambda_1 \rangle$ is a unit vector in the beam direction. The lepton trace (see below Eq. (7.3))can then be used to obtain the threshold cross section. The result is

$$\sigma_{\frac{1}{2},\frac{1}{2}} v_{rel} = \frac{8\pi}{3} \frac{\alpha^2 e_Q^2}{M^2} \qquad (7.15)$$

This is the transition probability for $\lambda_1 = \lambda_2 = \frac{1}{2}$. Since the Pauli spin wave function of the $q\bar{q}$ pair is

$$\alpha_1\beta_2 = \frac{1}{\sqrt{2}}\left[\frac{1}{\sqrt{2}}(\alpha_1\beta_2+\beta_1\alpha_2)\right] + \frac{1}{\sqrt{2}}\left[\frac{1}{\sqrt{2}}(\alpha_1\beta_2-\beta_1\alpha_2)\right]$$

the triplet state is only present half the time. To get the triplet bound state transition rate with color, we therefore multiply (7.15) by $2|\psi(0)|^2 \times 3$, obtaining (7.9).

The point about this last way of doing the calculation is to exhibit the nonrelativistic $q\bar{q}$ system explicitly. This will be important in allowing us to compute annihilation into photons or gluons from p states (see below).

2. Hadronic widths of Charmonium s-wave states

From the rates for $V \to e^+e^-$ we learn the square of the bound state wave function. Within the framework of the quark-color gluon gauge theory we can now discuss the annihilation of charmonium s-states into ordinary hadrons and use one more experimental number to determine the running coupling constant α_s. In later discussion it is useful to have the rates in terms of the square of the radial wave function and its derivatives. Thus we put $|R(0)|^2 = 4\pi|\psi(0)|^2$.

Then Eq. (7.9) reads

$$\Gamma(1^{--} \to e^+e^-) = \frac{4\alpha^2 e_Q^2}{M^2} |R(0)|^2 \qquad (7.16)$$

The charmonium annihilation into ordinary hadrons violates Zweig's rule, as discussed in Sect. IV. We saw that in color gluon gauge theories the annihilation involves an intermediate state of only gluons (see Fig. 7). If we assume that the gluons are quasi-free and turn into ordinary hadrons with essentially unit probability, we can calculate the hadronic annihilation of states like ψ and ψ' by computing their annihilation into gluons. Furthermore, if the coupling is weak, we can use lowest order perturbation theory. This means that we can transcribe QED results for positronium (Jauch and Rohrlich, 1955, Chapter 12). The $\ell = 0$ singlet spin states of positronium ($J^P = 0^-$) annihilate into two photons, while the $\ell = 0$ triplet spin states ($J^P = 1^-$) go into three photons. The decay rates are

$$\Gamma(0^- \to \gamma\gamma) = \frac{4\alpha^2}{M^2} |R(0)|^2 \qquad (7.17)$$

and

$$\Gamma(1^- \to \gamma\gamma\gamma) = \frac{16}{9\pi}(\pi^2 - 9)\frac{\alpha^3}{M^2} |R(0)|^2 \qquad (7.18)$$

where M is the mass of the state ($M \simeq 2m_e$). We state these without derivation, although the first one is derived in passing when we consider the $\ell = 1$ state annihilation.

In analogy with positronium we expect the triplet (1^-) and singlet (0^-) s-states to be almost degenerate in mass. We call the pseudoscalar analog of the ψ, the η_c. As you have heard from Gary Feldman, it is perhaps the state seen at DORIS at 2.7-2.8 GeV in $\gamma\gamma\gamma$. [We discuss the systematics of masses and mass splittings below.] Taking into account the quark charges e_Q and the color dimension, the decay rate for $\eta_c \to \gamma\gamma$ is, from (7.17),

$$\Gamma(\eta_c \to \gamma\gamma) = \frac{12\alpha^2 e_Q^4}{M^2} |R(0)|^2 \ . \qquad (7.19)$$

With $|R(0)|^2 \simeq 0.48$ GeV^3 from Table 3, $e_Q = \frac{2}{3}$, $M = 2.75$ GeV, this gives $\Gamma(\eta_c \to \gamma\gamma) \simeq 8.$ keV.

To obtain the annihilation rate of η_c into gluons it is necessary to replace α^2 with α_s^2. The recipe for the two-gluon annihilation is (Barbieri, Gatto, and Kögerler, 1976) $\alpha^2 e_Q^4 \to 2\alpha_s^2/9$. Thus we have

$$\Gamma(\eta_c \to \text{hadrons}) \simeq \Gamma(\eta_c \to gg) = \frac{8}{3}\frac{\alpha_s^2}{M^2} |R(0)|^2 \qquad (7.20)$$

Similarly the triplet state annihilation into three gluons can be transcribed from (7.18) according to $\alpha^3 \to 5\alpha_s^3/18$ (Appelquist and Politzer, 1975a):

$$\Gamma(\psi \to \text{hadrons}) \simeq \Gamma(\psi \to ggg) = \frac{40}{81\pi}(\pi^2 - 9)\frac{\alpha_s^3}{M^2} |R(0)|^2 \qquad (7.21)$$

The width (7.21) can be identified with the hadronic width of the ψ. Using (7.16) for the width into electron pairs, we find

$$\Gamma_h/\Gamma_e = \frac{5(\pi^2-9)}{18\pi} \frac{\alpha_s^3}{\alpha^2} \cdot \frac{(2/3)^2}{e_Q^2} \qquad (7.22)$$

The wave function at the origin and M cancel out; α_s can be determined from the ratio of widths. With the experimental value, $\Gamma_h/\Gamma_e = 10 \pm 1.5$ (corrected for second-order e-m decays), Eq. (7.22) yields

$$\alpha_s = 0.187 \pm 0.010 \qquad (7.23)$$

This is at least smaller than unity, justifying somewhat the weak coupling assumptions. With this value of α_s as the running coupling constant for the short-distance behavior at $M \approx 3$ GeV, the width (7.20) of the ψ's pseudoscalar partner is estimated to be

$$\Gamma_{\eta_c} \approx \Gamma(\eta_c \to gg) \approx 6.8 \text{ MeV} \qquad (7.24)$$

This is quite narrow, although not as narrow as the ψ and ψ'. In phenomenological terms it corresponds to a Zweig's rule suppression by a factor $\gtrsim 50$.

With α_s determined and $|\psi(0)|^2$ values known, Eqs. (7.20) and (7.21) can be used to calculate the expected widths of the η_c' and the ψ' into ordinary hadrons. For both states we have

$$\frac{\Gamma(\eta_c' \to \text{ord. had.})}{\Gamma(\eta_c \to \text{ord. had.})} \approx \frac{\Gamma(\psi' \to \text{ord. had.})}{\Gamma(\psi \to \text{ord. had.})} \approx \left(\frac{|R(0)|^2}{M^2}\right)_{\psi'} \Big/ \left(\frac{|R(0)|^2}{M^2}\right)_{\psi}$$

$$\approx \frac{2.4}{3.9} \times \left(\frac{3.1}{3.7}\right)^2 = 0.43$$

With $\Gamma(\psi \to \text{hadrons}) = 59 \pm 14$ keV, we find $\Gamma(\psi' \to \text{ordinary hadrons}) \approx 25$ keV. This corresponds to a branching ratio of $25/225 \approx 0.11$. Without the questionable ratio of masses this would be $36/225 \approx 0.16$. This is roughly consistent with the known facts about ψ' decay ($\sim$55% $\psi' \to \psi\pi\pi$ or $\psi\eta$; $\sim$22% $\psi' \to \gamma\chi$, $\chi \to$ hadrons; $\sim$4% $\psi' \to \gamma\chi \to \gamma\gamma\psi$; $\sim$19% presently unknown). For the η_c', we obtain $\Gamma(\eta_c' \to \text{ordinary hadrons}) \approx 2.9$ MeV. In passing we note that if (7.22) is applied to ϕ decay, for which $\Gamma(\phi \to \text{nonstrange hadrons})/\Gamma(\phi \to e^+e^-) \approx 588$, the coupling constant comes out to be $\alpha_s \approx 0.47$.

3. First orientation on wave functions and matrix elements with very simple model

The spectrum of charmonium states below 3.8 GeV is shown in Fig. 14. The well-established states and transitions are indicated by solid lines, the less well-founded by dashed lines. Arrows slanting to the right mean decay into ordinary hadrons. In the last section we discussed what could be said about the s-states from a knowledge of α_s and $|\psi(0)|^2$ alone. Now we turn to more detailed considerations of the energy spectrum, radiative transitions, etc. that require some knowledge of wave functions and potential. The lowest states

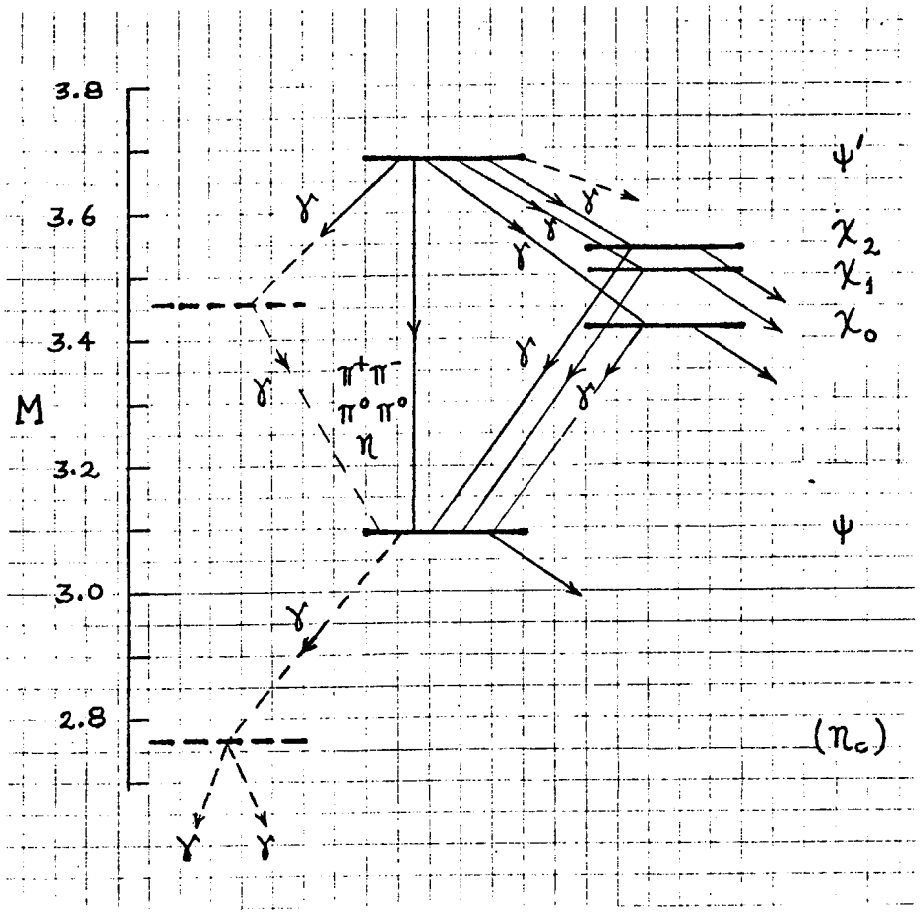

Fig. 14. Grotrian diagram of charmonium. Mass scale in GeV. Solid lines are well-established states or transitions, dashed lines less so. Short arrows to the right indicate transitions to ordinary hadrons.

in positronium are the $n = 1$ $^3S_1$ and $n = 1$ $^1S_0$ states. We expect from the (hyper) fine splitting of Eq. (6.11) that the $^1S_0$ lies lower than the $^3S_1$. This is the basis for the tentative identification of the state at $\sim$2.8 GeV as the $\eta_c(0^{-+})$. Deferring until later the question of the reasonableness of $\sim$0.3 GeV as a (hyper) fine splitting, we identify the $\psi(3.1)$ as the $n = 1$ $^3S_1$ state. It is natural in a potential model to identify the ψ' (3.7) as the $n = 2$ $^3S_1$ state. The intermediate states, labelled χ_0, χ_1, χ_2 in Fig. 14, are most naturally identified with the lowest lying p-states, namely $n = 2$ ^3P_J states, with $J = 0^{++}, 1^{++}, 2^{++}$. This assignment is reinforced by the following arguments:

(i) It was a property of quark confinement mechanisms that the potential energy between q and $\bar{q}$ increases with increasing separation. Since the Coulomb potential has the $n = 2$, $\ell = 0$ and $\ell = 1$ states degenerate, any potential that increases with r will depress the nodeless $\ell = 1$ state relative to the $\ell = 0$ state with its radial node (and therefore bigger kinetic energy).

(ii) The photon transitions $\psi' \to \gamma\chi$ are relatively strong ($\Gamma(\psi \to \gamma\chi) \approx 20$ keV), implying E1 transitions.

To see whether any of this makes even semi-quantitative sense we need some plausible wave functions. Note that, if the shape of the potential is chosen, the scale of matrix elements is set by the numerical value of $|R(0)|^2$. This is true, at least for relatively tightly bound states, because the Schrödinger equation can be written in terms

of a dimensionless radial coordinate, $\rho = \xi r$, where ξ is some combination of the reduced mass and the parameters of the potential. Then we have $|R(0)|^2 = \text{const.} \times \xi^3$, with the numerical value of the constant determined by the potential shape.

The simplest potential known to man is Hooke's law, the isotropic oscillator. The levels in Fig. 14 even look roughly as expected for such a potential, with the lowest χ state, at least, about half way between the two ψ states. The $\ell = 2$ state that is theoretically degenerate with the second $\ell = 0$ state has not been seen, but more realistic potential models have it lurking not far above 3.7 GeV. The radial wave functions that we need are the 1s, 2p and 2s:

$$R_{1s}(r) = \sqrt{\frac{4\xi^3}{\sqrt{\pi}}}\ e^{-\xi^2 r^2/2} \qquad (7.25a)$$

$$R_{2p}(r) = \sqrt{\frac{8\xi^3}{3\sqrt{\pi}}}\ \xi r e^{-\xi^2 r^2/2} \qquad (7.25b)$$

$$R_{2s}(r) = \sqrt{\frac{6\xi^3}{\sqrt{\pi}}}\left(1 - \frac{2}{3}\xi^2 r^2\right) e^{-\xi^2 r^2/2} \qquad (7.25c)$$

The scale parameter is $\xi = \sqrt{\mu\omega_o}$. Having chosen the potential shape, we could proceed to determine ξ from $|R(0)|^2$ for the $n = 1$, $\ell = 0$ state. With $|R(0)|^2 \simeq 0.48$, this gives $\xi \simeq 0.6$ GeV. We do not do this, however, because the exact value of $|R(0)|^2$ is somewhat sensitive to the detailed shape of the potential. Since our oscillator potential is only a very crude imitation of the actual potential, we aim rather for a global understanding, if that is possible. Thus we choose $\mu = m_c/2 \simeq 1.65/2$ GeV and ω_o, the oscillator spacing, as a rough mean between the values implied by the 1s - 2p spacing and the the 1s - 2s spacing, i.e. $\omega_o \simeq 0.33$ GeV. This gives $\xi = 0.52$ GeV. We thereby underestimate $|R_{1s}(0)|^2$ by a factor of 0.66, but that is quite adequate agreement for our purposes. [Our value, $|R_{2s}(0)|^2 \simeq 0.48\ \text{GeV}^3$, is also only in rough accord with the experimental $0.30\ \text{GeV}^3$.] In estimating matrix elements, etc. we use the wave functions (7.25), but in calculating transition rates we use the experimental energy differences in order to get at least the phase space factors correctly.

For electric dipole transitions, the relevant squares of matrix elements are

$$|\langle 2s|r|2p\rangle|^2 = \xi^{-2}$$
$$|\langle 2p|r|1s\rangle|^2 = \tfrac{3}{2}\xi^{-2} \qquad (7.26)$$

The latter value saturates the dipole sum rule from the ground state (the oscillator strength, $f_{ij} = 1$) because of the peculiarity of the E1 selection rules for a harmonic oscillator. It is therefore somewhat of an over-estimate of this matrix element.

4. Radiative transitions

The radiative transitions either shown in Fig. 14 or assumed to occur are E1 or M1 transitions. The absence of higher multipoles is either an exact statement (e.g., $\psi' \to \Upsilon\eta_c$; $1^- \to 0^-$; purely M1) or a consequence of the nonrelativistic Russell-Saunders approximation (e.g., $\psi' \to \gamma\chi_J$; $J = 1,2$; E1 because $L = 0 \to L = 1$).

(a) E1 transitions

The effective Hamiltonian describing the emission of a photon by the quark and anti-quark charges is the familiar form,

$$H_{int} = -\frac{ee_Q}{\sqrt{2k_o}}\,\vec{\epsilon}^{\,*}\cdot\left(\vec{v}_1 e^{-i\vec{k}\cdot\vec{r}/2} - \vec{v}_2 e^{i\vec{k}\cdot\vec{r}/2}\right) \qquad (7.27)$$

where $\vec{r} = \vec{r}_1 - \vec{r}_2$ is the relative coordinate. The velocities $\vec{v}_1$ and $\vec{v}_2$ are $\pm\dot{\vec{r}}/2$. If the potential energy is not velocity dependent, $\vec{r}$ can be replaced by $i\omega\vec{r}$ in the usual way. This yields

$$(H_{int})_{eff} = i\,e\,e_Q\sqrt{\frac{k}{2}}\,\vec{\epsilon}^{\,*}\cdot\vec{r}\,\cos\left(\frac{\vec{k}\cdot\vec{r}}{2}\right) \qquad (7.28)$$

The magnitude of $\vec{k}\cdot\vec{r}/2$ can be estimated from the value of $\xi \approx 0.5$ GeV and the typical photon energy of $\lesssim 0.3$ GeV. Thus $\langle\vec{k}\cdot\vec{r}/2\rangle < 0.3/(0.5\times 2) = 0.3$. Since $\cos(0.3) = 0.955$, we can safely set the cosine to unity and keep only the static E1 matrix element.

The calculation of the E1 transition probability for the transition from the triplet 2s state with $J = 1^-$ to the triplet p states of angular momentum J is an exercise in first-year quantum mechanics that I shall spare you. The result for the total transition probability is

$$\Gamma_J(E1) = \frac{4\alpha}{27}e_Q^2(2J+1)k^3|\langle 2p|r|2s\rangle|^2 \qquad (7.29)$$

We apply this result with our estimate (7.26) for the matrix element to the transitions $\psi' \to \gamma\chi_J$. The spin-orbit interaction of the gluon gauge theory implies an ordering of the p-states in energy with increasing J. Experiment supports this ordering. We assume it here. Table 4 contains the comparison of our crude estimate with the data presented by Feldman. The quark charge has been taken to be $e_Q = \frac{2}{3}$. The agreement can be considered satisfactory, in fact, better than we are entitled to have. A few comments:

Table 4

Radiative rates for E1 transitions, $\psi' \to \gamma\chi_J$

$M(\psi') = 3.684$ GeV, $\Gamma(\psi') = 228$ keV

M(GeV)	J	k(GeV)	Γ_J(keV)	Γ_{expt}(keV)
3.552	2	0.130	19.	18± 7
3.508	1	0.172	27.	21± 8
3.414	0	0.260	31.	23± 8

(a) A choice of $e_Q = \frac{1}{3}$ would lower the theoretical estimates by a factor of 4, perhaps outside the range of agreement (or disagreement) expected.

(b) The reverse ordering of states would, because of the $(2J+1)$ factor in (7.29), make the theoretical values in extremely poor agreement with the data. The rough constancy of the experimental widths is evidently due to the balancing compensation by the $(2J+1)$ and k^3 factors in the rate.

(c) The initially large estimates of the widths (Eichten et al., 1975; Appelquist et al., 1975) were due in some cases to very crude estimations and others to lack of knowledge of where the as yet unobserved p-states were located. For example, Eichten et al., using $k = 0.23$ GeV for all three p-states calculated $\Gamma(\psi' \to \gamma\chi_0) \simeq 25$ keV, with the others scaled proportionately by $(2J + 1)$ factors. Using 0.26 GeV, they would have obtained 36. keV, compared to our rough value of 31 keV and the experimental 23 ± 8 keV. A later paper (Eichten et al., 1976) gives revised estimates that are in the acceptable range. Some of the difference is from a fancier coupled channel calculation, but most of it is better values of the transition energies.

For the radiative transitions of the χ_J states to ψ, Eq. (7.29) is modified only by the replacement of $(2J + 1)$ by 3 and the matrix element $\langle 1s|r|2p\rangle$ instead of $\langle 2p|r|2s\rangle$. With the ψ mass at 3.095 GeV, the photon energies are 0.304 GeV, 0.389 GeV, and 0.428 GeV for $J = 0$, 1, 2, respectively. With the matrix element (7.26), the widths are 225 keV, 470 keV, and 625 keV. These are surely an over-estimate -- remember the selection rules for an oscillator. It is plausible that the ground state to first excited state will contribute perhaps $\frac{1}{2}$ to the dipole sum rule. We therefore make an educated guess that the widths are

$$\begin{aligned} \Gamma(\chi_2(3.552) \to \gamma\psi) &\simeq 300 \text{ keV} \\ \Gamma(\chi_1(3.508) \to \gamma\psi) &\simeq 230 \text{ keV} \\ \Gamma(\chi_0(3.414) \to \gamma\psi) &\simeq 100 \text{ keV} \end{aligned} \tag{7.30}$$

These are only very rough guesses. We show in the next sub-section how wrong or right they may be from sum rule arguments. For comparison, the calculation of Eichten et al. (1975), when corrected for the latest transition energies, gives 400 keV, 300 keV, 140 kev for the widths, the order being that of (7.30). The fancier Cornell calculation gives 320 keV, 200 keV and 90 keV (K. M. Lane, private communication).

(b) Dipole sum rules: upper and lower bounds on $\Gamma(\chi_J \to \gamma\psi)$, quark charges

In atomic physics sum rules of various sorts are powerful tools in estimating or setting bounds on various quantities of physical interest. The most famous is the Thomas-Reiche-Kuhr (dipole) sum rule for oscillator strengths. It can be applied to the bound states of the $q\bar{q}$ system as well. We show how it can be used to give upper and lower bounds to the radiative widths for $\chi_J \to \gamma\psi$. With data on the branching ratios, these latter bounds can be used to give lower limits on the total widths of the χ states. For the skeptic who is not sure what the quarks' electric charges are in charmonium, the sum rule can also eventually provide a relatively unambiguous determination.

First the upper bounds. The dipole sum rule for oscillator strengths from an initial state i to all final states

is

$$2\mu \sum_j \omega_{ji} |\langle j|\vec{r}|i\rangle|^2 = 3 \qquad (7.31)$$

where μ is the reduced mass, $\omega_{ji} = E_j - E_i$, and the matrix element is that of the vector $\vec{r}$. An upper bound can be placed on the radial matrix element for the $\psi \leftrightarrow \chi$ transition by assuming that it saturates the sum rule (analogous to our oscillator matrix element):

$$|\langle 2p|r|1s\rangle|^2 \leqslant \frac{3}{2\mu k}$$

In terms of the radiative widths for $\chi_J \to \gamma\psi$ this restriction reads

$$\Gamma(\chi_J \to \gamma\psi) < \frac{2\alpha k^2}{3\mu} e_Q^2 \qquad (7.32)$$

For the 3.508 GeV state, for example, $\Gamma(\chi_1 \to \gamma\psi) < 99$ keV for $e_Q = \frac{1}{3}$ and 4 times that for $e_Q = \frac{2}{3}$. Thus, when the total widths of the χ_J states are determined (and so the radiative partial widths), they can be tested against (7.32). If we are lucky and the widths are not too small, the factor of 4 difference between the two charge choices will make the test conclusive independently of uncertainty in the exact value of the reduced mass μ.

More interesting is the idea of a lower bound. For an arbitrary static central potential, including spin-orbit coupling, but not tensor forces, the general dipole sum rule yields more restrictive relations (Bethe and Salpeter, 1957, p. 256). The sum rule of interest to us is the one which sums the transitions from the 2p state to all n s states, as indicated in Fig. 15. The sum rule (Eq. (61.4) of Bethe and Salpeter) reads

$$2\mu \sum_n \omega_{ns,2p} |\langle ns|r|2p\rangle|^2 = -1 \qquad (7.33)$$

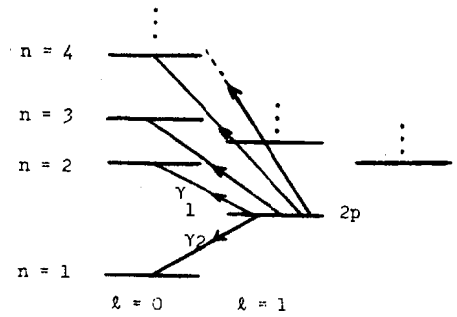

Fig. 15

The beauty of this sum rule lies in the negative sign on the right hand side and the fact that we already know the matrix element squared for one of the transitions, namely $\psi' \to \chi_J$. The negative sign shows that the $2p \to 1s$ transition dominates the sum rule ($\omega_{1s,2p} < 0$). By neglecting the $2p \to ns$ transitions for $n > 3$ on the left hand side, we get lower bounds on the $\chi_J \to \psi$ rates. From the rate formula (7.29) and $3/(2J+1)$ times it for $\chi_J \to \psi$,

we find the lower bound,

$$\Gamma(\chi_J \to \gamma_2\psi) \geqslant \frac{2\alpha k_2^2}{9\mu}\, e_Q^2 + \frac{3}{2J+1}\left(\frac{k_2}{k_1}\right)^2 \Gamma(\psi' \to \gamma_1\chi_J) \qquad (7.34)$$

Comparison with (7.32) shows that the first term here is $\frac{1}{3}$ of the upper bound. Note that the second term sets an absolute lower bound, independent of quark charges. Taking $m = 2\mu = 1.65$ GeV and the transition rates for $\psi' \to \gamma_1\chi_J$ from Table 4 we get the results shown in Table 5.

Table 5

Upper and lower bounds on the radiative widths for $\chi_J \to \gamma_2\psi$

(All masses and photon energies are in GeV; all widths are in keV; experimental widths for $\psi \to \gamma_1\chi$ from Table 4)

				Upper bound	Lower bounds		
J	M	k_1	k_2	$e_Q=2/3$	$e_Q=2/3$	$e_Q=1/3$	$e_Q=0$
2	3.552	0.130	0.428	480.	280.	160.	120.
1	3.508	0.172	0.389	400.	240.	140.	110.
0	3.414	0.260	0.304	240.	175.	110.	94.

The last column is just the second term in (7.34). It should correspond to an absolute lower bound, modulo corrections for tensor forces, relativistic effects, etc. Presently, these values have ∿30% experimental uncertainty, of course. In passing we note that $e_Q = \frac{1}{3}$ is uncomfortable, if not eliminated. One quarter of the upper bound quoted in Table 5 is of the order of, or even smaller than, the "absolute" lower bound for all three transitions.

With the (presently rather poorly known) branching ratios of 12.5±7.5% for $\chi_2(3552)$, 30±8% for $\chi_1(3508)$, and 5±3% for $\chi_0(3414)$ (Feldman, these lecturenotes), we can obtain rough lower limits on the <u>total</u> widths of the three p-states. With the "absolute" lower bound values from Table 5, and the branching ratio <u>plus</u> its error, we find

$$\begin{aligned}
\Gamma_{total}(\chi_2) &> \frac{0.120}{0.20} \simeq 0.6 \text{ MeV} \quad (\sim 2.2 \text{ MeV}) \\
\Gamma_{total}(\chi_1) &> \frac{0.110}{0.38} \simeq 0.3 \text{ MeV} \quad (\sim 0.8 \text{ MeV}) \\
\Gamma_{total}(\chi_0) &> \frac{0.094}{0.08} \simeq 1.2 \text{ MeV} \quad (\sim 3.5 \text{ MeV})
\end{aligned} \qquad (7.35)$$

The values in parentheses are those found from the $e_Q = 2/3$ lower bound in Table 5 and the central values of the branching ratios given above. "Upper" upper bounds can be similarly estimated by taking the upper bounds from Table 5 and the branching ratios <u>minus</u> their errors. These are

$$\begin{aligned}
\Gamma_{total}(\chi_2) &< \frac{0.480}{0.05} \simeq 9.6 \text{ MeV} \quad (3.8 \text{ MeV}) \\
\Gamma_{total}(\chi_1) &< \frac{0.400}{0.22} \simeq 1.8 \text{ MeV} \quad (1.3 \text{ MeV}) \\
\Gamma_{total}(\chi_0) &< \frac{0.240}{0.02} \simeq 12. \text{ MeV} \quad (4.8 \text{ MeV})
\end{aligned} \qquad (7.36)$$

Again the numbers in parentheses are obtained using the central values of the branching ratios.

The conclusion is that, if the bound $q\bar{q}$ picture has even approximate validity, the total widths of the χ_J states should be roughly 2-3 MeV for $J = 2$, 1 MeV for $J = 1$, and 3-4 MeV for $J = 0$. These estimates have both experimental and theoretical uncertainties in them, but they are probably correct to within a factor of 2 or 3 in either direction, and perhaps even better.

Incidentally, a smaller total width for the $J = 1$ p-state is understood in the color gauge gluon picture as a consequence of the necessity of emission of 3 gluons (Yang's theorem again) instead of two for $J = 0$ or 2. We consider what the charmonium model-predicts for these hadronic widths in the next section.

(c) M1 transitions

The effective Hamiltonian describing the emission of a photon by the quark and antiquark magnetic moments is

$$H_{int} = ie_Q\sqrt{\frac{k}{2}}\,\frac{e\hbar}{2mc}\left[e^{-i\vec{k}\cdot\vec{r}/2}\,\vec{\sigma}_1\cdot(\hat{k}\times\vec{\epsilon}^*) - e^{i\vec{k}\cdot\vec{r}/2}\,\vec{\sigma}_2\cdot(\hat{k}\times\vec{\epsilon}^*)\right] \tag{7.37}$$

We are here assuming that the quarks have $g = 2$, normal for spin $\frac{1}{2}$ Dirac particles. The transition probability is easily shown to be

$$\Gamma(\text{Magnetic}) = \frac{4}{3}e_Q^2\frac{\alpha k^3}{m^2}\left|\vec{S}_{fi}\right|^2(2J_f+1) \tag{7.38}$$

where

$$\vec{S}_{fi} = \left\langle f\left|\frac{1}{2}\vec{\sigma}_1 e^{-i\vec{k}\cdot\vec{r}/2} - \frac{1}{2}\vec{\sigma}_2 e^{i\vec{k}\cdot\vec{r}/2}\right|i\right\rangle$$

Since we are interested in triplet to singlet transitions, we do a tiny spin matrix element calculation and obtain

$$\left|\vec{S}_{fi}\right| = \left|\int d^3x\psi_f^*(\vec{r})\cos\frac{\vec{k}\cdot\vec{r}}{2}\psi_i(\vec{r})\right|$$

If both initial and final states are s-waves, only the spherically symmetric part of $\cos(\vec{k}\cdot\vec{r}/2)$ is relevant:

$$\left\langle\cos\frac{\vec{k}\cdot\vec{r}}{2}\right\rangle_{\text{Angles}} = j_0\left(\frac{kr}{2}\right) \approx 1 - \frac{k^2r^2}{24} + \frac{k^4r^4}{1920}\cdots$$

Then

$$\left|\vec{S}_{fi}\right| = \left|\int_0^\infty r^2dr\,R_f^*(r)\left(1 - \frac{k^2r^2}{24} + \ldots\right)R_i(r)\right| \tag{7.39}$$

There are two classes of transitions, allowed and forbidden. The allowed transitions are those between states that have essentially the same spatial wave function and differ only in the spin state, e.g. $\psi(n=1\ {}^3S_1) \to \gamma\eta_c(n=1\ {}^1S_0)$. If spin-orbit coupling and other spin-dependent effects are neglected in computing the wave functions, the initial and final radial wave functions are exactly the same. Then

$$\left|\vec{S}_{fi}\right|_{\text{allowed}} \approx 1 + 0\left(\frac{k^2\langle r^2\rangle}{24}\right)$$

and the transition probability is

$$\Gamma_{\text{allowed}}(M1) = \frac{4e_Q^2\alpha k^3}{3m^2}(2J_f+1) \tag{7.40}$$

With $e_Q = \frac{2}{3}$, m = 1.65 GeV, $M(\psi)$ = 3.095 GeV and $M(\eta_c)$ = 2.82 GeV, Eq. (7.40) gives a width for $\psi \to \gamma\eta_c$ of

$$\Gamma(\psi \to \gamma\eta_c) \approx 29.\ \text{keV} \qquad (7.41)$$

Feldman gives an upper limit on the branching ratio of $\psi \to \gamma\eta_c$ (2.8) of 0.03. With $\Gamma(\psi)$ = 69±7 keV, this implies $\Gamma(\psi \to \gamma\eta_c) < 2$keV, in gross contradiction with our estimate. There are at least two viewpoints that can be taken:

(a) One is that the very large spacing between the ψ and the η_c shows that the Russell-Saunders approximation is very poor. The spatial wave functions of singlet and triplet states are so different that the overlap integral (7.39) is quite small. If this is true, it means that we give up any simple estimation of M1 rates.

(b) Another point of view is that Eq. (7.40) is good and that the controversial state at 2.8 GeV, if real, is not the η_c. Then the upper limit of 2 keV for the width can be inserted into (7.40) to find the maximum allowable splitting between the ψ and η_c. The result is $\sim$0.10 GeV.

(c) Other views include the belief that (7.40), with its explicit dependence on quark mass and on assumptions about g-factor, is less trustworthy that the E1 rates that involve the quark charge. Perhaps we shall know from experiment which of the various viewpoints is valid soon.

The forbidden M1 transitions are even more problematical. The transition $\psi' \to \gamma\eta_c$, for example, involves the n = 2 and n = 1 s-state radial wave functions in (7.39). These wave functions are orthogonal (different eigenstates of the same Hamiltonian) if we, as usual, neglect spin-dependent forces. This means that the first term in the expansion of $j_0(kr/2)$ does not contribute. Keeping the lowest nonvanishing contribution $(-k^2r^2/24)$ gives the forbidden M1 width as

$$\Gamma_{\text{forbidden}}(M1) = \frac{e_Q^2}{432}\,\frac{\alpha}{m^2}\,(2J_f+1)k^7\,|\langle f|r^2|i\rangle|^2 \qquad (7.42)$$

Our harmonic oscillator wave functions (7.25) yield the estimate, $\langle 2s|r^2|1s\rangle = -(3/2)^{\frac{1}{2}}\xi^{-2}$. Thus

$$\Gamma_{\text{forbidden}}(M1) = \frac{e_Q^2\alpha}{288m^2}\,\frac{k^7}{\xi^4}\,(2J_f+1) \qquad (7.43)$$

For the $\psi' \to \gamma\eta_c(2.82)$ transition, Eq. (7.43) gives the rather small width,

$$\Gamma(\psi' \to \gamma\eta_c(2.82)) = 8.5\ \text{keV}$$

Three comments:

(a) This estimate is quite unreliable because of the simplicity of the assumed wave functions. Eichten et al. (1975) had $\sim$1 keV, also unreliable.

(b) The transition probability formula (7.42) is unreliable because

of the neglect of relativistic effects of the same order. Feinberg and Sucher (1975) considered the relativistic problem and found considerable dependence of the transition rate on the mixture of Dirac covariants in the potential. Factors of 10 or more away from the simple-minded (7.42) are possible.

(c) Experimentally, the upper limit on the partial width for $\psi' \to \gamma\, \eta_c(2.82)$ is $1.1 \times 10^{-2}\Gamma(\psi') \simeq 2.5$ keV.

The conclusion about radiative transitions and the simple nonrelativistic potential model is that the E1 radiative widths make adequate sense and reinforce the spin assignments for the states at 3.414 GeV (0^{++}), 3.508 GeV (1^{++}) and 3.552 GeV (2^{++}), determined experimentally from other data. Quark charges of $\pm 2/3$ seem necessary to make the theoretical widths in reasonable agreement with experiment. The sum rules can be used to give reasonably reliable upper and lower bounds on the radiative widths for $\chi_J \to \gamma\psi$. These, together with experimental branching ratios can delimit the total widths of the χ states.

On the other side of the ledger are the M1 transitions. These involve the pseudoscalar states - still not established in any semi-conclusive way. The disagreements and/or uncertainties here may change in time. At the moment, however, there is slight cause for concern.

5. Decay of p-states into gluons or photons

In the charmonium picture, the hadronic widths of the χ_J states are assumed to be given approximately by the annihilation of $c\bar{c}$ into two gluons for $J = 0, 2$ (Barbieri, Gatto, and Kögerler, 1976) and into three gluons or one gluon and a light quark pair for the $J = 1$ states (Barbieri, Gatto and Remiddi, 1976). These are analogous to the positronium QED calculations done long ago by Alekseev (1958). For p-wave states the transition rate is proportional to the square of the derivative of the radial wave function at the origin.

In line with our advertised purpose of teaching the reader how to calculate things, we sketch the key steps in the two gluon annihilation calculation.* As in Sect. VII.1, we consider the low energy limit of the $q\bar{q} \to gg$ cross section and then translate that into a transition probability for the bound state. The Feynman diagram is shown in Fig. 16, as are the momentum vectors in the c.m.s.

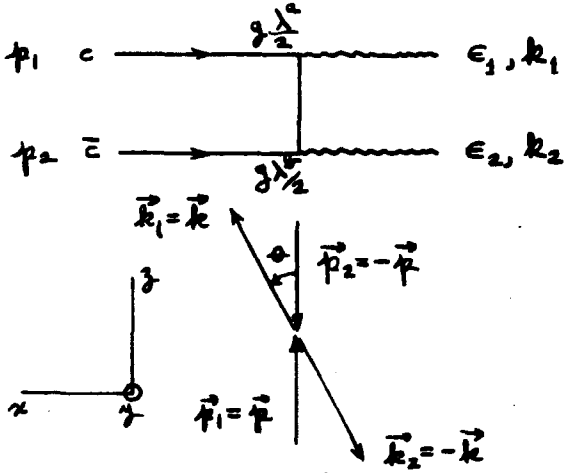

Fig. 16

*The reader who cares not how may proceed directly to Eq. (7.52) below.

Taking into account the SU(3) color couplings and the color singlet nature of the initial state (see Sect. VI.2), the matrix element is

$$\mathcal{M} = \frac{1}{4\sqrt{3}} \times 2\delta^{ab} g^2 \bar{v}_{\lambda_2}(p_2) \left\{ \begin{array}{c} \dfrac{\gamma\cdot\varepsilon_2(m - i\gamma\cdot(p_1 - k_1))\gamma\cdot\varepsilon_1}{m^2 - t} \\ \\ \dfrac{\gamma\cdot\varepsilon_1(m - i\gamma\cdot(p_1 - k_2))\gamma\cdot\varepsilon_2}{m^2 - u} \end{array} \right\} u_{\lambda_1}(p_1) \tag{7.44}$$

By the same transformation of spinors as in Sect. VII.1 this can be written in the c.m.s. as

$$\mathcal{M} = \frac{g^2}{2\sqrt{3}} \delta^{ab} (-1)^{\lambda_2 + \frac{1}{2}} u^{\dagger}_{\lambda_2}(\vec{p})\, \gamma_5 \left\{ \begin{array}{c} \text{Same as} \\ \text{in (7.44)} \end{array} \right\} u_{\lambda_1}(\vec{p}) \tag{7.45}$$

We proceed to make a nonrelativistic reduction by expanding in powers of the $q(\bar{q})$ momentum p. This will allow us to identify the $\ell = 0\ (0^{-+})$ and $\ell = 1\ (0^{++}, 2^{++})$ parts of the amplitude. To start we need the propagators in the c.m.s.:

$$m^2 - t = 2E^2(1 - \beta \cos\theta)$$

$$m^2 - u = 2E^2(1 + \beta \cos\theta)$$

where $\beta = p/E$ is the quark speed. There is a page of algebraic manipulation of the Dirac matrices that I omit. Keeping only pieces that contribute to order $(p)^0$ or $(p)^1$, the curly bracket in (7.44) becomes

$$\{\ \} = \frac{1}{2m^2} \left\{ \begin{array}{l} i\left[\vec{\gamma}\cdot\vec{\varepsilon}_1, \vec{\gamma}\cdot\vec{\varepsilon}_2\right]\vec{\gamma}\cdot\vec{k} \\ \\ -2i\left[\vec{p}\cdot\vec{\varepsilon}_1\vec{\gamma}\cdot\vec{\varepsilon}_2 + \vec{p}\cdot\vec{\varepsilon}_2\vec{\gamma}\cdot\vec{\varepsilon}_1 + \vec{p}\cdot\hat{k}\vec{\varepsilon}_1\cdot\vec{\varepsilon}_2\frac{\vec{\gamma}\cdot\vec{k}}{m}\right] \end{array} \right\} \tag{7.46}$$

The first term corresponds to the $\ell = 0$ contribution. Using

$$\left[\vec{\gamma}\cdot\vec{\varepsilon}_1, \vec{\gamma}\cdot\vec{\varepsilon}_2\right] = 2i\vec{\sigma}\cdot(\vec{\varepsilon}_1 \times \vec{\varepsilon}_2)$$

and $\gamma_5 \vec{\gamma} = -i\gamma_4 \vec{\sigma}$, it is a simple matter to show that this part gives an amplitude,

$$(\mathcal{M})_{\ell=0} = i\frac{g^2\delta^{ab}(-1)^{\lambda_2 + \frac{1}{2}}}{\sqrt{3}\, m} \vec{k}\cdot(\vec{\varepsilon}_1 \times \vec{\varepsilon}_2) \left\langle \lambda_2 | \lambda_1 \right\rangle \tag{7.47}$$

This is the familiar $\pi^0 \to \gamma\gamma$ matrix element. For the QED positronium calculation, $g^2\delta^{ab}/\sqrt{3} \to 2e^2$. The reader can carry on from here

to verify that the ^1S_o bound state annihilation rate (7.17) emerges correctly. (There two annoying factors of 2 -- one is in the relative velocity, already discussed; the other is involved with the two identical particles in the final state.)

The remaining terms in (7.46) are p-wave contributions. A two-component reduction gives

$$(\mathcal{M})_{\ell=1} = \frac{g^2\delta^{ab}}{\sqrt{3}}\,(-1)^{\lambda_2-\frac{1}{2}}\,\frac{p}{m}\left\langle \lambda_2 \left| \begin{array}{l} \hat{p}\cdot\vec{\varepsilon}_1\vec{\sigma}\cdot\vec{\varepsilon}_2 + \hat{p}\cdot\vec{\varepsilon}_2\vec{\sigma}\cdot\vec{\varepsilon}_1 \\ \\ +\,\vec{\varepsilon}\cdot\vec{\varepsilon}\;\hat{p}\cdot\hat{k}\;\vec{\sigma}\cdot\hat{k} \end{array} \right| \lambda_1 \right\rangle \tag{7.48}$$

Now comes the nitty-gritty. We must find the projections for a definite J value in the initial state. There are undoubtedly elegant ways of doing this, but it has been my personal experience that inelegant, brute-force methods are the quickest. Let us choose the initial helicities to be $\lambda_1 = \lambda_2 = \frac{1}{2}$. To make a list of helicity amplitudes for λ_3 and λ_4, the gluon helicities, we need explicit forms for $\vec{\varepsilon}_1$ and $\vec{\varepsilon}_2$. Remembering that they are final state quantities and so actually $\vec{\varepsilon}_1^*$ and $\vec{\varepsilon}_2^*$, using the Condon and Shortley convention for phases, and the coordinate axes in Fig. 16, we find

$$\vec{\varepsilon}_1^* = -\vec{\varepsilon}^*\,(\lambda_3 = +1),\ = \vec{\varepsilon}\,(\lambda_3 = -1)$$

$$\vec{\varepsilon}_2^* = \vec{\varepsilon}\,(\lambda_4 = +1),\ = -\vec{\varepsilon}^*(\lambda_4 = -1)$$

where

$$\vec{\varepsilon} = \frac{1}{\sqrt{2}}(\vec{e}_x\cos\theta + i\vec{e}_y - \vec{e}_z\sin\theta)$$

Armed with these polarization vectors, it is easy to write down the helicity amplitudes:

$$\left\langle \pm1,\pm1 \middle| (\mathcal{M})_{\ell=1} \middle| \tfrac{1}{2},\tfrac{1}{2} \right\rangle = -\frac{g^2\delta^{ab}}{\sqrt{3}}\,\frac{p}{m} \tag{7.49}$$

$$\left\langle \mp1,\pm1 \middle| (\mathcal{M})_{\ell=1} \middle| \tfrac{1}{2},\tfrac{1}{2} \right\rangle = \frac{g^2\delta^{ab}}{\sqrt{3}}\,\frac{p}{m}\,\sin^2\theta$$

Since the partial wave projections for angular momentum J involve the integral,

$$\langle \lambda_3\lambda_4 | \mathcal{M}^J | \lambda_1\lambda_2 \rangle = \frac{1}{2\pi}\int d\Omega\; D^J_{\lambda_a\lambda_b}(R_b)\,\langle \lambda_3\lambda_4 | \mathcal{M} | \lambda_1\lambda_2 \rangle\,,$$

where $\lambda_a = \lambda_1 - \lambda_2$, $\lambda_b = \lambda_3 - \lambda_4$, we see that the $\lambda_b = 0$ amplitudes correspond to $J = 0^{++}$ and the $\lambda_b = \pm 2$ amplitudes to $J = 2^{++}$ ($d^2_{20}(\theta) = \frac{\sqrt{6}}{4}\sin^2\theta$).

The low-energy cross section for the $\lambda_1 = \lambda_2 = \frac{1}{2}$ state to annihilate into two gluons through the $J = 0^{++}$ p-state is therefore given by

$$\sigma_{\frac{1}{2},\frac{1}{2}}(J = 0^{++}, \ell = 1) = \frac{1}{64\pi^2(4m^2)}\,\frac{m}{p}\cdot\underbrace{\frac{g^4}{3}\cdot 8\cdot\frac{p^2}{m^2}}_{\Sigma|\mathcal{M}|^2}\cdot 4\pi\cdot\frac{2}{2}$$

Sum over color indices

Sum over gluon helicities

Two identical particles

This gives

$$\sigma v_{rel} = \frac{16\alpha_s^2}{M^4} \cdot \frac{4\pi p^2}{3} \qquad (7.50)$$

where we have written $g^2/4\pi = \alpha_s$ and $M = 2m$ as the mass of the bound state to be.

The rule to go from velocity times cross section at threshold to bound state transition probability for a state with orbital angular momentum ℓ is to make the substitution,

$$\frac{4\pi}{2\ell+1} p^{2\ell} \to \left| \frac{(2\ell-1)!!}{\ell!} \frac{\partial^\ell}{\partial r^\ell} R_\ell(r) \right|_{r=0}^2 \qquad (7.51)$$

This can be obtained with the assumption that the amplitude is proportional to the wave function at zero separation, or its derivatives, one for each power of $\vec{p} \to -i\vec{\nabla}$, by examining the small r limit of the ℓth partial wave in a plane wave, remembering to separate off a normalized angular function. An alternative and less mysterious derivation is as follows (done here for $\ell = 1$). If the bound state wave function is $\psi(\vec{r})$, with Fourier transform,

$$\psi(\vec{p}) = \frac{1}{(2\pi)^3} \int d^3x \, e^{-i\vec{p}\cdot\vec{r}} \, \psi(\vec{r}) \, ,$$

then the bound-state transition amplitude, neglecting off-mass-shell effects of the binding, is

$$\mathcal{M}_{bound} = \int d^3p \, \mathcal{M}_\ell(\vec{p},\vec{k}) \psi^*(\vec{p})$$

where $\mathcal{M}(\vec{p},\vec{k})$ is the reaction amplitude for the "free-free" process.

The normalization can be checked by noting that for a plane wave, $\psi(\vec{r}) = e^{i\vec{p}_o\cdot\vec{r}}$, $\psi(\vec{p}) = \delta(\vec{p}-\vec{p}_o)$ and $\mathcal{M}_{bound}$ yields the expected result. Now suppose that near threshold $\mathcal{M}_\ell(\vec{p},\vec{k})$ has the limiting form, $\mathcal{M}_\ell(\vec{p},\vec{k}) = \mathcal{M}_{\ell 1} \vec{p}\cdot\hat{k}$, with $\mathcal{M}_{\ell 1}$ constant. Then

$$\begin{aligned} \mathcal{M}_{bound} &= \mathcal{M}_{\ell 1} \int d^3p \, \vec{p}\cdot\hat{k} \, \psi^*(\vec{p}) \\ &= \frac{\mathcal{M}_{\ell 1}}{(2\pi)^3} \int d^3x \, \psi^*(\vec{r}) \int d^3p \, \hat{k}\cdot\vec{p} \, e^{i\vec{p}\cdot\vec{r}} \\ &= \mathcal{M}_{\ell 1} \int d^3x \, \psi^*(\vec{r}) \, (-i\hat{k}\cdot\vec{\nabla}) \, \delta(\vec{r}) \\ &= i\mathcal{M}_{\ell 1} \, \hat{k}\cdot\vec{\nabla} \, \psi^*(0) \end{aligned}$$

Comparison of the total cross section near threshold with the total transition rate from $\mathcal{M}_{bound}$ leads to the correspondence (7.51).

For $\ell = 0$, Eq. (7.51) gives just $|R(0)|^2$ while for $\ell = 1$ it is $|R'(0)|^2$. There is also a spin factor. The helicity state $\lambda_1 = \lambda_2 = \frac{1}{2}$ is only $\frac{1}{2}$ triplet. Also, the product Y_{10} from the plane wave and χ_{10} for the triplet is only $1/3$ $J = 0^{++}$. Hence there is a factor of $6|R'(0)|^2$ to replace $4\pi p^2/3$ in (7.50). The rate for annihilation of $\chi_o(3.414)$ into 2 gluons is thus

$$\Gamma(\chi_o \to gg) \simeq \frac{96\alpha_s^2}{M^4} |R'(0)|^2 \qquad (7.52)$$

where $R'(0)$ is the derivative of the p-state wave function at the origin.

For the $J = 2^{++}$ p-state the calculation is exactly parallel.

We can indicate the numerical differences:

(i) The $\sin^4\theta$ angular distribution instead of isotropic gives a factor of $(32\pi/15)/4\pi = 8/15$.

(ii) The probability of $Y_{10}X_{10}$ being $J = 2$ is 2/3 instead of 1/3, giving a relative factor of 1/2.

The annihilation into 2 gluons of the $J = 2^{++}$ p-state is thus a factor of 4/15 times that of the $J = 0^{++}$ state:

$$\Gamma(\chi_2 \to gg) \simeq \frac{128}{5}\frac{\alpha_s^2}{M^4}|R'(0)|^2 \qquad (7.53)$$

Eqs. (7.52) and (7.53) are the results of Barbieri, Gatto and Kögerler (1976).

The student can modify the calculation for QED and compare her or his results with Alekseev's. For quarks with color, the recipe for obtaining 2-photon annihilation rates for χ_0 and χ_2 is to substitute $\alpha_s^2 \to 9\alpha^2 e_Q^4/2$ in (7.52) or (7.53). This gives

$$\begin{aligned}\Gamma(\chi_0 \to \gamma\gamma) &= \frac{256}{3}\frac{\alpha^2}{M^4}|R'(0)|^2 \\ \Gamma(\chi_2 \to \gamma\gamma) &= \frac{1024}{45}\frac{\alpha^2}{M^4}|R'(0)|^2\end{aligned} \qquad (7.54)$$

To estimate the widths into ordinary hadrons we need $R'(0)$ for the p-states. Our extremely naive oscillator wave function (7.25b) gives

$$|R'(0)|^2 = \frac{8}{3\sqrt{\pi}}\xi^5 \simeq 0.057\ \text{GeV}^5$$

for $\xi = 0.52$. With $\alpha_s = 0.2$, Eqs. (7.52) and (7.53) yield

$$\begin{aligned}\Gamma(\chi_0 \to gg) &\simeq 1.6\ \text{MeV} \\ \Gamma(\chi_2 \to gg) &\simeq 0.4\ \text{MeV}\end{aligned} \qquad (7.55)$$

Comparison with the "absolute" lower bounds (7.35) shows that these theoretical estimates are very close to the bound. A word of extreme caution here. The dependence of $|R'(0)|^2$ on the scale parameter as ξ^5 is a warning that estimates of these widths, even from semi-serious calculations, should not be trusted to better than an order of magnitude. Our simple oscillator estimate for $|R'(0)|^2$ is actually close to more reliable values. The purely linear potential of Eichten et al. (1975) gives $|R'(0)|^2 = 0.041\ \text{GeV}^5$, while the same model with a "Coulomb" potential of $-0.19/r$ in addition to the linear potential gives $|R'(0)|^2 = 0.067\ \text{GeV}^5$ (K. Gottfried and K.M. Lane, private communication). Barbieri, Gatto and Kögerler (1976) used $|R'(0)|^2 = 0.09$, an estimate obtained in their version of the $q\bar{q}$ bound-state calculation (Barbieri, Kögerler, Kunszt and Gatto, 1976).

For the $J = 1$ p-states the color gluon gauge theory estimate of the annihilation rate is much less certain. Barbieri, Gatto and Remiddi (1976) argue that the annihilation into one gluon and a light $\bar{q}q$ pair dominates the $J = 1^{++}$ rate, while the 3 gluon final state is most important for the $J = 1^{+-}$. Both of these transition rates involve logarithmic divergences at zero binding, with

$$\Gamma \simeq N \frac{\alpha_s^3}{M^4} |R'(0)|^2 \ell n \left(\frac{4m^2}{4m^2 - M^2} \right)$$

where N is a numerical constant ($128/3\pi$ for 1^{++} and $320/9\pi$ for 1^{+-}). With the logarithm estimated as $2\ \ell n\ (1/\alpha_s)$ one finds the annihilation rates for both $J = 1$ states to be roughly $1/3$ of that for the $J = 2^{++}$ state. Needless to say, these estimates are very speculative.

6. Systematics of the energy levels in charmonium

In our discussions in Chapter VI of the hadronic mass spectrum we did not treat the charmonium spectrum. We now turn briefly to that question, especially the (hyper) fine and spin-orbit and tensor force splittings.

For the $c\bar{c}$ system the color gauge theory model of Chapter VI led to the effective Hamiltonian (6.8a,b) or its phenomenological generalization (6.9). For the $\ell = 0$ states, the Fermi term in (6.8b) leads to a singlet-triplet mass difference of

$$\Delta M = \frac{8\alpha_s}{9m^2} |R(0)|^2 \qquad (7.56)$$

With $|R(0)|^2 = 0.48\ \text{GeV}^3$, $\alpha_s = 0.2$, $m = 1.65$ GeV, this gives $\Delta M \cong 31.$ MeV for the ψ-η_c splitting (De Rújula, Georgi, Glashow, 1975). The modification (6.9) replaces (7.56) with

$$\Delta M = \frac{2}{3m^2} \left\langle \nabla^2 V \right\rangle \qquad (7.57)$$

where $V(r)$ is the phenomenological central potential. Schnitzer (1976) has estimated that potentials giving at least an approximate description of the gross spectrum can increase the value of ΔM to of the order of 100 MeV at most. If the dimly seen state at 2.82 GeV is indeed the η_c, the splitting is a factor of nearly 3 larger than expected. Similarly the possible state at 3.455 GeV, seen so far only in $\psi' \to \gamma\chi \to \gamma\gamma\psi$ can perhaps be identified with the η_c' (for the arguments and difficulties, see Chanowitz and Gilman, 1976). If so, the singlet-triplet splitting is 0.230 GeV, much larger than anticipated.

Now turn to the p-states. The effective Hamiltonian (6.9) involves spin-orbit coupling, as well as the tensor force. The experimental intervals are in the ratio,

$$\frac{M_2 - M_1}{M_1 - M_0} = \frac{3.552 - 3.508}{3.508 - 3.414} = 0.47,$$

whereas for purely $\vec{L}\cdot\vec{S}$ coupling the ratio would be 2. Clearly the tensor force must be influential. Treating the $\vec{L}\cdot\vec{S}$ and tensor force terms in lowest order perturbation theory, we can make an empirical evaluation of their expectation values from the observed mass differences. Thus we have

$$M_2 = A + B - \frac{2}{5} C$$

$$M_1 = A - B + 2C$$

$$M_0 = A - 2B - 4C$$

where, according to (6.9),

$$B = \frac{3}{2m^2}\left\langle \frac{1}{r}\frac{dV}{dr}\right\rangle \qquad (7.58)$$

$$C = \frac{1}{12m^2}\left\langle \frac{1}{r}\frac{dV}{dr} - \frac{d^2V}{dr^2}\right\rangle$$

With the observed masses, we obtain

$$B = 34 \text{ MeV}, \qquad C = 10 \text{ MeV}$$

These values do not violate any a priori physical requirements. We expect both B and C to be positive on general grounds. Specific forms of $V(r)$ will, of course, put constraints on B and C that these values may not satisfy (e.g., the harmonic oscillator potential requires $B > 6C$).

Linear potential models give B values of the right order of magnitude, but under-estimate C by a factor of ~ 3 (e.g., $B = 52$ MeV, $C = 3.6$ MeV). This has led Schnitzer to an amusing speculation (Schnitzer, 1976b). An increase in the tensor-force coupling, and also in the Fermi term, in (6.9) can be achieved by assuming that the color gluon coupling to quarks has an anomalous "magnetic moment" contribution (Pauli term) in addition to the normal Dirac coupling. In nonrelativistic language this is equivalent to multiplying each "magnetic moment" by $(1 + a)$ where a is the "anomaly". Inspection of the classical Eq. (6.2) shows that the tensor force term and the Fermi term in (6.9) will each be multiplied by a factor $(1 + a)^2$. With $a \simeq 0.7$-1.0, these interaction terms will be compatible with the strength of the tensor force in the splitting of the p-states and the singlet-triplet splittings for the s-states.

The spin-orbit term, on the other hand, is not altered as much. The factor $(3/2m^2)$ in front of $(\frac{1}{r}\frac{dV}{dr})$ in (6.9) came from the "understandable" contribution $(1/m^2)$ that had its orgins in the $-\vec{\mu}\cdot\vec{B}$ of (6.3), plus a $(1/2m^2)$ part (the last terms in (6.7)) that came from the Pauli reduction of the Dirac operators for the individual quarks. Only the first term acquires a factor of $(1 + a)$. Thus the spin-orbit energy in (6.9) is multiplied only by a factor of $(1 + \frac{2a}{3})$. With $a \simeq 0.7$-1.0, the spin-orbit energy increases only by a factor of 1.5-1.7.

This "fix" of Schnitzer with an anomalous "magnetic" moment coupling is only suggestive, of course. It remains to be seen whether such a suggestion can endure closer scrutiny. Too much tinkering with the form of the potential reduces the significance of any resulting fit to the spectrum. Unfortunately, all that the freest of thinkers would say we know reliably is the very short-distance behavior of the interaction. There has been and will continue to be considerable arbitrariness in the exact form of the potential away from the origin, even if a nonrelativistic limit is granted. Clearly there are many calculations that will be done. Let us hope that the interplay of the more sensible among them and experiment will gradually increase our understanding of this part of the physics of the new particles.

VIII. Conclusions

There is no time to conclude. Charmonium seems to be a fair description of the new spectroscopy, at least below 3.7 GeV. The discovery of "hidden charm" in November 1974 and overt charm in June 1976 makes it fitting to end these lectures with a tribute to Mr. Charm himself. I give you Fig. 17.

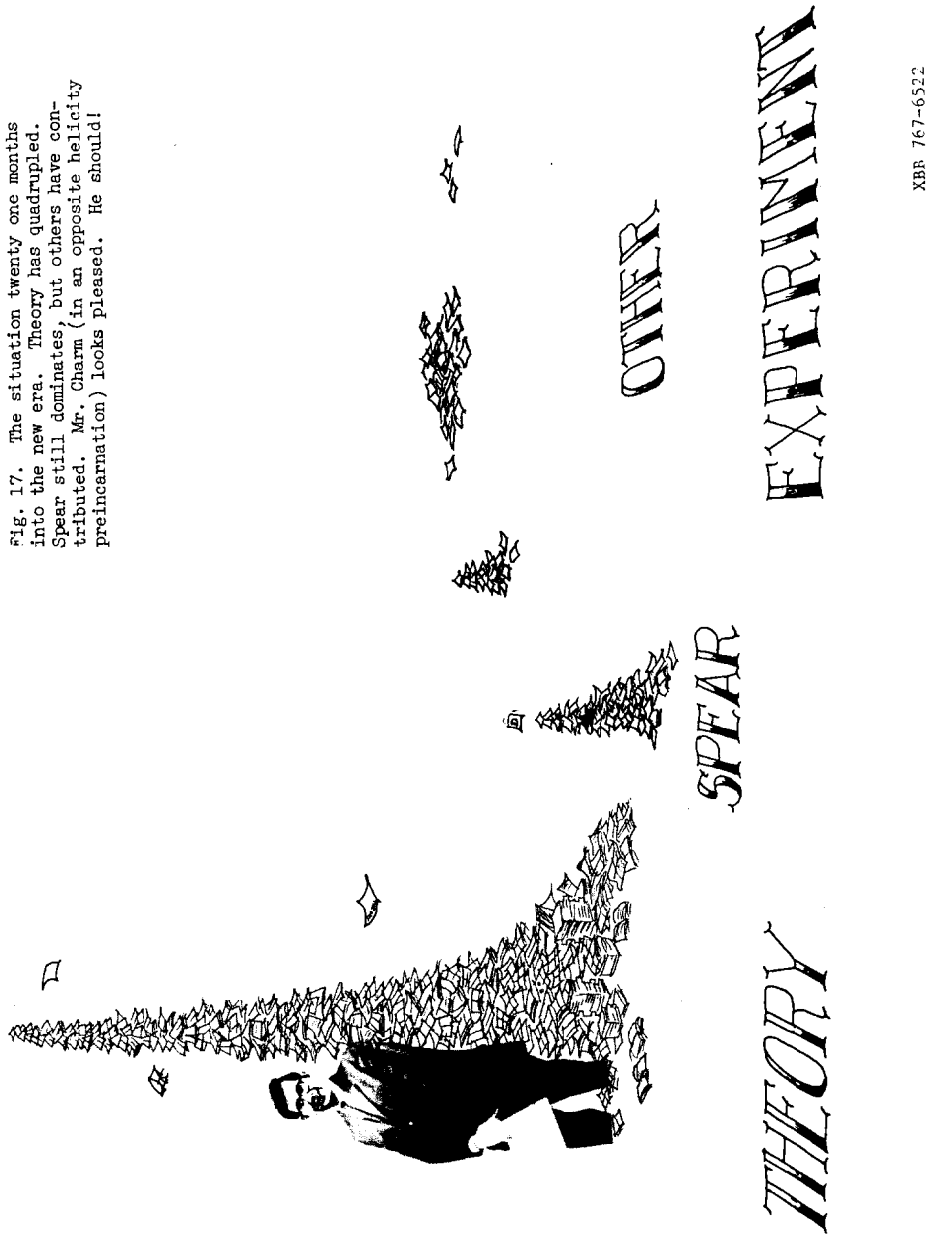

Fig. 17. The situation twenty one months into the new era. Theory has quadrupled. Spear still dominates, but others have contributed. Mr. Charm (in an opposite helicity preincarnation) looks pleased. He should!

XBB 767-6522

REFERENCES

1. Adler, S. L., 1969, Phys. Rev. 177, 2426.
2. Alekseev, A. I., 1958, Sov. Phys. JETP 7, 826.
3. Altarelli, G., N. Cabibbo, and L. Maiani, 1975, Nucl. Phys. B88, 285.
4. Appelquist, T., A. DeRújula, H. D. Politzer, and S. L. Glashow, 1975, Phys. Rev. Lett. 34, 365.
5. Appelquist, T., and H. D. Politzer, 1975a, Phys. Rev. Lett. 34, 43.
6. Appelquist, T., and H. D. Politzer, 1975b, Phys. Rev. D 12, 1404.
7. Barbieri, A., 1975, Weak and Electromagnetic Interactions at High Energies, Part A, Cargèse Summer Institute, June 1975, ed. M. Levy et al., Plenum Press (1976), p. 329.
8. Barbieri, R., R. Gatto, and R. Kögerler, 1976, Phys. Lett. 60B, 183.
9. Barbieri, R., R. Gatto, and E. Remiddi, 1976, Phys. Lett. 61B, 465.
10. Barbieri, R., R. Kögerler, Z. Kunszt, and R. Gatto, 1976, Nucl. Phys. B105, 125.
11. Bethe, H. A., and E. Salpeter, 1957, Quantum-Mechanics of One- and Two-Electron Atoms, Springer-Verlag, Academic Press, N. Y.
12. Bjorken, B. J., and S. L. Glashow, 1964, Phys. Lett. 11, 225.
13. Bolzan, J. F., K. A. Geer, W. F. Palmer, and S. S. Pinsky, 1975, Phys. Rev. Lett. 35, 419.
14. Breit, G., 1929, Phys. Rev. 34, 553.
15. Cazzoli, E. G., et al., 1975, Phys. Rev. Lett. 34, 1125.
16. Chaichain, M. and M. Hayashi, 1976, Phys. Lett. 61B, 178.
17. Chanowitz, M. S., and F. J. Gilman, 1976, SLAC-PUB-1746, LBL-4864 (May, 1976) (to be published).
18. Chew, G. F., and C. Rosenzweig, 1976, Nucl. Phys. B104, 290.
19. Coleman, S., and D. Gross, 1973, Phys. Rev. Lett. 31, 851.
20. DeRújula, A., H. Georgi, and S. L. Glashow, 1975, Phys. Rev. D 12, 147.
21. Eichten, E., K. Gottfried, T. Kinoshita, J. Kogut, K. D. Lane, and T.-M. Yan, 1975, Phys. Rev. Lett. 34, 369.
22. Eichten, E., K. Gottfried, T. Kinoshita, K. D. Lane, and T.-M. Yan, 1976, Phys. Rev. Lett. 36, 500.
23. Einhorn, M. B., and C. Quigg, 1975, Phys. Rev. D 12, 2015.
24. Feinberg, G., and J. Sucher, 1975, Phys. Rev. Lett. 35, 1740.
25. Freund, P. G. O., and Y. Nambu, 1975, Phys. Rev. Lett. 34, 1645.
26. Gaillard, M. K., and B. W. Lee, 1974, Phys. Rev. Lett. 33, 108.
27. Gaillard, M. K., and B. W. Lee, and J. L. Rosner, 1975, Rev. Mod. Phys. 47, 277.
28. Georgi, H. and S. L. Glashow, 1972, Phys. Rev. D6, 429.
29. Glashow, S. L., 1975, Scientific American 233, No. 4, 38.
30. Glashow, S. L., J. Iliopoulos, and L. Maiani, 1970, Phys. Rev. D 2, 1285.
31. Goldhaber, G., et al., 1976, Phys. Rev. Lett. 37, 255.
32. Gross, D., and R. Jackiw, 1972, Phys. Rev. D6, 477.
33. Gross, D., and F. Wilczek, 1973, Phys. Rev. Lett. 30, 1343.
34. Jackson, J. D., 1962, Elementary Particle Physics and Field Theory, Brandeis Summer Institute 1962, ed., K. W. Ford, W. A. Benjamin,

N. Y. (1963)., p. 354.

35. Jauch, J. M., and F. Rohrlich, 1955, The Theory of Photons and Electrons, Addison-Wesley, Reading, Mass.

36. Kingsley, R. L., S. B. Treiman, F. Wilczek, and A. Zee, 1975, Phys. Rev. D 11, 1919.

37. Kingsley, R. L., F. Wilczek, and A. Zee, 1976, Phys. Lett. 61B, 259.

38. Kokkedee, J. J. J., 1969, The Quark Model, W. A. Benjamin, N. Y.

39. Lee, B. W., 1975, Proc. Int. Symp. on Lepton and Photon Interactions at High Energies, Stanford University, August 21-27, 1975, ed. W. T. Kirk, SLAC (1976), p. 635.

40. Lee, B. W., 1976, Coral Gables Conf., Fermilab-Conf-76/20-THY/EXP (February, 1976).

41. Perl, M. L., et al., 1975, Phys. Rev. Lett. 35, 1489.

42. Peruzzi, I., et al., 1976, SLAC-PUB-1776, LBL-5340 (July, 1976) (to be published).

43. Politzer, H. D., 1973, Phys. Rev. Lett. 30, 1346.

44. Politzer, H. D., 1974, Phys. Rep. 14C, 130.

45. Pumplin, J., W. Repko, and A. Sato, 1975, Phys. Rev. Lett. 35, 1538.

46. Rosenzweig, C., 1976, Phys. Rev. D 13, 3080.

47. Schnitzer, H. J., 1975, Phys. Rev. Lett. 35, 1540.

48. Schnitzer, H. J., 1976a, Phys. Rev. D 13, 74.

49. Schnitzer, H. J., 1967b, Brandeis preprint (July 1976).

50. Steinberger, J., 1949, Phys. Rev. 76, 1180.

51. Törnqvist, N. A., 1976, LBL-5304, (June 7, 1976), submitted to Phys. Lett. B.

52. Weinberg, S., 1972, Phys. Rev. D 5, 1412. See also Phys. Rev. Lett. 27, 1688 (1971).

NEW PARTICLE PRODUCTION*

David Hitlin
Stanford Linear Accelerator Center
Stanford University, Stanford, California 94305

INTRODUCTION

These lectures deal with several specific topics in the area of new particle production. First, there is charmed particle production in e^+e^- annihilation. Next, photoproduction of ψ and ψ' and implications of these results for the photoproduction of charmed particles are discussed. Hadronic production of ψ and ψ' is then reviewed and again implications of these results for charmed particle production by hadrons are dealt with. Experimental evidence for the operation of the OZI rule in hadronic interactions is then reviewed. The final topic is a discussion of direct lepton production by hadrons and the relevance of this phenomenon to charmed particle production. Frequent reference will be made to results quoted by Jackson in his lectures at the Summer School portion of the Institute, and to material presented by Goldhaber, Glashow, Lederman, Lee, D. Meyer, H. Meyer, Schmüser, and Smith in the Topical Conference.

I. CHARMED PARTICLE PRODUCTION IN e^+e^- ANNIHILATION

While neutrino interactions had yielded several interesting indications of new phenomena which could most readily be explained by the introduction of a new hadronic quantum number,[1] and, indeed, a specific example of a $\Delta S = -\Delta Q$ reaction in the BNL 7-foot bubble chamber,[2] the most striking evidence for the existence of charm has appeared in e^+e^- annihilation.[3,4] The dramatic increase in R in the 4 GeV region[5] had been taken by many to be charm threshold, but characteristic features expected to be associated with the threshold, such as an increase in kaon production,[6] had not, and have not, as of this writing, been seen. Since a large body of data of the SLAC/LBL collaboration existed at 4.8 GeV, these data were examined[7] for narrow mass peaks in the $K^\pm\pi^\mp$, $K^o_S\pi^+\pi^-$, $\pi^+\pi^-$, K^+K^-, $K^\mp\pi^\pm\pi^\pm$, $K^o_S\pi^+$, and $\pi^+\pi^-\pi^\pm$ channels. π,K separation by time-of-flight was not attempted, on the grounds that the K momentum would on average be too high. In this search no significant enhancements were seen, and limits on charmed meson production × branching ratio in the range of a few tenths of a nanobarn were derived. These limits were close to the expected range, but did not exceed them.[8]

The use of time-of-flight information by the SLAC/LBL collaboration to obtain π,K separation in the 4 GeV region improved the signal to noise ratio sufficiently to show the existence of significant mass peaks, first in $K^\pm\pi$ and $K^\pm\pi^\mp\pi^+\pi^-$,[3] and soon thereafter in $K^+\pi\pi$.[4] We will review the features of these decays which lead to the assertion that they are examples of charmed meson decays, will discuss the production mechanism, and will then look at some future experimental prospects. There is a rich spectroscopy of new hadronic states to fill in, and a completely new term in the weak current to understand.

For our purposes, "charm" refers specifically to a new quantum number carried by a fourth quark which has those attributes necessary to implement the GIM mechanism[9] in, for example, the suppression of $K^o_L \to \mu^+\mu^-$ decay. Other schemes, involving more than four quarks, such as those of Harari,[10] will be dealt with, if at all, only in passing.

Figure 1 shows the behavior of the ratio $R = \sigma(e^+e^- \to \text{hadrons})/\sigma(e^+e^- \to \mu^+\mu^-)$ in the SPEAR/DORIS energy region.[5] The "step" in R, amounting to about two units, is clearly evident in the 4 GeV region. The explanation for the step in the charm scheme is that one has reached charm threshold. The structure at 4.03 GeV appears to be the best place to study charmed meson decays, as the region between phase space suppression on the one hand, and form factor suppression on the other, is relatively small.

Facts are accumulating rapidly, but let us summarize what is

*Work supported by the Energy Research and Development Administration.

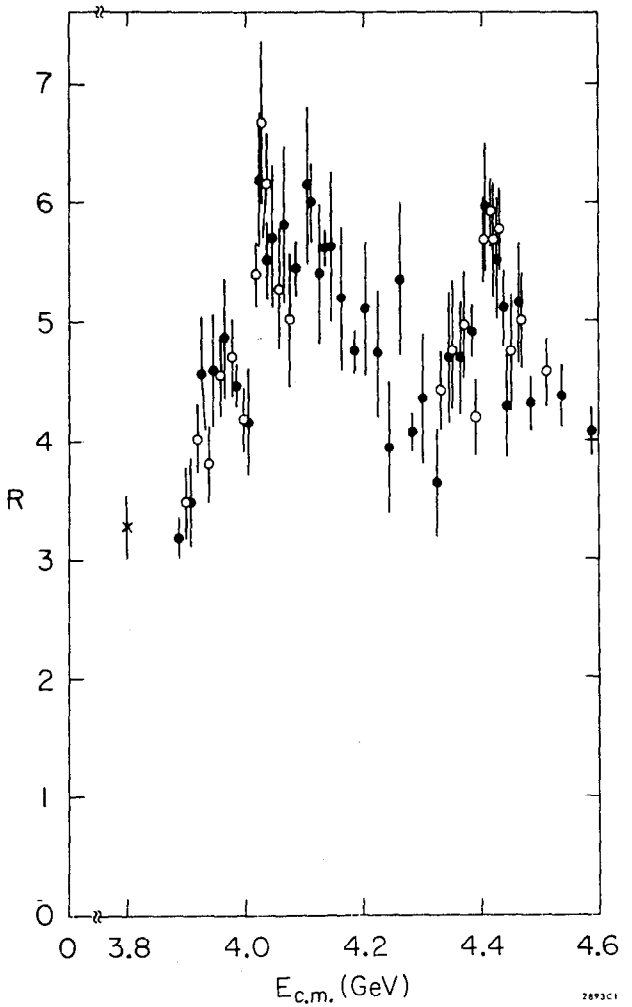

Fig. 1--Structure in $R = \sigma(e^+e^- \to \text{hadrons})/\sigma(e^+e^- \to \mu^+\mu^-)$ observed in the $\sqrt{s} = 4$ GeV region. (Ref. 5.)

experimentally established as of this writing. There is clear evidence for a D^o at a mass of 1865 ± 15 MeV and a D^+ at a mass of 1876 ± 15 MeV. The recoil spectra against these peaks indicates a D^{*o} and a D^{*+}, both with masses of about 2005 MeV. The D^o decays to $K^-\pi^+$ and $K^-\pi^+\pi^+\pi^-$, while the D^+ decays to $K^-\pi^+\pi^+$. Each of these branching ratios amounts to a few percent. Both D's are rather narrow. The decay modes seen thus far are presumably the Cabibbo favored ones; Cabibbo suppressed modes, such as $D^o \to \pi^+\pi^-$ have not been seen. The most likely spin assignment would be zero for the D's, one for the D*'s (see, however, Borchardt and Mathur[11]), but this has not been definitely established. No evidence for F production has yet been obtained.

The states to be expected in the charm scheme and the question of enhanced nonleptonic decays due to $\underline{20}$ dominance have been discussed in Jackson's lectures. Let us, therefore, discuss several other topics not touched upon there.

1. D,D* Production Ratios. Lane and Eichten[12] and De Rújula, Georgi, and Glashow[13] have shown that in a D production model in which a $c\bar{c}$ quark pair are made in e^+e^- annihilation and then mesons are formed by combining with light quarks from the vacuum with ℓs coupling results in a production ratio, just by counting spins, of $D\bar{D}:D\bar{D}^* + \bar{D}D^*:D^*\bar{D}^*$ of 1:4:7 close to threshold. These ratios may be modified by momentum dependent factors due to effects of the confining potential. Close[14] has shown, using a helicity formalism, that the 1:4:7 ratio is true only if all helicity amplitudes are equal and if one integrates over the polar angle, θ. For devices with particular acceptance, the detected production ratio may differ considerably from 1:4:7. One conclusion which remains unaltered, however, is that D* production in e^+e^- is greater than D production by a factor of 3 or so.

2. Electromagnetic Mass Splittings. The $D^+ - D^o$ and $D^{*+} - D^{*o}$ electromagnetic mass splittings have dramatic effects on the branching ratios of their

decay modes. There have been several calculations of these mass splittings, with predictions ranging from less than 5 to 15 MeV.

The first, and largest, estimate was made by De Rujula, Georgi, and Glashow.[13] Using their nonrelativistic bound state model (see Jackson, these proceedings), they assumed that the Coulomb part of the mass splittings between meson isodoublets was proportional to the product of the quark charges: $\delta \propto q_i q_j = 3:2:4$ for $\pi^+ - \pi^0 : K^+ - K^0 : D^+ - D^0$. Fitting the π^+-π^0 mass difference implies $\langle \frac{1}{r} \rangle = 1230$ MeV, which they use for all other pairs. It should be noted that this value is much larger than the 410 MeV derived by Schnitzer[15] from charmonium spectroscopy. The non-Coulomb part of the splitting, due to the u-d quark mass difference, is derived by fitting to the K^+-K^0 splitting. Summing these two contributions, DGG find 13 MeV for the D^+-D^0 splitting; they use 15 MeV in their branching ratio calculation.

This calculation has been criticized by several authors. Lane and Weinberg[16] question the applicability of the nonrelativistic atomic model to pions. They use instead Dashen's theorem, which says that the Coulomb contribution to the differences in the mass-squared is the same for K's and π's. After removing the Coulomb contribution to the quark mass difference, they calculate $\langle \frac{1}{r} \rangle = 350$ MeV, leading to a D^+-D^0 splitting of 6.7 MeV, which includes a 10% correction to $\langle \frac{1}{r} \rangle$ for heavy mesons. A similar analysis by Fritzsch[17] derives a similar result.

Celmaster,[18] using a perturbed harmonic potential, finds $M_{D^+} - M_{D^0} <$ 4 MeV. Sanchez Guillen,[19] using a fully relativistic model, finds 3 MeV. The (unweighted) Harvard average is 7 MeV. The D^{*+}-D^{*0} splittings should be comparable.

Because of the very small Q value of $D^* \to D\pi$ decay, relative branching ratios are very sensitive to these mass splittings. For example, with their 15 MeV estimate and with $M_{D^0} = 1.86$ and $M_{D^{*0}} = 2.00$, DGG calculate the branching ratio $D^{*+} \to D^0\pi^+$ to be $\geq 90\%$ of the total width of .5 - 1 MeV, whereas $D^{*+} \to D^+\pi^0$ is $\leq 10\%$ and $D^{*+} \to D^+\gamma \approx 1\%$. However, if $M_{D^+} - M_{D^0} = 7$ MeV and $M_{\pi^+} - M_{\pi^0} = 4.6$ MeV, the very small Q values involved can change these branching ratios dramatically. Calculations of Ono,[20] shown in Fig. 2, indicate that the relative rates $D^{-+} \to D^+\pi^0$ and $D^0\pi^+$ can vary over several orders of magnitude as the isodoublet mass splitting gets very small. While the recoil spectra seen in the 4 GeV region[21] are in qualitative agreement with the initial predictions of DGG, there are discrepancies in detail, at least some of which are due to this extreme sensitivity to the mass splittings.

3. Recoil Spectra. The spectrum of masses recoiling against a reconstructed D in e^+e^- annihilation is a rich area for studying the production mechanism and for determining the mass of higher D states.[22] These missing mass spectra contain real mass peaks corresponding to the D* mass (or any other meson made in conjunction with a D), and particularly near threshold, kinematic reflections which are artifacts of the details of production and decay. Fig. 3 summarizes the source of real and reflection peaks in the spectrum recoiling against D^0, D^+, and F^+ mesons.[23]

The details of the recoil spectra depend on several factors. First, there is the $D\bar{D}:D\bar{D}^* + \bar{D}D^*:D^*\bar{D}^*$ production ratio, which may depend on the polar angle θ, and thus will be seen differently in different detectors. Then there is an s dependence, due to production threshold effects and form factors. Finally, the relative magnitude of real and reflection peaks depends on the various $D^* \to$ D branching ratios, which are a sensitive function of the D^+-D^0 mass splitting.

4. Exotics. A most important piece of evidence supporting the charm interpretation of the 1876 MeV structure seen at SPEAR[4] has been that the peak was found in the exotic channel $K^\mp\pi^\pm\pi^\pm$ and not in $K^\pm\pi^\pm\pi^\mp$ or in doubly charged

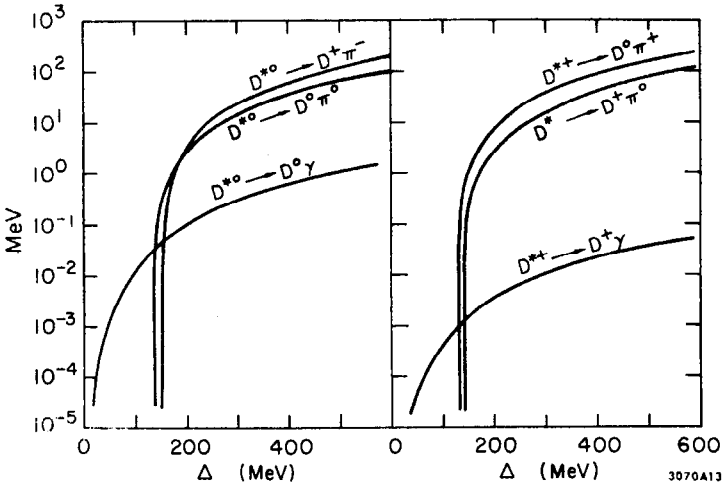

Fig. 2--Dependence of $D^* \to \gamma D$ and $D^* \to \pi D$ decay rates on $\Delta \equiv D^{*0} - D^0$. (Ref. 20.)

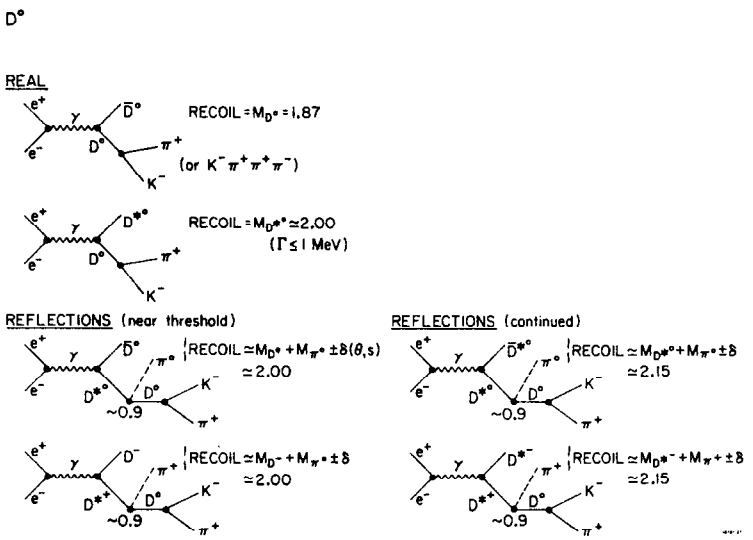

Fig. 3a--Genuine and kinematic reflection peaks expected in D^0 recoil spectra near threshold. (Ref. 23.)

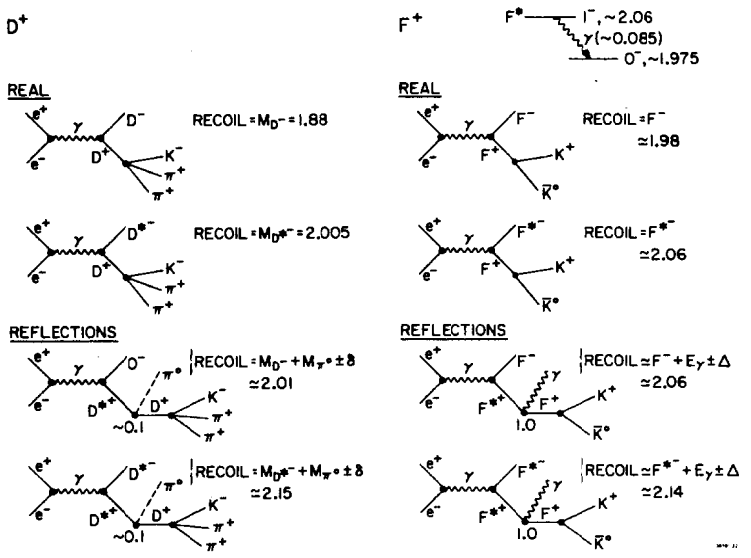

Fig. 3b--Genuine and kinematic reflection peaks expected in D^+ and F^+ recoil spectra near threshold.

modes like $K^{\mp}\pi^{\mp}$, $K^{\mp}\pi^{\mp}\pi^{+}\pi^{-}$, or $K^{\mp}\pi^{\pm}\pi^{\pm}\pi^{\pm}$. Since the $\cos\theta_c$ decay of a charmed quark is $c \to s\bar{u}d$, it is expected in the charm scheme that $D^+(c\bar{d}) \to K^-(s\bar{u})$ and not to $K^+(u\bar{s})$. If the new state were a high mass K*, the existence of the $K\pi\pi$ mode requires I = 3/2 or 5/2. No strange meson with $I > \frac{1}{2}$ has hitherto been observed, and further, the expected doubly charged modes are not seen.

The Λ_c interpretation[24] of the $\bar{\Lambda}\pi^-\pi^-\pi^+$ enhancement seen by the CIHF group[25] is similarly strengthened by the absence of $\bar{\Lambda}\pi^+\pi^+\pi^-$.

5. Parity Violation. There are several rather direct tests of the existence of parity violation in D decay, some of which have already been experimentally verified.

If the $K^{\pm}\pi^{\mp}$ and $K^{\pm}\pi^{\mp}\pi^{\mp}$ mass peaks belong to the same J=0 isomultiplet, then parity is violated since $P\left[(K\pi)_{J=0}\right] = +$, $P\left[(K\pi\pi)_{J=0}\right] = -$. The J^P of the $K\pi$ system is 0^+, 1^-, 2^+, etc., but for $K\pi\pi$ it may be natural or unnatural. For the natural sequence, the $K\pi\pi$ population on the edge of the Dalitz plot must vanish,[26] or parity is violated. Uniform population of the Dalitz plot has been demonstrated (see Goldhaber, these proceedings).

The observation of both $K^+\pi^-\pi^-$ and $K^0_S\pi^-$ or $K^+\pi^-$, $K^-\pi^+\pi^+\pi^-$ and $K^0_S\pi^+\pi^-$ is a clear manifestation of parity violation.

Parity violation can also, of course, be demonstrated by the existence of pseudoscalars, such as $\vec{p}_{beam} \cdot (\vec{k}_1 \times \vec{k}_2)(\vec{k}_1 - \vec{k}_2) \cdot \vec{p}_{beam}$ in two particle inclusive reactions (not 0^-) or $\vec{k}_1 \cdot (\vec{k}_2 \times \vec{k}_3)$ in three particle exclusive reactions.[27]

6. D^0-$\bar{D}^0$ Mixing. Since D^0 and $\bar{D}^0$ states can be connected by second order weak transitions, it is amusing to recapitulate the well-known $K^0, \bar{K}^0$ formalism.[28] The eigenstates of the system are

$$|D_1^0\rangle = \frac{1}{\sqrt{2}}(|D^0\rangle + |\bar{D}^0\rangle)$$

$$|D_2^0\rangle = \frac{1}{\sqrt{2}}(|D^0\rangle - |\bar{D}^0\rangle).$$

For a state which is initially pure D^0, we have

$$\frac{\Gamma(D^0 \to K^+\pi^-)}{\Gamma(D^0 \to K^-\pi^+)} = \tan^4\theta_c ,$$

whereas for a mixed state:

$$\frac{\Gamma(D_1^0 \to K^+\pi^-)}{\Gamma(D_1^0 \to K^-\pi^+)} = \tan^4\theta_c\left[1 + \frac{m_{D_1} - m_{D_2}}{2\lambda \sin^2\theta_c} + \frac{1}{\gamma}\left(\frac{\lambda_{D_1} - \lambda_{D_2}}{\lambda \sin^2\theta_c}\right)^2 + \frac{1}{2}\left(\frac{m_{D_1} - m_{D_2}}{\lambda \sin^2\theta_c}\right)^2\right].$$

It would appear to be very difficult to observe the consequences of $D^0, \bar{D}^0$ mixing, either in these hadronic decay modes or in semileptonic modes, due to the double Cabibbo suppression.

There are other models, however, in which D^0-$\bar{D}^0$ mixing is expected to be much larger.[29] The crucial test is the comparison of the charges of the K's in a sample of completely reconstructed $D^0\bar{D}^0$ events.

7. Semileptonic Decays. The semileptonic decay rate of $D \to K\ell\nu$ is typically estimated by using SU(4) to determine the matrix element of the vector current and assuming constant form factors,[30] or by scaling from $K \to \pi\ell\nu$. However, since the vector and pseudoscalar masses are not very different, the variation of the f_+ form factor may have a substantial effect on the rate. In the pole approximation for f_+, $f_+(t) = \frac{1}{(1-t/M_{F^*}^2)}$ varies substantially in the physical region $m_\ell^2 \leq t \leq (m_D - M_K)^2$; the naive rate estimate should be increased by a factor of 1.5.

The lepton spectra resulting from D decay are of some interest, both because of direct lepton signals seen in e^+e^- annihilation, and because of possible contributions to the direct lepton signal in hadronic collisions. Naively, it would appear that $D \to K\ell\nu$ should be the dominant semileptonic decay mode, but there is some evidence that this may not be the case. Fig. 4 shows the

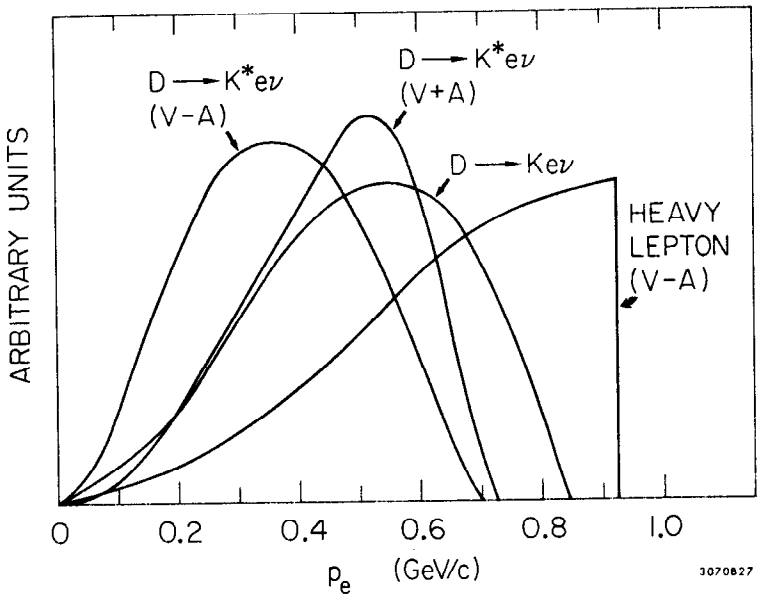

Fig. 4--Electron spectra in the center of mass resulting from $D \to Ke\nu$, $D \to K^*(890)e\nu$ for V-A and V+A coupling decays, and from decay of a V-A heavy lepton.

electron spectrum in the D center of mass for $D \to Ke\nu$ decay with constant form factors. Fig. 5 shows the same spectrum in the laboratory with a $\beta = .3$, a typical value for D production in the 4 GeV region. The DASP collaboration inclusive e^- spectrum[31] is shown superimposed, and clearly peaks at too low a momentum to be explained by this decay. The PLUTO collaboration has seen the $K^o_s e$ coincidences expected from D decay in the 4 GeV region;[32] their electron spectrum similarly peaks at low values of electron momenta. In order to produce a softer electron spectrum, a natural approach is to consider $D \to K^*\ell\nu$ or $D \to K(n\pi)\ell\nu$ decays. There is a great deal of uncertainty in the appropriate values of the four form factors involved in the $K^*\ell\nu$ mode. The matrix element has the general form

$$\langle K^*(q,\epsilon)|(V\mp A)_\lambda|D(p)\rangle = iF_1^V(t)\epsilon_{\lambda\alpha\beta\gamma}p^\alpha q^\beta \epsilon^\gamma \mp \left(F_1^A(t)\epsilon_\lambda + F_2^A(t)(p\cdot\epsilon)(p+q)_\lambda + F_3^A(t)(p\cdot\epsilon)(p-q)_\lambda\right).$$

Just as with the f_- contribution in $K\ell\nu$ decay, the contribution of the F_3^A is proportional to m_e and can be neglected. The F_1^V form factor can be derived from $\Gamma(\omega \to \pi^o\gamma)$. The other two axial form factors are highly model dependent. Hinchliffe and Llewellyn Smith[33] neglect F_2^A entirely, while Ali and Yang[34] estimate it using a hard pion approach. The center-of-mass electron spectra for $V \mp A$ couplings in $D \to K^*\ell\nu$ calculated by Ali and Yang are shown in Fig. 4, and the expected spectra in the 4 GeV region in e^+e^- annihilation are compared to the DASP electron spectrum in Fig. 5. . An even softer electron spectrum can be generated using $K^*(1420)\ell\nu$ decay.[35] An example is also shown in Figure 5. Uncorrelated $D \to K\pi\ell\nu$ and $K\pi\pi\ell\nu$ decays, in which the lepton spectra are mainly determined by phase space, also yield such soft e spectra.

Inclusive lepton spectra due to heavy lepton and charm decay can be distinguished by their shape and by the associated hadron multiplicity. For

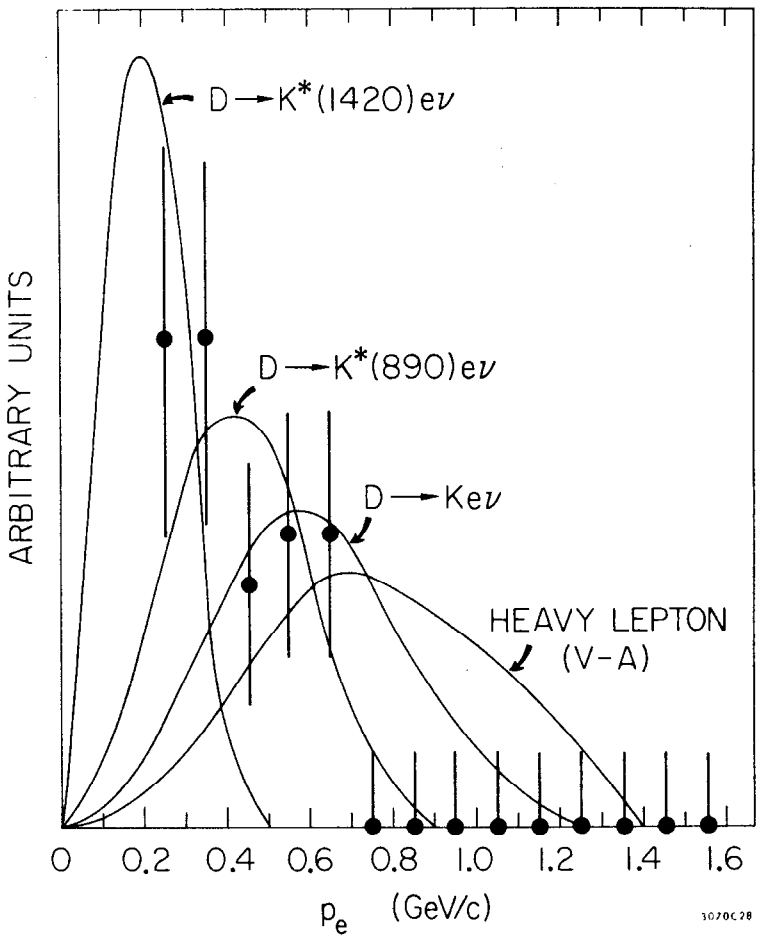

Fig. 5--Electron spectra in the laboratory ($\beta = 0.3$) resulting from $D \to Ke\nu$, $D \to K^*(890)e\nu$ (vector coupling), $D \to K^*(1420)e\nu$, and a V-A heavy lepton. DASP direct electron data shown for comparison (Ref. 31).

comparison V-A heavy lepton electron spectra are also shown in Figures 4 and 5.

The low momentum character of these electron spectra clearly requires the dominance of $K\pi\ell\nu$ (resonant or nonresonant) decay modes over $K\ell\nu$, a surprising result, since soft pion theorems and statistical arguments predict the opposite. A similar conclusion has been reached by Barger[36] in his analysis of ν induced μe events.

In the future, it appears possible to study the details of these weak couplings by a Dalitz plot analysis of the charged lepton-hadron spectra. This should be possible in $D \to K\ell\nu$, $D \to K^*(890)\ell\nu$ and $F \to \eta\ell\nu$ decays. The relative proximity of the higher charmed mesons (F, F*, scalar D) to the physical region for these decays implies substantial variation of the form factors with t. As an example, Fig. 6a shows the Dalitz plot of $D^0 \to K^+e^-\nu$ decay for a vector form factor, f_+, dominated by the F* pole. Fig. 6b shows the sensitivity of a Dalitz plot analysis of this decay to the extraction of the F* mass. The points are the results of a simulation of the decay using an F* mass of 2.1 GeV, for 500 events binned in 100 MeV bins. The curves are the t behavior of the f_+ form factor for several assumed mass values, with $f_+(0) \equiv 1$.

It thus appears to be possible to extract details of the form factors of these decays in much the way $K_{\ell 3}$ decay has been studied, and to in this way study the breaking of SU(4) × SU(4) symmetry of the weak hadronic currents.

The semileptonic decays of charmed baryons will also provide information on the structure of the weak current. These decays are likely to have a larger branching ratio than in the strange baryon case,[37] and the details of the spectra are sensitive to the coupling. For example, the mean electron momentum in $\Lambda_c^+ \to \Lambda^0 e^+ \nu$ is a sensitive measure of the type of coupling. This can be seen in Fig. 7 from Burwas and Ellis.[38]

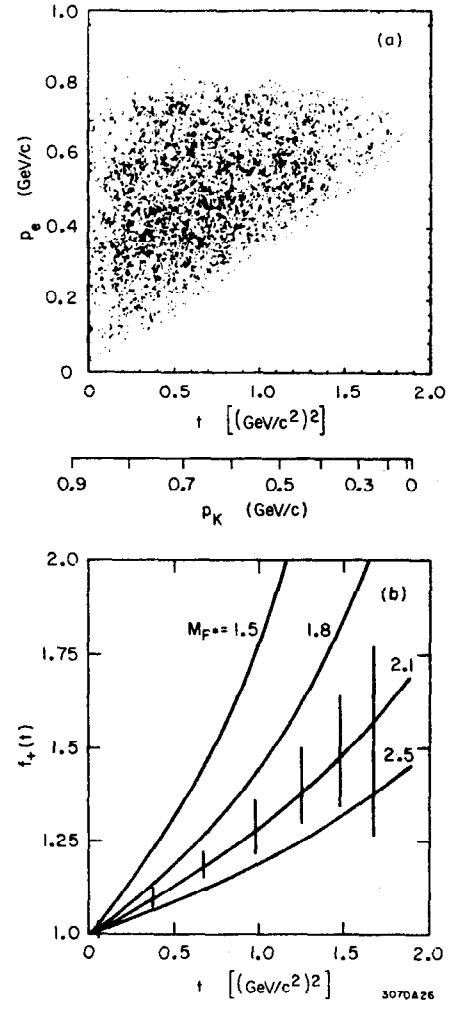

Fig. 6--(a) Dalitz plot for $D^0 \to K^+e^-\nu$ with t-dependence of the vector form factor (f_+) dominated by an F* pole mass of 2.1 GeV. (b) t-dependence of the f_+ form factor for several F* mass values. The "data points" show the sensitivity of a Dalitz plot of 500 events generated by a Monte Carlo calculation for the extraction of the pole mass.

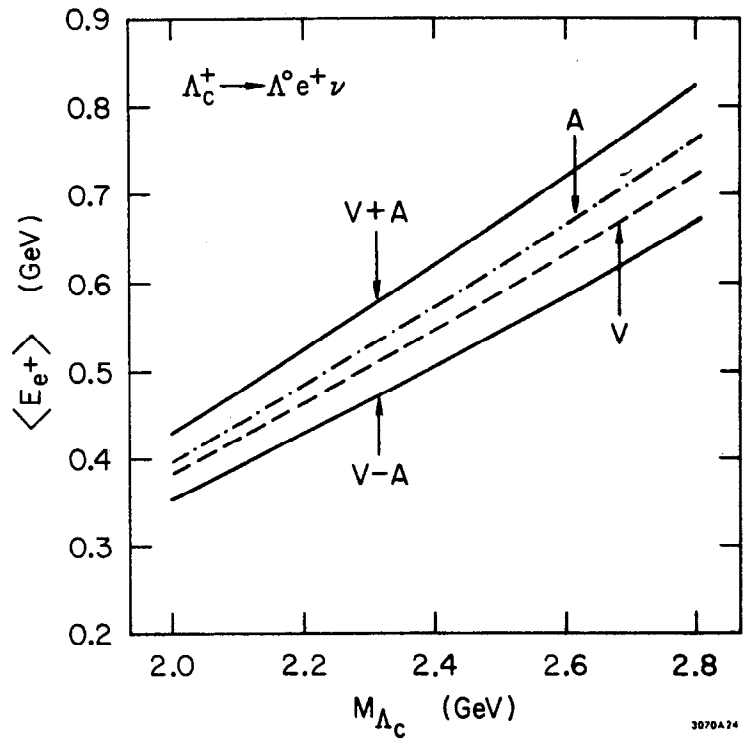

Fig. 7--Dependence of $\langle E_{e^+} \rangle$ in $C_0^+ \rightarrow \Lambda^0 e^+ \nu$ decay on various choices of the form of the decay coupling.

II. PHOTOPRODUCTION OF NEW PARTICLES

Important evidence on the hadronic nature of the ψ comes from photoproduction experiments. These also provide data which can be interpreted to place limits on the photoproduction of charmed particles. There is now data on the s and t dependence of ψ photoproduction from threshold out to 240 GeV.[39]

1. Psi Production. Since the ψ is clearly established as a vector meson,[10] it is natural to adopt the language of vector meson dominance to describe the photoproduction process. Let us follow Sivers, Townsend, and West (SWT),[40] who develop a formalism which explicitly allows for corrections to the VMD model. While the corrections can be calculated,[41] let us see how we can extract them from the experimental data itself. In the vector meson dominance model, ψ photoproduction is a diffractive process related to ψN elastic scattering:

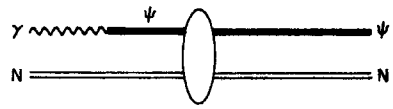

$$\frac{d\sigma}{dt}(\gamma N \rightarrow \psi N) = \lambda^2 \frac{3\Gamma_{\psi \rightarrow e^+e^-}}{\alpha M_\psi} \frac{d\sigma}{dt}(\psi N \rightarrow \psi N) .$$

Here λ is a parameter defined by STW describing the breakdown of VMD:

$$\lambda = \frac{\gamma_\psi(m_\psi^2) A(\psi N \rightarrow \psi N)\big|_{q^2=0}}{\gamma_\psi(0)\, A\,(\psi N \rightarrow \psi N)\big|_{q^2=m_\psi^2}} ,$$

λ clearly being unity in the VMD limit. $\Gamma_{\psi \rightarrow e^+e^-}$ is the partial rate of ψ into leptons measured in e^+e^- annihilation: $\Gamma_{\psi \rightarrow e^+e^-} = 4.8$ keV. Using the optical theorem, we can relate the differential cross section at t=0 to the total cross section:

$$\left.\frac{d\sigma}{dt}(\psi N \to \psi N)\right|_{t=0} = \frac{\sigma_{tot}^2(\psi N)}{16\pi}(1+\rho^2) ,$$

where ρ = Re A/Im A $\to 0$ as $s \to \infty$. We can then write the ψN total cross section in terms of measurable quantities:

$$\sigma_{tot}(\psi N) = \frac{1}{\lambda(1+\rho^2)^{\frac{1}{2}}}\left[\frac{\alpha M_\psi}{3\Gamma_{\psi\to e^+e^-}} 16\pi e^{-bt_{min}} \left.\frac{d\sigma}{dt}(\gamma N\to\psi N)\right|_{t_{min}}\right]^{\frac{1}{2}}$$

where

$$\frac{d\sigma}{dt} = \left.\frac{d\sigma}{dt}\right|_{t=0} e^{-bt} , \quad b = b(s).$$

Figure 8 shows the t dependence at 19 GeV measured by the SLAC-Wisconsin collaboration.[42] $\frac{d\sigma}{dt}$ has now been measured by four groups. Their results are summarized in Fig. 9. Note that $\left.\frac{d\sigma}{dt}\right|_{t=0}$ rises with s to a high energy value of about 40 nb/GeV^2. If we assume that $\rho = 0$ and $\lambda = 1$ at high s, we can conclude that $\sigma_{tot}(\psi N) \approx 1$ mb. This is certainly large enough to qualify the ψ as a member of the hadron family, but we have yet to ascertain the size of corrections to VMD.

A second experiment by the SLAC-Wisconsin collaboration[43] allows a test of the VMD assumption, by deriving $\sigma_{tot}(\psi N)$ from the A dependence of $\left.\frac{d\sigma}{dt}\right|_{t=0}$ using a procedure which is independent of VMD. We can define an effective A value for a nucleus which takes account of the possibility of multiple scattering within the nuclear volume:

$$A_{eff} = \frac{1}{\sigma_{tot}(\psi N)} \int_0^\infty [1-\exp(-\sigma_{tot}(\psi N)T(r'))]dr' .$$

$T(r')$ depends on the details of the nuclear model chosen, but a simple hard sphere model with radius $R = r_0 A^{1/3}$ suffices. In this model

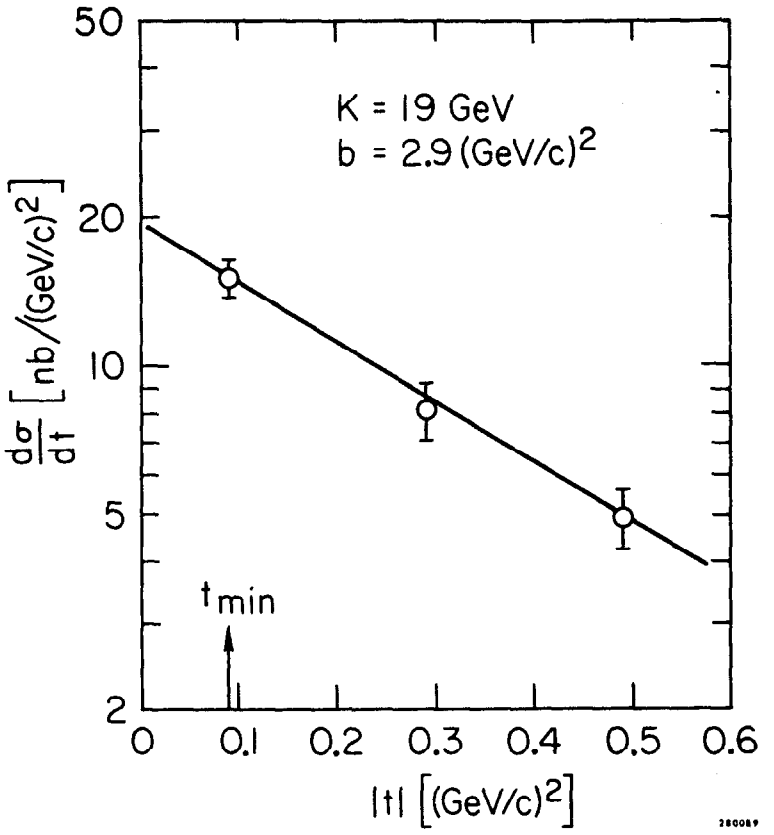

Fig. 8--The t-dependence of the ψ photoproduction cross section (Camerini et al., Ref. 42).

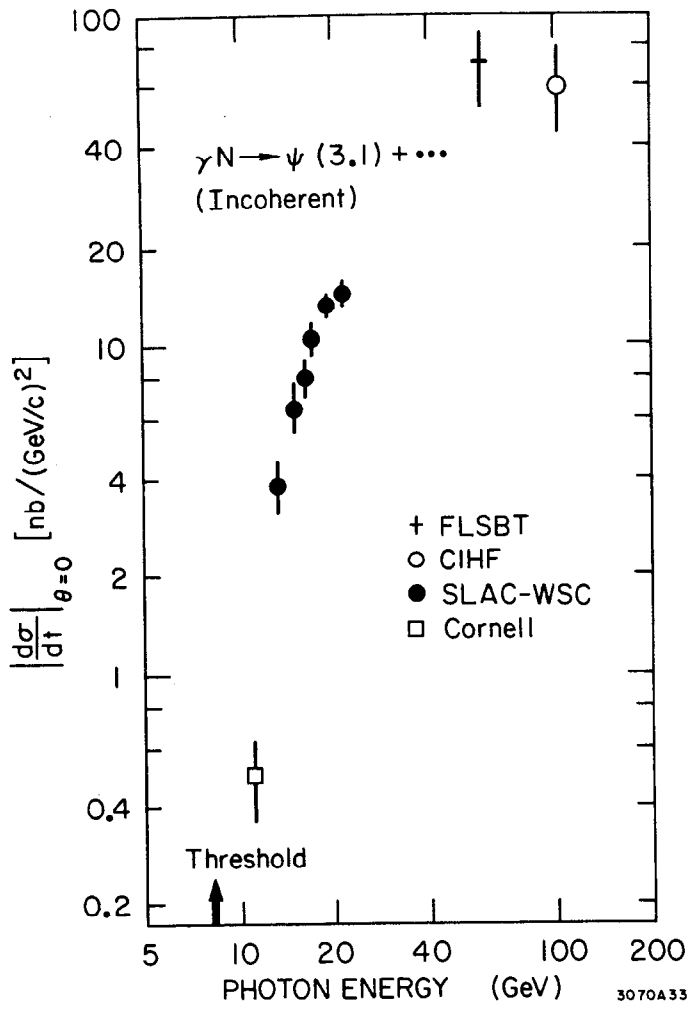

Fig. 9--The s-dependence of $d\sigma/dt$ at $\theta = 0$.

$$T(r') = \frac{3A}{2\pi R^3}(R^2 - r'^2)^{\frac{1}{2}} \qquad r' \leq R$$

$$= 0 \qquad r' > R .$$

Then

$$\frac{A_{eff}}{A} = 1 - \frac{9}{16\pi r_0^2}\sigma_{tot}(\psi N)A^{1/3} + \text{small corrections.}$$

Measurements on Be and Ta can then be interpreted to yield[43]

$$\sigma_{tot}(\psi N) = 3.48 \pm .79 \text{ mb} ,$$

a value substantially larger than the VMD estimate. We can then calculate λ:

$$\lambda = \frac{\sigma_{tot}(\psi N)_{VMD}}{\sigma_{tot}(\psi N)_{A\ dependence}} = .29 .$$

This value is in reasonable agreement with the corrections to VMD calculated by Aviv et al.[41] The larger value of $\sigma_{tot}(\psi N)$ establishes even further the hadronic behavior of the ψ. Fig. 10 compares σ_{tot} vs s for ρ, ϕ, and ψ.[44] It is interesting to note that the threshold behavior of $\sigma_{tot}(\psi N)$ is known in more detail than the others.

2. Relation to Charmed Particle Production. We can use these data to draw some conclusions about photoproduction of charmed particles. If we assume that $\rho \rightarrow 0$ at high energy, we can calculate

$$\frac{\sigma_{elastic}(\psi N)}{\sigma_{tot}(\psi N)} = \frac{1}{b\lambda}\left[\frac{\alpha M_\psi}{3\Gamma_{\psi \rightarrow e^+e^-}}\frac{e^{bt_{min}}}{16\pi}\frac{d\sigma}{dt}(\psi N \rightarrow \psi N)\Big|_{t_{min}}\right]^{\frac{1}{2}} \approx (4.5 \pm 1.4)\% .$$

This is somewhat smaller than the elastic production of other hadrons at high energy, which tends to fall in the range of 10-20%.

Further, at photon energies of 20 GeV, the inelastic cross section for ψ production is less than 20-30% of the elastic ψ production cross section. We can therefore conclude that the bulk of the inelastic cross section does not

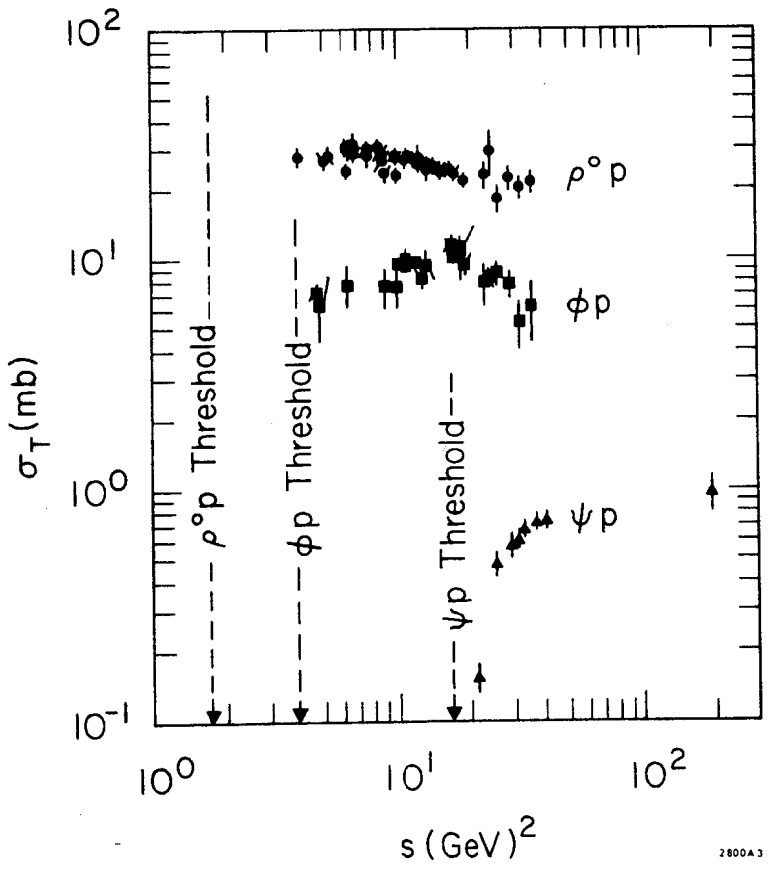

Fig. 10--The s-dependence of the total vector meson-nucleon cross sections. (Ref. 44.)

involve the ψ.[40] However, the $c,\bar{c}$ quarks carried by the ψ must appear in the final state, and they presumably do so in combination with uncharmed quarks. We may therefore conclude that

$$\sigma_{tot}(\psi N) \approx \sigma(\psi N \to D\bar{D} + X)\,!$$

Here $D,\bar{D}$ mean any state of nonzero charm. This conclusion is made even more tantalizing by the mysterious threshold behavior of $\frac{d\sigma}{dt}(\gamma p \to \psi p)$, which is shown in Fig. 11, since, for a D mass of 1.86 GeV, $D\bar{D}$ threshold in photoproduction is at $E_\gamma = 12$ GeV.

We can pursue this course a little further, noting that in the context of (corrected) VMD we can write

$$\sigma(\gamma p \to D\bar{D} + X) \approx \frac{\sigma_{tot}(\psi N)}{\sigma_{elastic}(\psi N)}\,\sigma(\gamma p \to \psi p) \approx \lambda \times 500\ \text{nb} \approx 150\ \text{nb},$$

whereas $\sigma_{tot}(\gamma p) = 120\ \mu$b for $E_\gamma > 20$ GeV. This conclusion is compatible with the observation at FNAL of a charmed baryon[25] (to be discussed below)(see also W. Y. Lee, these Proceedings), but is at odds with another result of the SLAC-Wisconsin experiments.

2.1 Experimental Information on Photoproduction of Charm. Fig. 12 shows the single arm inclusive muon yield at $E_\gamma = 8$, 12, and 20 GeV in the second experiment.[45] The extrapolation to zero decay path to remove the effect of normal hadronic decays results in an excess muon signal only at $E_\gamma =$ 20 GeV. With $\langle p_\perp \rangle = 1$ GeV, the ratio $\mu/\pi = 1.4 \times 10^{-4}$. This implies, if D mesons are the source of the muons, that

$$\sigma(\gamma p \to D\bar{D} + X) \times BR(D \to \mu) \approx 2\ \text{nb}.$$

However, if the branching ratio is taken to be 10%, then our previously derived result of 150 nb for D photoproduction implies a $\sigma \times$ BR of $\approx$ 15 nb. These two results are incompatible, but uncertainties in muon acceptance calculations due to unknown production mechanisms, coupled with unknown leptonic decay rates,

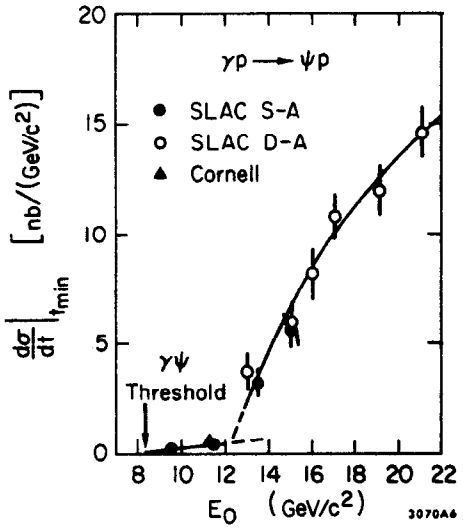

Fig. 11--The threshold behavior of the ψ photoproduction cross section.

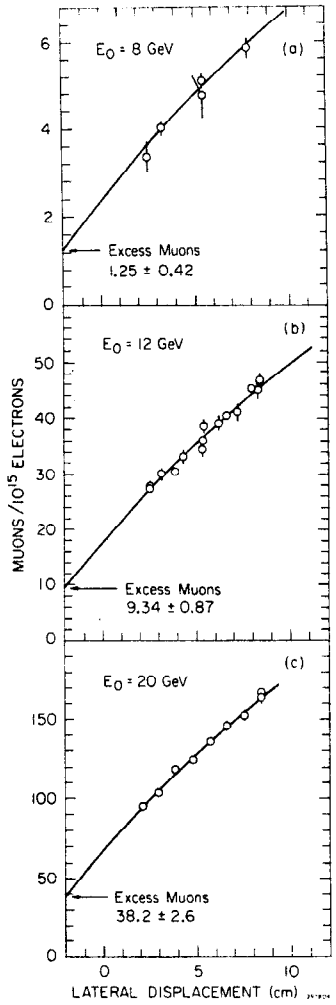

Fig. 12--Single arm inclusive muon yields in the SLAC-Wisconsin photoproduction experiment (Ref. 45).

are most likely responsible for the discrepancy.

Let us now turn to the very (photo)productive Columbia-Illinois-Hawaii-Fermilab (CIHF) experiment. Their most exciting result, of course, is the identification of a probable charmed (anti) baryon). Before briefly describing that result, however, there are several others from this experiment which have bearing on the question of new particle production. The first is a limit:[46]

$$\sigma(\gamma + \mathrm{Be} \to D\bar{D} + X) \leq 5 \text{ nb} .$$
$$\hookrightarrow K_S^0\pi$$

From the recent SPEAR result, $\mathrm{BR}(D^0 \to K\pi) \simeq 2\text{-}3\%$, we can conclude that

$$\sigma(\gamma + \mathrm{Be} \to D\bar{D} + X) \leq 150 - 250 \text{ nb} ,$$

which is consistent with our earlier conclusion.

The second is an enhancement in the dimuon spectrum[47] at $m_{\mu\mu} = 4.7$ GeV in the reaction

$$\gamma + \mathrm{Be} \to (4.7) + X \quad .$$
$$\hookrightarrow \mu^+\mu^-$$

The enhancement above the Bethe-Heitler background is statistically significant, but $\sigma \times \mathrm{BR}$ is small:

$$\frac{\sigma \times \mathrm{BR}(4.7 \to \mu\mu)}{\sigma \times \mathrm{BR}(\psi \to \mu\mu)} = .015 .$$

The third result is a preliminary one derived from a study of two track events with an identified μ and e.[48] There are two μe events with $M_{\mu e} > 1.1$ GeV, which, if real, imply a $\sigma \times (\mathrm{BR})^2 \times$ acceptance $= 4 \times 10^{-2}$ nb. This, it should be noted, is not likely to be relevant to the SPEAR μe events, but it could very well be the result of two leptonic decays of charmed particles.

There is now good evidence of photoproduction of charm, in this case a charmed baryon. The CIHF collaboration has observed a resonance decaying to $\bar{\Lambda}\pi^+\pi^-\pi^-$ in photoproduction. This is very likely the $\bar{\Lambda}_c$, the lowest mass charmed baryon and the only one to decay weakly. If the invariant mass of the $\bar{\Lambda}_c$ and an additional charged π are plotted, there is also evidence for an enhancement near 2.5 GeV, which is probably either the Σ_c or Σ_c^*. The close agreement of these masses with those observed in the Brookhaven neutrino event tends to confirm the conclusion that the 2.244 and 2.426 GeV mass combinations in that picture were indeed charmed states.

At this writing, the production cross section of the $\bar{\Lambda}_c$ has not been determined. For more details on the $\bar{\Lambda}_c$, see the lecture of W. Y. Lee in these Proceedings.

III. HADRONIC PRODUCTION OF NEW PARTICLES

In this section we will review the characteristics of ψ/J and ψ' production by hadrons and the implications of these data for the possibility of observing charmed particle production in hadronic reactions.

The inclusive cross section for ψ/J production by protons is shown in Fig. 13. It is seen to rise very rapidly with $\sqrt{s}$, so rapidly, in fact, that the simplest parton model ideas fail to reproduce the s dependence. The data of Fig. 13 are taken in different kinematic regions and with different targets.[49] In order to place them on a single graph, it is necessary to know the x, $p_\perp$, and A dependence of ψ/J production. The A dependence has been measured by the CIHF experiment[50] in a neutron beam at $\sqrt{s} = 24$ GeV, and found to be $A^{0.93\pm0.04}$, compared to that for $\rho+\omega$ production measured, in the same experiment, as $A^{0.62\pm0.03}$. Data on ψ/J production by pions are shown in Fig. 14.

The $p_\perp$ dependence of ψ/J production has been measured over a wide range of $\sqrt{s}$ and $p_\perp$, using both proton and π beams. These results are summarized in Table I. That the $p_\perp$ dependence is much more gradual than for other hadronic reactions is well established. It has also been shown by the CFSB group[51] that the x dependence of ψ/J production is flat for $\pm$ 0.06 about x = 0. More detailed information on the x dependence of ψ/J production by p and $\pi^\pm$

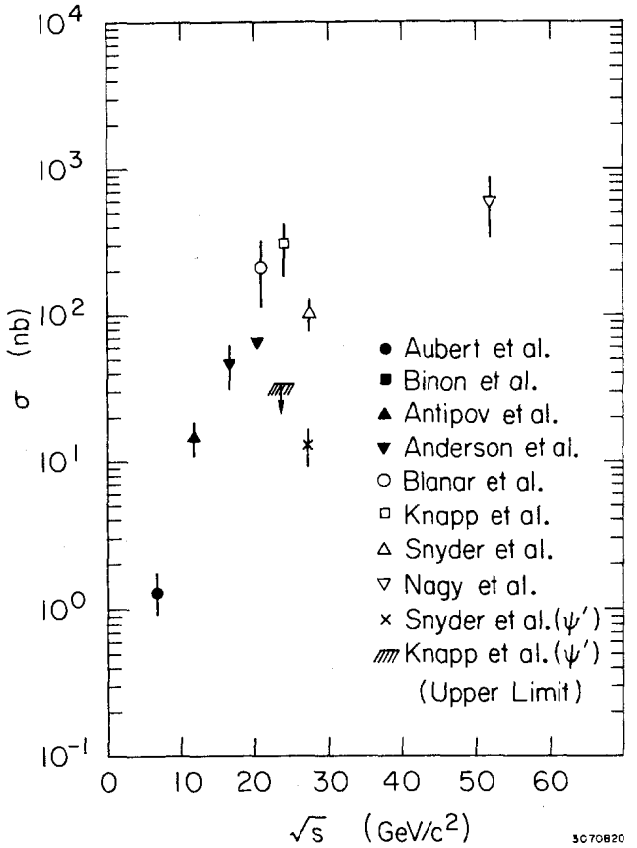

Fig. 13--s-dependence of the total cross section for ψ/J, ψ' production by protons and neutrons.

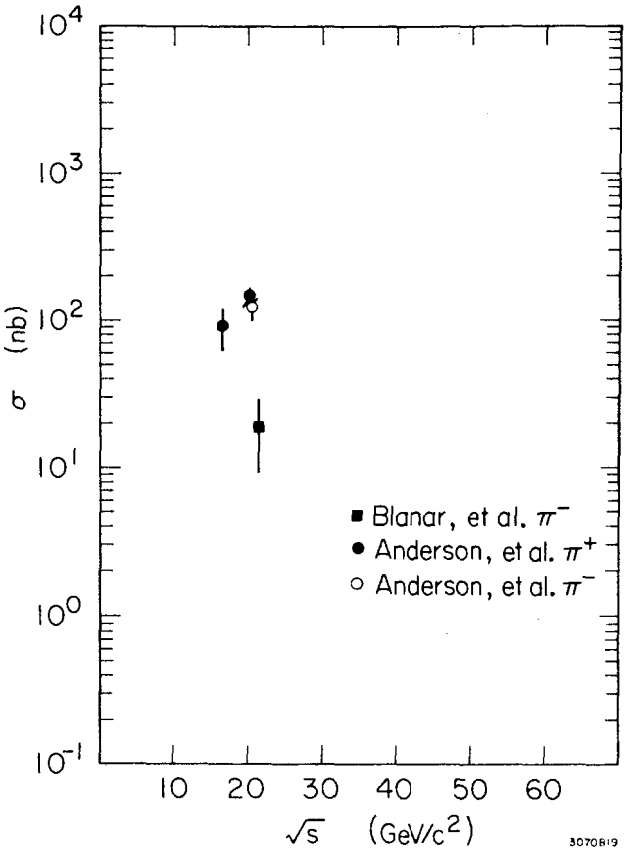

Fig. 14--s-dependence of the total cross section for ψ/J production by pions.

TABLE I

$p_\perp$ dependence of ψ/J production in p, n, and π interactions

exp	$\sqrt{s}$	$p_\perp$ range	$e^{-ap_\perp}$	$e^{-bp_\perp^2}$
p				
BNL-MIT	7.3	0 - 1.2		1.6
CP	16.8	0 - 2	1.97	
	20.5	0 - 2.5	1.97 ± .08	0.80 ± 0.06
NE	21.2	0 - 2	2.2 ± 0.5	1.1 ± 0.3
CIHF (n)	23.8	0 - 3	1.6 ± 0.2	excluded
CFSB	27.4	0 - 2	1.6 ± 0.35	1.1 ± 0.35
π				
CP (+)	16.8	0 - 2	1.7	
CP (+)	20.5	0 - 2.5	2.03 ± .15	0.88 ± 0.12
(-)	20.5	0 - 2.5	1.58 ± .13	0.59 ± .06
NE (-)	19.4	0 - 2	1.6 ± 0.2	0.81 ± 0.14

has recently been presented by the Chicago-Princeton[52] experiment.

The decay angular distribution has also been measured by the CFSB group, and appears to fit $1 + \cos^2\theta$ somewhat better than an isotropic decay. The Chicago-Princeton experiment, however, finds significant deviations from isotropy only in ψ/J production by protons on tin.

ψ' production has now been observed by the CFSB,[51] CIHF,[53] and Chicago-Princeton groups.[52] These data are also shown in Fig. 13.

1. Models of ψ/J Production by Hadrons and the OZI Rule. A successful model for ψ/J and ψ' production should presumably explain the s dependence of the cross section, the large $\langle p_\perp \rangle$, the ratio of cross sections for production by protons and pions, the operation of the OZI rule, and the fact that ψ' production is suppressed relative to ψ/J production. A further useful feature would be any predictions concerning the relation of ψ/J cross sections to charmed particle production cross sections.

1.1 Quark Fusion. One interesting approach to a model is the idea of $q\bar{q}$ fusion of Sivers,[54] Gunion,[55] Donnachie and Landshoff,[56] etc. In this model, to the extent the ψ/J consists of a $c\bar{c}$ pair, the hadronic production of ψ's alone is forbidden by the OZI rule, since the c quark content of the nucleon is presumably small (see Fig. 15a). In this model, the cross section for inclusive ψ/J production is given by

$$\sigma(pp \to \psi + \ldots) = \frac{8\pi^2}{3M_\psi^2} \sum_i \frac{g_{\psi i}^2}{4\pi} \tau \int_\tau^1 \frac{dx}{x} \left[f_i(x) \bar{f}_i\left(\frac{\tau}{x}\right) + f_i\left(\frac{\tau}{x}\right) \bar{f}_i(x) \right] ,$$

where

$$\tau = \frac{M_\psi^2}{s - s_{\text{threshold}}} .$$

The u,d quark distributions $f_i(x)$ are then obtained from the fits of Farrar[57] or Chu and Gunion.[58] The coupling is estimated by Sivers[54] to be

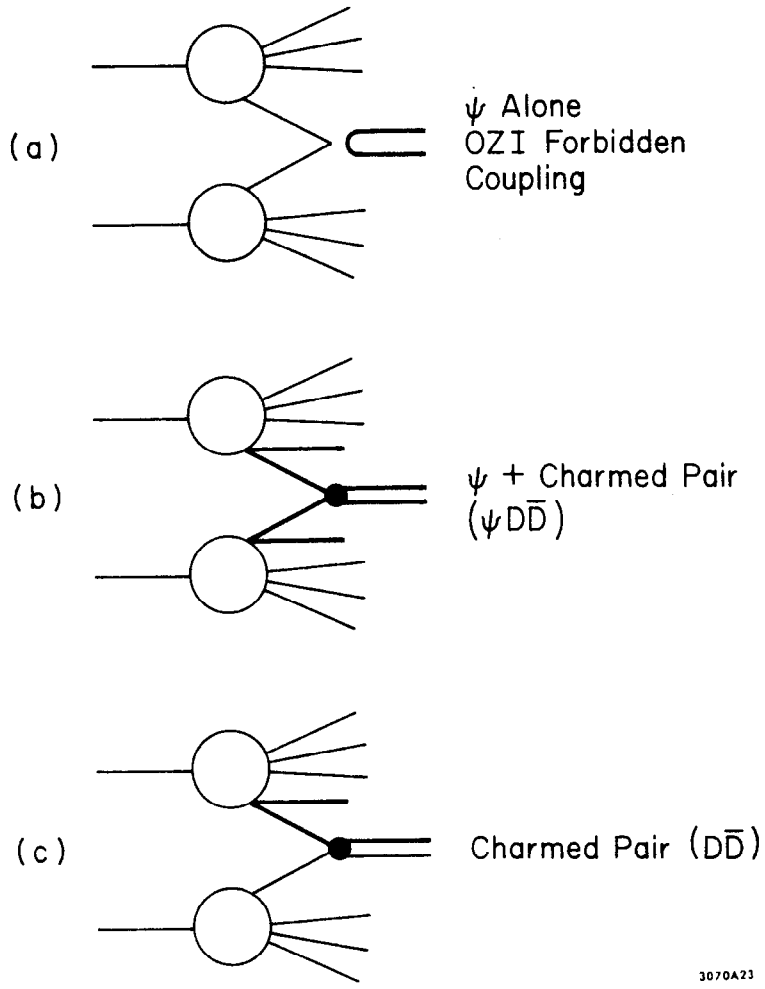

Fig. 15--Quark fusion diagrams for hadronic production of (a) the ψ/J alone, (b) ψ/J in conjunction with charmed particles, and (c) charmed particle pairs.

$$\frac{g^2_{u\bar{u}}}{4\pi} = \frac{g^2_{d\bar{d}}}{4\pi} = \frac{1}{2} R_{\psi} \frac{g^2_{\psi}}{4\pi} \frac{e^+e^-}{} \approx 1.3 \times 10^{-5} .$$

Alternatively, one can fit the cross section to low energy data. One finds, however, that the s dependence of this mechanism does not rise fast enough, failing by nearly an order of magnitude at $\sqrt{s} = 20$.

In order to boost the cross section, appeal is made to production from c quarks in the sea. Presumably, $g^2_{c\bar{c}}/4\pi$ is of order one. An estimate of the $f_c(x)$ can be made by analogy with strange quark distributions:

$$f_c(x) \simeq f_{\bar{c}}(x) \simeq \epsilon f_s(x) \simeq \epsilon \times 0.2 \times \frac{(1-x)^7}{x} .$$

Sivers obtains $\epsilon = .2$ for $g^2_{c\bar{c}}/4\pi = .5$. This mechanism then implies that $\sigma(pp \to \psi D\bar{D})$ is greater than $\sigma(pp \to \psi + X)$(Fig. 15b) and, further, that charmed particle production alone (Fig. 15c) will be larger than joint production with ψ/J: $\sigma(pp \to D\bar{D}X) > \sigma(pp \to \psi D\bar{D})$, since

$$\sigma(pp \to D\bar{D}X) \simeq \frac{4\pi^2}{3M_D^2} \frac{\bar{g}^2}{4\pi} \tau \int_{\tau}^{1} \frac{dx}{x} \sum_i \left[f_c(x) \bar{f}_i\left(\frac{\tau}{x}\right) + \bar{f}_c(x) f_i\left(\frac{\tau}{x}\right) + f_c\left(\frac{\tau}{x}\right) \bar{f}_i(x) + \bar{f}_c\left(\frac{\tau}{x}\right) f_i(x) \right].$$

1.2 Experimental Evidence for the OZI Rule. In this model, Sivers, for example, is able to obtain a reasonable fit to ψ/J inclusive production. A consequence of the model, however, is that inclusive $D\bar{D}$ production is predicted to be about $10^2 \times$ inclusive ψ/J production. Recent emulsion experiments call this prediction into question. This will be discussed further below. An interesting laboratory for testing these ideas is provided by hadronic ϕ production.[54] To the extent that the ϕ is composed of $s\bar{s}$ quarks, we can study the sea quark mechanism by comparing $\sigma(pp \to \phi$ alone) with $\sigma(pp \to \phi K\bar{K})$ and $\sigma(pp \to$ strangeness). The analogy is inexact, however, since OZI suppression is expected to be less stringent for ϕ's due to ϕ-ω mixing and the possible effect of intermediate states with a real $K\bar{K}$. Further, threshold effects in s are bound to

enter differently. With this in mind, we can briefly look at the experimental evidence in ϕ production. There are three relevant experiments. First, Blobel et al.[59] have investigated inclusive ϕ production by protons at $\sqrt{s} = 6.8$, measuring $\sigma(pp \to \phi + x) = 158 \pm 35\ \mu b$, and finding no strange particle enhancement in association with the ϕ. The Omega collaboration[60] has measured ϕ production in $\pi^- p$ at $\sqrt{s} = 6$, finding

$$\frac{\sigma(\pi^- p \to \phi K^+ K^- \pi^- p)}{\sigma(\pi^- p \to \rho^0 K^+ K^- \pi^- p)} = 0.45^{+0.25}_{-0.15},$$

so that the two Zweig-allowed processes are comparable.

The third experiment, by Donald et al.,[61] in $\bar{p}p$ at 3.6 GeV/c, does provide some support for the operation of the OZI rule. To the extent that the ϕ is $s\bar{s}$, the OZI rule predicts an enhancement of ϕ production in $\bar{p}p \to K^+K^-K^+K^-$:

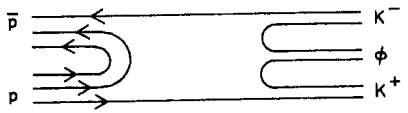

but no ϕ production in $\bar{p}p \to K^+K^-\pi^+\pi^-$. This statement is, of course, weakened by ϕ-ω mixing. Donald et al. find 12 of 16 $\bar{p}p \to K^+K^-K^+K^-$ events are in fact ϕK^+K^-, and that after cuts to remove $K^*(890)$ and ρ^0:

$$\frac{\sigma(\bar{p}p \to \phi\pi\pi)}{\sigma(\bar{p}p \to \omega^0\pi\pi)} = 0.009^{+0.004}_{-0.007},$$

in agreement with the mixing prediction. It should be noted, however, that $\bar{p}p$ experiments at lower momenta do not show significant enhancements of this type. Thus, while there is some evidence for the operation of the OZI rule in hadronic production, it is far from overwhelming.

Returning to the ψ,D production case, Fig. 16 shows the result of Sivers' calculations for ψ production in pp collisions.[54] While the sum of ψ alone and $\psi D\bar{D}$ cross sections provides a good fit to the data, the predicted cross section

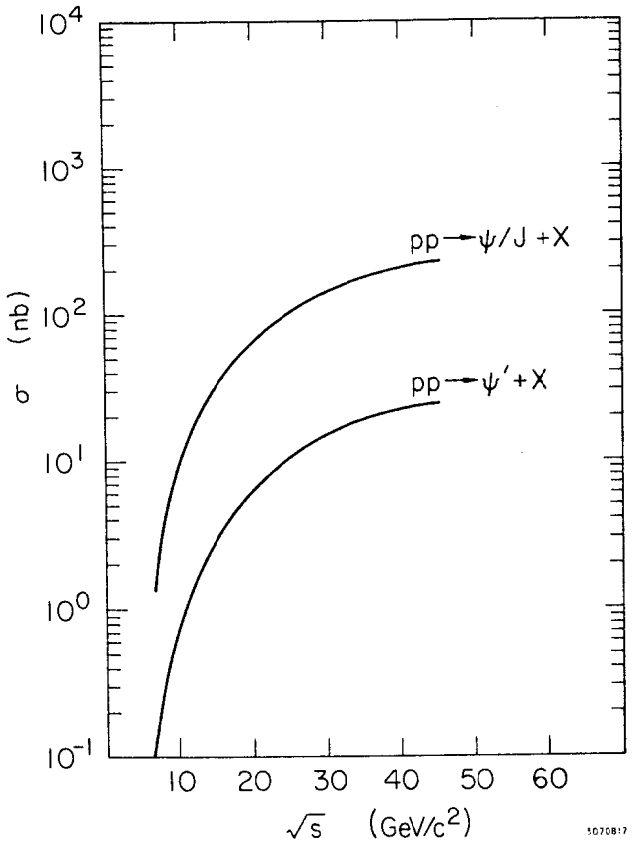

Fig. 16--Predictions of the quark fusion model of Sivers (Ref. 54) for the s-dependence of production by protons of the ψ/J alone, ψ/J in conjunction with charmed particles, and charmed particle pairs.

for inclusive D production is greater than 10 μb. This large a D production cross section would appear to be ruled out by a recent University College, London, emulsion exposure[62] to 300 GeV/c protons in which short tracks emerging from stars with lifetimes $\geq 10^{-14}$ seconds were searched for and not seen to level of less than 1 μb.

Another piece of experimental evidence which bears on the choice of production models comes from the neutron beam part of the CIHF experiment.[63] Events of the type $n + W \to \psi/J \;(\to \mu^+\mu^-) + X + \ldots \;(\to \mu^\pm)$ can, if π or K decay is ruled out as a source of the third muon, be indicative of the semileptonic decay of a charmed particle produced in association with the ψ/J. Two events of this type, which are consistent with π,K decay, were seen, so that a limit at 90% confidence level of

$$\frac{2\sigma(nW \to \psi D\bar{D})\ BR\ (D \to \mu + X)}{\sigma(nW \to \psi)} < 0.006$$

can be set for $x_F > 0.25$. If the semileptonic branching ratio is taken to be .1, we then have

$$\frac{\sigma(nW \to \psi D\bar{D})}{\sigma(nW \to \psi)} < .03,$$

which contradicts the quark fusion model.

1.3 Associated Production. At low energies, associated production of strange particles has a large cross section. For example, at $\sqrt{s} = 5$, $\sigma(\pi^- p \to K^o \Lambda^o) = 10\ \mu$b. By analogy, it should be possible to calculate the associated production of charm, in reactions such as $\pi^- p \to D^- \Lambda_c^+$ or $\pi^+ p \to \bar{D}^o \Sigma_c^{++}$. This has been done by Barger and Phillips[64] in a Regge model. They write

$$\frac{\frac{d\sigma}{dt}(\text{associated charm})}{\frac{d\sigma}{dt}(\text{associated strangeness})} = \left[\frac{\Gamma(1-\alpha_{D^*}(t))}{\Gamma(1-\alpha_{K^*}(t))}\right]^2 (\alpha' s)^{-2(\alpha_{K^*}(t)-\alpha_{D^*}(t))}.$$

The K* trajectory is well known:

$$\alpha_{K^*}(t) = 1 + .9(t-m^2_{K^*}) = .3 + .9t\ ,$$

but the D* trajectory

$$\alpha_{D^*}(t) = 1 + \alpha'_{D^*}(t-m^2_{D^*})$$

is, of course, not known. With different estimates of this trajectory, Barger and Phillips predict a rather small cross section for associated production, e.g., $\sigma(\pi^- p \to D^- \Lambda_c^+)$ is about 1 nb at $\sqrt{s} = 5$, falling to .01 nb at $\sqrt{s} = 20$.

1.4 Psi Production via Gluons. A third approach to hadronic production of ψ/J postulates that it is not directly produced in hadronic collisions, but rather results from the decay of C = +1 χ states which are more readily produced by the gluon component of the hadronic wave function.[65] In the charmonium model, the C = -1 ψ/J is produced by a three gluon coupling, while the $^3P\,\chi$ is produced by a two gluon mechanism:

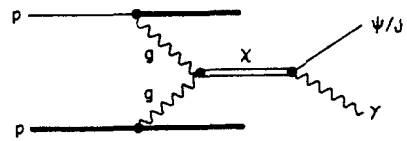

Since $\alpha_g \approx 0.2$, χ production should dominate ψ/J production. The cross section is then given by

$$\sigma = \sum_n \frac{8\pi^2}{M_n^3 P} \sum_J \sum_a \frac{\Gamma(n^3P_J \to gg)\Gamma(n^3P_J \to \psi + a)}{\Gamma_{tot}(n^3P_J)} \times \tau \int_\tau^1 \frac{dx}{x} f_g(x) f_g\left(\frac{\tau}{x}\right),$$

where the gluon x distribution is

$$f_g(x) = \frac{n+1}{16}\frac{1}{x}(1-x)^n\ .$$

The only n's which contribute to the sum must be those below charm threshold, or else $\Gamma(n^3P_J \to gg) \ll \Gamma_{total}(n^3P_J)$, since $n^3P_J \to gg$ violates the

OZI rule and is therefore assumed to be suppressed. The predominant χ decay is to $\psi/J + \gamma$ (or ω), since $\chi \to \psi + \pi$ is forbidden by isospin, $\chi \to \psi + 2\pi$ is forbidden by G parity and $\chi \to \psi$ + anything else is energetically forbidden.

This model can provide a good fit to the s dependence of ψ/J production, as shown in Fig. 17. It also explains several features of the reaction and makes other definite predictions. Since the ψ/J results from the decay of another state, the remarkable signal/noise ratio ($\sim$ 200 at BNL) can be understood. In a typical charmonium potential n = 3 lies at about 3.9 GeV. Thus only this level can feed the ψ', and the result is that ψ' production is small. Similarly, the hadronic production of ψ'', etc., states should be very small. In this context, the T(6 GeV) is not a bound state of standard SU(4) quarks. No joint production of ψ/J and charmed particles is predicted. Finally, some definite predictions about π and K production of ψ/J by this mechanism are possible.[66] For example, since the gluon distribution with $\pi^{\pm}$ are identical, one expects $d\sigma(\pi^+ T \to \chi + \ldots) = d\sigma(\pi^- T \to \chi + \ldots)$, for a target T of arbitrary isospin, whereas, since the $q\bar{q}$ annihilation mechanism is sensitive to valence quarks: $d\sigma(\pi^+ p \to \chi + \ldots) \leq \frac{1}{2} d\sigma(\pi^- p \to \chi + \ldots)$. Similar relations also hold for production by $K^{\pm}$. If the gluon distribution is SU(3) symmetric, then K and π production of χ should be equal. Finally, at x = 1, $f_g^N(x) \sim (1-x)^5$, whereas $f_g^{\pi}(x) \sim (1-x)^3$. If the fractional gluon momentum is $\sim$ 50% for π as well as N, then,at high energies, one expects

$$\frac{d\sigma}{dx_L}(\pi N) \approx \frac{d\sigma}{dx_L}(NN) \text{ at } x_L = 0, \text{ but}$$

$$\frac{d\sigma}{dx_L}(\pi N) \approx 6\,\frac{d\sigma}{dx_L}(NN) \text{ at } x_L = .6.$$

The recent Chicago-Princeton results lend some support to this picture.[67]

We end this section by noting an interesting scaling relation found by Gaisser, Halzen, and Paschos.[68] They write

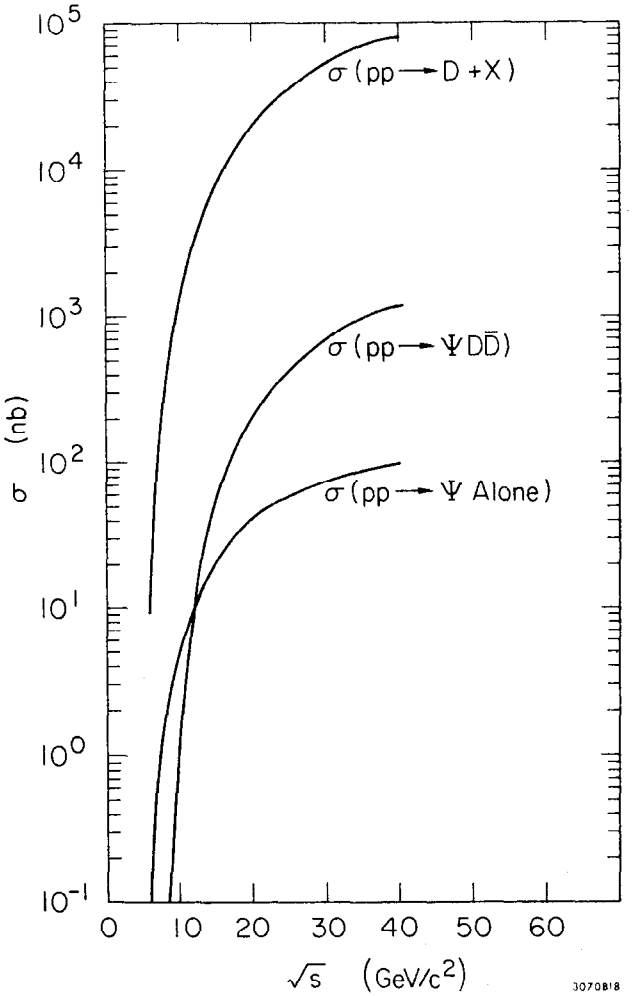

Fig. 17--Predictions of the gluon production mechanism for ψ/J of Carlson and Suaya (Ref. 65) for the s-dependence of production by protons of the ψ/J and ψ'.

$$\sigma(pp \to V + x) \equiv \sigma_V = \frac{\Gamma_V}{M_V^3} F\left(\frac{s}{M_V^2}\right) ,$$

which is valid for Γ_V/M_V small. The notion is that $F\left(\frac{s}{M_V^2}\right)$ is a universal function which describes the manufacture of a mass M_V out of the available energy $\sqrt{s}$. Then all differences between the production of vector mesons are contained in their hadronic widths. Referring to Fig. 18, we see that ϕ, ψ, and ψ' production fall on a universal curve, but note that $\psi' \to \psi\pi\pi$ is excluded from $\Gamma_{\psi'}$. This relation "explains" the small ratio $\sigma_{\psi'}/\sigma_{\psi}$ without the χ production mechanism and allows one to predict intermediate boson production cross sections at higher energies.

2. Production of the Υ. A narrow resonance in the e^+e^- spectrum produced by 400 GeV protons on Be has been reported by the CFSB collaboration[69] at a mass of 5.97 ± 0.05 GeV. The enhancement consists of 12 events at this mass corresponding to $\sigma \cdot B = (5.2 \pm 2.0) \times 10^{-3}$ nb/nucleon. It is a very narrow resonance with a $\sigma \approx 70$ MeV. This structure has been given the name Υ. The definite establishment of the Υ awaits further data on the $\mu^+\mu^-$ spectrum and improved e^+e^- data with better resolution, both by the same group.

The SLAC/LBL collaboration has searched the 6 GeV region at SPEAR for signs of the Υ.[70] The search was done in 4 MeV steps with ~ 60 hadron events/point. No enhancement was seen. Limits on Υ production in e^+e^- depend on its width. The cross section for a resonance is given by

$$\sigma(e^+e^- \to f) = \frac{\pi(2J+1)}{s} \frac{\Gamma_{ee}\Gamma_f}{(\sqrt{s}-m)^2 + \frac{\Gamma^2}{4}} .$$

At $\sqrt{s} = 6$ GeV, the beam width is ~ 4 MeV. If the resonance is narrow compared to this, then integrating over the resonance determines $(2J+1)\Gamma_{ee}\Gamma_{hadrons}/\Gamma$, while, if the resonance is wide, one determines

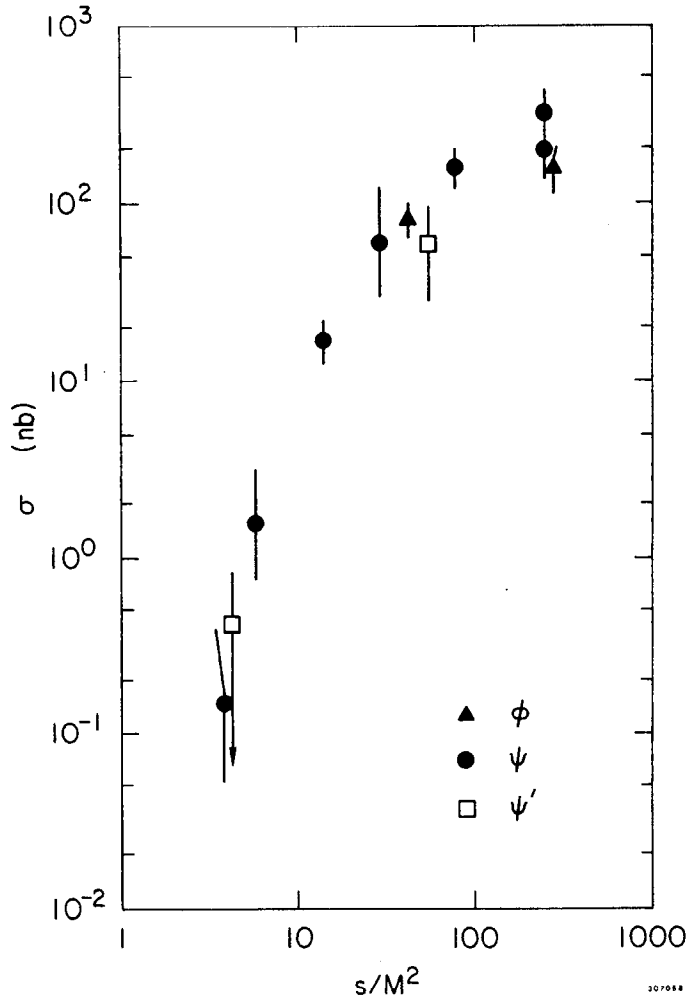

Fig. 18--The scaling relation for vector meson production. (Ref. 68.)

$(2J+1)\Gamma_{ee}\ \Gamma_{hadrons}/\Gamma^2$.

If J=1 is assumed, then the SPEAR search sets the following limits:

$$\text{for } \Gamma \ll 10 \text{ MeV}: \quad \frac{\Gamma_{ee}\Gamma_{hadrons}}{\Gamma} < 150 \text{ ev (90\% C.L.)}$$

$$10 \leq \Gamma \leq 50 \text{ MeV}: \quad \frac{\Gamma_{ee}\Gamma_{hadrons}}{\Gamma^2} < 1.5 \times 10^{-5}.$$

Since $\Gamma_{ee}/\Gamma \ll 1$ and $\Gamma_{hadrons}/\Gamma \simeq 1$, these are effectively limits on Γ_{ee} and Γ_{ee}/Γ, respectively. By comparison the known vector mesons have Γ_{ee} equal to several keV. These limits imply that the cross section for Υ production by protons is large. Since $(\sigma \cdot B_{ee})_\Upsilon = 5 \times 10^{-4} (\sigma \cdot B_{ee})_\psi$, we have $\sigma_\Upsilon \geq 3.5\ \sigma_\psi$. Two points which potentially weaken these conclusions should be made, however. First, it is known that Γ_{ee} of the $\psi(4.4)$ is only 440 eV, so small leptonic widths of vector mesons are not unprecedented. Second, were the Υ to have J = 0, the limits on production in e^+e^- would be a factor of three weaker, and, in addition, it is known that BR $(\eta \to \mu^+\mu^-) = 2.2 \times 10^{-5}$, so that a small leptonic width of a pseudoscalar meson might be expected.

3. Bump Hunting in Hadronic Reactions. As we have seen, the existence of a substantial body of experimental data on the hadronic production of the ψ/J has shed little light on the problem of charmed particle production by hadrons. Emulsion experiments, however, do constrain the total cross section for charm production to less than $\sim 1\ \mu b$. This leaves the hadronic bump hunter with a formidable task. As of this writing, no statistically significant mass peak has been seen in hadronic reactions.

Most such experiments have concentrated on two body final states.[71] In the conventional charm scheme the only such decay is $D^o \to K^-\pi^+$ at 1.86 GeV. Nonetheless, it is valuable to search in $\pi\pi$, πp, $\bar{p}p$ (a likely decay mode of the η_c) final states, and most experiments have done this. Three body final states include $D^+ \to K^-\pi^+\pi^+$, $K_s^o\pi^+$ at 1.87 GeV, $F^+ \to \pi^+\pi^+\pi^-$ (expected at $\sim$ 2 GeV), $D^{*+} \to D^o\pi^+ \to K^-\pi^+\pi^+$ at $\sim$ 2.02 GeV, and $\Lambda_c^+ \to \bar{K}^o p$, $\Lambda^o\pi$ at 2.25 GeV. If the total charm production cross section is taken as 1 μb and we use the SPEAR branching ratios for $D \to K\pi$, $K\pi\pi$ of 2-5%, the magnitude of the problem becomes clear: a likely σB of less than 20-50 nb. In typical FNAL two-body experiments performed so far, this corresponds to a peak of about 1% of background or less. The absence of 4σ peaks to this date is therefore not surprising.

There have been several bubble chamber experiments, which have looked for mass peaks in inclusive distributions and for evidence of associated production of charm.[72] These are far from having (what is now known to be) the required sensitivity. Counter experiments at BNL, CERN, and Fermilab have placed limits on σB which come closer to the needed sensitivity. For example, the MIT-BNL experiment[73] at $\sqrt{s} = 7.3$ places two-body limits on σB of as low as 1 nb at $M_{K\pi} = 2.25$ GeV. (No limits are quoted for the 1.8-2 GeV region.) If the s dependence of the charm production cross section is the same as that for ψ/J production, then this is still more than an order of magnitude above the expected σB. The Omega collaboration[74] has looked at two to five body final states in π^-p at $\sqrt{s} = 6$, setting limits as low as 35 nb at 95% confidence. These are summarized in Table II. At FNAL energies, there have been n, p, and π induced experiments.[75] As an example, the limits on σB placed by the MSU-OSU-Carleton collaboration in n+Be initiated final states are summarized in Fig. 19. A tantalizing peak in $M_{K^-\pi^+} = 1.86$ has been found in the Michigan-Purdue-Fermilab experiment,[76] but it is at the 3σ level and no corresponding peak is evident in $M_{K^+\pi^-}$ (see Fig. 20). This experiment differs from most others of this type in that it has its largest acceptance at x = 0.

Since the semileptonic branching ratios of charmed mesons are expected to

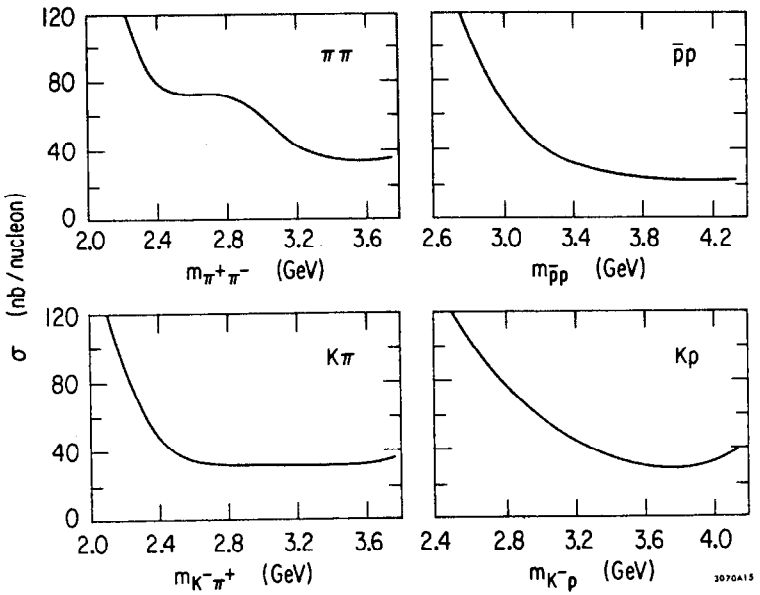

Fig. 19--Limits on hadronic production of two-body final states by 240 GeV/c neutrons (Abolins et al., Ref. 71).

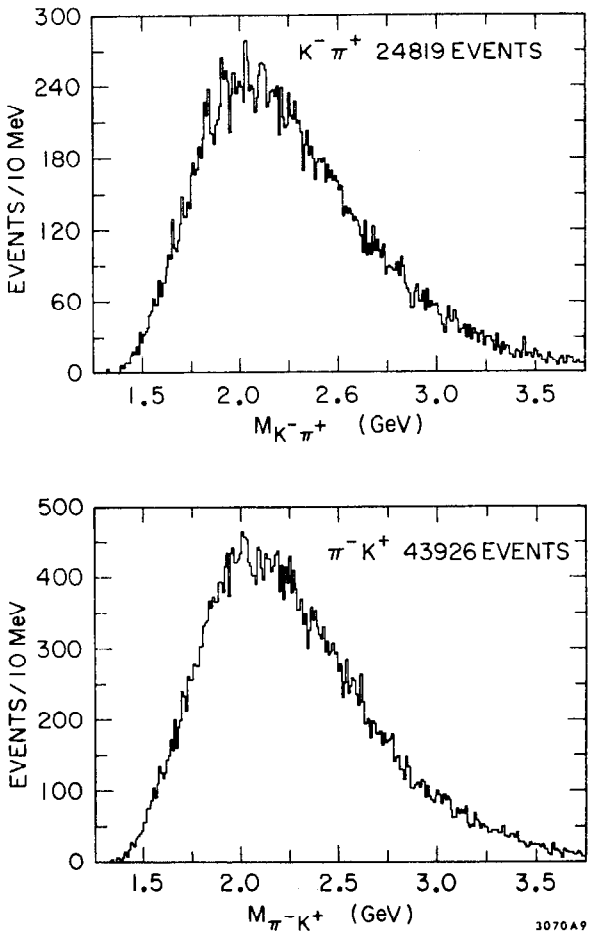

Fig. 20--$K^{\pm}\pi^{\mp}$ invariant mass spectra produced by 400 GeV/c protons (Bintinger et al., Ref. 71).

TABLE II

Limits on production of charmed hadrons in 19 GeV π^-p interactions (Ref. 74)

Charm reaction	Charm decays	Cross section upper limits (nb)		
		phase space	forward mesons	forward baryons
$\pi^-p \to D^-D^0p$	$D^- \to K^+\pi^-\pi^-; D^0 \to K^-\pi^+$	75	50	
$\pi^-p \to \bar{D}^0D^0\pi^-p$	$\bar{D}^0 \to K^+\pi^-; D^0 \to K^-\pi^+$	80	60	
$\pi^-p \to D^-C^+$	$D^- \to K^+\pi^-\pi^-; C^+ \to K^-p\pi^+$	65	80	200
$\pi^-p \to \bar{D}^0C^0$	$\bar{D}^0 \to K^+\pi^+\pi^-\pi^-; C^0 \to K^-p$	75	100	2000[a]
$\pi^-p \to \bar{D}^0C^0$	$\bar{D}^0 \to K^+\pi^-; C^0 \to K^-p\pi^+\pi^-$	65	1000[b]	55
$\pi^-p \to \bar{D}^0C^0$	$\bar{D}^0 \to K^+\pi^-; C^0 \to K^-p$	40	200	40
$\pi^-p \to D^-C^0\pi^+$	$D^- \to K^+\pi^-\pi^-; C^0 \to K^-p$	45	95	60
$\pi^-p \to \bar{D}^0C^+\pi^-$	$\bar{D}^0 \to K^+\pi^-; C^+ \to K^-p\pi^+$	55	120	60
$\pi^-p \to \bar{D}^0C^0\pi^+\pi^-$	$\bar{D}^0 \to K^+\pi^-; C^0 \to K^-p$	50	70	40

[a] 200 nb for $M_C + M_D > 4.0$ GeV for backward-produced mesons.

[b] 500 nb for $M_c > 2.3$ GeV and 300 nb for $M_c > 2.5$ GeV for backward-produced baryons.

be 15%, it is tempting to try to enrich a sample of hadronic events by requiring a coincident muon or electron. In practice the gain in sensitivity of such an experiment is limited by several factors. The improvement in trigger rate is held to $\sim 10^3$ by π decays, even at high energies, but even this is not realized, because a factor of 2 or 3 must usually be sacrificed in solid angle. The small semileptonic branching ratio and the fact that only one of the pair of D's produced is a candidate cost another factor of 20 or so. Such experiments thus can gain about 3-5 in sensitivity over untriggered experiments. This is sometimes realized in practice, and sometimes it is not.

As examples of this technique, we can cite the SLAC-Santa Cruz streamer chamber experiment[77] which used a 14 GeV π^+ beam on a polyethylene target and a μ trigger, setting limits in the 1-10 μb range on many different multihadron final states (up to five bodies). A similar experiment was performed in the FNAL streamer chamber by the SOD collaboration.[78] In this experiment, which utilized a 225 GeV π^- beam, enhancements in V^0's were searched for in coincidence with one and two high energy μ's. For $M_C = 3$ GeV, they set limits on $\sigma B_\mu^2 < 35$ nb. The MIT-BNL experiment[79] has searched for $K^-\pi^+\mu X$ final states in pBe reactions, seeing about 5 events per 12.5 MeV bin at 1.8-2.0 GeV. This allows them to set a limit on $\sigma B_\mu B_{K\pi} < .2$ nb, corresponding to a production cross section of the order of 100 nb. This experiment has also found that K^-e^+ coincidences in their double-arm spectrometer were 1% of π^-e^+ coincidences (note that this ratio is not $D \to Ke\nu/D \to \pi e\nu$), implying $\sigma_D B_e \leq 1$ nb. The idea of finding a charm signature by two semileptonic decays, resulting in μe coincidences, is currently being pursued in two experiments at the ISR.[80]

IV. DIRECT LEPTON PRODUCTION BY HADRONS

The subject of direct lepton production by hadrons has caused great excitement in recent years and has received many comprehensive reviews.[81] New data at low $p_\perp$, polarization measurements, and pair mass data, however, would seem to warrant a reexamination of the field and, in the context of these lectures, a discussion of the relevance of this phenomenon to the question of new particle production. For the sake of completeness, we will begin at the beginning, with some definitions, will summarize the available data, and will examine some attempts at an explanation of the phenomenon.

1. Definitions. "Direct leptons" are defined as those which are produced at or close to a production target but arise from "nontrivial sources". This far from clear definition must be made more specific by the enumeration of what is direct but trivial and direct yet nontrivial. The conventional classification of triviality is as follows:

Trivial: weak decays of π's, K's, hyperons.

Nontrivial: weak decays of charmed particles, heavy leptons, intermediate bosons.

Trivial: electromagnetic decays of ρ, ϕ, ω. Dalitz decays of π^o, η^o.

Nontrivial: electromagnetic decays of ψ/J, ψ', or new mesons (vector or otherwise).

Trivial: conversions of γ's from π^o.

Nontrivial: conversions of γ's from direct photon continuum.

It would seem that a more adequate definition for "trivial" would be "expected, as of mid-1974".

If the direct lepton is a muon, the background sources are π and K decay. The standard technique for measuring the background is the variation of the decay path before the muon filter and extrapolation to zero decay path. The sensitivity of this approach improves with beam energy and with transverse momentum, such that at FNAL energies and $p_\perp$ of 5 GeV/c or so μ/π ratios of 10^{-6} can be measured. Multiple scattering of the muons in the filter affects target reconstruction accuracy and can cause feeddown problems due to relatively poor $p_\perp$ resolution on a steeply falling spectrum.

If the direct lepton is an electron, the π and K backgrounds are less important than those arising from π^o or η^o Dalitz decays or conversion of photons from π^o decay in the target or surrounding material. This last background is removed by adding converter and extrapolating to zero length of conversion material. Dalitz decay backgrounds are dealt with by calculation. At low energies, electron detection is the more sensitive technique, the intrinsic sensitivity of the method not being a strong function of beam energy. If pairs can be detected, the sensitivity of the approach is extended still further.

2. Data. There is at present a great deal of data on direct lepton production. The kinematic regions covered by the measurements of the ℓ/π ratio are summarized in Figs. 21-23 for the ISR,[82-84] FNAL,[85-89] and lower energy machines,[90-94] respectively. Note that there are now data at low x extending from $p_\perp = .25$ GeV/c to 5.5 GeV/c and high x data at many energies. This extended range of data is quite important in arriving at a coherent explanation, as are the muon polarization measurements from Serpukhov[95] and Yale-FNAL[96,97] and the data on the pair origin of the single leptons from the Yale-FNAL[98] and Chicago-Princeton[99] experiments.

Before evaluating the contribution of trivial and nontrivial sources to the ℓ/π data, let us examine the s, $p_\perp$, and x dependence of the e/π and μ/π data. Figure 24 shows the s dependence of the μ/π ratio for data at $x \approx 0$ with $p_\perp >$ 1 GeV/c. The s dependence of the e/π ratio for $x \approx 0$ and $p_\perp > 1$ GeV/c is shown in Fig. 25. These μ/π and e/π data agree fairly well, both showing the threshold in $\sqrt{s}$ which would be characteristic of new particle production. The dominant contribution from the semileptonic decays of charmed mesons to the ℓ/π ratio should occur, as we shall see, just below $p_\perp = 1$ GeV/c. The new particle contributing the most to the ratio, especially beyond $p_\perp = 1.5$ GeV/c, is the ψ/J.

There is now a substantial amount of data at low $p_\perp$. The $p_\perp$ dependence of the e/π data is shown in Fig. 26. A vast range of center-of-mass energies is involved, from LASL energies up to $\sqrt{s} = 53$. No signal was seen at LASL, or in Winter's analysis of 19 GeV data. There does appear to be a signal at low s, low $p_\perp$, however, in the Penn-Stony Brook data. At high s, there is some discrepancy between the CHORMN data at 30° at the ISR and the revised CCRS data (at 90°). The background subtraction of the CCRS results has been changed, resulting in a decreasing e/π ratio with decreasing $p_\perp$, the original version[100] of these data fitted smoothly onto the CHORMN points. In the $p_\perp$ region in which

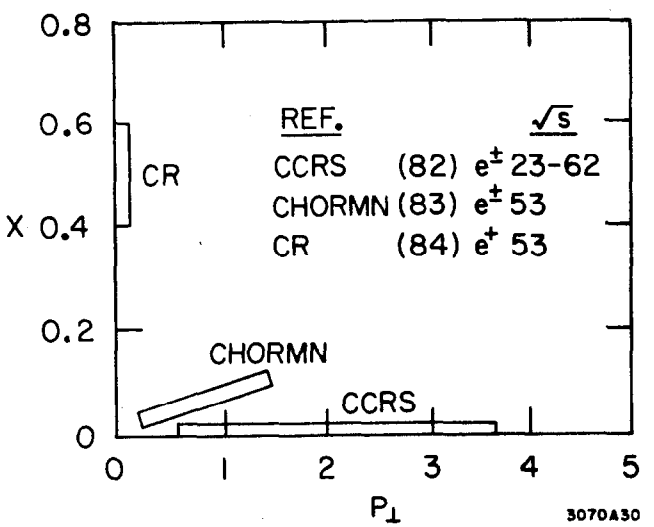

Fig. 21--ISR data on direct lepton production.

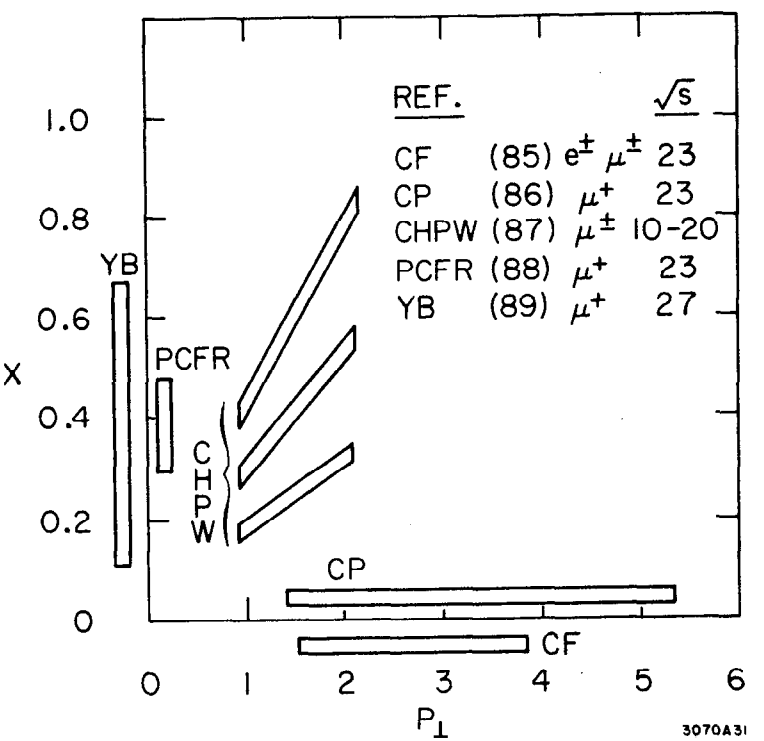

Fig. 22--Fermilab data on direct lepton production.

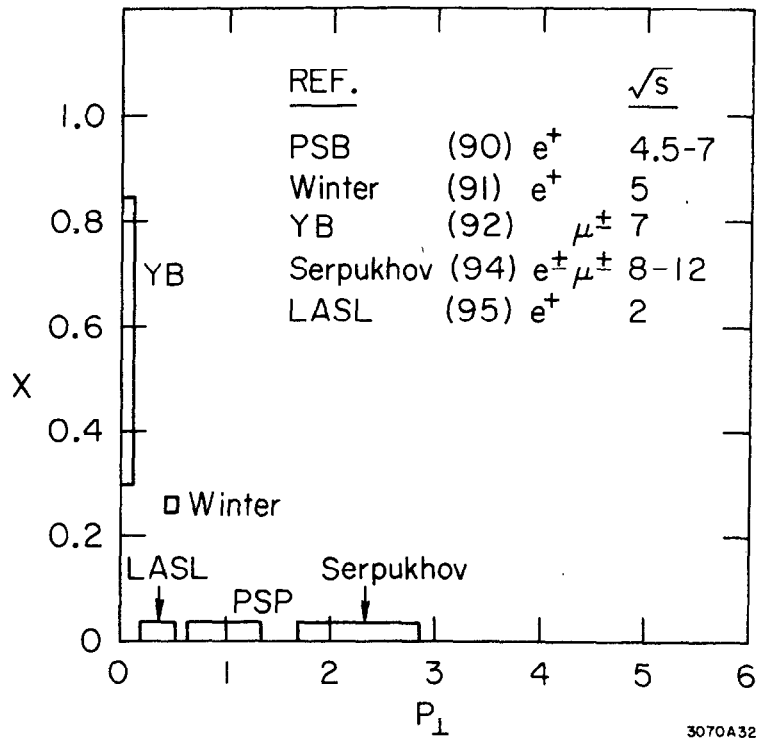

Fig. 23--Data on direct lepton production at machines below 30 GeV.

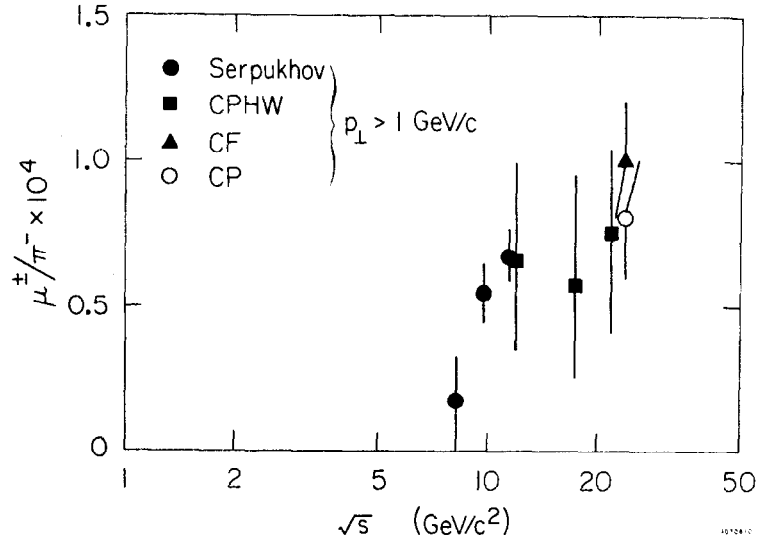

Fig. 24--s-dependence of the μ/π ratio for $p_\perp > 1$ GeV/c.

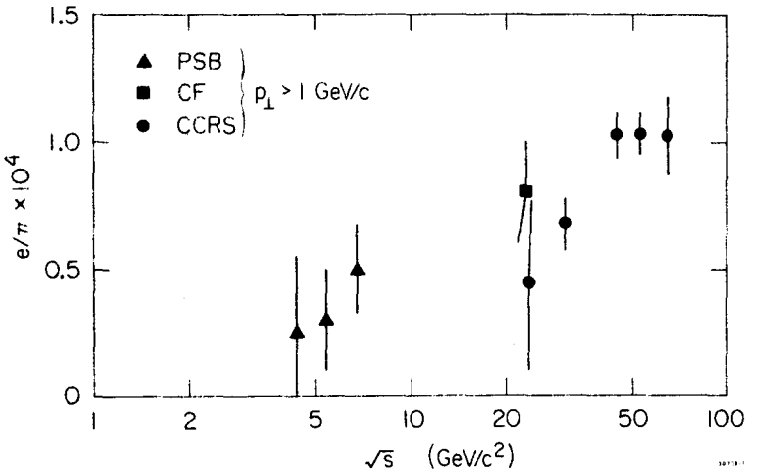

Fig. 25--s-dependence of the e/π ratio for $p_\perp$ > 1 GeV/c.

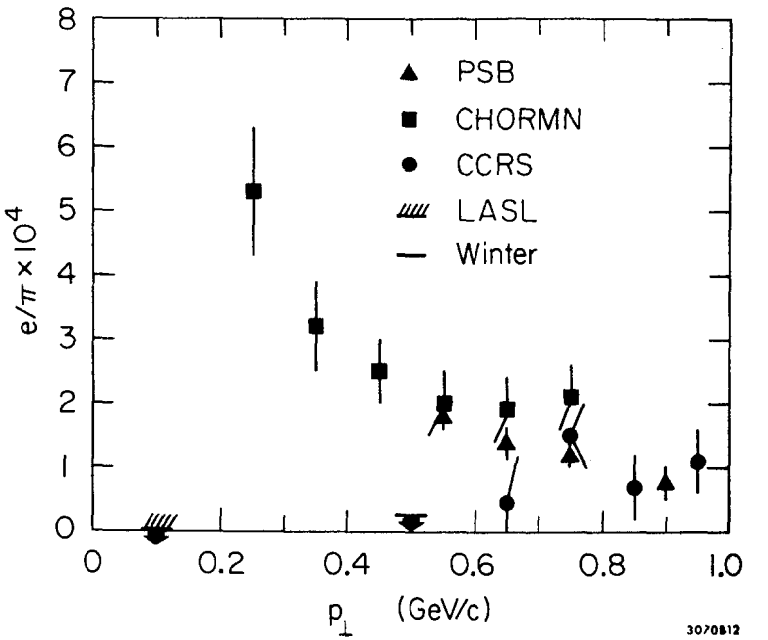

Fig. 26--$p_\perp$-dependence of the e/π ratio for $p_\perp$ < 1 GeV/c.

they overlap, the agreement of the CHORMN and PSB data is good.

The measurements of μ/π in the forward direction are shown in Fig. 27. The ratio falls off substantially as x_F approaches 1; this decrease will play an important part in any attempt at a global understanding of the ℓ/π data.

If the origin of the direct lepton signal is the weak decay of a charmed meson or heavy lepton, we would expect the muons to be longitudinally polarized. Since the purely leptonic decay of a pseudoscalar meson is inhibited by angular momentum considerations, semileptonic decay modes are expected to predominate so that V-A couplings produce a μ^+ with positive helicity. Despite the fact that a three body decay produces a yield of leptons which peaks at low $p_\perp$, for typical mass and meson production mechanisms, the ℓ/π ratio actually falls below 1 GeV/c, so that polarized muons are best sought somewhat above a $p_\perp$ of 1 GeV/c. One is faced in these experiments with the necessity to extrapolate the measured polarization to zero hadronic decay length. This has been done by a Yale-BNL group at FNAL[96,97] and in two experiments at Serpukhov,[95] which quote a joint result. The results are shown in Table III. The high energy

TABLE III

Longitudinal polarization of directly produced muons

Group	$\sqrt{s}$	$p_\perp$	p_μ	P
Yale-BNL	27	0 - 1	185	0.0 ± 0.10
	27	2.15	54	-0.15 ± 0.20
Serpukhov	12	2.0		
		2.8	21	-0.85 ± 0.36

results see no significant longitudinal polarization, while the Serpukhov experiments see a significant negative value. The Yale-BNL results are not strong evidence against the contribution of semileptonic decays of charmed particles to

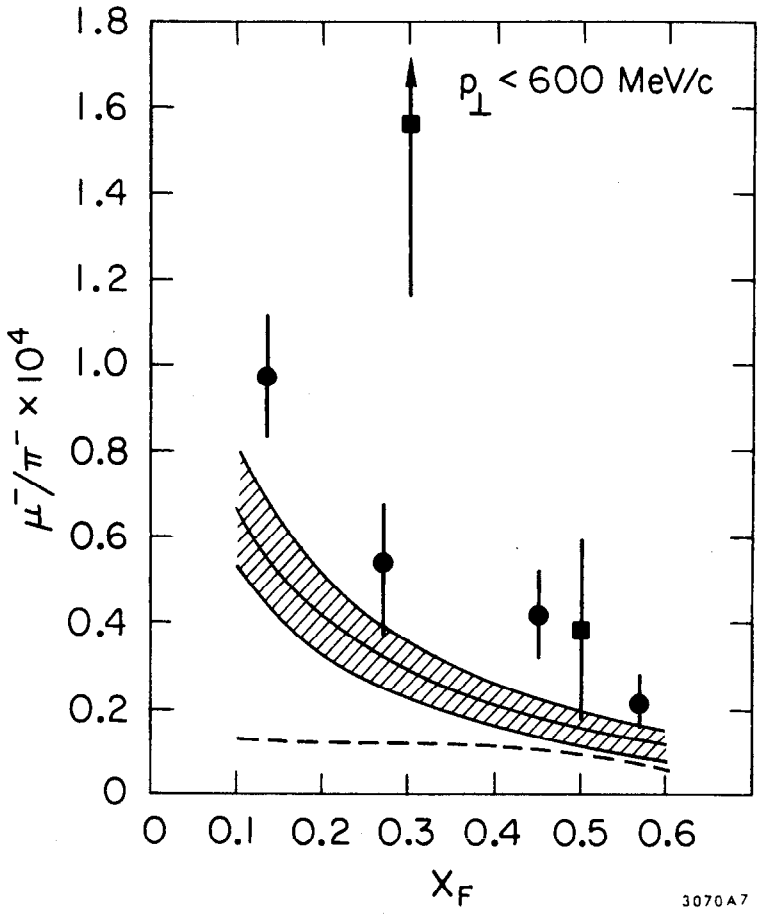

Fig. 27--Measurements of the μ/π ratio at high s as a function of Feynman x. Contribution of muon pairs to the ratio derived by Ref. 99 is shown superimposed.

the direct μ signal, as they bracket the region where the maximum contribution is expected. The Serpukhov result is difficult to interpret. No substantial contribution from charmed particles is expected at this $p_\perp$, even with V+A coupling. π and K decays can yield muons with negative polarization.

There are other features of the direct lepton signal, such as the strange A dependence of the phenomenon, the question of correlations, and the question of charge and lepton symmetry, which have been well summarized by Lederman[101] and will not be dealt with further here.

There have been many attempts to explain the direct lepton signal. It appears reasonably certain that as complex and wide ranging a phenomenon as this will be quantitatively understood in terms of many contributions. As we shall see, new particle production plays a role, but by "new particle" we can only with certainty mean the ψ/J; the contribution of charmed particles remains problematical. The new data at low $p_\perp$ and the large x data cannot be understood in terms of new particle production, but recent experiments on μ pair production may provide the answer here. Let us first find the size of the direct lepton signal due to known sources and then look at the characteristics of the remainder, considering possible sources.

3. Contributions to Direct Lepton Spectra

3.1 Vector Meson Contribution. It has long been clear that the leptonic decays of vector mesons make an important contribution to the direct lepton signal. New data have reinforced this contention and provided better values for cross sections and the $p_\perp$ dependence of production. Bourquin and Gaillard[102] have recently summarized these contributions in an empirical model of production in which the invariant cross section is given by

$$E\frac{d^3\sigma}{dp^3} = A\left(\frac{2}{E_\perp+2}\right)^{12.3} e^{-5.13/Y^{0.38}} \times \begin{cases} e^{-p_\perp}, & p_\perp < 1 \text{ GeV/c} \\ e^{-23(p_\perp - 1)/\sqrt{s}} e^{-1}, & p_\perp > 1 \text{ GeV/c} \end{cases}$$

with $p_\perp$ in GeV/c, $E_\perp = (m^2+p_\perp^2)^{\frac{1}{2}}$ in GeV/c^2, and

$$Y = \ell n\left(\frac{E_{max} + p_{L_{max}}}{E+p_L}\right) .$$

There appears to be reasonable evidence for the factorization assumption. In any case, at x = 0 this parametrization works well. The normalization constants A are chosen to fit available data. There is still some disagreement among ρ production cross sections; the suggestion of Bourquin and Gaillard that they could be reconciled by a $1+\cos^2\theta$ decay distribution has not been borne out by experiment. Nonetheless, their choice of $A_\rho = 5.5 \times 10^{-24}$ cm^2/GeV^2 is a decent fit to most data. Based on a single experiment at $\sqrt{s} = 5$ GeV, they choose $A_\omega = A_\rho$. ϕ production mechanisms, as we have seen, should involve the OZI mechanism, for which there is conflicting evidence. Weighing this evidence, Bourquin and Gaillard chose $A_\phi = .15\ A_\rho$, representing the operation of the OZI rule. In their model then, they, as a consequence, predict that, in central collisions at high energy, more than 50% of ϕ's produced should be accompanied by a $K\bar{K}$ pair. ψ/J production is similarly affected by the OZI mechanism, such that the appropriate normalization of the production of ψ/J alone is $A_{\psi/J} = .025\ A_\rho$. This gives a good fit to the data at low s, but is slightly too low at high s (ISR energies). This small discrepancy may be accounted for by the OZI allowed $\psi D\bar{D}$ production mechanism which we have also discussed above. One can set a limit on the $\psi D\bar{D}$ contribution by requiring agreement for $\langle p_\perp \rangle$ at $\sqrt{s} = 23$ and 53 GeV. This limits $\psi D\bar{D}$ to about 20% of ψ alone at $\sqrt{s} = 23$, but $\psi D\bar{D}$ can be a factor of 2 greater than ψ alone at higher s. In this model

$A_{\psi'} = A_{\psi/J}$ provides agreement with the Columbia-Fermilab data on ψ' production. Recently, Craigie and Schildknecht[103] have emphasized that the decays $\omega \to \pi^0 e^+ e^-$ and $\eta' \to \gamma e^+ e^-$ can make a significant contribution, although in the past this has been neglected with respect to the dominant $V^0 \to \ell^+ \ell^-$ decays.

Figure 28 shows the vector meson contributions to ℓ/π at x = 0, .3 and .5 at $\sqrt{s}$ = 23 in the Bourquin-Gaillard model. The x = 0 curves are compared to the Columbia-Fermilab and Chicago-Princeton data. The agreement for $2 \leq p_\perp \leq 4$ GeV/c is good, once the substantial contribution of the ψ/J is included. Below $p_\perp$ = 2 GeV/c, there is a discrepancy, which may be removed by the semi-leptonic charm decay contribution (see below).

The vector meson contributions at x = .3 and .5 do not account for the Yale-Brookhaven and CCFPR μ/π results shown. Models of the Bourquin-Gaillard type do not fit these data well. No substantial charmed meson contribution is, of course, expected at high x. Modifications of the production assumptions, for example relaxation of the factorization hypothesis, have been made by Hinchliffe and Llewellyn Smith,[33] but the agreement is still poor at high x. The continuum contribution at high x, shown in Figure 27, will be discussed below.

3.2 Charm Contribution. Can leptonic decays of charmed mesons account for the remaining excess at $p_\perp \lesssim 2$ GeV/c? The $p_\perp$ spectra lend some hope to this notion. The decay electron spectra of Fig. 4, for a D meson of mass 1.87 GeV, when folded with a representative D production spectrum, yield the $p_\perp$ distributions shown in Fig. 29 (from Hinchliffe and Llewellyn Smith). With the $D \to K^* e \nu$ spectrum of Yang and Ali,[34] using hard pion form factors and V-A or V+A coupling, it is possible to shift the peak from this decay contribution up or down slightly. The peaking of these distributions below $p_\perp$ = 1 GeV/c makes it very attractive to try to fit the CCRS and/or CHORMN data by adding semi-leptonic D decays to the vector meson contribution. This has been done by Bourquin and Gaillard, who considered $D \to Ke\nu$ decay only and by Hinchliffe

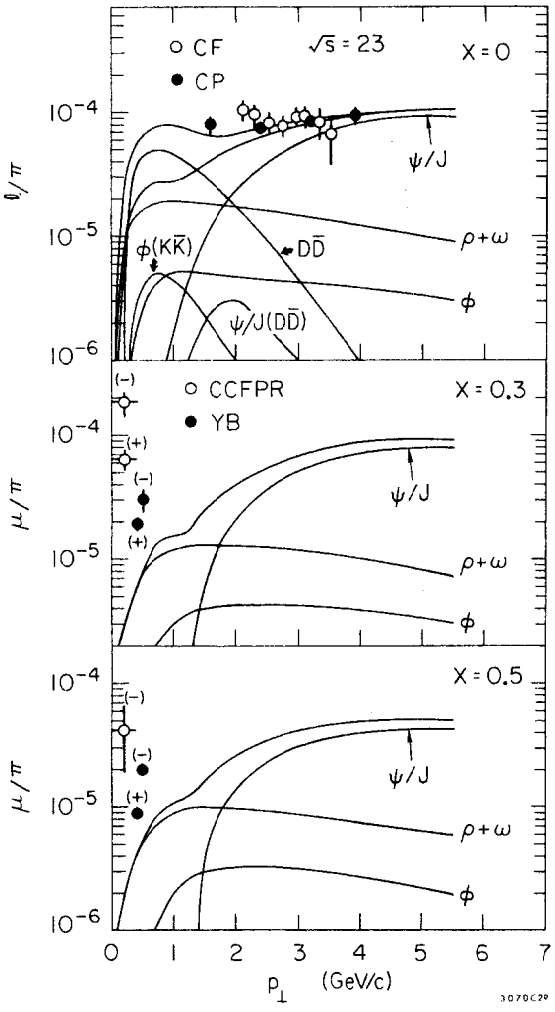

Fig. 28--Vector meson contributions to the ℓ/π ratio as a function of $p_\perp$ at $\sqrt{s}$ = 23 for x = 0, x = 0.3, and x = 0.5 (Ref. 102). Data of Refs. 85, 86.

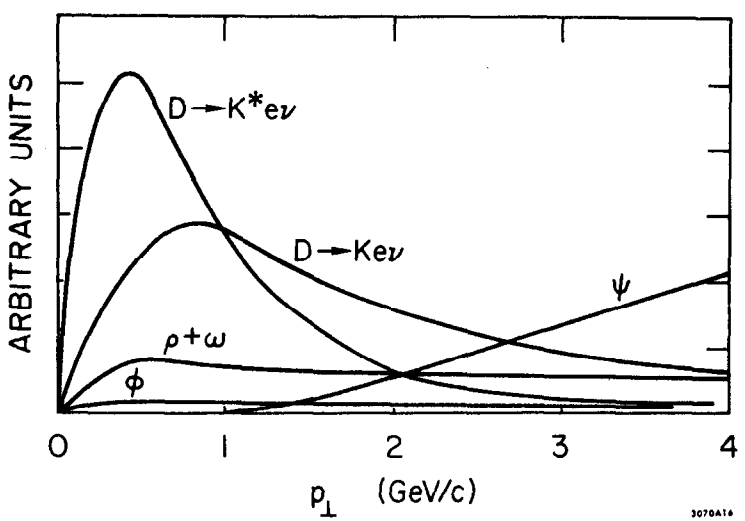

Fig. 29--Contribution to the $p_\perp$ dependence of the e/π ratio from D meson decays (Ref. 33).

and Llewellyn Smith, who also calculated the $D \rightarrow K^* e\nu$ contribution, but who did their fit using the CCRS data before it was revised. A fit of this type at $\sqrt{s} = 53$ is shown in Fig. 30. Clearly, neither attempt can account for the lowest $p_\perp$ CHORMN points (or for the high x data, because of the production characteristics).

Bourquin and Gaillard claim success in eliminating the discrepancy for $p_\perp \geq 1$ GeV/c by this mechanism. With a D mass of 1.8 GeV and $D \rightarrow Ke\nu$ only, they require $\sigma B = 3.6 \times 10^{-30} cm^2$ at $\sqrt{s} = 53$ GeV, and $0.8 \times 10^{-3} cm^2$ at $\sqrt{s} = 23$ GeV. For a branching ratio of 10%, this requires a production cross section of 8×10^{-3} cm^2 at $\sqrt{s} = 23$. The University College, London emulsion experiment[62] quoted above, however, sets a limit of $\lesssim 10^{-30}$ cm^2. It is, of course, not possible to claim that this represents a discrepancy until the D semileptonic branching ratio is actually measured. Hinchliffe and Llewellyn Smith find that they can reproduce some of the CHORMN rise at low $p_\perp$ with a $D \rightarrow K^* e\nu$ decay and a $\sigma B = 3 \times 10^{-29}$ cm^2 at $\sqrt{s} = 53$ GeV. This is probably in even worse contradiction to the emulsion experiment, and in addition requires that the $K^* e\nu$ (or $K(n\pi)e\nu$) modes dominate the $Ke\nu$, or else the agreement in the $p_\perp \simeq 1$ GeV/c region is spoiled. It is interesting that the DASP direct electron spectrum[31] also points to the same puzzling dominance of multipion semileptonic decay modes of the D.

Below $p_\perp$ of $\simeq .5$ GeV, neither vector mesons nor semileptonic decays of charmed particles are sufficient to explain the data. This is true of the CHORMN data at $\sqrt{s} = 53$, and of the FNAL μ data at $\sqrt{s} \simeq 23$. The Penn-Stony Brook signal at low s and $p_\perp < 1$ GeV/c is similarly not likely to originate from these sources.

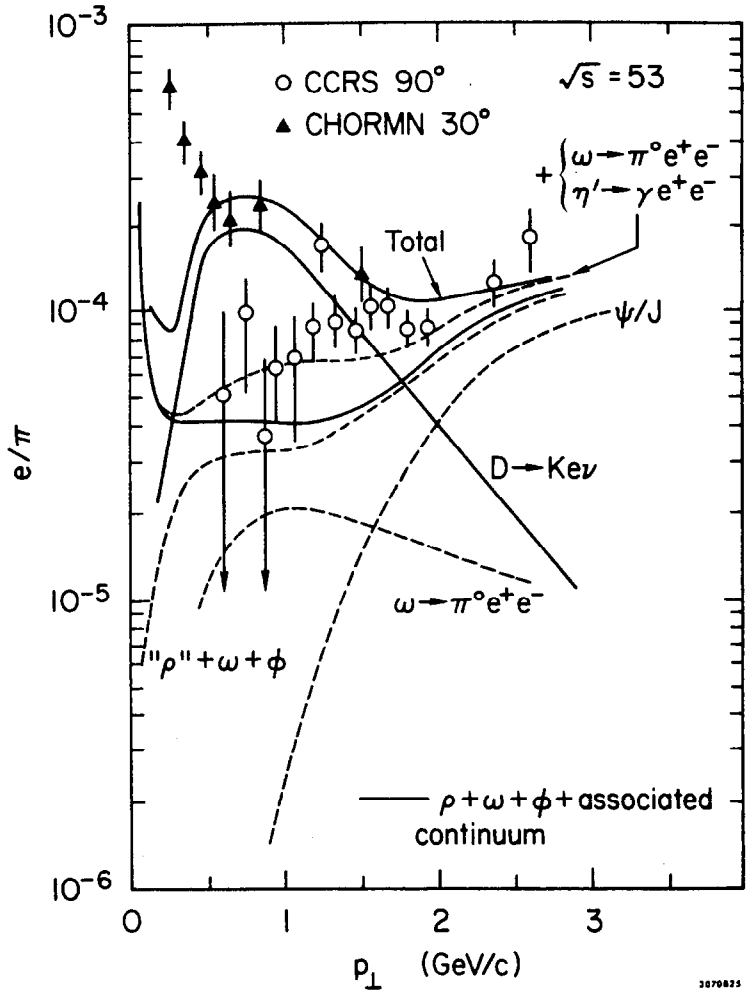

Fig. 30--Vector meson and possible charm contribution to the e/π ratio at $\sqrt{s} = 53$ (Refs. 102, 103). Data of Refs. 82, 83.

Lederman and White[104] have shown that the leptonic decay of a low mass (< 600 MeV) charged meson produced with σ. $B = 10^{-3}\sigma_\pi$ can explain many features of the ℓ/π data at low s and low $p_\perp$.

3.3 Continuum Contribution. There is now evidence for the operation of the Drell-Yan mechanism at very high $p_\perp$, although this will not be discussed in detail here. Several modifications have been made to extend these types of calculation to low $p_\perp$. M. Duong-van[105] has included the effect of the transverse momentum of the partons. Bjorken and Weisberg[106] have argued that lepton pairs are produced not only by valence quarks but also by newly produced quarks which have not yet combined to form hadrons. A similar approach by Ranft and Ranft[107] has produced a fit to the CHORMN data. Rückl[108] has been able to reproduce the low $p_\perp$ rise by considering the conversion of soft virtual bremsstrahlung. Several other attempts along these lines have been reviewed by Sullivan.[109]

It now appears that the higher energy anomalies at low $p_\perp$ and high x may be largely explained by the continuum pair mechanism. The Yale-FNAL experiment[98] showed indirectly that most single muons at high x and low $p_\perp$ originate from $\mu^+\mu^-$ pairs. Very recent Chicago-Princeton results[99] (see also A.J. Smith, these Proceedings) make an even stronger case for the pair origin of the single muons in these regions. The Chicago-Princeton group has used their data on $\mu^+\mu^-$ pairs produced by protons on Be at $\sqrt{s} = 16$ GeV to calculate the single muon contribution to the μ/π ratio by Monte Carlo techniques. Their spectrometer has a large acceptance in x_F and $p_\perp$, so that they have been able to make reliable extrapolations to $x_F = 0$. They find that at $x_F = 0$ the continuum contribution is 50% at $p_\perp = 1$ GeV/c and 30% at 2 GeV/c. This does not

completely explain the μ/π data: between .75 and 2 GeV/c, about 60% of the total is accounted for. It is in this region that the maximum contribution from $D \rightarrow Ke\nu$ decay is expected. Since D decay is now required to provide only about half as much of ℓ/π contribution as was needed without the measured continuum contribution, the prospects for a contribution due to charm are, if anything, enhanced.

The contribution of $\mu^+\mu^-$ pairs at $x_F > 0$, calculated by the Chicago-Princeton group, is compared with existing data in Fig. 27. The continuum contribution is quite important, and gives a reasonable account of the data.

4. Conclusion. In conclusion, it appears that the direct lepton phenomenon is now largely understood, or soon will be, as certain experimental discrepancies are resolved and measurements of charm production cross sections become available. It appears that the sources are varied, and that, as expected, new particle production does play a role. The dominant contribution at low $p_\perp$, at both low and high s, would appear to be continuum pairs, although low energy pair data are still not available. At intermediate values of $p_\perp$ at high s, there is some room for a contribution from semileptonic D decays. There are upper limits on charmed particle production which place restrictions on this contribution, but it cannot be ruled out that as much as 50% of the ℓ/π ratio in the $p_\perp \approx .5 - 1.5$ GeV/c region is the result of D decay, and this is, in fact, likely. At higher $p_\perp$, the contribution of the ψ/J is crucial to an understanding of the phenomenon. Recent extensions of the ℓ/π measurements to the $p_\perp = 4$-6 GeV region, not covered in this lecture, will allow further tests of our understanding of this phenomenon, and may even provide some surprises.

REFERENCES

1. A. Benvenuti et al., Phys. Rev. Lett. 34, 419 (1975), Phys. Rev. Lett. 35, 1199, 1203, 1249 (1975); B. C. Barish et al., Phys. Rev. Lett. 36, 939 (1976); J. von Krogh et al., Phys. Rev. Lett. 36, 710 (1976); H. Deden et al., Phys. Lett. 58B, 361 (1975); J. Blietschau et al., Phys. Lett. 60B, 207 (1976).
2. E. Cazzoli et al., Phys. Rev. Lett. 34, 1125 (1975).
3. G. Goldhaber et al., Phys. Rev. Lett. 37, 255 (1976).
4. I. Peruzzi et al., Phys. Rev. Lett. 37, 569 (1976).
5. J. Siegrist et al., Phys. Rev. Lett. 36, 700 (1976).
6. H. Lynch, SLAC Report No. SLAC-PUB-1750 (1976).
7. A. M. Boyarski et al., Phys. Rev. Lett. 35, 195 (1975).
8. M. Einhorn and C. Quigg, Phys. Rev. Lett. 35, 1114 (1975).
9. S. L. Glashow, J. Iliopoulos, and L. Maiani, Phys. Rev. D 2, 1285 (1970).
10. H. Harari, Proc. SLAC Summer Inst. in Particle Physics, 1975.
11. S. Borchardt and V. S. Mathur, Rochester Preprint COO-3065-149 (1976).
12. K. Lane and E. Eichten, Phys. Rev. Lett. 37, 477 (1976).
13. A. De Rújula, H. Georgi, and S. L. Glashow, Phys. Rev. Lett. 37, 398 (1976).
14. F. E. Close, Phys. Lett. 65B, 55 (1976).
15. H. Schnitzer, Phys. Rev. D 13, 74 (1976).
16. K. Lane and S. Weinberg, SLAC Report No. SLAC-PUB-1793 (1976).
17. H. Fritzsch, CERN-TH-2191 (1976).
18. W. Celmaster, Phys. Rev. Lett. 37, 1042 (1976).
19. J. Sanchez Guillen, Harvard Preprint HUTP-76/A170 (1976).
20. S. Ono, Phys. Rev. Lett. 37, 655 (1976).
21. G. Goldhaber, these Proceedings.
22. A. De Rújula, H. Georgi, and S. L. Glashow, op. cit.
23. A. De Rújula, Proc. Int. Neutrino Conf. 1976, Aachen, Germany, 8-12 June 1976.

24. B. W. Lee, C. Quigg, and J. L. Rosner, FERMILAB-PUB-76/71-THY.

25. B. Knapp et al., Phys. Rev. Lett. 37, 882 (1976); W. Y. Lee, these Proceedings.

26. B. W. Lee, C. Quigg, and J. L. Rosner, FERMILAB-PUB-76/63-THY.

27. A. De Rújula, S. L. Glashow, and R. Shankar, Phys. Rev. D 14, 752 (1976).

28. R. L. Kingsley et al., Phys. Rev. D 11, 1919 (1975); R. L. Kingsley, Rutherford Laboratory Preprint RL-76-065 (1976).

29. S. L. Glashow and S. Weinberg, Harvard Preprint HUTP-76/A158 (1976); R. L. Kingsley, op. cit.

30. M. K. Gaillard, B. W. Lee, and J. L. Rosner, Rev. Mod. Phys. 47, 277 (1975).

31. W. Braunschweig et al., Phys. Lett. B 63, 471 (1976).

32. J. Burmester et al., DESY 76/50 (1976).

33. I. Hinchliffe and C. Llewellyn Smith, Phys. Lett. 61B, 472 (1976) and Oxford Preprint TP-23/76 (1976).

34. A. Ali and T. C. Yang, DESY 76/39 (1976).

35. V. Barger, T. Gottschalk, and R. J. N. Phillips, Wisconsin Preprint COO-881-569 (1976).

36. V. Barger and R. J. N. Phillips, Phys. Rev. Lett. 36, 1226 (1976).

37. J. Ellis, M. K. Gaillard, and D. V. Nanopoulos, Nucl. Phys. B 100, 313 (1975).

38. A. Burwas and J. Ellis, Nucl. Phys. B 111, 341 (1976).

39. B. Gittleman et al., Phys. Rev. Lett. 35, 1616 (1975); U. Camerini et al., Phys. Rev. Lett. 35, 483 (1975); B. Knapp et al., Phys. Rev. Lett. 34, 1040 (1975); T. Nash et al., Phys. Rev. Lett. 36, 1233 (1976).

40. D. Sivers, J. Townsend, and G. West, Phys. Rev. D 13, 1234 (1976).

41. A. Donnachie and J. Randa, Manchester Preprint 76-0556 (1976); R. Aviv et al., Phys. Rev. D 12, 2862 (1975).

42. U. Camerini et al., op. cit.

43. R. L. Anderson et al., SLAC Report No. SLAC-PUB-1795 (1976).

44. V. Barger, Proc. Canadian IPP Int. Summer School, McGill University, Montreal, June 16-21, 1975.

45. D. M. Ritson, Proc. Vanderbilt Conf. on New Particles: Searches and Discoveries, Nashville, 1976, ed. R. Panvini.

46. W. Y. Lee, Proc. 1975 Int. Symposium on Lepton and Photon Interactions at High Energies, Stanford University, Aug. 21-27, 1975, ed. W. T. Kirk (SLAC, Stanford, 1975).

47. I. Gaines, Proc. Vanderbilt Conf. on New Particles: Searches and Discoveries, Nashville, 1976, ed. R. Panvini.

48. B. Knapp et al., preprint submitted to 18th Int. Conf. on High Energy Physics, Tbilisi, USSR, 15-21 Jul 1976.

49. J. J. Aubert et al., Phys. Rev. Lett. 33, 1404 (1974); Y. M. Antipov et al., Phys. Lett. 60B, 309 (1976); F. W. Busser et al., Phys. Lett. 56B, 482 (1975); B. Knapp et al., Phys. Rev. Lett. 34, 1044 (1975); K. J. Anderson et al., Phys. Rev. Lett. 36, 237 (1976); G. J. Blanar et al., Phys. Rev. Lett. 35, 346 (1975); E. Nagy et al., Phys. Lett. 60B, 96 (1975); F. Binon et al., CERN Preprint (1975).

50. M. Binkley et al., Phys. Rev. Lett. 37, 571 (1976).

51. H. D. Snyder et al., Phys. Rev. Lett. 36, 1415 (1976).

52. K. J. Anderson et al., preprint submitted to 18th Int. Conf. on High Energy Physics, Tbilisi, USSR, 15-21 Jul 1976.

53. M. Binkley et al., Phys. Rev. Lett. 37, 574 (1976).

54. D. Sivers, Nucl. Phys. B 106, 95 (1976).

55. J. F. Gunion, Phys. Rev. D 12, 1345 (1975).

56. A. Donnachie and P. V. Landshoff, CERN-TH-2166 (1976).

57. G. Farrar, Nucl. Phys. B 77, 429 (1974).

58. G. Chu and J. Gunion, Phys. Rev. D 10, 3672 (1974).

59. V. Blobel et al., Phys. Lett. 59B, 88 (1975).

60. P. L. Woodworth et al. (Omega Collaboration), Phys. Lett. 65B, 89 (1976).

61. R. Donald et al., Phys. Lett. 61B, 210 (1976).

62. D. Davis et al., quoted by D. Sivers, Rutherford Preprint RL-76-026 (1976).

63. M. Binkley et al., Phys. Rev. Lett. 37, 578 (1976).

64. V. Barger and R. J. N. Phillips, Phys. Rev. D 12, 2623 (1975).

65. C. Carlson and R. Suaya, WM-PP 10, PP-12 (1976); S. D. Ellis, M. Einhorn, and C. Quigg, Phys. Rev. Lett. 36, 1263 (1976); F. Halzen, Wisconsin Preprint COO-501 (1976).

66. S. D. Ellis, M. Einhorn, and C. Quigg, op. cit.

67. K. J. Anderson et al., Phys. Rev. Lett. 37, 799 (1976); K. J. Anderson et al., preprint submitted to 18th Int. Conf. on High Energy Physics, Tbilisi, USSR, 15-21 Jul 1976.

68. T. Gaisser, F. Halzen, and M. Paschos, BNL-21489 (1976).

69. D. C. Hom et al., Phys. Rev. Lett. 36, 1236 (1976).

70. H. Lynch, SLAC Report No. SLAC-PUB-1750 (1976).

71. D. Bintinger et al., Phys. Rev. Lett. 37, 732 (1976); E. J. Bleser et al., Phys. Rev. Lett. 35, 76 (1975); J. J. Aubert et al., Phys. Rev. Lett. 35, 416 (1975); M. A. Abolins et al., Phys. Rev. Lett. 37, 417 (1976); N. A. McCubbin, Proc. Vanderbilt Conf. on New Particles: Searches and Discoveries, Nashville, 1976, ed. R. Panvini.

72. For a summary of these results see R. Harris, in Proc. APS/DPF Seattle Meeting, Seattle, 1975, ed. H. J. Lubatti and P. Mochett.

73. J. J. Aubert et al., Phys. Rev. Lett. 35, 416 (1975).

74. B. Ghidini et al., Nucl. Phys. B 111, 189 (1976).

75. M. A. Abolins et al., op. cit.; E. J. Bleser et al., op. cit.; D. Bintinger et al., op. cit.

76. D. Meyer, these Proceedings; D. Bintinger, op. cit.

77. K. Bunnell et al., Phys. Rev. Lett. 37, 85 (1976).

78. V. Cook et al., Washington Preprint VTL-PUB-33 (1976).

79. U. Becker, Proc. Int. Neutrino Conf. 1976, Aachen, Germany, 8-12 June 1976.

80. ISR Experiments R605, R702.

81. J. Cronin, Lectures at the Int. School of Subnuclear Physics, Erice, 1975; L. M. Lederman, Proc. 1975 Int. Symposium on Lepton and Photon Interactions at High Energies, Stanford University, Aug. 21-27, 1975, ed. W. T. Kirk (SLAC, Stanford, 1975); B. Pope, Proc. Int. Conf. on High Energy Physics, Palermo, 1975.

82. F. W. Büsser et al., CERN Preprint 76-0672 (1976).

83. L. Baum et al., Phys. Lett. 60B, 485 (1976).

84. CERN-Rome Collaboration. Quoted by A. Staude, Proc. Int. Neutrino Conf. 1976, Aachen, Germany, 8-12 June 1976.

85. J. A. Appel et al., Phys. Rev. Lett. 33, 722 (1974).

86. J. P. Boymond et al., Phys. Rev. Lett. 33, 112 (1974).

87. D. Bintinger et al., Phys. Rev. Lett. 35, 72 (1975).

88. D. Bucholz et al., Phys. Rev. Lett. 36, 932 (1976).

89. L. B. Leipuner et al., Phys. Rev. Lett. 35, 1613 (1975).

90. E. Beier et al., Phys. Rev. Lett. 37, 1117 (1976).

91. K. Winter, Phys. Lett. 57B, 479 (1975).

92. L. Leipuner et al., Phys. Rev. Lett. 34, 103 (1975).

93. V. V. Abramov et al., Serpukhov Preprint IFVE 76-92 (1976).

94. A. Browman et al., Phys. Rev. Lett. 37, 246 (1976).

95. N. Z. Anisimova et al., Phys. Lett. 65B, 85 (1976).

96. L. Leipuner et al., Phys. Rev. Lett. 36, 1011 (1976).

97. M. J. Lauterbach et al., Brookhaven Preprint BNL-21852 (1976).

98. H. Kasha et al., Phys. Rev. Lett. 36, 1007 (1976).

99. K. J. Anderson et al., Phys. Rev. Lett. 37, 803 (1976).

100. F. W. Büsser et al., Preprint submitted to 1975 Int. Symposium on Lepton and Photon Interactions at High Energies, Stanford University, Aug. 21-27, 1975.

101. L. Lederman, op. cit.

102. M. Bourquin and J.-M. Gaillard, CERN Preprint 76-0393 (1976).

103. N. Craigie and D. Schildknecht, CERN-TH-2193 (1976).

104. L. Lederman and S. White, Phys. Rev. Lett. 35, 1543 (1975).

105. M. Duong-van, Phys. Lett. 60B, 287 (1976).

106. J. D. Bjorken and H. Weisberg, Phys. Rev. D 13, 1405 (1976).

107. J. Ranft and G. Ranft, Phys. Lett. 62B, 57 (1976).

108. R. Rückl, Max Planck Institute Preprint MPI-PAE/PTh 10/76 (1976).

109. J. D. Sullivan, Proc. Vanderbilt Conf. on New Particles: Searches and Discoveries, Nashville, 1976, ed. R. Panvini.

A DEMOCRITEAN APPROACH TO ELEMENTARY PARTICLE PHYSICS

H. Pierre Noyes

Stanford Linear Accelerator Center
Stanford University, Stanford, California

I. INTRODUCTION.

Theoretical physicists are caught in a maze of exciting experimental results. Many of us are charmed by the situation, and not a few believe that "charm" is Ariadne's thread, which will guide us out of this labyrinth to a decisive confrontation. Like the elusive quarks to which it is tied, and the concept of "strangeness" which led us to them, this thread can be counted on to lead us around many new corners into new puzzles. But this discovery also gives us an opportunity to ask whether some of the puzzles are of our own making, whether we might not climb up over the walls rather than being confined to using familiar search strategies.

The approach I take in this seminar is first to listen to some of our critics. We claim to be studying the basic phenomena on which all natural science rests, yet[1]

> "...good mathematical physicists who are not in the field make no attempt to master it – or else have made an attempt and given it up. ... It seems that to think particle physics you have to give assent to a private language which is only compatible with the language of the rest of physics at the expense of following a whole series of very complicated rules of procedure."

I trust that most of you are sensitive enough to our delicate relationships to sources of both public and private funds to realize that this type of evaluation could easily lead to our supply train being cut off at the pass.

Our problem goes deeper than the use of technical jargon. We often fail to formulate our hypotheses in such a way that they can be disproved. Indeed, some of us may even do this deliberately.[2,3] When we ask our experimental colleagues to test one of our hypotheses, we should first ask ourselves whether we have specified a possible outcome which would convince us that our hypothesis was wrong. We should also be prepared to take the responsibility for our mistakes when experiment goes against us, and to try to pinpoint past mistakes in framing and presenting new hypotheses. Of course I am stating the obvious; I wish this obvious statement had more connection with practice.

Many of us are unaware of the non-trivial connections between the acausal aspects of quantum mechanics and the disillusionment with deterministic science and its accompanying technology following World War I.[4] I know from sad experience that few physicists now assent to the proposition that quantum mechanics is not the product of experimental experience and hence innocent of philosophy, let alone Forman's contention[4] that it is at least partly the result of an active search within physics for a rupture with the past capable of breaking the chains of classical determinism. Even fewer take the trouble to study available historical records before making dogmatic statements.

I realize that mentioning criticism from outside our own "charmed" circle carries little weight with many of you. But Einstein is still a name that I can conjure with. He never accepted the radical rupture with classical causality incorporated in quantum mechanics.[5] Yet his criticisms did not bear experimental fruit until the 1960's. As I will discuss below, his chosen experiment crusis went against his philosophical

conclusions. Paradoxically, many physicists have chosen to ignore his criticism of quantum mechanics, while swallowing at one gulp his acceptance of the space-time continuum. In contrast, Bridgman[6] abstracted from Einstein the methodology which he judged to have led to success - the operational approach - and then used this weapon to attack the foundations of both general relativity and quantum mechanics. Most of Bridgman's criticisms are still unanswered, but as I indicate below some of them can be approximately met. Yet I find Bridgman's belief that by adopting operational definitions physics can disentangle itself from the quagmire of philosophy at best a naive faith.

Of more immediate technical interest to the problems of elementary particle physics is the discussion of quantum electrodynamics by Bohr and Rosenfeld.[7] This theory (QED) forms a bridge between classical and quantum physics thanks to the fact that, assuming sources with continuously variable mass and charge, the only dimensional constants which enter the theory are c and $\hbar$. Thus, the wavelength of the radiation can be arbitrarily large compared to the detection apparatus, and the structure of the theory can be explored using classically describable equipment. Quantum mechanics enters the analysis only through the assumption that the positions and momenta of the parts used to detect the electromagnetic radiation obey the Heisenberg uncertainty relations. Two years of work enabled Bohr and Rosenfeld to construct the limits of measurability of the electromagnetic field in finite volumes (not at points) by designing sufficiently complicated (conceptual) apparati, and proved that these limits coincide with the commutation relations derived more simply via "second quantization." But if mass (as they point out) or charge are quantized, the scale invariance of the theory disappears, and with it the correspondence limit on which their derivation is based. Consequently, from an operational point of view, there is no available justification for the second quantization of the "matter field." This suggests that we should be cautious in accepting any aspect of current "quantum field theories" that cannot be related to observable "massless" radiation. In particular, the properties of Feynman diagrams that have served as a heuristic guide - even in S-matrix theory - are suspect.

II. METHODOLOGY

Although my introductory remarks are critical of current theory, my intent is not to be destructive. Quantum field theory has provided a guide to the experimental discovery of many new and exciting phenomena. Our problem is more an embarrassment of riches than a poverty of possibilities. Under like circumstances, it has often proved useful to pare down the number of hypotheses needed to correlate the data to a minimum (Occam's Razor) and to relate these hypotheses as closely as possible to laboratory operations actually carried out (Bridgman's operational analysis). Once this analysis has been performed, it might prove possible to synthesize new structures which have previously been obscured by the bric-a-brac. A complementary approach is to try to isolate a few philosophical principles which are compatible with the analysis, and to explore what minimal set of hypotheses might be added in order to synthesize from them an explanatory structure capable of meeting the problems posed.

Fortunately, several decades of work by a few philosophers, theorists, and experimental physicists have considerably narrowed the field of

theories we need to consider if we wish to make use of experimental results usually interpreted by conventional quantum mechanics as a first approximation. Many of these results can be explained by introducing "local hidden variables" which are classically describable, but subject to unknown randomizing forces analogous to the collisions between point molecules in classical statistical mechanics. However, Bell has shown that if these randomizing forces are not themselves subject to macroscopic correlations (e.g., changing their effect at one slit when the other slit is opened or closed in a double slit experiment), the assumption of statistical independence limits the type of statistical correlation possible in the measurement of <u>two</u> systems. For example, if a spin-0 system decays to two spin-$\frac{1}{2}$ systems whose correlated polarizations are subsequently measured by two polarimeters, the correlated prediction of <u>any</u> local hidden variable theory must lie within the shaded triangle indicated in Figure 1. In contrast, quantum mechanics predicts the unique correlation curve cos 2θ, which lies <u>outside</u> this region for half the observable range. Hence, an experimental measurement of this curve in the critical interval can either <u>disprove</u> the quantum mechanical prediction or <u>disprove</u> the whole class of local hidden variable theories considered by Bell.

This is a specific example of the "Einstein-Podolsky-Rosen" paradox which Einstein raised as a criticism of quantum mechanics. In a classical deterministic theory, if one spin is measured at one detector and the original system determines the sum of the two spins, we can <u>predict</u> from one measurement what the result will be in the second detector, even though the two detection events cannot be connected by a light signal. In contrast,

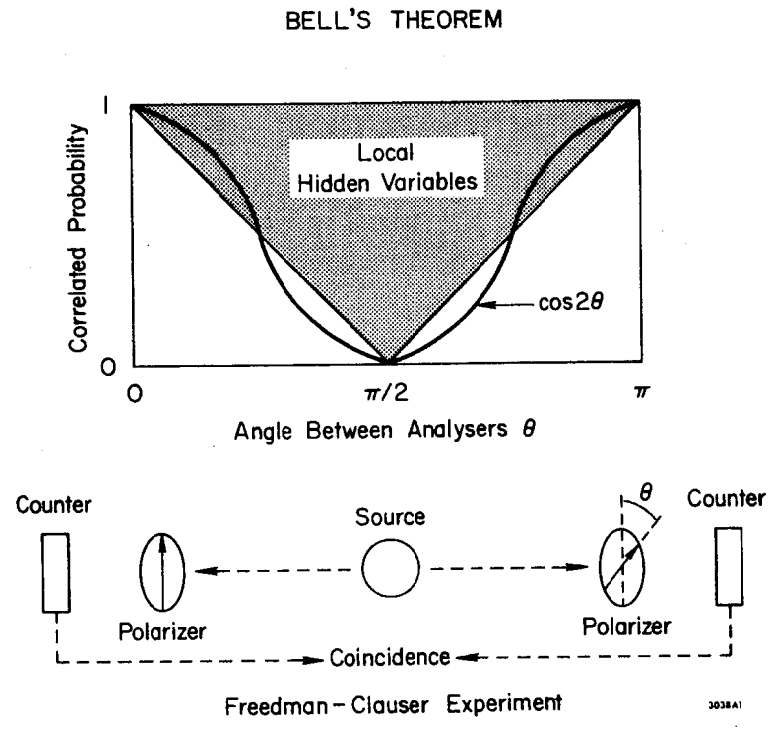

Fig. 1 Local hidden variable theories allow correlations only inside the triangle, while quantum mechanics predicts the unique curve, cos 2θ. The Freedman-Clauser result gives the quantum mechanical curve and excludes local hidden variable theories.

quantum mechanics predicts that if one particle is detected, there is a statistical correlation between that measurement and what happens at the other detector, even though no causal chain (with $v < c$) can connect the two detections. Thus, the quantum mechanical prediction is non-local in a way that is irreconcilable with relativistic causality, no matter how we introduce local randomization.

A closely related experiment (in a higher spin system) has been performed by Freedman and Clauser.[9] Their result is consistent with the quantum mechanical prediction, and excludes local hidden variable theories with high probability. Of course, it is always possible to introduce non-local hidden variables which can describe any macroscopic correlation one wishes - but this really does seem to be multiplying hypotheses unnecessarily; if we adopt Occam's Razor, we should accept the quantum mechanical explanation, or something equivalent to it.

If we ignore for the moment the preparation of the correlated system and the structure of the two polarimeters and detectors, the only technical apparatus we need to describe the experimental result is the wave function for two free particles and the Born interpretation of the wave function giving the statistical probability (including correlations) of detecting the two particles. So we concentrate now on the interpretation of this wave function, and in particular its time-development. We have discussed this in detail elsewhere[10], initially following Phipps's critique[11,12] of the passage from classical to quantum mechanics. In classical Hamilton-Jacobi theory, we have not only the dynamical variables $\underline{p}_k, \underline{q}_k$ but also the initial constants of the motion $\underline{P}_k, \underline{Q}_k$. In the usual "derivations" of quantum mechanics, these degrees of freedom are apparently lost. As he justly remarks[13]:

> "There is nothing to be happy about in a theory that claims to embody a formal "Correspondence," yet absent-mindedly mislays half the classical canonical variables in the process, then covers its nakedness with a fog of blather about "mind," which could just as well be the "God" whose sensorium provided Newton with such convenient cover in circumstances of like embarrassment. I'm pretty absent-minded myself, but when it comes to counting parameters I'll take on any performing horse (or non-performing physicist)."

Phipps has shown that, in the quantum limit he defines, these degrees of freedom can be retained, and provide the conventional Schroedinger wave function with a phase factor $\exp -i\Sigma \underline{P}_k \cdot \underline{Q}_k$. Thus, in this limit, the predictive consequences of the usual theory are retained; by assuming that the randomness of quantum processes arises from the abrupt change in these parameters when "virtual" processes are completed and join the fixed past Phipps supplies not only a natural explanation of the severance of phase chains but also a quantal basis for the second law of thermodynamics. This was the original starting point for my interest in the "Fixed Past-Uncertain Future" interpretation of quantum mechanics.[10] (See Figure 2.)

I have noted[14] that when one starts from scattering boundary conditions these parameters occur naturally, if one requires translational invariance. The scattering process is then attributed to an abrupt change in these parameters. If one sums all such changes consistent with (macroscopic) energy and momentum conservation in such a way as to preclude their occurrence as hidden variables, one recovers the usual scattering formalism, with the significant difference that the T-matrix is now an arbitrary function which one can use to describe any quantum process with N_A free particles in and N_B free particles out. The description

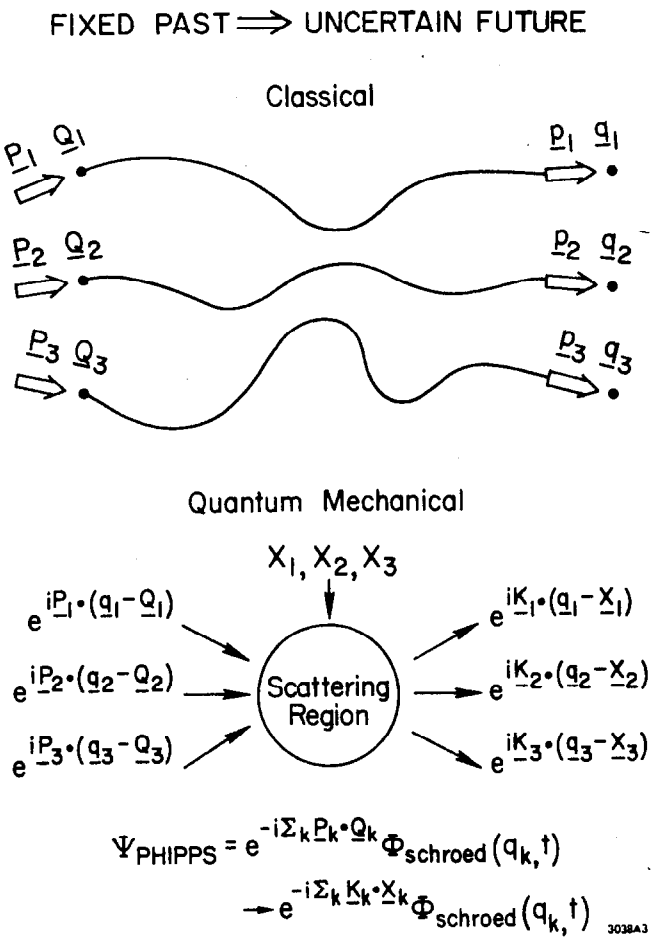

Fig. 2 Classical Hamilton-Jacobi theory contains both the constants of the motion $\underline{P}_k$, $\underline{Q}_k$ and the dynamical variables $\underline{p}_k$, $\underline{q}_k$. Ordinary quantum mechanical presentations discuss only the latter variables. Phipps retains the constants of the motion as a phase factor of the Schroedinger wave function, and interprets their sudden change (in the quantum limit) as the source of quantum mechanical irreversibility.

is covariant if T (after removing the usual phase space factors) is a Lorentz scalar, but is not necessarily the matrix element of some "interaction." In fact it need not even be unitary. Thus, we have explicitly exhibited a quantum mechanical scattering formalism in which the kinematic (descriptive) element is cleanly separated from the dynamics (calculation of T). In the paper[14] I go part way toward Bridgman's operational requirements in that my description is carried through using only counts in detectors, plus devices to change energy and momentum; my description is "Democritean" in that, with those exceptions, it contains only particles and the void. By introducing external e.m. fields in the usual way one can then, to first order in $e^2/\hbar c$, describe the operative devices, and by extrapolation to atomic dimensions, their structure. As Finkelstein has pointed out[15], one can define momemtum via De Broglie wavelength, using a grating; since a regular array of detectors is a grating, we could further simplify our operational procedure.

III. AN INTERMEDIATE DYNAMICAL THEORY

Our immediate task is to construct a dynamical theory using only the covariant multiparticle wave function for free particles of finite mass containing the associated, and empirically tested, connections between mass, energy, and momentum. For this purpose we can adopt the simple, but profound, analysis used by Wick[16] to derive the range of nuclear forces in Yukawa's meson theory. If the trajectories of two systems are defined precisely enough so that they coincide within a region of linear dimension r during a time δt, the limiting velocity of special relativity tells us that they can be coherent in this region only if $r < c\delta t$. Applying the Heisenberg uncertainty relation, we find

that $c\delta t \leq \hbar c/\delta E$. If these two systems communicate with some particle of finite mass m, Heisenberg's principle and the mass-energy relation allow this particle to be present if $\hbar c/\delta E \leq \hbar/mc$. If, following Newton, we assume that the overall process conserves momentum, when the two systems subsequently separate so far that the uncertainty relation will no longer support the presence of the particle of mass m, they do not need to share their momenta in the same way as they did initially, and hence can scatter (cf. Figure 3). We further predict that if the energy of the initial system is high enough, the particle of mass m can emerge in the final state along with the two initial systems. The importance of this derivation for our theory is that this Wick-Yukawa mechanism can generate scattering between free particle systems without the necessity of introducing the concept of "interaction." Thus, we can hope to generate at least a partial theory of quantum scattering by making empirical observations of two-particle scattering, and use these observations as input for a dynamical scheme to calculate the behavior of systems containing three or more particles.

This picture of scattering processes already has profound qualitative implications, even in the "non-relativistic" regime where there is no particle creation. In a classical scattering theory based on finite-range "forces", we can study the effects of pairwise scatterings in dilute systems, and then predict uniquely and deterministically the effect of a double scattering in which one of the particles in the first scattering subsequently scatters from a third particle (cf. Figure 4). However, in a quantum mechanical system, study of two-particle scatterings does not allow us to predict uniquely and unambiguously the wave function within

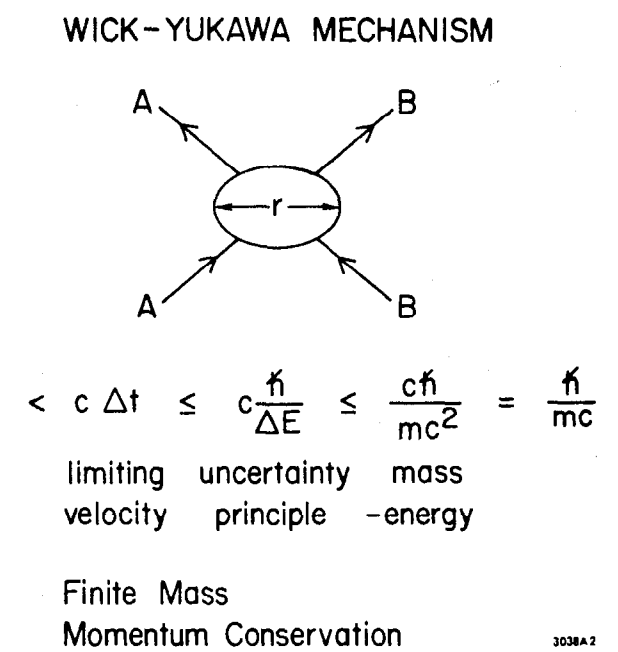

Fig. 3 Wick's derivation of the range of forces in Yukawa's meson theory using only the uncertainty relations and special relativity.

the range of forces. Further, since the scattering process is statistical, the wave function emerging from the first scattering can interfere with this unknown wave function in the second scattering, making the result both unpredictable and irreversible. I have called this the "eternal triangle effect" for reasons discussed elsewhere[17,3]. Perhaps even more surprising is the fact that the non-local effect caused by the presence of the third particle (even with structureless particles, zero angular momentum, and strictly finite range "potentials") does not fall off with the range of forces, but exists throughout a region of dimension $|a|/R$, where a is the two-body s-wave scattering length and R the range of forces. In fact Efimov[18] has proved in this case that even when the two-body systems contain no bound state, this effect generates a number of three-body bound states which goes to infinity like $(1/\pi)\ln|a|/R$ as $|a|$ goes to infinity. In this limit the bound state spectrum corresponds precisely to the two-body bound state spectrum generated by a "potential" which falls off like $1/r^2$. Note that this effect depends only on the on-shell scattering parameter a, and is independent of the details of the potential inside the range R; it therefore should persist in a "zero-range" theory, providing that limit can be well defined in the three-body problem.

As an intermediate step toward a zero-range theory we first consider the covariant boundary condition model for three-particle systems developed by Brayshaw[19,20,21,22]. Two-body scattering data are fitted using a boundary condition at finite radius, whose analytic structure is prescribed by the Faddeev-type three-body equations in which these amplitudes will be used. Outside this radius the hadrons are described, as in a zero-range theory, by free particle wave functions; the inside region may be thought of as the regime that can only be described by quarks, whose function in this model is simply to provide the boundary condition. Brayshaw's results for the non-strange three-hadron systems are summarized in Figure 5. Starting from the π-π $I=0$ s-waves at a few hundred Mev (the ϵ_0 region) the boundary condition radius is found to be $\hbar/4m_\pi c$. Using this to calculate the $I=1$, 0^- 3π state, he finds[19] that there is a three-body bound state close in mass to m_π; if this is identified with the π, the model then predicts the $I=1$ s-wave π-π scattering length to be $a^0_0 \sim 0.23\ \hbar/m_\pi c$, in rather good agreement with other estimates of this poorly known parameter. We know from other work that of the three parameters a^0_0, m_ρ, and Γ_ρ only one is independent, so this calculation also determines the π-π $I=1$ p-wave, or "rho-meson." Given the rho, it is then possible to calculate the $I=0$, 1^- 3π system and find[19] a single resonance at the position of the ω; adding the $K\bar{K}$ channel sharpens this resonance to about the observed width. Using the ρ it is possible to get the A_2, while using both the ρ and the π-π s-wave it is also possible to get the A_1 and explain why the A_1 is so difficult to detect experimentally.[22] Thus, all the low-lying states of the 3π system can be obtained using only the one parameter $r_{\pi\pi}$. Equally, or perhaps even more, significant is the fact that Brayshaw can prove that the model yields no other low-lying bound states or resonances in this system.

We know from other work that, given the π-π and π-N phase-shifts, the main features of the $\pi\pi$N system emerge, so Brayshaw has not yet examined this system using his model. Further, if one accepts the Chew-Low

ETERNAL TRIANGLE EFFECT

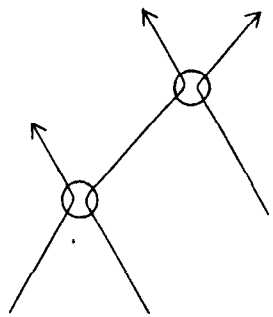

Classical Determinism

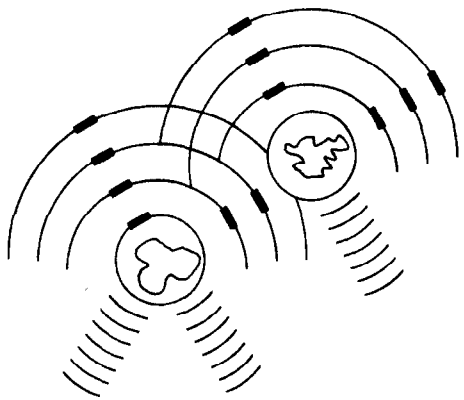

Quantum Mechanical Irreversibility
+
Statistical Prediction

3038A4

Fig. 4 For finite range systems, study of the scattering of pairs allows a unique prediction of double scattering in a three particle system. For the quantum mechanical three-body problem, the interference between the scattered wave from the first scattering interferes with the second scattering, making the result not only statistically unpredictable but also novel. Thus, the future cannot be unambiguously predicted from the past, and systems evolve. The effect does not fall off with the range of forces R, but instead depends on the dynamical scattering length a and its ratio to R.

NON-STRANGE THREE-HADRON SYSTEMS

COVARIANT BOUNDARY CONDITION MODEL (BRAYSHAW)

		Input	Predicted States	
3π	0^-	"ϵ_o" $\rightarrow r_{\pi\pi} = \frac{\lambda\!\!\!^{-}}{4m_\pi c}$	π	No others.
		(conventional a: $\rightarrow \rho$)	$a_0^0 \sim .23 \frac{\lambda\!\!\!^{-}}{m_\pi c}$, ρ	
	1^-	$\rho \rightarrow m_\omega$		
		+ $K\bar{K} \rightarrow$ sharp	ω	
	2^-	ρ, d wave spectator	A_2	
		+ $K\bar{K}$		
	1^+	ρ, "ϵ_o" $\rightarrow$ pole but no sharp peak	A_1	
$\pi\pi N$		(tied down by dispersion theory)		
πNN		P_{11} bound state at M; G^2		
		$r_{\pi N} = \lambda\!\!\!^{-}/Mc$		
		$r_{NN} = \lambda\!\!\!^{-}/2m_\pi c$ $\quad {}^1f = .3, \rightarrow {}^d(a_t, r_t)$		
		${}^3f = 1.8 \rightarrow$ "singlet d" (a_s, r_s)		
NNN		$a_t, r_t, d_s, r_s \rightarrow {}^t$ (7.2 MeV)		

$$r_{\pi\pi} = \frac{\lambda\!\!\!^{-}}{4m_\pi c} \qquad r_{\pi N} = \frac{\lambda\!\!\!^{-}}{mc} \qquad r_{NN} = \frac{\lambda\!\!\!^{-}}{2m_\pi c}$$

Fig. 5 Summary of Brayshaw's results for three-hadron systems; using the covariant boundary condition model, in conjunction with familiar dispersion-theoretic results almost completely determines the low lying three-hadron states.

bootstrap[23] connecting the P_{11} and P_{33} states, the pion-nucleon mass ratio and G^2 are at least approximately co-determined by self-consistency. In a boundary condition model, the associated πN radius is approximately $\lambda\!\!\!^{-}/M_n c$. For the $NN\pi$ system we need, in addition to the P_{11} state already discussed, the NN radius of $\lambda\!\!\!^{-}/2m_\pi c$ and the logarithmic derivative for the singlet and triplet NN S-waves above pion production threshold. As we have shown[20], these suffice to determine the most important features of the nuclear force - the deuteron and "singlet deuteron." Unpublished work by Brayshaw shows that many other features of the NN phase shifts also emerge in a satisfactory way[21], as well as interesting properties of πd scattering and related phenomena. Finally, since we now have calculated the singlet and triplet nucleon scattering lengths and effective ranges, Brayshaw[19] can calculate the NNN system, and finds a triton at about -7.2 Mev, which is as good or better than the binding energy obtained with "realistic nucleon-nucleon potential models." We conclude that the covariant boundary condition model goes a long way toward explaining all of the most significant features of the low-lying states of non-strange three-hadron systems.

Although the basic physics underlying Brayshaw's thinking is that inside the boundary radii lie super-strong quark systems which communicate with the external hadrons in first approximation only through the boundary condition parameters, the actual values of the radii required by experiment - $\lambda\!\!\!^{-}/4m_\pi c$, $\lambda\!\!\!^{-}/M_n c$, $\lambda\!\!\!^{-}/2m_\pi c$ - correspond precisely to the a priori estimate of where the $\pi\pi$, πN, and NN systems become so strongly "interacting" that the two-particle incident channels get lost in a hadronic soup. Thus, it may be possible to think of the boundary condition radii as a convenient way of parameterizing this estimate, or equivalently as the radii of the "diffractive discs" generated by unitarity due to the opening of particle production channels at high energy. Thus, lacking any evidence for free quarks, Occam's Razor would advise us to try to construct a model which has only free particles, plus the unitarity requirements of particle production. I am actively engaged in trying to construct such a model as a zero-range limit of the successful boundary condition model, but so far all my efforts contain flaws. I therefore must confine myself here to indicating how such a theory might go, with no guarantee that it will be successful.

The conceptual outline of my zero-range theory is indicated in Figure 6. The starting point for hadrons would be to postulate that the π is a bound state of the nucleon-antinucleon system, and then try to calculate the nucleon as a bound state of a nucleon plus a nucleon-antinucleon pair, using the pion bound state in the nucleon-antinucleon channel as the only input. The kinematics would be the same as for Brayshaw's successful π - 3π bound state calculation (three equal masses), but with different quantum numbers and different dynamical input. If this works, the self-consistency condition would determine a relation between the residue at the bound state pole (G^2) and the m_π/M_n mass ratio. The second relation would come from the Chew-Low bootstrap, leaving no free parameters in the theory. By introducing particle production processes, I should then be able to predict the boundary condition radii, and start to reproduce Brayshaw's successes from a theory including anti-nucleons, and hence some approximation to crossing, without relying on phenomenology.

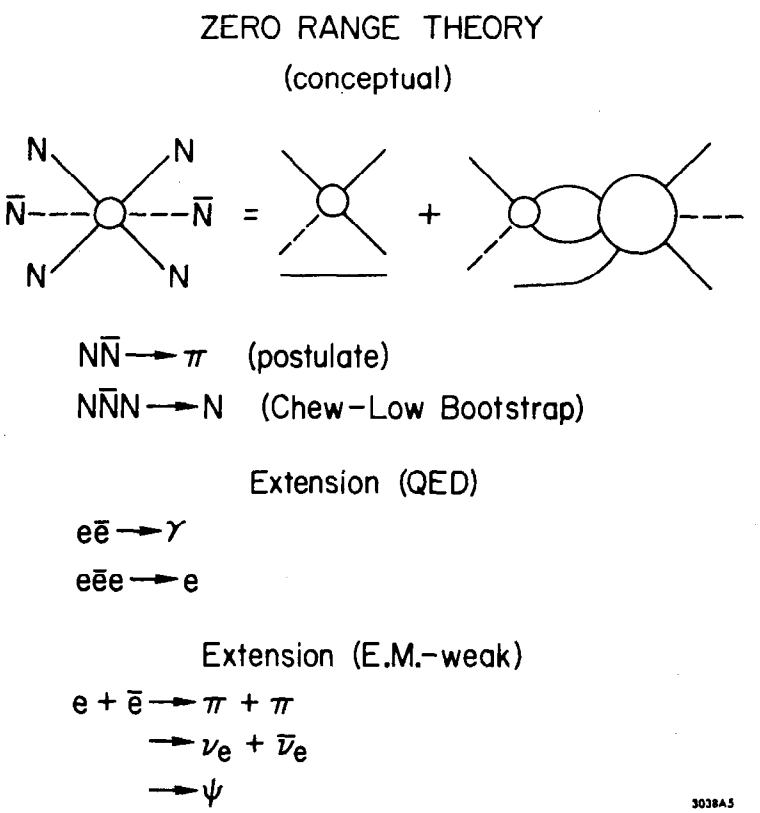

Fig. 6 Summary of a conceptual zero range theory (see text).

If the hadronic calculations work, the next step will be to attempt to construct a theory for charged particles, starting from the assumption that the photon is a 1⁻ zero mass bound state of a spin $\frac{1}{2}$ particle and its antiparticle. The consistency condition would then be that this bound state generates the particle as a bound state of a particle and a particle-antiparticle pair. In this instance, I would have to be able to reconstruct the renormalized perturbation theory of QED up to the point where hadronic processes enter. Since even Compton scattering, from this point of view, is a five-body problem, you can see why I intend to start with hadrons rather than QED. To bring hadrons into the QED calculation, I would initially limit the high energy behavior by adding to the assumption that γ is a bound $e\bar{e}$ state; the inelastic threshold $e\bar{e} \to \pi\pi$ will then serve to remove ultraviolet divergences. Weak interactions enter through the channel $e\bar{e} \to \nu_e, \bar{\nu}_e$, which can be fixed phenomenologically using the Gipsy. Note that by always formulating the theory in terms of two-body on-shell unitary amplitudes, and equations which generate three (or more) particle unitary on-shell states, I need never encounter infinite quantities. This, basically, is what I mean by a Democritean theory - one which at each stage contains only a finite number of free particles of finite energy.

Although the program just outlined may, in time, generate the equivalent of "coupling constants" self-consistently, it is by no means guaranteed of success. I therefore find it useful to think of coupling constants in another way, which I arrived at by a generalization of an argument given by Dyson.[24] The renormalized perturbation series for QED can be viewed as an expansion in the number of particle-antiparticle pairs

which can be present in the system. If this number of pairs $N_{q\bar{q}}$ is confined to a volume whose linear dimension is their own Compton wavelength, the corresponding electrostatic energy is $\approx N_{q\bar{q}}\, e^2/(\lambda\!\!\!^{-}/mc) = N_{q\bar{q}}\,(e^2/\lambda\!\!\!^{-}c)mc^2$. If we are using a theory in which like charges attract, which corresponds to replacing e^2 by $-e^2$ in the QED series, once we go beyond 137 terms this electrostatic energy can suck additional pairs out of the vacuum with a net gain in energy, and the energy of the system collapses to minus infinity. Dyson argued that this proved that the QED series is not absolutely convergent. I would use the same observation to conclude that we cannot, by electromagnetic measurement, define what we mean by more than 137 charged particle pairs within their own Compton wavelength. So stated, $\lambda\!\!\!^{-}c/e^2$ becomes a restriction on operationally definable particle number, and hence a "Democritean" definition of what I mean by a "coupling constant."

The generalization of this particulate definition to other "interactions" is immediate (cf. Figure 7). $N_{Gp} \sim 10^{38}$ is the maximum number of gravitating protons which can be defined within their own Compton wavelength using gravitational measurements. In this case the Dyson singularity is not mathematical but physical - they disappear down a Laplacian[25] black hole. Similarly, the maximum number of pions which can be defined hadronically within their own Compton wavelength is 10 (using $f^2 \sim 0.1$, rather than 0.08, to compensate for the exponential in the Yukawa potential). For superstrong interactions we can only define isolated systems with quark number 0 or 3. Thus, we have a Democritean description of the familiar sequence 3, 10, 137, $\sim 10^{38}$. If we wish to go behind the apparatus of free particle scattering theory at zero range

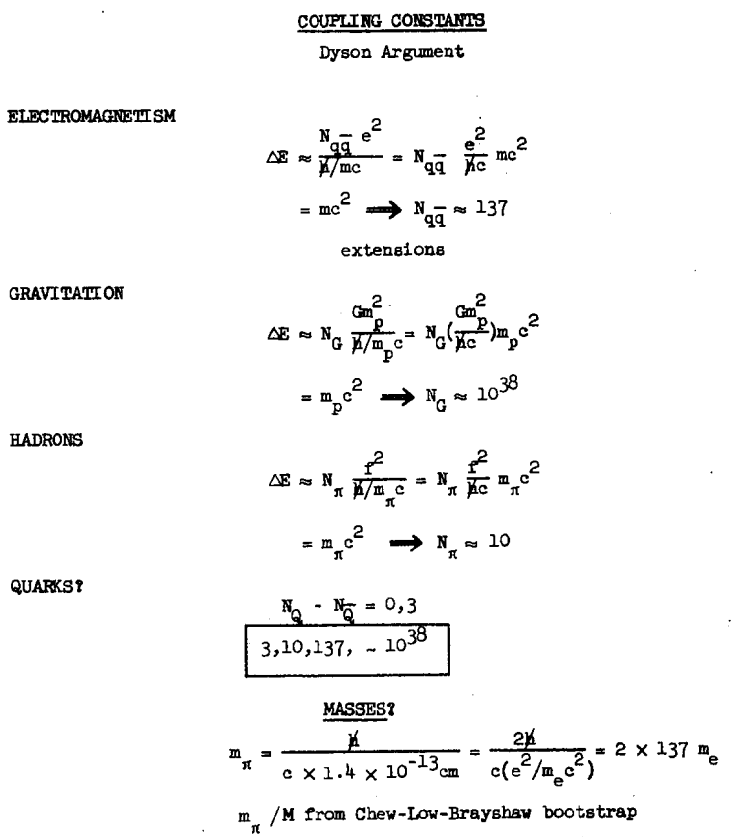

Fig. 7 Basic numbers to be explained by a Democritean theory derived by a generalization of Dyson's argument (see text).

sketched above to a still more fundamental theory, we might start by trying to see how these particular particle numbers arise.

With regard to mass values, we fasten on the unexplained numerical coincidence that $m_{\pi^0} = 2(137)m_e$. A glimmer of explanation might come from the fact, invoked above, that the first anelastic threshold which cuts off (and hence "renormalizes") the QED series for electrons is $e\bar{e} \to 2\pi^0$. But these π's are also, by the Dyson argument, the maximum number of electron-positron pairs we can meaningfully discuss in terms of QED. It is therefore tempting to assume that the π^0 is a "bound state" of 137 electron-positron pairs. Since the number is odd, the ground state should be 0^-. If we add $e\bar{\nu}_e$ or $\bar{e}\nu_e$ we might get the $\pi^\pm$ as well as the π^0. Charge 2 systems would be unstable, thus "explaining" the iso-triplet character of the pion. Since we hope to get m_π/M_n from the Chew-Low bootstrap, this leaves only one mass to be chosen (e.g., m_e or M_p). But we need one mass to be chosen arbitrarily in order to relate our elementary picture to macroscopic measurements. The units of length and time are then $\hbar/mc$ and $\hbar/mc^2$. These are again allowed since a Democritean theory requires[3] a limiting velocity, and the fixed past-uncertain future aspect of quantum mechanics (and experience) require $\hbar$. Thus, if we can generate the sequence 3, 10, 137, $\sim 10^{38}$ from fundamental philosophical principles, we have a chance of building up constructively to the skeletal theory we have arrived at by applying Occam's Razor to existing quantum scattering theory. A possible route to accomplish this is outlined in the next section.

IV. A CONSTRUCTIVE APPROACH

So far our discussion has concentrated on the dynamical aspects of quantum mechanics, and more specifically on the operational analysis of what we mean by a particle into whether or not a particle detector fired (i.e., passed through the detector during a spacial and temporal interval defined by the characteristics of the detector) or did not. More careful analysis of quantal phenomena, which cannot be developed here, has led me to the conclusion that <u>all</u> quantum effects which do not support a "classical" description based on the concept of a space-time continuum can be resolved into such dichotomic (yes-no) events. I take the possibility of analyzing any complicated description into a system of discrete choices as a necessity of rational thought. An old characterization of this materialist philosophy is that "atoms and the void suffice." To make this fundamental Democritean postulate somewhat less polemical, I phrase it as:

"SOMETHING DIFFERS FROM NOTHING" (I)

Starting from this necessity, we recognize, experientially, that not all discriminations are made (can be made?) "simultaneously", and hence that we must meet a sequence of choices, which (again experientially) can be modified by previous discriminations. Causal theories assert that this experience is unreal in the sense that these sequences, being determined by the initial discrimination, are already contained in the initial discrimination. Thus, there is only one choice - whether the world exists or not. Thus, causal theories end up by being anti-rational in our sense, since nothing determines the difference between something and nothing until an additional postulate is added. This may be a good starting point for a mystical philosophy - or madness - but quantum mechanics has provided us with a rational alternative. If we accept the existence of sequential discriminations, and hence in a primitive sense time, we still do not have to believe that the past determines the future. In fact, if we accept the

analysis of the Freedman-Clauser experiment given above, we can rationally make the postulate that:

"PAST SEQUENCES DETERMINE NOW ONLY FUTURE PROBABILITIES" (II)

If we take (I) and (II) seriously, this commits us to what I have described as the fixed past-uncertain future interpretation of quantum mechanics, or some philosophical equivalent. This should not sound too heretical to most quantum physicists. Indeed, when I discussed this with Rudolph Peierls a few years ago, he stated his objection to my calling this an "interpretation" of quantum mechanics by saying "But that is quantum mechanics."

These two philosophical postulates still do not suffice, for me, to indicate the direction in which to develop a theory. We still need some way to discriminate sequences, or order within a sequence, or both. For my third basic postulate, I rely on historical experience within natural philosophy to recognize that the start of new and exciting developments has often been connected with isolating aspects of sequences which, more or less, recur and which can be used to give further structure to the description of the past. The most general way I have thought of to isolate this aspect of successful theories is to postulate that:

"SEQUENCES CONSERVE SOMETHING" (III)

Historical examples of this principle are easy to cite. Quantitative predictive astronomy in Chaldea grew out of the recognition, in temple records, that the helical risings of planets and other astronomical objects recurred at regular periods which could be recovered by numerical analysis. Leucippus and Democritus postulated that the invariant objects were atoms. Ptolemy based his astronomical system on the principle of circular motion. For Copernicus, Ptolemy had not been precise enough in applying this principle (because of the use of equants), and insisted on couching his description in terms of uniform circular motion, thus finding some simplicity in centering the motion of the solar system on the center of the earth's orbit, rather than on the earth. Kepler made his system fully heliocentric, and arrived at the conservation of elliptical paths, equal areas in equal times, and the ratio of the cubes of the radial distances to the squares of periodic times. For Descartes, who broke the circle, the basic principle was the conservation of uniform linear motion. For Newton it was conservation of linear and angular momentum. For Lavoisier, mass; for Dalton, atomic mass; for Helmholtz, energy; for Einstein, mass-energy; for Bohr and Sommerfeld, adiabatic invariants. Any of you can supply equally cogent examples. These principles and examples are summarized in Figure 8.

To proceed from these principles to a specific physical theory we therefore seek first for conserved quantities which have so far survived the buffeting of intense experimental investigation, and try to state the goal of the theory which could connect back to the regularities left behind after our surgical application of Occam's Razor.

My choice of candidates for conserved quantum numbers is given in Figure 9. These are quantized charge, baryon number, muon number, electron number, and (for "spin-$\frac{1}{2}$ particles") the z-component of spin at a single locus. Many direct and indirect tests of each of these conservation laws have been performed. I trust all of you will agree that if we found an exception we would be on the track of new and exciting physics. So this postulate meets my own criterion of being disprovable by

CONSTRUCTIVE APPROACH

Democritean Postulate

"Something differs from nothing"

(atoms and the void suffice)

Evolutionary Postulate

"Past sequences *determine* now *only* future possibilities"

(fixed past → uncertain future)

Conservation Postulate

"Sequences conserve something"

Historical Examples

Chaldean astronomers: periods of Helical risings

Leucippus, Democritus: atoms

Ptolemy: circular motion

Copernicus: uniform circular motion

Kepler: ellipses, equal areas in equal times, R^3/T^2

Descartes: uniform linear motion

Newton: linear and angular momentum

Lavoisier: mass Dalton: atomic mass

Helmholtz: energy Einstein: mass-energy

Bohr-Somerfeld: adiabatic invariants

Fig. 8 Basic postulates of the constructive approach.

CANDIDATES FOR

CONSERVED QUANTUM NUMBERS

Charge
Baryon number
Muon number
Election number
z component of spin
at a single locus

BASIC SYSTEMS

$p, n, \mu, \nu_\mu, e, \nu_e$ + antiparticles + spin → 256 possibilities at one locus

COMPOSITE SYSTEMS

$\pi \supset N\uparrow\ \bar{N}\downarrow$ etc.

$\gamma\uparrow \supset e\uparrow\ \bar{e}\uparrow,\ \nu_e\uparrow\ \bar{\nu}_e\uparrow$

$g\uparrow \supset \nu_e\uparrow\ \bar{\nu}_e\uparrow\ \nu_\mu\uparrow\ \bar{\nu}_\mu\uparrow$

Goal is to account for

3, 10, 137, ~ 10^{38}

~ 10^5 (weak decays): ~~of~~ cosmological?

256 saturation

Fig. 9 Absolutely conserved particulate quantum numbers, and how they might be combined to describe more complicated systems.

experiment, yet possible in terms of the framework for discussion I have set forth. The minimal content of this seminar, for those who do not take any of the rest of it seriously, is, I hope, the suggestion that theories should make this assumption fundamental, and experiments should strive vigorously to disprove it.

The next step is to exhibit physical systems that are well defined operationally and which isolate the dichotomic (yes-no) choices implied by these conservation laws. For these I select the proton, neutron, muon, electron, their respective antiparticles, and (since they are all spin-$\frac{1}{2}$) their spin states (explored via the exclusion principle). The baryons (p,n) illustrate the charged-neutral dichotomy. The leptons (μ,e) illustrate the muon-electron dichotomy. The fact that one pair is charged-neutral and the other charged-charged illustrates the (secondary) baryon-lepton dichotomy, and provides a first clue for dynamics. A second dynamical clue is that the leptons (but, so far as we know, not the baryons) also have neutral counterparts (neutrinos) that are not "particles", if we use mass as a defining characteristic of a particle, but still carry the muon-electron quantum number dichotomy. Using also the particle -antiparticle and spin-up spin-down dichotomies, the exclusion principle then tells us that there can be 256 distinct systems at a single locus. Everything else is to be built up by sequences of comparisons ("time") and additional loci ("space").

Although we now have a descriptive quantal system to identify the "illustrations" and discriminate between these 256 possibilities operationally, we must obviously carry out sequences of comparisons, and in the course of these operations define what we mean by different "loci." In this process we can expect to encounter complex systems which will not have the same fundamental descriptive significance but which can persist long enough to cause "counts in detectors", and hence be described as "particles" in a more directly experimental sense. For the hadrons, the lowest mass system will be the pion - a 0^-, I=1 system which in terms of quantum numbers is a bound state of a nucleon-antinucleon pair, but ultimately unstable. For the leptons, if the success of QED is any guide, we know that there is a massless 1^- "bound state" of $e\bar{e}$, which can enter quantum particulate phenomena due to "pair creation", and is further restricted by having a "correspondence limit" in "classical" electromagnetic fields. From the point of view of quantum numbers, it could just as well be a $\nu_e\bar{\nu}_e$ state, and thus provide a link to the "weak interactions." With this as a guide, we can speculate that the other "classical field" has a quantum "graviton" describable as a $\nu_e\bar{\nu}_e\nu_\mu\bar{\nu}_\mu$ system in a 2^- state. The only phenomenon then left over that does not have a particulate description would be the CP-violating "super-weak" decay. One possibility is that this phenomenon arises cosmologically due to the accumulation of time-ordered events during the evolution of the universe, and hence is not directly related to "interactions" described in terms of particulate systems. Linking cosmology to the elementary particle parameters is an old game. A recent example is the fact noted by Hoyle and Narlikar[26] that the Hubble radius in units of the pion Compton wavelength ($\sim 10^{40}$) is associated with the number which, in our language, we would call the maximum number of pions we could define by gravitational means within their own Compton wavelength.

We have now abstracted to a dimensionless level a few specific numbers which we view as the task of a fundamental theory to derive

and which, by reversing the abstractions used above, we might hope to use to "derive" all of physics as we now understand it. These are (1) the sequence 3, 10, 137, ~ 10^{38} as the maximum number of particles we can operationally define within their own Compton wavelength using quark, hadronic, electromagnetic or gravitational means of identification; (2) saturation of exact quantal description without requiring spatial extension at 256 possibilities; (3) explanation of the instability of systems with respect to "weak decays" in terms of some number of order 10^5; (4) cosmological explanation due to time development of the Hubble constant and the K_L-K_S "super-weak" transitions.

Although for this audience I have presented these requirements inductively starting from familiar facts in elementary particle physics and cosmology, they were in part arrived at by another route, to which I now turn. Some time ago Amson, Bastin, Kilmister, and Parker-Rhodes presented a deductive scheme[27] which yields the sequence 3, 10, 137,~10^{38} and terminates. I initially arrived at the generalization of the Dyson argument given above in trying to understand how a sequence of pure numbers could have anything to do with "coupling constants"[3], and this year noted that the number 256, which also occurs in their theory, has a very natural connection with the absolute particulate conservation laws listed above. I therefore conclude by discussing a few pieces of their scheme in the hope that it will stimulate further thinking along these lines for some of you.

From the point of view I have been developing, I like to state the basic postulate of Amson, Bastin, Kilmister, and Parker-Rhodes as:

"THINGS ARE THE SAME OR DIFFERENT" (III')

I call it III' rather than IV because it is not obviously equivalent to my conservation postulate, but also is not obviously independent of it. In formal logical terms, it would be interesting to derive one from the other or to find what additional postulates are needed to incorporate both in the same system. In a primitive sense, it appears to be different because it includes the concept of identity, while my conservation postulate does not explicitly require such a concept. I have made a brief case above for the importance of conservation laws in physics, but the concept of identity has also proved powerful, particularly in quantum mechanics - as in the phenomena we associate with Bose-Einstein and Fermi-Dirac statistics, and the Gibbs paradox. I do not have time here to explore the deep philosophical issues involved in the choice between III or III', or their ordering in a deductive scheme if they both turn out to be logically compatible with II.

If we start introducing mathematical concepts, postulate I (SOMETHING DIFFERS FROM NOTHING) we can start off with the symbols 0,1. One aim of Amson, Bastin, Kilmister, and Parker-Rhodes is to construct hierarchies based on this symbolization. Their basic postulate (III') then defines the logical operation of symmetric difference, or the arithmetic operation of addition, modulo 2 (cf. Figure 10). To extend this operation to more complicated systems they introduce columns containing only zeros and ones, and combine these, elementwise, to form a third column (cf. Figure 10). This defines a symmetric operation on columns, with interesting group properties which are proved in their paper.[27] Although their initial paper can be read without introducing any fundamental distinction between 0 and 1, it is convenient to distinguish the null column (all zeros); from

COMBINATORIAL BASE HIERARCHY

OF

AMSON, BASTIN, KILMISTER, and PARKER-RHODES

DISCRIMINATORY POSTULATE

"Things are the same or different"

(Discriminating between the same things produces a different result than discriminating between different things.)

2 elements (0,1)

$0 + 0 \to 0,\ 0 + 1 \to 1,\ 1 + 0 \to 1,\ 1 + 1 \to 0$

Columns

$$B_n(x,y) = \begin{pmatrix} x_1 \\ \vdots \\ x_n \end{pmatrix} + \begin{pmatrix} y_1 \\ \vdots \\ y_n \end{pmatrix} \to \begin{pmatrix} x_1+y_1 \\ \vdots \\ x_n+y_n \end{pmatrix}$$

$B_n(x,x) = (0)_n$; $B(x,y) = B(y,x)$

Exclude null column

Lowest level (4 elements)

Non-trivial results $\begin{pmatrix}1\\0\end{pmatrix} + \begin{pmatrix}0\\1\end{pmatrix} \to \begin{pmatrix}1\\1\end{pmatrix}$

$\begin{pmatrix}1\\1\end{pmatrix} + \begin{pmatrix}1\\0\end{pmatrix} \to \begin{pmatrix}0\\1\end{pmatrix}$

$\begin{pmatrix}0\\1\end{pmatrix} + \begin{pmatrix}1\\1\end{pmatrix} \to \begin{pmatrix}1\\0\end{pmatrix}$

Fig. 10 Starting point of the combinatorial base hierarchy.

our Democritean point of view this distinction is not just convenient but necessary for the interpretations we intend to make.

Although various hierarchies can be constructed in this way, the one which concerns us - the combinatorial base hierarchy - starts from columns of height 2. Excluding the null column, the trivial result $B_n(x,0) = (x)_n = B_n(0,x)$, and taking account of the symmetry we have three possibilities, given in Figure 10. These form a "discriminately closed set" in the sense that any two members of the set combine under the binary operation to give a third member of the set. In the paper[27] they show that it is also possible to define three discriminately closed subsets, which are given in Figure 11. This is most easily done in terms of a mapping isomorphism onto non-singular 2×2 matrices of which these are eigenvectors; but there is also a logical definition which does not require matrix multiplication.

The middle level of the hierarchy can be obtained by rearranging the mapping matrices as columns with four elements and finding the discriminately closed set. This contains $2^3-1 = 7$ columns, out of the $4^2 = 16$ possibilities, which are exhibited in Figure 11. Again there are the same number of discriminately closed subsets, just as at the lowest level there are $2^2 - 1 = 3$ columns (and DCsS) out of $2^2 = 4$ possibilities. Repeating the construction gives the last level of the hierarchy with $2^7 - 1 = 127$ columns out of $16^2 = 256$ possibilities. Although the construction is non-unique in terms of a specific labeling of slots in the columns, the cardinal numbers of DCsS are provably unique. The last level of the hierarchy <u>is</u> the last because attempted repetition of the construction, provably, should yield $2^{127} - 1 \sim 10^{38}$ columns which obviously cannot be

Lowest Level (cont'd)

$2^2 - 1 = 3$ discriminately closed subsets (DCsS)

$$\begin{pmatrix}1\\0\end{pmatrix};\ \begin{pmatrix}0\\1\end{pmatrix};\ \begin{pmatrix}1\\0\end{pmatrix},\ \begin{pmatrix}0\\1\end{pmatrix},\ \begin{pmatrix}1\\1\end{pmatrix}$$

Mapping Isomorphism

$$\begin{pmatrix}1&1\\0&1\end{pmatrix}\begin{pmatrix}1\\0\end{pmatrix}=\begin{pmatrix}1\\0\end{pmatrix};\ \begin{pmatrix}1&0\\1&1\end{pmatrix}\begin{pmatrix}0\\1\end{pmatrix}=\begin{pmatrix}0\\1\end{pmatrix}$$

$$\begin{pmatrix}1&0\\0&1\end{pmatrix}\ \begin{pmatrix}1\\0\end{pmatrix},\ \begin{pmatrix}0\\1\end{pmatrix},\ \begin{pmatrix}1\\1\end{pmatrix}=\begin{pmatrix}1\\0\end{pmatrix},\ \begin{pmatrix}0\\1\end{pmatrix},\ \begin{pmatrix}1\\1\end{pmatrix}$$

Middle Level

$$\begin{pmatrix}1&1\\0&1\end{pmatrix}\to\begin{pmatrix}1\\0\\1\\1\end{pmatrix};\ \begin{pmatrix}1&0\\1&1\end{pmatrix}\to\begin{pmatrix}1\\1\\0\\1\end{pmatrix};\ \begin{pmatrix}1&0\\0&1\end{pmatrix}\to\begin{pmatrix}1\\0\\0\\1\end{pmatrix}$$

$$\begin{pmatrix}1\\0\\1\\1\end{pmatrix},\begin{pmatrix}1\\1\\0\\1\end{pmatrix},\begin{pmatrix}1\\0\\0\\1\end{pmatrix}\to\begin{pmatrix}0\\1\\1\\0\end{pmatrix},\begin{pmatrix}0\\0\\1\\0\end{pmatrix},\begin{pmatrix}0\\1\\0\\0\end{pmatrix},\begin{pmatrix}1\\1\\1\\1\end{pmatrix},\begin{pmatrix}1\\1\\0\\1\end{pmatrix},\begin{pmatrix}1\\0\\1\\1\end{pmatrix},\begin{pmatrix}1\\0\\0\\1\end{pmatrix}$$

$4^2 = 16$ elements $\quad 2^3 - 1 = 7$ DCsS

Last Level

$16^2 = 256$ elements $\quad 2^7 - 1 = 127$ DCsS

Why Last?

$$2^{127} - 1 > (256)^2$$

Fig. 11 The three levels of the hierarchy.

exhibited in terms of the 256^2 possibilities.

These results are summarized in Figure 12. The connection with physics is attempted by noting that the construction "preserves information" (explicitly discriminate closure) in passing from one level to another, and that if the successively articulated systems are considered together, including lower levels, the construction generates the cardinal sequence 3, 10, 137, $\sim 10^{38}$ for which we are looking. Further, since the levels intercommunicate, this need only be a first approximation to the "coupling constants" when we go to more complicated sequences. Interestingly, the failure to close at the $(256)^2$ level, and hence the generation of unstable sequences at that level, gives us an estimate of $\sim 10^5$ for the inverse "coupling constant" that could correspond to "weak decays." Finally, the last level at which indefinite repetition of the comparison between columns can occur contains only 256 possibilities, and hence might be connected with the number we arrived at above from the absolute particulate conservation laws.

It is clearly a long way from this kind of abstract mathematical system to an elementary particle theory capable of being <u>disproved</u> by experiment, but to me it looks like a promising beginning which could, in principle, provide an explanatory framework for <u>all</u> of physics. The scheme is much richer in structure than I have been able to explain in this very brief account. As an example, let me show, at the middle level, how we might start to use it to explain the "stability" of certain structures. Assume we start with some random assemblage of the 16 possible columns. Discriminating between two identical columns leads to a null result, but the other columns fall into either an open or a closed

SUMMARY OF

COMBINATORIAL BASE HIERARCHY

Lowest Level

$2^2 = 4$ columns $2^2 - 1 = 3$ DCsS

Middle Level

$4^2 = 16$ columns $2^3 - 1 = 7$ DCsS

Last Level

$16^2 = 256$ columns $2^7 - 1 = 127$ DCsS

Termination

$(256)^2 < 2^{127} - 1$

TENTATIVE CONNECTIONS WITH PHYSICS

1. Information preservation

   3; $3 + 7 \rightarrow 10$; $10 + 127 \rightarrow 137$, Max $2^{127} - 1 + 127 \approx 10^{38}$

   $\Longrightarrow$ 3, 10, 137, $\sim 10^{38}$

2. Comparisons at $(256)^2$ level fail to close indicates instability

   $\Longrightarrow$ $(256)^2 \sim 10^5$ for instability

3. Termination at 256

   $\Longrightarrow$ absolute particulate conservation laws

Fig. 12 How the combinatorial base hierarchy might connect to physics.

set (cf. Figure 13). Discriminating any two of the members of the open set leads to a member of the closed set, as can be readily checked. But, as we have already seen, once in the closed set one never gets out of it. So, statistically, we will settle down from 15 to 7 possible columns. But if this goes on within the closed set, as can also be seen from Figure 13, we will settle down from 7 to 3 columns. These, except for zeros which can no longer change, are just the three members of the lowest level! Thus, there is a natural ordering of processes once one adds some rule (in this case randomness) to the scheme. Whether this will provide a useful clue to the dynamics only the uncertain future can decide.

Conclusion

I hope to have shown you that by taking some thought it is possible to at least approach very fundamental questions in physics, and in that way open for consideration new schemes that, though firmly grounded in experimental fact, need not lead to conventional conclusions. Whether this is physics - which I prefer to call natural philosophy - or poetry I leave for you to decide. If you reach the latter conclusion, I rest my defense on the words of John Keats:

> "... and if it is so that it [poetry] is not so fine a thing as philosophy – For the same reason that an eagle is not so fine a thing as a truth – Give me this credit - Do you not think that I strive to know myself." [28]

STABILIZATION

AT THE MIDDLE LEVEL

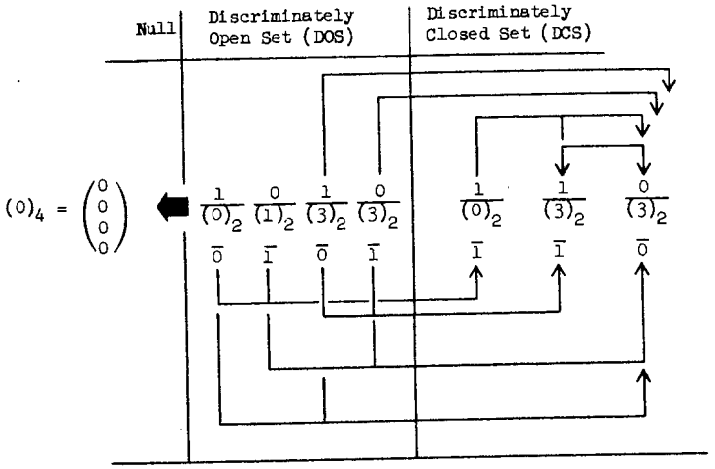

$$(0)_2 = \begin{pmatrix}0\\0\end{pmatrix}$$

$$(1)_2 = \begin{pmatrix}1\\1\end{pmatrix}$$

$$(3)_2 = \begin{pmatrix}1\\0\end{pmatrix}, \begin{pmatrix}0\\1\end{pmatrix}, \begin{pmatrix}1\\1\end{pmatrix}$$

Fig. 13 Stabilization at the middle level (see text).

REFERENCES

1. E. W. Bastin, report to the Science Research Council (of the U.K.) April, 1976.
2. J. M. Ziman, Public Knowledge (Cambridge University Press, London, 1968).
3. H. P. Noyes, "Non-Locality in Particle Physics," SLAC-PUB-1405 (Rev. November 1975).
4. Paul Forman, "Weimar Culture, Causality, and Quantum Theory, 1918-1927: Adaptation by German Physicists and Mathematicians to a Hostile Intellectual Environment." Historical Studies in the Physical Sciences 3,1 (1971).
5. P. Schlipp, ed. Albert Einstein, Philosopher-Scientist (Library of Living Philosophers, Vol. 7, Open Court, LaSalle, Illinois, 1969)
6. P. W. Bridgman, The Logic of Modern Physics, Macmillan, New York, 1928; The Nature of Physical Theory, Princeton University Press, Princeton, 1936.
7. N. Bohr and L. Rosenfeld, Kgl. Danske Vidensk. Selskab, Math-Fys. 12, No. 8 (1933).
8. J. S. Bell, Physics 1, 195 (1965).
9. S. J. Freedman and J. F. Clauser, Phys. Rev. Letters 28, 938 (1972).
10. H. P. Noyes, Foundations of Physics 5, 37 (1975), Erratum 6, 125(1976).
11. T. E. Phipps, Jr., Dialectica 23, 189 (1969).
12. _____, Foundations of Physics 3, 435 (1973).
13. T. E Phipps, private communication, quoted in SLAC-PUB-1351, "Fixed Past and Uncertain Future: An Exchange of Correspondence Between Pierre Noyes, John Bell, and Thomas E. Phipps, Jr." (Stanford Linear Acceperator Center, Stanford, California, 1973.)
14. H. P. Noyes, Foundations of Physics 6, 83 (1976).
15. D. Finkelstein, private communication.
16. G. C Wick, Nature 142, 993 (1938).
17. H. P. Noyes, Bull. Am. Phys. Soc. 16, 20 (1971).
18. V. Efimov, Phys. Letters 33B, 563 (1970).
19. D. D. Brayshaw, Phys. Rev. D11, 2583 (1975).

20. D. D. Brayshaw and H. P. Noyes, Phys. Rev. Letters 34, 1582 (1975).

21. D. D. Brayshaw, "A New Dynamics of NN Scattering," SLAC-PUB-1686 (December 1975).

22. D. D. Brayshaw, Phys. Rev. Letters 36, 73 (1976).

23. G. F. Chew, Phys. Rev. Letters 9, 233 (1962).

24. F. J. Dyson, Phys. Rev. 85, 631 (1952).

25. P. S. Laplace, Exposition du Systeme du Monde, Vol. II (Paris, 1795), p. 305 (English translation: W. Flint, London, 1809). I am indebted to E. Guth for finding this reference for me. It is quoted in W. C. Misner, K. S. Thorne, and J. A. Wheeler, Gravitation (E. H. Freeman, San Francisco, 1970), as follows: "A luminous star, of the same density as the earth, and whose diameter should be 250 times larger than that of the Sun, would not, in consequence of its attraction, allow any of its rays to arrive at us; it is therefore possible that the largest luminous bodies in the universe may, through this cause, be invisible."

26. F. Hoyle and J. V. Narlikar, Action at a Distance in Physics and Cosmology, Freeman, San Francisco (1974).

27. Ted Bastin, Studia Philosophica Gandensia 4, 77 (1966).

28. John Keats - Letter 159 (Rollins' numbering) - journal - letter of February 14 - May 3, 1819, to George and Georgiana Keats in America.

ALL COUPLING CONSTANT METHODS FOR STUDYING CUTOFF FIELD THEORIES*

M. Weinstein
Stanford Linear Accelerator Center
Stanford University, Stanford, California 94305

I. INTRODUCTION

Recently we have seen a marked increase of interest in the problem of finding classical and semiclassical solutions to relativistic field theories. The reasons for this renewal of interest in classical problems are quite varied. For some[1] the interest in semiclassical solutions to field theories lies in the hope that they can provide a calculational procedure for discussing relativistic bound state problems. In particular the "holy grail" pursued by these people is the goal of being able to convincingly reconcile the apparent successes of the naive quark model with the fact that one has not yet been able to identify quarks as final states in any physical process. (One example of this sort of thinking was the original SLAC bag model.[2]) For others, the interest in semiclassical solutions to field equations lies in the fact that they indicate one has only begun to catalogue the bestiary of peculiar objects which can exist in a theory by virtue of the existence of topological conservation laws. Whatever one's reasons as a result of this work we have begun to appreciate that more phenomena can (and probably do) occur in a quantum field theory, than are ever dreamed of in perturbation theory.

Because of our desire to understand questions raised by the study of semiclassical solutions to field equations and our desire to calculate the spectrum of states belonging to any given non-Abelian color gauge theory of strong interactions, people have begun to seriously attack the task of developing new—all coupling constant methods—for computing the properties of quantum field theory. It is my goal in these lectures to present a simple exposition of the approach to this problem which has been developed here at SLAC by Sid Drell, Shimon Yankielowicz[3] and myself.

Since I would like my discussion to be understandable to anyone familiar with elementary quantum mechanics some coverage of background material will be necessary. Moreover, in order to be able to discuss the ideas I want to develop, in an arena uncluttered by infinite numbers of fields and indices, I will never discuss—except in my "smooth talk" at the end—a field theory which has any hope of having something to do with particle physics; instead my discussion will be limited to a "toy" theory defined in one-space one-time dimension. I will show you, however, that this theory has a rich structure and can serve both as a useful framework on which to hang our discussion of nonperturbative calculational techniques, and as a model which should enable you to understand, in simple terms, what afficianados of the sport mean when they talk about

(i) phase transitions and critical behavior,

(ii) "semiclassical" or "quantum" kinks—or solitons, and

(iii) lattice theories and their connection to continuum field theories.

Hopefully, as an added cultural benefit, our discussion of nonperturbative calculational techniques should leave you with an idea as to one way in which "renormalization group" ideas can be useful in discussing a field theory. Unfortunately, the way in which these concepts, developed by Wilson and Kadanoff[4] within the context of path-integral language (and the ideas developed in the Hamiltonian discussions of Kogut and Susskind[5]) relate to our use of these ideas is not at all clear. For this reason, I don't know how transferable the material developed in my lectures will be to other contexts—but, that is your problem. At least, the general words will look the same, and so you can fool yourself into thinking you understand them when you hear them again.

*Work supported by the Energy Research and Development Administration.

By way of giving credit where credit is due, I would like to say that the naive treatment to the "toy" model I will discuss in detail, was worked out independently by us, Stoeckly and Scalapino[6] and R. B. Pearson.[7] Moreover, as I will explain later, Bob Pearson made a very important contribution to the development of the more sophisticated calculational techniques which form the backbone of our approach.

II. OUTLINE

Since our discussion will be somewhat lengthy and will be divided into separate topics I will try to follow the dictum of "first telling you what I am about to do, then doing it, and finally telling you what I did! " To begin, let me give you some idea as to how these talks will proceed. To do this I will now present an outline of the material I will cover in the order in which I will cover it. This outline will be of immense benefit to the readers of the written version of this talk since it will enable them to decide what sections they do not wish to read. Unfortunately, it will be somewhat less useful to you, since I am going to discuss all of the material—but you could of course make a deal with your neighbor and have him wake you up for the interesting parts.

The general plan of these lectures will be the following:

A. Heuristics. Since most of the nonperturbative properties of the "toy" model I will discuss are quantum field theory analogues of what happens in more familiar physical systems, I will begin by discussing the ideas to be developed in later sections by talking about the way these ideas relate to a ferromagnet. My purpose in this discussion is to give a semiconcrete and intuitive explanation of what I will mean by the terminology I will use for the rest of my lectures.

B. Classical Field Theory Analogue. Following this brief discussion, I will spend a short time discussing a classical relativistic field theory which has properties analogous to—though not exactly the same as—a ferromagnetic system. This will be the model we will quantize and reduce to our "toy" model. My goals in this discussion will be to

(i) identify the critical coupling constant in this model,

(ii) discuss the degeneracy properties or long range order of the ground state for different values of the coupling constants, and

(iii) show that the classical theory possesses "soliton" or "kink" states of significant interest.

C. The Connection Between Cutoff Field Theories and Lattice Models. Having presented the classical version of this field theory I will turn to the general question of quantization. The purpose of the discussion in this section is to explain the problems encountered if one proceeds in familiar ways, and to explain why we reformulate our problem as a lattice theory. The discussion presented here will lay down a general framework, but specific detailed examples of what I am talking about will not be given in my talk. A more detailed discussion of some points will appear in appendices to the written version of this talk.

D. A Lattice Analogue of Continuum ϕ^4 Theory. Building upon the remarks of the preceding discussion, I will write down a quantum mechanical lattice version of the classical ϕ^4 theory. My principle purpose at this point is to present a brief, heuristic, discussion of why we can simplify this model—to the "toy" model I referred to—without losing any important physics.

E. Analysis of Toy Model I. In this section we turn to a serious study of the properties of our "toy" theory. We begin with a statement of exact results known for this model. Then we discuss within the framework of perturbation theory how some of these exact results can be understood (the real proof is based upon methods which are very special to this model and devoid of any physical insight).

F. Analysis of Toy Model II: Nonperturbative Methods. This is the key section of my lectures. It is the place I will explain our variational approach and the way in which it leads us to "renormalization group" transformations. This discussion will be developed in two states: first, I will set forth the general idea and give a simple implementation of this idea. Second I will present a more sophisticated and more powerful way of implementing the same idea. The comparison of approximate and exact results for the model in question will be discussed.

G. Smooth Talk. This section summarizes the discussion of the previous section and extends the notion to other more relevant models.

III. HEURISTICS

Before plunging into a discussion of abstract field theories let us try and see how the concepts I will focus on apply to a discussion of a real physical system, namely, a ferromagnet at zero temperature, a system which exhibits spontaneous magnetization. One typically says that since the direction of the average magnetization of this system at any point in space is the same as at any other point, this system has a ground state which exhibits "long range order." The magnitude of the magnetization is referred to as the "order parameter."

One aspect of this system can be appreciated without knowing anything about the detailed dynamics of the system. This is the fact that the basic Hamiltonian of the system is rotationally invariant, and so the energy of the ground state of the magnet cannot depend upon the direction in which the magnetization points. Hence, we say that the ground state of the system is infinitely degenerate. The general idea to be gleaned from this observation is that if there is a state of a system which has the lowest possible energy, and if in this state the expectation value of some operator—like the magnetization—is nonvanishing, then because the magnetization rotates under symmetry transformations of the theory (i.e., transformations which leave the Hamiltonian unchanged) this state must have degenerate partners. Whenever, during these talks, I refer to a system being in an ordered phase I will mean that it has a degenerate (either infinitely or finitely degenerate) ground state.

To understand what I mean when I discuss critical coupling constants for a theory let us discuss some of the microscopic physics of a ferromagnet. (Please be warned that this is by way of analogy and my discussion of a ferromagnet is by no means complete or even necessarily really correct.) At any rate, the point is that in a ferromagnet there are two competing effects taking place. Presuming that the bulk magnetization is due to an aligning of atomic electron spins, there is the magnetic moment—magnetic moment interaction which tends to align these spins antiparallel to one another—and "exchange forces" which tend to make the atomic electron spins align parallel to one another. Whenever the strength of the exchange terms dominate the magnetic interactions the system is ferromagnetic, i.e., its ground state is degenerate and exhibits long range order. Clearly, if we adjust the strength of the "exchange terms" relative to magnetic terms we eventually reach a point beyond which there is no "spontaneous magnetization" (i.e., the order parameter goes to zero) and so the ground state becomes unique. The value of "coupling constant" or "exchange term strength" at which the ground state changes from being degenerate to unique is what we refer to as the critical coupling constant. As we go through this point we say that the system undergoes a phase transition from an ordered to a disordered phase.

Finally, let us note that the analogue of the ever popular "kink" or "soliton state" in this system is the magnetic domain wall, i.e., that small transition region between two larger regions whose bulk magnetization points in different directions.

IV. A CLASSICAL FIELD THEORY ANALOGUE

To sharpen our definitions and to make more precise statements about "soliton" or "kink" states, let us turn to a discussion of a classical relativistic field theory which has properties quite similar to the ferromagnetic system. The specific features I want to focus your attention upon are:

(i) as one varies a "coupling constant" in this system the ground state goes from being degenerate to nondegenerate, and that at the same time the system goes from an "ordered" to "disordered" state,

(ii) for those values of coupling constant which correspond to having a unique ground state the only elementary excitations of the system are "small vibrations." However, when the system has a doubly degenerate ground state, there are two types of elementary excitations—small vibrations and solitons. Furthermore, near the critical point the soliton becomes the more important excitation.

The theory I will consider is defined either by the Lagrangian density

$$\mathcal{L}(\phi(x), \partial_\mu \phi(x)) = \frac{1}{2}(\partial_\mu \phi(x))^2 - \lambda(\phi^2(x) - f)^2 \qquad (4.1)$$

where $\mu=0, 1$, or equivalently by the Hamiltonian

$$H = \int_{-\infty}^{+\infty} dx \left\{ \frac{\Pi^2(x)}{2} + \frac{(\nabla\phi(x))^2}{2} + \lambda(\phi^2(x) - f)^2 \right\}, \qquad (4.2)$$

where

$$\Pi(x) \stackrel{\text{def}}{=} \partial_0 \phi(x) \quad \text{and} \quad \nabla\phi(x) \stackrel{\text{def}}{=} \partial_1 \phi(x) \ .$$

If we observe that H is a sum of positive terms we see that the field configuration, ϕ_0, having the lowest possible energy must correspond to $\partial_0\phi_0 = \Pi = 0$ and $\nabla\phi_0 = 0$, i.e., ϕ_0 must be both time independent and independent of 'x'. Inspection of the term $\lambda(\phi^2 - f)^2$ shows that the nature of the groundstate is quite different depending upon whether f is greater or less than zero. If $f \leq 0$ then the lowest possible value $\lambda(\phi^2 + |f|)^2$ can take is $\lambda|f|^2$, and this is achieved for $\phi_0 = 0$. Hence the lowest state of the system for $f \leq 0$ is unique and is invariant under the transformation $\phi(x) \to -\phi(x)$, which is an invariance of H. If, however, $f > 0$ then the lowest value $\lambda(\phi^2 - f)^2$ can take is zero, and this occurs for either of two possibilities: namely $\phi_0 = \pm\sqrt{f}$. Hence for $f > 0$ the ground state of this classical system is doubled. This is consistent with the fact that the $+\sqrt{f}$ configuration gets mapped into the $-\sqrt{f}$ configuration by the symmetry $\phi \to -\phi$. Recalling our ferromagnetic analogy we say that the system undergoes a phase transition at a critical value of the coupling constant f, namely $f_c = 0$.

Note that for the classical theory the value of 'λ' is irrelevant insofar as the degeneracy properties of the ground state are concerned, and so a natural question to ask is "what role, if any does λ play in determining the structure of the theory?" The answer, of course, is that λ is involved in determining the "mass of small vibrations about the ground state." To see this most easily for the case $f \leq 0$ assume that we are examining a small disturbance at t=0, i.e., $\delta\phi(x, 0)$. It is easy to show that this vibration is stable, in that if the initial disturbance at t=0 is small enough it stays small. Thus, one need only keep the linear terms in the equation of motion as a first approximation to the time development of the system. In this way one finds small vibration solutions of frequency squared $\omega(k)^2 = k^2 + m^2$, where the k=0 mass is $m = (\lambda f)^{1/2}$. Similarly, for the case $f > 0$ one can ask what the mass of small vibrations about either one of the states, $\phi_0(f) = \pm\sqrt{f}$, is. As before linearizing the equations of motion tells us that $m = (8\lambda f)^{1/2}$. In either of these cases one can proceed to analyze the problem of finding the true time dependent response to a small displacement by constructing a perturbation series built upon these plane waves. It is in this sense that one refers to the small vibrations of mass, $m = (8\lambda f)^{1/2}$, as the fundamental excitations of the system.

Having said all this let us now note that the $f \leq 0$ case is distinguished from the $f > 0$ case in an important way. That is, for $f > 0$ there are also exact solutions

to the time independent equations of motion different from $\phi_0 = \pm\sqrt{f}$, i.e., there are solutions to

$$-\nabla^2\phi(x) + 4\lambda\phi(x)\,(\phi^2(x) - f) = 0 \quad , \tag{4.3}$$

which are not found in the perturbation expansion, and which have an energy which differs from the ground state energy by a finite amount. These are the so-called "kinks" or "solitons" and are of the general form

$$\phi_{\substack{\text{kink}\\(\text{antikink})}} = \pm\sqrt{f}\,\tanh\left(\sqrt{2\lambda f}\;(x-x_0)\right) \quad . \tag{4.4}$$

Since this function corresponds to the field configuration shown in Fig. 1, we see that it is just a region of "finite width" joining two "ground state configurations." That this is the direct analogue of a domain wall in the ferromagnet is obvious if we think of $\phi = +\sqrt{f}$ as magnetization pointing up and $\phi = -\sqrt{f}$ as magnetization pointing down.

The really important observation which I would like to make about the "kink" state is that direct substitution of (4.4) into (4.2) yields an energy for the kink which is $E_{\text{kink}} \cong (\lambda f^3)^{1/2}$. Comparing this to the plane wave of k=0 we see that $E_{\text{kink}}/m_{(\text{small vib})} \cong f$; hence, for $f \ll 1$, the kink becomes a much lower energy excitation of the system than the so-called "small vibration." This means, of course, that for $f \ll 1$ the perturbation analysis, in terms of plane wave "small vibrations" about $\phi_0 = \pm\sqrt{f}$, breaks down because the effects of forming "kink-antikink" states, such as that shown in Fig. 2, must be taken into account.

To summarize, we have learned that our classical analogue

(i) exhibits phase transitions from an ordered to disordered phase at a critical coupling $f_c = 0$;

(ii) in the ordered state this theory has both "plane wave" or "small vibration" excitations of mass $m \cong (\lambda f^3)^{1/2}$;

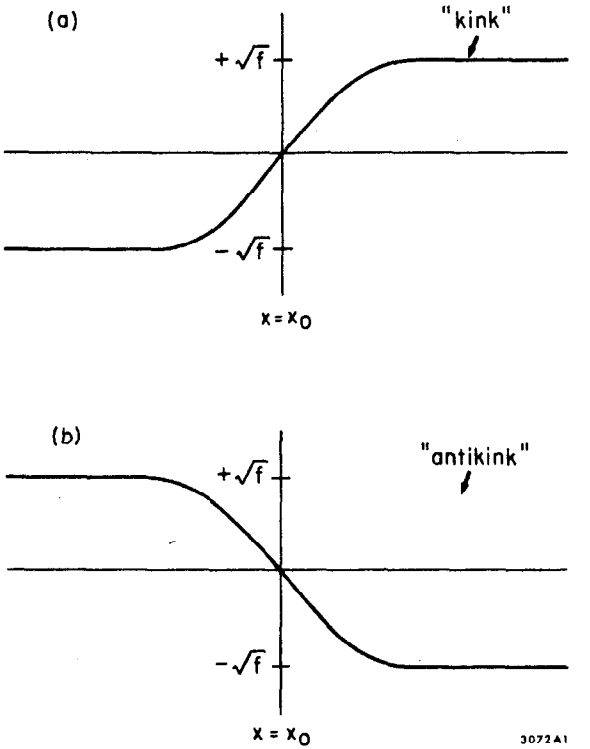

Fig. 1

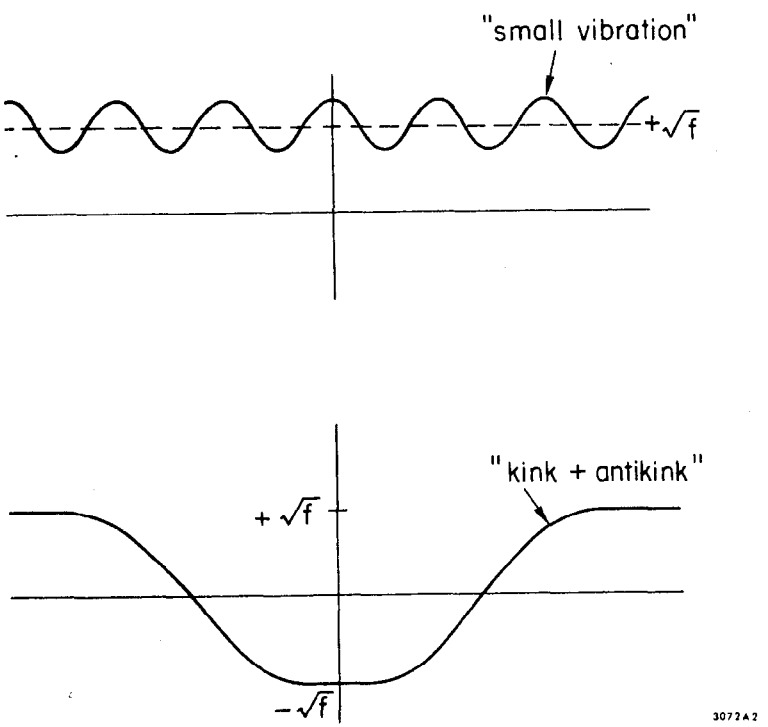

Fig. 2

(iii) the kink state cannot be found from the "perturbation" or "small vibration analysis";

(iv) in the limit $f \ll 1$, when $m_{kink}/m \ll 1$ the usual perturbation analysis breaks down completely because "kinks" and "antikinks" become the lowest lying excitations.

Obviously we could take the Hamiltonian of (4.2) and impose the commutation relations $[\Pi(x), \phi(y)] = -i\delta(x-y)$ in order to quantize the theory. However, our classical discussion already warns us that in the interesting region $f \ll 1$ the usual perturbation methods must fail.

V. ON THE CONNECTION BETWEEN FIELD THEORIES AND LATTICE MODELS

Having argued that we will need to go beyond perturbation theory to study the region $f \ll 1$, we are immediately confronted by the problem of renormalization. We all know that if one adopts the usual perturbation theory approach to dealing with a formal continuum Hamiltonian one does not obtain finite answers unless one resorts to the trick of multiplicative renormalization. Unfortunately, while the infinities encountered in perturbation theory are there whether or not one is dealing with the perturbation expansion, the only well developed method for removing them is tied inextricably to the perturbative approach. Moreover, except for a few special cases no convincing nonperturbative ways for removing these divergences have been put forth. In order to develop a nonperturbative way of computing in a theory free of divergences we find it necessary to abandon—at least temporarily—one or another of our cherished ideas. Our approach will be to abandon manifest (but not practical) Poincare invariance and avoid ultraviolet divergences by establishing a finite momentum space cutoff. Moreover, since we shall be interested in studying phase transitions and other properties which are associated with subtleties of taking infinite volume limits, we will initially define each theory in a box in position space and study the infinite volume limit

afterwards. Actually, what we will really do is study a theory defined on a lattice. Of course, logical completeness requires that I prove to you that studying theories with fixed momentum and spatial cutoffs are equivalent to lattice theories; unfortunately, finiteness of time militates against my doing so. Anyway, as amusing as this correspondence is, my real aim is to tell you what one does with a lattice theory once one has it and not how one goes about finding that lattice theory (or class of lattice theories) which can be shown to be unitarily equivalent to a given cutoff continuum field theory. Hopefully, you will allow me to assure you that such a correspondence can be made and let it go at that for now (in Appendices I and II the way one constructs such an equivalence is described for both free scalar and free fermion field theories, and the way one carries out the same program for interacting theories is clearly indicated). Establishing this correspondence in detail will be irrelevant to this talk anyhow, since for simplicity's sake I will not discuss the theory which is the true unitary equivalent of cutoff ϕ^4 theory at all. Instead I will write down a lattice ϕ^4 theory which at the classical level has properties which are essentially the same as the continuum model we have been discussing, and quantize it. Clearly, even if we make this simplification we still must answer the question, "What do you do with a lattice theory once you have it?", since at first blush strong and intermediate coupling lattice theories are no easier to solve than their continuum counterparts.

VI. A LATTICE ANALOGUE OF CONTINUUM ϕ^4 THEORY

A. The Model. In the sections to follow we shall discuss a simple version of lattice ϕ^4 theory, which will be based upon a nearest neighbor definition of the gradient of a field $\phi(j)$, i.e., $(\nabla\phi)(j) \stackrel{\text{def}}{=} (\phi(j+1) - \phi(j))$. For those of you who are aware of the fact that in general our SLAC collaboration spends its time singing the praises of a different definition of the gradient, let me hasten to assure you that we have not changed our affections. However, since both definitions are equally simple to work with, and since for scalar fields—as opposed to fermion fields—there is no crucial difference between the two definitions, I adopt the more familiar one so as to minimize the number of new ideas I will ask you to get used to in a short time. I want to emphasize, however, that the methods I will use to study the lattice ϕ^4 theory can be applied to either the theory I will write down, the one using our favorite definition of the gradient or the lattice model truly equivalent to cutoff continuum ϕ^4 theory with roughly equal simplicity, and with roughly the same results.

The theory we will study is defined by

$$H = \Lambda \sum_{j=-N}^{+N} \left[\frac{\Pi(j)^2}{2} + \lambda(\phi(j)^2 - f)^2 + \frac{1}{2}(\phi(j+1) - \phi(j))^2 \right], \tag{6.1}$$

where $\Pi(j) = \partial_0 \phi(j)$. We can look upon this as a classical theory of a field defined as a function of a discrete set of points, instead of as a function of a continuum variable 'x'. As in the continuum case we note that H is a sum of positive terms and so the field configurations of lowest energy correspond to $\Pi(j)=0$ and $(\phi(j+1) - \phi(j)) = 0$ (i.e., $\phi(j)$ is a constant). Therefore, the analysis of the structure of the ground state of this theory for $f \leq 0$ and $f > 0$ is the same as the analysis of the continuum theory. In fact the only significant difference between (6.1) and the continuum version of the model is that, for convenience, all fields and coupling constants have been rescaled by dividing by the appropriate powe of inverse lattice spacing $\Lambda \stackrel{\text{def}}{=} 1/a$, so as to make them dimensionless. In this way all of the dimensions of H come from the single explicit factor of mass, Λ, which appears in front of the sum. With this definition one quantizes this model by specifying the equal time commutation relations

$$\left[\Pi(j_1),\ \phi(j_2)\right] = -i\delta_{j_1, j_2} \ . \tag{6.2}$$

Assuming without further ado that the classical physics of this model is essentially equivalent to the physics of the continuum model, what I will now

attempt to do is convince you that (at least for some range of λ and f) this model can be still further simplified without losing the physics we are interested in. The resulting "toy" model will be the one we will study in detail. In order to formulate this argument it becomes convenient to divide H into two terms,

$$H_1 = \Lambda \sum_j \left[\frac{\Pi^2(j)}{2} + \phi^2(j) + \lambda(\phi^2(j) - f)^2 \right] , \qquad (6.3)$$

and

$$H_2 = \Lambda \sum_j [-\phi(j)\ \phi(j+1)] . \qquad (6.4)$$

Having done this we then observe that H_1 is a sum of commuting terms, $H_1(j)$. Thus, the problem of diagonalizing H_1 reduces to the problem of finding the eigenstates of $H_1(j)$.

Since, $[\Pi(j), \phi(j)] = -i$, it is obvious that in the basis in which $\phi(j)$ is diagonal $\Pi(j)$ can be written as $\frac{1}{i}\frac{\partial}{\partial\phi(j)}$ and so, solving the eigenvalue problem specified by each $H_1(j)$ is equivalent to solving the Schrœdinger equation

$$\left\{ -\frac{\partial^2}{\partial\phi^2} + \lambda\left(\phi^4 + \left(\frac{1}{\lambda} - 2f\right)\phi^2 + f^2\right)\right\} \Psi_n(\phi) = E_n \Psi_n(\phi) \qquad (6.5)$$

this is just the same as solving the elementary quantum mechanical problem of a particle of mass, m=1, in a double potential well.

I will now try and convince you that so long as we require $(\lambda f^3)^{1/2} >>> (\lambda f)^{1/2} >> 1$, then one can for the purpose of discussing the low lying eigenstates of this theory replace our ϕ^4 theory by a model having only two levels at a site. In order to see why this is so let us consider Fig. 3 which shows that the height of the potential barrier at $\phi=0$ is λf^2 and that the minima of the potential occurs at $\phi_{min} = \pm\sqrt{f - 1/2\lambda}$, where $V(\phi_{min}) = \frac{1}{\lambda}(1 - 1/4\lambda)$. Now the double well problem should be familiar to you from elementary quantum mechanics, where it was studied as a first example of tunneling. For our purposes in this discussion it

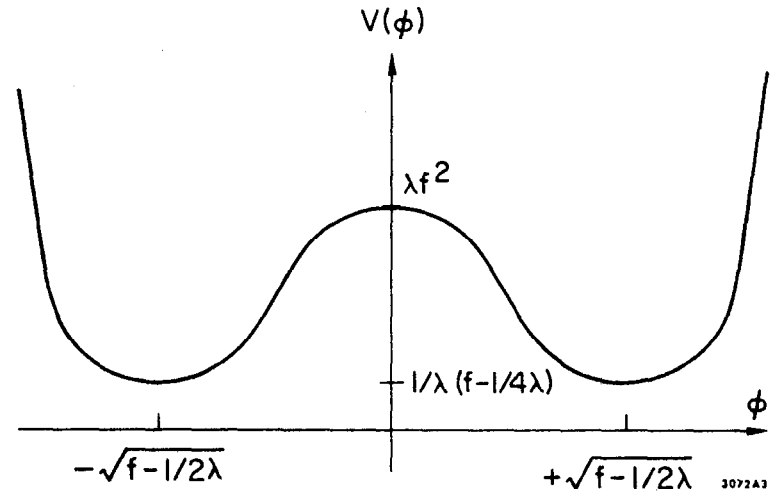

Fig. 3

suffices to recall a few basic facts about this problem, namely:

(i) The eigenstates of the problem can be divided into states which are even or odd under the transformation $\Psi_n(\phi) \rightarrow \Psi_n'(+\phi) = \Psi_n(-\phi)$.

(ii) The first even and odd states are split in energy by an amount proportional to exp {-(height of barrier) × (width of barrier)} which is on the order of exp $\left\{-\lambda f^3\right\}$. Hence for $(\lambda f^3)^{1/2} >> 1$ the two lowest states of our single-site Schrœdinger problem are nearly degenerate.

(iii) When the first two levels are nearly degenerate one can use naive harmonic oscillator wave functions centered about either minimum to estimate the energy gap to the next level. This argument tells us that the energy of the next level will be essentially $(\lambda f)^{1/2}$ so long as $\lambda f^2 >> (\lambda f)^{1/2}$—or equivalently, so long as $(\lambda f^3)^{1/2} >> 1$. In other words, so long as we satisfy this inequality, the gap between *the first two nearly degenerate levels and the next eigenstate of the* system can be made as large as desired.

Assuming that we restrict attention to the case $(\lambda f^3)^{1/2} >> 1$ and $(\lambda f)^{1/2} >> 1$, let us try and see what we expect the groundstate of $H=H_1+H_2$ to be like. In this case the groundstate of H_1 is simply given as the product over all j's of the lowest state for each $H_1(j)$. Clearly, by far the most important effect of $H_2 = -\sum_j \phi(j)\,\phi(j+1)$ is to mix this state with states of the same form except having odd parity levels at two adjacent sites "j" and "j+1". Since the lowest even and odd levels are essentially degenerate and since these mixing effects stay finite no matter how large we make $(\lambda f^3)^{1/2}$, for sufficiently small splittings, it behooves us to restrict attention to the two lowest states at each site and to replace $H_2 = -\sum_j \phi(j)\,\phi(j+1)$ by a product of matrices defined for sites "j" and "j+1" which mix these two nearly degenerate levels.

B. A Final Simplification. The previous argument tells us that for large $(\lambda f^3)^{1/2}$ we can replace $H=H_1+H_2$ by an analogue theory of the form

$$H^{(toy)} = \Lambda \sum_j \left[\begin{pmatrix} -\epsilon/2 & 0 \\ 0 & +\epsilon/2 \end{pmatrix}(j) - \Delta \begin{pmatrix} 0 & 1 \\ 1 & 0 \end{pmatrix}(j) \begin{pmatrix} 0 & 1 \\ 1 & 0 \end{pmatrix}(j+1) \right]$$

$$\stackrel{\text{def}}{\equiv} H_1^{(toy)} + H_2^{(toy)} \tag{6.6}$$

In case the passage from what we have said up to now to (6.6) was too rapid let me explain the analogue in greater detail. The term

$$H_1^{(toy)} = \Lambda \sum_j \begin{pmatrix} -\epsilon/2 & 0 \\ 0 & +\epsilon/2 \end{pmatrix}(j) \tag{6.7}$$

is the replacement for H_1 in (6.3). It merely says that in our analogue system we assume that we have two states or spins, $|\downarrow(j)\rangle$ and $|\uparrow(j)\rangle$, at each site—corresponding to the even and odd parity states of our original theory—and that in the absence of H_2 these states are split in energy by an amount "ϵ" (of course ϵ is some complicated function of λ and f which will not need to be further specified). In other words $H_1^{(toy)}$ is a transcription of the single-site part of H into a theory of spins on a lattice. Obviously,

$$H_2^{(toy)} = -\Lambda \sum_j \left\{ \Delta \begin{pmatrix} 0 & 1 \\ 1 & 0 \end{pmatrix}(j) \begin{pmatrix} 0 & 1 \\ 1 & 0 \end{pmatrix}(j+1) \right\}$$

$$= -\Lambda \sum_j \left\{ \Delta \sigma_x(j)\, \sigma_x(j+1) \right\} \tag{6.8}$$

is just a transcription of H_2 to this spin language. To see why it must have this particular form we need only recall that the operator $\phi(j)$ is odd under the transformation $\phi \rightarrow -\phi$. Hence matrix elements of $\phi(j)$ taken between two even states, or two odd states, must vanish identically. If we restrict attention to the two nearly degenerate eigenstates of $H_1(j)$ then the only matrix element $\phi(j)$ has between these states is $\langle even|\phi(j)|odd\rangle = \langle odd|\phi(j)|even\rangle\, \Delta^{1/2}$. (Note that since only two states are involved one can always choose the relative phase of $|odd\rangle$

and |even> so this matrix element is real.) Therefore, if we think of the two states as $|\downarrow(j)\rangle$ and $|\uparrow(j)\rangle$, $\phi(j)$ can be replaced by $\Delta^{1/2}$ times the matrix which flips spin down to spin up and vice versa, i.e., $\sigma_x(j) = \begin{pmatrix} 0 & 1 \\ 1 & 0 \end{pmatrix}(j)$. Thus we are led to study the theory defined by (6.6), with ϵ and Δ chosen arbitrarily.

VII. ANALYSIS OF THE TOY MODEL: I

A. Exact Results. Having specified the "toy" model we wish to study in detail, the question arises as to whether or not we have oversimplified our original problem and lost all of the interesting nonperturbative phenomena we were out to find. Let me hasten to reassure you that this is not so. This model can be solved exactly and one can show that it has all sorts of interesting properties. Before listing the facts which we know to be true, let me address a question which comes up when one discusses properties of solvable models. "Why study an exactly solvable model in one-space one-time dimension, when we all know the methods for solving these models exactly never work anywhere else?" This is a good question—fortunately (I think) I have a good answer. I couldn't care less about the way in which one goes about solving this model exactly! As I am sure you suspected, the method of obtaining an exact solution to this model involves performing a Pauli-Jordan transformation followed by a Bogoliubov transformation and this method does not generalize to higher dimensions. Even worse, so far as I am concerned, while it allows you to study the properties of this model exactly it leaves you with no "nuts and bolts" feeling for what is going on. However, it is not the model that I care about, but rather the approximate techniques I will use to discuss it. Unlike the techniques used to solve this model exactly, our methods are easily generalizable to any model in any number of space dimensions, and perhaps even more importantly they do give you a feeling for the nuts and bolts of the theory. The only drawback to these methods is that although they seem intuitively reasonable they are after all only approximate calculations. Therefore, it is enormously important to begin by trying them out on a theory for which an exact solution is known in order to see whether or not they really work. With this comment in mind let us list some interesting properties of the theory defined in (6.6).

(i) The theory defined in (6.6) exhibits a phase transition at the point $\epsilon = 2\Delta$. One can rigorously show that for $\epsilon \leq 2\Delta$ the groundstate—or lowest energy eigenvalue—of H is twofold degenerate, whereas for $\epsilon > 2\Delta$ the groundstate is unique.

(ii) Since the overall scale of H plays no role in the detailed physics only the ratio $\epsilon/\Delta \stackrel{\text{def}}{=} y$ matters, and so $y_c = 2$ is the critical coupling constant of this theory. In effect y_c plays the role of "f" in the classical ϕ^4 model.

(iii) The transformation

$$U = \exp\left(\frac{i\pi}{2}\sum_j \sigma_z(j)\right) = \prod_j (i\sigma_z(j)) \tag{7.1}$$

is the unitary transformation which plays the role, in this quantum theory, of the classical transformation $\phi \to -\phi$. (This is so since we have seen that $\sigma_x(j) = \begin{pmatrix} 0 & 1 \\ 1 & 0 \end{pmatrix}(j)$ is the toy theory equivalent to the operator $\phi(j)$ and it is easy to see that

$$U\sigma_x(j)\,U^{-1} = -\sigma_x(j) \quad .) \tag{7.2}$$

(iv) As in the classical theory we can label states according to their transformation properties with respect to U. In particular the two-dimensional space of states spanned by the degenerate eigenvectors of H, for $\epsilon \leq 2\Delta$, can be generated by eigenvectors of U which we will call |even> and |odd>. Clearly $\langle \text{even}|\sigma_x(j)|\text{even}\rangle = \langle \text{odd}|\sigma_x(j)|\text{odd}\rangle = 0$ since $U\sigma_x U^{-1} = -\sigma_x$, but in general $\langle \text{even}|\sigma_x(j)|\text{odd}\rangle$ has no reason to

vanish. If it does not vanish it is useful to form the combinations

$$|\pm\tilde{f}> = \frac{1}{\sqrt{2}}\{|\text{even}> \pm |\text{odd}>\} \tag{7.3}$$

for which

$$U|\pm\tilde{f}> = |\mp\tilde{f}> \tag{7.4}$$

and for which

$$<\pm\tilde{f}|\sigma_x(j)|\pm\tilde{f}> = \pm <\text{even}|\sigma_x(j)|\text{odd}> \tag{7.5}$$

is nonvanishing. These states are the quantum analogues of the classical states $\phi_0(f) = \pm\sqrt{f}$, and it can be shown that the "order parameter" or "magnetization" satisfies

$$<\pm\tilde{f}|\sigma_x(j)|\pm\tilde{f}> = \pm\left(1-\left(\frac{y}{y_c}\right)^2\right)^{1/8} \tag{7.6}$$

for $y \leq y_c$, where $y \stackrel{\text{def}}{\equiv} \epsilon/\Delta$ and $y_c = 2$. The exponent 1/8 in (7.6) is an important critical exponent of this model.

(v) For $\epsilon > 2\Delta$ the groundstate of the system is unique and develops continuously from the state we have called |even>.

(vi) For $\epsilon \ll 2\Delta$ the lowest lying physical excitations of definite momentum are "kinks", i.e., states which are clearly identifiable as moving "domain walls." The "single kink" spectrum is given by

$$E_{\text{kink}}(k_n) = \Lambda\sqrt{(2\Delta-\epsilon)^2 + 8\Delta\epsilon\sin^2\left(\frac{k_n}{2}\right)} \tag{7.7}$$

where k_n is the dimensionless lattice momentum, $k_n = \frac{2}{(2N+1)}n$. In the infinite volume limit, i.e., $N \to \infty$, k_n becomes a continuous variable running over $-\pi \leq k \leq \pi$. (As an aside it is worth noting that (7.7) explains what I mean by the lattice theory abandoning manifest Lorentz invariance but keeping practical Lorentz invariance. It follows from (7.7) that this simple theory, near the critical point $\epsilon = 2\Delta$, approximates a Lorentz invariant theory arbitrarily closely. To see how this works first define the dimensional momentum $\kappa = \sqrt{2\epsilon\Delta}\,\Lambda k$ so that k runs from $-\pi\Lambda$ to $+\pi\Lambda$, and define a mass $M_0 = \Lambda(2\Delta-\epsilon)$. Next rewrite

$$E_{\text{kink}}(k) = \sqrt{M_0^2 + 8\Delta\epsilon\Lambda^2\sin^2\left(\frac{\kappa}{2\sqrt{2\epsilon\Delta}\,\Lambda}\right)} \tag{7.8}$$

Thus we see that approaching the critical point from below as yields a relativistic theory of "kinks", in that if M_0 is held finite say 1 GeV and Λ is taken arbitrarily large, say 10^{100} GeV, then until we reach values of κ on the order of 10^{100} GeV our spectrum is essentially relativistic.)

(vii) For $\epsilon > 2\Delta$ the lowest lying physical excitations are "particle-like", in that they are identifiable as moving disturbances in a uniform groundstate as opposed to a moving interface between two "groundstate" configurations. The 1-particle spectrum, remarkably enough, is given by the same formula

$$E_{\text{particle}}(k_n) = \Lambda\sqrt{(\epsilon-2\Delta)^2 + 8\Delta\epsilon\sin^2\left(\frac{k_n}{2}\right)}$$

(therefore, approaching the critical point from above defines a relativistic theory of particle excitations).

(viii) The groundstate energy density, $\mathscr{E}_0(y)$ can be calculated exactly and one can prove that $\partial^2\mathscr{E}_0(y)/\partial y^2$ has a singularity at the critical point $y_c = 2$.

B. A Simple Derivation of Some of These Results. I will not even attempt to explain how these exact results are derived as that would be a seminar in itself. Anyhow, as I have said, even if you know how to solve this theory you don't really get the feeling that you understand what is going on. I would like

to try and give simple arguments to show

(i) for $\epsilon \ll 2\Delta$ the groundstate of H is doubled whereas for $\epsilon \gg 2\Delta$ the groundstate is unique;

(ii) the elementary excitations for $\epsilon \ll 2\Delta$ are "kink-like" in plane wave states, whereas for $\epsilon \gg 2\Delta$ they are "particle-like" plane wave states.

In order to carry out this discussion it will prove convenient to rewrite (6.6) as

$$H = -\frac{\epsilon}{2}\Lambda\left(\sum_j \begin{pmatrix} 1 & 0 \\ 0 & -1 \end{pmatrix}(j)\right) + \Lambda\sum_j\left[\begin{pmatrix} 0 & 0 \\ 0 & \epsilon \end{pmatrix}(j) - \Delta\begin{pmatrix} 0 & 1 \\ 1 & 0 \end{pmatrix}(j)\begin{pmatrix} 0 & 1 \\ 1 & 0 \end{pmatrix}(j+1)\right] \tag{7.8}$$

and to drop the term $-\frac{\epsilon\Lambda}{2}\left[\sum_j \begin{pmatrix} 1 & 0 \\ 0 & 1 \end{pmatrix}(j)\right]$, since it is just a multiple of the unit matrix. Having done this let us consider what happens when we look at H for $\epsilon = 0$ (i.e., look at $H(\epsilon = 0)$).

In this case we observe that H can be exactly diagonalized, since all of the terms $\sigma_x(j)\sigma_x(j+1)$ commute with one another. It is therefore convenient to go to a new set of single-site states, namely

$$\begin{aligned} |\rightarrow(j)\rangle &= \frac{1}{\sqrt{2}}(|\uparrow(j)\rangle + |\downarrow(j)\rangle) \\ |\leftarrow(j)\rangle &= \frac{1}{\sqrt{2}}(|\uparrow(j)\rangle - |\downarrow(j)\rangle) \end{aligned} \tag{7.9}$$

so that the complete set of states of the form

$$\ldots |\rightarrow(j)\rangle\ |\rightarrow(j+1)\rangle \ldots\ |\rightarrow(j+p)\rangle \ldots$$

or

$$\ldots |\leftarrow(j)\rangle\ |\leftarrow(j+1)\rangle \ldots\ |\leftarrow(j+p)\rangle \ldots$$

or

$$\ldots |\rightarrow\rangle\ |\rightarrow\rangle\ |\leftarrow\rangle\ |\leftarrow\rangle \ldots$$

will all be eigenstates of $H(\epsilon = 0)$. Observing that

$$\sigma_x(j)\,|\rightarrow(j)\rangle = +|\rightarrow(j)\rangle$$

and

$$\sigma_x(j)\,|\leftarrow(j)\rangle = -|\leftarrow(j)\rangle \tag{7.10}$$

we can evaluate the eigenenergy of each such configuration, since each term $-\Delta\sigma_x(j)\sigma_x(j+1)$ gives a factor of $-\Delta$ whenever the "j" and "j+1" spins point in the same direction and a factor of $+\Delta$ whenever they point in the opposite direction. If, for the sake of definiteness, we restrict ourselves to finite volume, so that our lattice has a finite number of sites (i.e., $\sqcup = 2N+1$) then the two states

$$\ldots |\rightarrow\rangle|\rightarrow\rangle \ldots |\rightarrow\rangle \ldots \overset{\text{def}}{\equiv} |\Rightarrow\rangle_0$$

and

$$\ldots |\leftarrow\rangle|\leftarrow\rangle|\leftarrow\rangle \ldots |\leftarrow\rangle \ldots \overset{\text{def}}{\equiv} |\Leftarrow\rangle_0$$

are clearly the eigenstates of $H(\epsilon=0)$ having the lowest possible energy, namely $E_0 = -2N\Delta$. Since there are two distinct configurations having this energy we see that for $\epsilon = 0$, the groundstate of this theory is degenerate. Moreover, since $\phi(j)$ corresponds to $\Delta^{1/2}\sigma_x(j)$ in this model and the expectation value of $\Delta^{1/2}\sigma_x(j)$ in each of these states is nonvanishing—more precisely

$${}_0\langle\Rightarrow|\sigma_x(j)|\Rightarrow\rangle_0 = -{}_0\langle\Leftarrow|\sigma_x(j)|\Leftarrow\rangle_0 = \Delta^{1/2} \tag{7.11}$$

we see that the order parameter in these states is $\Delta^{1/2}$. Hence, we see that for $\epsilon = 0$ our theory has the same sort of groundstate degeneracy as the classical model with $\pm\sqrt{f}$ corresponding to $\pm\Delta^{1/2}$.

In addition to the groundstates of the $H(\epsilon=0)$ Hamiltonian let us see if we can identify the low lying "kink states" or "magnetic domain configurations." This is trivial since it is clear that configurations like

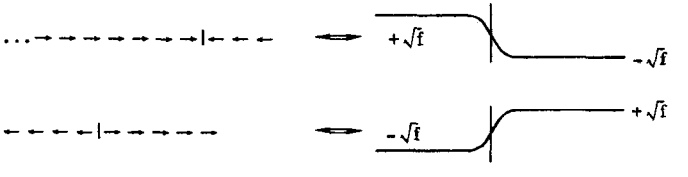

or

which represent two adjacent blocks of oppositely aligned spins, clearly correspond to "antikink" and "kink" configurations of the classical theory. Since in such a configuration only one pair of adjacent spins are antiparallel the energy of any state like this is

$$E_{1\ \text{kink}} = E_{1\ \text{antikink}} = -2N\Delta + 2\Delta = E_0 + 2\Delta \quad , \tag{7.12}$$

so these states represent "mass=2Δ" configurations. Higher states corresponding to more domains, e.g.,

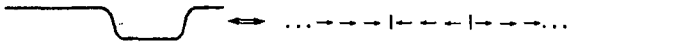

or

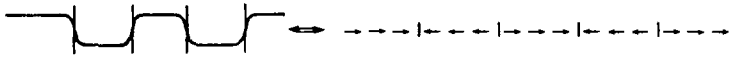

are "multiple kink-antikink" configurations which have higher "mass". In fact, since each mismatched pair of spins contributes +Δ to the energy whereas a matched pair in the groundstate contributes -Δ we see that the general rule for calculating the energy of any such configuration is to count the number of interfaces, N_i, and multiply this by +2Δ to get the difference in energy between multiple kink-antikink configurations and the groundstate. Note further that the energy depends only upon the number of interfaces and not their location.

With these features of the H(ϵ=0) case in mind let us develop a perturbation theory discussion of what happens for very small but nonzero "ϵ". In other words let us treat the term

$$V = \epsilon \sum_j \begin{pmatrix} 0 & 0 \\ 0 & 1 \end{pmatrix}(j) \tag{7.13}$$

as a perturbation on the term

$$-\Delta \sum_j \sigma_x(j)\, \sigma_x(j+1) \tag{7.14}$$

Looking at any of the terms in V we see that

$$\epsilon \begin{pmatrix} 0 & 0 \\ 1 & 1 \end{pmatrix}(j)|\rightarrow (j)\rangle = \frac{\epsilon}{2}|\rightarrow (j)\rangle - \frac{\epsilon}{2}|\leftarrow (j)\rangle$$

and

$$\epsilon \begin{pmatrix} 0 & 0 \\ 0 & 1 \end{pmatrix}(j)|\leftarrow (j)\rangle = \frac{\epsilon}{2}|\leftarrow (j)\rangle - \frac{\epsilon}{2}|\rightarrow (j)\rangle \quad , \tag{7.15}$$

hence in the $|\rightarrow\rangle$, $|\leftarrow\rangle$ basis H can be rewritten as

$$H = \sum_j \left\{ -\Delta \begin{pmatrix} +1 & 0 \\ 0 & -1 \end{pmatrix}(j) \begin{pmatrix} +1 & 0 \\ 0 & -1 \end{pmatrix}(j+1) - \frac{\epsilon}{2}\begin{pmatrix} 0 & 1 \\ 1 & 0 \end{pmatrix}(j) \right\} + \frac{\epsilon}{2}\,\mathbf{1} \quad . \tag{7.16}$$

It follows that applying V to any eigenstate of H(ϵ=0) gives us a linear combination of states all of which come from flipping one spin in the original state. Let us analyze what happens to the various eigenstates of the H(ϵ=0) Hamiltonian in first order perturbation theory. To begin with, consider as our initial state the state $|\Longrightarrow\rangle$ of all spins to the right. Then $V|\Longrightarrow\rangle$ is the state shown in Fig. 4 and is orthogonal to the original state $|\Longrightarrow\rangle$. This means there is no first order shift in the groundstate energy. Clearly the same is true for the state $|\Longleftarrow\rangle$ and so $|\Longrightarrow\rangle$ and $|\Longleftarrow\rangle$ stay degenerate to first order, at an energy $E_0 = -2N\Delta$.

Focusing on 1-kink or 1-antikink states yields a different result. If we consider Fig. 5 we see that if we let V operate on a state of this form, the interface gets moved one step to the right or one step to the left or a new pair of interfaces is created. The matrix elements linking the 1-kink or 1-interface state to a 3-interface state does nothing to shift the energy of this state to first order in ϵ. However, the matrix elements which link a 1-interface state to a different 1-interface state do cause a first order shift in the energy since all of these states are degenerate, at energy $E_0 + 2\Delta$. Recall that the rule for doing degenerate perturbation theory is to first diagonalize V as restricted to the degenerate states and then compute the first order shift for each state $|\psi_n\rangle$, which will be $\delta E_n = \langle\psi_n|V|\psi_n\rangle$. The diagonalization of V in the 1-kink or

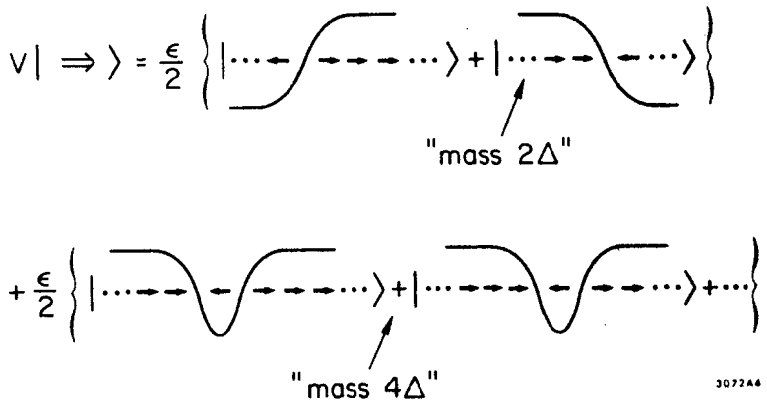

Fig. 4

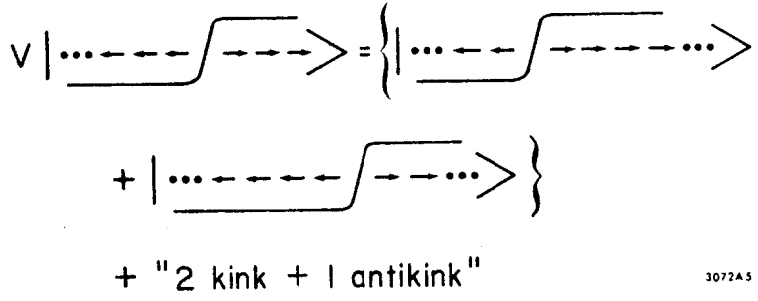

Fig. 5

antikink sector is easily accomplished in the infinite volume limit, $N\to\infty$, because, denoting by $|\psi_j\rangle$ the 1-kink state whose interface lies between 'j' and 'j+1',

$$V|\psi_j\rangle = -\frac{\epsilon}{2}\left(|\psi_{j+1}\rangle + |\psi_{j-1}\rangle\right) \quad . \tag{7.17}$$

Thus, if we form the states

$$|\psi_k\rangle = \sum_j e^{ikj}|\psi_j\rangle \tag{7.18}$$

we see that

$$V|\psi_k\rangle = -\frac{\epsilon}{2}\left(e^{-ik} + e^{+ik}\right)|\psi_k\rangle = -\epsilon\cos(k)|\psi_k\rangle \tag{7.19}$$

It follows that the states $|\psi_k\rangle$, which correspond to "plane wave kink states" or kinks of definite momentum 'k', do get a first order shift in energy; to this order we have

$$H|\psi_k\rangle = E_{1\ \text{kink}}(k) = \left\{E_0 + (2\Delta - \epsilon\cos(k))\right\}|\psi_k\rangle \tag{7.20}$$

Obviously the results for 1-antikink states are identical. (Note that it becomes necessary to measure all energies with respect to the groundstate energy $E_0 = -2N\Delta$ when N goes to infinity in order to obtain finite quantities.)

To summarize, for small enough ϵ the two-fold degeneracy of the groundstate persists, and the lowest lying excitations of the system are single kink or antikink states of momentum 'k'. Moreover (7.20) tells us that the k=0 kink or antikink state has the lowest energy and the "mass" of this state is $(2\Delta-\epsilon)$; this happens to agree with the exact answer.

To conclude our analysis let us consider the limit $\Delta=0$ or $\epsilon/\Delta \gg 1$. It is clear that in this case the groundstate is the state having all spins down. Having any spin up costs an energy ϵ. In this limit the groundstate is thus unique and the lowest energy particle-like excitations of the system correspond to the (2N+1)-degenerate states having all but 1 spin down. Applying a small Δ/ϵ perturbation analysis to this case we find that to first order in Δ/ϵ the spectrum of "plane wave" states of "particle" type is $E(k) = E_0 + (\epsilon - 2\Delta\cos(k))$. Once again this agrees with the exact solution in that for $\epsilon \gg 2\Delta$ we see that the mass of the k=0 state is $\epsilon - 2\Delta$. Since we have established that this theory changes from a theory with a two-fold degenerate groundstate and plane wave kinks as the lowest lying excitations, to a theory with a unique groundstate and particle-like plane wave excitations, as we go from $\epsilon < 2\Delta$ to $\epsilon > 2\Delta$ it follows that it must undergo a phase transition for some critical value of ϵ. What the perturbation analysis cannot tell us is the value of $\epsilon/2\Delta$ at which this happens, nor—for example—the behavior of $\langle\sigma_x(j)\rangle$ as we approach this critical point.

VIII. ANALYSIS OF TOY MODEL II: NONPERTURBATIVE METHODS

In this section we turn to an approximate analysis of our "toy" model by variational techniques in an attempt to calculate the properties of the theory for all values of ϵ/Δ. Since guessing a trial wave function for a theory as complicated as this one is a nontrivial feat we shall not do this "at one fell swoop," but shall devise an iterative constructive procedure for finding a suitable infinite parameter trial state. In order to explain the motivation behind the procedure I will set forth allow me to remind you of certain general properties of variational calculations carried out for what I will call a "linear trial wave function."

A. A General Theorem. Assume that we have a Hamiltonian, H, defined on a specific Hilbert space, $\mathscr{H}$. Next, let $|\psi_n\rangle$ stand for any set, in general not a complete set, of orthonormal states in $\mathscr{H}$. We define a "linear trial state with respect to the set $|\psi_n\rangle$" to be a normalized linear combination of the form

$$|\psi^{\text{trial}}\rangle \stackrel{\text{def}}{\equiv} \sum_n \alpha_n|\psi_n\rangle \tag{8.1}$$

where the $\{\alpha_n\}$'s are any set of complex numbers such that

$$\langle\psi^{\text{trial}}|\psi^{\text{trial}}\rangle = \sum_n |\alpha_n|^2 = 1 \tag{8.2}$$

The question we wish to answer once one has chosen a specific set of $\{\alpha_n\}$'s is "for which choice of $\{\alpha_n\}$'s is the expectation value

$$E(\alpha_1,\ldots) \equiv \langle\psi^{\text{trial}}|H|\psi^{\text{trial}}\rangle = \sum_{n,m} \alpha_n^*\alpha_m\langle\psi_n|H|\psi_m\rangle \qquad (8.3)$$

minimized?"

Due to the constraint equation, (8.2), we cannot proceed to solve this problem by differentiating $E(\alpha_1,\ldots,\alpha_n,\ldots)$ with respect to the $\{\alpha_n\}$'s and straightforwardly equating the results to zero. Rather we must introduce a Lagrange multiplier λ and minimize the unconstrained expression

$$\langle\psi^{\text{trial}}|H|\psi^{\text{trial}}\rangle - \lambda\langle\psi^{\text{trial}}|\psi^{\text{trial}}\rangle$$

$$= \sum_{n,m} \alpha_n^*\alpha_m\left\{\langle\psi_n|H|\psi_m\rangle - \lambda\delta_{nm}\right\}$$

$$\stackrel{\text{def}}{=} \sum \alpha_n^*\alpha_m (H^{TR}-\lambda\mathbb{1})_{n,m} \quad . \qquad (8.4)$$

One then solves the resulting equations

$$\sum_m H^{TR}_{nm}\alpha_m = \lambda\alpha_n \quad , \qquad (8.5)$$

$$\sum_n \alpha^*_n H_{nm} = \lambda\alpha^*_m \qquad (8.6)$$

and

$$\sum_n \alpha_n^*\alpha_n = 1 \qquad (8.7)$$

for λ and α_n's. Clearly the solution to this problem is to observe that the α_n's must be the coefficients of the normalized eigenvectors of the matrix H^{tr}_{nm}—which we shall refer to as a truncated or effective Hamiltonian—and the parameter λ must be chosen to be the corresponding eigenvalue. Of course, if the states $|\psi_n\rangle$ are a complete orthonormal set, then (8.27) just says that the linear trial states which extremize the energy are the exact eigenstates of H.

The lesson to be learned from this exercise that if we are faced with the problem of diagonalizing a Hamiltonian which we cannot handle by simple methods, by cleverly choosing a set of orthonormal states (not a complete set) we reduce the problem of finding the groundstate of our system to the problem of finding the groundstate of an effective Hamiltonian. If we are fortunate this effective or truncated Hamiltonian will be amenable to analysis by familiar methods. This notion should be firmly fixed in your minds since it forms the backbone of everything which follows. Our aim will be to develop an algorithm for cleverly choosing a class of states which is intuitively well suited to the problem of finding an accurate upper bound on the groundstate energy of H, and which at the same time leads to an H^{tr} which can be studied by simple means.

B. A Simple Minded Algorithm for Choosing $|\psi_n\rangle$'s. In order to be more concrete let us discuss one example of an algorithm for choosing an orthonormal set of $|\psi_n\rangle$'s. To begin, recall that the space of states corresponding to the Hamiltonian of (6.6) is spanned by the set of wavefunctions formed by taking arbitrary tensor products of states having either spin up, $|\uparrow(j)\rangle$, or spin down, $|\downarrow(j)\rangle$, at each point. Our procedure will be to find a new complete set of states which span the same space and then thin this new set out in some way. We will try to do this in such a way as to keep states which we have good reason to believe are most important in the expansion of the true groundstate of H.

As a guide to making such a choice of $|\psi_n\rangle$'s let us, as indicated in Fig. 6, divide the lattice into disjoint boxes each of which contains two lattice sites. Clearly, one way to get a set of states which span our Hilbert space is to take the four states $|\downarrow\downarrow\rangle$, $|\uparrow\uparrow\rangle$, $|\uparrow\downarrow\rangle$, and $|\downarrow\uparrow\rangle$ associated with each box and then to form from these states four different orthonormal vectors—say for example

$$\frac{(|\uparrow\uparrow\rangle+|\downarrow\downarrow\rangle)}{\sqrt{2}} \quad , \quad \frac{(|\downarrow\downarrow\rangle-|\uparrow\uparrow\rangle)}{\sqrt{2}} \quad , \quad \frac{(|\uparrow\downarrow\rangle+|\downarrow\uparrow\rangle)}{\sqrt{2}} \quad , \text{ and } \frac{(|\downarrow\uparrow\rangle-|\uparrow\downarrow\rangle)}{\sqrt{2}} \quad .$$

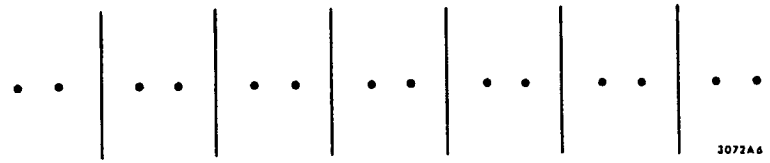

Fig. 6

It is then obvious that we can take a basis for the full Hilbert space, states formed by taking the product over boxes of one of these new vectors for each box. In general the subclass of states, $|\psi_n>$, used to form our linear trial wave functions will be defined by restricting ourselves to two of the four states in each box when forming product states. The key question will be how to decide on which two states in each box to throw away.

One way to throw away states is on the basis of the following overly simple argument. Begin by deleting from the Hamiltonian all terms $-\Delta\sigma_x(j)\,\sigma_x(j+1)$ for which j and j+1 do not lie within the same box. In this event the resulting Hamiltonian can be diagonalized by diagonalizing any one of the single box Hamiltonians

$$H_{(box)} = \epsilon\left\{\begin{pmatrix}0&0\\0&1\end{pmatrix}\otimes\begin{pmatrix}1&0\\0&1\end{pmatrix}+\begin{pmatrix}1&0\\0&1\end{pmatrix}\otimes\begin{pmatrix}0&0\\0&1\end{pmatrix}\right\}$$

$$-\Delta\begin{pmatrix}0&1\\1&0\end{pmatrix}\otimes\begin{pmatrix}0&1\\1&0\end{pmatrix}$$

$$=\sum_{j=1}^{2}\left\{\begin{pmatrix}0&0\\0&\epsilon\end{pmatrix}(j)\right\}-\Delta\sigma_x(1)\,\sigma_x(2) \qquad (8.8)$$

The Hamiltonian $H_{(box)}$ acts on the four possible states $|\downarrow\downarrow>$, $|\uparrow\uparrow>$, $|\uparrow\downarrow>$ and $|\downarrow\uparrow>$. As an aid to diagonalizing this problem let us observe that $H_{(box)}$ is invariant under a rotation about the z-axis of π. More specifically the unitary transformation

$$U^{(box)} = e^{i\frac{\pi}{2}\sum_{j=1}^{2}\sigma_z(j)} = -\sigma_z(1)\,\sigma_z(2) \qquad (8.9)$$

commutes with $H_{(box)}$; since,

$$U\sigma_z(j)\,U^{-1} = \sigma_z(j); \quad U\sigma_x(j)\,U^{-1} = -\sigma_x(j) \qquad (8.10)$$

Because of this $H_{(box)}$ can only mix states having the same eigenvalue of U, hence the state $|\downarrow\downarrow>$ only mixes with $|\uparrow\uparrow>$ and the state $|\uparrow\downarrow>$ only mixes with $|\downarrow\uparrow>$.

This reduces the problem of diagonalizing $H_{(box)}$ to the problem of diagonalizing two 2×2 matrices; namely

$$M_1 = \begin{bmatrix} \langle\downarrow\downarrow|H_{box}|\downarrow\downarrow\rangle & \langle\downarrow\downarrow|H_{box}|\uparrow\uparrow\rangle \\ \langle\uparrow\uparrow|H_{box}|\downarrow\downarrow\rangle & \langle\uparrow\uparrow|H_{box}|\uparrow\uparrow\rangle \end{bmatrix} = \begin{bmatrix} 0 & -\Delta \\ -\Delta & 2\epsilon \end{bmatrix} \tag{8.11}$$

and

$$M_2 = \begin{bmatrix} \langle\downarrow\uparrow|H_{box}|\downarrow\uparrow\rangle & \langle\downarrow\uparrow|H_{box}|\uparrow\downarrow\rangle \\ \langle\uparrow\downarrow|H_{box}|\downarrow\uparrow\rangle & \langle\uparrow\downarrow|H_{box}|\uparrow\downarrow\rangle \end{bmatrix} = \begin{bmatrix} \epsilon & -\Delta \\ -\Delta & \epsilon \end{bmatrix} \tag{8.12}$$

Diagonalizing M_1 and M_2 is a trivial exercise and the four eigenfunctions and eigenvalues are given in Table I.

Table I

State	Energy	Energy Relative to Lowest State
$\frac{1}{\sqrt{1+a^2}}(\lvert\downarrow\downarrow\rangle + a\lvert\uparrow\uparrow\rangle)^* \equiv \lvert\downarrow'\rangle$	$\epsilon - \sqrt{\epsilon^2+\Delta^2}$	0
$\frac{1}{\sqrt{2}}(\lvert\uparrow\downarrow\rangle + \lvert\downarrow\uparrow\rangle) \equiv \lvert\uparrow'\rangle$	$\epsilon - \Delta$	$\sqrt{\epsilon^2+\Delta^2} - \Delta$
$\frac{1}{\sqrt{2}}(\lvert\downarrow\uparrow\rangle - \lvert\uparrow\downarrow\rangle)$	$\epsilon + \Delta$	$\sqrt{\epsilon^2+\Delta^2} + \Delta$
$\frac{1}{\sqrt{1+a^2}}(-a\lvert\downarrow\downarrow\rangle + \lvert\uparrow\uparrow\rangle)$	$\epsilon + \sqrt{\epsilon^2+\Delta^2}$	$2\sqrt{\epsilon^2+\Delta^2}$

*$a = (\sqrt{\epsilon^2+\Delta^2} - \epsilon)/\Delta$.

Step (i) of our general procedure will be to choose this set of four eigenstates as the new orthonormal system which we will use to construct a basis for $\mathcal{H}$. Step (ii), the thinning out procedure, is simply accomplished if we argue—with some justification—that when we add back the terms linking different boxes the most important part of the true groundstate will be spanned by states formed by restricting ourselves to the two lowest energy states in Table I for each box. Having made this statement, we need only construct the truncated or effective Hamiltonian for this choice of linear trial wave functions and see if we can solve it.

Let us begin our computation of $H^{(tr)}$ by labelling each box by an integer 'p' and computing the truncated form of the part, H_1, of the Hamiltonian in (6.6) which does not contain terms $-\Delta\sigma_x(j)\,\sigma_x(j+1)$ where 'j' and 'j+1' are in different boxes. Since our procedure for constructing the $|\psi_n\rangle$'s was to keep for each 'p' the two lowest eigenstates of the $H^{(box)}(p)$ corresponding to that box it is clear that we can write $H_1^{(tr)}$ as

$$H_1^{(tr)} = \sum_p H_{box}^{(tr)}(p) = \sum_p \begin{pmatrix} \epsilon - \sqrt{\epsilon^2+\Delta^2} & 0 \\ 0 & \epsilon - \Delta \end{pmatrix}(p) \tag{8.12}$$

This is perhaps better written as

$$H_1^{(tr)} = \sum_p \left\{ \left(\epsilon - \sqrt{\epsilon^2+\Delta^2}\right)\begin{pmatrix} 1 & 0 \\ 0 & 1 \end{pmatrix}(p) + \begin{pmatrix} 0 & 0 \\ 0 & \sqrt{\epsilon^2+\Delta^2} - \Delta \end{pmatrix}(p) \right\} \tag{8.13}$$

to make it look like the expression in (7.8). The next task which faces us is to compute the truncated version of H_2 which is the sum over all terms $-\Delta\sigma_x(j)\,\sigma_x(j+1)$ which couple different boxes. In order to compute $H_2^{(trunc)}$ all we need to do is see how any one such terms acts on one of the $|\psi_n\rangle$'s we are considering. Since any one of the $|\psi_n\rangle$'s is a state of the form $\prod_{boxes} |\psi_p\rangle$ where the $|\psi_p\rangle$'s can be either of the first two levels in Table I, the way in which a term of the type $-\Delta\sigma_x(j)\,\sigma_x(j+1)$ acts on a $|\psi_n\rangle$ is to flip one spin in each of two adjacent boxes. Therefore, in order to compute the truncated version of this term, we need only compute the overlap of the state in the pth box obtained by flipping one spin in

$$|\psi_0(p)\rangle = \frac{(|\downarrow\downarrow\rangle + a|\uparrow\uparrow\rangle)}{\sqrt{1+a^2}} \tag{8.14}$$

with the state

$$|\psi_1(p)\rangle = \frac{(|\downarrow\uparrow\rangle + |\uparrow\downarrow\rangle)}{\sqrt{2}} \quad . \tag{8.15}$$

Clearly, since $\sigma_x(j)$ is Hermitian and 'a' is real the truncated form of $\sigma_x(j)$ will be symmetric too. Actually since the term we wish to compute is $-\Delta\sigma_x(j)\sigma_x(j+1)$ we should note that $\sigma_x(j)$ will flip the right spin in a box whereas $\sigma_x(j+1)$ will flip the left spin, so in principle we must compute the overlap for each of these cases separately. In fact the calculations will give identical results.

The actual computation is quite trivial. Assuming 'j' lies in the pth box we find

$$\sigma_x(j)|\psi_0(p)\rangle = \sigma_x(j)\left[\frac{1}{\sqrt{1+a^2}}(|\downarrow\downarrow\rangle + a|\uparrow\uparrow\rangle)\right]$$

$$= \frac{1}{\sqrt{1+a^2}}\left[|\downarrow\uparrow\rangle + a|\uparrow\downarrow\rangle\right] \tag{8.16}$$

and so

$$\langle\psi_1(p)|\sigma_x(j)|\psi_0(p)\rangle = \frac{(1+a)}{\sqrt{2}\sqrt{1+a^2}} \tag{8.17}$$

Similarly

$$\sigma_x(j+1)|\psi_0(p+1)\rangle = \frac{1}{\sqrt{1+a^2}}\left[|\uparrow\downarrow\rangle + a|\downarrow\uparrow\rangle\right] \tag{8.18}$$

and so

$$\langle\psi_1(p+1)|\sigma_x(j+1)|\psi_0(p+1)\rangle = \frac{(1+a)}{\sqrt{2}\sqrt{1+a^2}} \tag{8.19}$$

It follows from (8.14)-(8.19) that for 'j' in the pth box

$$\sigma_x^{(tr)}(j) = \frac{(1+a)}{\sqrt{2(1+a^2)}}\sigma_x(p) \tag{8.20}$$

and

$$\sigma_x^{(tr)}(j+1) = \frac{(1+a)}{\sqrt{2(1+a^2)}}\sigma_x(p+1) \quad . \tag{8.21}$$

Thus, we have reduced the problem of finding the best upper bound which one can obtain by choosing trial states from the set of states spanned by forming all possible tensor products of the lowest two states in Table I, to the problem of diagonalizing a new Hamiltonian, $H^{(tr)}$. Interestingly enough $H^{(tr)}$ has exactly the same form as the original Hamiltonian but different coefficients. To be precise

$$H^{(tr)} = \sum_p \left[c_1\begin{pmatrix}1&0\\0&1\end{pmatrix}(p) + \epsilon_1\begin{pmatrix}0&0\\0&1\end{pmatrix}(p) - \Delta_1\begin{pmatrix}0&1\\1&0\end{pmatrix}(p)\begin{pmatrix}0&1\\1&0\end{pmatrix}(p+1)\right] \tag{8.22}$$

where

$$c_1 = \epsilon - \sqrt{\epsilon^2(\Delta^2} \tag{8.23}$$

$$\epsilon_1 = \sqrt{\epsilon^2+\Delta^2} - \Delta \tag{8.24}$$

and

$$\Delta_1 = \frac{\Delta(1+a)^2}{2(1+a^2)} \tag{8.25}$$

At this point we face one of two possibilities. Either the values of ϵ_1 and Δ_1 are such that we can treat the resulting effective Hamiltonian, H_1, by perturbation theory for $\epsilon_1/\Delta_1 > 1$ or $\epsilon_1/\Delta_1 < 1$; or, we say that we still have too large a class of orthonormal wave functions and we carry out the same procedure as we just went through, but this time for the Hamiltonian H_1. It is a straightforward exercise to convince oneself that each successive restriction of our class of trial wave functions leads us to a new effective Hamiltonian of the same form as the original Hamiltonian, but the coefficients of this effective Hamiltonian are given in terms of the ones obtained from the previous calculations. The general result is that after 'n' successive truncations our variational problem reduces to the

problem of diagonalizing an effective lattice Hamiltonian

$$H_n^{(tr)} = \sum_j \left[d_n \begin{pmatrix} 1 & 0 \\ 0 & 1 \end{pmatrix}_j + \epsilon_n \begin{pmatrix} 0 & 0 \\ 0 & 1 \end{pmatrix}_j - \Delta_n \begin{pmatrix} 0 & 1 \\ 1 & 0 \end{pmatrix}^{(j)} \begin{pmatrix} 0 & 1 \\ 1 & 0 \end{pmatrix}^{(j+1)} \right] \tag{8.26}$$

where

$$\begin{aligned} \epsilon_{n+1} &= \sqrt{\epsilon_n^2 + \Delta_n^2} - \Delta_n \quad , \\ \Delta_{n+1} &= \frac{\Delta_n}{2} \frac{(1+a_n)^2}{(1+a_n^2)} \quad , \\ a_n &= \sqrt{\left(\frac{\epsilon_n}{\Delta_n}\right)^2 + 1} - \left(\frac{\epsilon_n}{\Delta_n}\right) \quad , \\ c_{n+1} &= \epsilon_n - \sqrt{\epsilon_n^2 + \Delta_n^2} \quad , \end{aligned} \tag{8.27}$$

and

$$d_{n+1} = c_{n+1} + 2d_n \quad .$$

where, referring back to Eq. (6.6) and Eq. (7.8) we see that $d_0 = -\epsilon/2$. Hopefully, at some state of this process one of the $H_n^{(tr)}$'s will prove to have a ratio of ϵ_n/Δ_n which is solvable or can be handled in perturbation theory. In any event we shall borrow from Wilson and Kadanoff and call the process of generating a new effective Hamiltonian from the one which was obtained in a previous step a "renormalization group transformation." The recursion relations given in (8.26)-(8.27), which define the parameters in $H_n^{(tr)}$ obtained from successive iterations, will be referred to—for want of a better name—as renormalization group equations.

C. Analyzing the Renormalization Group Equations. The preceding discussion reduced the problem of constructing a set of $|\psi_n\rangle$'s by means of a successive thinning out process, to the equivalent problem of computing a series of renormalization group transformations on the coefficients of an effective Hamiltonian. In order to extract all of the information contained in (8.26)-(8.27) the recursion relations must be studied numerically. However, there are several points which can be understood without putting these equations on a computer. First, we note that both (ϵ=0, Δ arbitrary) and (ϵ arbitrary, Δ=0) are fixed points of the renormalization group transformation since in either case $\epsilon_n = \epsilon$ and $\Delta_n = \Delta$ for all 'n'. In fact, we have already seen that both of these cases can be solved exactly and it is easy to convince oneself that our algorithm for constructing the groundstate wave function constructs the exact eigenstate for these two cases. Second, we observe that a great deal of information can be extracted without completely solving the renormalization group equations if we know whether the ratio ϵ_n/Δ_n increases or decreases with successive iterations. In order to see if this happens let us define

$$y_n \stackrel{\text{def}}{\equiv} \left(\frac{\epsilon_n}{\Delta_n}\right) \tag{8.28}$$

and going back to (8.26)-(8.27) we see that 'y_{n+1}' is a function of 'y_n' alone. To be precise

$$y_{n+1} = \frac{2\left(\sqrt{1+y_n^2} - 1\right)\left(1 - 2y_n\left(\sqrt{1+y_n^2} - y_n\right)\right)}{\left(1 + \sqrt{1+y_n^2} - y_n\right)^2} \stackrel{\text{def}}{\equiv} F(y_n) \tag{8.29}$$

If we now wish to see if $y_n = \epsilon_n/\Delta_n$ increases or decreases with each iteration we need only study the function

$$R(y) \stackrel{\text{def}}{\equiv} F(y) - y \tag{8.30}$$

and see what it looks like for all 'y'. R(y) is plotted in Fig. 7, and we obtain useful information from the general shape of the curve alone. For example, since a "fixed point" of the transformation is a value of ϵ and Δ which reproduces itself under the renormalization group transformation, we must have that $F(y) = F(\epsilon/\Delta) = 0$, unless of course $\epsilon/\Delta = \infty$ and then $F(\infty) > 0$ cannot reduce this value. Hence Fig. 7 shows that there are three fixed points for our transformation;

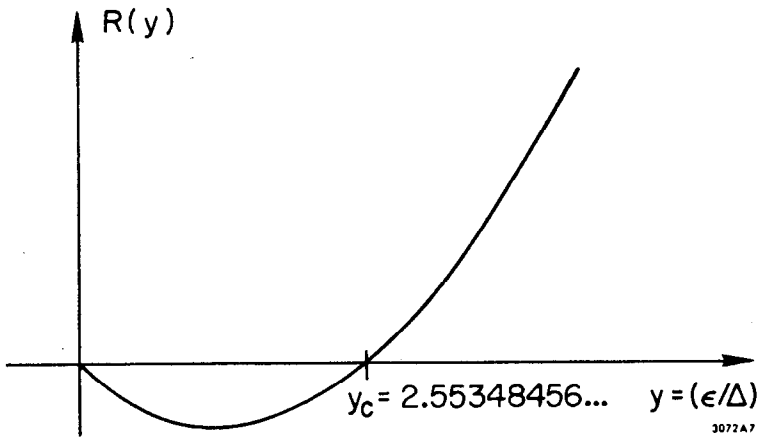

Fig. 7

namely, $\epsilon/\Delta=0$, $\epsilon/\Delta=\infty$ and $\epsilon/\Delta=2.55348456\ldots$. Actually, $F(y)=0$ only requires that the ratio (ϵ/Δ) is unchanged by the iteration and so if $\epsilon_{n+1}=\lambda\epsilon_n$ and $\Delta_{n+1}=\lambda\Delta_n$, i.e., if the Hamiltonian reproduces itself up to an overall scale factor, we will also have a zero of $F(y)$. As we have seen $y=0$ and $y=\infty$ are true fixed points of (8.26)–(8.27), and more careful analysis shows that $y=2.55\ldots$ is a point at which the Hamiltonian is reproduced up to a scale factor λ (y_c), which is another critical constant of the theory.

There is additional qualitative information which can be extracted from $F(y)$. In particular, $F(y)=0$ implies that the ratio (ϵ/Δ) decreases for that iteration and so the new (ϵ'/Δ') or y' lies to the left of the y we started with. Since, as shown in Fig. 7, $F(y)$ is negative for $y<y_c$ we see that if we start at any point in this range successive iterations of our truncation procedure will drive us to form for the effective Hamiltonian which we have studied in perturbation theory. On the other hand, since $F(y)>0$ for $y>y_c$ we conclude that successive iterations drive us to $y=\infty$ which implies $\Delta/\epsilon>>1$ which is another form of the Hamiltonian which we have studied in perturbation theory. Hence we conclude that all theories for which $y<y_c$ are theories with a degenerate groundstate, etc.; whereas, all theories for which $y>y_c$ are theories with a unique groundstate. Clearly y_c is the point at which the nature of the groundstate changes, and so y_c is the <u>critical point</u> of this theory. Note, that the result $y_c=2.55348\ldots$ is obtained from our simple procedure is not too bad since $y_c^{(exact)}=2$ is the exact answer. The fixed points $y=0$ and $y=\infty$ are usually referred to the stable fixed points of the <u>renormalization group transformation</u> and the fixed point at $y=y_c$ is called an <u>unstable fixed point</u>. Notice, the fact that at $y=y_c$ the Hamiltonian continues to reproduce itself up to a scale factor says that at a critical point the physics going on at different length scales is essentially the same.

Certainly, there is more information to be gleaned from the recursion relations in (8.26)-(8.27) than one obtains from plotting F(y) alone. In particular, these relations allow us to compute ϵ_n and Δ_n separately. If one examines the result of iterating (8.24)-(8.27) one finds that for initial values, $\epsilon_0/\Delta_0 < y_c$, the successive renormalization group transformations lead to $\lim_{n\to\infty} \epsilon_n = 0$ and $\lim_{n\to\infty} \Delta_n = \Delta_\infty(\epsilon_0/\Delta_0) \neq 0$, whereas for $(\epsilon_0/\Delta_0) > y_c$, $\lim_{n\to\infty} \epsilon_n = \epsilon_\infty(\epsilon_0/\Delta_0) \neq 0$ and $\lim_{n\to\infty} \Delta_n = 0$. The next question is how to use this information to calculate the order parameter $<\sigma_x(j)>$.

The answer to this question is easily divined once one realizes that as we carry out a succession, say N, renormalization group transformations we are effectively finding, by direct construction, those two states within a block of size $(2)^N$-sites which have the lowest energy. Now, for $y < y_c$, in the limit $N\to\infty$ we have shown $\epsilon_N \to 0$ and $\Delta_N \to \Delta$, and so the two states we construct in this limit are degenerate. Since we construct these states by keeping one state which is even under U and one state which is odd, we need only refer to our discussion of exact results, in particular Eq. (7.5), to see that the quantity we want to compute is

$$\lim_{N\to\infty} <\psi^N_{even}|\sigma_x(j)|\psi^N_{odd}> \stackrel{def}{\equiv} <\sigma_x(j)>$$

Going back to the discussion leading to (8.20) we see that because $\left[\sigma_x(j)\right]^{tr}$ is a purely off-diagonal 2×2-matrix calculating $<\psi^{(1)}_{even}|\sigma_x(j)|\psi^{(1)}_{odd}>$ is the same as computing

$$\left[\sigma_x(j)\right]^{1st\text{-}trunc.} = \frac{(1+a_1)}{\sqrt{2(1+a_1^2)}}\begin{pmatrix}0 & 1\\ 1 & 0\end{pmatrix} = \sqrt{\frac{\Delta_1}{\Delta_0}}\begin{pmatrix}0 & 1\\ 1 & 0\end{pmatrix} \tag{8.31}$$

Hence in sucessive transformations we find that

$$\left[\sigma_x(j)\right]^{Nth\text{-}trunc.} = \prod_{p=1}^{N}\sqrt{\frac{\Delta_p}{\Delta_{p-1}}}\begin{pmatrix}0 & 1\\ 1 & 0\end{pmatrix} = \sqrt{\frac{\Delta_n}{\Delta_0}}\begin{pmatrix}0 & 1\\ 1 & 0\end{pmatrix} \tag{8.32}$$

This argument therefore tells us that if $\Delta_\infty \equiv \lim_{N\to\infty} \Delta_n$ then the order parameter for a theory such that $y_0 = \epsilon_0/\Delta_0 < y_c$, is given by

$$\tilde{f}\left(\frac{\epsilon_0}{\Delta_0}\right) = \sqrt{\frac{\Delta_\infty}{\Delta_0}} \quad . \tag{8.33}$$

Explicit numerical iteration of (8.26)-(8.27) shows that a very good fit to

$$\tilde{f}\left(\frac{\epsilon_0}{\Delta_0}\right) = \tilde{f}(y_0) = \left(1 - \left(\frac{y}{y_c}\right)^2\right)^{.39} \tag{8.34}$$

with $y_c \cong 2.55348456\ldots$. Considering that we have been so crude in our calculations the agreement of this with the exact answer

$$\tilde{f}_{exact}(y) = \left(1 - \left(\frac{y}{2}\right)^2\right)^{.125} \tag{8.35}$$

is not too bad.

Nevertheless, the advertised virtue of this method is that one gets a good nuts and bolts feeling for what is going on and so one can see how to do better. In the next section we will show how a simple modification of our approach does produce a significant improvement in results.

D. Nonperturbative Analysis: A More Sophisticated Algorithm. Now that we have seen how a variational procedure based upon successive truncation of a space of "linear trial wave functions" leads one to a renormalization group transformation, let us go on to analyze how one can modify our truncation algorithm to produce better results. In this case "better" will mean a better calculation of the groundstate energy and a better calculation of the general behavior of the order parameter $<\sigma_x(j)>$. Actually, we will find that we worsen the prediction of the critical temperature in the process. We are pretty sure that we know why this happens and I will try to explain the reason in more detail at a later point in our discussion. In any event, the improvement in critical exponent by a factor of 2 and the improvement in the qualitative behavior of the groundstate energy

density with respect, y, is even more dramatic. We will see this when we plot $-\partial^2 \mathcal{E}_0/\partial y^2$ and observe that the calculation I am about to describe can see that $\mathcal{E}_0(y)$ possesses a singularity in its second derivative at the critical point—a result which cannot be obtained from a more naive calculation.

As interesting as these results are, however, I do not wish to focus your attention too closely on them. The key point I wish to make in this discussion is that the variational technique based upon the use of linear trial wave functions can be systematically improved upon and that the procedure for implementing this methodically is not much more difficult than the original naive procedure.

To begin, let us note that there are in fact two distinctly different pieces to our algorithm, both susceptible to change and improvement. First we committed ourselves to grouping lattice sites into boxes containing two sites each. We then constructed "box states" and thinned out our complete set by throwing away two out of the four possible states per box. Clearly we could easily generalize this approach both by grouping things into bigger boxes and by keeping more states. However, for now let us assume that this part of our procedure will be left unmodified so that successive truncations of our space of trial wave functions shall always lead to an effective Hamiltonian of the same form as the original one. Having committed ourselves to this procedure, let us turn to the question of improving upon our algorithm for throwing away states. Obviously, although our algorithm for throwing away states based upon a diagonalization of the appropriate two site Hamiltonian is intuitively appealing, it is by no means sacred. Moreover, it certainly neglects important physics. This notion is completely born out if one looks at the argument between the exact answer and the simple method for small ϵ/Δ.

Under these conditions the question becomes "what can we do to correct these defects?" The answer is "adopt a procedure which keeps these small effects." In order to develop such a procedure let us recall that once we noted the invariance of the theory with respect to the transformation U we were led to classify states according to their U eigenvalues. Hence we divided the "box" states into two classes; e.g., $\{|\uparrow\uparrow>, |\downarrow\downarrow>\}$ and $\{|\downarrow\uparrow>, |\uparrow\downarrow>\}$. We then decided to adopt a procedure for choosing one state from each class and truncated H with respect to this choice. The first question to raise is "Why choose a member from each class? Why not choose two members from the same class?" If we did this we would immediately find that, since $\sigma_x(j)$ cannot link members of the same class, at the first iteration the term Δ_1 would be zero and then H_1 could be exactly diagonalized. It would then be trivial to show this procedure would be constructing a poor class of variational wave functions since the remaining box-box interactions would be rendered inoperative and therefore would not be available for lowering the energy. This argument tells us that we must choose one member of each class, but does not tell us which member to choose.

It is apparent that the most general procedure we could adopt is to decide to form two states

$$|\psi_0> = \cos(\theta)|\downarrow\downarrow> + \sin(\theta)|\uparrow\uparrow>$$

and (8.36)

$$|\psi_1> = \cos(\phi)|\downarrow\uparrow> + \sin(\phi)|\uparrow\downarrow>$$

and compute the new truncated Hamiltonian in terms of the unknown angles θ, ϕ. This would lead to an effective Hamiltonian H_1 of the form

$$H_1 = \sum_p \Big[c_1(\epsilon_0, \Delta_0, \theta, \phi) \begin{pmatrix} 1 & 0 \\ 0 & 1 \end{pmatrix}(p) + \epsilon_1(\epsilon_0, \Delta_0, \theta, \phi) \begin{pmatrix} 0 & 0 \\ 0 & 1 \end{pmatrix}(p) - \Delta_1(\epsilon_0, \Delta_0, \theta, \phi) \begin{pmatrix} 0 & 1 \\ 1 & 0 \end{pmatrix}(p) \begin{pmatrix} 0 & 1 \\ 1 & 0 \end{pmatrix}(p+1) \Big] \quad (8.37)$$

where

$$c_1 = \epsilon_0 - (\epsilon_0 \cos(2\theta) + \Delta_0 \sin(2\theta)) \quad (8.38)$$

$$\epsilon_1 = \epsilon_0 \cos(2\theta) + \Delta_0(\sin(2\theta) - \sin(2\phi)) \quad (8.39)$$

and

$$\Delta_1 = \Delta_0 \cos(\theta - \phi) \sin(\theta + \phi) \tag{8.40}$$

Clearly this procedure could be worked out without deciding upon θ and ϕ in advance. In fact, on general grounds one would expect that a different choice of θ and ϕ to be appropriate for different values of ϵ and Δ. Since each renormalization group transformation produces new values of ϵ_n and Δ_n, we probably should assume that θ and ϕ are arbitrary functions of ϵ and Δ. In this way we make an essentially independent choice of θ and ϕ at each iteration. Once one allows this freedom in the choice of θ and ϕ at each stage of the calculation, the question becomes one of adopting a physical criterion for fixing these two functions. To do this we will make use of a clever observation made by Bob Pearson at FNAL. He suggested we choose $\theta(\epsilon, \Delta)$ and $\phi(\epsilon, \Delta)$ to be functions of ϵ_n/Δ_n) alone, since the overall scale of the Hamiltonian could not matter, and then work out the renormalization group transformations in terms of $\theta(\epsilon/\Delta)$ and $\phi(\epsilon/\Delta)$. If we adopt this prescription we can write the result of the n+1st renormalization group transformation as

$$H_{n+1} = \sum_p \left[d_{n+1} \begin{pmatrix} 1 & 0 \\ 0 & 1 \end{pmatrix}(p) + \epsilon_{n+1}(\epsilon_n, \Delta_n) \begin{pmatrix} 0 & 0 \\ 0 & 1 \end{pmatrix}(p) \right.$$
$$\left. - \Delta_{n+1}(\epsilon_n, \Delta_n) \begin{pmatrix} 0 & 1 \\ 1 & 0 \end{pmatrix}(p) \begin{pmatrix} 0 & 1 \\ 1 & 0 \end{pmatrix}(p+1) \right] \quad ; \tag{8.41}$$

where

$$c_{n+1} = \epsilon_n - (\epsilon_n \cos(2\theta(\epsilon_n/\Delta_n)) + \Delta_n \sin(2\theta(\epsilon_n/\Delta_n))) \tag{8.42}$$

and

$$d_{n+1} = 2d_n + c_{n+1} \quad ,$$

$$\epsilon_{n+1} = \epsilon_n \cos(2\theta(\epsilon_n/\Delta_n)) + \Delta_n(\sin(2\theta(\epsilon_n/\Delta_n)) - \sin(2\phi(\epsilon_n/\Delta_n))) \tag{8.43}$$

and

$$\Delta_{n+1} = \Delta_n \cos(\theta(\epsilon_n/\Delta_n) - \phi(\epsilon_n/\Delta_n)) \sin(\theta(\epsilon_n/\Delta_n) + \phi(\epsilon_n/\Delta_n)) \quad . \tag{8.44}$$

To fix the unknown functions $\theta(\epsilon/\Delta)$ and $\phi(\epsilon/\Delta)$ we decide at some stage, N, to compute the groundstate energy of H_N, and require that the arbitrary functions θ and ϕ be chosen to minimize this quantity. In order to give a more explicit formulation of this idea let us examine Eqs. (8.42)-(8.44). We can easily convince ourselves that ϵ_n and Δ_n stay bounded in magnitude at least under a wide class of choices of $\theta(\epsilon/\Delta)$ and $\phi(\epsilon/\Delta)$—but that the term proportional to d_{n+1} increases by a power of 2 for each iteration. Hence, for N sufficiently large this term swamps the remainder of the Hamiltonian. This divergence in the coefficient of the unit matrix is just the renormalization group transformation's way of telling us that translation invariance of the groundstate implies that its energy is proportional to the volume of the lattice times a finite number, $\mathscr{E}_0$. This number, $\mathscr{E}_0$, is called the groundstate energy density. Since ϵ_n and Δ_n do not grow with this factor of 2^N, and since each point of the effective Nth-lattice is 2^N-points in the original lattice, it is not hard to convince yourself that the energy density is the limit

$$\mathscr{E}_0 = \lim_{N \to \infty} \left(\frac{1}{2^N} d_N \right) \tag{8.45}$$

or, from (8.42),

$$\mathscr{E}_0 = \lim_{N \to \infty} \sum_{n=0}^{N} \left(\frac{c_n}{2^N} \right) \quad . \tag{8.46}$$

A precise statement of our full procedure is to first parametrize the two unknown functions $\theta(\epsilon/\Delta)$ and $\phi(\epsilon/\Delta)$ in terms of a small number of unknown parameters. Next, carry out the recursion implied by (8.45) and (8.46)—say one hundred times—in order to compute the groundstate energy density, to one-part in $(2)^{100}$. This gives us $\mathscr{E}_0^{(N=100)}$ as a function of the unknown parameters, so we finally vary over these parameters to minimize $\mathscr{E}_0^{(N=100)}$. By this procedure the "renormalization group" algorithm, as well as all quantities of interest, are constructed by a variational procedure. Hence, the only arbitrary

input is the choice of the way in which we group sites and the general choice of the number of states we decide to keep.

E. A Discussion of Results. It will surprise no one that the procedure just outlined must be carried out numerically, but this is done quite easily and Figs. 8-10 summarize the results of a simple two parameter calculation done for the starting Hamiltonian

$$H_0 = \sum_j \left[-\frac{\epsilon_0}{2} \begin{pmatrix} 1 & 0 \\ 0 & 1 \end{pmatrix}(j) + \epsilon_0 \begin{pmatrix} 0 & 0 \\ 0 & 1 \end{pmatrix}(j) - \Delta_0 \sigma_x(j)\, \sigma_x(j+1) \right] \tag{8.47}$$

Because of a symmetry argument based upon invariance of H_0 under any reflection taking the lattice into itself we chose to fix $\phi(\epsilon/\Delta)$ to be a constant equal to $\pi/4$. Therefore, only $\theta(\epsilon/\Delta)$ had to be determined. The choice of $\theta(\epsilon/\Delta)$ was constrained by the fact that for $\epsilon=0$ and any Δ we know that choosing $\theta(\epsilon/\Delta=0)=\pi/4$ leads to a construction of the exact wave function; and the same is true, if for $\Delta=0$, we make the choice $\theta(\epsilon/\Delta=\infty)=0$. These considerations led us to parametrize $\theta(\epsilon/\Delta)$ as:

$$\theta(\epsilon/\Delta) = \frac{\pi}{4}\left[1 - \frac{(\tanh(\rho(\epsilon/\Delta) - u) - \tanh(-u))}{(1 - \tanh(-u))}\right] \tag{8.48}$$

since this function is $\pi/4$ at $\epsilon/\Delta=0$ and vanishes as $\epsilon/\Delta \to \infty$. The parameters ρ and u were the free parameters with respect to which we minimized the ground-state energy density, (8.46). In Fig. 8 we show a comparison of our calculation of the groundstate energy density to the exact answer. Values of ϵ smaller than 1 and greater than 3 are suppressed because for these regions agreement is much better than one-part in 10^3. Examination of these curves shows that our worst disagreement with the exact answer is on the order of 3%. This is a significant improvement over the naive calculation. In Fig. 9 we compare our computation of $f(\epsilon/\Delta)$ with the exact answer. As shown the critical value of ϵ/Δ is now at $(\epsilon/\Delta) \cong 2.75$ which is, as we noted at the outset, somewhat worse than the naive calculation. Interestingly the form of $f(\epsilon/\Delta)$ can be fit to a power law

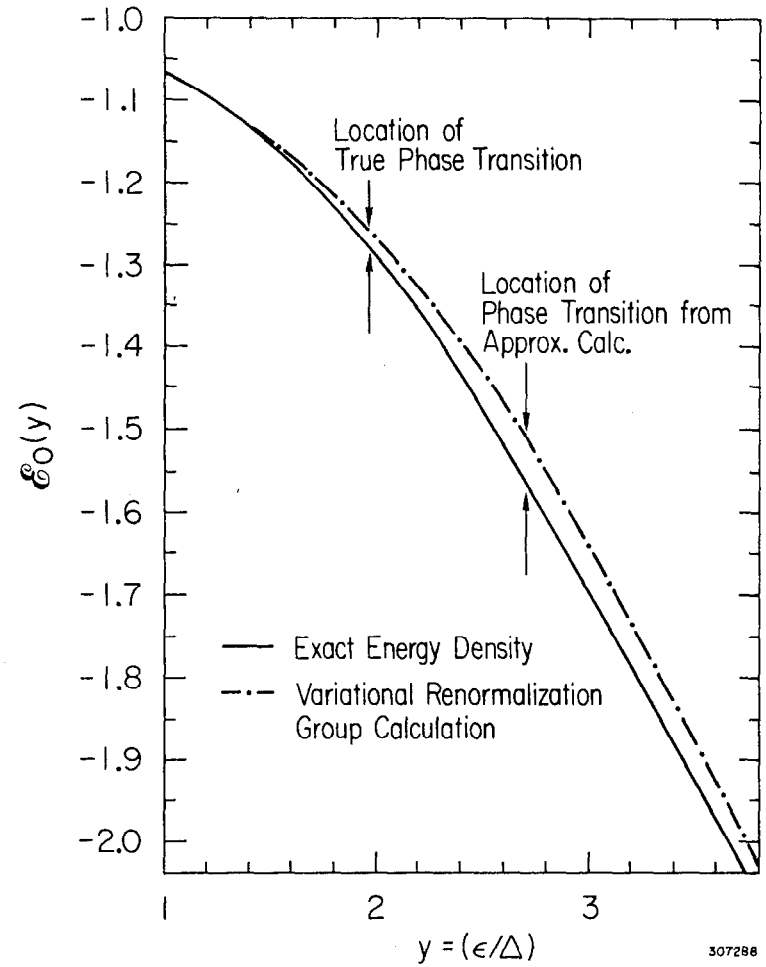

Fig. 8

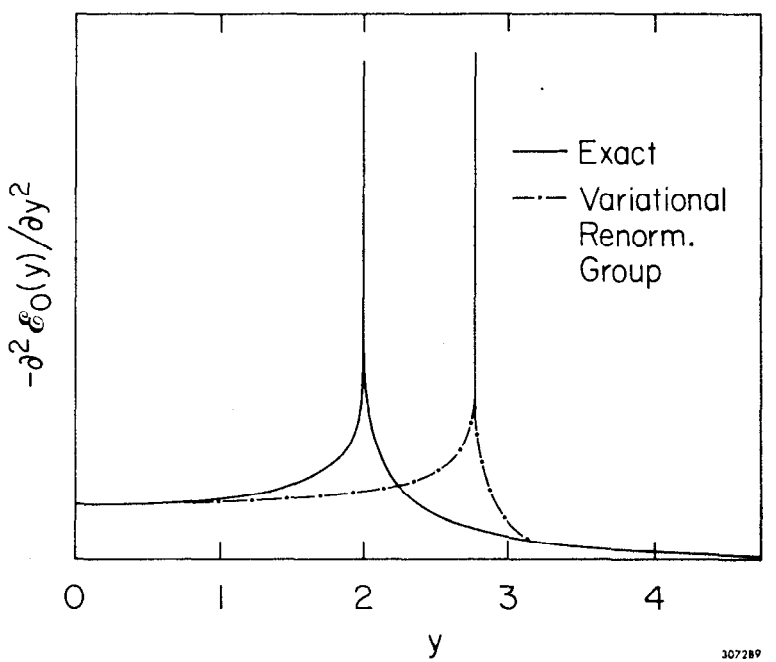

Fig. 9

of the form

$$\tilde{\gamma}(\epsilon/\Delta) = \left(1 - \left(\frac{y}{y_c}\right)^2\right)^{.21}$$

Note that the critical exponent of 0.21 is a significant improvement over the naive approximation answer of 0.4. I want to emphasize that these calculations are the simplest ones I could think of doing to demonstrate the method and can clearly be improved upon by improving the choice of $\theta(\epsilon/\Delta)$. Surprisingly, even five parameter variation forms for $\theta(\epsilon/\Delta)$ doesn't improve the calculation of the critical point much, although the critical exponent becomes smaller ≈ 0.17. There seems to be a good physical reason for this which is related to the fact that because we work on two sites the function $\phi(\epsilon/\Delta)$ becomes trivial for symmetry reasons, and so the eigenstates of U corresponding to +1 and -1 are not being treated equally. Intuitively, what one would guess is that in order to get the best possible groundstate energy density below the critical point the renormalization group calculation wants to make (ϵ/Δ) small as rapidly as possible, so that Δ approaches its fixed form as quickly as possible. If both $\theta(\epsilon/\Delta)$ and $\phi(\epsilon/\Delta)$ could both vary this could be accomplished while at the same time allowing each individual level to attain a lower energy. Since, however, $\phi(\epsilon/\Delta)$ is forced to be $\pi/4$ as a consequence of the aforementioned symmetry property of the two site truncation process, $\theta(\epsilon/\Delta)$ has to behave somewhat incorrectly in order to produce the best groundstate energy. This artificial situation doesn't arise if one works with blocks of three sites at a time, a procedure which has many other theoretical arguments to recommend it. A computation of this sort based on a 3-site block is quite straightforward, and will be carried out in the near future to see if our understanding of what is really happening is as good as I am arguing it is.

Finally let us discuss the curves shown in Fig. 10. As shown the ground-state energy density has the property that ∂^2 (groundstate energy density/$\partial\epsilon^2$ exhibits a singularity at y_c=2, the true critical point. This is really quite a subtle property of the theory and as you can see our variational results also exhibit a singularity at the calculated critical point. Moreover there seems to be, given the crudeness of our procedure, remarkable similarity in the general shape of the curves. It is worth noting that the naive renormalization group procedure discussed first misses this singularity completely.

IX. "SMOOTH-TALK", OR "WHERE DO WE GO FROM HERE?"

The preceding discussion completes our analysis of the "toy model." I would like to spend the remainder of this talk summarizing what I hoped you learned from this discussion and relating it to other already published work which we have done at SLAC.[3] In a sense, these papers on strong coupling lattice theories, should have followed the discussion I have just presented—and so you might think of this talk as paper 0 in our series.

As I indicated at the outset my real interest in the "toy model" I analyzed by the variational—or "renormalization group"—methods was not in the physics of the model but rather in the methods themselves. Hopefully, from this example you have been immediately led to generalize the technique to any field theory; nevertheless, at the risk of overstating the obvious, allow me to list those points which I feel summarize the important features of our discussion.

First we argued that to begin analyzing nonperturbative effects in any field theory one must formulate the theory in a way which does not implicitly make use of the weak coupling expansion. We contended—without giving the proof—that one way to do this was to formulate the theory with a volume and momentum cutoff, a procedure which is completely equivalent to formulating the theory on a lattice.

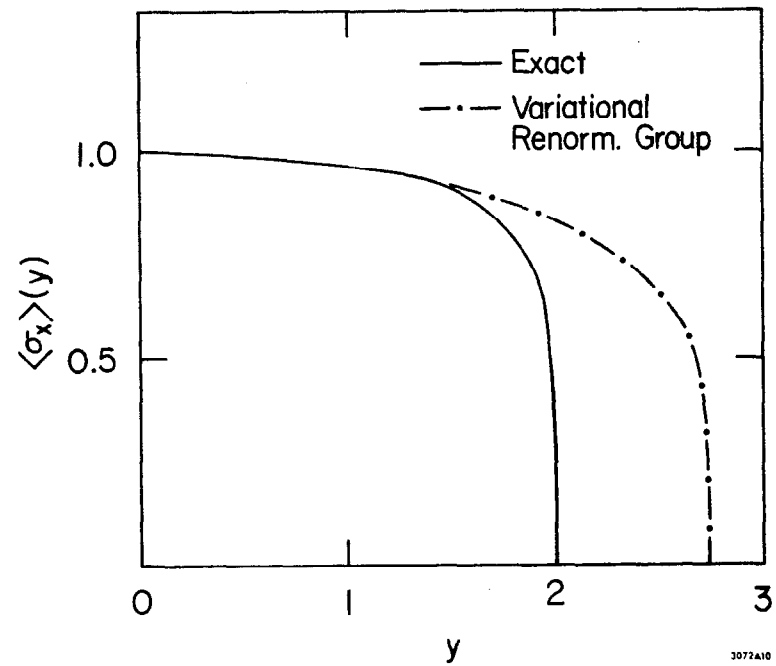

Fig. 10

Second, we argued one could study the resulting lattice problem by variational methods. We then showed that a variational procedure which could be adopted was one based upon linear trial wave functions, and we showed that the problem of finding a good basis for constructing such trial-wave functions was equivalent to a renormalization group calculation in which the renormalization group itself had to be determined by means of a variational procedure. In effect, the arbitrary input to a calculation was the way in which one grouped single sites into blocks of sites and the assumption of how many states one keeps at each truncation.

Having derived the specific form of the renormalization group transformations for the set of assumptions made in the second step, the next question is to analyze what happens to the form of the truncated or effective Hamiltonian as we thin out our family of linear trial wave functions. As we saw in the specific example, the key first point to understand in these transformations is what happens to the strength of the gradient (site-site recoupling) terms relative to the single-site terms in the Hamiltonian.

Quite generally, it proves useful to study the function which gives the change in the ratio of the single-site couplings to the gradient after a finite number (one or a thousand) interactions, since, as we saw in our "toy model" one can tell a great deal about qualitative features of a theory from this information alone. Suppose, for the sake of argument, we assume that there is only one single-site coupling constant in a theory. Then, defining 'y' to be the strength of the single-site coupling to the gradient term, we can plot the general form of the function R(y) = (change of y in finite number of iterations). A few examples of imaginable R(y)'s are given in Figs. (11a)-(11c) so that we may make a few general remarks about what one would conclude from each picture.

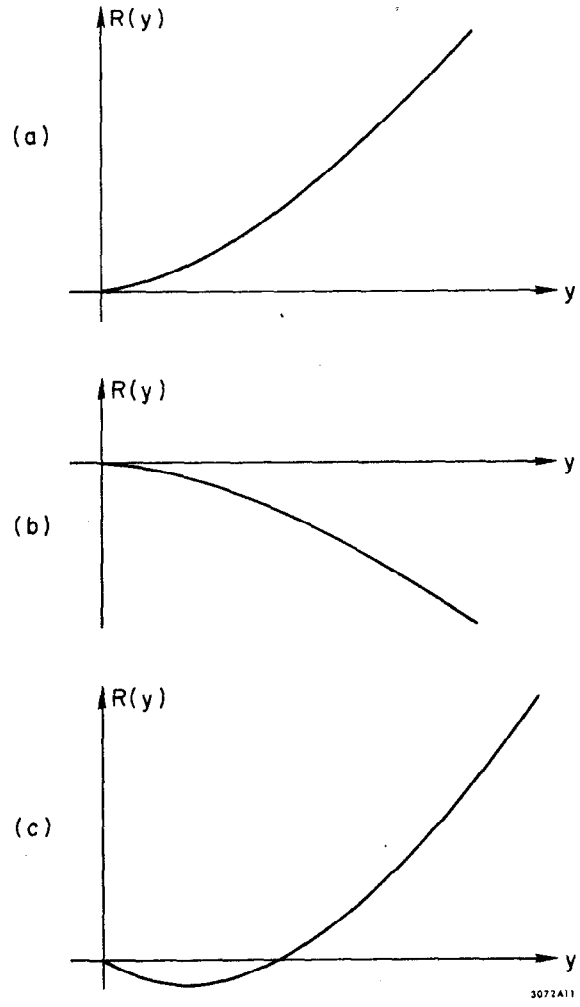

Fig. 11

In Fig. 11a we see that $R(y) \geq 0$ for all values of $0 \leq y \leq \infty$. If a theory has this sort of R(y) we can conclude two things. First, the points y=0 and y=∞ are the only fixed points of the theory. The Hamiltonian at y=0, i.e., zero coupling constant, is a "free field theory," and can be presumably solved exactly, the y=∞ Hamiltonian is solved by solving the single-site Schrœdinger problem. Second, we observe that if we start at some finite value of y successive iterations drive us to larger value of y (i.e., $R(y) > 0$) hence, eventually our problem can be studied by treating the gradient terms as a perturbation on the single-site terms. Hence, in any theory for which $R(y) > 0$ we can conclude that the low energy (or long-wavelength) physics is described by an effectively strong-coupling constant Hamiltonian. One other thing which follows from this discussion is that the mass gap in such a theory will be given by calculating the gap between the first two eigenstates of the effective single-site Schrœdinger problem, and will, therefore, be a function of the effective single-site coupling "g_∞". In general, since the scale of H_0 is set by the cutoff Λ, this means that the lowest mass gap in the theory will be $\approx \Lambda g_\infty$ and so to have practical Lorentz invariance—which we will take to mean that the scale of physical masses should be negligible with respect to the maximum momentum—we are only interested in theories for which $g_\infty \ll 1$, or in other words $g_\infty \Lambda \approx 1$ GeV (for the sake of argument). Since the Hamiltonian at a fixed point reproduces itself up to a scale factor, if one finds a critical point (or fixed point) for which this scale factor, ρ, is less than unity, then by iterating the overall scale of H_N as $N \to \infty$ is $\Lambda \rho^N$. This tells us that the critical theory has no mass gap. This also implies that choosing y close enough to the critical point guarantees that for the first M iterations, H_M, will stay fixed up to a factor of ρ^M and then it will start changing rapidly to its limiting form. Therefore, heuristically we argue that in order to get a practically relativistic theory one needs to start from a value near this fixed point so as to get a scale for $H^M = \rho^M \Lambda \approx 1$ GeV.

It follows from this discussion that for a case like Fig. 11a one need only compute the parameter ρ for the case y=0 to decide whether or not a "practically relativistic" limit exists for the theory in question. If $\rho < 1$ then one can take the cutoff Λ arbitrarily large keeping the mass of the lowest states fixed by taking the original "bare" coupling towards zero as a function of Λ. This would therefore be an example of a theory whose short distance behavior is "free" but whose long wavelength behavior is not.

If we next look at R(y) for Fig. 11b we come up with the opposite conclusion. If $R(y) < 0$ then each successive set of N-iterations will make it smaller. Hence the large wavelength or low energy physics of this theory is given by weak coupling perturbation theory, whereas the single-site or short distance behavior is governed by a strong coupling constant.

Figure 11c tells us that the two different cases can occur depending upon the starting value for y, i.e., whether $y_0 < y_c$ or $y > y_c$. This is of course the form of R(y) calculated for our toy model and so I can refer you back to our discussion of the way in which the exact case leads to an effectively relativistic theory in order to clarify the kind of information you can get from this picture.

Finally, we have reached the point in our discussion where we can understand why the material in Ref. 3 is relevant. As we have seen for cases (11b) and (11c), after a large number of iterations, it becomes necessary to know the solution of the strong coupling lattice theory. The discussion we give (we, meaning Drell, Yankielowicz, and me) for the case of strong coupling fermion theories on a lattice was to show that if a renormalization group calculation of self-coupled fermion, or color-gauge theories leads us to an R(y) of the form shown in Figs. 11b and 11c, then our analysis of these models becomes important. For the case of color gauge theories in particular—where the folklore based upon continuum perturbation theory and asymptotic freedom leads us to conjecture that

Fig. 11b is the relevant form of R(y)—the fact that the infinite or very large coupling analysis of the color gauge theory leads to a "zeroth order spectrum" of physical particles makes the need to study these theories more carefully even greater. To summarize, although much remains to be done along the lines presented in this talk, the analysis of Ref. 3 tells us that if we are lucky the large distance behavior of lattice color gauge theories of strong interactions could be very, very amusing.

APPENDIX A

A. On the Equivalence of Cutoff and Free Field Lattice Theories.

Case I: Boson theory: As an example of the way in which a continuum field theory can be converted to an equivalent lattice-field theory let us study the two simple cases of (i) a free scalar field, and (ii) a free fermion field. In order to maintain a simple notation I shall work things out for the particular case of one space-one time dimensional theories, the generalization of this trick to higher dimensions is discussed in Ref. 3.

To begin let us consider the free massive scalar field theory defined by the Lagrangian density

$$\mathscr{L}(\phi, \partial_\mu \phi) = \frac{1}{2}(\partial_\mu \phi(x))^2 - \frac{\mu^2}{2}\phi^2(x) \tag{A.1}$$

and the canonical equal time commutation relations

$$\left[\Pi(x,t),\ \phi(y,t)\right] = -i\delta(x-y)$$

where

$$\Pi(x,t) \overset{\text{def}}{\equiv} \frac{\delta \mathscr{L}}{\delta(\partial_0 \phi)} = \partial_0 \phi(x,t) \quad . \tag{A.2}$$

In order to discuss the quantum mechanical theory we proceed canonically to construct the Hamiltonian

$$H = \int_{-\infty}^{+\infty} dx \left\{\Pi(x)\, \partial_0 \phi(x) - \mathscr{L}\right\}$$
$$= \int_{-\infty}^{+\infty} dx \left[\frac{\Pi^2(x)}{2} + \frac{(\nabla\phi(x))^2}{2} + \frac{\mu^2}{2}\phi^2(x)\right] \tag{A.3}$$

maintaining the commutation relations specified in Eq. (A.2).

As promised our first step will be to assume that the theory under consideration is defined in a finite volume, i.e., a box of length L. Hence, we think of the functions $\phi(x)$ and $\Pi(x)$ as defined on the interval $-L/2 \le x \le L/2$ and so we can expand these functions with respect to the complete set of functions, $e^{ik_n x}$, where

$$k_n \overset{\text{def}}{\equiv} \left(\frac{2\pi}{L}\right) n \tag{A.4}$$

for arbitrary integer n. To be specific we write

$$\phi(x) \equiv \frac{1}{\sqrt{L}} \sum_{n=-\infty}^{+\infty} e^{ik_n x} \phi(k_n); \qquad \phi(k_n) = \frac{1}{\sqrt{L}} \int_{-L/2}^{+L/2} dx\, e^{-ik_n x} \phi(x) \tag{A.5}$$

and

$$\Pi(x) = \frac{1}{\sqrt{L}} \sum_{n=-\infty}^{+\infty} e^{+ik_n x} \Pi(k_n); \qquad \Pi(k_n) = \frac{1}{\sqrt{L}} \int_{-L/2}^{+L/2} dx\, e^{-ik_n x} \Pi(x) \tag{A.6}$$

so that

$$H = \sum_{n=-\infty}^{+\infty} \left[\frac{1}{2}\Pi(k_n)\Pi(-k_n) + \frac{\left(k_n^2+\mu^2\right)}{2}\phi(k_n)\phi(-k_n)\right] \tag{A.7}$$

It follows from Eqs. (A.5) and (A.6) that

$$\left[\Pi(k_n), \phi(-k_n)\right] = -i\delta_{k_n, k_m} \quad . \tag{A.8}$$

Although we will not use this fact later it is worth noting that we can transform H to the form of a function of 'k' times a number operator by defining $\omega_k = \sqrt{k^2+\mu^2}$ and writing

$$\phi(k) = \frac{1}{\sqrt{2\omega_k}} \left(a_{-k} + a_k^+\right) \tag{A.9}$$

and

$$i\Pi(k) = \sqrt{\frac{\omega_k}{2}} \left(a_{-k} - a_k^+\right) \tag{A.10}$$

so that

$$\left[a_{k_n}^+, a_{k_m}\right] = \delta_{k_n, k_m} \tag{A.11}$$

so that H becomes

$$H = \sum_n \sqrt{k_n^2+\mu^2} \left(a_k^+ a_k + \frac{1}{2}\right) \tag{A.12}$$

Having collected the formulae needed to discuss a theory in finite volume, we now impose a maximum momentum cutoff by assuming $-k_{max} \leq k_n \leq k_{max}$. The easiest way to define k_{max} is to let $L = (2N+1)a$ where "a" has the dimensions of length and then rewrite Eq. (A.4) as

$$k_n = \frac{2\pi}{(2N+1)a} n \qquad \text{for} \quad -N \leq n \leq N \tag{A.13}$$

In this way we can define the cutoff mass $\Lambda = 1/a$ and for $N \to \infty$, $k_{max} \to \pi\Lambda$. Having adopted these definitions it is a trivial matter to show that the cutoff version of the Hamiltonian defined in Eq. (A.7) is unitarily equivalent to a lattice Hamiltonian. To do this one need only define

$$\frac{1}{\Lambda^{1/2}} \phi(j) = \sum_{n=-N}^{+N} \frac{e^{-i\left(\frac{k_n}{\Lambda}\right) j}}{\sqrt{2N+1}} \phi(k_n)$$

and

$$\Lambda^{1/2} \Pi(j) = \sum_{n=-N}^{+N} \frac{e^{-i\left(\frac{k_n}{\Lambda}\right) j}}{\sqrt{2N+1}} i\Pi(k_n) \tag{A.14}$$

where $-N \leq j \leq N$, and $\phi(j)$ and $\Pi(j)$ are dimensionless.

It is a simple exercise to show that

$$\left[\Pi(j), \phi(j')\right] = -i\delta_{jj'}$$

so this transformation preserves the canonical commutation relations, and that

$$H = \Lambda\left[\sum_j \frac{1}{2}\left(\Pi(j)^2 + \left(\frac{\mu^2}{\Lambda^2}\right)\phi(j)^2\right) + \sum_{j_1 j_2} \frac{D(j_1-j_2)}{2} \phi(j_1)\phi(j_2)\right] \tag{A.15}$$

where

$$D(j_1-j_2) = \frac{1}{(2N+1)} \sum_n \left(\frac{k_n}{\Lambda}\right)^2 e^{i\frac{k_n}{\Lambda}(j_1-j_2)} .$$

Since Eq. (A.15) defines a theory of a scalar field defined on (2N+1) lattice sites we have completed our task of establishing the desired correspondence. Note, the amusing feature of this formulation of the lattice theory is that in the limit $(2N+1) \to \infty$ the only way in which this theory fails to be a relativistic theory is that the spectrum $\sqrt{k^2+\mu^2}$ cuts off a maximum momentum, k_{max}. This completes our discussion of the scalar free field.

APPENDIX B

Free Fermion Case. The continuum finite volume fermionic theory starts from a Hamiltonian

$$H = \int_{-L/2}^{+L/2} dx\ \psi^+(x)\left\{\frac{1}{i}\alpha\nabla + \beta m\right\}\psi(x) \tag{B.1}$$

and canonical equal time anticommutation relations

$$\{\psi^+(x),\ \psi(y)\} = \delta(x-y) \tag{B.2}$$

Proceeding as in the case of the free field we define

$$\psi(x) = \sum_n \frac{e^{ik_n x}}{\sqrt{L}}\,\psi(k_n)\ ; \qquad \psi(k_n) = \frac{1}{\sqrt{L}}\int_{-L/2}^{+L/2} dx\, e^{-ik_n x}\,\psi(x)$$

and

$$\psi^+(x) = \psi(x)^+ = \sum_n \frac{e^{-ik_n x}}{\sqrt{L}}\,\psi^+(k_n) \tag{B.3}$$

where k_n is given by Eq. (A.4). It is then a simple exercise to show that

$$H = \sum_n \psi^+(k)\left\{\alpha\cdot k + \beta m\right\}\psi(k) \tag{B.4}$$

Clearly this can be solved in the usual way by writing

$$\psi(k) = u(k)\,b(k) + v(-k)\,d_k^+ \tag{B.5}$$

where u(k) and v(k) satisfy

$$\begin{aligned}(\alpha k + \beta m)\,u(k) &= E(k)\,u(k)\quad ,\\ (\alpha k + \beta m)\,v(-k) &= -E(k)\,v(-k)\end{aligned} \tag{B.6}$$

with $E(k) = \sqrt{k^2+m^2}$.

Having established the finite volume formulation we now established a k_{max} cutoff as in the boson case and find that the free cutoff continuum model is unitarily equivalent to a lattice Hamiltonian

$$H = \Lambda\left[\sum_{j_1 j_2}\left(-\frac{1}{i}\,\delta'(j_1-j_2)\right)\psi^+(j_1)\,\alpha\psi(j_2) + m\sum_j \psi^+(j)\,\beta\psi(j)\right] \tag{B.7}$$

where

$$\psi(j) = \frac{1}{\sqrt{2N+1}}\sum_n e^{-i\left(\frac{k_n}{\Lambda}\right)j}\,\psi(k)$$

and[8]

$$-\delta'(j_1-j_2) \overset{\text{def}}{=} \frac{1}{(2N+1)}\sum\left[i\left(\frac{k_n}{\Lambda}\right)e^{i\left(\frac{k_n}{\Lambda}\right)(j_1-j_2)}\right].$$

This completes our analysis of the two free fields of interest. Obviously the same procedure leads to an equivalent lattice formulation of any interacting field theory (except for those involving gauge fields where some additional questions arise which will not be addressed in these lectures). Deriving the correct form of the Hamiltonian which is truly equivalent to say cutoff continuum ϕ^4 theory is left as an exercise to the student.

REFERENCES

1. A partial list of people who have worked on this problem is R. F. Dashen, B. Hasslacher, and A. Neven, Phys. Rev. D 10, 4130 (1974); 10, 4114 (1974); 10, 4138 (1974); L. D. Faddeev and L. A. Takhtjan, Dubna report No. E2-7998 (unpublished); A. M. Polyakov, L. D. Landau Institute report (1974) (unpublished); N. Christ and T. D. Lee, Phys. Rev. D 12, 1606 (1975); T. D. Lee and G. C. Wick, ibid. 9, 2291 (1974).
2. W. A. Bardeen, M. S. Chanowitz, S. D. Drell, M. Weinstein, and T. M. Yan, Phys. Rev. 11, 1094 (1975); M. Creutz and K. S. Soh, ibid. 12, 443 (1975).
3. S. D. Drell, M. Weinstein, and S. Yankielowicz, Phys. Rev. D 14, 487 (1976);

4. A review of the ideas of Kadanoff and Wilson can be found in "Lectures on the application of Renormalization Group Techniques to Quarks and Strings," Leo P. Kadanoff, PRINT-76-0772 (Brown). First of five lectures at University of Chicago, "Relativistically Invariant Lattice Theories," K. G. Wilson, CLNS-329 (February 1976, Coral Gables Conference); "Quarks and Strings on a Lattice," K. G. Wilson, CLNS-321 (November 1975, Erice School of Physics); K. G. Wilson and J. Kogut, Phys. Rev. 12, 75 (1974); L. P. Kadanoff, Critical Phenomena, Proceedings of the International School of Physics "Enrico Fermi," Course LI, edited by M. S. Green (Academic, New York, 1972).

5. For a discussion of the ideas of these authors as applied to more physical models, as well as references to earlier works see T. Banks, S. Raby, L. Susskind, J. Kogut, D.R.T. Jones, P. N. Scharbach, and D. K. Sinclair, CLNS-339 (July 1976); J. Kogut, D. K. Sinclair, and L. Susskind, CLNS-336 (June 1976); L. Susskind, PTENS 76/1 (January 1976); L. Susskind and J. Kogut, Phys. Reports 23C, 331 (1976).

6. Exact solutions to the toy model we discuss appear in recent publications of B. Stoeckly and D. J. Scalapino, Phys. Rev. B 11, 205 (1975); D. J. Scalapino and B. Stoeckly, UCSB preprint (May 1976) and an earlier analysis of this model is P. Pfeuty, Ann. Phys. (N.Y.) 57, 79 (1970).

7. R. B. Pearson (private communication, to be published).

8. For the afficiandoes it is worth observing that with the definition of $\nabla\psi$ given in Eq. (B.6) (i.e., $(\nabla\psi)(j) = -\sum\delta'(j-\ell)\psi(\ell)$) the free field spectrum of a fermionic theory is exactly that of the continuum theory. Hence one encounters no doubling of states and one still preserves the full chiral invariance of the massive theory.

OBSERVATION OF NEUTRINO AND ANTINEUTRINO ELASTIC SCATTERING FROM PROTONS*

H. H. Williams

University of Pennsylvania

and

D. Cline, A. Entenberg, W. Kozanecki, A. K. Mann,

D. D. Reeder, C. Rubbia, J. Strait and L. Sulak

Department of Physics
Harvard University
Cambridge, Massachusetts 02138

Department of Physics
University of Pennsylvania
Philadelphia, Pennsylvania 19174

Department of Physics
University of Wisconsin
Madison, Wisconsin 53706

Abstract

We have observed 30 events of the process $\nu p \to \nu p$ with a background expectation of 7 events. The ratio $\sigma(\nu p \to \nu p)/\sigma(\nu n \to \mu^- p)$ is measured to be 0.17 ± 0.05 for $0.3 < q^2 < 0.9$ $(\mathrm{GeV/c})^2$, where $-q^2$ is the square of the four-momentum transfer to the proton. We have also observed 22 events of the process $\bar{\nu} p \to \bar{\nu} p$ with a background expectation of 8 events. The ratio $\sigma(\bar{\nu} p \to \bar{\nu} p)/\sigma(\bar{\nu} p \to \mu^+ n)$ is 0.2 ± 0.1 for the same q^2 interval. These two measurements yield a ratio $\sigma(\bar{\nu} p \to \bar{\nu} p)/\sigma(\nu p \to \nu p) = 0.4 \pm 0.2$, where the error is statistical. This difference between neutrino and antineutrino scattering suggests that the hadronic neutral current displays a significant parity-violating interference and that a purely vector Lorentz structure is unlikely.

The development of renormalizable gauge-invariant theories of the weak interaction and the discovery of weak, neutral current interactions as predicted by them has led to two very exciting predictions: the unification of weak and electromagnetic interactions, and the existence of new quantum numbers. The second prediction, the existence of particles with new quantum numbers, has now been spectacularly confirmed.[1] Nonetheless, it is clear that further verification of the gauge theories and an accurate understanding of the new phenomena will require detailed measurements of neutral current reactions.

Since nature has been sufficiently kind as to provide us with an electromagnetic and charged weak interaction of the simple current-current form, it is natural to anticipate that the weak neutral-current interaction may also be of this form:[2]

$$H' = \frac{G}{\sqrt{2}} \bar{\nu} \gamma_\mu (1 + \gamma_5) \nu \, J_\mu^{NC}.$$

It then remains to determine the space-time (i.e. vector, axial-vector) and isospin properties of the hadronic neutral current J_μ^{NC}.

The elastic scattering of neutrinos (antineutrinos) by protons, $\nu_\mu(\bar{\nu}_\mu) + p \to \nu_\mu(\bar{\nu}_\mu) + p$ is one of the foremost reactions of interest for studying the structure of J_μ^{NC} primarily because of its simplicity. Theoretical predictions[3] for this process are straightforward and do not involve the many model-dependent assumptions that invariably follow when one attempts to predict the cross sections for final states with more than one hadron present. Furthermore, the process is free from "complications" arising from new particle thresholds that may be present at higher energies.

Specifically, if the weak hadronic neutral current has a V, A

Lorentz structure and if one assumes time reversal invariance and the absence of second class currents, the matrix element for $\nu p \to \nu p$ can be written[3] in terms of three form factors g_V, g_A, and f_V,

$$\langle p' \mid J_\mu^{NC} \mid p \rangle \propto \bar{u}_{p'} \left[g_V \gamma_\mu + g_A \gamma_\mu \gamma_5 + i (p + p')_\mu f_V \right] u_p,$$

where p and p' are the initial and final 4-momenta of the proton and each of the form factors is a function only of $-q^2 \equiv (p' - p)^2$. The differential cross section corresponding to this matrix element is

$$d\sigma^{\nu,\bar{\nu}}/dq^2 = \frac{G^2}{4\pi} \left\{ (g_A^2 - g_V^2) q^2 / 2E_\nu^2 + (g_A \pm g_V)^2 \right.$$

$$+ (1 - q^2/2mE_\nu)^2 (g_A \mp g_V)^2$$

$$\left. + (2 - q^2 (m + 2E_\nu)/2mE_\nu^2) \left[(4m^2 + q^2) f_V^2 - 4mf_V g_V \right] \right\}$$

where E_ν is the incident neutrino energy, m is the proton mass, and G is the weak coupling constant. Each term in the expression for $d\sigma/dq^2$ has a different (q^2, E_ν) dependence, thus allowing one to unfold the form factors by measuring the q^2 shape at different E_ν.

Most importantly, the $\nu - \bar{\nu}$ cross section difference

$$d\sigma^{\nu}/dq^2 - d\sigma^{\bar{\nu}}/dq^2 \propto g_A g_V (2 - q^2/2mE_\nu) q^2/mE_\nu$$

directly measures the parity-violating interference term $g_A g_V$. Sensitivity to this difference is largest for $q^2 \sim E_\nu \sim m$, i.e., 1 GeV neutrinos and the $q^2 \approx .5 - 1\ (\mathrm{GeV/c})^2$. On the other hand, the inherent strength of the interaction is most clearly seen at $q^2 = 0$ since $d\sigma/dq^2$ becomes independent of both E_ν and the dipole masses, and is the same for ν's and $\bar{\nu}$'s. It is therefore desirable to measure the differential cross section over as large a range of q^2 as possible.

Previous attempts[4] to measure neutrino elastic scattering have been hampered by high neutron background, poor pion-proton separation, and/or low statistics. The addition of shielding does not necessarily eliminate the neutron background problem because of the presence of ν-induced neutrons in equilibrium with neutrinos. In this experiment the problem is significantly alleviated by using a detector of such large size that ν-induced neutrons can be absorbed or detected through their interactions in the outer regions of the detector.

The experiment was performed at Brookhaven National Laboratory in a "wide-band" horn-focused neutrino beam. Figure 1 shows the calculated ν and $\bar{\nu}$ flux distributions which peak sharply at $E_{\nu,\bar{\nu}} \approx 1$ GeV.[5] The incident ν beam has a time structure reflecting the basic RF structure of the accelerator; namely, 12 pulses of 35 ns duration separated by 220 ns. This time structure is very useful for eliminating background from neutrons produced more than ≈ 20 m from the detector since those neutrons will in general arrive out-of-time with the incident neutrinos.

The target-detector (Fig. 2a) consists of 12 calorimeter modules containing a total of 33 tons of liquid scintillator.[6] Each module (Fig. 2b) is divided into sixteen 19cm x 23cm x 2.6m cells comprising the primary fiducial volume and two 38cm x 46cm x 2.6m cells at the top and bottom which are used as a software veto. For an energy deposition greater than 3 MeV in a given cell, precise timing and the energy depositions are recorded for each tube. Events may be localized to an accuracy of ± 10cm in two dimensions solely from the hodoscopic nature of the calorimeters. Position information in the third dimension, i.e. along the length of the cell, is obtained from the difference in the arrival times of the scintillation light at the phototubes at each end of the cell, and also by comparision of the relative pulse heights from

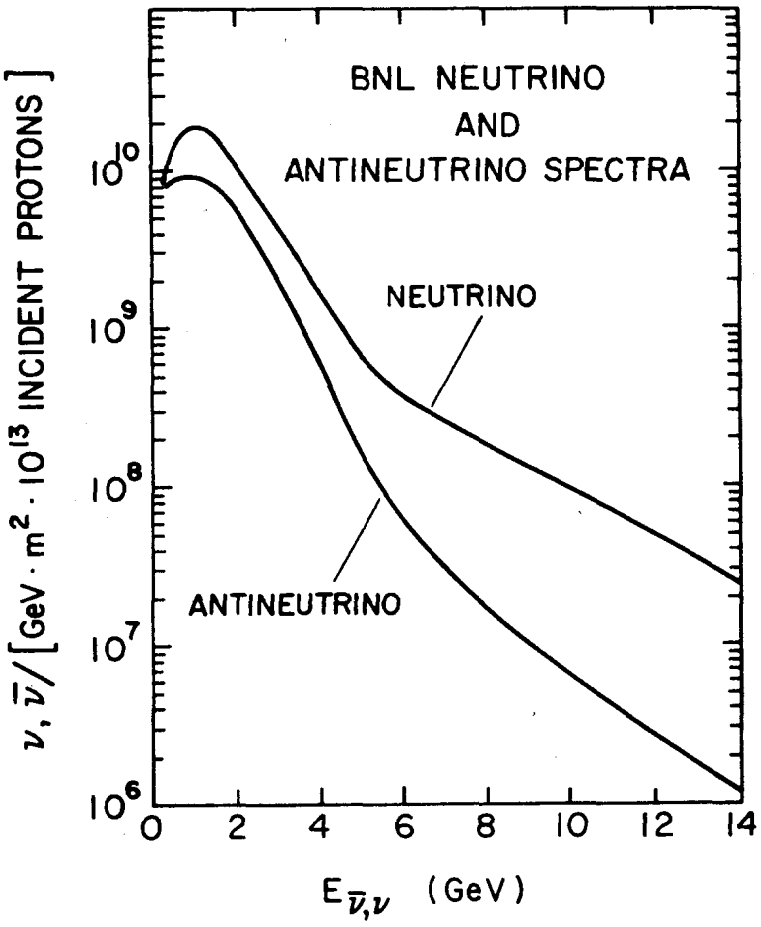

Fig. 1 - Calculated ν and $\bar{\nu}$ spectra for the BNL beam.

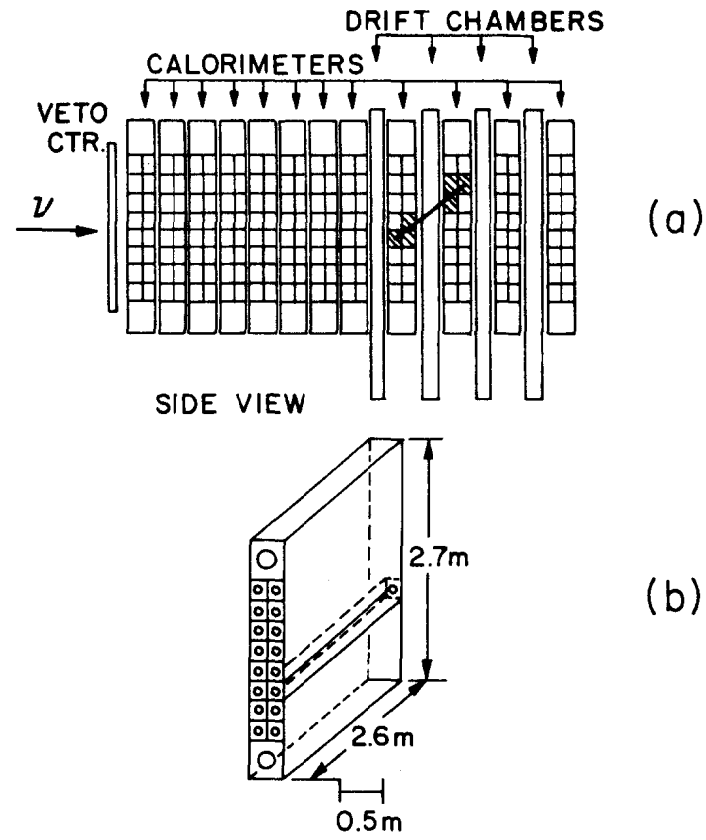

Fig. 2 - (a) Side view of the apparatus showing a typical recoil proton event.
(b) Diagram of a single calorimeter module.

the two phototubes. Each of these techniques yields a position resolution of approximately ± 12 cm.

The front half of the detector utilizes a close packed geometry to be fully sensitive to neutrons and charged particles entering from the sides, top and bottom. For example, a neutron passing through the detector would signal itself by interacting in several, separated cells. The last half of the detector has 4 drift chambers[7] interspersed among the calorimeters. Each chamber contains two x-planes and two y-planes so that the angle as well as position of any tracks exiting from a module may be determined. We have measured a single gap efficiency of 98% for particles with an angle of up to 60° relative to the beam direction. The entire apparatus is housed in a blockhouse of 1.5 m thick heavy concrete to shield against neutrons. A 2.4 m x 3.5 m liquid scintillator counter upstream of the first calorimeter is used to veto charged particles.

The calorimeters and drift chambers are continuously calibrated by accepting beam associated muons along with neutrino induced triggers; in addition, vertical cosmic ray events, recorded between machine bursts, monitor the pulse height and timing of each phototube in the system.

To estimate the cosmic ray background, the detector is enabled between beam bursts for a period of time equal to the duration of the beam spill. None of the events recorded during this gate satisfy the criteria imposed on neutrino-induced candidates.

Candidates for elastic ν scattering have a very simple and clean signature; namely, a single track originating and stopping in the liquid, in time with the RF structure of the accelerator, and whose range and energy loss is consistent with that of a proton. The kinetic energy, T_p, of the proton is directly proportional to the total pulse height in the calorimeters, and for an initial proton at rest, the momentum transfer-squared to the proton is simply $q^2 = 2 M_p T_p$.

The initial selection criterion for neutral current events is containment, i.e. that neither the veto counter nor any cell in the farthest upstream calorimeter fires, and no energy deposition occurs within 40 cm horizontally or 46 cm vertically of the edge of any module nor in the most downstream 20 cm of the detector. From a data sample representing 1.8×10^{18} protons incident on the ν-target, events were selected which contained a single track that originated and stopped in the scintillator, and had an energy greater than 100 MeV.

The distribution of event times, i.e. the time at which an event occurs relative to the time of beam extraction, is presented in Fig. 3a for charged-current ν interactions (not contained) and indicates clearly the RF structure of the ν-beam. Shown in Fig. 3b is a scatter plot of total (kinetic) energy, T, versus the event time measured with respect to the nearest RF bunch for all contained events (for a fraction of the total data sample). For energies > 150-160 MeV, virtually all events are in-time. For T < 150 MeV, there exists a substantial number of out-of-time events, presumably neutron induced. For this reason, and also because the proton-pion separation becomes increasingly ambiguous in this energy region, we have excluded from the analysis those events with T < 150 MeV.

Figs. 4a and 4b show, respectively, a charged-current ν interaction and a proton recoil typical of the candidates for neutrino elastic scattering. The events indicate the extent to which information from

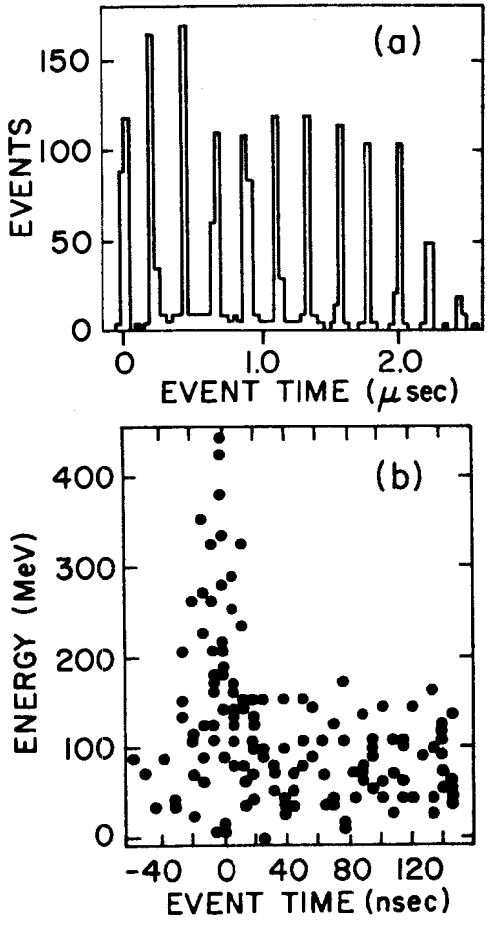

Fig. 3 - (a) Distribution of event times (charged current events) illustrating the time structure of the ν beam.
(b) Scatter plot of total (kinetic) energy vs. event time (modulo 220 ns) for contained events.

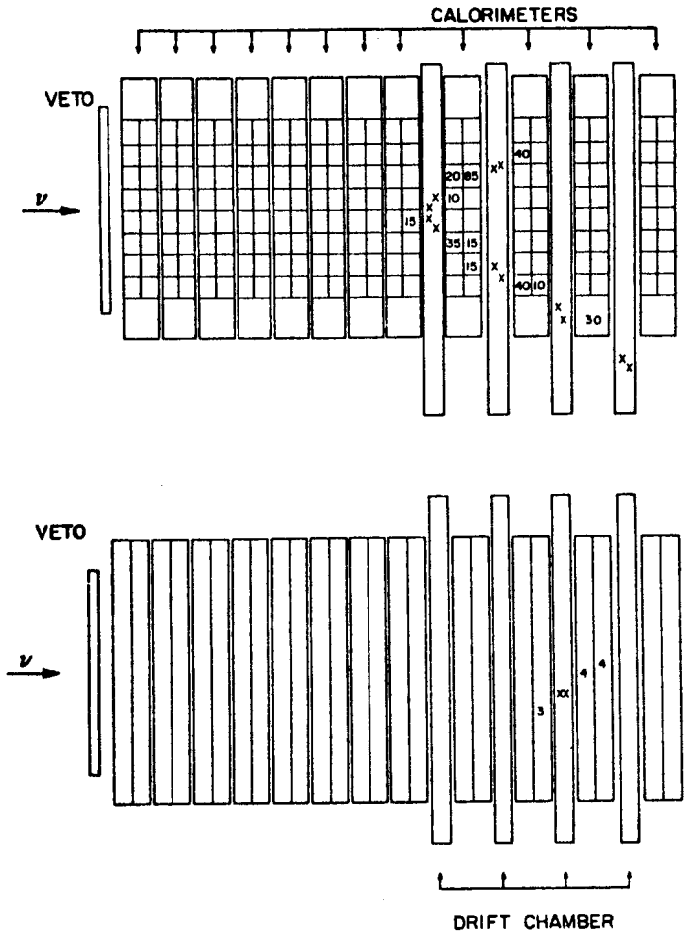

Fig. 4 - (a) Side view of charged current event. The energies deposited in each cell are indicated (in MeV).
(b) Typical candidate (top view) for neutrino-proton elastic scattering. The position of the numbers indicates the position of the track as deduced from the timing information. The value of the numbers indicates which cell fired.

the calorimeters both complements and reinforces the drift chamber information.

For selected single track events, the measured range, the pattern of energy depositions, and the total energy identify the particle. For each event, the total energy and angle of the track are known and it is therefore possible to calculate both the range of the particle and the energy loss expected in each cell (except the first) for either the proton or pion hypothesis; these calculated values are then compared with those observed. Since the range and energy loss for protons typically differ from that for pions by more than a factor of two, the particle identification is relatively unambiguous. For example, shown in Fig. 5 is a plot of range versus energy for events selected as protons. It illustrates that a rather clean identification of protons may be achieved from range information alone. A more quantitative discrimination is achieved by comparison of the calculated and observed energy depositions in each cell, examples of which are shown in Fig. 6. Finally, the results of fits to the proton and pion hypothesis are presented in Fig. 7. The χ^2 is on the average greater than the degrees of freedom because of the Landau distribution and calibration errors. A clear separation occurs, however, for all but 15% of the events.

We obtain in this manner 30 single particle events identified as protons. Fig. 8 shows a plot of event time (module 220 ns) for the selected protons. The distribution is identical to that for charged current events, and strongly supports the view that the protons are neutrino induced. Shown in Figs. 8b, c are the vertex distributions for the proton events along the length of the detector and in the plane normal to the incident beam; within statistical error both distributions are

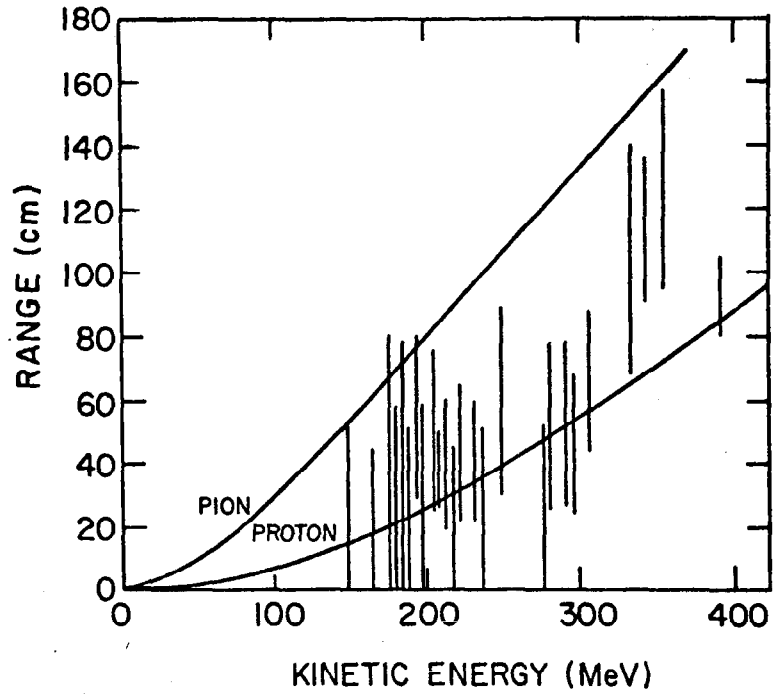

Fig. 5 - Plot of range vs. energy for the selected p events (several events have been omitted for clarity). Each line indicates the measured range of the particle as determined by the number of cells that fire.

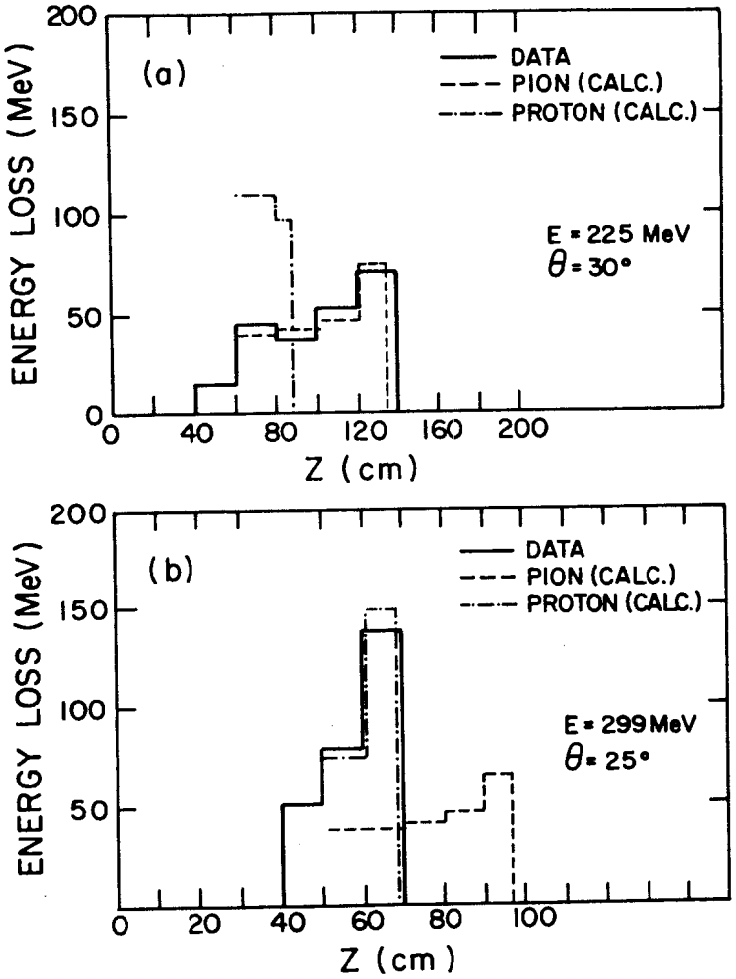

Fig. 6 - Comparison of the observed and calculated energy loss, dE/dz, as a function of z, the coordinate along the ν-beam direction, for pion and proton hypotheses. (a) Pion. (b) Proton.

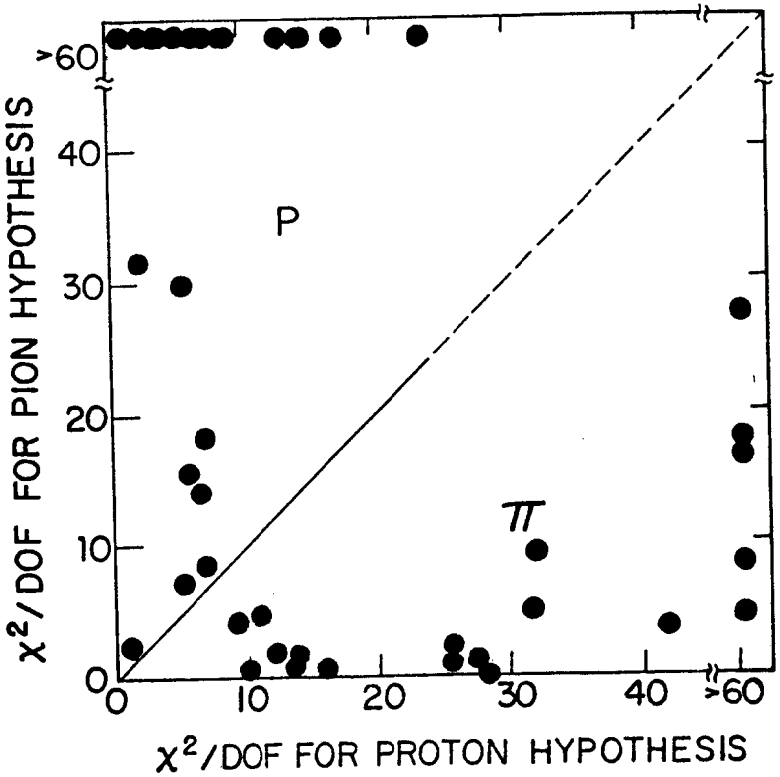

Fig. 7 - Results of fits of the calculated to the observed energy depositions for proton and pion hypotheses.

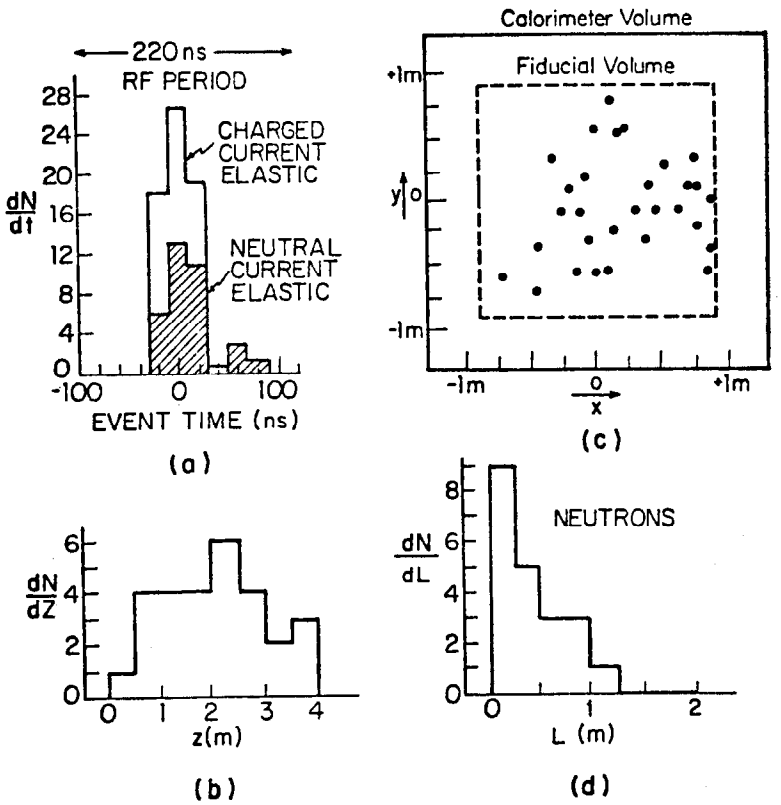

Fig. 8 - (a) Distribution of event times for single protons (shaded) compared to that for a sample of charged current elastic events.
(b) Distribution of p vertices along the beam direction, and
(c) in the plane normal to the beam direction.
(d) Distribution of the distance, L, between successive interactions for neutron events.

uniform. In contrast, these distributions would exhibit rapid attenuation away from the edges of the calorimeter if the events were neutron induced. As an example, the distribution of event vertices transverse to the beam direction for neutron-induced events is presented explicitly in Fig. 13 and discussed in detail in connection with the $\bar{\nu}$ event sample. The observed attenuation is confirmed by an independent estimate of the neutron interaction length, obtained from the distribution of distances between interactions for neutron events with multiple interactions. This distribution, presented in Fig. 8d, indicates a neutron interaction length of ≈ 40 cm. We conclude that the background from neutrons is small.

Additional confirmation that the events arise from ν elastic scattering is obtained from the angle-energy correlation of the protons. Although the energy spectrum of the ν beam extends from .5 to > 10 GeV, the flux is sharply peaked at 1 GeV; approximately sixty percent of the quasielastic events produced correspond to ν energies between 0.5 and 1.5 GeV. For the reaction $\nu p \rightarrow \nu p$, the majority of the recoil protons should then satisfy the correlation between angle and kinetic energy dictated by elastic scattering for incident neutrinos of this energy range. It is seen from Fig. 9a which is a plot of kinetic energy versus angle for the selected protons, that the events lie in the expected region.

In contrast, recoil protons produced via the reaction $np \rightarrow np$ by ν-induced neutrons entering from the front of the apparatus would populate predominantly the region of the plot corresponding to $E_\nu < 0.6$ GeV. Fig. 9b shows the distribution of recoil protons expected from ν-induced neutrons.[8]

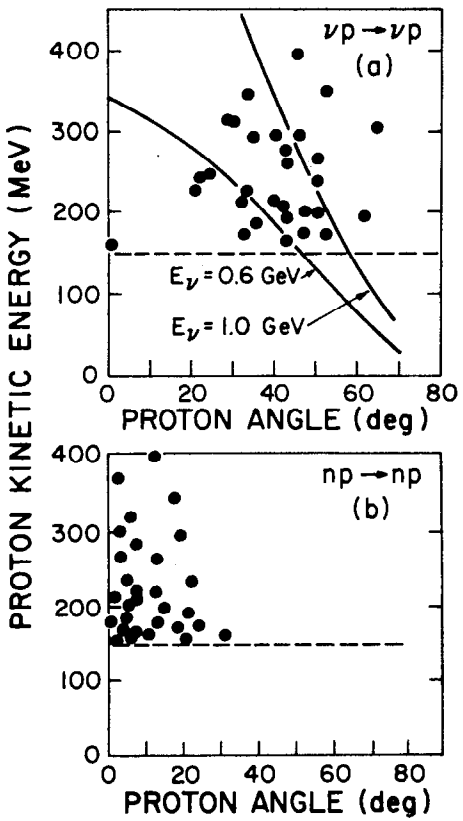

Fig. 9 - (a) Kinetic energy vs. angle for $\nu p \rightarrow \nu p$ candidates. The uncertainty in the energy is $\pm$ 15%. The absence of events below 150 MeV is due to the energy cut. Kinematic curves for $\nu p \rightarrow \nu p$ are shown for two neutrino energies.

(b) Expected distribution for recoil protons produced via the reaction $np \rightarrow np$ by ν-induced neutrons.

We estimate, from Figs. 8 and 9, that at most three of the events could be neutron-induced.

Background from the ν-induced reactions $\nu n \rightarrow \nu \pi^- p$ and $\nu n \rightarrow \mu^- p$ is determined by multiplying the number of such events detected by the probability that the pion or muon escapes detection. In a scan of 75% of the data, only 10 events were found with an identified proton plus a second track that did not veto the event because of the containment criterion. In eight of these events, the second particle was observed in the drift chambers, while in two it was contained within a calorimeter module. From the drift chamber efficiency and the finite cell size, we estimate at most two events in which the second particle is unobserved.

The reaction $\nu p \rightarrow \nu p\pi^o$ in which the π^o is not detected constitutes another source of background. The observed number of $p\pi^o$ events in the sample and the calculated photon detection efficiency imply at most two events with an unseen π^o.

Events from the reaction $\nu n \rightarrow \nu n$ would appear in our sample if np charge exchange occurs in the target nucleus or if it occurs after the neutron leaves the nucleus provided that the de-excitation of the target goes undetected (i.e. <3 MeV of energy is visibly deposited in the scintillator). The background from n charge exchange <u>in</u> the nucleus is largely offset by the loss of valid $\nu p \rightarrow \nu p$ events due to p charge exchange. The net correction is estimated to be $\approx$ 10%.[9] Furthermore, the total background from $\nu n \rightarrow \nu n$ may be estimated empirically by observing the fraction of $\bar{\nu} p \rightarrow \mu^+ n$ events with a valid p signature. This approach indicates a background of less than 20% and will allow a detailed correction as a function of q^2 in the future. We have not made any

correction at the present time.

In summary then, we have observed a total of 30 events that possess the required characteristics of neutrino-proton elastic scattering; the background is estimated to be 3 events from $np \to np$, 2 events from $\nu n \to \mu^- p$ and $\nu n \to \nu \pi^- p$ and 2 events from $\nu p \to \nu p\pi^0$. After subtraction, the number of $\nu p \to \nu p$ events for $0.3 < q^2 < 0.9$ $(GeV/c)^2$, when corrected for detection efficiency and compared with the number of quasielastic events in the same q^2 interval, yields a cross section ratio $\sigma(\nu p \to \nu p) / \sigma(\nu n \to \mu^- p)$ of 0.17 ± 0.05, where the error is statistical. This value is consistent with most of the broken gauge-symmetry models involving the weak neutral current,[3,17] and agrees well with the value 0.23 ± 0.09 obtained recently by W. Lee et al.[4]

The q^2-distribution for the observed events, corrected for detection efficiency (calculated both analytically and by Monte Carlo), is presented in Fig. 10.[10] Also shown is the q^2-distribution for a sample of quasi-elastic events, $\nu n \to \mu^- p$. For $q^2 > 0.3$, the selection requirements for $\nu n \to \mu^- p$ and $\nu p \to \nu p$ are identical except for the presence of a muon; for $q^2 < 0.3$, $\nu n \to \mu^- p$ candidates were primarily identified by their muon signature. The observed shape of the q^2-distribution for $\nu n \to \mu^- p$ and the measured ratio of $\nu n \to \mu^- p$ to the total cross section, 0.25 ± 0.03, are consistent with previous measurements.[11,12] Fig.11 shows the incident ν energy distribution for the observed quasi-elastic events. It agrees well with the calculated spectrum.

To the extent that the elastic charged current $d\sigma/dq^2$ distribution agrees well with past measurement, the energy calibration, effects due to Fermi motion and resolution, etc. appear to present no significant problem.

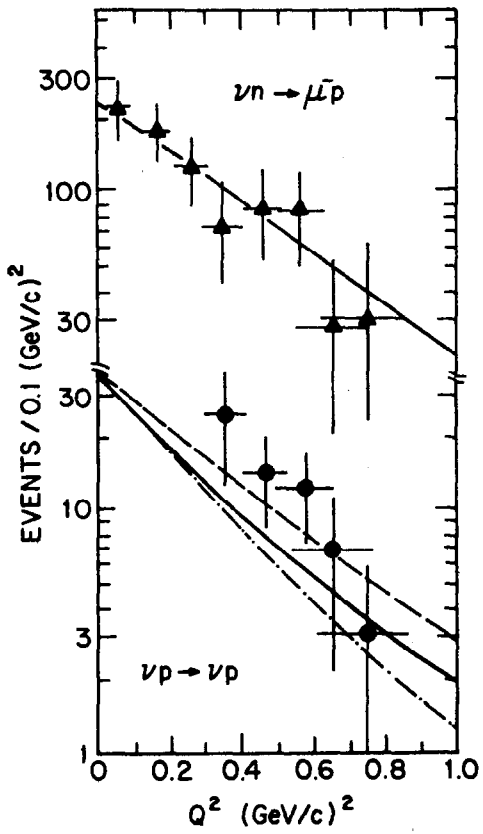

Fig. 10 - Observed q^2-distributions for $\nu n \to \mu^- p$ and $\nu p \to \nu p$, corrected for geometric acceptance. The $\nu p \to \nu p$ data has the 23% background estimate subtracted uniformly in q^2. The solid line (top) is the calculated q^2-distribution for $m_A = 0.9$ GeV/c^2 and $m_V = 0.84$ GeV/c^2. The predictions of the Weinberg-Salam model for $\nu p \to \nu p$ are compared to the data for $\sin^2\theta_w = 0.2$ (dashed line), 0.3 (solid line), and 0.4 (dash-dot line).

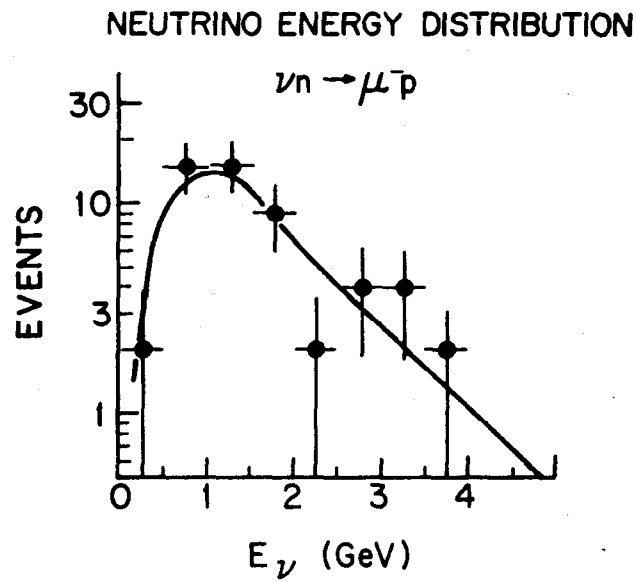

Fig. 11 - Neutrino energy distribution for a sample of $\nu n \rightarrow \mu^- p$ events. The solid lines show the expectation for the spectra of Fig. 1 and total cross sections calculated with $m_V = 0.84$ GeV/c^2 and $m_A = 0.95$ GeV/c^2.

We have also measured the elastic scattering of anti-neutrinos by protons employing very similar selection criteria and cuts as for the neutrino measurement; 22 in-time proton recoils were observed with an estimated background of 8 events. The anti-neutrino reaction is more difficult to observe because the $\bar{\nu}$ flux is lower than the ν flux by 60%, and the cross section (according to our measurement) is approximately $2\frac{1}{2}$ times smaller than for neutrino elastic scattering.

Fig. 12a shows the distribution of event times for the 31 proton recoils, 9 of which lie outside the ± 30 ns timing cut. The vertex distribution of the in-time events along the beam direction is shown in Fig. 12b; it is consistent with a uniform distribution indicating the events cannot have been produced by neutrons entering the front of the apparatus.

A careful comparison of the distribution of event vertices transverse to the beam direction (X-Y distribution) obtained for n-induced events with that obtained for the elastic scattering candidates is presented in Figs. 13 and 14 as evidence that the events were not induced by neutrons entering the sides of the apparatus. Fig. 13 shows the X-Y distribution for proton recoils which occur out-of-time, and are therefore presumably n-induced. Only events with $T_p > 135$ MeV have been included. The distribution exhibits a very distinct peaking towards the edges of the calorimeter. This is illustrated quantitatively in Fig. 13b which shows the number of events per square meter as a function of the radial distance from the center of the calorimeter. The distribution is consistent with a neutron interaction length of approximately 40 cm as was independently determined from the study of neutron events with multiple interactions.

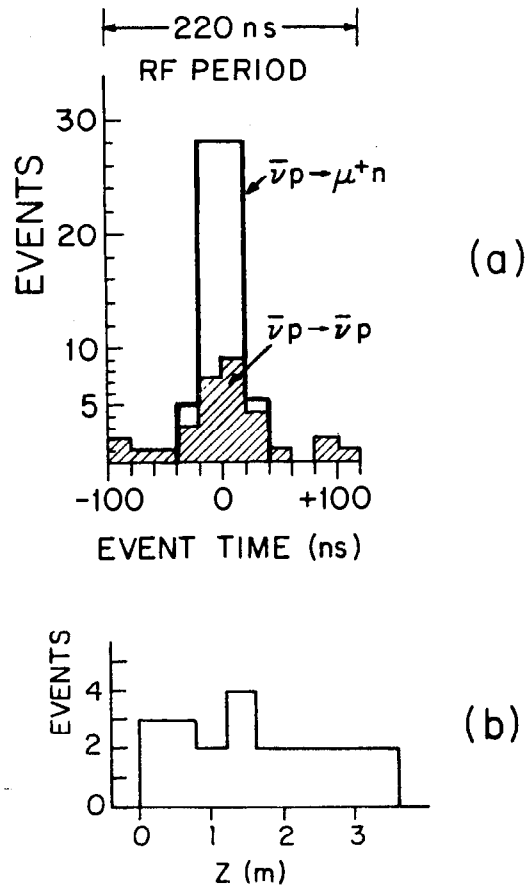

Fig. 12 - (a) Distribution of event times for single protons (shaded) observed during $\bar{\nu}$ exposure compared to that for a sample of $\bar{\nu}p \rightarrow \mu^+ n$ events.
(b) Distribution of event vertices along the beam direction.

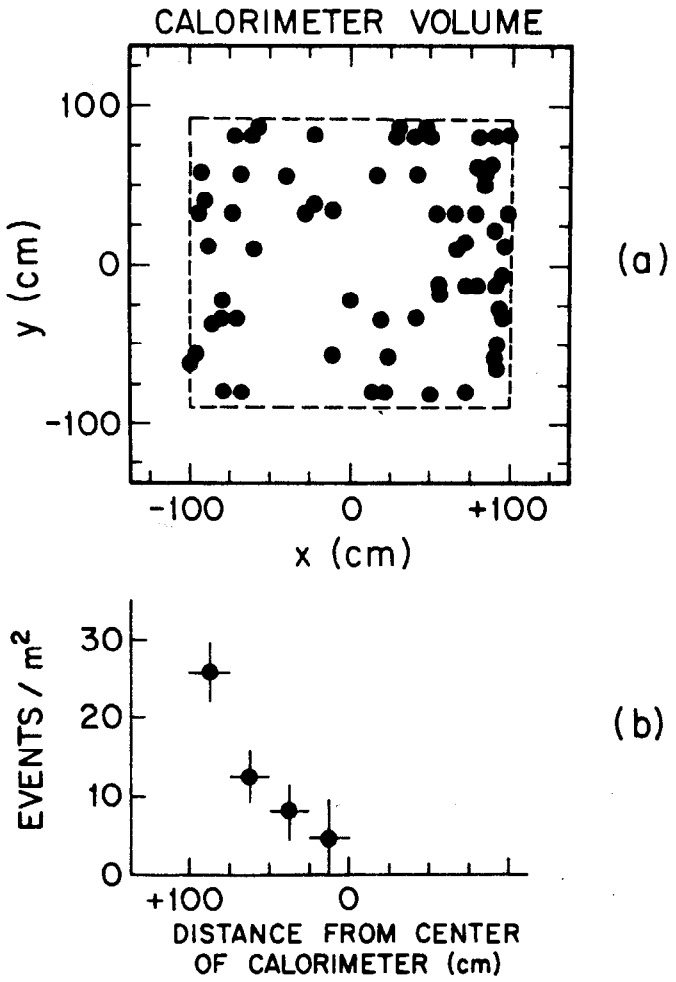

Fig. 13 - (a) Distribution of n-induced proton recoils in the plane normal to the direction of the incident ν's.
(b) Distribution of same events as in (a) as a function of the distance from the center of the calorimeter.

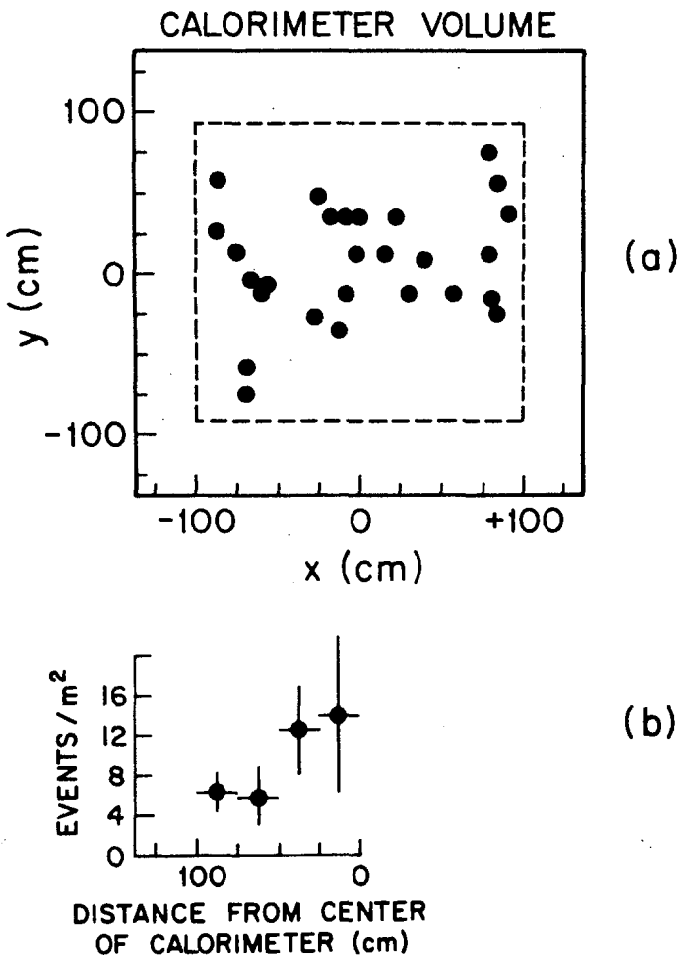

Fig. 14 - (a) Distribution of $\bar{\nu}p \to \bar{\nu}p$ candidates in the plane normal to the direction of the incident ν's.
(b) Distribution of same events as in (a) as a function of the distance from the center of the calorimeter.

In contrast, the X-Y distribution of the in-time elastic scattering candidates, shown in Fig. 14, exhibits no attenuation away from the edges and in fact peaks slightly at the center. The latter effect is to be expected for events produced uniformly across the detector since the geometric acceptance decreases towards the edge of the fiducial volume. We determine an upper limit on the n-background by making the very conservative assumption that all of the events within 20 cm of the dashed line in Fig. 14a are n induced; then the measured neutron attenuation illustrated in Figure 13b implies that at most 6 of the selected 22 events could be n-induced.[13]

Background from other neutral current channels is determined in the same way as described for the ν events and is estimated to be at most 1 event from $\bar{\nu}\, n \to \bar{\nu}\, \pi^- p$ and 1 event from $\bar{\nu}\, p \to \bar{\nu}\, p\pi^0$. The contribution from $\bar{\nu}\, p \to \mu^+ n$ is estimated to be negligible.

The correlation between angle and kinetic energy of the recoil protons is presented in Fig. 15. As for the ν reaction, the majority of the events lie in the region expected for elastic scattering induced by antineutrinos with an energy spread characteristic of the BNL beam.[14] The calculated antineutrino spectrum is peaked at 1 GeV; approximately 60% of the $\bar{\nu}\, p \to \mu^+ n$ events correspond to $\bar{\nu}$ energies between 0.5 and 1.7 GeV.

In conclusion we have observed a total of 22 events that possess the required characteristics of antineutrino-proton elastic scattering.[15] After a background subtraction of 8 events, the corrected number of $\bar{\nu}\, p \to \bar{\nu}\, p$ events for $0.3 < q^2 < 0.9$ $(\mathrm{GeV}/c)^2$, relative to the number of quasi-elastic events in the same q^2 interval, yields a cross section ratio $\sigma(\bar{\nu}\, p \to \bar{\nu}\, p)/\sigma(\bar{\nu}\, p \to \mu^+ n)$ of 0.2 ± 0.1 where the error is

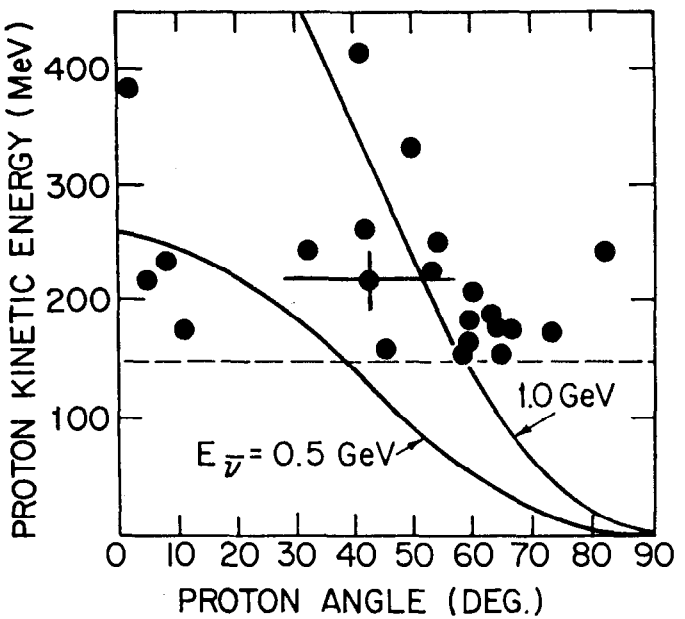

Fig. 15 - Kinetic energy versus angle for the $\bar{\nu}p \rightarrow \bar{\nu}p$ candidates. A typical error bar shows the uncertainty in the energy ($\pm$ 10%) and in angle ($\pm$ 15°). The absence of events below 150 MeV is due to the energy cut. Kinematic curves for $\bar{\nu}p \rightarrow \bar{\nu}p$ are shown for two antineutrino energies.

statistical.

Charged current events of the type $\bar{\nu} p \rightarrow \mu^+ n$ have been observed in the same sample as the $\bar{\nu} p \rightarrow \bar{\nu} p$ events. Although it is not possible to determine the q^2 for each event since in general the n will deposit only a fraction of its energy in the scintillator, one may compare the observed energy distribution to that expected for a given q^2 distribution of $\bar{\nu} p \rightarrow \mu^+ n$. The q^2_{vis}-distribution for the detected $\bar{\nu} p \rightarrow \mu^+ n$ events is presented in Fig. 16 where $q^2_{vis} \equiv 2 m_n T_{vis}$ with T_{vis} the visible energy deposited by the neutron. This distribution is compared to that expected for a V-A current, corrected for neutrons which leave the detector without depositing all of their energy in $np \rightarrow np$ collisions and for saturation effects of the scintillator. The data is consistent with dipole form factors characterized by masses $m_V = 0.84$ GeV/c^2 and $m_A = 0.9 \pm 0.2$ GeV/c^2, in agreement with an earlier measurement.[16] The relative normalization of $\bar{\nu} p \rightarrow \bar{\nu} p$ to $\bar{\nu} p \rightarrow \mu^+ n$ has been determined both by this technique and also by simply counting the total number of $\bar{\nu} p \rightarrow \mu^+ n$ interactions and assuming the events to be distributed in q^2 according to previous measurements.[16] The two techniques give similar results.

The q^2-distribution for the $\bar{\nu} p \rightarrow \bar{\nu} p$ events, corrected for geometric acceptance, is displayed in Fig. 17. The 35% background has been subtracted by arbitrarily assuming it to be uniform in q^2. This distribution is compared with the q^2-distribution for $\bar{\nu} p \rightarrow \mu^+ n$.

Despite the low statistics, it is interesting to compare the observed differential cross sections for ν and $\bar{\nu}$ elastic scattering with theoretical predictions. The curves in Figs. 10 and 17 present the predictions of the Weinberg-Salam model for $\sin^2 \theta_w = 0.2$, 0.3 and 0.4. The model is in satisfactory agreement with both the ν and $\bar{\nu}$ data.

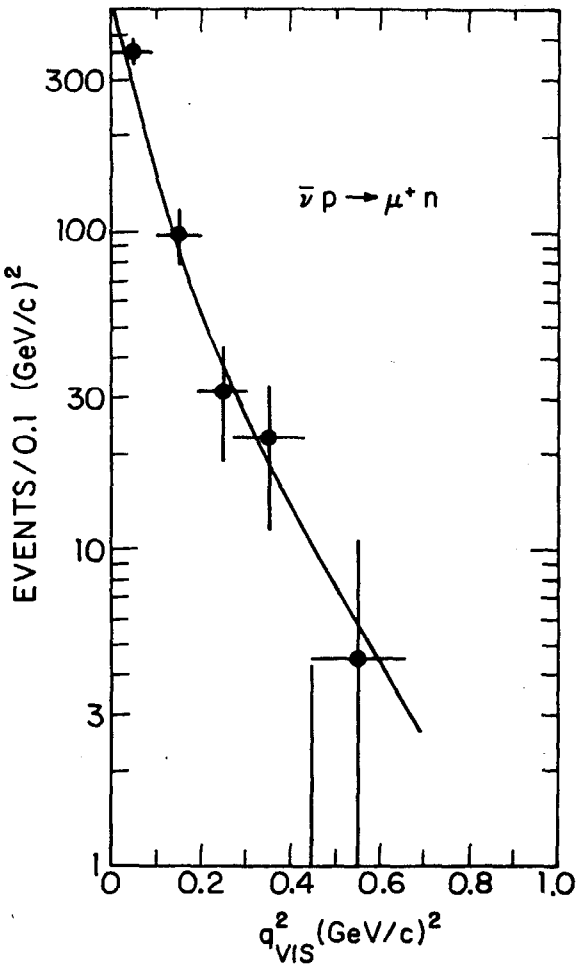

Fig. 16 - The observed q_{vis}^2 distribution for $\bar{\nu}p \rightarrow \mu^+ n$. The solid line is the q^2 distribution, corrected for the undetected neutron energy, for dipole form factors characterized by $m_A = 0.9$ GeV/c^2 (the best fit) and $m_V = 0.84$ GeV/c^2. The horizontal error bars in this figure and in Fig. 17 represent the uncertainty in the energy measurement.

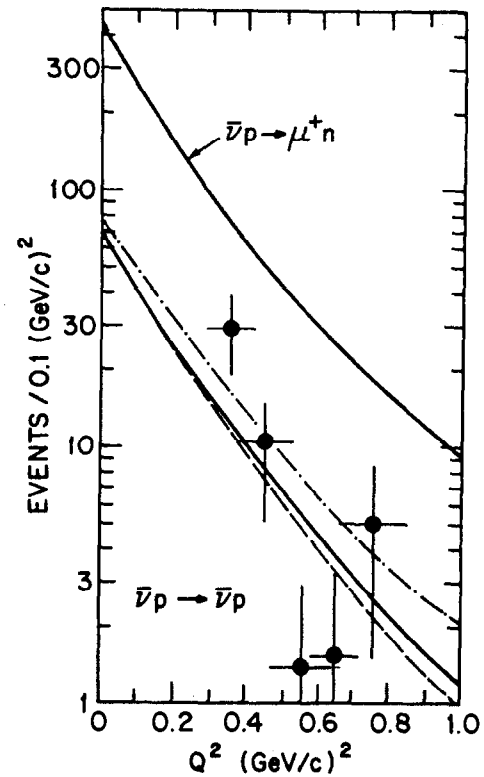

Fig. 17 - Observed q^2 distribution for $\bar{\nu}p \rightarrow \bar{\nu}p$, corrected for geometric acceptance, where the 35% background, arbitrarily assumed to be uniform in q^2, has been subtracted. The solid line representing $\bar{\nu}p \rightarrow \mu^+ n$ is the parent q^2 distribution for the line in Fig. 16. The predictions of the Weinberg-Salam model for $\bar{\nu}p \rightarrow \bar{\nu}p$ are compared to the data for $\sin^2\theta_w = 0.2$ (dashed line), 0.3 (solid line), and 0.4 (dash-dot line).

This is also illustrated in Fig. 18 which compares the measured values of R_ν and $R_{\bar{\nu}}$ with the theoretical predictions for $0.3 < q^2 < 0.9$ $(GeV/c)^2$. Comparisons of the data to a number of other theoretical models have been made by Albright et al, Barnett, Sidhu, Barger and Nanopoulos, and Fishbach et al.[3,17]

One may obtain a direct comparison of the ν and $\bar{\nu}$ elastic scattering rates from the measured values of R_ν and $R_{\bar{\nu}}$ if the ratio of the charged current elastic cross sections is known. We calculate the ratio $\sigma(\bar{\nu} p \to \mu^+ n)/\sigma(\nu n \to \mu^- p) = 0.34$ for $m_V = 0.84$ and $m_A = 0.9$ GeV/c^2 in the interval $0.3 < q^2 < 0.9$ $(GeV/c)^2$ for the BNL spectra. This yields

$$\sigma(\bar{\nu} p \to \bar{\nu} p)/\sigma(\nu p \to \nu p) = 0.4 \pm 0.2,$$

where the error is statistical only. The systematic error, which is dominated by the error on the background subtraction, is evaluated to be approximately 25%. Note that most corrections, -- e.g., nuclear effects, reasonable changes in the calculated neutrino spectrum, a 20% increase in m_A -- cancel to first order in the ratio of the cross sections. If the neutral hadronic current were parity-conserving, this ratio would be unity, suggesting that the hadronic neutral current displays a significant parity-violating interference term and that a purely vector form is unlikely at the level of $2\frac{1}{2}$ - 3 standard deviations. More generally this result excludes at the same level of confidence any pure coupling, S, P, T, V or A, since that would require equal ν and $\bar{\nu}$ cross sections.

The predictions of the Weinberg-Salam model for this ratio are presented in Fig. 19.

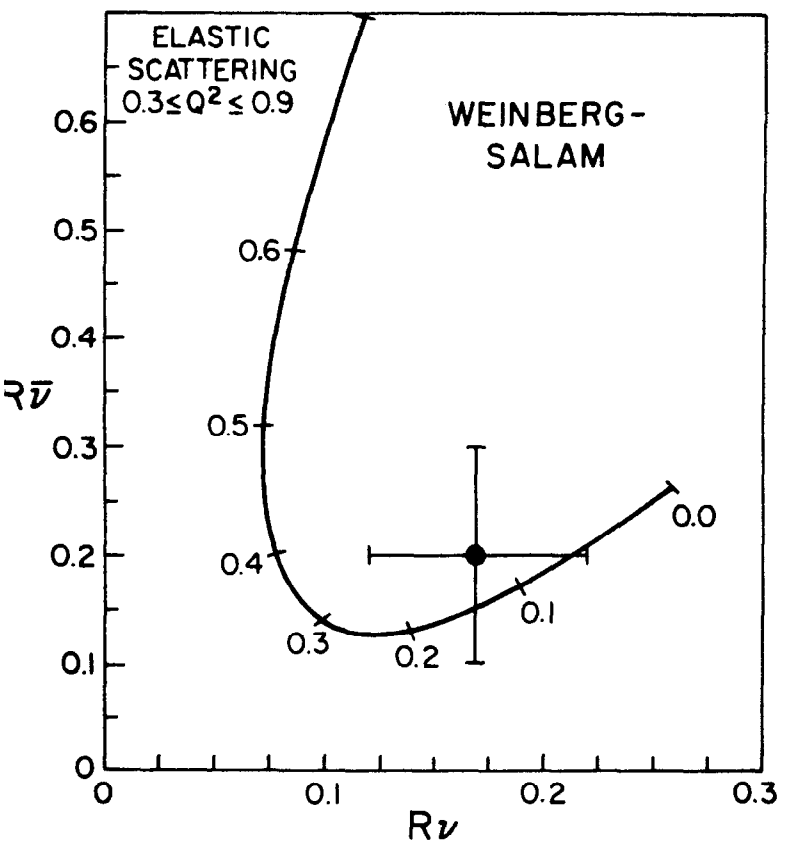

Fig. 18 - Comparison of the prediction of the Weinberg-Salam model for $R_\nu = \sigma(\nu p \to \nu p)/\sigma(\nu n \to \mu^- p)$ and $R_{\bar{\nu}} = \sigma(\bar{\nu} p \to \bar{\nu} p)/\sigma(\bar{\nu} p \to \mu^+ n)$, $(0.3 < Q^2 < 0.9$ $(GeV/c)^2$ and averaged over the BNL $\nu,\bar{\nu}$ spectrum) with the measured values. The calculation assumes $m_V = 0.84$ and $m_A = 0.9$ GeV/c^2.

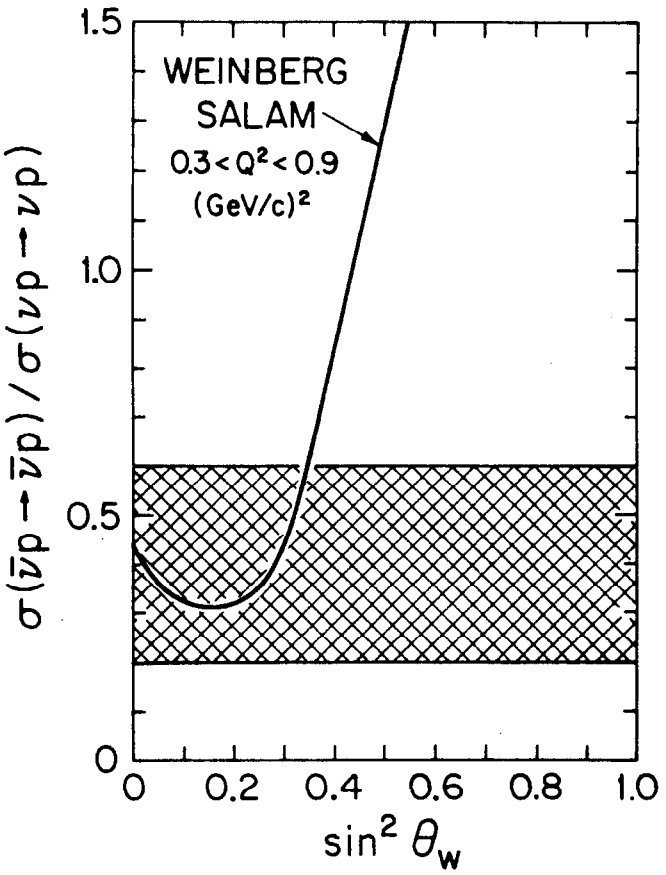

Fig. 19 - Comparison of the ratio $\sigma(\bar{\nu}p \to \bar{\nu}p)/\sigma(\nu p \to \nu p)$ predicted by the Weinberg-Salam model with the measured ratio. The same Q^2 cuts and values of m_V and m_A were assumed as in Fig. 18.

From a general phenomenological point of view one may ask what can be deduced from the elastic scattering data about the structure of the weak neutral current independent of any specific model. Bjorken has illustrated in his lectures at this summer school that if one assumes the weak neutral current to be composed of an arbitrary mixture of vector and axial vector currents, $V^{I=0}$, $V^{I=1}$, $A^{I=0}$, $A^{I=1}$ with the indicated isospin properties, then the elastic scattering data, when combined with inelastic neutral current data, begin to put significant restrictions on the structure of the current. We are currently analyzing a ν data sample approximately five times as large as the one presented here, and will have a comparable $\bar{\nu}$ sample soon. This additional data should put very significant restrictions on the structure of the neutral current in the near future.

We thank the staffs of Brookhaven National Laboratory and the Physics Departments at Harvard, Pennsylvania, and Wisconsin Universities for their support of this experiment. One of us (HHW) would like to thank in particular C. Albright, J. D. Bjorken, B. Kayser, E. A. Paschos, S. P. Rosen, D.P. Sidhu, and J. Smith for numerous discussions concerning the interpretation of the data.

References

* Work supported in part by the U. S. Energy Research and Development Administration.

1. A. Benvenuti et al., Phys. Rev. Lett. 35, 1203 (1975); E. G. Cazzoli et al., Phys. Rev. Lett. 34, 1125 (1975); J. von Krogh et al., Phys. Rev. Lett. 36, 710 (1976) and Proceedings of the International Conference on the Production of Particles with New Quantum Numbers, edited by D. B. Cline and J. J. Kolonko (University of Wisconsin, Madison, 1976), p. 302; G. Goldhaber et al., Phys. Rev. Lett. 37, 255 (1976) and report in these Proceedings; B. Knapp et al.; Phys. Rev. Lett. 37, 882 (1976); W. Lee, report in these Proceedings.

2. One must, of course, remain open-minded to the possibility of a neutral current interaction that transforms as S, P or T. However, this experiment and the results of F. Merritt et al., La Physique du Neutrino a Haute Energie (Ecole Polytechnique, Paris, 1975), p. 291, exclude pure (S, P) or pure T as a possibility.

3. S. Weinberg, Phys. Rev. D5, 1412 (1972); J. J. Sakurai and L. F. Urrutia, Phys. Rev. D11, 159 (1975); A. DeRujula, H. Georgi, and S. L. Glashow, Phys. Rev. D12, 3589 (1975); S. L. Adler and S. F. Tuan, Phys. Rev. D11, (1975); F. Martin, preprint PAR/LPTHE 75/12, Laboratoire de Physique Theorique et Hautes Energies, Paris (1975); E. Fischbach, J. T. Gruenwald, S. P. Rosen, H. Spivack, and B.Kayser, Phys.Rev. Lett. 37, 582 (1976). See also reference (17).

4. D. C. Cundy et al., Phys. Lett. 31B, 478 (1970); P. Schreiner et al., in Proc. XVII Int. Conf. on High Energy Physics, London, England, edited by J. R. Smith (Rutherford High Energy Laboratory, Didcot, Berks, England, 1974), p. IV-123; B. Escoubes et al., Colloq. Int. CNRS 245, 256 (1975); W. Lee et al., Phys. Rev. Lett. 37, 186 (1976) and report in these Proceedings.

5. The neutrino and antineutrino spectra have been calculated by T. Tso at Brookhaven National Laboratory using the Sanford-Wang parameterization of π and K spectra (BNL 11299 JRS/CLW-1 and JRS/CLW-2).

6. Results from this experiment have been previously reported in D. Cline, A. Entenberg, W. Kozanecki, A. K. Mann, D. D. Reeder, C. Rubbia, J. Strait, L. Sulak, and H. H. Williams, Phys. Rev. Lett. 37, 252 (1976), ibid. 37, 648 (1976); H. H. Williams et al., Proceedings of the International Conference on the Production of Particles with New Quantum Numbers, edited by D. B. Cline and J. J. Kolonko (University of Wisconsin, Madison, 1976), p. 415; L. Sulak et al., Neutrino Conference Aachen (1976), in print. Additional details of the calorimeters may be found in L. Sulak, Proceedings of the Calorimeter Workshop, edited by M. Atac (Fermi National Accelerator Laboratory, Batavia, Ill., 1975), p. 155.

7. D. C. Cheng et al., Nucl. Instr. and Meth. 117, 157 (1974).

8. The distribution of recoil protons presented in Fig. 9b has been calculated in two ways: 1) the momentum and angular distribution of the incident neutrons was assumed to be consistent with that observed for nucleons produced by ν-interactions in the BNL 7' BC and 2) the angle of the neutrons relative to the ν-beam direction was taken to be zero and the momentum distribution was deduced from neutron interactions, at energies < 150 MeV, in our apparatus. The two techniques give consistent results.

9. S. L. Adler, Institute for Advanced Study, Princeton, N. J. (private communication).

10. The detection efficiency for E_ν = 1 GeV and for tracks which go through at least one drift chamber, is approximately 0.2, 0.45, and 0.33 for q^2 = 0.35, 0.55, and 0.75 $(GeV/c)^2$, respectively.

11. The value, 0.25 ± 0.03, that we determine for the ratio of the total quasi-elastic cross section to the total cross section, integrated over the BNL neutrino energy distribution, is consistent with that obtained from data taken with the BNL 7' BC. M. J. Murtagh, BNL, private communication.

12. W. A. Mann et al., Phys. Rev. Lett. 31, 944 (1973); E. G. Cazzoli et al., Proceedings of Neutrino Conference-Aachen (1976).

13. The fiducial volume from which the final 22 $\bar{\nu} p \to \bar{\nu} p$ candidates were selected was chosen to be smaller than the area indicated by the dashed lines in Fig. 14; therefore 5 of the 27 events in Fig. 14 (those near the edges) were excluded outright. The n background in the remaining 22 events is at most 6 events.

14. For the majority of events in Fig. 15, the proton angle is determined solely from the calorimeter information and is therefore subject to a statistical and systematic error of approximately 15°.

15. A possible additional source of background is the reaction $\nu p \to \nu p$ due to residual ν's in the $\bar{\nu}$ beam. From the $q^2_{\nu,p}$-distribution for $\nu p \to \mu^+ n$, we can place a conservative upper limit of 10% on the contamination of ν's in the $\bar{\nu}$ beam. The calculated ν contamination is approximately 5%.

16. M. Rollier et al., Colloq. Int. CNRS 245, 349 (1975).

17. C. H. Albright, C. Quigg, R. E. Schrock, and J. Smith, Phys. Rev. D14, 1780 (1976); R. M. Barnett, Harvard University preprint (1976); D. P. Sidhu, Brookhaven National Laboratory preprint BNL-21511 (1976); V. Barger and D. V. Nanopoulos, University of Wisconsin preprint (1976).

Recent Results from Counter-Spark Chamber Neutrino Experiment at BNL*

C.Y. Pang
Physics Department
University of Illinois at Urbana-Champaign
Urbana, Illinois 61801

INTRODUCTION

In this talk I will discuss the following subjects:

1) the first observation of the reaction $\nu_\mu + p \to \nu_\mu + p$ and the measurement of the ratio

$$R_{el} = \frac{\sigma(\nu_\mu + p \to \nu_\mu + p)}{\sigma(\nu_\mu + n \to \mu^- + p)}$$

2) the study of the reactions $\nu_\mu + N \to \nu_\mu + N' + \pi^\circ$ and $\bar{\nu}_\mu + N \to \bar{\nu}_\mu + N' + \pi^\circ$

3) the observation of $\nu_\mu + N \to \mu + e + \ldots$.

The results are obtained by the Columbia-Illinois-Rockefeller Collaboration in an experiment conducted at Brookhaven National Laboratory.[1] I will first describe the BNL ν-beam and the detector layout. The physics results will then be presented.

ν-BEAM AND DETECTORS

The layout of the BNL ν-area is shown in Figure 1. 29 GeV protons are extracted and impinge on a sapphire target. A focusing horn system is followed by 150 ft. of drift space and 100 ft. of iron shield. The neutrino beam consists of 12 to 13 rf bunches per pulse, each bunch $\sim$ 35 ns wide and separated by 220 ns. The average proton beam intensity during our run was 4×10^{12} protons/pulse. The $\nu(\bar{\nu})$ flux was calculated by T.T. Tso[2] and is shown in Figure 2. As will be

---

* Work supported in part by Energy Research & Development Administration

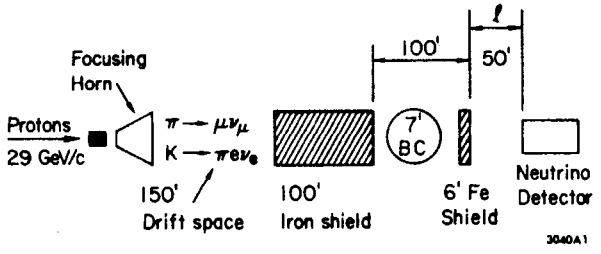
Focusing
Horn
Protons
29 GeV/c
$\pi \rightarrow \mu\nu_\mu$
$K \rightarrow \pi e\nu_e$
150'
Drift space
100'
Iron shield
100'
50'
ℓ
7'
BC
6' Fe
Shield
Neutrino
Detector
3040A1

Fig. 1

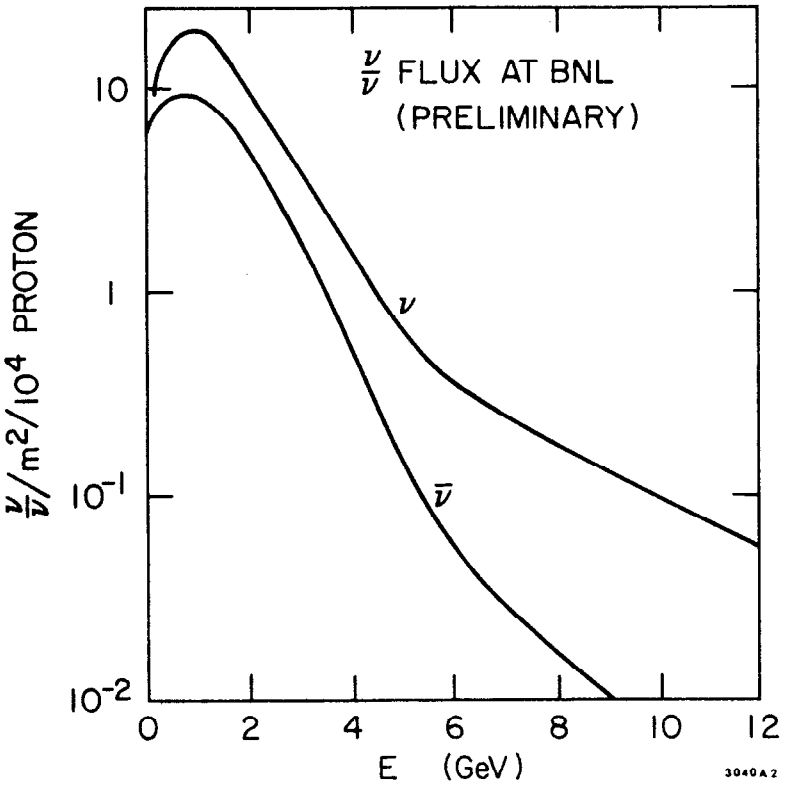
$\frac{\nu}{\bar{\nu}}$ FLUX AT BNL
(PRELIMINARY)
$\frac{\nu}{\bar{\nu}}$/m^2/10^4 PROTON
10
1
10^{-1}
10^{-2}
ν
$\bar{\nu}$
0
2
4
6
8
10
12
E (GeV)
3040A2

Fig. 2

seen later, there is good agreement between the calculated results and our measurements of the flux.

The detector shown in Figure 3 consists of 26 modules of narrow gap optical spark chambers interspersed with liquid and solid scintillation counters. Twenty-one spark chamber modules are each composed of 7 aluminum plates 6 ft. x 6 ft. x 1/4 inch. The remaining five modules are composed of 7 aluminum plates 8 ft. x 8 ft. x 1 inch. The chambers are photographed in two views in narrow angle stereo. The total weight of the detector is 26 tons and the 4 ft. x 4 ft. fiducial mass is 8 tons.

The spark chambers were fired at the end of each beam spill and their memory time kept well over the spill time. Plexiglass Cerenkov detectors were inserted into the iron shield and were used to start the time-of-flight clock and open the system gate upon arrival of muons from the target. The pulse height and time-of-flight were recorded for each counter.

OBSERVATION OF THE REACTION $\nu_\mu + p \to \nu_\mu + p$

We report the first observation of the elastic neutral current reaction

$$\nu_\mu + p \to \nu_\mu + p \qquad (1)$$

and the measurement of the ratio

$$R_{el} = \frac{\sigma(\nu_\mu + p \to \nu_\mu + p)}{\sigma(\nu_\mu + n \to \mu^- + p)} \quad . \qquad (2)$$

To establish the observation of reaction (1), which manifests itself as a single stopping track in our chambers, the following experimental issues must be settled:

1) Is the single track a proton, and if it is,
2) is it induced by ν's or by neutrons. If it is indeed induced by ν, then
3) can the track be simulated by well-known ν-reactions such as

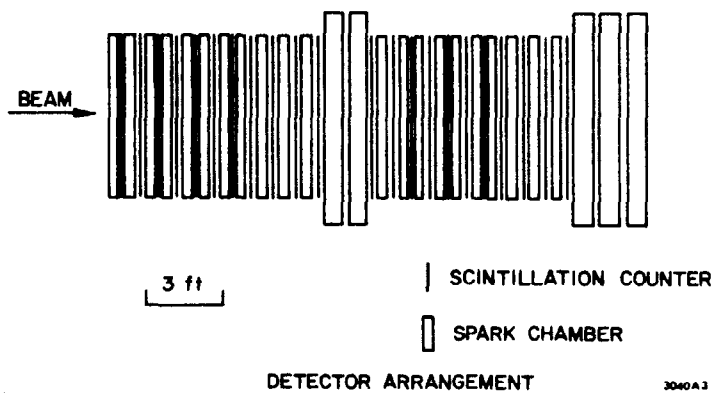

Fig. 3

$\nu p \rightarrow \nu p\pi^\circ$ with the π° not detected in our apparatus. If it is not, then we have observed reaction (1).

The film was scanned for 1 and 2-prong events with a minimum visible track length of 2 inches of Al for either track. Events were measured and reconstructed in space and a 4 foot x 4 foot fiducial cut imposed. The reconstructed events were then matched to the scintillation counters hit by that event and TOF and pulse height information were obtained.

A muon is defined as either a straight track with range greater than 2 interaction lengths, a straight track exiting the detector, or a stopping track with visible multiple scattering. A proton is defined as a stopping track with no visible interaction and a track length equivalent to between 2 inches and 20 inches of Al. A proton track is also required to have at least 5 sparks in the chambers and hits in at least 2 adjacent counters for pulse height measurements.

Candidates for the quasi-elastic reaction ($\nu n \rightarrow \mu^- p$) are then events with 1 muon and 1 proton. Candidates for the elastic reaction (reaction (1)) are events with a single proton. In both reactions, we require no additional charged tracks or neutrals pointing back to the vertex.

The reactions under discussion in this report are produced in C and Al nuclei instead of free protons. In order to demonstrate that we have indeed observed the quasi-elastic reaction, we show in Figure 4A the distribution in ϕ, the angle between the transverse proton direction and the plane made by $\vec{P}_\nu$ and $\vec{P}_\mu$. Figure 4B shows the angular distribution of the muon as well as the Monte Carlo prediction. The inputs to this Monte Carlo are the well-known quasi-elastic dynamics[3] and the neutrino spectrum calculated from 7 foot bubble chamber data. Figure 4C shows the measured neutrino energy spectrum for quasi-elastic events.

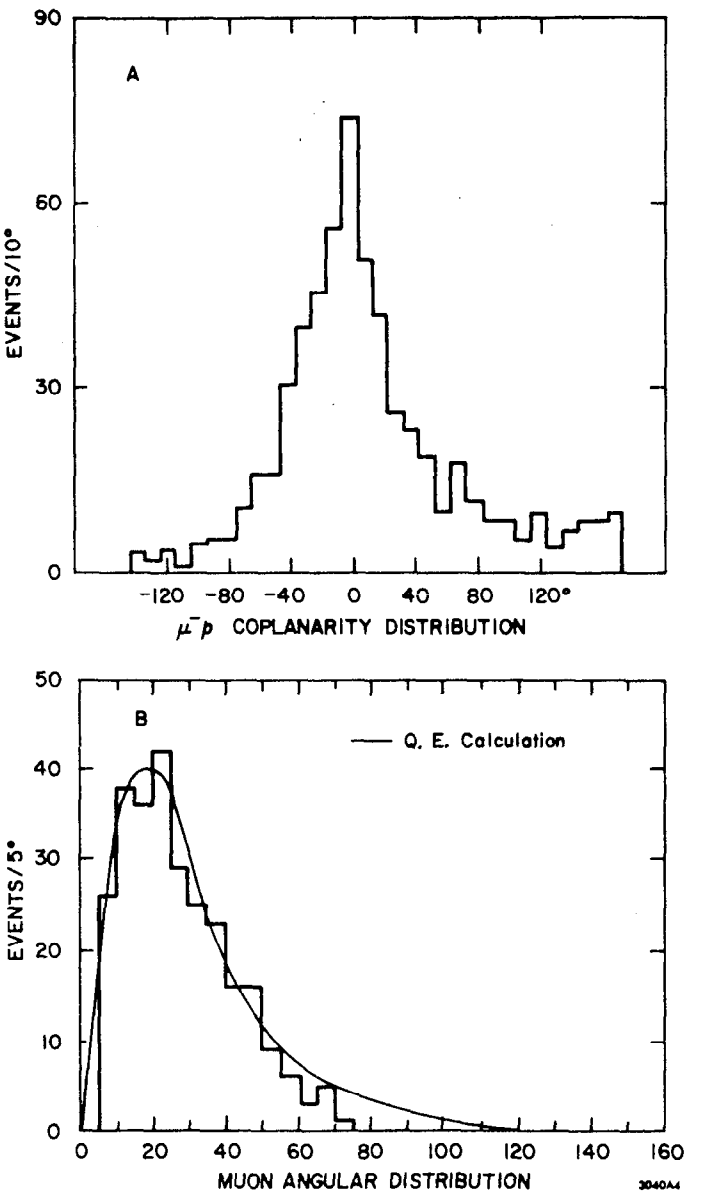

Fig. 4

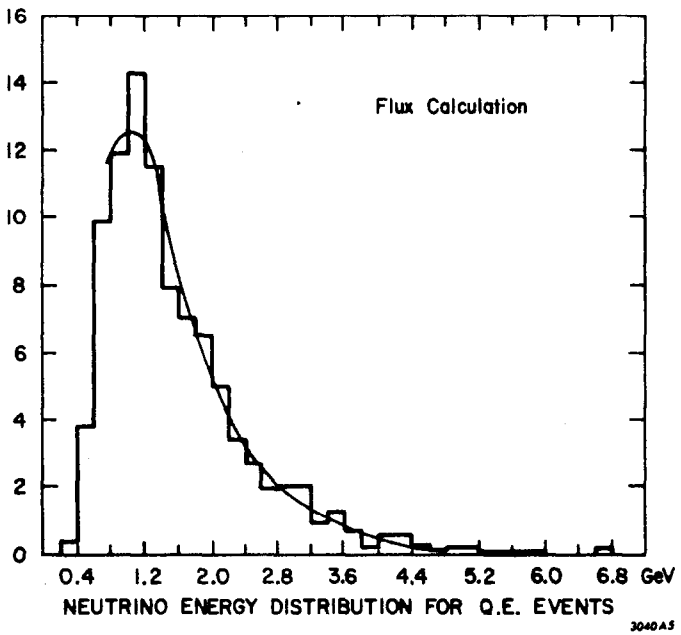

Fig. 4c

The Monte Carlo calculation also includes the effect of Fermi momemtum of the initial nucleon. Based on these distributions, we believe that we have observed quasi-elastic events.

One of the major issues in this experiment is to show that the single straight track identified as a proton is induced by a neutrino and not a neutron. Since the detector is located far from all sources of neutrons, we measure the TOF of events to differentiate neutron from neutrino-induced reactions. Figure 5B shows the TOF for all proton tracks. An in-time signal is observed above a substantial background. Using a right-handed coordinate system centered on the chambers with y up and z along the neutrino beam, we define an azimuthal angle ϕ in the x,y plane with $\phi = 0$ along the x axis. We find that the background is strongly correlated with events interacting high in the detector (positive y) with azimuthal angles ($-30 < \phi < -150°$) towards the ground. We make the following cuts to reduce the neutron background:

Reject events with

a. $y > 0.3$ ft - $35° > \phi > -150°$

$|x| > 1.5$ ft $0° > \phi > -180°$

b. $P_p < 550$ MeV/c and $\theta_p < 25°$

The first cut reduces "sky shine" background while the second enhances the elastic signal since most protons from elastic events are expected to have a proton angle of > 25°. The TOF distribution for quasi-elastic events is shown in Figure 5A.

A fast neutron background may still produce events in and near the rf bucket. In our study of the $\nu_\mu p \to \nu_\mu p\pi^\circ$ reaction, we are quite sensitive to $np \to np\pi^\circ$ contamination. Based on the distribution of $\nu N \to \nu N\pi^\circ$ events along five interaction lengths of apparatus, we estimate a background of < 5% for neutrons with > 1 GeV/c momenta. Using the measured cross sections for $np \to pn$ and $np \to np\pi^\circ$, we compute a

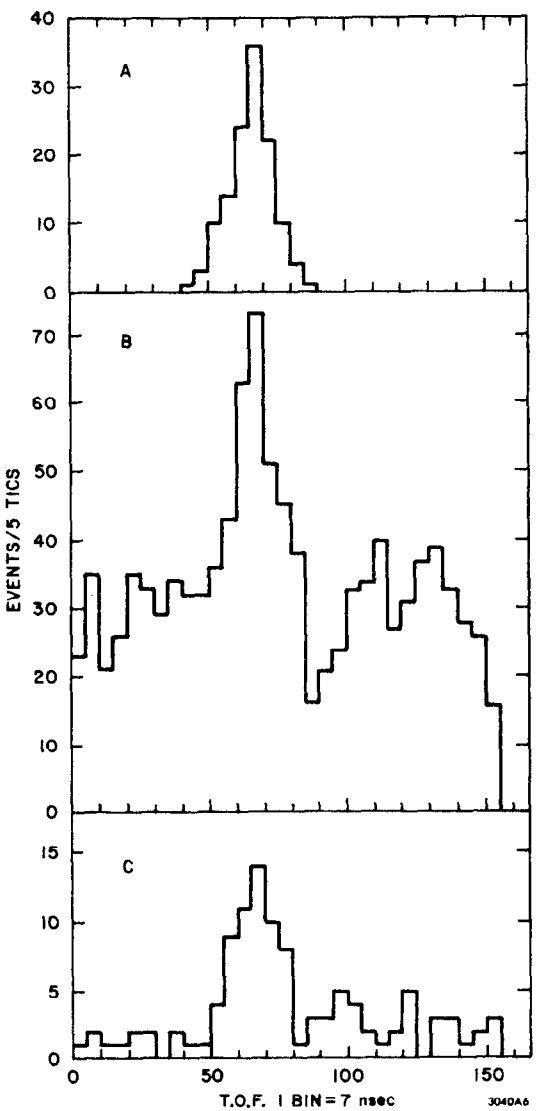

Fig. 5

negligible background due to np → pn near the rf bucket. The other possible background is due to neutrinos interacting near the detector and producing prompt neutrons. The apparatus is supported 7 feet above the ground with no nearby masses so that the ground is the only source of such events. Since a neutron from the ground would produce protons with upward azimuthal angles and would have to pass through 2-3 interaction lengths to interact in the top half of the detector, such a source would produce ∿ 8 times as many upward pointing protons in the bottom half of the apparatus as in the top. The number of observed events pointing up is 17 for $y < 0$ and 14 for $y > 0$. We conclude there is negligible background from this source. From Figure 5C we have 55 events in 6 bins centered on the rf bucket. We estimate the residual sky shine background to be 12 events, assuming a flat subtraction. We obtain 92 $\nu_\mu n \to \mu^- p$ and 43 $\nu_\mu p \to \nu_\mu p$ candidates.

Protons and pions can be separated in our apparatus by pulse height. In the energy range of interest, protons are ∿ twice minimum ionizing while pions remain minimum ionizing over most of their range. In determining the pulse height for each track, we average the pulse height of the last two counters. Figure 6A shows the pulse height distribution of in-time elastic candidates, protons from quasi-elastic events, and minimum ionizing particles. Because our counters are thin, pions do not stop in them so that the average sampled energy loss is very close to minimum ionizing. The total sample of pions which can contribute to the elastic signal will have a pulse height distribution which is given by minimum ionizing particles. A pulse height cut of > 12 then reduces the pion background by a factor of 3. After pulse height cuts we obtain 77 $\nu_\mu n \to \mu^- p$ and 38 $\nu_\mu p \to \nu_\mu p$ candidates. The neutron background is now estimated to be 10 events.

Another source of background for the $\nu_\mu p \to \nu_\mu p$ reaction is

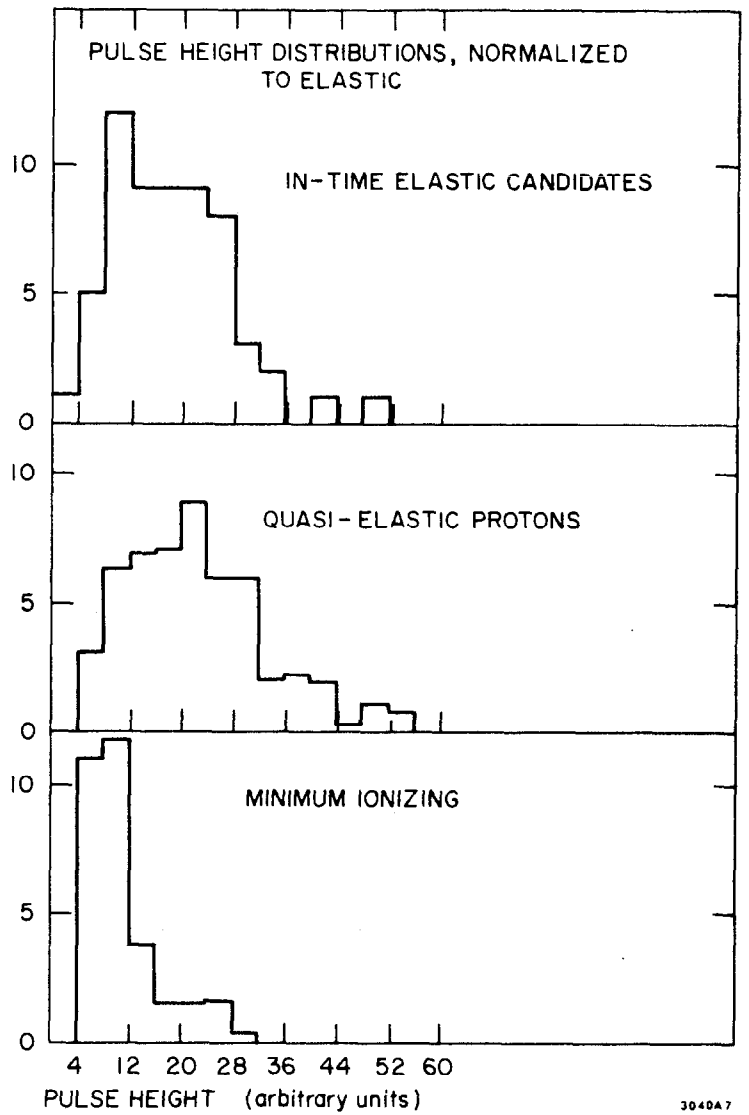

Fig. 6A

$\nu_\mu n \to \mu^- p$ events where the μ^- escapes detection. This correction is (0.08 ± 0.02) of the observed quasi-elastic signal (see Figure 4B).

After pulse height cuts, of 38 elastic candidates, 10 are estimated to be due to residual sky shine, 6 due to the wide angle muon problem, and 3 due to pion contamination if $I(\pi N) = 1/2$. Thus 19 events remain if $I(\pi n) = 1/2$ and 21 if $I(\pi N) = 3/2$. As to the statistical significance of whether we have observed the elastic reaction, we have 4.4 and 5.1 σ, respectively. Increasing the pion contamination by a factor of two does not change the statistical significance of our data. The systematic errors are believed to be smaller than the statistical ones. We conclude that we have clearly observed neutral currents. For the measurement of R_{el}, our statistical errors are larger, and we find $R_{el'} = 0.23 \pm 0.09$. Previous searches for this reaction[4] have obtained $R_{el} = -0.08 \pm 0.20$ by S.J. Barish et al., and an upper limit of $R_{el} = 0.12 \pm 0.06$ by Cundy et al.

There are several theoretical predictions of this ratio.[5] Using the Weinberg-Salam (W.S.) model, the prediction is $R_{el} = 0.07$ for $\sin^2\theta_w = 0.4$ and $0.3 < q^2 < 1.0$ GeV^2. We have observed the reaction $\nu_\mu p \to \nu_\mu p$ but our measurement of R_{el} is not sufficiently accurate to rule out any particular model. The q^2 distributions are shown in Figure 6B. The elastic events have been corrected for background subtraction. Within the detector acceptance both CC and NC show similar q^2 behavior.

Once the reaction $\nu_\mu p \to \nu_\mu p$ is observed, the reaction $\nu_\mu n \to \nu_\mu n$ should also occur ($x = \sigma(\nu n \to \nu n)/\sigma(\nu p \to \nu p) \approx 1.5$ in the W.S. model).[6] Some final state neutrons from this reaction can charge exchange $\nu_\mu n \to \nu_\mu (n \to p)$ and mimic the reaction $\nu_\mu p \to \nu_\mu p$. Then $R_{el} \cong R_{el}^{obs.} (1 - x\varepsilon)$ where $R_{el}^{obs.}$ is the observed $\sigma(\nu_\mu p \to \nu_\mu p)/\sigma(\nu_\mu n \to \mu p)$ ratio and ε is the probability that a neutron will charge exchange and produce a proton within our kinematical cuts. ε is not well-known, but if we

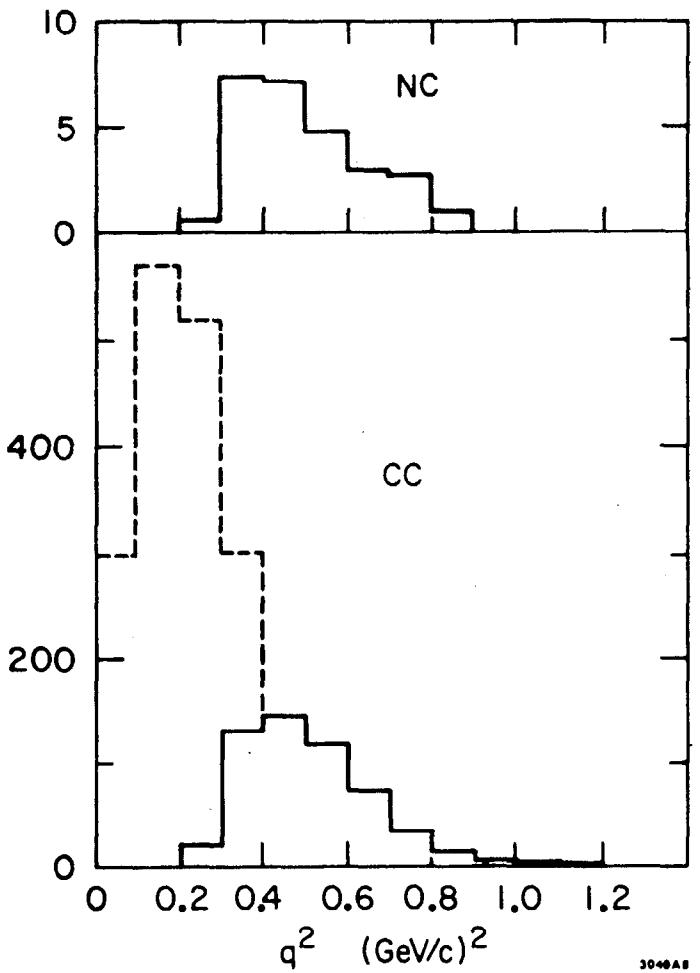

Fig. 6B

conservatively take it to be 0.1 the $R_{el} = 0.23(1-1.5x0.1) = 0.2$ so that this is a small effect.

SINGLE π° PRODUCTION

We report on the measurement of the ratios

$$R_o' = \frac{\sigma(\nu N \to \nu N'\pi^\circ)}{2\sigma(\nu N \to \mu^- N''\pi^\circ)}$$

$$\bar{R}_o' = \frac{\sigma(\bar{\nu}N \to \bar{\nu}N'\pi^\circ)}{2\sigma(\bar{\nu}N \to \mu^+ N''\pi^\circ)}$$

The method of analysis has been reported earlier.[7] The accepted events are with one or two showers greater than 10 sparks ($\gtrsim$ 100 MeV in energy). Based on the study of the TOF and event distribution along the detector the neutron background is found insignificant in the π° reactions. Assuming that $\sigma(\nu n \to \nu n\pi^\circ) = \sigma(\nu p \to \nu p\pi^\circ)$, we obtain

$$R_o' = 0.17 \pm 0.04$$

$$\bar{R}_o' = 0.39 \pm 0.18 \quad .$$

Because the target is not composed of free nucleons we must correct the theoretical predictions for charge exchange effects. These effects have been calculated by Adler, Nussinov and Paschos.[8] In the W.S. model with $\sin^2\theta_W = 0.35$ they predict

$$R_o' = 0.20$$

$$\bar{R}_o' = 0.25$$

which are not inconsistent with the observed ratios.

The $\pi^\circ p$ mass, which is sensitive to the isospin I = 3/2 and I=1/2 amplitudes in the C.C. and N.C. final states, can be constructed using the methods described in reference 7. In order to eliminate the poo. resolution inherent with low energy showers, to reduce misidentification of a spectator nuclear breakup proton as the target proton, and to reduce nuclear rescattering of protons in our sample, we impose two cuts:

a) The proton must stop inside the detector with a momentum

$\geq$ 650 MeV/c and a polar angle $\leq$ 80°. The first cut reflects the fact that the momentum distribution of breakup and rescattered tracks lies below 650 MeV/c while the second is the kinematic limit for the proton.

b) The momentum of the π° must be greater than 250 MeV/c.

With these cuts, the mass resolution in our detector is $\sim$ 100 (MeV^2).

Another factor which must be considered is misidentification of C.C. and N.C. final states. Such misidentification is due to C.C. events with wide angle muons that are not detected in our apparatus. Although, with no p_p or p_π cuts, this correction is 10% of the observed number of C.C. events, wide angle muons are strongly correlated with a small $\theta_{\pi^\circ p}$ hadronic system. The contamination of N.C. by C.C. events is therefore much greater at small $\theta_{\pi^\circ p}$. Figures 7a and 7b show the C.C. and N.C. mass distribution for p_p > 650 MeV/c and $\theta_{\pi^\circ p}$ < 20°. We expect this region to show strong C.C. contamination in the N.C. events and we indeed observe Δ production both in the C.C. and N.C. data. Figures 7c, 7d, 7e, and 7f show the C.C. and N.C. mass distributions for $\theta_{\pi^\circ p}$ > 20° where rescattering and C.C. contamination are believed to be small. We observe clear Δ production in C.C. but not in the N.C. data. The data, however, is not yet statistically significant.

OBSERVATION OF THE REACTION $\nu_\mu N \to \mu + e + \ldots$

In our detector, electrons and gamma rays can be separated by two parameters: the straight track length at the origin of the shower and the conversion point. Electrons typically show $\sim$ 1 radiation length (r.l.) of straight track before showering while for γ's the visible straight track is much shorter (> 0.3 r.l.). Electrons originate at the vertex while γ's convert away with a conversion length of 11.5 cm of Al. Charged hadrons can be separated from muons in the detector because they interact with a visible interaction length of 25 cm. of Al.

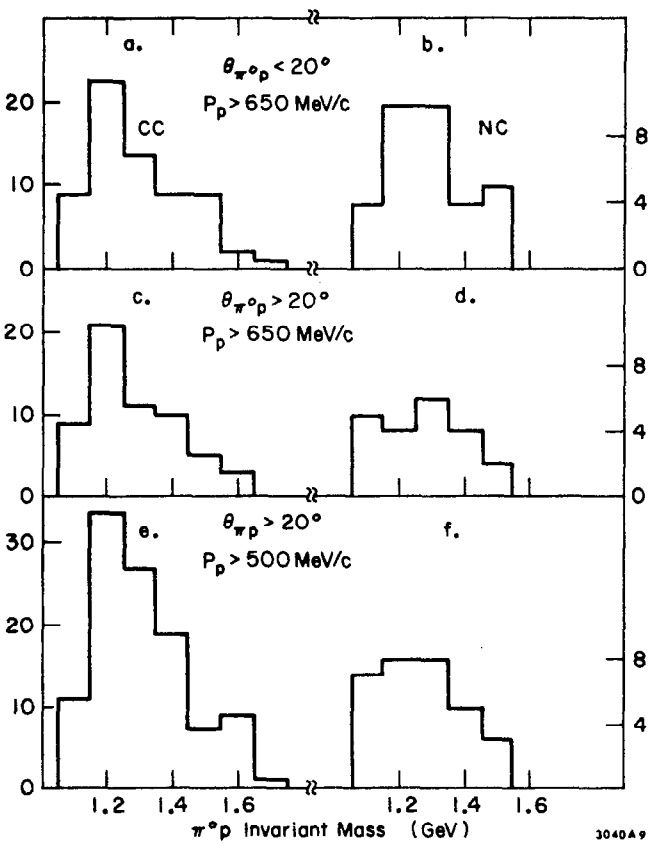

Fig. 7

Events with electromagnetic showers in the data sample could be due to four processes:

a) $\nu_\mu N \to \mu^- \pi^\circ + \ldots$

b) $\nu_\mu N \to \nu_\mu \pi^\circ + \ldots$

c) $\nu_e N \to e^- + \ldots$

d) $\nu_\mu N \to \mu e + \ldots$

In the case of reactions a and b, we note that the π° spectrum is a rapidly falling function of π° energy. Furthermore, the efficiency for seeing both γ's from π° decay in our detectors increases with π° energy. To search for electrons, we cut at $E_{\pi^\circ} > 500$ MeV and demand no visible second shower.

We now demonstrate that the detector responds to γ's and electrons as expected. Figure 8 shows the distribution of the range of the longest non-interacting track vs. shower energies. Events corresponding to reaction c) lie predominantly in region II since they have no associated muon. We should observe an enriched electron signal in this region. Events corresponding to reaction a) will lie in region I and we expect negligible contribution from reaction c) in this region. Figure 9 shows the length of straight track (s.t.) at the origin of showers vs. the conversion distance (c.d.) of showers separately for the three regions of Figure 8. Figure 10 shows the γ-ray conversion distribution determined by selecting a sample of 2γ events with $M_{\gamma\gamma} < 250$ MeV. Only events with at least one shower with $E_\gamma > 500$ MeV were used. Using this distribution and the number of showers with s.t. > 0.75 and c.d. > 0.45 we calculate that the γ-ray contamination in region II for events with s.t. > 0.75 and c.d. < 0.45 is 2 events.

It is clear that after these cuts we are left with a sample of ν_e induced events and a small γ background. By selecting events in this region consistent with $\nu_e n \to e^- p$ where the proton candidate stops in the

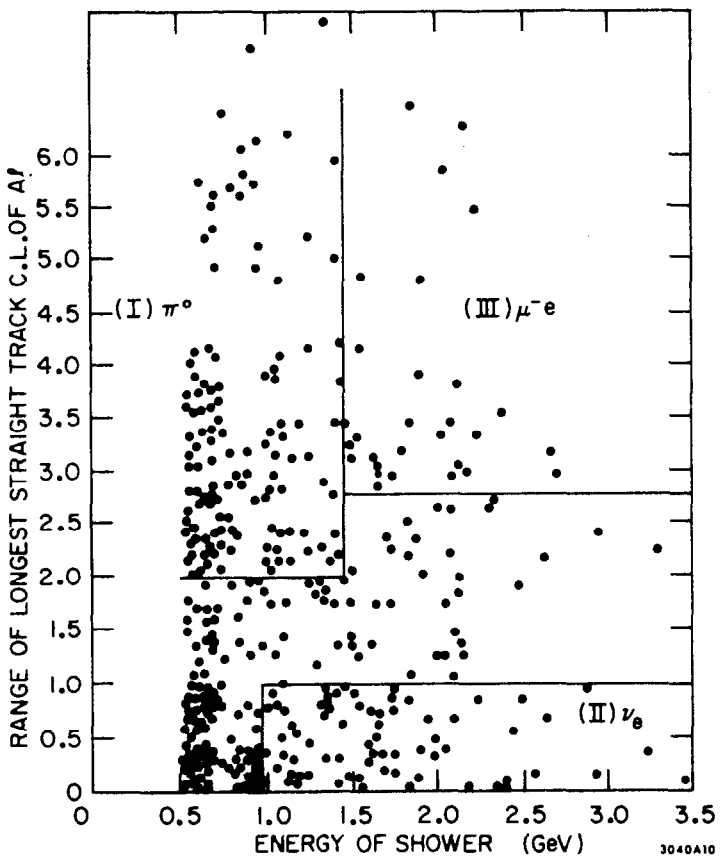

Fig. 8

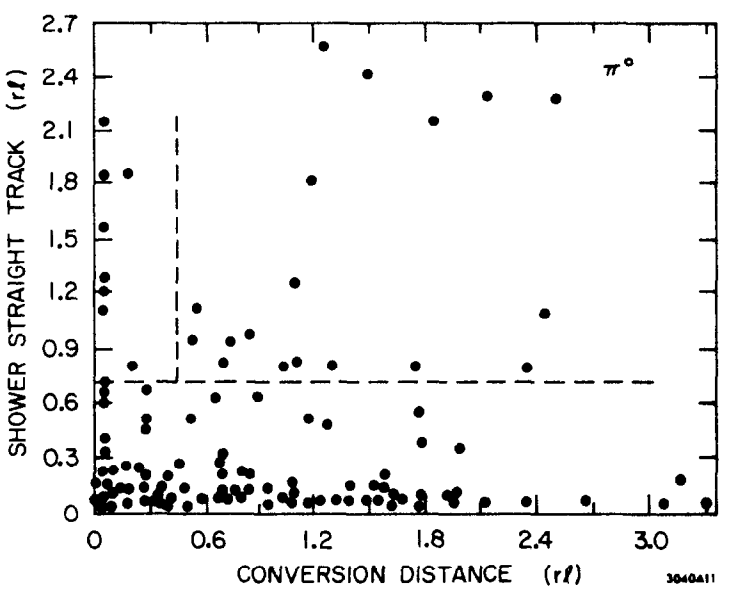
SHOWER STRAIGHT TRACK (rl)
CONVERSION DISTANCE (rl)
π°
0
0.3
0.6
0.9
1.2
1.5
1.8
2.1
2.4
2.7
3.0
3040A11

Fig. 9A

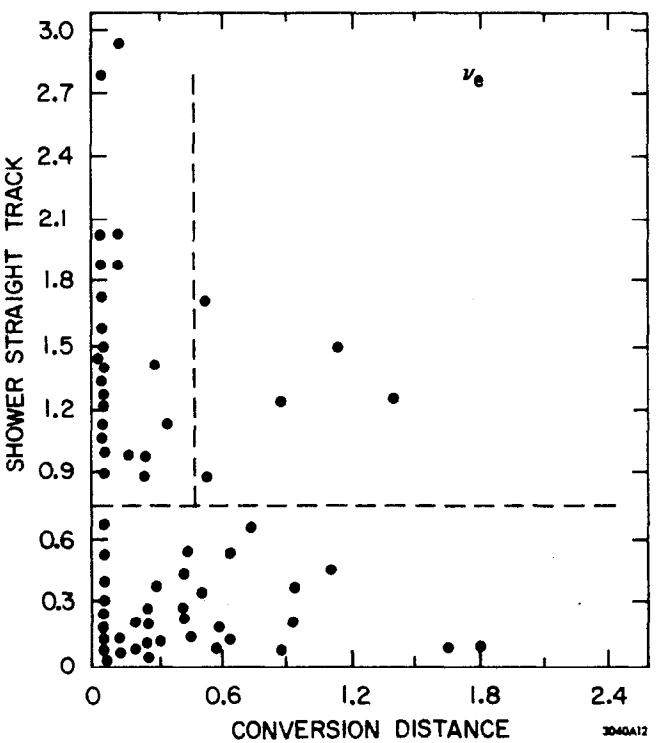
SHOWER STRAIGHT TRACK
CONVERSION DISTANCE
νe
0
0.3
0.6
0.9
1.2
1.5
1.8
2.1
2.4
2.7
3.0
3040A12

Fig. 9B

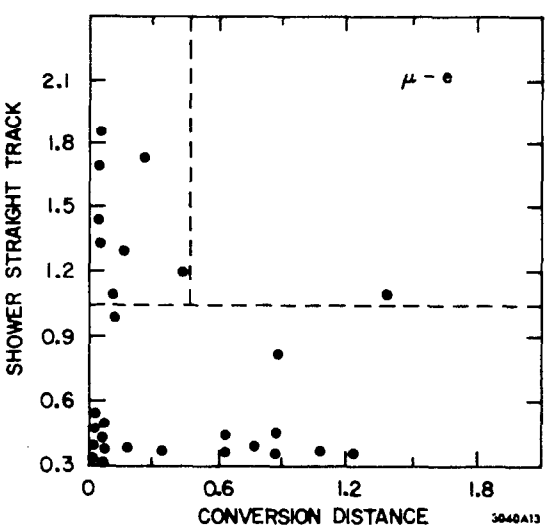
μ - e
SHOWER STRAIGHT TRACK
2.1
1.8
1.5
1.2
0.9
0.6
0.3
0
0.6
1.2
1.8
CONVERSION DISTANCE
3040A13

Fig. 9c

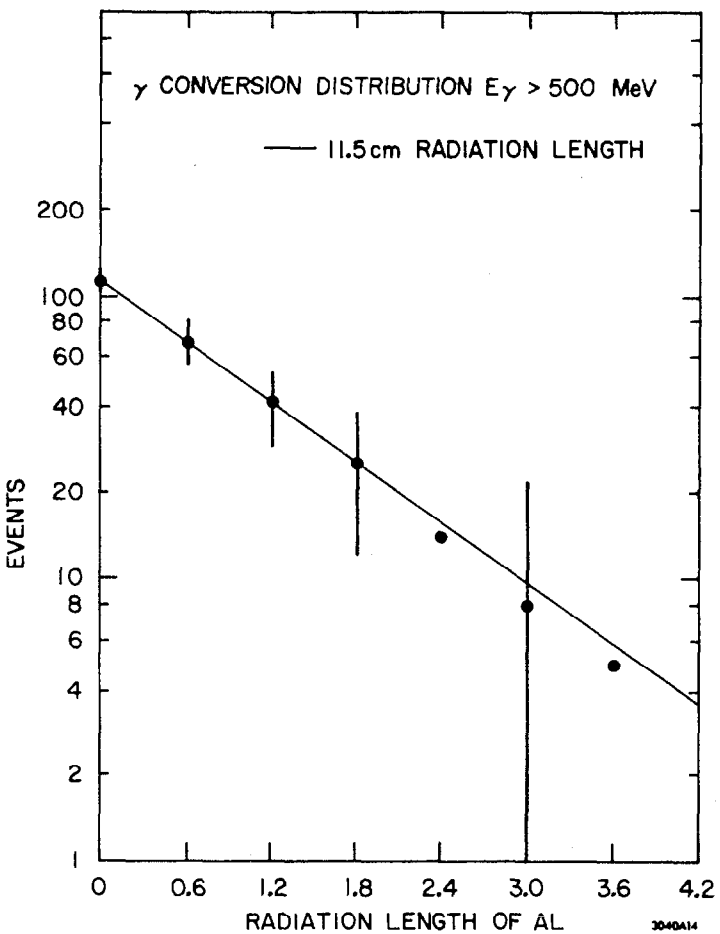
γ CONVERSION DISTRIBUTION Eγ > 500 MeV
11.5 cm RADIATION LENGTH
EVENTS
200
100
80
60
40
20
10
8
6
4
2
1
0
0.6
1.2
1.8
2.4
3.0
3.6
4.2
RADIATION LENGTH OF AL
3040A14

Fig. 10

detector with p_p > 550 MeV/c, E_e > 1 GeV and the electron and proton are coplanar and then compare with $\nu_\mu n \to \mu^- p$ candidates with identical cuts, we find the ratio of ν_e to ν_μ flux is 0.01 ± 0.005, in agreement with expectation.

Figure 11 shows the range of the longest non-interacting track vs. the shower energy distribution for electron-like showers (s.t. > 0.75 r.l., c.d. < 0.45 r.l.). In region III we observe 7 events separated from the rest in longest track length. Out of 28 candidates with E_e > 1.5 GeV we have 7 events with straight tracks > 2.7 collision lengths of Al. If all 7 tracks were hadrons, we would expect to have observed ∿ 70 events with interacting tracks. We observe 1. Therefore, all 7 straight tracks are muons with a maximum contamination of 0.2 events. We now turn to whether these events could be due to γ's. Figure 9C shows the shower straight-section vs. conversion length distribution for region III of Figure 8. We observe a clear electron signal corresponding to the 7 events. Since after s.t. cuts, we have 7 "e" + μ events with 1 "e" + μ with the "e" converting away from the vertex, we find the probability that all "e"'s are really gamma rays is extremely small. We believe that at least 4 out of 7 "e"'s are genuine electrons. We conclude that we have observed μe events. The observed rate with respect to the total observed rate, without correcting for detection efficiency etc., is μe/all $\simeq 3\times10^{-4}$.

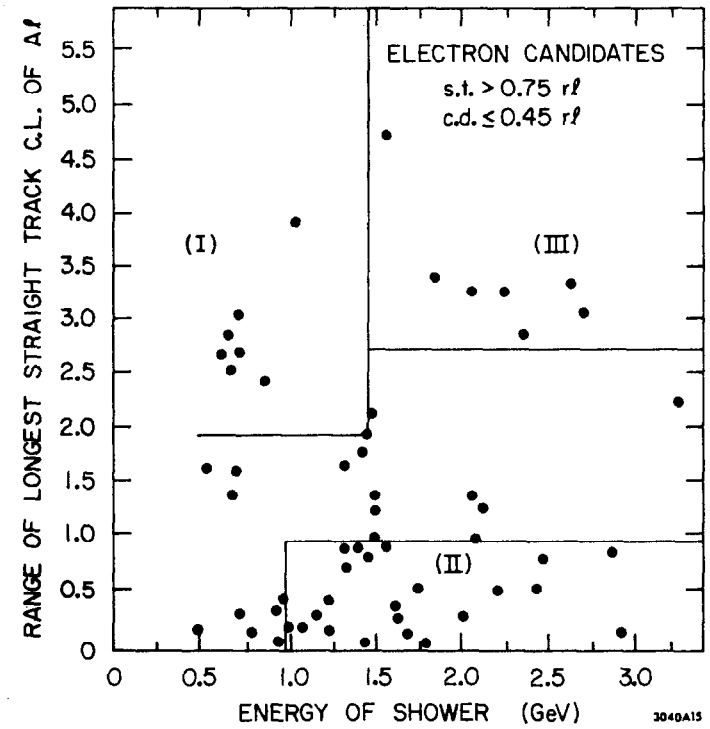

Fig. 11

REFERENCES

1. The members of this collaboration are W. Lee, E. Maddry, P. Sokolsky, L. Teig, A. Bross, T. Chapin, L. Holloway, L. Nodulman, T. O'Halloran, C. Pang, K. Goulianos and L. Litt.

2. M. Murtaugh, private communication.

3. T.D. Lee, C.N. Yang, Phys. Rev. Lett. 4, 307 (1960). C.H. Llewellyn-Smith, Phys. Rpts. 3, 261 (1972).

4. D.C. Cundy et al., Phys. Lett. 31B, 478 (1970); S.J. Barish et al., paper submitted to XVII International Conference on High Energy Physics (London, 1974).

5. S. Weinberg, Phys. Rev. D5, 1412 (1972); M.A.B. Beg, A. Zee, Phys. Rev. Lett. 30, 675 (1973); J.J. Sakurai, Phys. Rev. D9, 250 (1974); J.J. Sakurai, L.F. Urratia, Phys. Rev. D7, 159 (1975); S. Adler, Sixth Hawaii Topical Conference in Particle Physics (August 1975), to be published.

6. C. Quigg, K. Albright, and J. Smith, FNAL Preprint.

7. W. Lee, in Proceedings of the XVII International Conference in High Energy Physics (London, 1974); W. Lee *et al.*, in La Physique du Neutrino à Haute Energie (Paris, 1975), p. 205; P. Sokolsky, in Proceedings of the Division of Particles and Fields (Seattle, 1976).

8. S.L. Adler, S. Nussinov, and E.A. Paschos, Phys. Rev. D9, 2125 (1974); S.L. Adler, Phys. Rev. D9, 229 (1974).

RECENT RESULTS IN μe EVENTS AND NEUTRAL CURRENT IN GARGAMELLE

Paul Musset

CERN
1211 Geneva 23
Switzerland

We present some of the most recent results obtained by the Gargamelle collaboration:

Aachen, III Physikalisches Institut der Technischen Hochschule

Brussels, Interuniversity Institute for High Energies ULB-VUB

CERN, Geneva

Palaiseau, Laboratoire de Physique Nucleaire des Hautes Energies, Ecole Polytechnique

Milano, Instituto di Fisica dell'Universita and INFN

Orsay, Laboratoire de l'Accelerateur Lineaire

London, University college.

Two main subjects will be discussed. First, the study of the isospin and space properties of the neutral weak current has recently led to evidence for an isovector contribution and for a parity violation effect. Second, the study of the events which includes a μ^- and an e^+ has been completed. A strange particle is observed to be emitted in most cases and the observations are well fitted by the hypothesis of the existence of a "charm" quantum number.

1. PROPERTIES OF THE NEUTRAL WEAK CURRENT

The first evidence for neutrino reactions without muons in the final state was found more than three years ago[1]. These reactions are currently attributed to the existence of a neutral weak current. Nevertheless, because of technical difficulties, the detailed study of the neutral weak current is still in infancy[2]. We report here some of our investigations on both the isospin and space property of the neutral weak current.

1.1 Isospin properties of the neutral weak current

The isospin properties of the neutral weak current have been investigated in a simple channel, the one pion channel[3]. On a target made of neutrons and protons, there are four possible reactions :

$$\nu \text{ (or } \bar{\nu}) + p \rightarrow \nu \text{ (or } \bar{\nu}) + p + \pi^0 \qquad (1)$$

$$\nu \text{ (or } \bar{\nu}) + p \rightarrow \nu \text{ (or } \bar{\nu}) + n + \pi^+ \qquad (2)$$

$$\nu \text{ (or } \bar{\nu}) + n \rightarrow \nu \text{ (or } \bar{\nu}) + p + \pi^- \qquad (3)$$

$$\nu \text{ (or } \bar{\nu}) + n \rightarrow \nu \text{ (or } \bar{\nu}) + n + \pi^0 \qquad (4)$$

If the transition is an isoscalar ($\Delta I = 0$) transition, there is only one amplitude and the Clebsch-Gordon coefficients give the respective rates of (1):(2):(3):(4) = 1:2:2:1. Summing on an equal number of protons and neutrons, the relative rates of occurrence of the various charges of the pions are

$$\pi^0:\pi^-:\pi^+ = 1:1:1$$

We restrict ourselves to the test of a pure isoscalar transition since an isovector ($\Delta I = 1$) contribution would add two supplementary amplitudes, and there would be no relation between the rates of occurrence of the various charges. Furthermore, in order to avoid possible biases due to the π^+/p ambiguity, only the ratio $\pi^0:\pi^-$ was measured.

The number of protons is not exactly equal to the number of neutrons in the freon CF_3Br used in Gargamelle. Consequently, the hypothesis of a pure isoscalar transition leads to the ratio

$$Q = \pi^o:\pi^- = 0.9:1.$$

Once the pions have been emitted in the neutrino interaction, they may subsequently reinteract inside the nucleus, and then they may undergo charge exchange. In the hypothesis of the $\Delta I = 0$ transition, a very interesting property exhibits itself, namely the fact that the charge exchanges do not alter at all the rate of occurence of the different charge states of the pions. Consider the four charge-exchange reactions:

$$\pi^o + p \to \pi^+ + n \qquad (5)$$

$$\pi^o + n \to \pi^- + p \qquad (6)$$

$$\pi^+ + n \to \pi^o + p \qquad (7)$$

$$\pi^+ + p \to \pi^o + n \qquad (8)$$

The reactions (5) and (6) are equal by charge symmetry as are reactions (7) and (8). The reactions (5) and (7) are equal because they are time reversed processes, as are reactions (6) and (8). Hence the four reactions are equal. Let us call α the probability that a pion emitted inside a nucleus undergoes one of these reactions. It is possible to construct a reinteraction matrix which gives the rates of occurrence of the various charges after the interactions as a function of the rates before the reinteraction.

This matrix

	0	−	+
0	$1-2\alpha$	α	α
−	α	$1-\alpha$	0
+	α	0	$1-\alpha$

indicates a null overall effect and Q is still the same after the reinteraction of the pions. The experimental number can be compared with that prediction, once corrected for detection efficiencies. The π^o are detected by the observation of 2 γ-rays and the π^- are identified as interacting tracks.

The neutrino and antineutrino runs give respectively

$$\nu: Q > 1.4 \pm 0.2$$

$$\bar{\nu}: Q > 2.1 \pm 0.4$$

These numbers are to be considered as lower limits, since the neutron background exhibits a measured Q-value of 1. Hence, the neutron contribution can only make Q lower. Our conclusion is that the neutral weak current has at least an important isovector component. An isoscalar component is not excluded by the data. Nevertheless, in the hypothesis of a pure final state with isospin $I_f = 3/2$ which is produced by a $\Delta I =$ transition, Adler, Nussimov and Paschos[4] have calculated the effects of the reinteraction within the frame of the Salam-Weinberg theory[5] and predicted a Q value of 1.8 in that case, compatible with our observations.

1.2 Space properties of the neutral weak current

The space properties of the neutral weak current have been investigated through the measurement of the ratios of neutral-to-charged currents inclusive reactions R and $\bar{R}$

$$R = \frac{\sigma(\nu + N \to \nu + H)}{\sigma(\nu + N \to \mu^- + H)} \qquad \bar{R} = \frac{\sigma(\bar{\nu} + N \to \bar{\nu} + H)}{\sigma(\bar{\nu} + N \to \mu^+ + H)}$$

a) Selection of events

The principle of these measurements is to compare two categories of events, the NC (neutral current) and CC (charged current) events, with the smallest possible background and with reduced biases. The background is reduced by requiring that the N.C. events consist of positively identified hadrons with a visible energy greater than 1 GeV. The C.C. events consist of the same hadronic part, plus one (and only one) muon candidate. The use of the ratios NC/CC offers the advantage of minimizing the biases produced by flux measurements, energy measurements, etc.[6].

Since the previous analyses, increased statistics and a more refined study of the corrections are now available.

Table 1 gives the numbers of observed events, together with the calculated numbers of events coming from the following corrections :

1. The number of events due to the neutron background is calculated from a Monte-Carlo method which generates and propagates neutrons on the material both in front of and all around the fiducial volume.

2. There is a small correction which is due to neutral currents events feeding the CC channel, because a π^- which leaves or stops without interaction has not been identified.

3. Finally, a few NC events in the antineutrino beam are in fact produced by the neutrino contamination, whereas the anti-neutrino contamination is negligible in the neutrino beam.

The last column gives the corrected numbers of events, with a resolution of the π^+/p ambiguity which is described below.

Note that the average incident neutrino energy of the NC and CC events is about 4 GeV, an energy at which the behaviour of the inelastic charge-currents events can be tested to agree rather well with the hypothesis of scaling.

b) Effect of the corrections

In order to obtain the final values of R and $\bar{R}$, various assumptions or corrections have to be made. It is important to be sure that they cannot lead to systematic errors. The correction for the cut in hadronic energy will be made below in the framework of a model. Since this question is discussed separately, let us examine other possible sources of biases: the π^+/p ambiguity, the selection criteria and the measurement errors in energy.

The π^+/p has been treated in a statistical manner based on the sample of pions identified by δ-rays, and on the sample of stopping protons identified by range-curvature.

If only two extreme hypotheses are used, viz. that all the positive ambiguous tracks are pions, or protons, the values for R and $\bar{R}$ are found to be respectively :

	R	$\bar{R}$
π	0.22	0.59
p	0.27	0.52

These numbers give an impression of the importance of this effect. The statistical method mentioned above gives the final result :

$$R = 0.25 \pm 0.03 \qquad \bar{R} = 0.56 \pm 0.07$$

where the errors do not include systematic effects.

A second consideration is relevant to the evaluation of R and $\bar{R}$, i.e. the fact that the events are selected with all the hadrons identified could be the source of some small differences in the two categories NC and CC. This effect can be investigated by weighing each event according to the probability that the hadronic tracks interact.

The results obtained for R (0.26) and $\bar{R}$ (0.60) show that the effect of the selection criteria is in fact negligible.

Before going to the correction due to the hadronic energy cut, let us see if any systematic effect could come from the fact that the hadronic energy is not measured with an infinite precision. Errors in momenta measurements and losses of neutrals could affect the fraction of events rejected by the energy cut, thus leading to a misestimate of the correction. Since the E_H hadronic energy cut is reflected by a $y = \frac{E_H}{E\nu}$ cut, it was assumed that the differential cross section $\frac{d\sigma}{dy}$ can vary from a constant to a $(1 - y)^2$ dependence.

No effect of more than 5% was found on the percentage of events rejected by the cut, showing that this effect is negligible.

Taking all possible biases into account in the evaluation of the errors, the values for R and $\bar{R}$ uncorrected for the hadronic energy cut are:

$$R = 0.25 \pm 0.04 \qquad \bar{R} = 0.56 \pm 0.08$$

c) Comparison with models

In order to compare the observed values of R and $\bar{R}$ with theoretical models, we have corrected R and $\bar{R}$ for the effect of the energy cut, according to the following assumptions: the scaling hypothesis is valid[7], the charged and neutral currents have only contributions from V and A, and the target consists of spin 1/2 constituents. This leads to the well-known simple forms for the differential charged-current cross sections

$$\frac{d\sigma_c}{dy} = \frac{G^2 ME}{\pi}\left[a_c + b_c (1-y)^2\right] \quad \frac{d\bar{\sigma}_c}{dy} = \frac{G^2 ME}{\pi}\left[b_c + a_c (1-y)^2\right]$$

The measurements of the charged-current total cross sections give

$$a_c = 0.48 \pm 0.05 \qquad b_c = 0.02 \,{}^{+0.04}_{-0.02}$$

The neutral currents cross sections have the same form under the same assumptions :

$$\frac{d\sigma_n}{dy} = \frac{G^2 ME}{\pi}\left[a_n + b_n (1-y)^2\right] \quad \frac{d\bar{\sigma}_n}{dy} = \frac{G^2 ME}{\pi}\left[b_n + a_n (1-y)^2\right]$$

By integrating the effect of the hadronic energy cut over the neutrino and antineutrino spectra, the ratios R and $\bar{R}$ gives a_n and b_n, once a_c and b_c are known from the charged-current cross sections.

$$a_n = 0.116 \pm 0.024 \qquad b_n = 0.034 \pm 0.011$$

It is possible to obtain corrected values for R and $\bar{R}$ under the assumptions:

$$R_{corr} = 0.26 \pm 0.04 \qquad \bar{R}_{corr} = 0.39 \pm 0.06$$

where the errors include the effects of all the possible biases discussed above.

In the case of parity conservation, one should have $a_n = b_n$ since a and b respectively measure the contribution of V-A, (V + A) and respectively V + A (V - A) on partons(anti-partons). The result $a_n - b_n = 0.082 \pm 0.026$ is more than 3 σ away from this hypothesis. On the contrary, the results agree very well with the Salam-Weinberg model completed by a model of the nucleon[8] which gives (Figure 1)

$$\sin^2\theta_W = 0.31 \pm 0.06 \quad \text{from the R value}$$

$$\sin^2\theta_W = 0.33 \,{}^{+0.05}_{-0.08} \quad \text{from the } \bar{R} \text{ value.}$$

We would like to stress that such a good agreement between two independent measurements is not trivial. It does strongly support the hypothesis that the neutral current phenomenon is related to the Weinberg-Salam theory.

We conclude from the data that the parity conservation in the neutral weak current interaction is not favoured, and that the best value of the Weinberg parameter is

$$\sin^2\theta_W = 0.32 \pm 0.05$$

d) Result of the leptonic neutral current experiment

From the three unambiguous events found in the search for the reaction $\bar{\nu}_\mu + e^- \to \bar{\nu}_\mu + e^-$, a cross section value can be deduced

$$\sigma_{tot} = (0.10 \,{}^{+0.21}_{-0.09})\ 10^{-41}\ E_{CM}^2$$

where the errors are at a 90 % C.L.

In the Salam-Weinberg theory this gives a limit for the Weinberg parameter

$$\sin^2\theta_W < 0.4$$

a value which is consistent with the measurements in the semi-leptonic channel.

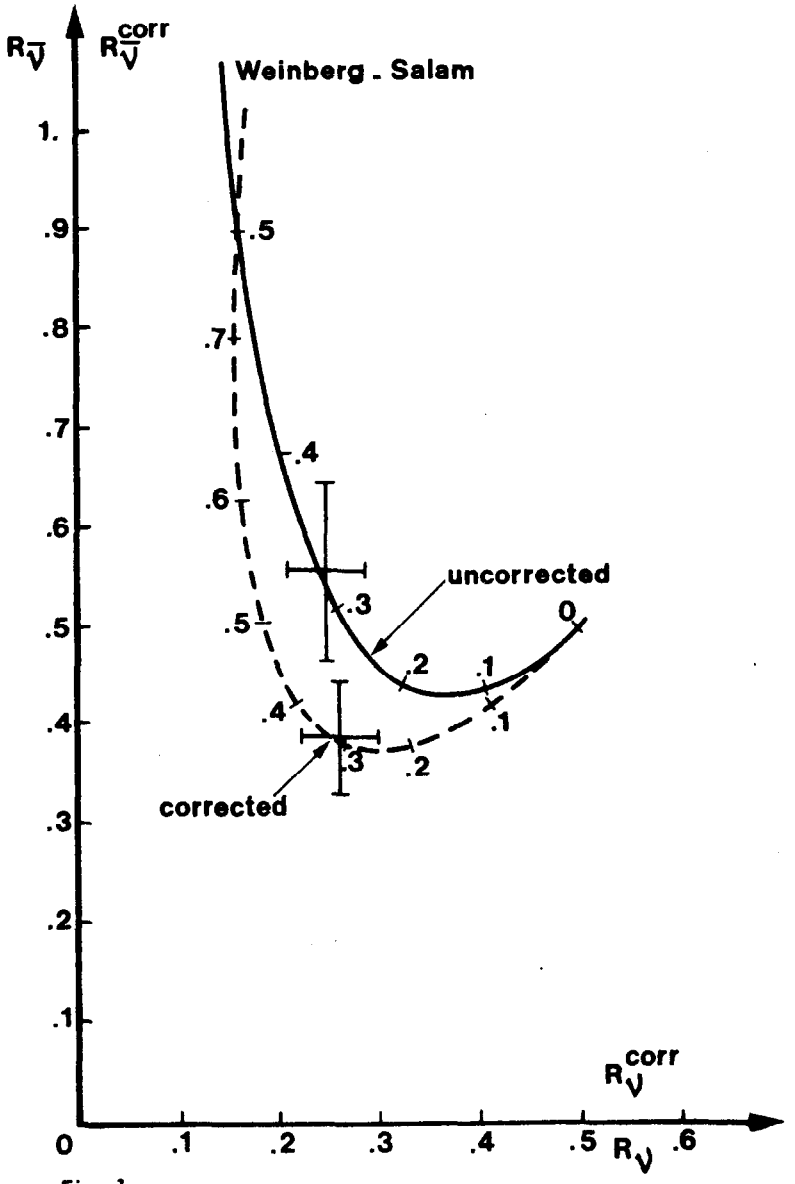

Fig. 1

2. THE CHARMED CURRENT

For the last three years, the evidences for a neutral weak current have been accumulated in neutrino ($\Delta S = 0$) reactions, whereas the absence of a neutral weak current has long been known from the case of the $\Delta S = 1$ transitions. One of the rare theoretical hypothesis which was able to deal with this apparent contradiction, i.e. the hypothesis of charm[9], resisted the experimental tests for many years.

More recently, the observation of one event produced in a $\Delta S/Q = -1$ reaction at Brookhaven, the dimuon events observed at Fermi Lab, and the first $\mu^- e^+ V^0$ event observed in Gargamelle, gave first support to the charm hypothesis[10].

To be significant, evidence for a new process has to come from more than one event. This is the reason the last neutrino run with Gargamelle was done with an increased synchrotron intensity.

A charmed hadron can be singly produced by a charmed current in neutrino reaction :

$$\nu_\mu + N \to \mu^- + C + \text{hadrons}.$$

In order to detect a possible charmed particle, a search was made of a characteristic semi-leptonic decay mode :

$$C \to S + e^+ + \nu_e$$

The strange particle S, of strangeness - 1, can be a Λ or a K, and may be detected by the clear signature of a V^0 ($\Lambda^0 \to \pi^- + p$, $K_s^0 \to \pi^+ + \pi^-$).

The positron, which is required to have an energy $E_e > 200$ Mev, is identified by a characteristic bremsstrahlung and spiralization.

The identification probability of such a decay is then ~ 100 %.

Among 40,500 charged current events of total energy above 1 GeV, three such unambiguous events have been detected[11]. A fourth event also deserves some concern but has unfortunately a positron energy either just above or below the cut, depending upon the method used.

The kinematics of the three events is shown in the following table (units are GeV).

	E_{vis}	Q^2_{vis}	W_{vis}	P_μ	P_e	$M_{\Lambda E}$	P_Λ	M_{Ke}	P_K
I	3.6	.61	2.5	.18	.25	1.2	2.1	0.65	1.8
II	3.9	1.9	2.1	1.1	.89	1.9	1.1	1.6	1.4
III	6.1	3.7	2.6	.9	.77	2.0	3.7	-	-

In order to know whether these events are due to charm or if they are caused by some background, the study of all the related channels has been made.

The following table gives the number of observed events in the different channels, together with the number of events expected from the various sources of background.

	Number of observed events	Background due to $\nu_e(\bar{\nu}_e)$	Background due to γ's and Dalitz	Total number of background
$\mu^-e^+V^o$	3	$.01 \pm .005$	$.11 \pm .05$	$.12 \pm .05$
μ^-e^+	16	$.6 \pm .2$	6.5 ± 2.5	7.1 ± 2.5
e^-e^-	25	9 ± 2	16.5 ± 4	25.5 ± 4.5
e^-V^o	6	3 ± 1	-	3 ± 1

The main source of background is due to asymmetric pairs of γ-rays materialized close to the neutrino vertex. The probability of such a close materialization has been measured in the present experiment to be $P = (4.1 \pm .7)$ % in a sample of $\sim 10^3$ γ-rays.

In the same sample of γ-rays, the probability of observing only the positron or the electron from the pair was found to be respectively $\alpha_+ = (1.5 \pm .3)$ % and $\alpha_- = (4.4 \pm .6)$ %.

A small background is also produced by ν_e and $\bar{\nu}_e$ interactions which lead to an e^- or an e^+ in the final state, together with a non-interacting π^- mistaken as a μ^-.

From the table above, it is clear that the 3 (4) $\mu^-e^+V^o$ events cannot be explained by the background, for such an interpretation has a probability of $\leq 2.10^{-4}$. The 16 μ^-e^+ events can be partially explained by the "7 background events", but it is expected that, in addition, some of the strange particles emitted in the channel μ^-e^+S will not be detected (K^o_L, $K^o_s \to \pi^o + \pi^o$, $\Lambda^o \to n + \pi^o$, $\Sigma^\pm$, $K^\pm$). The number of 16 μ^-e^+ events is compatible with a sum of the "7 background events" plus a number of events ($\sim$ 6-9) expected from the μ^-e^+S channel.

Finally, the channels e^-V^o and μ^-e^- can be explained by the background only. Consequently, the events in the various channels can have a consistent interpretation.

There is a large correlation between the e^+ and the V^o in the μ^-e^+ channel since, if there were no correlation at all, it could be deduced that 255 μ^-e^+ would have been expected on the basis of the 3 observed events, whereas only 16 μ^-e^+ events are seen.

Let us remark that the background interpretation of the $\mu^-e^+V^o$ events is also rejected by the consideration that it would imply the observation of 10 $\mu^-e^-V^o$, whereas none are seen.

Our conclusion is that a new weak current has been observed, which leads to the simultaneous or quasi-simultaneous production of a positron and a strange particle in addition to the ordinary muon.

We are not in a position to directly measure the mass of a charm particle assuming that the existence of charm is the interpretation of our observations. Nevertheless, the quantities measured are in agreement with what is expected from charm production by neutrino. The cross section calculations[12], mainly charmed-baryon production, give the right order of magnitude for the number of observed events if the semi-leptonic branching fraction is ~ 0.2. Note also that the sign of the positron (no electron) is in agreement with the charm scheme.

Finally, one V^o is identified as a Λ^o (Figs. 2a, 2b). In addition, among the 16 $\mu^- e^+$ events one shows the decay $\Lambda^o \to \pi^o + n$, with the detection of 2 γ-rays pointing apart from the neutrino vertex together with a neutron star.

If this new kind of neutrino reaction has to be identified with charm, a mass of a charmed baryon (C and C^*) in the region of 2.5 GeV is expected from the W-values observed.

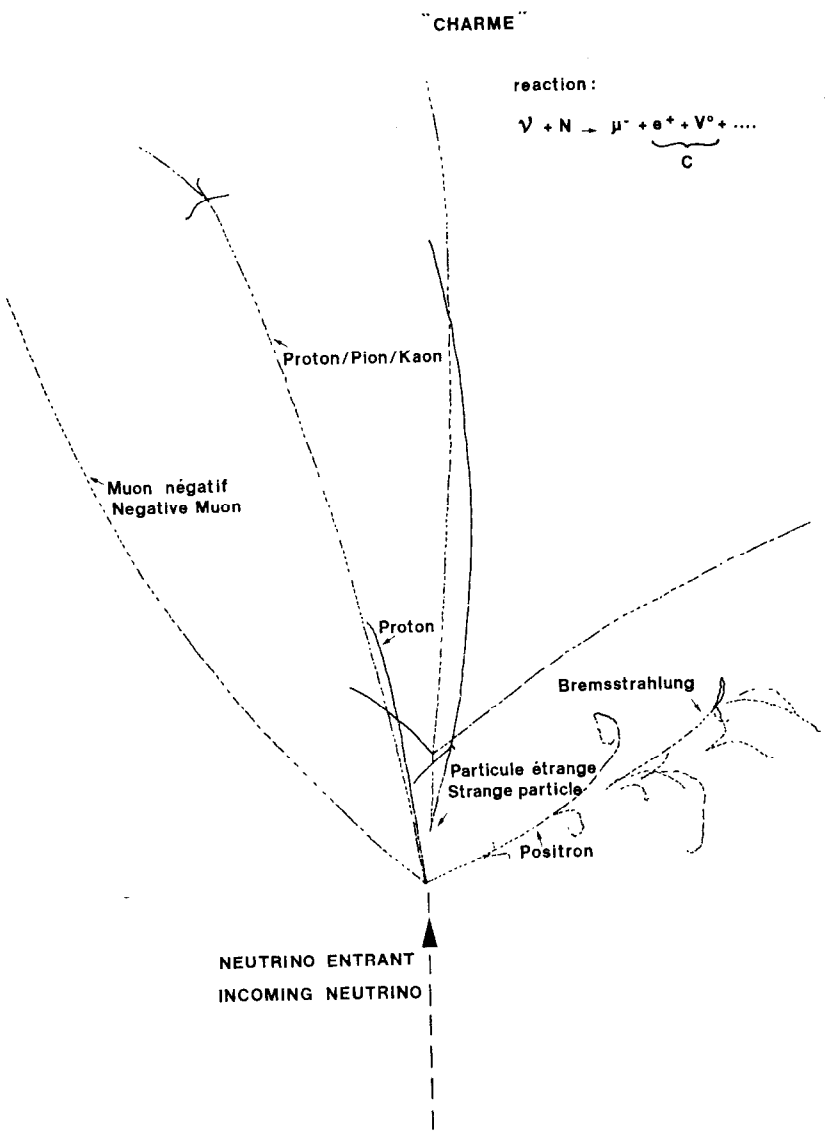

Fig. 2a

"CHARME" reaction :

$\nu + N \rightarrow \mu^- + \underbrace{e^+ + V^\circ}_{C} + \ldots$

Fig. 2b

REFERENCES

(1) F.J. Hasert et al., Phys. Let. 46B, n° 1, 138 (1973)

A. Benvenuti et al., Phys. Rev. Let. 32 800 (1974)

S.J. Barish et al., Phys. Rev. Let. 33 448 (1974)

B.C. Barish et al., Phys. Rev. Let. 34 538 (1975)

L.G. Hyman (p. 183), W.Y. Lee (p. 205), M.J. Murtagh (p. 239) in "La Physique du Neutrino à Haute Energie", Paris 1975.

(2) The experimental results are analyzed in connection with their theoretical implication in :

L. Wolfenstein "Phenomenology of Neutral Currents" COO-3066-39

J.J. Sakurai "Neutral currents without gauge theory prejudices" CERN/TH 20 99.

(3) G.H. Bertrand-Coremans et al., Phys. Let. 61B, n° 2, 207 (1976)

(4) S.L. Adler, S. Nussinov and E.A. Paschos, Phys. Rev. D.9, 2125 (1974).

(5) A. Salam and J.C. Ward, Phys. Let. 13, 168 (1964)

W. Weinberg, Phys. Rev. Let. 19, 1264 (1967)
Phys. Rev. Let. 27, 1688 (1971)
Phys. Rev. D5, 1412 (1972)

(6) F.J. Hasert et al., Nucl. Phys. B73, 1 (1974)

(7) J. Bjorken and E. Paschos, Phys. Rev. D1, 3151 (1970)

(8) L.M. Sehgal, Nucl. Phys. B65, 141 (1973)

(9) B.J. Bjorken and S.L. Glashow, Phys. Let. 11, 255 (1964)

D. Amati, H. Bacry, J. Nuyts and J. Prentki, Il Nuovo Cimento X34 1731 (1964)

S.L. Glashow, J. Iliopoulos and L. Maiani, Phys. Rev. D2, 1285 (1970)

G. Snow, Nucl. Phys. B55, 445 (1974)

A. de Rujula et al., Rev. Mod. Phys. 46, 391 (1974)

G. Altarelli, N. Cabibbo, L. Maiani, R. Petronzio, Phys. Let. 48B, 435 (1974)

M.K. Gaillard, B.W. Lee and J.L. Rosner, Rev. Mod. Phys. 47, 277 (1975)

M.K. Gaillard, S.A. Jackson and D.V. Nanopoulos, CERN/TH 0249 (1975)

(10) B. Aubert et al., XVII Int. Conf. on High Energy Phys., London 1974, V 117.

A. Benvenuti et al., Phys. Rev. Let. 34, 419 (1975)
" " " 35, 1249 (1975)

B.C. Barish, Symposium on Lepton and Photon Interactions, Stanford (1975).

E.G. Cazzoli et al., Phys. Rev. Let. 34, 1125 (1975)

U. Nguyen Khac, "La Physique du Neutrino à Haute Energie" Paris 1975

H. Deden et al., Phys. Let. 58B, n° 3, 361 (1975)

(11) J. Blietschau et al., Phys. Let. 60B, n° 2, 207 (1976)

(12) J. Finjord and P. Ravndal, Phys. Let. 56B, 61 (1975)

R.E. Schrock and B.W. Lee, Fermi Lab. Pub. 75/80 THY (1975)

Characteristics of $\mu^- e^+ K^\circ$ Events Produced by a Neutrino Beam

W. F. Fry
Department of Physics
University of Wisconsin
Madison, Wisconsin 53706

in collaboration with

A. Barbaro-Caltieri, P. Bosetti, G. Lynch, J. Marriner

F. Solmitz and M. L. Stevenson

Lawrence Berkeley Laboratory
University of California
Berkeley, California 94720

and

D. Cundy, D. Haidt, G. Harigel and H. Wachsmuth

CERN
1211 Geneva 23
Switzerland

and

R. Cence, F. Harris, S. I. Parker, M. Peters,

M. Peters, V. Peterson and V. Stenger

Department of Physics
University of Hawaii
Honolulu, Hawaii 96822

and

U. Camerini, D. Cline, J. von Krogh, R. J. Lovesles,

J. Mapp, R. H. March and D. D. Reeder

Department of Physics
University of Wisconsin
Madison, Wisconsin 53706

I. Introduction

Historically, the heavy liquid bubble chamber has been extremely useful in studies of the weak interaction, both studies of weak decay processes and of neutrino interactions. Among the attributes of this instrument are: excellent detection of neutral particles, complete comverage of solid angle for charged particles, and measurement of kinematic quantities of charged particles. The technique is uniquely suited for a sensitive search for new phenomena in neutrino interactions particularly when a new energy regime can be explored. Using the 15' bubble chamber at Fermi National Accelerator Laboratory (FNAL) together with the 300 GeV proton accelerator and associated neutrino beams we have obtained 80,000 pictures of the bubble chamber filled with a Neon-hydrogen mixture and exposed to a focussed neutrino beam.

One goal of the early analysis was motivated by the observation by the Harvard-Pennsylvania-Wisconsin-FNAL collaboration of neutrino induced events with two muons in the final state.[1] A search for events with a muon and an electron in the final state was made in the bubble chamber film and a sample of events has been isolated. Early results from the study have been previously reported.[2] Similar studies have been reported by BNL[3] and the Gargamelle collaboration.[4]

II. Experimental Details

The 300 GeV proton beam was extracted from the accelerator and directed on a Beryllium target one interaction length long. The resultant spray of positive mesons was focussed by two horns.

A typical burst of 6 x 10^{12} protons produced ν_μ neutrinos. This beam produced about one neutrino event per ten frames. This study also found the electron antineutrino ($\bar{\nu}_e$) flux to be about one order of magnitude smaller than ν_e. Although the absolute flux is difficult to determine by calculation, the relative contribution can be determined to about 20%.

For this exposure the FNAL chamber was filled with a mixture of neon andhydrogen (20% neon by volume). The density of this mixture is 0.281 gm/cm^3, the radiation length (λ_R) is 116. cm, and the characteristic interaction length is about 3 m.

An important feature of this chamber is the addition of apparatus to distinguish muons from charged hadrons. This External Muon Identifier (EMI) consists of 24 proportional wire chambers each 1 meter square in area located behind and outside the vacuum vessel of the chamber. Metallic zinc has been placed between the coils such that an additional four interactions lengths is provided. A track is extrapolated from the sensitive volume of the bubble chamber through the absorber and the magnetic field to the position of the wire chambers. The track is called a muon if there is an isolated "hit" in the wire chambers near the position of the extrapolated track. A hadron will interact in the absorber and the shower of secondary particles will record multiple hits in the wire chambers which have little correlation with the extrapoalted parent track. The misidentification of a true muon as a hadron is due mainly to chamber inefficiency and is about 1%. The misidentification of a hadron as a muon is due chiefly to the "punch through" of the energetic shower into the wire chambers and the accidental correspondence of one hit to the parent track. The probability of incorrectly identifying a muon is thus dependent on the number and energy of the hadrons produced in the ν interaction.

III. Scanning

In the study of rare event type phenomena it is imperative that the scanning and selection process be well understood in order that the results will be quantitatively meaningful. In the experiment reported here, the procedure involved scanning of a segment of the film by physicists and subsequent scanning and rescanning by professional scanners. All candidates for neutrino interactions of all types were studied by physicists, looking for events where an identifiable positron or electron was associated with the neutrino interaction. An electron is said to be identified if it exhibited one or more of the electromagnetic phenomena; (1) visible bremmstrahlung where the change in momentum was clearly discernible by visual inspection of the curvature (abbreviated as V.B.S.), (2) visible brammstrahlung accompanied by the conversion of the γ ray into an electron pair or compton electron (abbreviated as V.B.S._e.p.), (3) non-visible brammstrahlung plus electron pair where the electron pair did not point to the vertex but tangentially to the electron track or (4) the superposition of an electron pair on the track in question (triplet) which comes from the bremmstrahlung and conversion of the γ ray in a short distance so that the electron pair is superimposed on

on the incident electron.

Because there is a finite probability that the electron pair, for some of the above processes could come directly from the main vertex, it was necessary to apply an origin-electron pair distance criteria such that this background would be less than 10 percent of the signal.

IV. Electron Detection Efficiency

The detection efficiency for electrons and its energy dependence was determined from a study of electron pairs. In this study an electron apri must satisfy the following criteria: (1) zero opening angle and (2) point to a vertex in a chamber. The following quantities were recorded: (1) the type and number of electromagnetic processes which lead to its identification as an electron (if it was identified), (2) its position in the chamber and (3) its momentum. The chamber was divided into five zones along the length of the chamber. The detection efficiency was determined for each zone. to set the average detection efficiency each zone was weighted by its volume and the average taken. The results are tabulated in Table I.

Table 1

Electron Detection Efficiency

	Det. Efficiency	
$100 < p < 300$ MeV/c	0.29 ± 0.08	
$300 < p < 800$ MeV/c	0.47 ± 0.01	
$800 < p < 3000$ MeV/c	$0.52 \pm .08$	0.48 ± 0.07
$3000 < p < 5000$ MeV/c	$0.41 \pm .11$	

Table II

Topology of the Events

Event Number	How e^+ Ident.	μ^- Ident.	K°_S	K°_L	$K^\pm$	$\pi^\pm$	$L^\pm I^\pm S^\pm$
1	1 NVB + PR 1 VB + PR	EMI	+ -				
2	1 NVB + PR 2 VB + PR	Geom Miss of EMI	+ -				
3	2(VB + PR) Annih + PR	EMI	+ -				
4	1 Delta 1 VB 1 Trid	Geom Miss $L^\mp(2.8)$ in EMI	+ -				
5	1(VB - PR) INVB + C δ)-2) at VTX	EMI	+ -, oo	$1d(1I^{o}?$	$1I^+)$		
6	INVB + C INVB + PR	EMI	+ -	$1d(1I^{o}?$	$1I^+)$		
7	INVB + CPR IVB + CPR		Λ(+-)			1^+d	
8	IVB + PR	Geom Miss EMI		$1I \rightarrow \Lambda$ $1I \rightarrow K^\circ\pi?$	1^-d		
9	INVB + PR IVB KINK or VB	EMI	+ -	1I, 1n		$3I^+$ $1^-CH\ 1^-(K)$	$2L^+, 6\gamma$
10	IVB = PR	EMI	o o				
11	INVB + PR IVB + PR	EMI	or Λ				
12	2(VB + PR)	EMI			1^+d		
13	INVB + PR IVB + PR	EMI	or Λ(+-)				

NVB	Non Visible Trems.	L	Leaving Track
VB	Visible Brems.	I	Interacting "
TRID	$e^\pm$ Pair on e^+ Track	S	Stopping "
PR	Electron-Positron Pair	S	Stopping "
CPR	Close " " "	d	Decay
n	Neutron	CH	Charge Exchange
γ	e^- pair from Prim VTX		

TABLE III

LEPTON AND STRANGE PARTICLE KINEMATICS

ID#	E_{vis}	Momenta μ^-	Momenta e^+	K°_S	K°_L	$K^\pm$	Visible Q^2	Visible ν	Visible x	Visible y	Visible W^2
1	33	14	1.6	6.1			.13	18	.004	.56	35
2	12	3.4	1.1	3.1			1.6	8.1	.10	.71	15
3	26	21.8	2.2	1.6			6.2	3.1	1.	.12	.4
4	28	9.3	5.2	5.8			7.2	18	.21	.66	28
5	98	53	2.1	$^{+-oo}_{4.4,}$	2.1		.21	39	.003	.41	75
6	24	15	.4	2.2	3.3		5.5	7.8	.37	.34	10
7	15	$^{ss}_{2.0}$	5.6	1.2Λ			.16	12	.007	.86	24
8	20	(.80)	3.9		$^{3.6}_{4.6}$	.6	16	18	.49	.96	18
9	97	$^{ss}_{9.3}$	5.7	38	1.0		9.4	87	.058	.90	154
10	21	14.1	1.3	$^{oo}_{1.1}$			1.2	5.7	.11	.29	10
11	30	26.2	1.4	1.6 or Λ			2.7	2.9	.49	.10	3.6
12	61	$^{ss}_{17.9}$	4.0			±25	.70	42	.009	.70	78
13	42	33.6	.80	1.5 or Λ			3.8	7.3	.29	.17	10

ss "SAME SIDE" MUON

TABLE IV

MASS, MOMENTUM, CORRELATIONS $\perp$ TO $\vec{\nu}$ INC

ID#	M	POSITRON			STRANGE			EVENT		TOTAL
1	.70	-.018	.006	.019	-.552	.776	.952	1.897	.512	1.964
2	.81	-.051	-.040	.065	.277	-.924	.965	-.170	.234	.289
3	1.04	-.321	-.503	.597	.180	-.862	.881	.108	-.951	.957
4	.70	-.187	-.499	.531	-.279	-.550	.617	.260	.102	.279
5	.60 .69	.007	-.256	.257	-.089 .272	-.205 .556	.229 .619	-.369	.234	.437
6	.66 .67	-.047	.067	.081	.143 .024	-.219 -.573	.261 .573	-.091	-.807	.812
7	(1.5	-.390	-.843	.929	.320	-.221	.389	.033	-.581	.581
8	.85 .75 1.4K	-.052	-.213	.219	-.082 -.371 .026	-.629 -.391 -.241	.634 .539 .242	.407	1.052	1.129
9	1.3 2.1	.054	-.577	.580	.249 .049	1.296 -.254	1.320 .259	-.019	-1.251	1.252
10	1.08	.379	-.416	.562	-.002	.327	.327	-.740	-.487	.886
11	1.38(K)	.397	.288	.491	-.194	-.925	.945	.678	-.990	1.200
12	1.89	-.334	.482	.587	.210	.068	.221	.062	-.593	.596
13	95K (1.5^)	.420	-.164	.451	-.104	-.024	.107	-.240	-.814	.849

Although a quantitative study of study of the detection efficiency 5 GeV/c has not been made, the fact that electron neutrino events have been found which has electrons up to about 100 GeV/c and about at the correct rate is considered to show that this detection efficiency cannot be greatly lower than at 5 GeV/c.

All events which had an electron of either sign were taken as electron candidates and treated separately from all of the other neutrino interactions. Each of these events were then examined under high magnification to see if there was any evidence for a V° or a charged $K^{\pm}$ meson. Since the most striking characteristics of the dilepton events is the number of V° decays, the question arises as to whether the higher percentage of V'c comes from a more detailed study under higher magnification of the electron events. It was fund that an additional V° was found by this more detailed study of the vertex in only 10 percent of the cases and hence their effect is small.

V. Characteristics of $e^+\mu^-$ Events

Some of the more obvious characteristics of the events are given in the following tables of those where a e^+ is clearly identified and a μ^- is clearly identified by the EMI or where there is a μ^- candidate.

VI. Rate of μ^-e^+/CC

The production rate of μ^-e^+ events for the cuts $E_{e^+} \geq .8$ GeV and $E_{vis} > 5$ GeV can be estimated by connecting for the electron detection efficiency which has been given previously. The contribution of neutral currents in the denominator has been subtracted

if the partial cross section is to be compared to the charged current cross section. To obtain the true production rate, however, two more corrections have to be made.

a. Loss of events due to simulated Dalitz pairs.

True μ^-e^+ events will be lost in our selection process if the positron, combined with one of the negative non-interacting hadrons in the reaction, gives a mass $m(e^+L^-) < m(\pi^\circ)$. This loss was determined empirically by studying events with Dalitz pairs, where both $e^\pm$ were identified. For these events, the positron simulated a Dalitz pair with a leaving negative track in approximately 20% of the times.

B. Loss of events at energies $E_{e^+} < .8$ GeV.

Unfortunately, this loss cannot be determined experimentally since it depends on the mechanism by which the positrons are being produced. If the positron originates indeed from the decay of a particle with a mass of several GeV, the momentum spectrum of the positron will extend to quite small values and the effect of the $E_{e^+} \geq .8$ GeV cut will be substantial. It has been estimated using 3-body decay of a 2-GeV mass particle, that approximately 50% of the events might be lost with this cut.

An estimate for the total rate is then

$$\mu^-e^+/CC \tilde{=} 1.5\%.$$

VII. Strange Particles

The k multiplicity m that has been found in $e^+\mu^-$ events, to be meaningful, must be compared to that found in "normal" charged current interactions. A sample of charged current interactions have been studied looking for associated V's which come from decays of Λ°, k_S° and k_L°. The results of this study is summarized in the following table. An attempt was made to eliminate neutral currents in this sample.

Since 85% of the V's in the μ^-e^+ events are k° decays it is interesting to compare the ratio of various k° decays to charge current interactions in the $e^+\mu^-$ events with that in the charge currents. This comparison is shown in Table IV.

The total V°/(Interaction) in $(e^+\mu^-)$ compared to V°/(CC int.) is a ratio of 0.93/0.05.

Table III

Number and Type of V Events in

"Normal" charged Current ν Interactions in 20% Neon

Decay Mode	Number	Number of v's/CC
k°_S	19	19/970 = .02
Λ°	28	28/970 = .03
K°_L	2	2/970 = .002
$K^\circ_S\Lambda^\circ$	2	2/970 = .002
$K^\circ_S K^\circ_S$	0	
total	51	5%

(Total sample CC = 970)

Table IV

Comparison of V Event Rates in $e^+\mu^-$ Events with CC Events

Decay Mode in V° Events	V's in $e^+\mu^-$ number	N/event	V° in CC
$k^\circ_S(\pi^+\pi^-)$	6	6/13 = 46%	2%
$\Lambda^\circ(p\pi^-)$	2	2/13 = 15%	3%
K°_L	1	1/13 = 8%	0.2%
$K^\circ_S(\pi^+\pi^-)\ K^\circ_L$	1 (K°_L int)	1/13 = 8%	0 → ≤ 0.1%
*$k^\circ_S(\ ^+\ ^-)$, k°_L, k°_L	2	2/13 = 15%	0 → ≤ 0.1%
one or more v's/event		12/13 = 92%	5%

*The k°_L decay is taken in both $(e^+\mu^-)$ events and (CC) events even though it may come from a charge exchange of a $k^\pm$.

A more detailed analysis of the strange k particle production in $(e^+\mu^-)$ now follows.

IX. k° Phenomena

Although the available data on strange particle production in the $e^+\mu^-$ events is somewhat meager, it is enough to give some important results. The most quantitative results come from the k° phenomena while the evidence for charged k mesons is at best only collaborative.

The most definitive mode of identification of the k° is its two body decay; $k^\circ_S \to \pi^+ + \pi^-$. Typically it is a 3C fit to a vertex. The mean error in the invariant mass is about 25 MeV in this bubble chamber so that the chance coincidence of a neutron background event is negligible.

It is important to note that in two cases the V° has been identified as a Λ° and not a k°. In two other cases there is a k°-Λ° ambiguity. One possible source for the Λ°'s is the production of Λ°'s by a k° meson which was produced in the initial neutrino interaction. A crude estimate of this probability gives a snumber which is crudely consistent with the 2 Λ° events observed. (The two Λ°-k° events which are ambiguous are more likely to be k° than Λ° from a statistical consideration of probabilities).

Perhaps the simplest way to estimate the mean number of neutral k mesons produced per event is to use only the $k^\circ_S\pi^+\pi^-$ mode's and correct for the branching ratio. It will be assumed that the numbers of k°_S and k°_L are equal and that the branching ratio of $k^\circ_S\pi^+\pi^-$ to k°_S total is 2/3, this gives the efficiency for detecting

a $k^{\circ}_{s,L}$ as 1/3. The total number of events with one k°_{s} or others V's in addition is 7 out of a total of 14 $e^{+}\mu^{-}$ events. This gives for the average multiplicity of k° production

$$M(k_{sL}) = 7/13 \times 3 = 1.6 \pm 0.8$$

We know there is a loss at short lifetimes so this value is perhaps too small by about 15 percent.

X. Other Electron Phenomena

In the scanning, all tracks were examined to see if there was an electromagnetic process which would identify it as an electron track; either as an electron or a positron. Five processes lead to the production of electrons or positrons; namely:

1) Genuine $\mu^{-}e^{+}$ (or $\mu^{+}e^{-}$ from $\bar{\nu}$ contamination).
2) ν_e interactions and hence an absence of a muon.
3) Dalitz pairs from π° or η°.
4) High energy knock knock-on electrons along a track very close to the neutrino vertex, and
5) Electron pairs where the conversion of the γ occurred to close to the ν interaction that the gap could not be observed. If the pair is very asymmetric the lower energy electron or positron may be unobserved and hence only one electron of either sign seen.

Background classes 3, 4 and 5 can be reduced to a level below the $\mu^{-}e^{+}$ signal by a suitable choice of electron energy and asymmetry parameters as was discussed in the section on backgrounds.

The number of electrons and positrons which are consistent with or identified as Dalitz pairs as estimated from the average number of pions in normal neutrino interactions. There are about 4-5 Dalitz pair candidates for each identified $e^{+}\mu^{-}$ events.

There is a non-negligible contamination of electron neutrinos in the muon neutrino beam. No quantitative measure of the ratio of electron to muon neutrinos has been made, but an estimate can be obtained from the ratio of k/π from the proton horn target. This gives a ratio of about 3 percent. This is in agreement with the number that are tentatively identified as electron neutrino interactions.

XI. Summary and Conclusions

The most important properties of the $\mu^{-}e^{+}$ events are summarized in the following paragraphs.

a) The most striking characteristics of the $\mu^{-}e^{+}$ events is the high k° multiplicity. A search for decays of charged k mesons is clearly less conclusive but the results are consistent with the charged multiplicity being equal to the neutral multiplicity. The best estimate for the average neutral k multiplicity is about 1.6 $K^{\circ}/\mu^{-}e^{+}$ events. This is to be compared with an observed k° multiplicity of .06 for the charged current neutrino interactions, based on the $\pi^{+}\pi^{-}$ decay mode of the K°_{s} (19 events in 970 c.c ν_μ interactions).

b) The Λ° production is much lower than the k° production. It is possible that the observed Λ°'s come entirely from secondary $\bar{k}^{\circ}$ interactions in the target nucleus. The $k^{\circ}/\Lambda^{\circ}$ ratio associated

with the μ^-e^+ events corrected for the probability of observing each, is found to be 8 while in ν_μ c.c. interaction this ratio is fund to be 1.36. Clearly the strange particle production is different for the μ^-e^+ events than in the ν_μ c.c. events.

c) The total rate of production of $e^+\mu^-$/cc is estimated to be 1.5%.

d) There is no evidence for any energy dependence in the production of the μ^-e^+ events, although te statistics are poor.

e) The values of x and y are not significantly different for the μ^-e^+ events than for c.c. ν_μ interactions.

f) The ratio of the momenta of the two leptons is a significantly large number $\langle p_\mu \rangle / \langle p_e \rangle = 6.6$ suggesting that the two leptons do not come from the same vertex.

g) The remaining ν interactions which have an electron and not a muon are consistent with the interactions of electron neutrinos.

The K° multiplicity is consistent with the semi leptonic decay of a charmed particle into a k meson, electron and a neutrino.

References and Footnotes

1. A. Benvenuti, D. Cline, W. T. Ford, R. Imlay, T. Ling, A. Mann, R. Orr, D. D. Reeder, C. Rubbia, R. Stefanski, L. Sulak and P. Wanderer, Phys. Rev. Letters 35, 1199 (1975), 35, 1203 (1975), 35, 1249 (1975).
2. J. von Krogh, W. Fry, U. Camerini, D. Cline, R. J. Loveless, J. Mapp, R. H. March, D. D. Reeder, A. Barbaro-Galtieri, P. Bosetti, G. Lynch, J. Marriner, F. Solmitz, M. L. Stevenson, D. Haidt, G. Harigel, H. Wachsmuth, R. Cence, F. Harris, S. I. Parker, M. Peters, V. Peterson and V. Stenger, Phys. Rev. Letters 36, 710 (1976).
3. E. G. Cazzoli et al. Phys, Rev. Lett. 34, 1125 (1975).
4. M. Haguenauer; Proceedings of the International Conference on Production of Particles with New Quantum Numbers (held at Madison, Wisc.) (P330) 1976.

SEARCH FOR NEW PARTICLES PRODUCED IN $\bar{\nu}_\mu$ NUCLEON INTERACTIONS IN THE 15-FOOT BUBBLE CHAMBER*

F. A. Nezrick
Fermi National Accelerator Laboratory
Batavia, Illinois 60510

October 1976

*Work supported by the United States Energy Research and Development Administration. This experiment was performed by the following group:
J. P. Berge, F. A. DiBianca, H. Emans, R. Hanft, C. Kochowski,
F. A. Nezrick, W. G. Scott, W. Smart and W. Venus, Fermilab;
V. V. Ammosov, A. G. Denisov, P. F. Ermolov, V. A. Pitukhin,
Y. G. Rjabov, E. A. Slobodyuk, and V. I. Sirotenko, IHEP, Serpukhov;
V. I. Efremenko, P. A. Gorichev, V. S. Kaftanov, V. D. Khovansky,
G. K. Kliger, V. Z. Kolganov, S. P. Krutchinin, M. A. Kubantsev,
S. V. Mironov, A. N. Rosanov, and V. G. Shevchenko, ITEP, Moscow;
C. T. Coffin, R. N. Diamond, H. French, W. Louis, B. P. Roe,
A. A. Seidl and D. Sinclair, University of Michigan.

INTRODUCTION

Preliminary results are presented on searches for new particles produced in the interaction of antineutrinos with nucleons in the 15-ft bubble chamber. Indirect tests for new particle production are made by investigating the x and y distributions of all charged current events and by investigating the general properties of events with neutral strange particles. Direct tests of new particle production are made by searching for dilepton events and by looking for peaks in the invariant mass distributions of events involving neutral strange particles.

EXPERIMENTAL CONFIGURATION

This experiment utilized the 15-ft bubble chamber filled with a 21% atomic neon-hydrogen mixture (X_o = 110 cm) exposed to the horn focused antineutrino beam. The incident proton energy was 300 GeV and the average intensity was 8.5×10^{12} protons per pulse. The proton spill time was 20 μseconds which optimally matched the good focusing time of the horn system. The horn system focused negative particles ($\pi^- \rightarrow \mu^- \bar{\nu}$) and defocused positive particles ($\pi^+ \rightarrow \mu^+ \nu$). To suppress even more the neutrino background in the antineutrino beam an "absorptive plug" was placed downstream of the first horn to remove the wrong sign mesons which passed through the hold in the horn. Figure 1 shows the relative importance of the "absorptive plug" in reducing the neutrino background. In this experiment the neutrino contamination was less than 4% of the total flux.

The external muon identifier (EMI) was used in this experiment. The EMI consists of approximately 600 gms cms^{-2} of zinc absorber and magnet coils inside the vacuum vessel of the bubble chamber followed by 23 m^2 of multiwire proportional chambers.[1] Muon candidates seen in the bubble chamber are extrapolated to the EMI in an attempt to match them with fitted coordinates in the proportional chambers.[2]

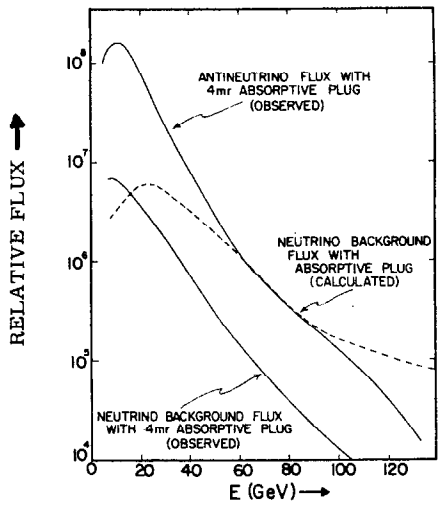

Fig. 1: Relative neutrino background flux with and without use of 4 mr absorptive plug compared with the antineutrino flux.

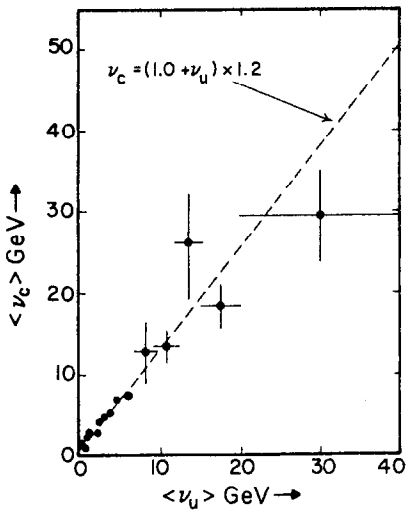

Fig. 2: Correction for missing hadronic energy.

Because of the geographical scale of this collaboration and our desire for a speedy result the bubble chamber film distribution received special attention. The entire quantity of film was copied using the direct reversal technique.[3] There are no identified differences in measurements from the original or copied film. Each nation received 50% original film and 50% copied film but was responsible for scanning and measuring only the original film. The copied film was used for cross checking.

DATA ANALYSIS

Event Scan Selection: The film was scanned for all neutral induced events with a total momentum, (charged plus neutral), Σp_x, along the neutrino beam direction greater than ~ 1 GeV. Events consisting of a single charged track only were not included in the scan. Therefore the elastic events $\bar{\nu} + P \rightarrow \mu^+ + n$ were not detected but those with observed V^o were recorded. About 3000 neutral candidates were found in the scan. Each of the four groups was responsible for scanning and measuring 25% of the total data. The Hydra Geometry program[4] was used for geometrical reconstruction.

Muon Selection: The EMI is used to identify the muon tracks. After the event is measured in the bubble chamber all tracks which could be muons are extrapolated to the EMI. From the extrapolated position in the EMI, the multiple scattering circle (the tracks penetrate about ~ 600 g/cm^2 of absorber between the fiducial volume and the EMI) and the position of the nearest actual recorded hit in the EMI, the confidence levels C_H of the track being a hadron and C_μ of the track being a muon are calculated. The track is taken as an identified muon if it has $C_H < 10\%$ and $C_\mu > 4\%$.

Antineutrino Energy Determination: In the charged current events the antineutrino energy is the sum of the momenta in the neutrino direction of the muon, charged hadrons and neutral hadrons. For

antineutrino interactions on the average only ~ 25% of the total energy goes into hadrons ($< y > \gtrsim 0.25$) and only about one-third of that into neutral hadrons. In this experiment a large fraction of the neutral energy is undetected. The following is a procedure to correct the antineutrino energy for the energy missing in neutrals.

Assume that on the average the neutral hadrons in the hadron shower are symmetrically distributed around the mean charged hadron direction. Then for a sample of events, with a certain average fraction of the hadronic shower momentum undetected, on the average the same fraction of longitudinal momentum, P_L^H, and transverse momentum, P_T^H, will be undetected. Due to Fermi motion and undetected nuclear fragments we do not expect transverse momentum balance in individual events. However for a sample of events if there were no missing neutrals the mean transverse momentum of the muon $< P_T^\mu >$ and hadrons $< P_T^H >$ should balance in the antineutrino-muon plane. Therefore the mean transverse imbalance in the antineutrino-muon plane is used to correct for the missing hadronic longitudinal momentum.

We calculate the corrected antineutrino energy as follows. The uncorrected energy transfer between the leptons and hadrons ν_u from the visible energy deposited in the detector is given by

$$\nu_u = \Sigma\ P_L^H$$

where P_L^μ and P_L^H are the longitudinal momentum of the muon and hadrons.

For fixed intervals of ν_u calculate $f = < P_T^H > / < P_T^\mu >$ in the antineutrino-muon plane and $< \nu_u >$. The mean corrected energy transfer ν_c for each interval is given by

$$< \nu_c > = \frac{< \nu_u >}{f}$$

The mean corrected energy transfer for intervals of the mean uncorrected energy transfer is given in Figure 2. The distribution is well fitted by the correction formula $\nu_c = 1.2\ (\nu_u + 1.0)$. All events are corrected for missing hadronic energy using the correction formula. We see the correction involves a 20% scaling plus an additive 1.2 GeV which could account for unseen nuclear recoil and spallation nucleons. The antineutrino energy is then the sum of the muon energy and the corrected hadronic energy.

INDIRECT TESTS OF NEW PARTICLE PRODUCTION

A. x and y Distributions

Consider the antineutrino-nucleon interaction described by the antineutrino and muon with energies E and E_μ and a virtual boson propagator carrying the energy $\nu = E - E_\mu$ and four momentum $Q^2 = 4EE_\mu \sin^2 \frac{\theta_{\mu\nu}}{2}$. The scaling variables are defined as $x = Q^2/2m\nu$ and $y = \nu/E$. In the scaling region the cross section for "neutrino" - nucleon scattering is of the form

$$\frac{d\sigma^{\nu,\bar{\nu}}}{dxdy} = \frac{G^2 ME}{\pi}\left[F_2(x)\ (1-y) + 2xF_1(x)\frac{y^2}{2} \mp xF_3(x)y(1 - \frac{y}{2})\right]$$

where F_1, F_2 and F_3 are the hadronic structure functions. Assuming charge symmetry invariance and the Callan-Gross relation $\left(F_2(x) = 2 \times F_1(x)\right)$ the cross section can be written:

$$\frac{d\sigma^{\nu}}{dxdy} = \frac{G^2 ME}{\pi}\left[q(x) + \bar{q}(x)\ (1 - y)^2\right] \qquad (1)$$

$$\frac{d\sigma^{\bar{\nu}}}{dxdy} = \frac{G^2 ME}{\pi}\left[q(x)\ (1 - y)^2 + \bar{q}(x)\right] \qquad (2)$$

with $q(x) = \frac{1}{2}\left[F_2(x) + xF_3(x)\right]$ and $\bar{q}(x) = \frac{1}{2}\left[F_2(x) - xF_3(x)\right]$. Within the quark-parton model $q(x)$ and $\bar{q}(x)$ are interpreted as the probabilities of the quark and antiquark being involved in the interaction and carrying the momentum fraction x. The relative momentum fraction of the nucleon carried by the antiquarks is expressed in the jargon of this subject by

$$B(x) = \frac{xF_3(x)}{F_2(x)} = 1 - \frac{2\ \bar{q}(x)}{q(x) + \bar{q}(x)}$$

Re-expressing equations 1 and 2 in terms of B and integrating over x gives

$$\frac{d\sigma^{\nu}}{dy} = \frac{G^2ME}{\pi} \int F_2(x)\,dx \left[(1 - y + \frac{y^2}{2}) + By\ (1 - \frac{y}{2})\right] \quad (3)$$

$$\frac{d\sigma^{\bar{\nu}}}{dy} = \frac{G^2ME}{\pi} \int F_2(x)\,dx \left[(1 - y + \frac{y^2}{2}) + By\ (1 - \frac{y}{2})\right] \quad (4)$$

As seen from equations 1 and 2 if the antiquark contribution to the interaction is negligible then the neutrino y-distribution will be constant and the antineutrino y-distribution will be $(1 - y)^2$. A sensitive determination of B comes from the antineutrino y-distribution in the high-y region which is dominated by the antiquark contribution. We also expect the relative antiquark contribution to affect primarily the low x region ($x < 0.2$) because of the rapidly decreasing ratio of $xF_3(x)/F_2(x)$ for small x.[5]

Let us now look at the experimental data for the y-distributions. The following data cuts were applied to the 3000 candidates described in the data analysis section to produce an unbiased antineutrino data set with well determined parameters:

1. Identify μ^+: One positive track must be identified by the EMI as a muon, i.e., $C_H < 0.10$ and $C_\mu > 0.04$.

2. Cut neutral background (n, K^O, etc.): Previous studies[6] show that most of the neutron, K^O, and other neutral background has an energy of less than 10 GeV. Therefore we require $E_c > 10$ GeV.

3. Well measured events: Require the event be greater than 65 cm from the downstream wall of the chamber to allow adequate measurement length for the tracks.

4. Good EMI Efficiency: For good EMI acceptance and to reduce hadron background we require that the muon candidate have a momentum greater than 4 GeV.

5. Good resolution of ν_c: Events with $\nu_u < 1$ GeV are cut from the sample (1) because of the large fractional correction for missing hadron energy[7] and (2) because the small ν region is biased from the scanning loss of elastic events.

Applying these data cuts to the antineutrino candidates produced 493 charged current antineutrino events between 10 GeV and 200 GeV. The y-distribution for these events has been corrected for the EMI geometrical efficiency which was calculated using Monte-Carlo events. The EMI geometrical efficiency as a function of x and y is given in Table I.

TABLE I

EMI Geometrical Acceptance Variation with x and y for Mean Antineutrino Energy of 20 GeV

y \ x	0.0 - 0.2	0.2 - 0.4	0.4 - 0.6	0.6 - 0.8	0.8 - 1.0
0.0 - 0.2	0.98	1.00	0.95	0.94	0.96
0.2 - 0.4	0.94	0.99	0.93	0.88	0.96
0.4 - 0.6	0.93	0.94	0.93	0.81	0.80
0.6 - 0.8	0.96	0.96	0.79	0.75	0.73
0.8 - 1.0	0.43	0.36	0.25	0.21	0.19

The y-distribution for all events between 10 GeV and 200 GeV with $0.0 < x < 1.0$ is inconsistent with a pure $(1 - y)^2$ distribution. A maximum likelihood fit gives $B = 0.79 \pm 0.06$. The y-distribution for $0.0 < x < 1.0$ and the different antineutrino energy intervals 10-30 GeV and 50-200 GeV are given on Figures 3a, 3b and 3c respectively and are compared with the theoretical y-distribution with $B = 0.8$. No apparent variation with energy is observed. The mean antineutrino energy in the 50-200 GeV distribution is about 62 GeV. Note that the fitted range of the y-distribution as shown by the data points on Figure 3 vary with antineutrino energy consistent with the $\nu_u > 1$ GeV and $P_\mu > 4$ GeV data cuts. The maximum likelihood fit to the y-distributions in the three energy intervals was made and the B values are given as a function of energy on Figure 4. From these data alone there is no evidence of an energy dependence of B. The data are

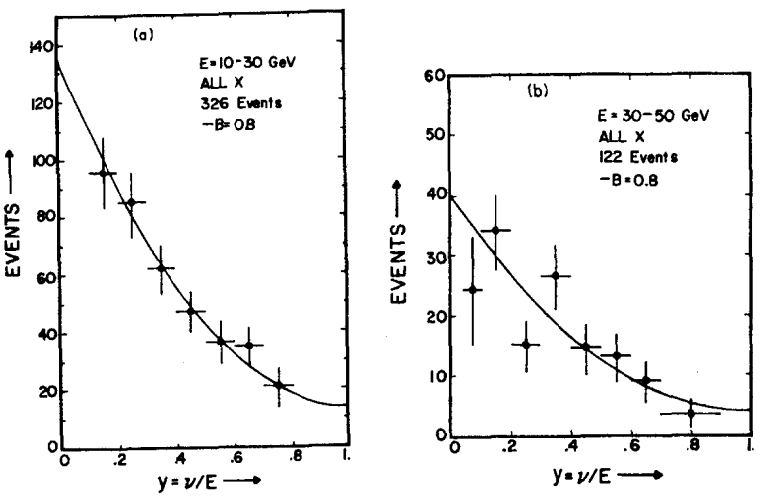

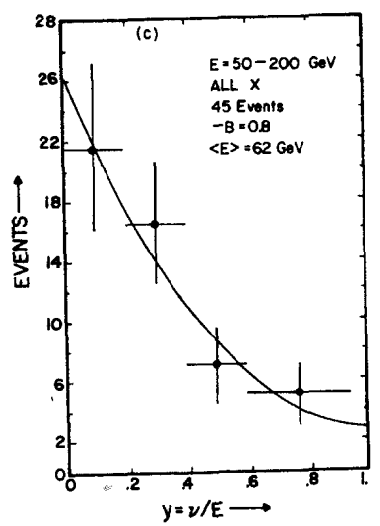

Fig. 3: Antineutrino y-distributions for events with $0 < x < 1.0$ in the antineutrino energy intervals:

(a) $10 < E < 30$ GeV
(b) $30 < E < 50$ GeV
(c) $50 < E < 200$ GeV

The solid line is from Eq. 4 normalized to the data and with $B = 0.8$.

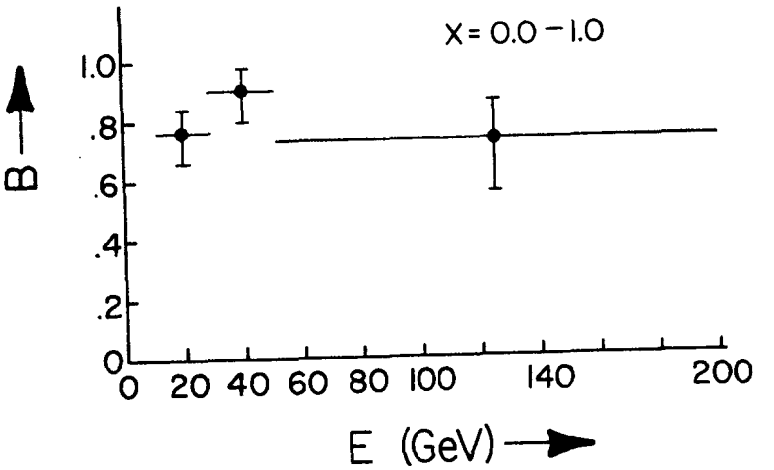

Fig. 4: B values as a function of antineutrino energy from maximum likelihood fits to data of Fig. 3a, 3b and 3c. The data are plotted in the middle of the energy intervals.

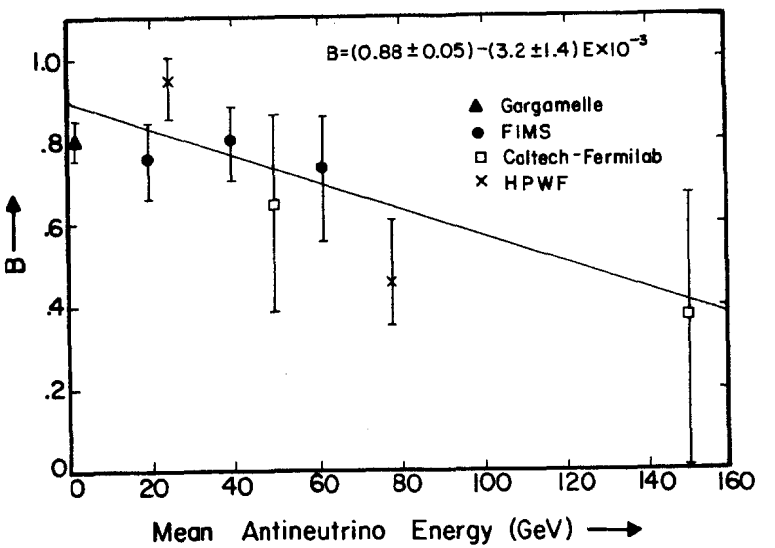

Fig. 5: B values as a function of antineutrino energy from Table II. The data are plotted at the mean of the energy interval. Solid curve is a least squares fit to the world data.

consistent with B = 0.79 ± 0.06 independent of energy which gives a relative antiquark contribution to the interaction $\frac{\bar{q}}{q + \bar{q}}$ = 0.10 ± 0.03.

Let us compare the world data on B values for antineutrino interactions as a function of energy. Table II summarizes the present situation. The graphical presentation of these data is given in Figure 5. A least squares fit gives[8]

$$B = (0.88 \pm 0.05) - (3.2 \pm 1.4)\ E \times 10^{-3}.$$

TABLE II

B Values from Antineutrino Experiments

Experiment	Approximate Mean Energy (GeV)	Fitted B Value $B = 1 - \frac{2\bar{q}}{q + \bar{q}}$
This experiment	20	$0.76\ ^{+\ 0.08}_{-\ 0.10}$
Fermilab-ITEP-Michigan-Serpukhov (FIMS)	40	$0.90\ ^{+\ 0.08}_{-\ 0.10}$
	62	$0.73\ ^{+\ 0.12}_{-\ 0.18}$
Gargamelle (GGM)[9]	1.5	0.80 ± 0.06
Caltech-Fermilab (CF)[10]	50	$0.64\ ^{+\ 0.22}_{-\ 0.26}$
	150	$0.36\ ^{+\ 0.30}_{-\ 0.36}$
Harvard-Penn-Wisconsin-Fermilab (FPWF)[11]	25	0.95 ± 0.10
	78	$0.45\ ^{+\ 0.15}_{-\ 0.10}$

Consider now the x dependence of B as determined from the y-distribution. For each of the three energy intervals of Figure 3 a maximum likelihood fit to B was made to the y-distributions for the x intervals 0.0-0.1, 0.1-0.2, 0.2-0.4 and 0.4-1.0. The fitted B values are given in Figure 6. Assuming that B is not a function of antineutrino energy, the data of Figure 6 are folded together to give the x dependence of Figure 7. Also given in Figure 7 is the x dependence

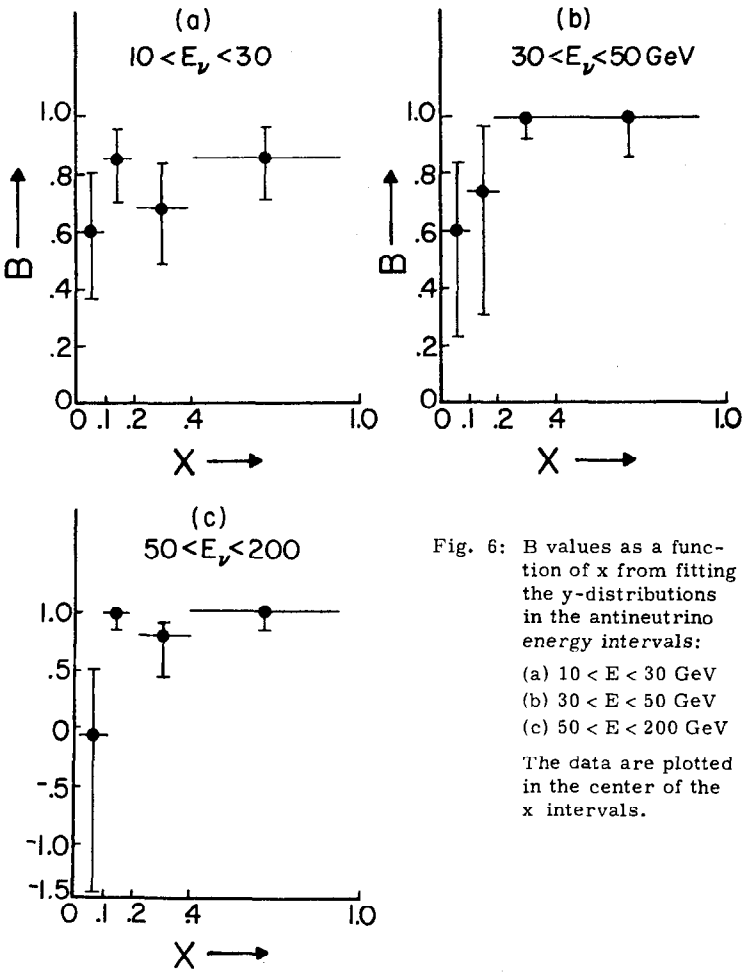

Fig. 6: B values as a function of x from fitting the y-distributions in the antineutrino energy intervals:
(a) 10 < E < 30 GeV
(b) 30 < E < 50 GeV
(c) 50 < E < 200 GeV
The data are plotted in the center of the x intervals.

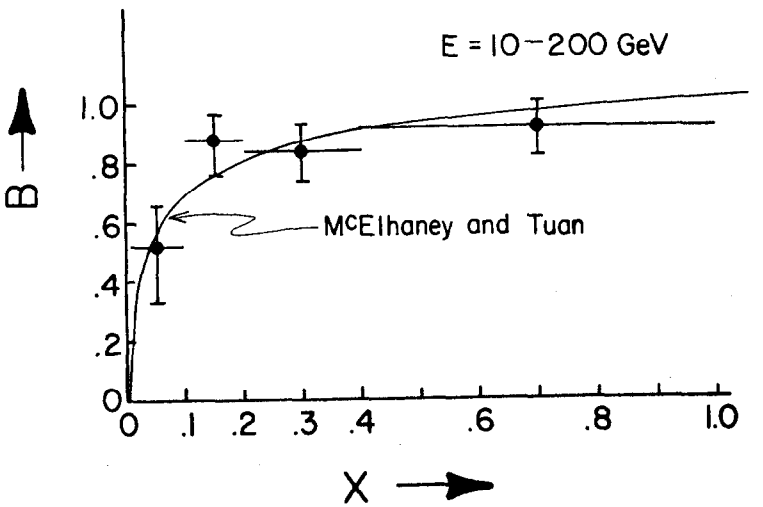

Fig. 7: Fitted B values as a function of x for antineutrino events for all energies, $10 < E < 200$ GeV.

of B as predicted by McElhaney and Tuan[12] which also fits well the Gargamelle data[9]. Even at high energies the antiquark contribution to the interaction is dominant at small x, ($x \lesssim 0.15$).

The $x = Q^2/m\nu$ distribution (quark momentum distribution) will be examined for three antineutrino energy intervals; 10-30 GeV, 30-50 GeV and 50-200 GeV. The x-distributions are corrected for EMI geometrical acceptance. For each energy interval only the events in the y-range unaffected by the P_μ and ν_u cuts are used. For example in the $10 < E < 30$ GeV ($50 < E < 200$ GeV) range $y_{min} = \nu_c^{min}/10$ GeV $= 2.4/10 = 0.3$ (0.1) and $y_{max} = E - P_\mu^{min}/E = 10-4/10 = 0.6$ (0.9). The x-distributions for the three energy intervals are given in Figure 8. The data are compared with F_2^{ed} (SLAC)[13] normalized for $x > 0.2$ where the antiquark contribution in the antineutrino data is negligible. In all three x-distributions, the data show an excess of events compared to F_2^{ed} for $x < 0.2$ and good agreement for $x > 0.2$. Is this low x behavior an anamoly? Probably not!

Expressing the differential cross section for antineutrino-nucleons and electron-nucleons in terms of the weights of up quarks (u), down quarks (d), and strange quarks (s) gives

$$\frac{d\sigma^{\bar{\nu}N}}{dx} \propto u + d + 3(\bar{u} + \bar{d}) \cos^2\theta_c + 6\,\bar{s} \sin^2\theta_c$$

$$\frac{d\sigma^{eN}}{dx} \propto u + d + (\bar{u} + \bar{d}) + \frac{2}{5}(s + \bar{s}).$$

Assuming all the sea components have equal weight and neglecting the Cabbibo angle gives:

$$\frac{d\sigma^{\bar{\nu}N}}{dx} \propto u + d + 3(\bar{u} + \bar{d})$$

$$\frac{d\sigma^{eN}}{dx} \propto u + d + \frac{7}{5}(\bar{u} + \bar{d})$$

Therefore in the region where the antiquark contribution is negligible ($x > 0.2$) we expect agreement between the antineutrino x-distribution and the electron x-distribution. As the antiquark contribution

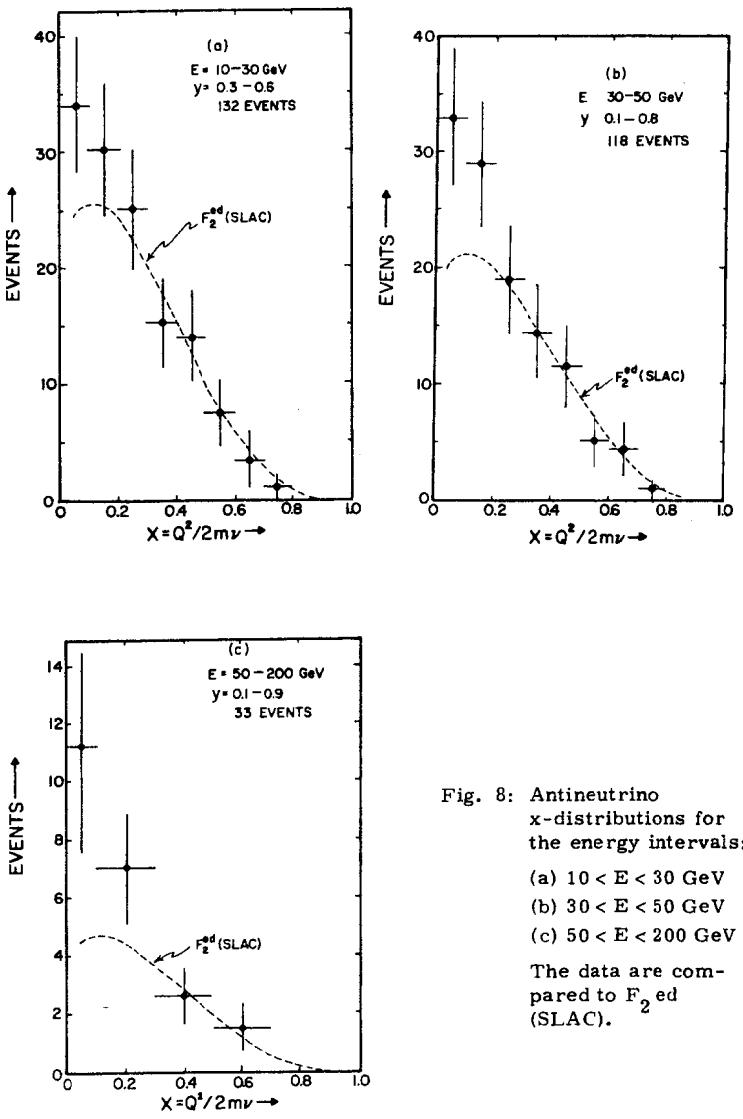

Fig. 8: Antineutrino x-distributions for the energy intervals:
(a) $10 < E < 30$ GeV
(b) $30 < E < 50$ GeV
(c) $50 < E < 200$ GeV
The data are compared to F_2^{ed} (SLAC).

becomes important ($x < 0.2$) we expect the antineutrino x-distribution to lie above $F_2^{ed}(x)$. The B values determined from the antineutrino excess at low x are in agreement (within errors) with the B values determined from the y-distribution.

B. Properties of Events with Neutral Strange Particles

This is a very preliminary analysis of events with neutral strange particles produced by antineutrino interactions. Most of the events are produced from a nuclear target (Ne). No correction is at present made for nuclear absorption, etc.

All events with two-prong "associated" secondary stars were considered as events with V^o (Λ^o, K_S^o) candidates. All V^o candidates were processed through Hydra geometry and through Hydra kinematics for three-constraint kinematic fits to the K^o or Λ^o mass hypothesis. Eighty-five events were found inside the 21 m^3 fiducial volume of the chamber which fit either K^o or Λ. Requiring that the antineutrino energy be greater than 10 GeV and that there be an EMI identified muon in the event produced a charged current sample of 588 events[14] of which 41 contain a K^o and/or a Λ. The energy distribution of the V^o events is given on Figure 9. The dashed line gives the shape of the energy distribution of the antineutrino charged current events in this experiment. There is no strong energy threshold above 10 GeV for a new strange particle production channel.

What is the relative rate of neutral strange particles produced in antineutrino-nucleon interactions? The observed distribution of V^o events is given in Table III. The events with a Λ^o or K^o are considered observed if they have kinematic fits to $\Lambda^o \to p\pi^-$ or $K^o \to \pi^+\pi^-$. For example there were five events with an identified K^o and an identified Λ^o, i.e. two V^o's. The corrections for neutral decay modes and for particles decaying outside the chamber are given in Table IV. The distribution of the corrected number of V^o events is given in Table III.

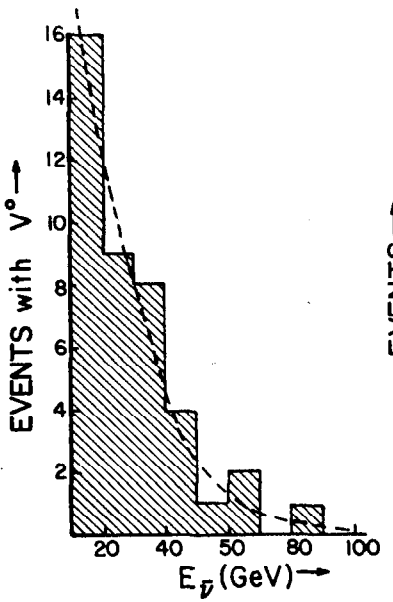

Fig. 9: Energy distribution of V^o events.

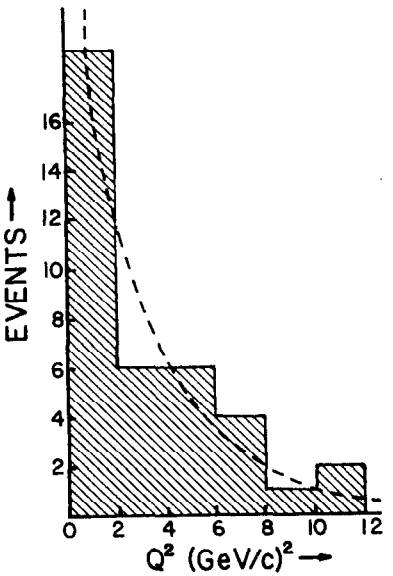

Fig. 10a: Q^2 distribution of V^o events.

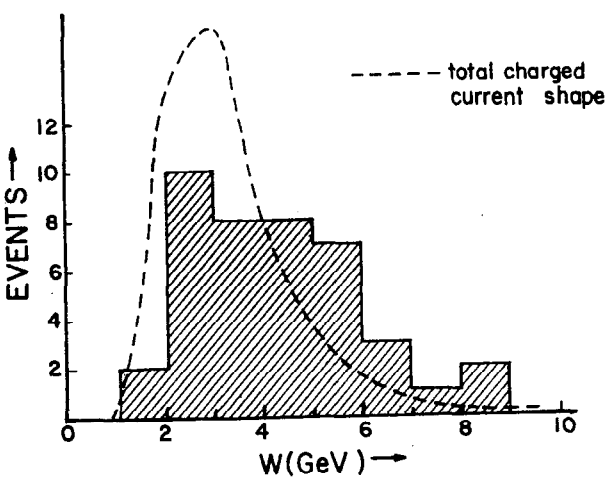

Fig. 10b: W distribution of V^o events.

TABLE III

The Observed and Corrected Distribution of Neutral Strange Particle Events

Class	Number of Events Observed	Number of Events Corrected
Λ^o	21	17 ± 9.
K^o	14	22 ± 17
$K^o + \Lambda^o$	5	22 ± 10
$K^o + K^o$	1	9 ± 9
TOTAL	41 ± 6.4	70 ± 13

TABLE IV

Probability of Observing Strange Particle Decay Mode A Coming from Source B

A \ B	Λ^o	K^o	$\Lambda^o + K^o$	$K^o + K^o$
Λ^o	2/3	0	4/9	0
K^o	0	1/3	1/9	4/9
$K^o + \Lambda^o$	0	0	2/9	0
$K^o + K^o$	0	0	0	1/9

Applying additional corrections of 10% for the loss of V^o which decay too close to the event vertex to be resolved and 10% for V^o events lost from processing inefficiency gives the total corrected number of 85 ± 16 events containing one or more V^o's in the charged current sample of 588 events. Therefore (14.5 ± 3)% of the charged current antineutrino-nucleon events above 10 GeV contain one or more neutral strange particles. In a previous experiment[16] it was found that (16 ± 3)% of the charged current neutrino-proton events above 10 GeV contain one or more neutral strange particles.

The momentum transfer, Q^2, distribution and invariant mass, W, distribution are given in Figure 10 and compared with the total charged current distributions. There is a tendency for the strange particle events to be produced at slightly higher W than the charged current events. This tendency was not statistically significant in the neutrino-proton V^o interactions.[16] The V^o enhancement with increasing W can be better seen in Figure 11. It is clear that strange particle production does increase with increasing W and to first order the increase is independent of the particle which excites the nucleon be it a neutrino, antineutrino, photon or electron. The x and y distributions for the neutral strange particle events are given in Figure 12 and are compared with the shape of the total antineutrino charged current event sample. The shaded part of the distribution represents the V^o events with W > 5 GeV. The total V^o sample has an x and y distribution consistent with the charged current events. However, the V^o events with W > 5 GeV are concentrated at higher than average y values.

DIRECT TESTS OF NEW PHENOMENA

A. Search for μ-e Events

Recently evidence has been reported[17,18] for neutrino induced events with both a positron and a negative muon in the final state. At high energy these events are reported to occur at a level of ~1% of all neutrino interactions. There is evidence that the rate of strange particle production in these events is anomalously high. Herein we report on a search for similar events produced in the antineutrino experiment.

The antineutrino events were selected as described in the Data Analysis section. After the events were measured, all events with $\Sigma P_x > 7.5$ GeV/c were examined by physicists searching for evidence

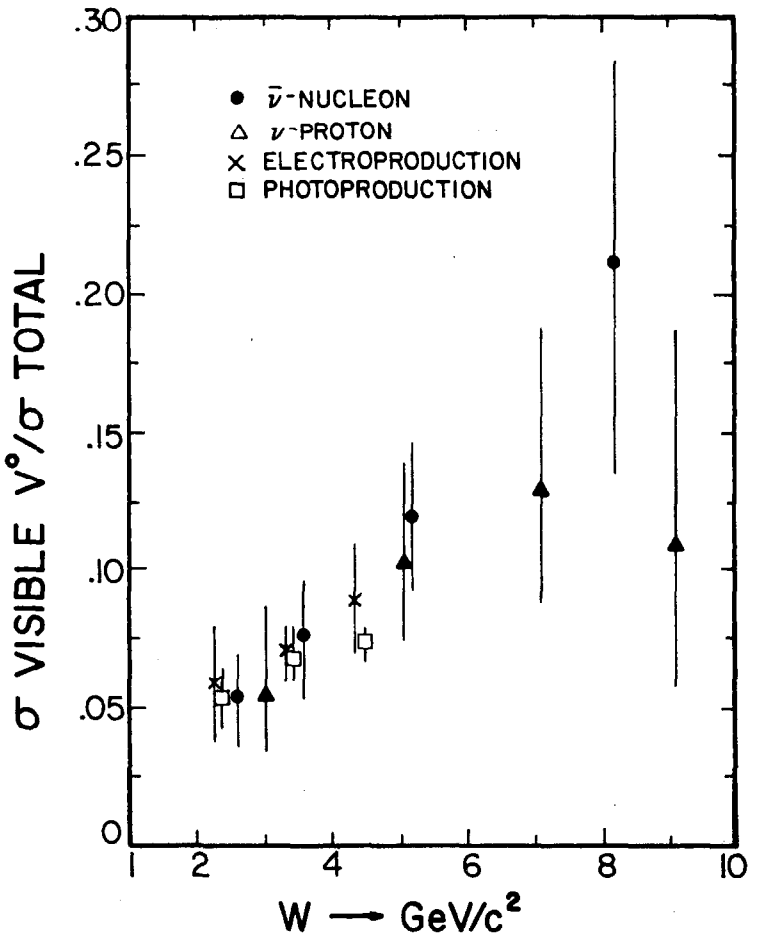

Fig. 11: The relative fraction of antineutrino charged current events with V^o's as a function of W. Comparison is made with neutrino-proton interactions, electroproduction and photoproduction.

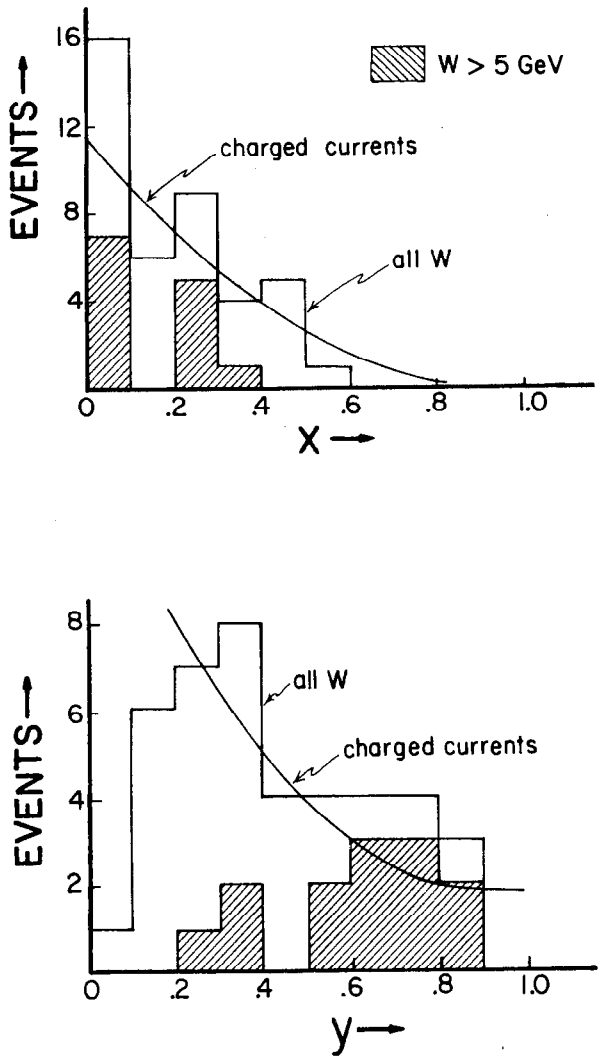

Fig. 12: x and y distributions for all V^0 events. The solid curve shows the shape of the total charged current x and y distributions. The shaded area shows V^0 events with W > 5 GeV.

of electrons or positrons at the primary vertex. Each track was examined carefully under high magnification (X70) over its entire length. Any track which spiralled smoothly to a point in the liquid or which had any visual indication of catastrophic energy loss - bremstrahlung (sudden curvature changes and/or converted pairs), tridents, large δ-rays, or annihilation (in the case of positrons) - was considered an electron or positron candidate. Each electron or positron candidate was measured and fitted over its entire length to find evidence of radiative energy loss. Electron or positron candidates which showed definite evidence of energy loss inconsistent with any other mass assignment were considered as identified.

In order to measure the detection efficiency for electrons produced with the same spatial distribution as the events in the bubble chamber, physicists examined both tracks of each electron-positron pair produced within 20 cms of the primary vertex of an event. Each track was examined to see whether it would have been classified as an electron or positron candidate using the same criteria as were used for tracks from the primary vertex. Figure 13 shows the measured electron detection efficiency as a function of the electron energy E_e. This efficiency decreases with increasing E_e to an approximately constant value of 0.70 ± 0.08 for $E_e > 800$ MeV.

As the electron energy decreases the number of expected background events becomes large as discussed below. Therefore events with electrons or positrons at the interaction vertex with $E_e < 200$ MeV are not considered further. After removing electron-positron pairs 12 events have an electron or positron apparently originating at the interaction vertex. These events are listed in Table V. The energies E_e are determined from curvature measurements corrected where appropriate for detected bremstrahlung.

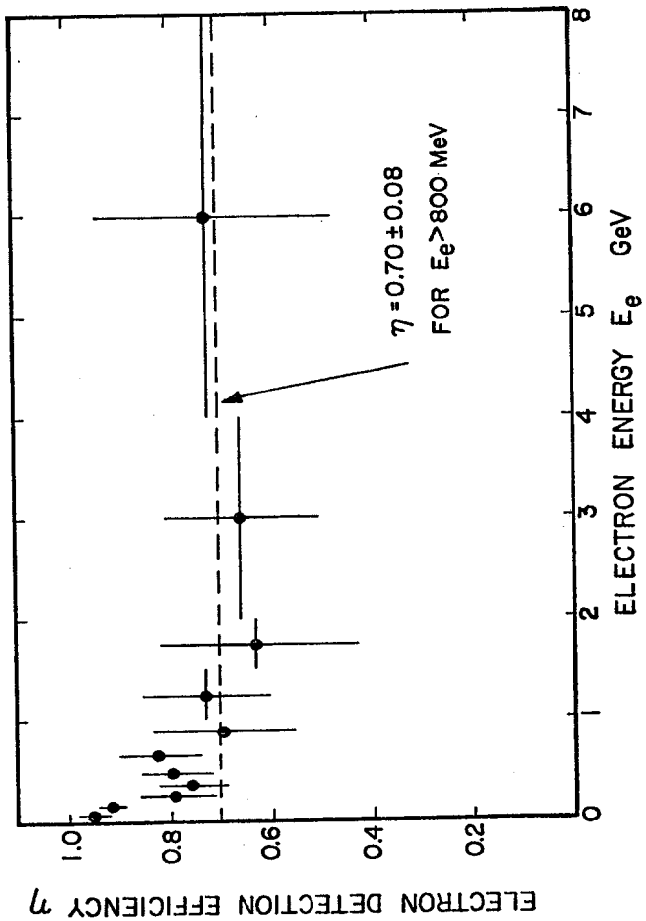

Fig. 13: The electron detection efficiency determined from a study of electron positron pairs plotted as a function of electron energy E_e.

TABLE V

List of Events with Single Electrons or Positrons with E_e > 200 MeV

Event Number	ΣP_x	E_e	EMI Muon	V^o
1	26 GeV/c	1.4 ± 0.1 GeV e^+	None	None
2	8 GeV/c	2.0 ± 0.1 GeV e^+	None*	None
3	21 GeV/c	12 ± 2 GeV e^+	None	None
4	33 GeV/c	32 ± 7 GeV e^+	None*	None
5	54 GeV/c	35 ± 5 GeV e^+	8.7 GeV μ^+	None
6	56 GeV/c	56 ± 13 GeV e^+	None*	None
7	68 GeV/c	67 ± 10 GeV e^+	None*	None
8	32 GeV/c	1.2 ± 0.01 GeV e^-	17.3 GeV μ^+	None
9	10 GeV/c	6.3 ± 0.4 GeV e^-	None	None
10	42 GeV/c	31 ± 8 GeV e^-	None	None
11	55 GeV/c	37 ± 12 GeV e^-	None	4 GeV/c K^o_s
12	153 GeV/c	130 ± 40 GeV e^-	None*	None

*All secondaries identified as hadrons in the bubble chamber.

Five events have all tracks other than the electron or positron identified as hadrons in the bubble chamber. Only events 5 and 8 have a muon identified by the EMI and are considered as μe candidates. Event 11 has a 4 GeV/c K^o_s; no other event shows any evidence for a strange particle.

In order to assess the significance of the two μe candidates consider the following backgrounds:

1. Electron neutrinos and antineutrinos are expected to be present in the beam at about the 1% level. Events 3 through 7 and 9 through 12 in Table V have leading electrons or positrons and are very likely to be ν_e or $\bar{\nu}_e$ induced events. A ν_e or $\bar{\nu}_e$ event can simulate a μe event when a hadron is misidentified as a muon by the EMI. The

probability that a hadron is misidentified as a muon by the EMI is estimated to be ~3%. With the assumption that all the events in Table V are ν_e or $\bar{\nu}_e$ induced, this background is estimated to be ~0.03 μ^+e^+ and ~0.15 μ^+e^- events. The importance of suppressing the ν_e background is clearly evident.

2. The film quality is such that a close in Compton electron vertex (within about 2 cm of the interaction vertex) may not be resolved. This background has been estimated from the measured gamma spectrum. Figure 14 shows the expected number of charged current events with close in Compton electrons with $E_e > E_{min}$.

3. Events with asymmetric gamma conversion within 2 cm of the primary vertex or asymmetric Dalitz pairs having an undetected electron or positron, apparently have a single positron or electron at the interaction vertex. With the assumption that electrons or positrons with $E_e < 5$ MeV are always undetected the expected number of such events has been estimated from the observed spectrum of Dalitz pairs and close in pairs and is shown in Figure 14. As E_e decreases below 200 MeV the background from both sources 2) and 3) increases rapidly.

4. Small angle K_{e3} decays are estimated from the observed number of K^o_s decays and decay kinematics to contribute 0.02 e^- and 0.04 e^+ background events.

Event 5 is the only μ^+e^+ candidate. In addition to the μ^+ and the e^+ in this event there are two negative hadrons. Interpreted as a $\bar{\nu}_\mu$ charged current event the estimated antineutrino energy $E_{\bar{\nu}}$ is 64 GeV, and the estimates for the scaling variables are x = 0.001 and y = 0.86. However the presence of a high energy leading e^+ suggests that this event may be a $\bar{\nu}_e$ event with a positive hadron misidentified as a muon even though the expected number of such events is only ~0.03.

Event 8 is the only μ^+e^- candidate. Events of the type μ^+e^- are of the particular interest because the lepton configuration is

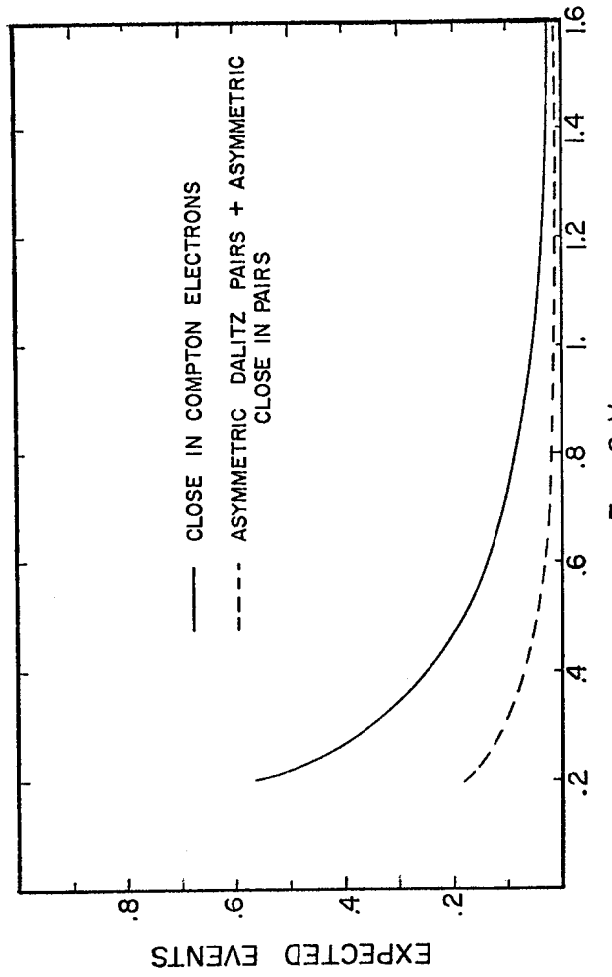

Fig. 14: The expected number of background events with $E_e > E_{min}$ due to close in Compton electrons and due to asymmetric Dalitz pairs and close in pairs.

charge conjugate to the configuration $\mu^- e^+$ observed in neutrino interactions as reported in References 16 and 17. In addition to the μ^+ and e^- there are 4 positive hadrons and 2 negative hadrons in this event. Interpreted as a $\bar{\nu}_\mu$ event the estimates for the antineutrino energy and the scaling variables are given by $E_{\bar{\nu}}$ = 36 GeV, x = 0.066 and y = 0.51. The combined background from all sources 1-4 considered above for $E_e > 1.2$ GeV is 0.2 ± 0.2 events. In fact for this particular event there is a small track of unknown sign at the interaction vertex which could be a positron with energy ~2 MeV which would indicate that the electron is part of a very asymmetric Dalitz pair. See Figure 15. The electron track overlaps 4 other tracks at the interaction vertex and it cannot be excluded that it is due to a Compton electron. The event is not considered compelling evidence for $\bar{\nu}_\mu$ induced μ^+e^- events.

Table VI shows the upper limit at 90% confidence for the yields of μ^+e^- and μ^+e^+ events relative to all antineutrino charged current

TABLE VI

Upper Limits for Antineutrino Induced μe Events as a Function of Energy (90% Confidence Level)

$E_{\bar{\nu}}$	Charged Current Events	$\sigma(\mu^+e^-)/\sigma(\mu^+X)$	$\sigma(\mu^+e^+)/\sigma(\mu^+X)$	$\sigma(\mu eV^o)/\sigma(\mu^+X)$
>10 GeV	1120	0.5%	0.5%	0.3%
>20 GeV	630	0.9%	0.9%	0.5%
>30 GeV	330	1.7%	1.7%	1.0%
>40 GeV	160	2.1%	3.6%	2.1%

events based on a single candidate in each case. Note that our maximum data sample has been used in this analysis. The upper limit on the relative yield of μe events with associated neutral strange particles detected via charged decay modes (V^o) is also given based on zero

Fig. 15: High magnification view of the vertex of the μ^+e^- candidate. The radius of curvature of the curling lepton track at the vertex is about 2 MeV/c.

candidates. The number of charged current events has been corrected for missing single track events.[19] No correction has been applied for EMI acceptance; the assumption is made that the EMI acceptance for μe events is the same as for all other charged current antineutrino events. The upper limits have been corrected for the electron detection efficiency $\eta = 0.70$. The upper limits are applicable for electrons with energies $E_e > 200$ MeV and for muons with energy above 4 GeV.

B. Search for μ-μ Events

We will present very preliminary results on the direct dimuon production by antineutrinos interacting in hydrogen-neon. The search naturally divides itself into two studies. The first study is for the sample of dimuons where one muon is fast ($P_\mu > 4$ GeV/c) and therefore identified by the EMI and the other muon is slow and decays and is identified in the bubble chamber (fast-stopping dimuons). The second study is for the sample where both muons are fast and are identified by the EMI (fast-fast dimuons).

Fast-Stopping Dimuons: The 1157 events with $\Sigma P_X > 7.5$ GeV studied in the μe search are further studied here. In several independent physicist scans all events were searched for continuous tracks which terminated in an identified electron as described in the previous section. These events contained direct electrons from the primary vertex, π-μ-e decays and μ-e decays. The direct electron candidates were used in the μ-e dilepton analysis.

Here we consider the events with π-μ-e and μ-e tracks which are trapped in the bubble chamber. The bubble chamber is basically a sphere of 1.8m radius with a magnetic field of 30 Kg. In principle a 1.5 GeV/c track can be trapped within the chamber and decay. In practice however the muon trapping efficiency drops to 10% for antineutrino events for muons of 600 MeV/c (muon range of 740 cm). Therefore in this study we restrict the slow muon to have a momentum of less than 600 MeV/c.

There were several events with very slow stopping positive tracks. In every case, these were ambiguously identified as stopping π^+ from observation of the unmistakable π^+-μ^+-e^+ chain. We measured and fit these tracks in order to gain some appreciation of the power of our Geometry program in separating slow π^+ from slow μ^+ orbits. It was found that for stopping tracks shorter than about 15 cm, there is inadequate difference between the quality of the fits for the μ mass and the π mass assumptions to allow convincing separation. In the fast-stopping dimuon study we therefore exclude all μ candidates with $P_\mu < 0.1$ GeV/c (corresponding to a μ with residual range of 22 cm). However in the present data sample there were no muon candidate in this momentum region.

The events were scanned at almost life-size. In the 23% atomic Neon-Hydrogen mix the range of the μ from a π decay at rest is ~ 3 mm on the scanning table. Because of foreshortening due to dip and possible μ alignment with the incident direction of the decaying pion it is frequently difficult to separate the π-μ-e decay chain from the μe decay at rest. Since it is difficult to visually detect angle changes less than 5° on a slow track, it is impossible to separate π-μ decays in flight with a trapped μ subsequently decaying at rest from μ-e decays. For these reasons the nature of the track ending in an electron was in most cases not determined at the scanning stage.

We measured every candidate track that did not have an unambiguous π-μ-e or an obvious kink from the production point down to the electron vertex with many points per view. The tracks were then fit starting at the production vertex in increasing arc length, looking for deviation in angle and momentum of the downstream orbit from the prediction of the fit to the upstream orbit larger than that predictable from multiple

scattering. This process largely eliminates π-μ decays in flight. In the remaining events, the transition point between the parent track and the electron track was discernable. Using the range-momentum relation for pions and muons allowed the separation of the remaining sample into probable stopping pions with invisible daughter muons and probable stopping muons. Three probable stopping muon events were found.

The properties of the three stopping muon events are given in Table VII. Events 2 and 3 are interpreted as antineutrino charged current high-y events with y values of 0.990 and 0.985. Observing two high-y events is consistent with B = 0.8. Event 1 is an apparent $\mu^+\mu^+$ event. Observing one such event is consistent with the estimated

TABLE VII

Properties of Antineutrino-Nucleon Events with Identified Stopping Muons

Event No.	ΣP_X	Stopping Muon Momentum	Fast EMI Muon Momentum
1	11.4 GeV	170 MeV/c μ^+	6 GeV/c μ^+
2	17.8 GeV	174 MeV/c μ^+	None
3	8.2 GeV	126 MeV/c μ^+	None

background from early and small angle π-μ decay in flight. No $\mu^+\mu^-$ events were found with one fast muon (P_μ > 4 GeV/c) and one or more slow muons (P_μ < 0.6 GeV/c). For antineutrino energies greater than 10 GeV a 90% confidence level upper limit on the production rate of $\mu^+\mu^-$ events within the above momentum ranges is about 3% of all charged current events. This limit has been corrected for the geometrical trapping efficiency for the slow stopping muon and for the μ^- capture probability. The $\mu^+\mu^-$ background is estimated to be about 0.3 events with the above cuts.

Fast-Fast Dimuons: We report here preliminary results on a search for events with two or more tracks identified as muons by the EMI. The data set used here is approximately the same as used in the μ-e search. The previously described EMI muon selection procedure (C_H < 10%, C_μ > 4% and P_μ > 4 GeV) was applied to each leaving track of the event which did not interact in the chamber. An acceptable multiple muon candidate satisfied the following conditions: the muon candidates did not have the same hit in the EMI, the time coincidence of "muon hits" in the EMI was within 111 nsec, each muon candidate had a momentum greater than 4 GeV/c and the total antineutrino energy was greater than 10 GeV. With these conditions the total efficiency for detecting the leading muon is ~75%. The total efficiency for detecting the non-leading muon is ~70%. Eleven dimuon candidates were found which satisfied the above conditions: 1(++), 5(+-), 5(-+) and 0(--) where the signs refer to the charge of the leading and non-leading muon candidates.

The dominant background in this procedure to select dimuon events is the normal charged current event accompanied by a pion punching-through to the EMI and being misidentified as a muon. The momentum spectrum of the non-leading muon candidates was calculated by applying an estimate[20] of the punch-through probability to the observed spectrum of π^+ and π^- mesons in the charged current events which exit the chamber without interacting. The observed and calculated integral spectra for the non-leading muon are given in Table VIII.

TABLE VIII

Number of Observed Dimuon Candidates and Calculated Background as a Function of the Momentum P' of the Non-leading "muon"

P' (GeV/c)	N(++) obs.	N(++) calc.	N(+-) obs.	N(+-) calc.	N(-+) obs.	N(-+) calc.	N(--) obs.	N(--) calc.
> 2	3	3.5	9	5	7	3.5	0	1.1
> 4	1	2	5	3	5	3	0	0.8
> 6	0	1	3	1.5	5	2	0	0.5
> 10	0	0.3	1	0.7	3	1	0	0.2
> 20	0	0.07	0	0.25	0	0.2	0	0.1

For events with P' > 4 GeV/c, 11 dimuon candidates were observed with a calculated background of 8.8 events. The observed number of dimuon candidates is not statistically significant above the estimated background. Only one dimuon candidate with P' > 4 GeV/c (P_{μ^+} = 11 GeV/c, P_{μ^-} = 18 GeV/c, $E_{\bar{\nu}}$ = 180 GeV) has an associated neutral strange particle, a K^o.

Assuming all the dimuon candidates in Table VIII with P' > 4 GeV/c are real dimuon events and folding in the total muon identification efficiencies, the 90% confidence level upper limits for the relative rates of dimuon production with and without a V^o in antineutrino reactions is given in Table IX. The dimuon rates are relative to the charged current sample which has been corrected for missing one-prong events. The upper limits are given in Table IX for dimuon production above antineutrino energies of 10-40 GeV.

It should be noted that assuming that the momentum spectrum of the non-leading muon in dimuon events is similar to the momentum spectrum of hadrons produced in single muon events, the requirement that the non-leading muon have P_μ > 4 GeV will suppress the apparent dimuon rate at lower antineutrino energies (~20-30 GeV).

It is clear that this type of analysis can be improved by using higher density neon-hydrogen chamber fittings and by an improved EMI.

TABLE IX

90% Confidence Level Upper Limits for Antineutrino Induced Dimuon Events as a Function of Energy

$E_{\bar{\nu}}$ (GeV)	$\frac{\sigma(\mu^+\mu^-X)}{\sigma(\mu^+X)}$	$\frac{\sigma(\mu\,\mu^+X)}{\sigma(\mu^+X)}$	$\frac{\sigma(\mu^+\mu^\pm V^o)}{\sigma(\mu^+X)}$
10	1.4%	0.6%	0.35%
20	2.4	1.1	0.6
30	4.2	2.0	1.2
40	5.8	4.3	2.4

C. Study of the Strange Particle Invariant Mass Spectra

A preliminary analysis is reported on semi-inclusive invariant mass spectra of 3-7 prong charged current events above 10 GeV with one or more observed neutral strange particles. This sample consists of about 500 charged current events including 17 Λ, 12 K^o and 2 $K^o\Lambda$ events.

Semi-inclusive invariant mass distribution, were studied for the combinations in brackets for the following reactions:

$\bar{\nu}N \to \mu^+ (\gamma\gamma)X$
$\to \mu^+ (\Lambda\gamma)X$
$\to \mu^+ (\Lambda\pi^+)X$
$\to \mu^+ (\Lambda\pi^-)X$
$\to \mu^+ (\Lambda 2\pi^+)X$
$\to \mu^+ (\Lambda\pi^+\pi^-)X$
$\to \mu^+ (\Lambda 2\pi^-)X$
$\to \mu^+ (\Lambda\pi^+ 2\pi^-)X$
$\to \mu^+ (\Lambda 2\pi^+\pi^-)X$
$\to \mu^+ (\Lambda 2\pi^+ 2\pi^-)X$
$\to \mu^+ (\Lambda 3\pi^+\pi^-)X$

$\bar{\nu}N \to \mu^+ (K^oP)X$
$\to \mu^+ (K^on)X$
$\to \mu^+ (K^o\pi^+)X$
$\to \mu^+ (K^o\pi^-)X$
$\to \mu^+ (K^o 2\pi^+)X$
$\to \mu^+ (K^o\pi^+\pi^-)X$
$\to \mu^+ (K^o 2\pi^-)X$
$\to \mu^+ (K^o\pi^+ 2\pi^-)X$
$\to \mu^+ (K^o 2\pi^+\pi^-)X$
$\to \mu^+ (K^o 2\pi^+ 2\pi^-)X$
$\to \mu^+ (K^o 3\pi^+\pi^-)X.$

For this analysis all unidentified charged tracks were taken as pions.

The ($\gamma\gamma$) mass distribution for all charged current events with two gamma rays is given in Fig. 16a. The π^o peak has a width of ±15 MeV centered at 130 MeV. The ($\Lambda\gamma$) mass distribution is given in Fig. 16b. There is some indication for the production of Σ^o (1190). A search was made of all the other invariant mass distributions for resonances with a width of $\lesssim$ 50 MeV. From a preliminary analysis, no narrow peaks were found which contained 4 or more events above background.

There is evidence from SPEAR for the existence of a charmed meson D^o ($\bar{D}^o$) with a mass ~1.87 GeV. In antineutrino interactions we might therefore expect to produce the $\bar{D}^o$ which could decay $\bar{D}^o \to \bar{K}^o\pi^+\pi^-$. Figure 16c shows the ($K^o\pi^+\pi^-$) mass distribution. There is no evidence for the production of $\bar{D}^o$ by antineutrinos. The upper limit on the cross section, relative to all charged current events, times branching ratio for the mode $\bar{D}^o \to K^o\pi^+\pi^-$ is about 1.5%.

CONCLUSIONS FROM ANTINEUTRINO-NUCLEON INTERACTIONS

1. y distribution study - The relative antiquark content of the nucleon is energy independent; $\frac{\bar{Q}}{Q+\bar{Q}} = 0.10 \pm 0.03$.
2. x distribution study - The x distribution is consistent with F_2^{ed} (SLAC) for $x \geq 0.2$ and is energy independent.
3. Properties of V^o events - The relative fraction of charged current events above 10 GeV with one or more V^o is 14.5 ± 3%, increases with increasing W and is consistent with νp interactions.
4. μ-e search - The upper limit on the production of μ-e events by antineutrinos is $\frac{\sigma(\mu^+e^-X)}{\sigma(\mu^+X)} < 0.5\%$ for $E_\nu > 10$ GeV.

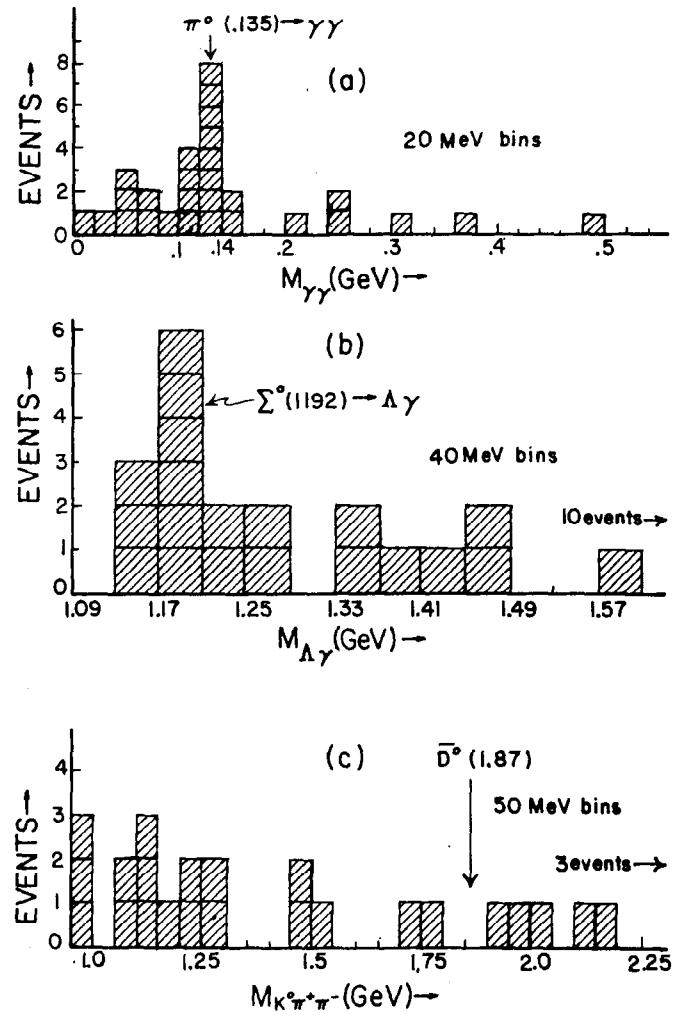

Fig. 16: Invariant mass distributions for (a) $\gamma\gamma$ combinations from all charged current events with 2 γ-rays converted. (b) $\Lambda\gamma$ distribution for all Λ events. (c) $K^o\pi^+\pi^-$ distribution for all K^o events.

6. μ-μ search - For antineutrino interactions greater than 10 GeV, the μ-μ upper limit is

$$\frac{\sigma(\mu^+\mu^- X)}{\sigma(\mu^+ X)} = \begin{cases} < 3\% & P_{\mu^+} > 4 \text{ GeV} \quad P_{\mu^-} < 0.6 \text{ GeV} \\ < 1.4\% & P_{\mu^+} > 4 \text{ GeV} \quad P_{\mu^-} > 4 \text{ GeV} \end{cases}$$

7. V^o invariant mass spectra study - No evidence was found for new narrow resonances. The upper limit (cross section x branching ratio) on the relative yield of $\bar{D}^o$ in antineutrino interactions is 1.5%.

WHAT IS IN THE FUTURE

The present experiment based on approximately 1,000 charged current antineutrino interactions lacks the statistical sensitivity to make strong conclusions on 1) the high-y anamoly, 2) the μ-e production, 3) the μ-μ production and 4) peaks in the strange particle invariant mass plots. During the first quarter of 1977 this experiment expects with additional running at Fermilab to increase its statistics by almost an order of magnitude. With the improved statistics and improved identification power of a heavier neon-hydrogen mixture it is anticipated that it will be possible to obtain definitive answers to some of the most important outstanding questions in present day experimental antineutrino physics.

FOOTNOTES AND REFERENCES

1. R. J. Cence, et al., University of Hawaii Report UH 511 217 76: Lawrence Berkeley Laboratory Report LBL-4816 (to be published in Nuclear Instruments and Methods).
2. In this experiment a muon is considered to be identified by the EMI if the muon confidence level for the match is greater than 4% and if the hadron confidence level is less than 10%.
3. Film copied at Eastman Kodak Co., Oakbrook, Illinois.
4. Hydra Geometry, Hydra Application Library, CERN.
5. H. Deden, et al., Nucl. Phys. B85, 269 (1975).
6. J. W. Chapman, et al., Phys. Rev. D. 14, 5 (1976).
7. A large fractional error in ν_c for small ν values has a negligible effect on the $y = \nu/E$ distribution but a large effect on the $x = Q^2/2m\nu$ distribution.
8. The difference between this fit and the fit reported earlier at the 1976 International Conference on Neutrino Physics, Aachen by F. Nezrick is the use here of the older Gargamelle determination of B determined from the y distribution study.
9. D. H. Perkins, Proceedings of the 1975 International Symposium on Lepton and Photon Interactions at High Energies, Stanford.
10. Results reported at the 1976 International Conference on Neutrino Physics, Aachen. The result was presented in terms of α where $B = 1-2\alpha$.
11. Results reported at the 1976 International Conference on Neutrino Physics, Aachen.
12. R. McElhaney and S. F. Tuan, Phys. Rev. D8, 2267 (1973).
13. A. Bodek, thesis, MIT, 1973 (unpublished).
14. Slightly different data sets have been used in the different sections of this paper. They are all unbiased sets with slightly more statistics in some studies. In each case the data set will be explicitly stated.
15. The total corrected number of V^o events is independent of the number of observed ΛK events, i.e., 3/2 (Λ events observed) + 3 (K events observed) - 3 (KK events observed).
16. J. P. Berge, et al., Phys. Rev. Lett. 36, 127 (1976).
17. H. Deden et al., Phys. Lett. 56B, 361 (1975).
18. J. Von Krogh, et al., Phys. Rev. Lett. 36, 710 (1976).
19. The missing single track events are expected to be largely confined to the region of small y. The number of missing events is estimated assuming a y-distribution of the form $dN/dy = (1 + y$

$+ y^2/2) - By(1 - y/2)$ with $B = 0.8$ and extrapolating to $y = 0$. The correction is 14% for $E_{\bar{\nu}} > 10$ GeV and less at higher energies.

20. We appreciate V. Z. Peterson making available to us the results of Monte Carlo punch-through calculations performed by A. Grant at Cern.

CALT 68-564
ENERGY RESEARCH AND
DEVELOPMENT REPORT

DIMUON PRODUCTION IN HIGH ENERGY NEUTRINO AND ANTINEUTRINO INTERACTIONS*

B. C. Barish, J. F. Bartlett, A. Bodek, K. W. Brown, D. Buchholz†,
Y. K. Chu, F. Sciulli, E. Siskind, L. Stutte,
California Institute of Technology, Pasadena, California 91125

E. Fisk, G. Krafczyk, D. Nease
Fermilab, Batavia, Illinois 60510

and

O. Fackler
Rockefeller University, New York, N.Y. 10021

Talk presented by L. Stutte at the SLAC Topical Conference, Stanford Linear Accelerator Center, Palo Alto, California, Aug. 11-13, 1976.

* Work supported in part by the U.S. Energy Research and Development Administration. Prepared under Contract E(11-1)-68 for the San Francisco Operations Office.

† Now at Northwestern University, Evanston, Illinois.

I. Introduction

We have examined a sample of high energy neutrino and antineutrino induced events for evidence of dimuon production. The data were obtained in the fall of 1975 using the Caltech-Fermilab apparatus[1] and the narrow-band dichromatic neutrino beam.[2] Since the primary purpose of this run was a measurement of the charged current total cross-section, the data cover a wide range of separate incident neutrino energy settings of the beam between 30 and 215 GeV, corresponding to hadron beam energy settings of 80-250 GeV. The spill time was long enough ($\sim$1 sec) to allow for an independent ascertainment of the incident neutrino flux. The run resulted in approximately 20,000 charged current events for which all kinematic quantities are calculable.

Some of the important features of our experiment relevant to dimuon production are:

1) the dichromatic beam - The events obtained are mostly high energy ($\gtrsim$ 30 GeV) and can be separated into samples of neutrino and antineutrino induced events, since the beam is sign-selected.

2) a dense target-detector - The packing fraction of the calorimeter is ~50% (e.g. the density $\rho \sim 4$ gm/cm^3), minimizing extra muons from π or K decay.

3) good muon detection - Muons are identified with good acceptance down to $E_\mu \sim 3$ GeV, since the Fe target also serves as a muon identifier.

4) small solid angle magnet - This is an important limitation in the data since most of the kinematic quantities can be measured for only a fraction of the events.

Some of the questions we hope to answer with these data include:

1) Are the new data consistent with previously reported data or dimuon production?[3,4]

2) How do neutrino- and antineutrino-induced dimuon events compare?

3) What is the energy dependence of the dimuon production rate?

4) What is the evidence for trimuon production?

The results are still preliminary and this paper is just a progress report. The dimuon data presented here are completely uncorrected for acceptance or detection efficiency. The background calculations are also preliminary and the estimates are shown for comparative purposes. No background subtraction has been applied to the data.

The scan for the dimuon events has just recently been completed, while the single muon event scan is still in progress. Roughly 10-30% of the single muon charged current events have been measured (depending on the energy) so that the total numbers of single muon events have been estimated. Energy calibrations are still being completed and thus there is an uncertainty of ± 20 % in the hadron energy. For the data presented here, the major importance of this uncertainty is in the calculation of the π and K decay background level relative to the data.

II. General Features of Events and Backgrounds.

Figures 1 a,b show two dimuon candidates obtained with the beam set to transport a positive 190 GeV/c secondary hadron beam through the decay pipe. The neutrinos enter from the left and interact in the 140 ton steel target. Scintillation counters located every 4" of steel were used to measure the final state hadron energy E_H using calorimetry techniques.[5] The angles of the final state muons θ_μ were determined with magnetostrictive spark chambers. For those muons which did not stop in or exit from the target prematurely, the muon energy E_μ was determined by measuring their deflection in the steel toroidal magnetic spectrometer situated downstream of the calorimeter.

Figure 1a shows an event with rather large hadron energy in which both muons enter the spectrometer. The total energy observed (~ 180 GeV) is so

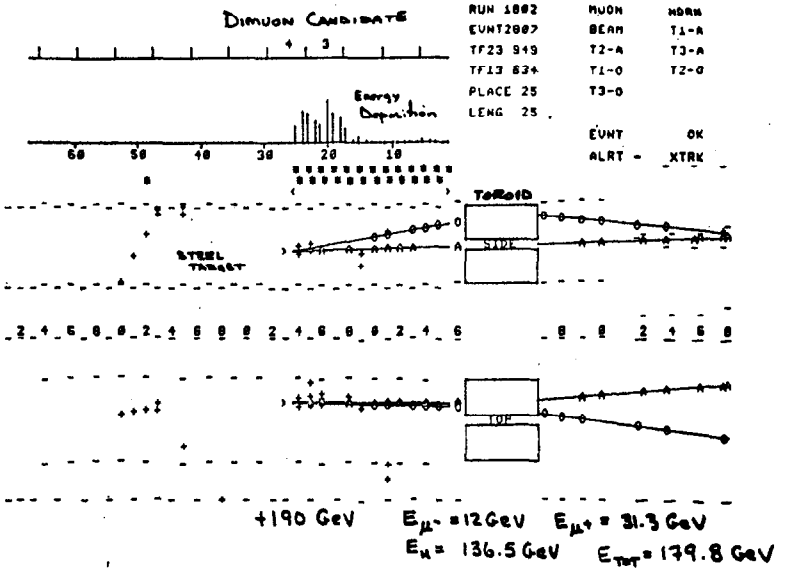

Fig. 1a

Example of dimuon candidates at +190 GeV in the Caltech-Fermilab detector. Both muons enter the magnetic spectrometer.

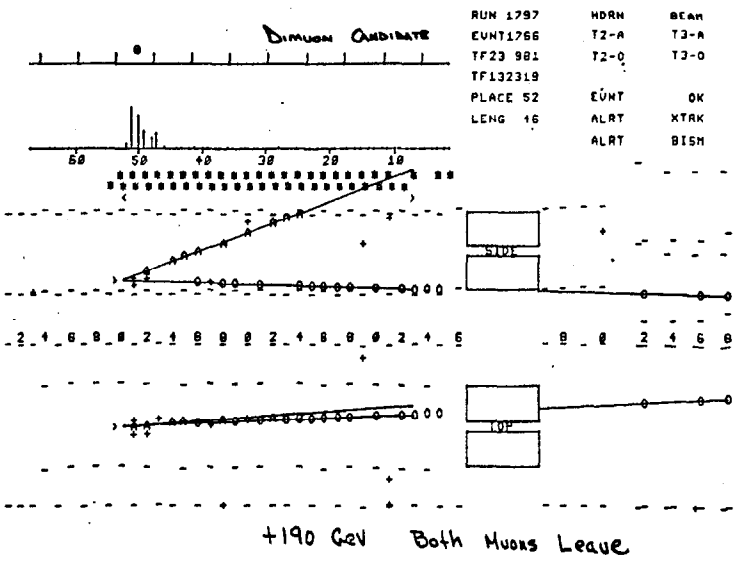

Fig. 1b

Example of dimuon candidates at +190 GeV in the Caltech-Fermilab detector. Both muons miss the target.

large that this event must have come from a kaon-decay neutrino ($\langle E_{\nu_K} \rangle = 171$ GeV). Figure 1b shows perhaps a more typical event in which both muons leave the target and the total energy observed is a lower limit.

Figure 2 shows a dimuon event obtained with the beam set at -190 GeV (antineutrino running). As in Figure 1a, both muons enter the spectrometer. At -190 GeV the negative pion decay antineutrinos have $\langle E_{\bar{\nu}_\pi} \rangle = 56$ GeV, so this event with 132 GeV of observed energy is again consistent only with a kaon decay antineutrino, ($\langle E_{\bar{\nu}_K} \rangle = 150$ GeV).

Figure 3a,b shows the integrated number of observed 2μ events as a function of the second muon energy $E_{\mu 2}$ with $E_{\mu 2} > E$. This implicity requires a penetration in steel of about 2 meters. The neutrino and antineutrino data are shown separately, but are summed over the incident neutrino energies. All dimuon candidates are plotted which satisfy the following restrictions:

a) at least one muon entered the spectrometer and

b) the second muon has an observed energy greater than 3 GeV/c

as determined by the distance traversed in the steel target.

The most likely source of background for dimuon events is an ordinary charged current event with an extra muon resulting from the decay of a pion or kaon produced in the hadronic cascade. In order to estimate an upper limit to this background we used a Monte Carlo program to simulate the hadronic cascade through several generations until the shower was completely absorbed in the target-calorimeter. The final state hadron distributions in the initial neutrino interaction were chosen to match multiplicity and energy distributions for charged hadrons measured in Fermilab bubble chamber neutrino experiments.[6] The resulting probability curves are then folded with the measured hadron energy (E_{had}) distributions at each incident neutrino energy to obtain the expected number of background 2μ events

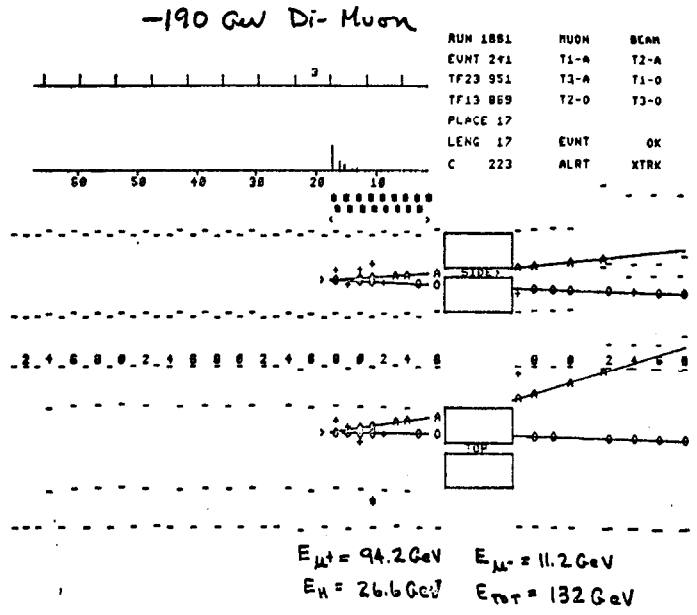

Fig. 2

An example of a dimuon candidate in anti-neutrino running at -190 GeV.

originating from π and K decays. The smooth curves plotted in figure 3a,b are the results of this background calculation. The transverse momentum dependence of the secondary decay muons is not included in this calculation, even though real decay muons at large angles ($\theta_{\mu 2} \geq 250$ mrad) will not typically pass the penetration requirement. Therefore, this calculation probably represents an upper limit to background from this source.

For both neutrinos and antineutrinos, a) this data is consistent with our previous results,[3] and b) the events with a high energy "extra" muon cannot adequately be explained on the basis of the π and K decay background calculation. For example, for incident antineutrinos and $E_{\mu 2} > 15$ GeV, we observe 5 events and expect a background of at most 0.4 events. It should be emphasized that this calculation has not yet been empirically tested, although work is in progress to do so.

III. Energy Dependence of Dimuon Production.

The total observed energy distributions for single muon events at ± 190 GeV are shown in Figures 4 a,b. The curves are drawn to guide the eye only; however, the two peak energy structure of the dichromatic beam is apparent. For antineutrinos, the lower $\bar{\nu}_K$ yield, reflecting the lower K^- yield, is evident.

Also shown on these figures (with a magnified scale) are the observed energy distributions for dimuon events. Though the statistics are not really adequate to be definitive regarding the structure of the dimuon observed energy distribution, these distributions are consistent with the single muon distributions shown in the same figures. Indeed, this would be the case if the missing final state lepton carried off only a small fraction of the incident energy. In the following, we assume that the observed dimuon events can be classified into two distinct energy bands, depending on their total energy.

FIGURE 3a
Neutrino-Induced Dimuon Events

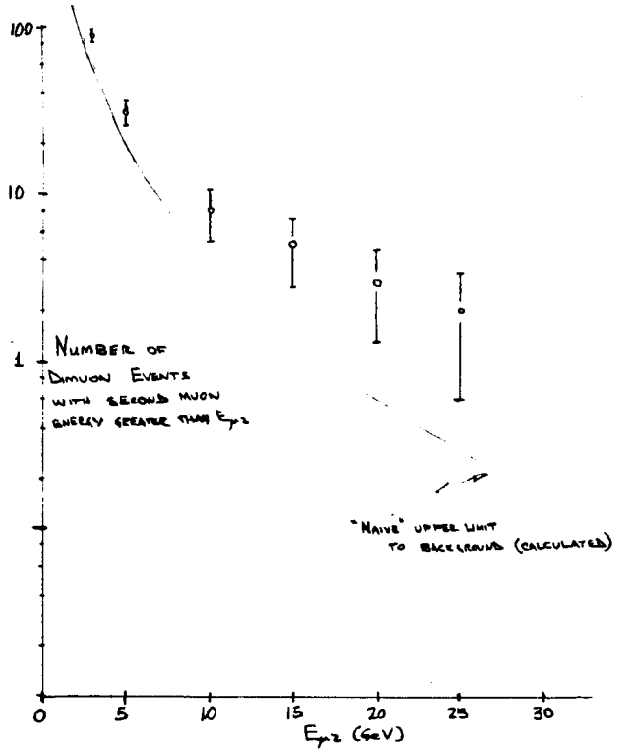

Fig. 3a

The number of 2μ events with $E > E_{\mu 2}$ as a function of $E_{\mu 2}$ for events in which the first muon entered the spectrometer. The curve is an upper limit to the number of events expected from π and K decay neutrino running.

FIGURE 3b
Antineutrino-Induced Dimuon Events

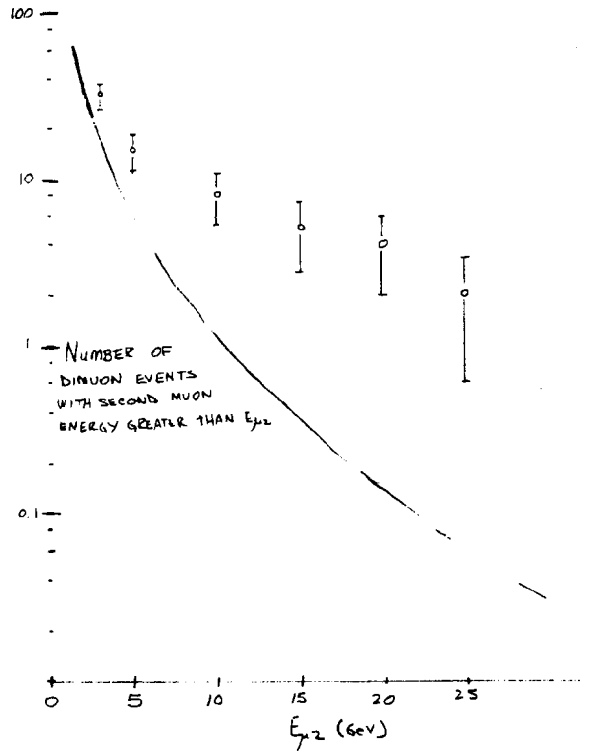

Fig. 3b

The number of 2μ events with $E > E_{\mu 2}$ as a function of $E_{\mu 2}$ for events in which the first muon entered the spectrometer. The curve is an upper limit to the number of events expected from π and K decay antineutrino running.

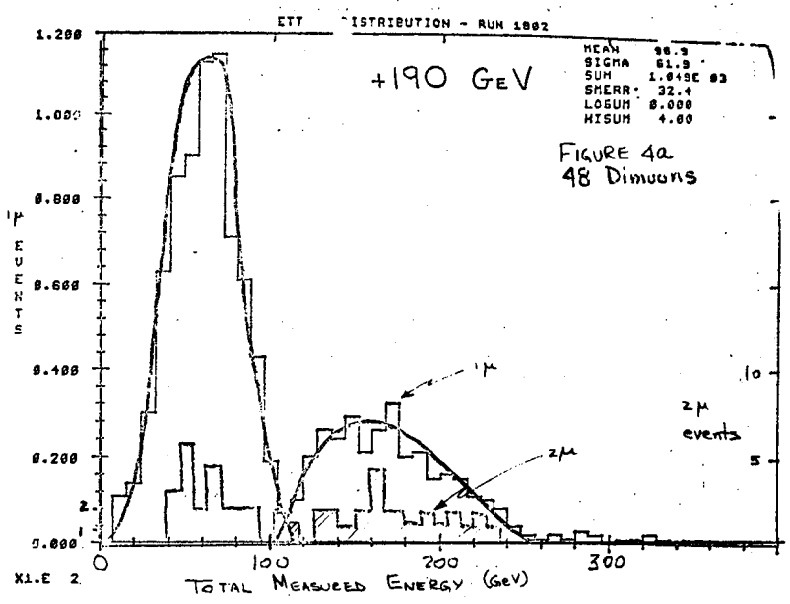

Fig. 4a

Observed total energy distributions for single muon events. Cross hatched data (magnified scale) are the observed dimuon energy distributions with $E_{\mu 2} > 3$ GeV.

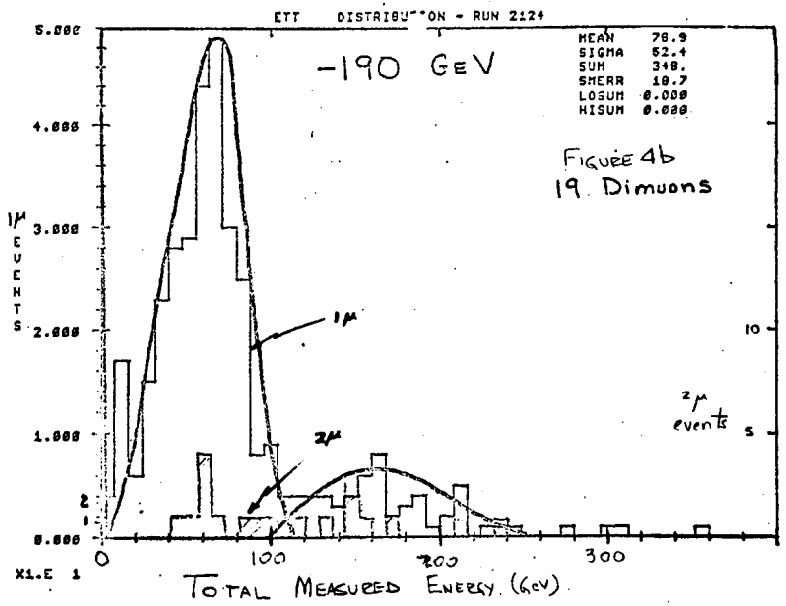

Fig. 4b

Observed total energy distributions for single muon events. Cross hatched data (magnified scale) are the observed dimuon energy distributions with $E_{\mu 2} > 3$ GeV.

The observed ratio of double to single muon events ($\sigma_{\mu\mu}/\sigma_{\mu}$) is shown as a function of average incident neutrino beam energy for neutrinos and antineutrinos in Figures 5 a,b, respectively, for all events in which a) the first muon entered the spectrometer and b) the observed energy of the second muon $E_{\mu 2} > 3$ GeV. Also shown on these figures are previous results from this experiment at +170 GeV[3] and from the Harvard-Penn-Wisconsin-Fermilab Experiment.[4] The HPWF data has been corrected for scanning efficiency and acceptance, whereas the CITF data has not.

This observed $\sigma_{\mu\mu}/\sigma_{\mu}$ ratio increases with energy. Extrapolation to the behavior of the integrated $\sigma_{\mu\mu}$ cross-section should be approached with some caution, however. For example, background from π or K decay would also increase with energy. Even if the events were all "real", the entire increase might be due to an increase in the acceptance of the apparatus with higher neutrino energy. Before drawing any conclusions on the energy dependence of the dimuon signal, a more definitive background estimate and a more complete efficiency calculation are required. It should be noted that a complete efficiency calculation requires some physics knowledge of the production mechanisms (e.g. how many μ's are below 3 GeV as a function of energy?)

In the entire 2μ sample, 20 events had both muons traverse the spectrometer. Eight of the 20 events were antineutrino-induced and 12 were neutrino-induced. All 8 of the antineutrino-induced events had opposite sign muons ($\mu^+\mu^-$). Two of the neutrino-induced events had same sign muons ($\mu^-\mu^-$).

IV. Trimuons

To date there has been no reported observation of trimuon (3μ) production in neutrino and antineutrino data. In this sample we have observed a few trimuon candidates with the requirement that a) the first muon enter

Fig 5a

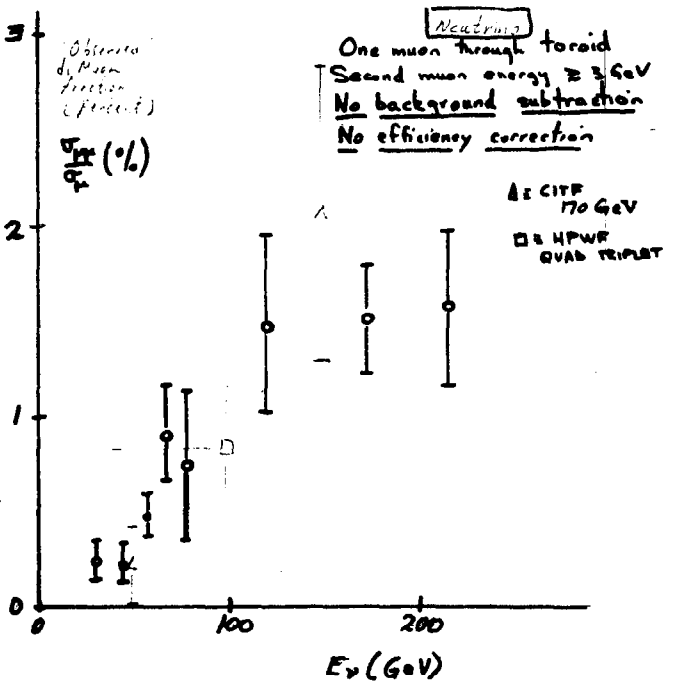

Fig. 5a

The ratio $\sigma_{\mu\mu}/\sigma_{\mu}$ as a function of energy for the requirements that the first muon entered the spectrometer and $E_{\mu 2} > 3$ GeV. Previous CITF data (Δ) from reference 3, HPWF data (□) from reference 4.

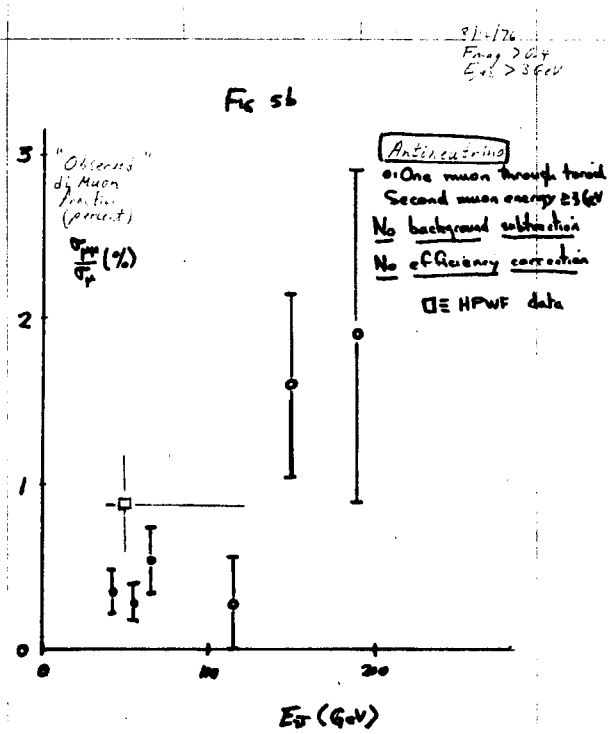

Fig. 5b

The ratio $\sigma_{\mu\mu}/\sigma_{\mu}$ as a function of energy for the requirements that the first muon entered the spectrometer and $E_{\mu 2}>3$ GeV. Previous CITF data (Δ) from reference 3, HPWF data (□) from reference 4.

the spectrometer, and b) $E_{\mu 2}$ and $E_{\mu 3}$ each be greater than 3 GeV.

The two best candidates, found in the +190 GeV running, are shown in Figure 6 a,b. Some of the kinematic quantities calculated for these events are indicated on the figures.

The obvious question is whether or not these events are explained by conventional mechanisms. In the following, we estimate possible sources, using the total number of 1μ and 2μ events in the + 190 and +250 GeV/c running. Three possible sources of 3μ events are:

1) Simultaneous π or K decay at the hadronic vertex to produce 2 extra muons (figure 7a). An upper limit to the expected number of events from this process is .03; this source is considered very unlikely.

2) Neutrino induced dimuon production with a π or K decay at the hadronic vertex to produce an extra muon (figure 7b). An upper limit to the expected number of events from this background is .04 and this explanation too is very unlikely.

3) "Direct" dimuon production at the hadronic vertex or from nuclear interactions in the hadronic shower (figure 7c). The uncorrected neutrino trimuon production rate relative to the single muon rate is on the order of 3×10^{-4}. In hadronic collisions the prompt μ/π ratio is $\sim 10^{-4}$. If this prompt muon signal in hadronic collisions is dimuon production, then this rate is comparable to the neutrino induced trimuon signal. This is a possible explanation for the neutrino induced trimuon signal.

V. Conclusions

In summary we see a definite signal for dimuon production in both the neutrino and antineutrino data over a wide range of energies. Whether or

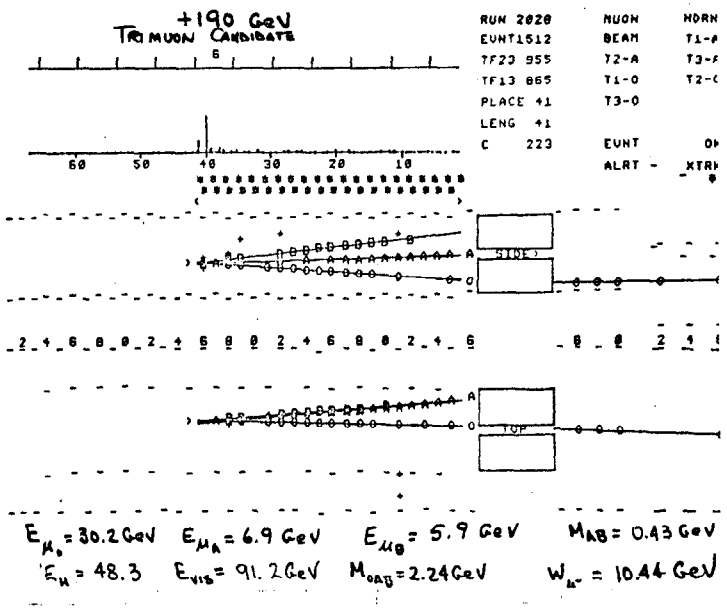

Fig. 6a
Trimuon Candidate at +190 GeV.

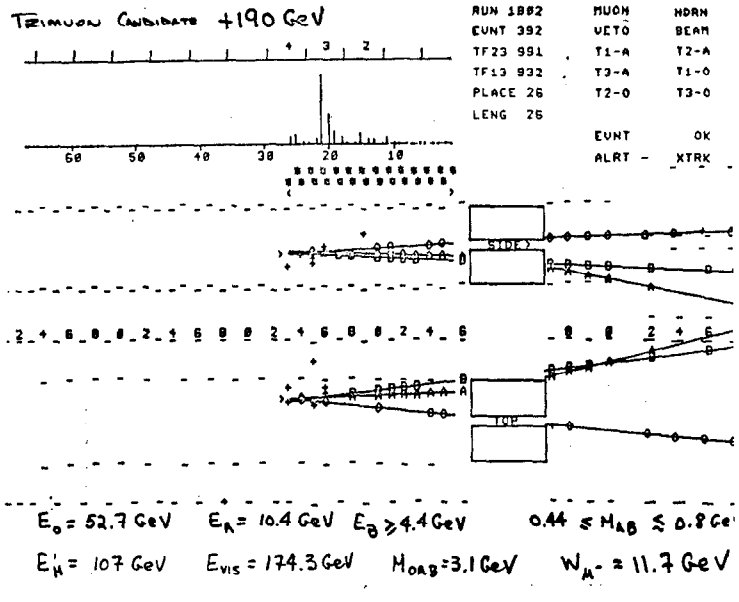

Fig. 6b
Trimuon Candidate at +190 GeV.

FIGURE 7 - TRIMUON MECHANISMS

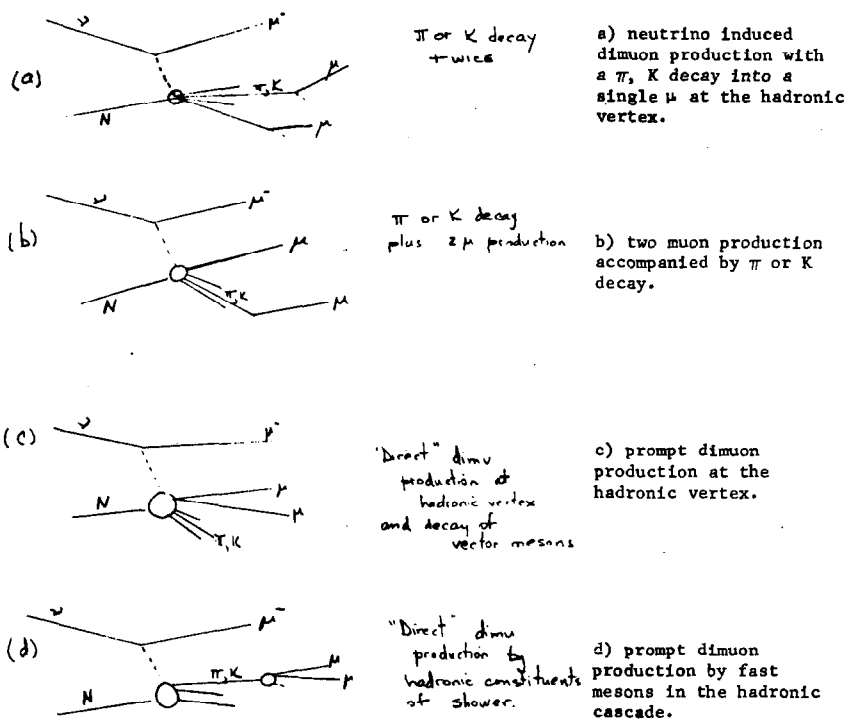

Fig. 7
Possible trimuon sources.

not we can draw any conclusions regarding the energy dependance of this signal will have to await more detailed treatment of the data and more effort on the effect of the apparatus acceptance. The uncorrected neutrino and antineutrino dimuon production rate relative to the single muon rate reaches about 1.5% at high energy.

Two good candidates for trimuon production were observed at +190 GeV/c. The trimuon production rate relative to the single muon production rate is of order 3×10^{-4}.

References

1. B. C. Barish, CALT 68-835, published in Proceedings of the Sixth Hawaii Topical Conference in Particle Physics, p.213, (1975).

2. B. C. Barish, et al., Fermilab Proposal No. 21, and P. Limon, et al., Nucl. Inst. and Meth. 116, 317 (1974).

3. B. C. Barish, et al., Phys. Rev. Lett. 36, 939 (April, 1976), and A. Bodek, Proceedings of the Summer Institute on Particle Physics, SLAC, (July 1975).

4. A. Benvenuti, et al., Phys. Rev. Lett. 18, 1199 (Nov. 1975) and Phys. Rev. Lett. 19, 1249 (Nov. 1975).

5. B. C. Barish, et al., Nucl. Inst. and Meth. 116, 413 (1974) and Nucl. Inst. and Meth. 130, 49 (1975).

6. P. Berge, et al., FNAL Report No. FERMILAB-PUB-75/84 (unpublished).

STUDY OF CHARMED MESONS AT SPEAR

Gerson Goldhaber

Department of Physics and Lawrence Berkeley Laboratory
University of California, Berkeley, California 94720

I. PRODUCTION AT SPEAR

The data I will discuss here comes from the SLAC-LBL magnetic detector at SPEAR. This detector as well as event selection techniques have been described earlier,[1] and I will thus confine myself to some details about the time-of-flight system only.

Early in May 1976 we observed a narrow peak in two neutral decay modes[2] $K\pi(1865)$ and $K3\pi(1865)$ based on the study of ~ 29,000 hadronic events from the E_{cm} region 3.9 - 4.6 GeV. In this talk I will discuss this data as well as new data from two additional runs at SPEAR at E_{cm} = 4.028 GeV and E_{cm} = 4.415 GeV, taken during May - June 1976. These consisted of ~ 25,000 and ~ 26,000 hadronic events respectively. The energies were chosen to lie at the two prominent peaks of the R plot ($R = \sigma_{hadron}/\sigma_{\mu\mu}$) shown in Fig. 1.

In June 1976, from a study of the 4.028 GeV data, for which the ratio of signal to background for the new mesons is considerably improved over the earlier 3.9 - 4.6 GeV data, we observed the charged decay mode[3] $K^{\mp}\pi^{\pm}\pi^{\pm}(1876)$.

The entire sample analyzed here thus corresponds to ~ 80,000 hadronic events identified in the detector. In the present analysis we have confined ourselves to hadronic events with three or more observed prongs.

Summary of Data Sample (Preliminary)

E_{cm} (GeV)	Hadronic Events	Integrated Luminosity (nb^{-1})
3.9 - 4.6 pre-May 1976	~ 29,000	~ 1830
4.028	~ 25,000	~ 1280
4.415	~ 26,000	~ 1630
3.9 - 4.6 all	~ 80,000	~ 4740

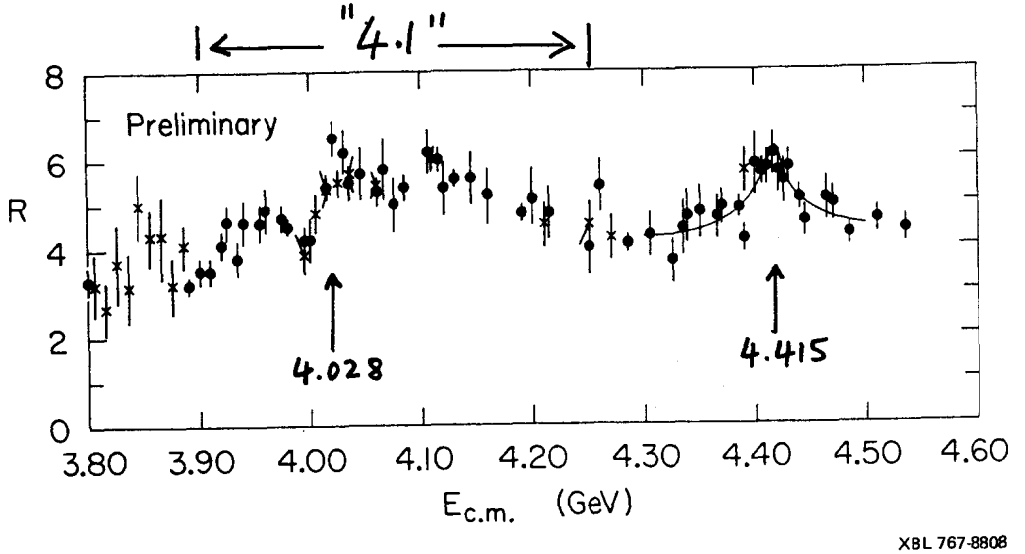

Fig. 1. The ratio $R = \sigma_{had}/\sigma_{\mu\mu}$. The distribution corresponds to the pre-May 1976 data sample. The location of the two new high-statistics points 4.028 and 4.415 is also indicated.

The Particle Identification Methods by Time of Flight

An important innovation used in this study was the application of time-of-flight (TOF) information to help identify hadrons. The TOF system includes 48 2.4 cm × 20 cm × 260 cm Pilot Y scintillation counters arranged in a cylindrical array immediately outside the tracking spark chambers at a radius of 1.5 m from the beam axis. Both ends of each counter are viewed by Amperex 56 DVP photomultiplier tubes (PM); anode signals from each PM are sent to separate TDC's, ADC's, and latches. Pulse height information is used to correct times given by the TDC's. The collision time is derived from a pickup electrode that senses the passage of the 0.2 ns long beam pulses; the period between successive collisions is 780 ns. Run-to-run calibrations of the TOF system are performed with Bhabha scattering ($e^+e^- \rightarrow e^+e^-$) events. The rms resolution of the TOF system is $\sigma_t = 0.4$ ns.

Typical time difference between a π and a K in the Kπ signal is only about 0.5 ns. We have used the following two techniques to extract the best possible information on particle identity. To apply these methods, tracks are required to have good timing information from both PM's, consistent with the extrapolated position of the track in the counter.

A. Direct Particle Identification by TOF

In this method we calculate two χ^2 values for each observed track. The first is related to the probability that the track is a π,(χ^2_π) and the second to the probability of the track being a K,(χ^2_K). Here χ^2_i is defined by:

$$\chi^2_i = (t_i - t_M)^2/\sigma_t^2$$

where $i = \pi,K$; t_i is the time calculated for mass i from measured momentum; t_M is measured TOF. If the track satisfies the criteria $\chi^2_K < 3$, $\chi^2_K < \chi^2_\pi$ the track is called a K. If $\chi^2_\pi < \chi^2_K$ the track is called a π; the track is also called a π when no reliable TOF information is available as when, for example, more than one track hits the TOF counter. There are also a small number of nucleons and antinucleons which have been identified but these do not play a part in the present analysis.

B. The Weight Method

In the weight method each track is assigned a weight corresponding to its probability of being a π and a second weight corresponding to its probability of being a K. These are determined from the measured momentum and TOF assuming a Gaussian probability distribution with standard deviation 0.4 ns. Tracks with net (π plus K) probability less than 1% are rejected. (This eliminates most of the nucleons.) Then, the relative π-K probabilities are renormalized so that their sum is unity, and two-particle combinations are weighted by the joint probability that the particles satisfy the particular π or K hypothesis assigned to them. In this way, the total weight assigned to all $\pi\pi$, Kπ, and KK combinations equals the number of two-body combinations and no double-counting occurs.

To be more specific, we define

$$W_\pi \propto e^{-\chi^2_\pi/2}$$

and $$W_K \propto e^{-\chi^2_K/2}$$

with the normalizing condition

$$W_\pi + W_K = 1 \ .$$

In the study of the two-body system, for example, each pair of particles with total charge zero gets entered into three graphs:

in $M(\pi^\pm\pi^\mp)$ we enter $W_{\pi_1}W_{\pi_2}$

in $M(K^\pm\pi^\mp)$ we enter $W_{K_1}W_{\pi_2}$ and $W_{\pi_1}W_{K_2}$

in $M(K^\pm K^\mp)$ we enter $W_{K_1}W_{K_2}$.

In our earlier publications[2,3] we have used method B, the weight method. This method allowed us to give a quantitative assessment of the reliability of the K particle assignments in Kπ(1865). In what follows we will use method A which lends itself more readily to the study of scatter plots. We will also show a comparison between the two methods which demonstrates that for the study of mass plots they do not differ in any essential features.

C. Summary and Nomenclature

At the moment we have no "rigorous proof" that we are indeed dealing with charmed mesons.[4] However, every clue we have uncovered, so far, points in the direction of charm. It is becoming clear that we are dealing with those particles which are correlated with the broad $\psi(4.1)$ resonance and thus very likely with the property that is still "hidden" at the lower energies corresponding to the ψ/J and ψ'.

I will discuss the following about the new particles we have observed:

a. Observation of a threshold: $E_{th} > 3.1$ GeV.

b. Associated production: the particles are produced exclusively in association with another particle of equal or larger mass.

c. Exotic final state: the charged particle decays into an exotic final state. Incidentally, this is the first clearly established case of an exotic final state.

d. Experimental width: from the direct mass measurement of $K\pi(1865)$ we showed that the width is $\Gamma < 40$ MeV/c^2; by including information on the recoil system this can now be reduced to $\Gamma < 5$ MeV.

e. I-spin multiplet: the proximity in mass of the neutral and charged particles in both the ground state and first excited state is evidence that we are dealing with I-spin multiplets.

f. Parity violation in the decay: from a comparison of $K\pi\pi$ and $K\pi$ we give evidence for parity violation, and hence weak decay.

g. Search for Cabibbo forbidden decay modes: we note an indication, in the $\pi^+\pi^-$ channel, at the 1.5 standard deviation level (i.e., not statistically significant).

h. Semi-leptonic decay modes: evidence for these from work at DESY was presented at this Topical Conference.[5]

I could now proceed and call these new particles M^o, M^+, M^{o*}, M^{+*}, etc. where M stands for a new meson, but I will not do so. For clarity and ease of comparison I will use the nomenclature D^o, D^+, etc. introduced for charmed particles,[4] with the understanding that we do not have complete proof as yet[6] that our observed particles are indeed the mesons of charm theory. Our situation is somewhat analogous to the case of the discovery of the Ω^-. The observed particle has most of the properties predicted for the 10th baryon of the Δ-decuplet while to date no spin and parity measurements are available to check the theoretical prediction $J^P = 3/2^+$.

II. THE ESTABLISHED DECAY MODES

A. Threshold Behavior for the $K^{\mp}\pi^{\pm}$ Decay Mode

In Fig. 2 we show the $K^{\mp}\pi^{\pm}$ mass distribution for three energy regions: the ψ/J, the ψ', and the $E_{cm} = 3.9 - 4.6$ GeV region. The $K^*(890)$ signal shows up clearly in all of them; however the $K\pi(1865)$ signal occurs only for the 3.9 - 4.6 GeV region. Figure 3 shows the $M = 1500 - 2500$ MeV/c^2 region in detail. In these figures the ψ data corresponds to $\sim$ 150,000 hadronic events and the ψ' data to 350,000 hadronic events. We note that of these $\sim$ 72,000 hadronic events correspond to second-order electromagnetic interaction and these at least could be a source for the $K\pi(1865)$ signal. We consider the absence of any such signal a clear indication that the $K\pi(1865)$ does not get produced below a threshold energy E_{th}. Thus $E_{th} > 3.1$ GeV. In Figs. 2, 3 we also show the $E_{cm} = 4.028$ GeV data. For this energy the signal-to-background ratio is much larger than for the overall 3.9 - 4.6 GeV region. The $K\pi(1865)$ particle thus appears specifically associated with the peak in R.

In Fig. 4 we show the $K\pi$ signal for all the $E_{cm} = 3.9 - 4.6$ GeV data with a cut on the recoil mass at $M_{recoil} > 1800$ MeV. This selection tends to reduce the background while the signal remains unaffected. Also shown in Fig. 4 are the kinematic reflections in the "$\pi^+\pi^-$" and "K^+K^-" mass distributions which occur because of K misidentification or lack of TOF information, in which case the track is assigned the pion mass. With the present statistics we note clear "kinematic reflection"

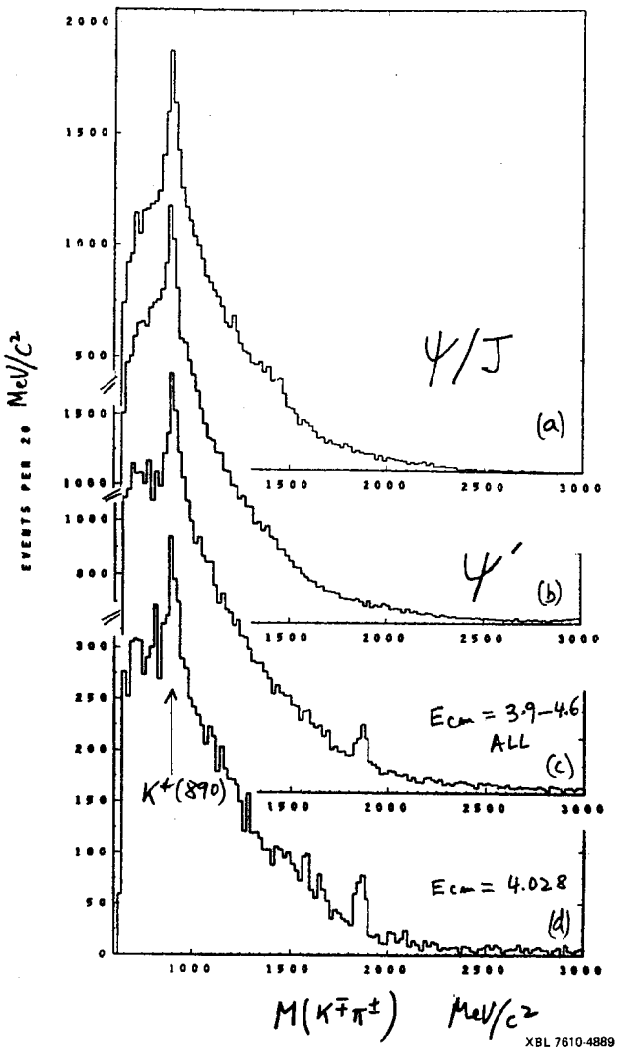

Fig. 2. A composite of the Kπ mass distribution for the ψ/J region, the ψ' region and the E_{cm} = 3.9 - 4.6 GeV region (all data) as well as the E_{cm} = 4.028 GeV data separately.

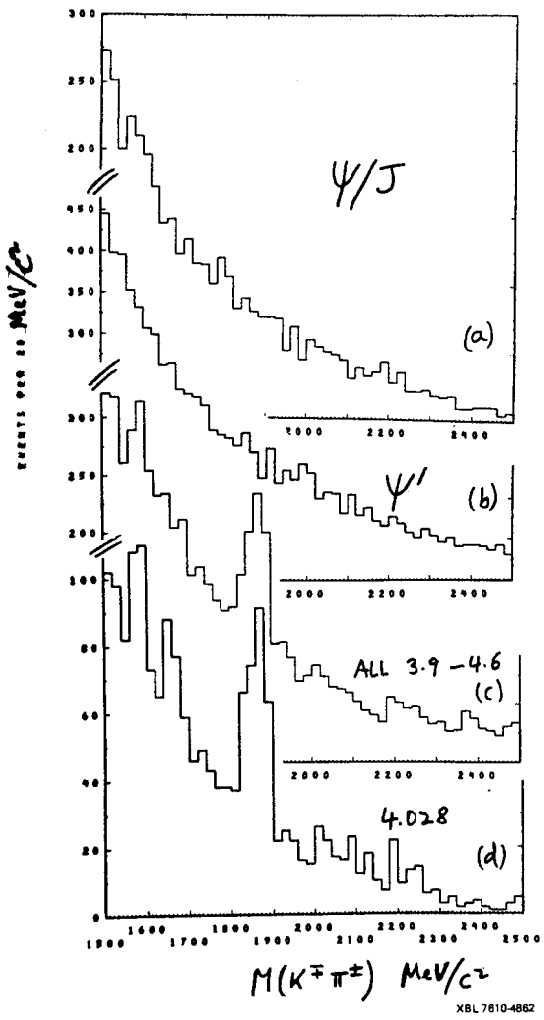

Fig. 3. Detail of the Kπ mass spectrum in the M = 1500 - 2500 MeV/c^2 region for the same data samples as in Fig. 2.

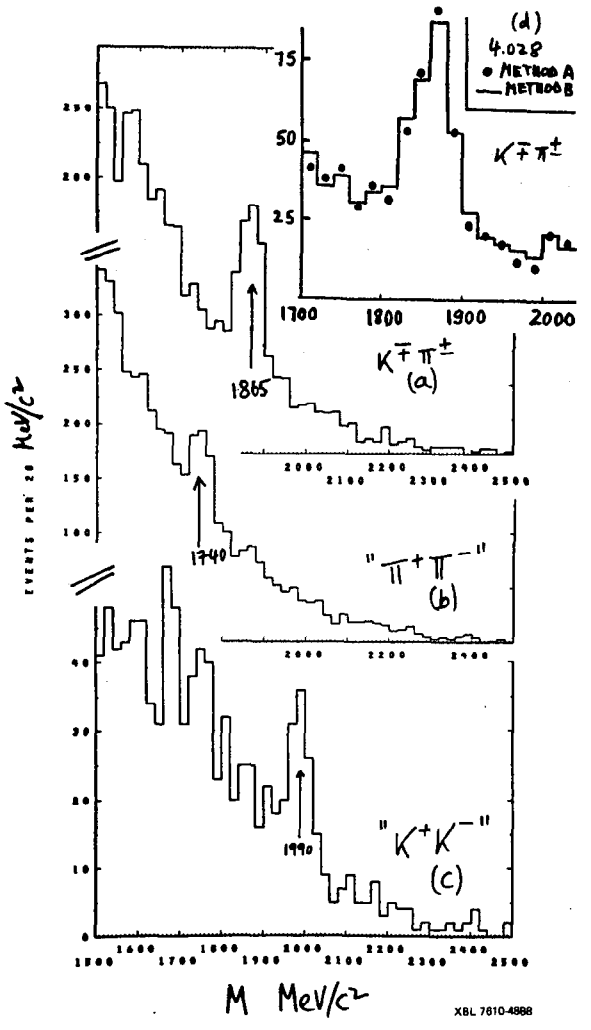

Fig. 4. The two-body mass distributions with $M_{recoil} > 1800$ MeV/c for all data. (a) $K^{\mp}\pi^{\pm}$, (b) "$\pi^+\pi^-$," (c) "K^+K^-" and insert (d) which shows the $K^{\mp}\pi^{\pm}$ distributions as obtained by the two TOF methods for the $E_{cm} = 4.028$ GeV data only.

signals at 1740 MeV/c^2 for "$\pi\pi$" and 1990 MeV/c^2 for "$K\bar{K}$." We note that the momentum of the two-body system in such a kinematic reflection signal is not altered by the mass assignment to the track. We will make use of these additional events below in connection with the recoil spectrum.

The $K^{\mp}\pi^{\pm}$ signal is taken from the experimental mass distribution region $M(K\pi) = 1820 - 1900$ MeV/c^2. Background is estimated from two equal width side bands $M(K\pi) = 1700 - 1780$ MeV/c^2 and $M(K\pi) = 1940 - 2020$ MeV/c^2, a total of twice the width of the signal region. This gives a total signal after appropriate background subtraction ($\frac{1}{2} N_{bgnd}$) of 340 ± 47 events. The "$\pi^+\pi^-$" and "K^+K^-" reflection signals are obtained in a similar fashion and give signals of 159 ± 30 and 46 ± 11 events respectively. Thus if we ascribe all these three contributions to $K\pi(1865)$ we get 545 ± 57 events.

B. The $(K3\pi)^0$ Decay Mode

In Fig. 5 we show the $K^{\mp}\pi^{\pm}\pi^{+}\pi^{-}$ mass distribution. The $K3\pi(1865)$ signal suffers from a much more severe background problem than the $K\pi(1865)$ signal. We will comment on this in connection with the recoil mass study below. The $K3\pi$ signal was determined for the mass interval 1860 - 1900 MeV/c^2 with two equal side bands for background determination. We find 325 ± 67 events in the signal after background subtraction.

C. The Charged Exotic Decay Mode $K^{\mp}\pi^{\pm}\pi^{\pm}(1876)$

In Fig. 6 we show a comparison of the exotic decay mode $K^{\mp}\pi^{\pm}\pi^{\pm}$ and the non-exotic mode $K^{\mp}\pi^{+}\pi^{-}$.

Here "exotic" stands for the fact that the I-spin of the final state is $I = 3/2$ or $5/2$ rather than $I = 1/2$ as is the case for all known K^*'s. Such a final state cannot be formed out of a $q_i\bar{q}_j$ pair where here q_i ($\bar{q}_j$) stands for any of the three "old-fashioned" quarks (anti-quarks). Another way of describing the "exotic" nature of this final state is that the charge of the K is opposite to the charge of the entire $K\pi\pi$ final state. In terms of the charm model[4] the Cabibbo-favored decays involve

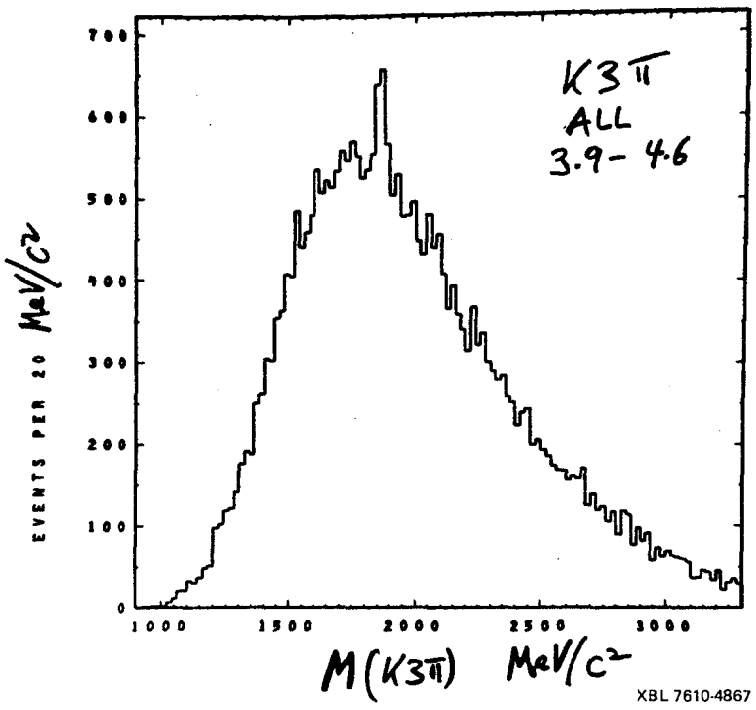

Fig. 5. The $K^{\mp}\pi^{\pm}\pi^{+}\pi^{-}$ mass distribution for the E_{cm} = 3.9 - 4.6 GeV region (all data).

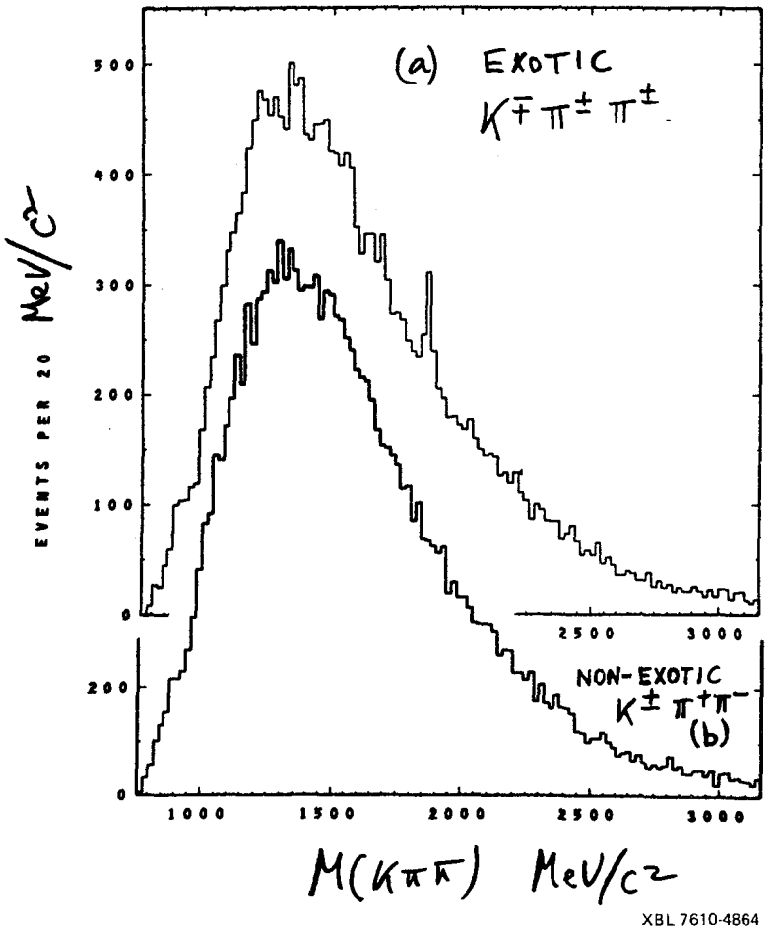

Fig. 6. Comparison of the exotic ($K^{\mp}\pi^{\pm}\pi^{\pm}$) and non-exotic $K^{\mp}\pi^{+}\pi^{-}$ mass distributions for all data.

a c-quark transforming into an s-quark with $\Delta C = \Delta S$. Thus the D^+ with $C = 1$ and $S = 0$ decays to a system with $C = 0$, $S = -1$ and positive charge, which is exotic. The exotic $K\pi\pi$ signal was determined from the mass interval 1840 - 1920 MeV/c^2. Here background estimates come from the non-exotic channel over the same mass interval, scaled by 1/2. We find 160 ± 35 events in the signal after background subtraction.

III. THE RECOIL SYSTEMS

We find that the $(K\pi)^o$, $(K3\pi)^o$ and $K^{\mp}\pi^{\pm}\pi^{\pm}$ signals are associated with a very distinct recoil spectrum. This can be illustrated in a scatter plot of the final state mass M versus the recoil mass M_{recoil}. In Fig. 7 we show the scatter plot for the $K^{\mp}\pi^{\pm}$ mass distribution and in Fig. 8 for the $K^{\mp}\pi^{\pm}\pi^{\pm}$ mass distribution. The scatter plots shown correspond to the E_{cm} = "4.1" GeV region; i.e., E_{cm} = 3.9 - 4.25 GeV, including the data at 4.028 GeV. We note a strong correlation between M and M_{recoil}. This is in agreement with the charm theory expectation that M is essentially a δ-function, on our energy scale, and thus the observed width in M is entirely due to our instrumental resolution. Thus when the measured M value is too large the corresponding M_{recoil} value is too small and vice versa. This then gives rise to the observed correlation. Here M_{recoil} is defined by:

$$M^2_{recoil} = (E_{cm} - \sqrt{p^2 + M^2})^2 - p^2$$

where M and p are the measured effective mass and momentum of the final state considered. Alternately if we consider M as a δ-function, we can substitute a nominal fixed value of $M_{K\pi}$ = 1865 MeV and $M_{K\pi\pi}$ = 1872 MeV for M respectively.

In Fig. 9a we show the M_{recoil} distribution as measured directly and in Fig. 9b with $M_{K\pi}$ fixed for all the data. In Fig. 9a only the Kπ signal with identified K mesons is shown. On the other hand in Fig. 9b we have also added in the signal from the "$\pi^+\pi^-$" and "K^+K^-" kinematical reflections illustrated in Fig. 4. This is possible as only the experimental quantities

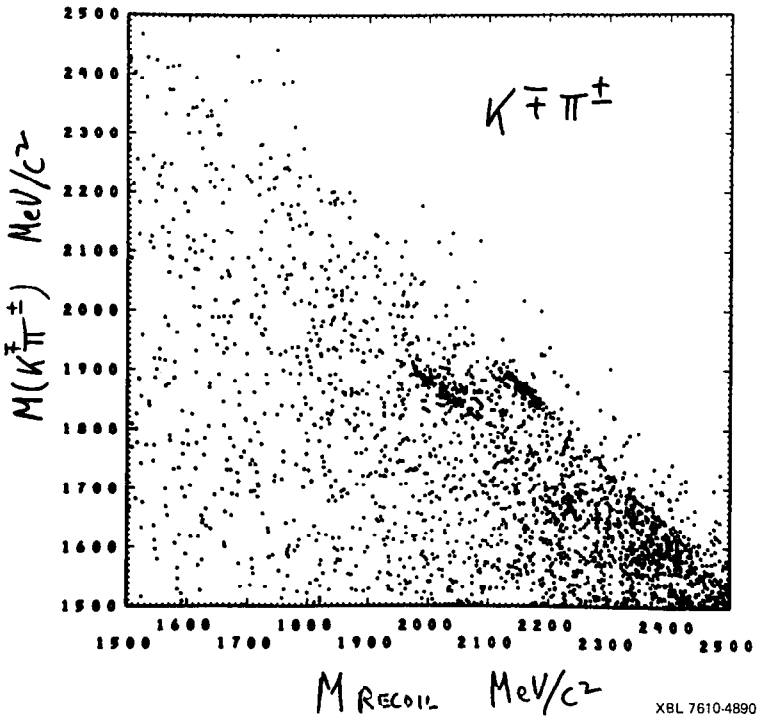

Fig. 7. Scatter plot $M(K^{\mp}\pi^{\pm})$ versus M_{recoil} for the "4.1" GeV data E_{cm} = 3.9 - 4.25 GeV.

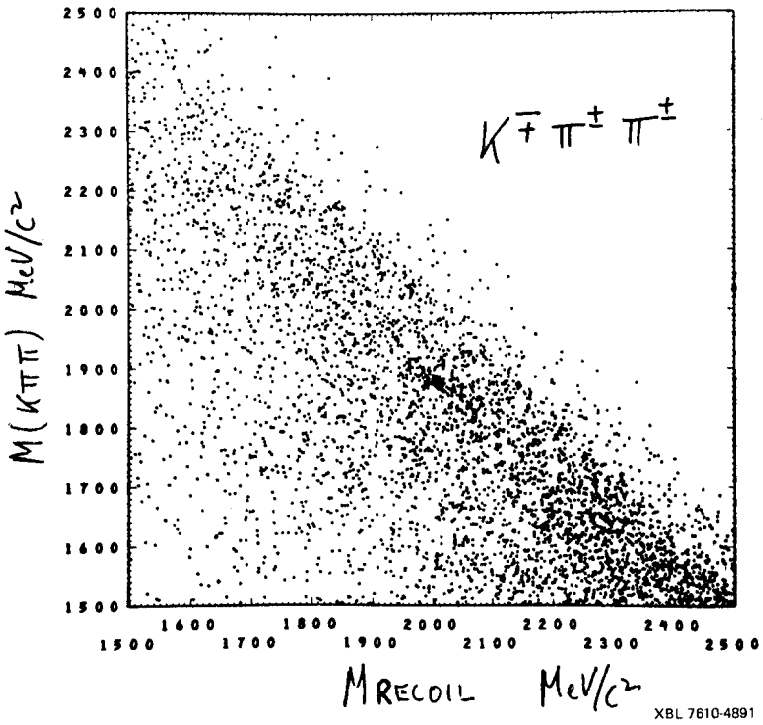

Fig. 8. Scatter plot $M(K^{\mp}\pi^{\pm}\pi^{\pm})$ versus M_{recoil}. Data sample as in Fig. 7.

E_{cm} and the momentum p are used to calculate M_{recoil}. The addition of these signals increases the available statistics, but more important, removes biases due to the fact that the reliability of K identification decreases with increasing K momentum. In the distributions in Figs. 9a and 9b the corresponding background has been subtracted. The background was evaluated from the population of two bands on either side of the signal. In Fig. 9a the background bands were subtracted directly without concern for slightly different kinematical boundaries. In Fig. 9b M_{recoil} for the background events was evaluated with the same fixed $M_{K\pi}$ value. This "scales" the kinematic boundaries. Because of the subtraction procedure the statistical errors corresponding to the histograms in Fig. 9 are not given by $\sqrt{N}$ but rather by $\sim\sqrt{1.2N}$ to $\sim\sqrt{1.8N}$.

Some caution must be used in interpreting the four prominent structures in Fig. 9b. Namely, we must remember that the data samples added together in this figure have a highly non-uniform integrated luminosity distribution from E_{cm} = 3.9 - 4.6 GeV. In particular the second and third peaks come largely from the 4.028 GeV data. We observe peaks in M_{recoil} at $\sim$ 1860 MeV/c^2, $\sim$ 2005 MeV/c^2, $\sim$ 2145 MeV/c^2 and $\sim$ 2430 MeV/c^2. Of these the fourth peak is still being studied. An interpretation suggested[7] for the first three peaks is as follows:

$$e^+e^- \rightarrow D^0\overline{D^0} \qquad (1)$$

$$e^+e^- \rightarrow D^0\overline{D^{*0}} \text{ and charge conjugate} \qquad (2)$$

$$e^+e^- \rightarrow D^{*0}\overline{D^{*0}} \ . \qquad (3)$$

A priori, an alternate possibility exists for the third peak; viz.,

$$e^+e^- \rightarrow D^0\overline{D^{**0}} \text{ and charge conjugate} \ . \qquad (3')$$

We will discuss these interpretations in more detail below and in particular show evidence for the strong preference of interpretation (3) over (3'). The recoil spectrum against the $(K3\pi)^0$ mass peak shows consistent features (not shown here) but suffers statistically from the very substantial background subtraction.

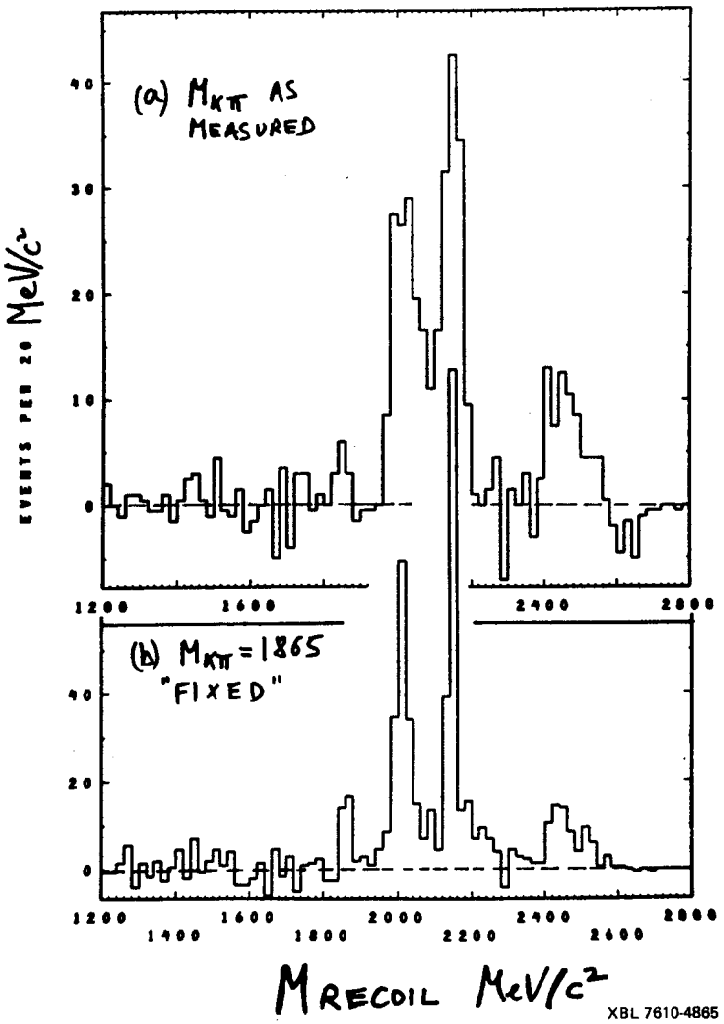

Fig. 9. (a) M_{recoil} distribution for the $K^{\pm}\pi^{\mp}$ signal as measured. (b) M_{recoil} distribution for the $K^{\pm}\pi^{\mp}$ signal, as well as the kinematic reflection signals "$\pi^+\pi^-$" and "$K\bar{K}$," for fixed $M_{K\pi}$ = 1865 MeV/c^2. Each distribution is background subtracted as discussed in the text. E_{cm} = 3.9 - 4.6 GeV all data.

In Fig. 10 we show the corresponding M_{recoil} distribution for the exotic channel $K^{\mp}\pi^{\pm}\pi^{\pm}$. In this case the background is deduced from the non-exotic channel $K^{\pm}\pi^{+}\pi^{-}$. In this case we again have a more severe background subtraction as well as a lower statistical significance on the signal (~ 160 events). The very prominent peak observed at M_{recoil} ~ 2012 MeV/c^2 can be interpreted as

$$e^+e^- \rightarrow D^+D^{*-} \text{ and charge conjugate .} \qquad (4)$$

There are indications in the data for the presence of the other three peaks observed in the recoil spectrum against the D^0. In particular there is some evidence for

$$e^+e^- \rightarrow D^{*+}D^{*-} , \qquad (5)$$

$$\text{or} \qquad \rightarrow D^+D^{**-} \text{ and charge conjugate ,} \qquad (5')$$

only much weaker relative to reaction (4). This feature is clearer if we compare the recoil spectra for "fixed" masses at E_{cm} = 4.028 GeV. In Fig. 11 we show these recoil spectra for the $(K\pi)^0$, $(K3\pi)^0$ and $(K\pi\pi \text{ exotic})^{\pm}$ signals each with the appropriate background subtraction.

IV. MASSES, WIDTHS AND MASS DIFFERENCES

For mass determination we focus on a single energy: E_{cm} = 4.028 GeV. We can then consider momentum distributions p of the two-particle system. In Fig. 12a we show the momentum spectrum for $K^{\mp}\pi^{\pm}$, together with the kinematic reflections "$\pi^+\pi^-$" and "$K\bar{K}$", in 10 MeV intervals. In Fig. 12b the same for the $K^{\mp}\pi^{\pm}\pi^{\pm}$ system. The background level is sketeched in on these.

In Fig. 13a and 13b we show these same distributions in 20 MeV intervals, with background subtracted.

A. Momentum Values

Several peaks stand out prominently:

$$p_1 = 765 \pm 12 \text{ MeV/c,}$$

$$p_2 = 560 \pm 8 \text{ MeV/c}$$

with a "satellite structure" ~ 50 MeV/c lower,

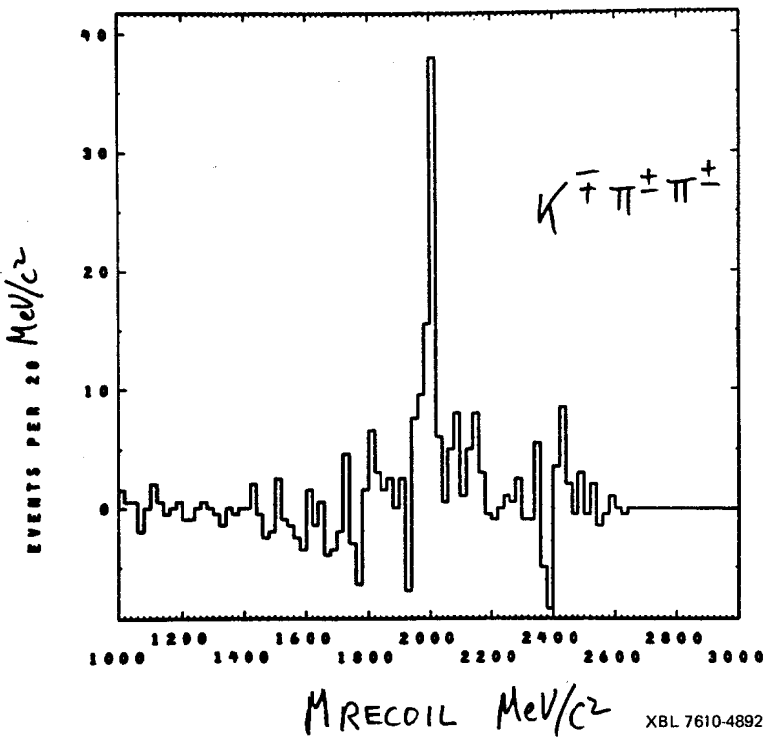

Fig. 10. M_{recoil} distribution for the $K^{\mp}\pi^{\pm}\pi^{\pm}$ signal as measured. The background subtraction comes from the same mass cuts on the non-exotic $K\pi\pi$ channel.

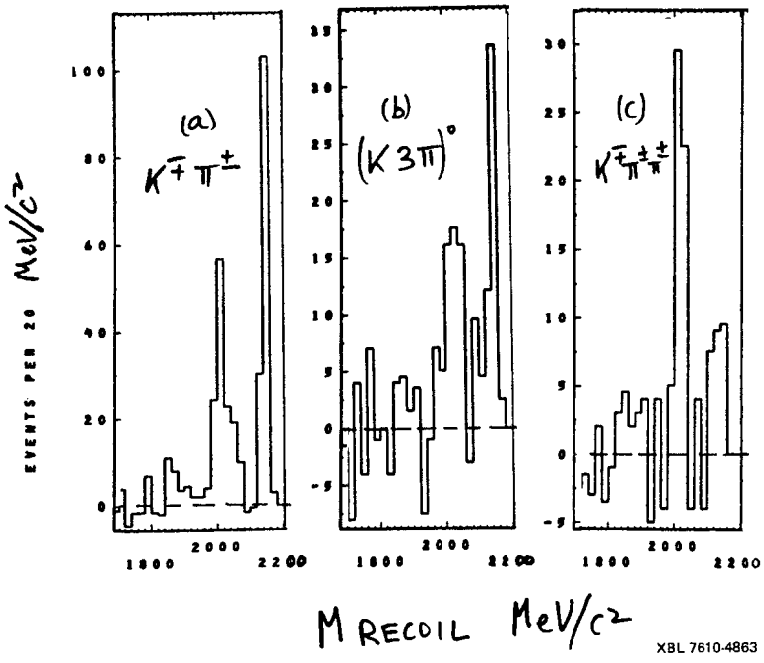

Fig. 11. The recoil spectra at E_{cm} = 4.028 GeV against $(K\pi)^{0}$, $(K3\pi)^{0}$ and $(K\pi\pi \text{ exotic})^{\pm}$ for fixed masses with background subtraction.

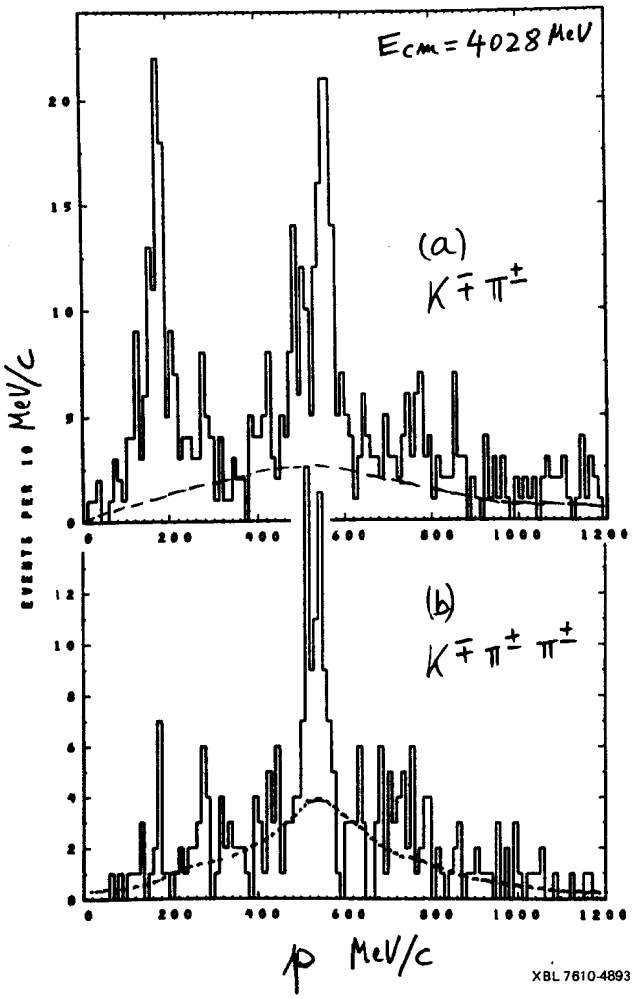

Fig. 12. Momentum spectra at E_{cm} = 4.028 GeV in 10 MeV/c intervals. (a) Signals observed in the two-body systems $K^{\mp}\pi^{\pm}$ as well as kinematic reflections "$\pi^{+}\pi^{-}$," "$K^{+}K^{-}$." (b) For the signal observed in $K^{\mp}\pi^{\pm}\pi^{\pm}$. The dashed curves indicate background levels.

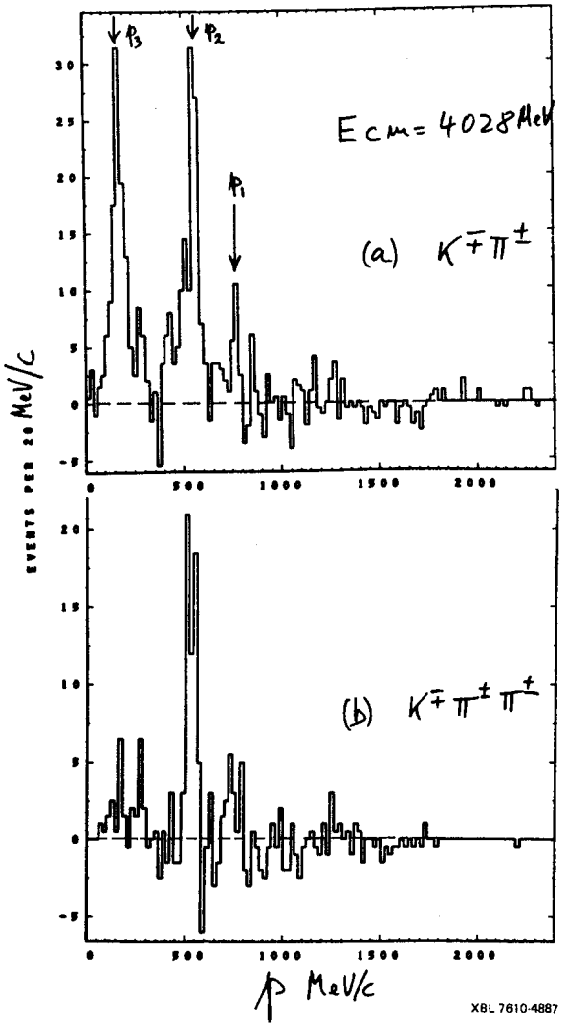

Fig. 13. The same spectra as in Fig. 12, now in 20 MeV/c intervals and with background subtraction.

$$P_3 = 178 \pm 8 \text{ MeV/c}, \quad \Gamma_3 = 35 \pm 8 \text{ MeV/c}$$

for the neutral distributions and

$$P_4 = 535 \pm 10 \text{ MeV/c}$$

for the charged distribution. Here the indices correspond to the reactions quoted above. The errors are estimates of the precision to which the central values are known including an allowance for systematic errors in the momentum scale. Finally the incident energy is

$$E_{cm}/2 = E_o = 2014 \pm 2.7 \text{ MeV} .$$

Here the error has three components added in quadrature: ± 2 MeV from the 0.1% uncertainty in the absolute energy calibration, ± 1.4 MeV beam spread from synchrotron radiation effects, and ± 1 MeV variation (which is known from flip coil measurements) in precise run-to-run beam settings. As far as widths of distributions are concerned the latter two errors contribute in quadrature giving $dE_o = 1.7$ MeV.

B. D^{*o} Decay

The possibilities for D^{*o} decay with charm conservation are:

$$D^{*o} \rightarrow D^o + \pi^o \qquad (6)$$

$$D^{*o} \rightarrow D^o + \gamma \ . \qquad (7)$$

The Q value for π^o production is so small that we can ask which of these two decay modes is the predominant one. Here $Q_{\pi^o} = M_{D^{*o}} - M_{D^o} - m_{\pi^o}$. We also note that the $D^{*o} \rightarrow D^+ \pi^-$ decay will be ruled out by energy conservation.

In Figs. 14a,b we show momentum spectra resulting from Monte-Carlo calculations for reactions (2) and (3) with D^{*o} decays according to (6) and (7) respectively. These were calculated at $E_{cm} = 4028$ MeV and for M_{Do} and $M_{D^{*o}}$ values as indicated. It is clear that the shape of the peak centered at p_3 is a sensitive function of whether we are dealing with π^o or γ decay of D^{*o}. For π^o decay (Fig. 14a) we get an essentially Gaussian distribution while for γ decay (Fig. 14b) we get a distribution with $dN/dp^2 =$ constant or $dN/dp \propto p$. It can be noted from a comparison of Fig. 12a with Fig. 14 that the predominant decay mode is π^o decay; however

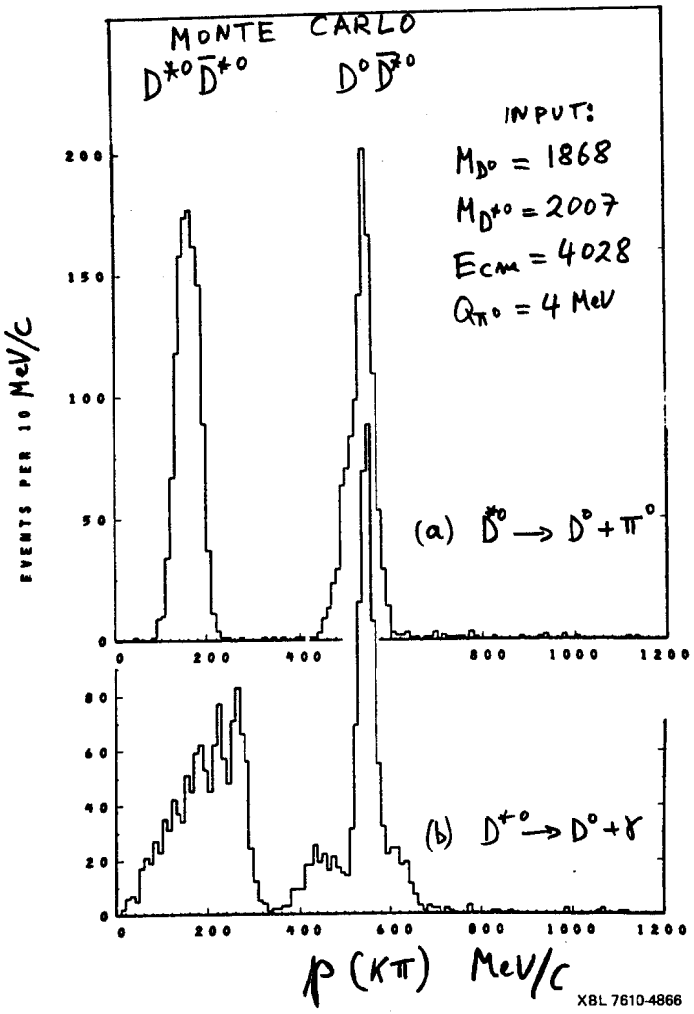

Fig. 14. Momentum spectra from Monte-Carlo calculation simulating the detector at SPEAR. (a) $D^{*o} \rightarrow D^o + \pi^o$. (b) $D^{*o} \rightarrow D^o + \gamma$.

there is evidence for appreciable γ decay as well. A preliminary estimate for $\Gamma(D^{*o} \to D^o\gamma)/\Gamma(D^{*o} \to D^o\gamma \text{ and } D^o\pi^o)$ is $\sim 35-45\%$.

C. Mass Determinations

We can quote the following preliminary values. From reaction (1) using p_1 we get a mass estimate for M_{Do} from $M_{Do}^2 = E_o^2 - p_1^2$

$$M_{Do}(1) = 1863 \pm 5.3 \text{ MeV}/c^2 \ .$$

Here the error is arrived at from $dM_{Do}(1) = 1.1\, dE_o - 0.4\, dp_1$. From reaction (2) using p_2 we get a relation between M_{Do} and M_{D*o} from $2E_o = E_{Do} + E_{D*o}$. In a linear approximation this is given by:

$$M_{Do}(2) + M_{D*o} = 3869 \pm 6.4 \text{ MeV} \ .$$

Here the error is arrived at from

$$dM_{Do}(2) = 2.1\, dE_o - 0.6\, dp_2 - dM_{D*o} \ .$$

From reaction (3) we get

$$M_{D*o}^2 = E_o^2 - \left(p_3 \frac{M_{D*o}}{M_{Do}}\right)^2 \ .$$

This gives:

$$\boxed{M_{D*o} = 2005 \pm 3 \text{ MeV}/c^2}$$

where the error comes from

$$dM_{D*o}(3) = dE_o - 0.1\, dp_3 \ .$$

Using this M_{D*o} value in the relation for $M_{Do}(2)$ we get

$$\boxed{M_{Do} = 1864 \pm 5.4 \text{ MeV}/c^2} \ .$$

Here $dM_{Do}(2,3) = 1.1\, dE_o - 0.6\, dp_2 + 0.1\, dp_3$.

The resulting value for $Q_{\pi o}$ is

$$Q_{\pi o} = 6 \pm 5.1 \text{ MeV}$$

where the error comes from $dQ_{\pi o} = 0.6\, dp_2 - 0.2\, dp_3$ since the dependence on dE_o (essentially) cancels here.

The experimental width Γ_3 is a very sensitive function of $Q_{\pi o}$. In particular the observed width Γ_3 fits best with a $Q_{\pi o}$ even lower than 6 MeV. Aside from the experimental resolution the contributions to the width Γ_3 come from $Q_{\pi o}$, Γ_{Do}, Γ_{D*o}, and $dE_o = 1.7$ MeV (the portion contributing to the broadening of the distribution). This places more stringent limits on Γ_{Do} and Γ_{D*o} of < 5 MeV. From charm theory Γ_{Do} is expected to be $\ll 1$ eV (weak decay) while Γ_{D*o} is of typical electromagnetic width because of the very low $Q_{\pi o}$ value.

Finally from reaction (4) and p_4 we get a relation between M_{D+} and M_{D*+} which in a linear approximation becomes:

$$M_{D+} + M_{D*+} = 3883 \pm 7.3 \text{ MeV} \ .$$

Here the error is arrived at from:

$$dM_{D+}(4) = 2.1\, dE_o - 0.6\, dp_4 - dM_{D*+} \ .$$

This yields $(M_{D+} + M_{D*+}) - (M_{Do} + M_{D*o}) = 14 \pm 7.7 \text{ MeV}/c^2$, where now the error in E_o cancels. We have no reliable experimental determination for δ and δ^* where we define $\delta = M_{D+} - M_{Do}$ and $\delta^* = M_{D*+} - M_{D*o}$. Here $\delta + \delta^* = 14 \pm 7.7 \text{ MeV}/c^2$. If from theory δ and δ^* are considered approximately equal[7,8,9] we get

$$\delta \approx \delta^* \approx 7 \pm 4 \text{ MeV}/c^2 \ .$$

If on the other hand as suggested by Ono[10] $\delta \approx \delta^* + 3 \text{ MeV}/c^2$,

$$\delta \approx 8.5 \pm 4 \text{ MeV}/c^2$$

and $$\delta^* \approx 5.5 \pm 4 \text{ MeV}/c^2 \ .$$

As shown in Fig. 11c we have an indication for reaction (5); this gives an upper limit on M_{D*+}, namely E_o; i.e.,

$$M_{D*+} < 2014 \text{ MeV}/c^2 \ .$$

This limit is consistent with the δ^* values quoted above.

D. Does p_3 Correspond to $D^{*o}D^{*o}$ or D^oD^{**o}?

With the value for M_{D*o} given above $Q = E_{cm} - 2M_{D*o} = 18$ MeV, and $p(D^{*o}) = 191$ MeV/c. This represents a phenomenal rise from threshold for reaction (3), a p-wave process. In fact it has been suggested[11] that perhaps process (3'), with D^{**o} a $J^P = 1^+$ state with mass $M(D^{**o}) = 2146 \text{ MeV}/c^2$ and s-wave production, could be occurring. From a very preliminary study of the M_{recoil} spectrum at $E_{cm} = 4.415$ GeV we find however no evidence for a recoil mass peak near $2146 \text{ MeV}/c^2$ but find

instead a broad peak at $M_{recoil} \approx 2200$ MeV/c^2 and $\Gamma \approx 80$ MeV/c^2. These values are completely consistent with values expected from reaction (3).

E. Study of an Individual Event

We have studied individual events to try and find examples of "complete" events; viz.,

$$e^+e^- \to \overline{D^o} \quad D^{*o}$$
$$\quad \hookrightarrow K^+\pi^- \quad \hookrightarrow D^o\pi^o$$
$$\qquad\qquad\qquad \hookrightarrow K^-\pi^+ \quad .$$

We have observed one clear-cut case at $E_{cm} = 4028$ MeV (see Fig. 15). This event gives a good fit to the above assumption and has been further constrained by a hand calculation to demand equal masses for the D^o and $\overline{D^o}$. This gives

$$M_{D^o} = 1866.5 \text{ MeV}/c^2$$
$$M_{D^{*o}} = 2006.7 \text{ MeV}/c^2 \quad .$$

The event does not fit a missing γ-ray.

This result lies well within the errors of the mass determinations given above. Figure 16 shows a sketch of the (central values) of the relations between M_{D^o}, $M_{D^{*o}}$, M_{D^+}, $M_{D^{*+}}$, δ and δ^* as well as the above event.

V. THE τ-θ PUZZLE REVISITED; EVIDENCE FOR PARITY VIOLATION FROM $D^\pm$ DECAY

A study of the $D^\pm \to K\pi\pi$ Dalitz plot shows that the plot is compatible with a phase space distribution, does not appear to die off on the boundaries as a natural spin parity assignment would, and is specifically incompatible with J^P assignments of 1^- or 2^+. These observations, coupled with the observation of the $K\pi$ decay of the D^o, a final state of natural spin parity ($J^P = 0^+, 1^-, 2^+, \ldots$), and the belief that the neutral and charged particles are members of the same isomultiplet, suggest parity violation in the decay of the D's.

A. Appearance of Dalitz Plot

In order to obtain a relatively clean sample of the decay $D^\pm \to K^\mp\pi^\pm\pi^\pm$

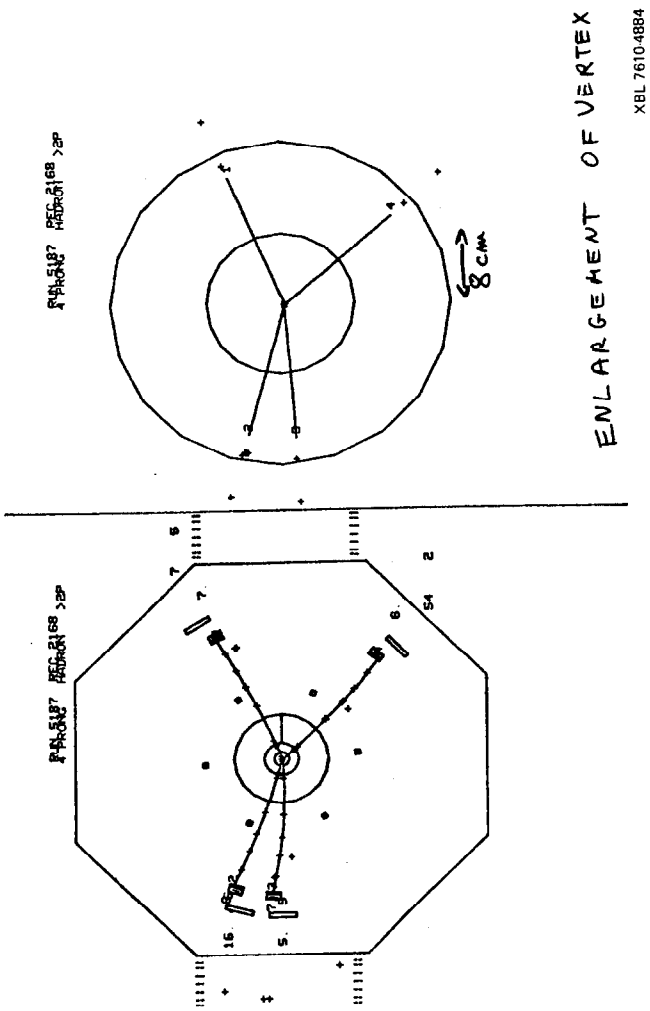

Fig. 15. Computer reconstruction of an example of $e^+e^- \to \overline{D^o}D^{*o}$, $\overline{D^o} \to K^+\pi^-$, $D^{*o} \to D^o\pi^o$, $D^o \to K^-\pi^+$. The right-hand part is an enlargement of the vertex region showing no measurable path length for D^o and $\overline{D^o}$ decay.

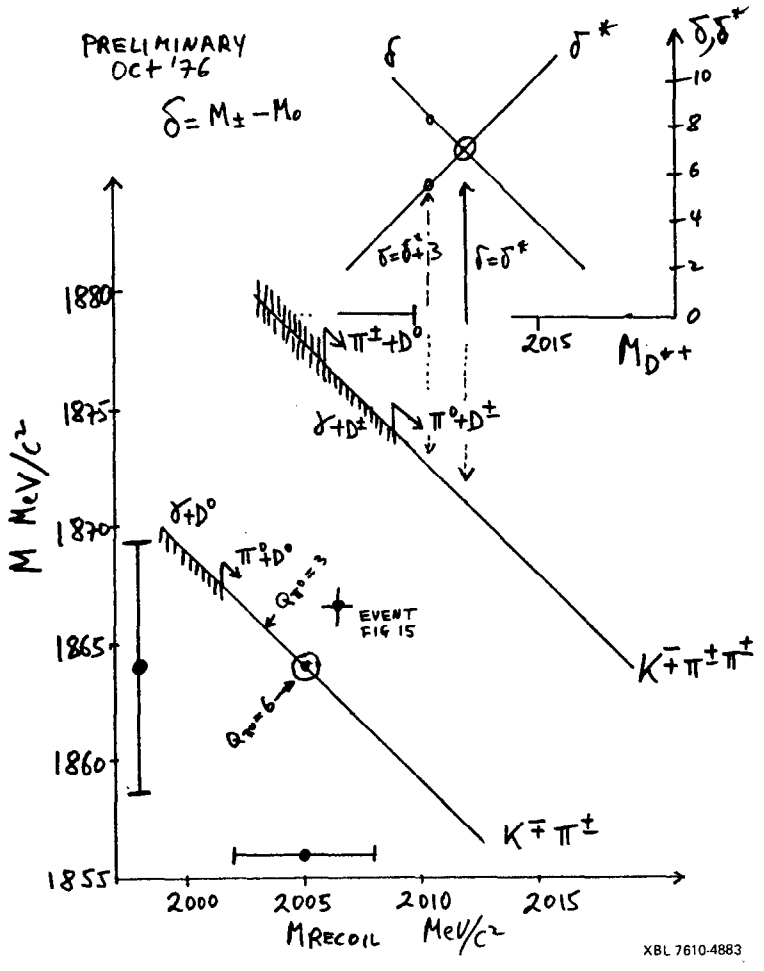

Fig. 16. Sketch of the relations between M_{D^0} and $M_{D^{*0}}$, M_{D^+} and $M_{D^{*+}}$. The $\pi^0 D^0$, $\pi^0 D^\pm$ and $\pi^\pm D^0$ thresholds are indicated by shading. The inset shows δ and δ^* as a function of $M_{D^{*+}}$ for the "best values" of $M_{D^0} = 1864$ and $M_{D^{*0}} = 2005$ MeV/c^2. For clarity the central values are only shown.

we apply mass and missing mass cuts to three-body combinations for data taken between $3.9 < E_{cm} < 4.25$ GeV. The cuts are $1860 < M_{K\pi} < 1920$ MeV/c^2 and $1960 < M_{recoil} < 2040$ MeV/c^2 (see Fig. 17). From this selection we obtain a sample of 126 events of which we estimate 58 events to be background. In Fig. 18a we present the Dalitz plot for these 126 events, choosing the Dalitz variables:

$$X_{Dalitz} = \frac{\left|T_{\pi_1} - T_{\pi_2}\right|}{\sqrt{3}\,Q} \quad ; \quad Y_{Dalitz} = \frac{T_K}{Q}$$

with T being D rest frame kinetic energies and $Q = T_{\pi_1} + T_{\pi_2} + T_K$. Figure 18b shows a background Dalitz plot consisting of non-exotic $K\pi\pi$ combinations, $K^\pm\pi^+\pi^-$, with identical kinematic cuts. Both the signal and background plots appear uniformly populated without either boundary zeros or zeros along the y axis as expected for natural spin parity assignment. In order to specifically rule out the states 1^- and 2^+ we have performed Monte-Carlo simulations using the simple, phenomenological matrix elements presented by Zemach.[12]

B. The 1^- Matrix Element

For the case of $J^P = 1^-$ we construct an axial vector amplitude symmetric under the exchange of the two pions. A simple representation is provided by: $(T_{\pi_1} - T_{\pi_2})(\vec{\pi}_1 \times \vec{\pi}_2)$ where $\vec{\pi}$ represents a D rest frame pion momentum. For the case of unpolarized production one then expects an intensity proportional to $|T_{\pi_1} - T_{\pi_2}|^2 |\vec{\pi}_1 \times \vec{\pi}_2|^2$.

For comparison with the data we have divided the Dalitz plot into the four discrimination regions[13] of Fig. 19a. These regions are nearly evenly populated by phase space whereas the 1^- matrix element strongly populates region 3 at the expense of regions 1 and 4. Figure 20a compares the background subtracted region populations of the data to the populations expected in the 1^- model, both distributions normalized to the phase space Monte Carlo.

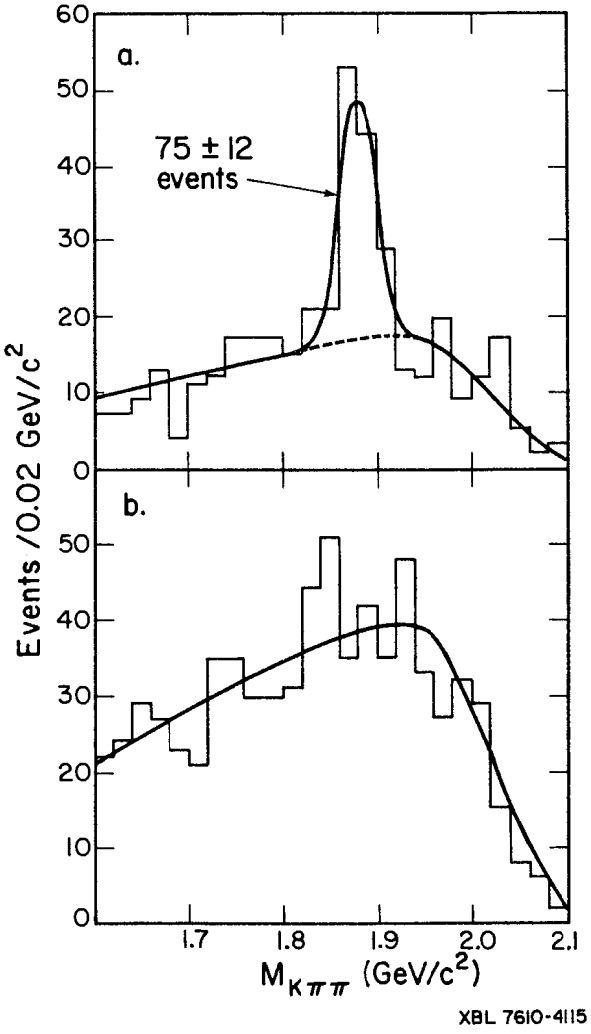

Fig. 17. The Kππ distribution for the "4.1" GeV region with an M_{recoil} cut 1960 - 2040 MeV/c^2. (a) Exotic, (b) non-exotic.

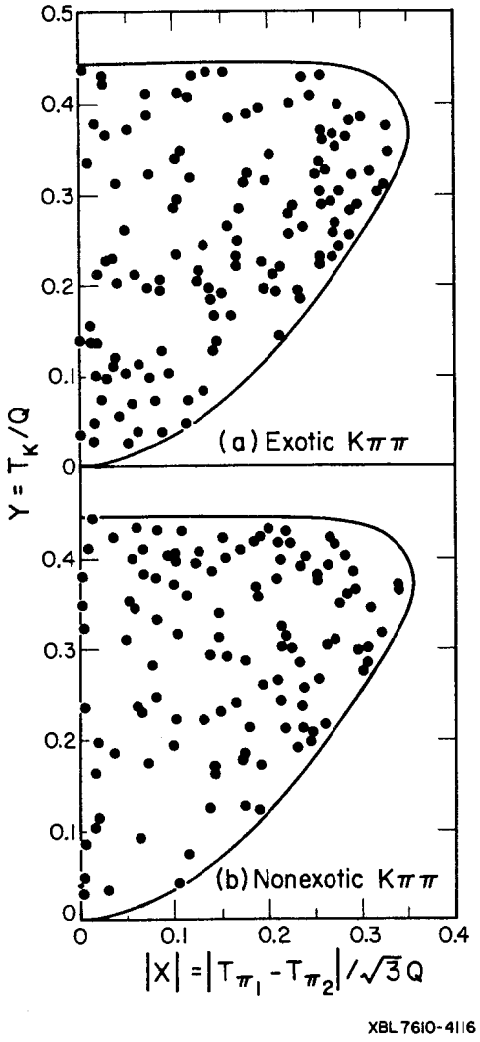

Fig. 18. Dalitz plots, folded around y-axis, for the Kππ system with mass cuts M(Kππ) = 1860 - 1920 MeV/c^2 and the selections given in Fig. 17. (a) Exotic, (b) non-exotic.

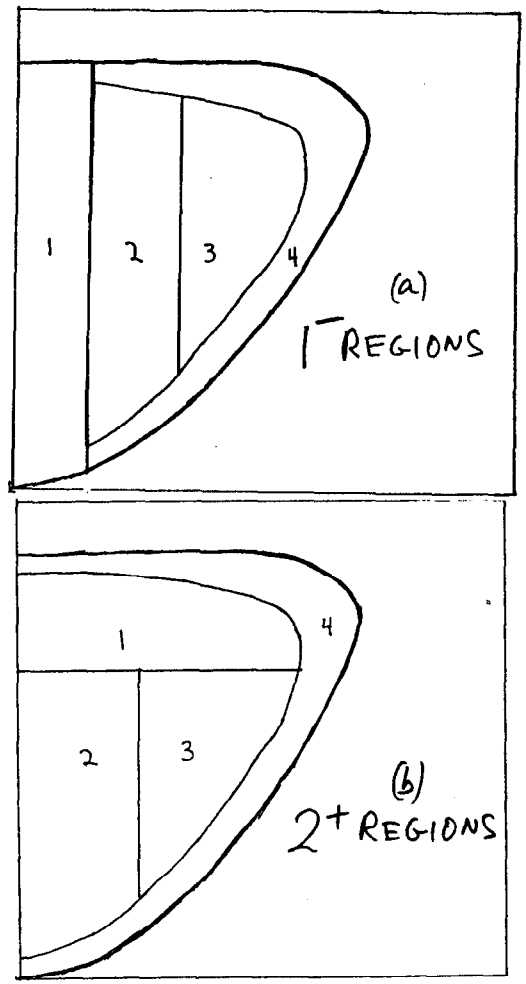

Fig. 19. The discrimination regions on the Dalitz plot selected for effective separation between phase space and (a) a 1^- matrix element, (b) a 2^+ matrix element.

C. The 2^+ Matrix Element

Again following Zemach[12] we construct a symmetric, traceless second-rank tensor which is also symmetric under the exchange of the two pions. A simple example is provided by: $A^{ij} = \Delta\pi^i q^j + \Delta\pi^j q^i$ where $\vec{\Delta\pi}$ is the difference of the pion momenta and $\vec{q}$ is their cross product.

For unpolarized production one expects intensity proportional to

$$\sum_i \sum_j A^{ij} A_{ji} \quad \text{or} \quad |\vec{\pi}_1 - \vec{\pi}_2|^2 |\vec{\pi}_1 \times \vec{\pi}_2|^2 \ .$$

The discrimination regions for the 2^+ matrix elements are shown in Fig. 19b. Comparison of the region populations to the data is shown in Fig. 20b.

The χ^2 comparison between phase space and the respective 1^- and 2^+ matrix elements are given on Fig. 20.

We have thus demonstrated from a study of the $K\pi\pi$ Dalitz plot that this three-body final state is incompatible with J^P assignments of either 1^- or 2^+. $J^P = 0^+$ is not an allowed state of three pseudoscalars. Since the presumed isomultiplet state, D^o, decays into two pseudoscalars, a final state of natural spin parity, we conclude there exists evidence for parity violation in the decays of the D's, which implies that we are dealing with a weak decay.

VI. THE PRODUCT OF CROSS SECTION AND BRANCHING RATIO

We have searched for the charmed particle signal at all the energies from the ψ/J up to $E_{cm} = 7.8$ GeV. I have already shown in Figs. 2 and 3 the absence of any D^o signal in the $K^{\mp}\pi^{\pm}$ decay mode at the ψ and ψ'. Above $E_{cm} \sim 3.9$ GeV where we begin to observe a D^o signal the cross section rises rapidly to a maximum value of $\sigma \cdot BR = 0.6 \pm 0.1$ nb (preliminary) for the $K^{\mp}\pi^{\pm}$ decay mode at $E_{cm} = 4.028$ GeV. This is followed by a rapid drop off by a factor of ~ 3 at 4.4 GeV. Beyond 4.6 GeV the cross section drops off further to a level where we either cannot observe a signal at all or can just barely recognize it. The preliminary $\sigma \cdot BR$ distribution is shown in Fig. 21. To obtain $BR(K^{\mp}\pi^{\pm})$ one needs to

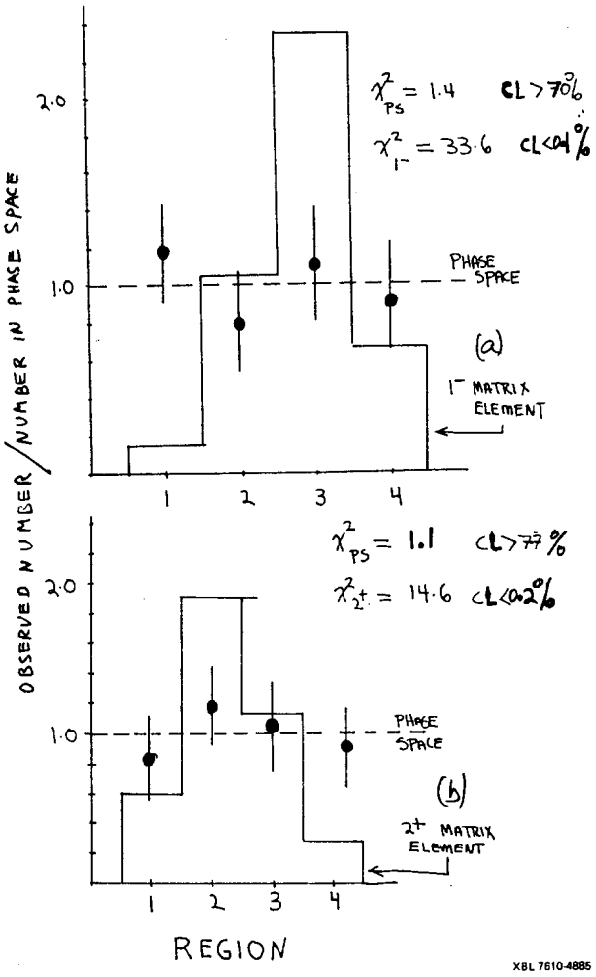

Fig. 20. Comparison of background subtracted populations in the four discrimination regions (a) the 1^- model, (b) the 2^+ model, with all distributions normalized to phase space Monte-Carlo calculations. The respective χ^2 values and confidence levels are also shown.

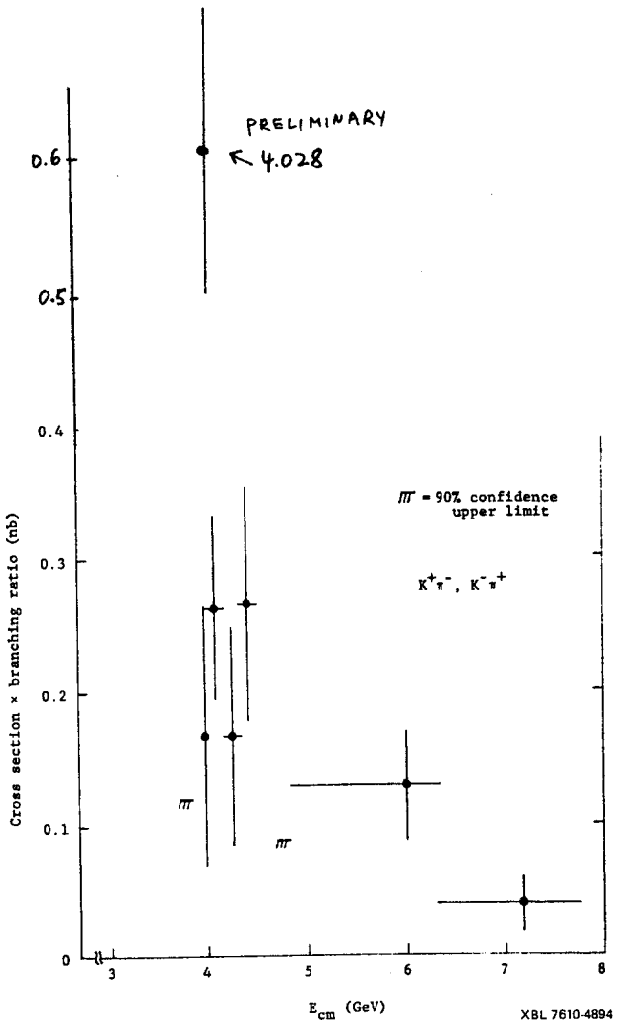

Fig. 21. $\sigma \cdot BR$ for $K^{\mp}\pi^{\pm}(1865)$ production.

study "complete" events like the one illustrated in Fig. 15. This study is in progress. As "complete" events are very rare, this indicates that $BR(K^{\mp}\pi^{\mp})$ is small, of the order of a few percent.

$\sigma \cdot BR(K^{\mp}\pi^{\pm}\pi^{\pm}) \approx 0.3 \pm 0.15$ nb at $E_{cm} = 4.028$ GeV, evaluation at other energies is in progress. Finally $\sigma \cdot BR(K3\pi)$ is approximately 2 to 3 times larger than $\sigma \cdot BR(K^{\mp}\pi^{\pm})$ but the detailed study is not complete as yet.

VII. SEARCH FOR A CABIBBO FORBIDDEN DECAY MODE

According to charm theory[4] the decay $D^{o} \to K^{-}\pi^{+}$ proceeds with a $BR \propto \cos^2\theta$ while the decay $D^{o} \to \pi^{-}\pi^{+}$ proceeds with a $BR \propto \sin^2\theta$ where θ is the Cabibbo angle. We have searched for a $\pi^{-}\pi^{+}$ signal with optimal cuts on the recoil system. We find an indication at the 1.5 standard deviation level giving $BR(D^{o}(\overline{D^{o}}) \to \pi^{+}\pi^{-})/BR(D^{o}(\overline{D^{o}}) \to K^{\mp}\pi^{\pm}) = 6.5 \pm 4\%$ (see Fig. 22). Thus the effect is not established as yet.

The results presented here are the work of the LBL-SLAC collaboration at SPEAR, whose members are: F. M. Pierre, G. S. Abrams, M. S. Alam, A. M. Boyarski, M. Breidenbach, W. C. Carithers, W. Chinowsky, S. C. Cooper, R. G. DeVoe, J. M. Dorfan, G. J. Feldman, C. E. Friedberg, D. Fryberger, G. Hanson, J. Jaros, A. D. Johnson, J. A. Kadyk, R. R. Larsen, D. Lüke, V. Lüth, H. L. Lynch, R. J. Madaras, C. C. Morehouse, H. K. Nguyen, J. M. Paterson, M. L. Perl, I. Peruzzi, M. Piccolo, T. P. Pun, P. Rapidis, B. Richter, B. Sadoulet, R. H. Schindler, R. F. Schwitters, J. Siegrist, W. Tanenbaum, G. H. Trilling, F. Vannucci, J. S. Whitaker, and J. E. Wiss.

We wish to thank the SPEAR operating staff for their enthusiastic efforts in successfully carrying out the runs at 4.028 and 4.415 GeV under new conditions and very limited time. We also wish to thank the LBL and SLAC computer centers for their help in facilitating the data analysis. Finally I wish to thank Ms. Christina Frank for her meticulous work in typing and compiling this report.

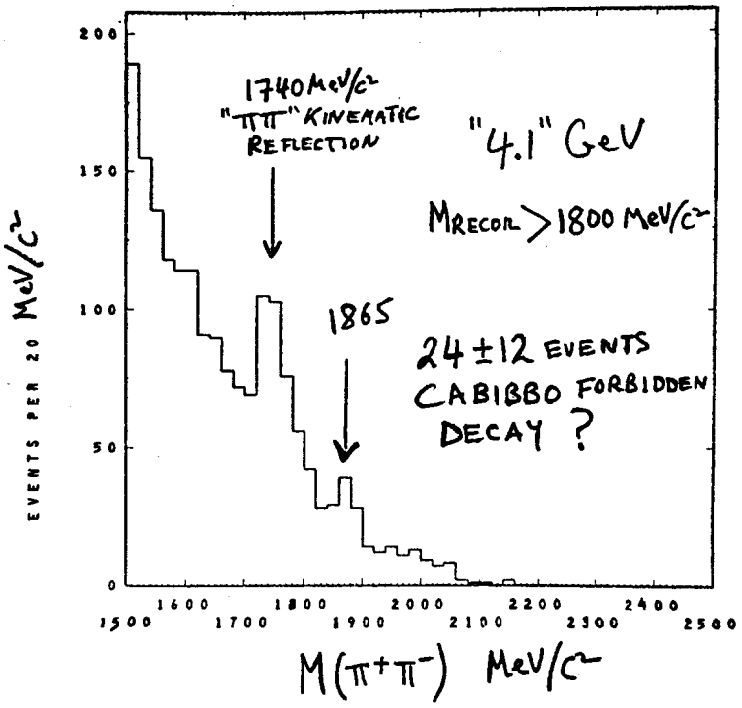

Fig. 22. $M(\pi^{+}\pi^{-})$ distribution for the "4.1" GeV region with a cut of $M_{recoil} > 1800$ MeV/c^2. We note the kinematic reflection signal centered at 1740 MeV/c^2 as already shown in Fig. 4b, as well as a possible small excess of events consistent with 1865 MeV/c^2.

REFERENCES AND FOOTNOTES

1. J.-E. Augustin et al., Phys. Rev. Lett. 34, 233 (1975); J.-E. Augustin et al., Phys. Rev. Lett. 34, 764 (1975).
2. G. Goldhaber, F. M. Pierre et al., Phys. Rev. Lett. 37, 255 (1976).
3. I. Peruzzi, M. Piccolo et al., Phys. Rev. Lett. 37, 569 (1976).
4. S. L. Glashow, J. Iliopoulos, and L. Maiani, Phys. Rev. D2, 1285 (1970); S. L. Glashow, Experimental Meson Spectroscopy, A.I.P. Conf. Proc. No. 21, Particles and Fields Subseries No. 8, p. 387 (1974). For more details, see also M. K. Gaillard, B. W. Lee, and J. L. Rosner, Rev. Mod. Phys. 47, 277 (1975); A. De Rujula, H. Georgi, and S. L. Glashow, Phys. Rev. D12, 147 (1975); M. B. Einhorn and C. Quigg, Phys. Rev. D12, 2015 (1975). Earlier indications of possible charmed particle production have come from experiments involving neutrino interactions, as well as from cosmic-ray emulsion studies. See, for example: A. Benvenuti et al., Phys. Rev. Lett. 34, 419 (1975); E. G. Cazzoli et al., Phys. Rev. Lett. 34, 1125 (1975); J. Blietschau et al., Phys. Lett. 60B, 207 (1976); J. von Krogh et al., Phys. Rev. Lett. 36, 710 (1976); B. C. Barish et al., Phys. Rev. Lett. 36, 939 (1976); K. Niu et al., Prog. Theor. Phys. 46, 1644 (1971).
5. See talks by D. Meyer and by P. Smusser for results from DESY presented at this topical conference.
6. For an alternate interpretation of the entire psion family, in terms of a color model, see G. Feldman and P. T. Mathews, The Discovery of Coloured Kaons?, Imperial College London Preprint ICTP/75/17, July 1976. Also a review by O. W. Greenberg and C. A. Nelson, Color Models of Hadrons, University of Maryland preprint PHYS.PUB.77-047.
7. A. De Rujula, H. Georgi, and S. L. Glashow, Phys. Rev. Lett. 37, 398 (1976); K. Lane and E. Eichten, Phys. Rev. Lett. 37, 477 (1976).
8. K. Lane and S. Weinberg, Phys. Rev. Lett. 37, 717 (1976). See also H. Fritzsch, Phys. Lett. 63B, 419 (1976).
9. D. B. Lichtenberg, Phys. Rev. D12, 3760 (1975).
10. S. Ono, Phys. Rev. Lett. 37, 655 (1976).
11. M. Suzuki, private communication. Also, J. Finkelstein and S. S. Pinsky, Columbia University preprint COO-1545-198.
12. C. Zemach, Phys. Rev. B133, 1201 (1964). See also B. Lee, C. Quigg, and J. Rosner, Tests for Weak Decays of Charmed Particle Candidates, Fermilab preprint 76/63 Thy.
13. The inner boundary of region 4 is a contour of constant (and small) $|\vec{\pi}_1 \times \vec{\pi}_2|$.

Limits on Charmed Particle Production in Hadron Collisions

D. I. Meyer
University of Michigan

The title of my talk should really be "Why Hadron Interactions are the Worst Place to Look for Charmed Particles." I will supply you with numerous excuses illustrated by slide, graphs, calculations, etc., and try to be realistic about the probability for seeing the charmed states from hadron collisions in the future. I will also talk about various by products of the experiment. The experiment was a collaboration of FNAL, Purdue, and Michigan by the group shown in Fig. 1.

The problem of seeing charmed particles in hadron interactions can be stated simply. There are many other hadrons around expecially those that when analyzed in pairs give low effective mass. I hope therefore it will become clear as I proceed that the failure thus far to detect charmed particles in hadron collisions is not surprising.

Now that the charmed particles have been discovered their production cross section in hadron collisions is of considerable interest. The theoretical interpretation of hadronic production of ψ's is complicated by Zweig's rule. Thus the cross section for pair production of charmed particles becomes of importance.

E-357 PARTICLE SEARCH

FERMILAB:
- D. BINTINGER
- D. JOVANOVIC
- R. LUNDY

UNIVERSITY OF MICHIGAN
- C. AKERLOF
- P. ALLEY
- D. KOLTICK
- R. LOVELESS
- D. MEYER
- R. THUN

PURDUE UNIVERSITY
- R. DITZLER
- D. FINLEY
- F. LOEFFLER
- E. SHIBATA
- K. STANFIELD

The apparatus in our experiment is a canonical double arm spectrometer shown in Fig. 2. It has drift chambers to measure the opening angle and momentum of the particles, three Cerenkov counters in each arm for particle identification and a steel hadron shield in the rear so that we can detect ψ's for a direct calibration of the mass and mass resolution as well as for a cross section comparison with the other FNAL ψ experiments. Let me emphasize that beam rate, solid angle and background due to other beam particle interactions are not the limitation for an experiment of this type in the mass range below a few GeV. The data rate is set by the computer read in time.

The drift chambers were exceedingly reliable; they gave 250μ resolution using an Argon – 10% CO_2 mixture. We did not struggle for better space resolution because the limitation on mass resolution was determined by uncertainty in the opening angle caused by multiple scattering in the $\check{C}$ counters.

To convince ourselves and others that the apparatus works as designed hadron data and $\psi \to \mu^+\mu^-$ data were taken simultaneously. The ψ mass spectra is shown in Fig. 3. The absolute mass is in agreement with the Spear result and comparable in accuracy. The measured resolution agrees with that expected from calculations of multiple scattering. The cross section is measured only over a limited x and $p_\perp$ range. It agrees very well with the Columbia-Stony Brook data measured in roughly the same x and $p_\perp$ range. If a distribution of

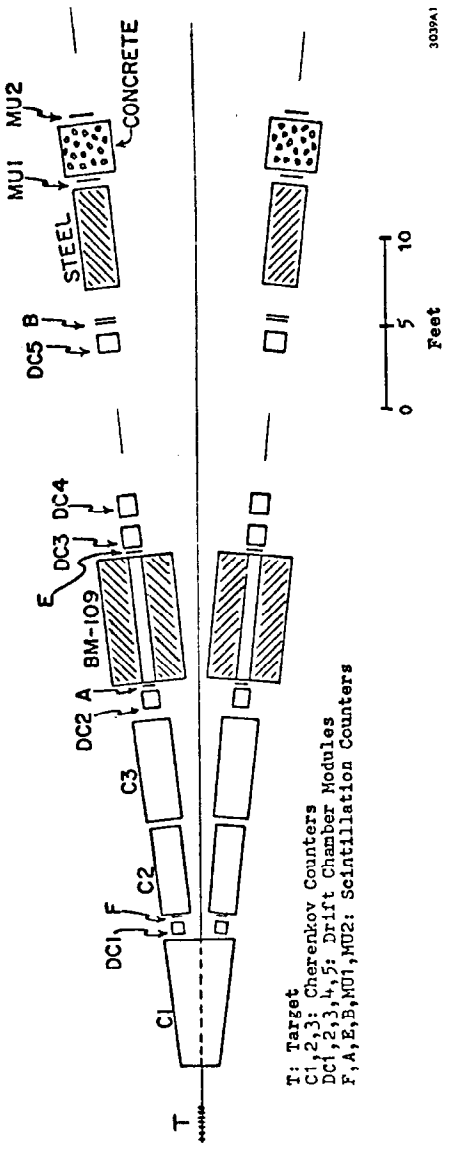

Fig. 2

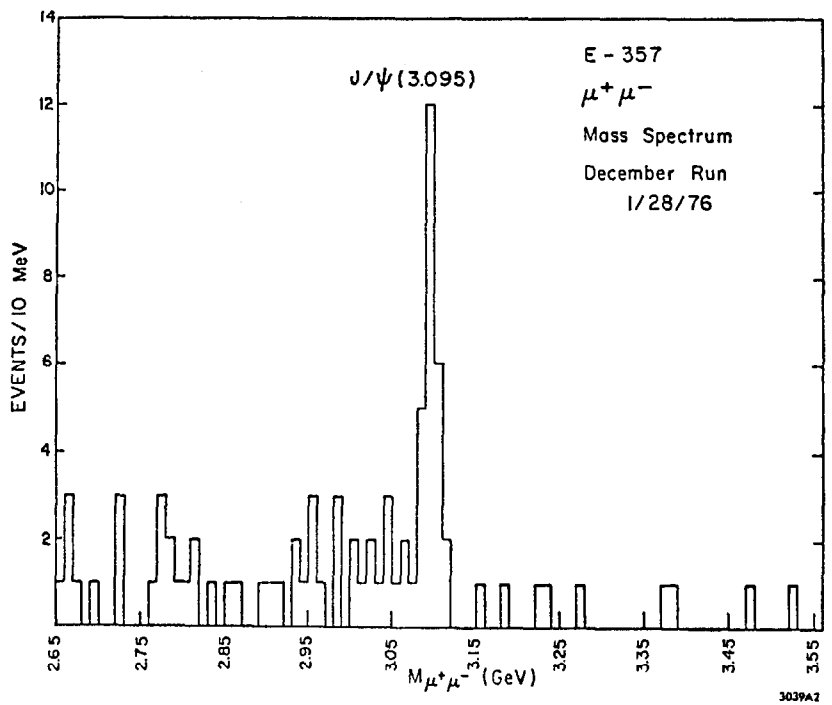

Fig. 3

$(1-x)^{3.4}e^{-1.6\ p_\perp}$ is used as indicated by other experiments the total production cross section is 10.7 ± 2.4 nb in agreement with other FNAL experiments.

Before looking at the hadron results I will first describe the Cerenkov identification. The three Cerenkov counters in each arm were calibrated for efficiency by running them all at the same index of refraction. The maximum inefficiency as measured by asking how often one of the three counters did not record a particle when the other two did was typically 99%. The counters were then set to the proper gas pressures. For a given momentum particle only three patterns of triggers corresponding to π, K or p are allowed. By studying the number and distribution of disallowed patterns estimates of the fraction of misidentified particles were made. These disallowed patterns were almost entirely due to gamma-ray conversions associated with the same primary event in the target as that being measured. After these Cerenkov corrections (they were typically ~10%) our particle ratios agree very well with those of Cronin et. al.

Next let me turn to ϕ production. Because each of the spectrometer arms subtends a reasonable solid angle the $\phi^\circ \to K^+K^-$ can be detected in one arm and a second particle K, π, or p in the other arm. In Fig. 4 is shown the ϕ signal obtained. The natural width of the ϕ is 4.2 GeV. The observed width agrees with our resolution calculations. Fig. 5 shows the ϕ/π^- ratio as a function of $p_\perp$. The ratio increases with $p_\perp$ consistent with that

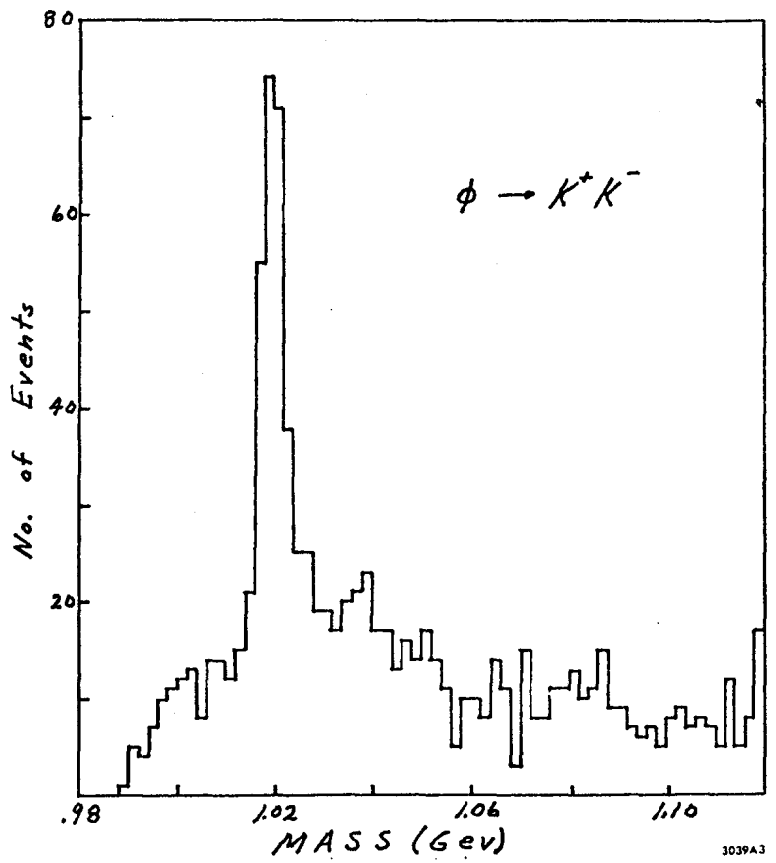
80
60
40
20
No. of Events
$\phi \rightarrow K^+K^-$
.98
1.02
1.06
1.10
MASS (Gev)
3039A3

Fig. 4

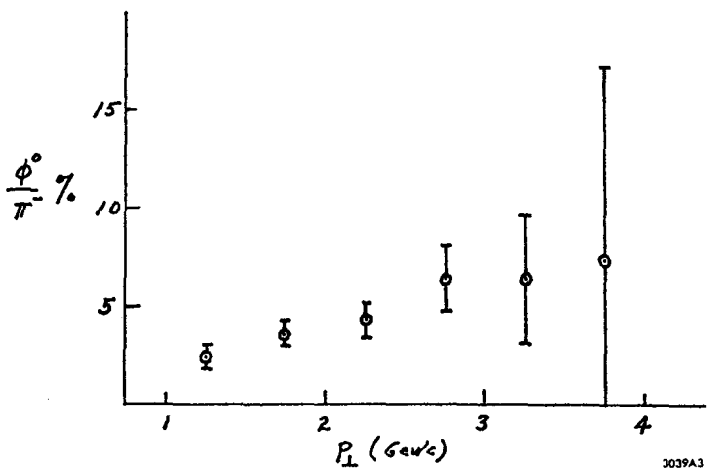
15
10
5
$\frac{\phi^\circ}{\pi^-}$ %
1
2
3
4
$P_\perp$ (Gev/c)
3039A3

Fig. 5

for other heavy particles. From data taken using Pb and Be targets an average $A^{1.1}$ dependence for ϕ production is found in this $p_\perp$ region.

The ϕ data can also be used to make a check on Zweigs rule. The ratio $\phi K^\pm/\phi\pi^\pm$ should be larger than $\pi^- K^\pm/\pi^-\pi^\pm$ ($\phi K^\pm$ means ϕ in one arm $K^\pm$ in the other, etc.) Because there are on the average so many particles produced in a 400 GeV collision it is difficult to calculate apriori how large an enhancement would be expected. In the average event there is about 60% probability of charged K's being produced in a 400 GeV collision. However by Zweigs rule the ϕ should always be produced with both a K^+ and a K^-. Thus an extremely crude guess might give an enhancement of around 1.5 to 2 in K's associated with ϕ's. The measured ratio is

$$\frac{\phi K^\pm/\phi\pi^\pm}{\pi^- K^\pm/\pi^-\pi^\pm} = 1.5 \pm .3 \ .$$

Thus there is an enhancement of K's associated with ϕ's but this result is statistically weak and there is no simple way of making a definite Zweig's rule prediction of what enhancement to expect.

Turning to the modes where D's should be seen the hadron mass spectra are shown in Fig. 6 for π^+K^- and $K^+\pi^-$. When this data was taken the position of the D was not known so the magnet settings were optimized at somewhat too high a mass for maximum sensitivity. Notice that there is a bump in the data at about 1.86 GeV mass however there are clearly other bumps at other masses also.

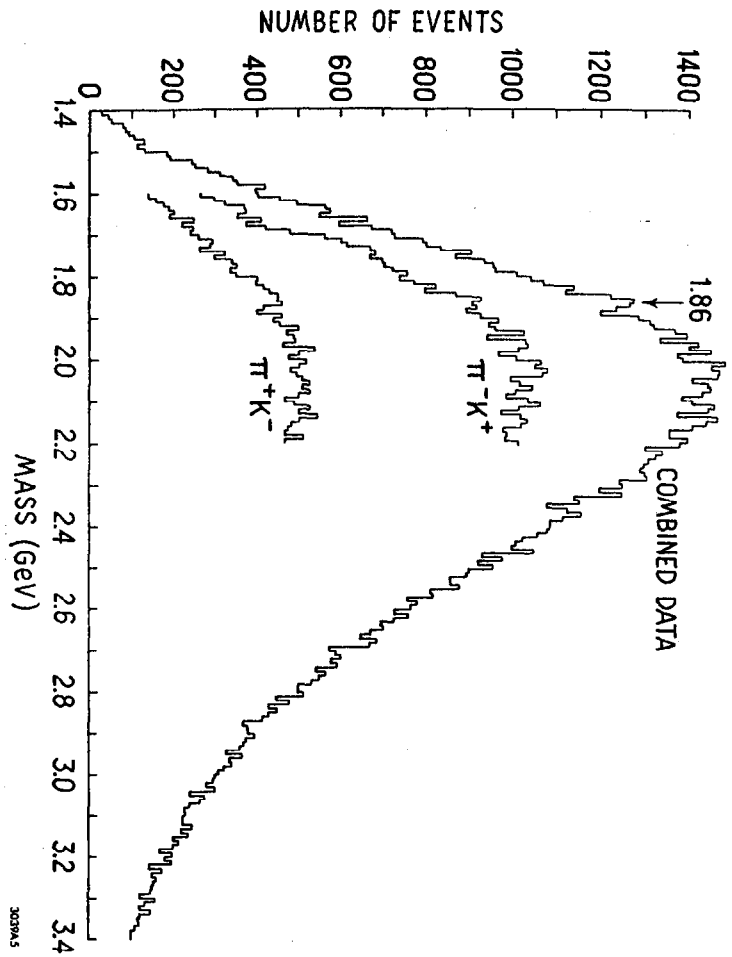

Fig. 6

The 1.86 bump is statistically the most significant but not by very much.

In Fig. 7 details of the region around 1.86 are shown. (Fig. 7 contains some data and corrections not in Fig. 6.) If a smooth curve is drawn through the data the statistical significance of the bump is found to be about 2.5 standard deviations.

The bump is too small to be considered anything other than a statistically amusing observation, but I would like to use it to illustrate the difficulty of observing charmed particles in hadron collisions. The bump is about 5% of the background hadron mass spectra. The absolute cross section times branching ratio corresponds to a few hundred nanobarns if the x and $p_\perp$ distributions are similar to the ψ. For reasonable assumptions about branching ratio the production cross section would be 5 to 10 μb. If the peak is real a factor of 5 more data would make it statistically believable and this will be collected in the present run. More likely the effect is spurious and the real cross section is an order of magnitude smaller requiring 100 times more data. Even if such data could be collected in a reasonable time the signal would be a fraction of a percent of background and great care would be needed to eliminate systematic effects.

Clearly the problem in seeing charmed states is with physical background from non-resonant hadron production. By a combination of optimizing the system for a

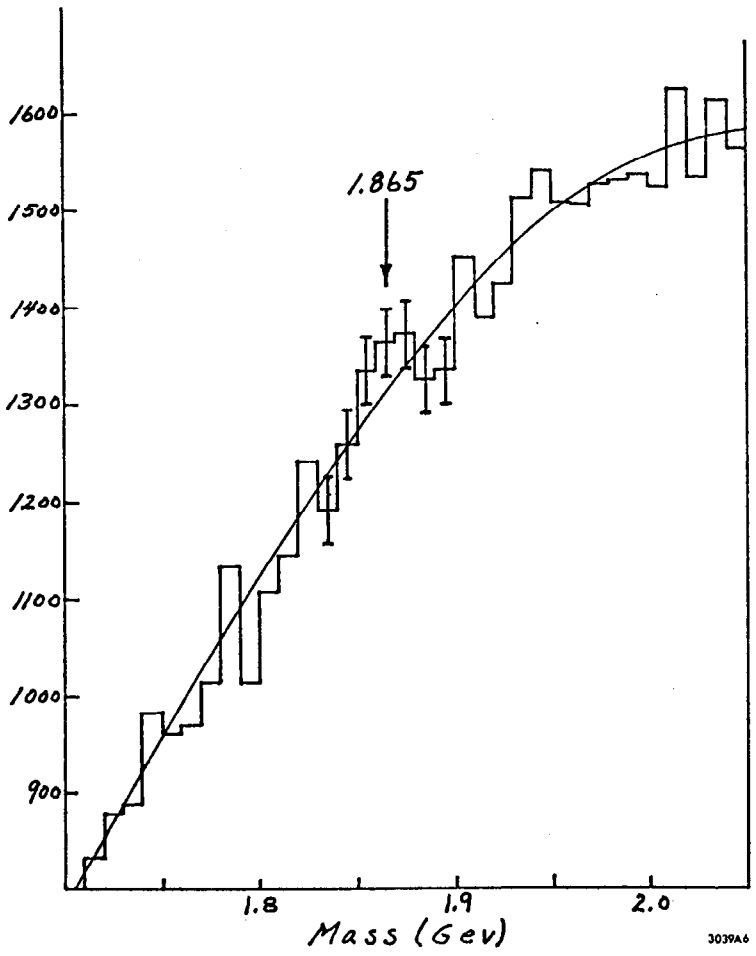

Fig. 7

mass of 1.86 GeV, speeding up the computer and specializing the trigger to the πK modes an order of magnitude more data can be obtained in a reasonable running time. However the natural thing to do is look around for some signature characteric of the D would cut into the background without cutting out the signal. The two obvious signatures which come to mind are prompt μ's which might be associated with some of the D decays and the fact that the D lifetime should be around $10^{-12} - 10^{-13}$ seconds.

Making use of the lifetime is difficult because 10^{-13} seconds corresponds in our experiment to a distance of 300 microns. Nevertheless an attempt has been made to use this signature. The set up used is shown in Fig. 8. Also shown is the fraction of the charmed events detected as a function of lifetime. In practice the veto downstream from the target cut the background ratio by a factor of around 100 while vetoing the signal by an estimated factor of 2. Thus a significant gain in sensitivity is obtained for lifetimes greater than 10^{-12} sec. Data was taken very rapidly because many fewer events were read into the computer than without the veto. The remaining background was due primarily to Λ and $\bar{\Lambda}$ decays downstream from the veto counter. No sign was seen of any charmed signal. The one positive result of the experiment was an exceedingly clean Λ and $\bar{\Lambda}$ signal. This is shown in Fig. 9. The $\bar{\Lambda}/\Lambda$ ratio was about 1/3. For a mean life $> 10^{-11}$ sec. a limit can be set on $D\bar{D}$ production $\sigma \cdot BR < 100$ nb. and at 10^{-12} $\sigma \cdot BR < 300$ nb. for

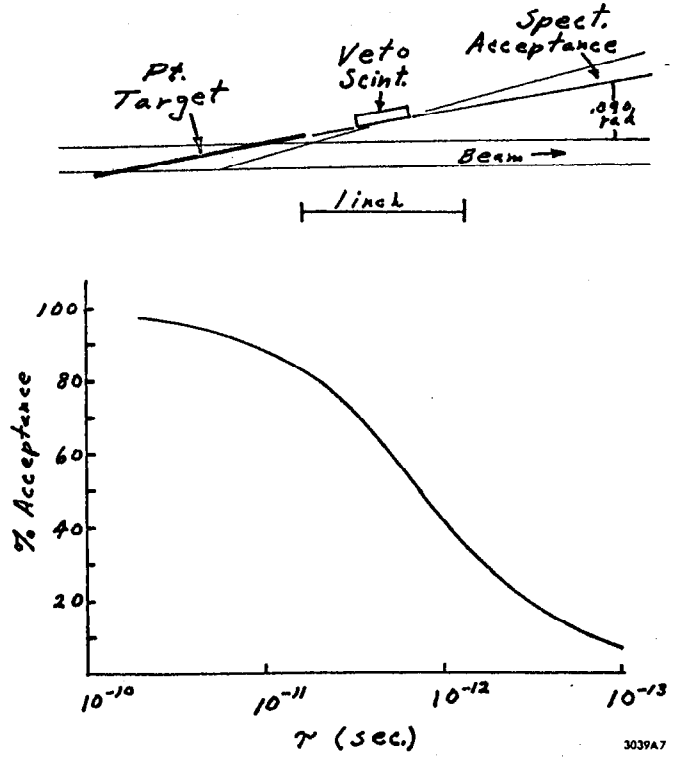

Fig. 8

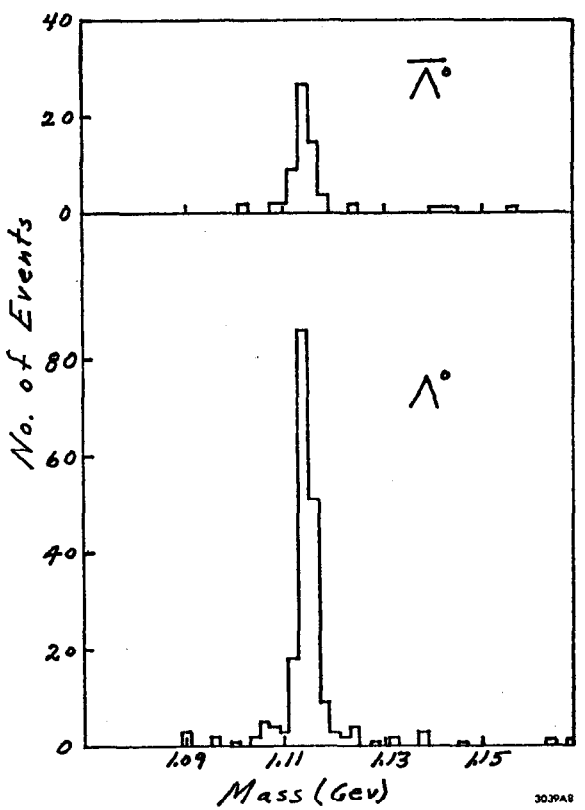

Fig. 9

a four standard derivation effect.

To exploit the other D signature this week an experimental run was started using a trigger which requires a prompt μ in addition to two hadrons. The set up is shown in Fig. 10. There are approximately 16 feet of steel in two sections as a hadron shield. One is immediately downstream from the target with holes to match the beam and the aperture of the two spectrometer magnets. The μ counters subtend about 50% of the solid angle in the center of ma.. There is a limit to what can be gained by this technique. A fraction of π's decay before they are absorbed, this fraction is difficult to estimate but even optimistically is at the least 1/1000. The branching ratio of D's into modes with leptons is not huge. The largest gain in sensitivity one can expect is therefore around an order of magnitude.

Our present run will take date simultaneously with and without a prompt μ signature. Whether it will be sufficient to detect a charmed signal is unclear.

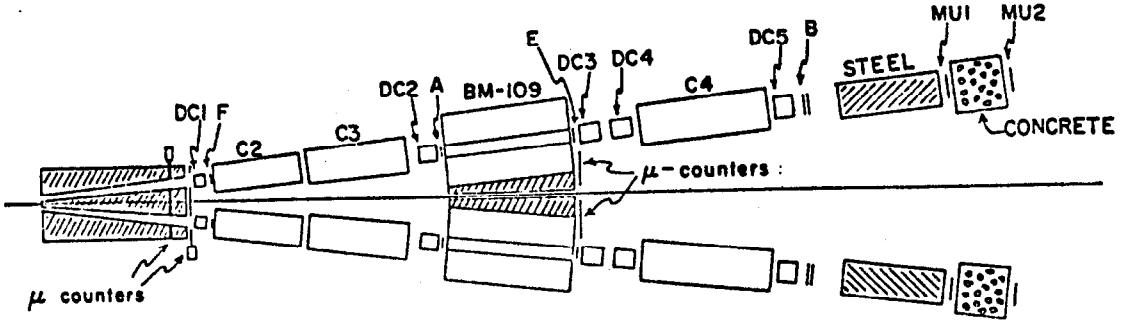

C : Cherenkov
DC: Drift Chamber Module

3039A9

Fig. 10

New Particle Production from DASP at DORIS

P.Schmüser, II. Institut für Experimentalphysik der Universität
Hamburg, Germany

In my talk I want to report new results obtained by the DASP collaboration[1] at the DESY storage ring DORIS. Since a detailed description of the double arm spectrometer DASP has been given in Ref.2, I will only discuss those features of the apparatus which are important for the present measurements.

Three Photon Final State and Evidence for X(2.8)

The nonmagnetic inner detector of DASP has been used to study e^+e^- annihilation into three photons at cms energies around 3.1 and 3.7 GeV. This detector which is shown in Fig. 1 consists of scintillation counters, multiwire proportional chambers, lead converters, proportional tube chambers and lead-scintillator shower counters. It covers more than 70% of 4π. The basic detection unit is a scintillation counter hodoscope, a lead sheet 5 mm thick and a tube chamber with three (in some cases two) layers of signal planes which measure the position of a track to $\pm$ 5 mm ($\pm$ 7.5 mm). The inner detector is subdivided into 6 sections. Each section is made out of four layers of this basic unit, followed by a sandwich shower counter. The direction of charged tracks and photons can be measured to $\pm 2^\circ$. The photon energy resolution is around 30% (FWHM) at 1 GeV. The detection efficiency is 50% for photons of 50 MeV and close to 100% above 100 MeV.

Three-photon final states have been investigated in order to look for radiative decays

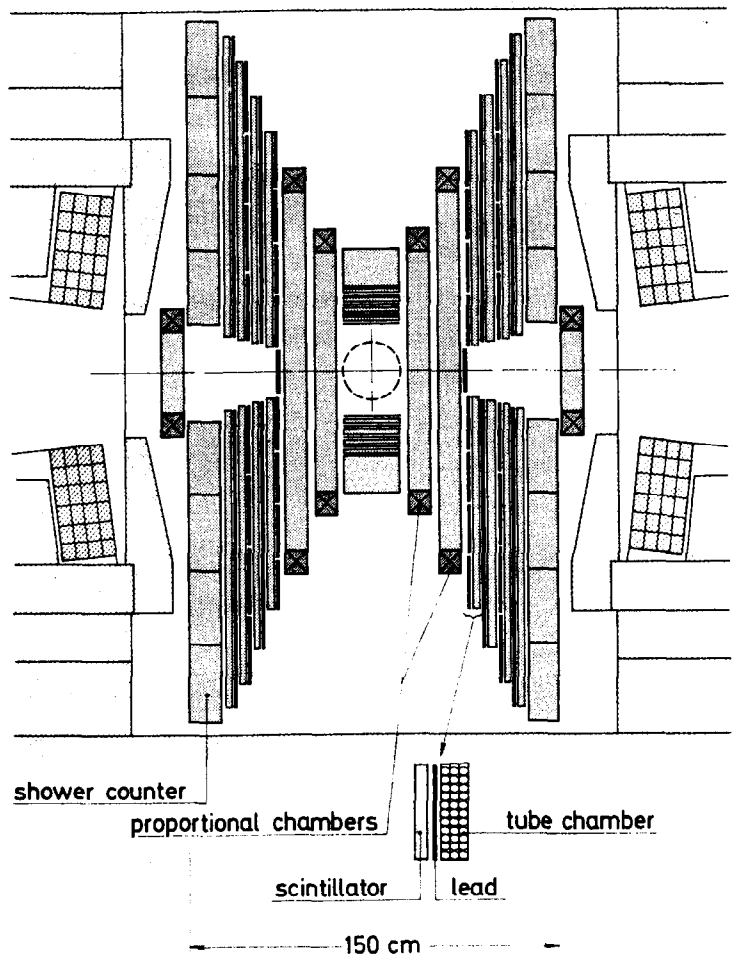

Fig. 1 - The inner detector of DASP viewed along the beam direction.

$$J/\psi \text{ (or } \psi') \rightarrow M \ \gamma$$

where M is a meson having a $\gamma\gamma$ decay mode. The most serious background is produced by the QED reaction $e^+e^- \rightarrow \gamma\gamma\gamma$, a much smaller background by direct decays of the resonances into three photons[3]. These background processes do not lead to bumps in the two photon effective mass spectra.

The apparatus was triggered on showering tracks in two different sections of the inner detector. Events were selected by requiring three observed photons and no additional tracks. At the J/ψ resonance, 149 3γ-candidates were found for an integrated luminosity $L = 421\ nb^{-1}$. At the ψ', 57 candidates were found for $L = 475\ nb^{-1}$. The statistics at the J/ψ has been doubled since the 1975 Lepton Photon Symposium[2].

For genuine three photon events the three momentum vectors have to lie in a plane. Events with missing tracks will in general not be coplanar. The directions of the photons are not well determined by the tube chambers alone since the electromagnetic showers have a large lateral spread. They can be calculated from the well measured conversion points of the photons in the tube chamber system, and the position of the e^+e^- interaction point. This was taken from multihadron data collected during the same experiment. A plane was fitted to the three conversion points and the interaction point. The χ^2 distribution of the one-constraint fit (see Fig. 2) demonstrates that the 3γ sample contains little background from beam-gas interactions and multihadron events. A χ^2 cut of 2.7 was applied. At 3.1 GeV, 39 of the 149 events were rejected, among them about 10-12 genuine 3γ events. The remaining 110 events contain only a very small background.

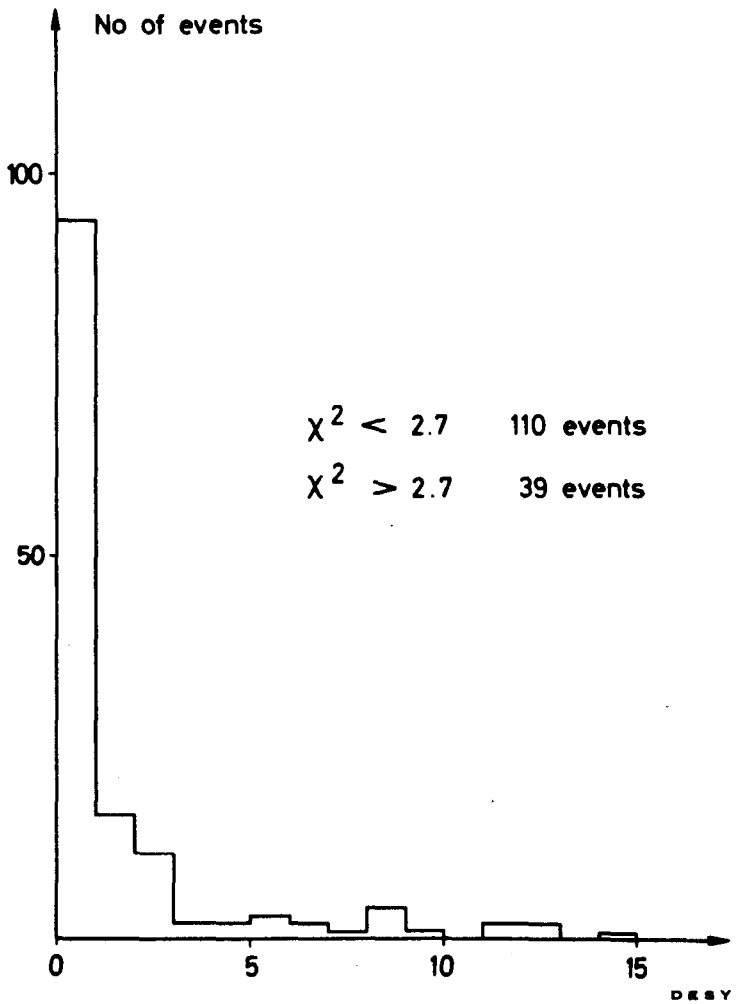

Fig. 2 - $e^+e^- \rightarrow \gamma\gamma\gamma$ at 3.1 GeV: χ^2 distribution for a fit of a plane through the conversion points of the three photons and the interaction point.

Knowing the directions of the photons from the fit and the cms energy the photon energies can be computed. In Fig. 3 the measured photon energies are plotted vs the calculated energies. They agree well within the resolution of the shower counter. This is additional evidence that the 3γ samples contains little contamination from multi-π^0 events with undetected tracks.

For each γγγ event, three two-photon effective masses are calculated; only two are independent. Fig. 4 is a Dalitz plot of the 3.1 GeV data where the high mass solution is plotted horizontally, the low mass solution vertically. Each 3γ event enters only once. A minimum opening angle of 30° between any two photons was required in order to remove possible π^0 contamination.

The Dalitz plot shows a dense population towards high γγ masses. This is largely due to the QED reaction $e^+e^- \to \gamma\gamma\gamma$. The three-photon annihilation can be considered as a radiative correction to the two-photon annihilation. Therefore most QED events will contain two high-energy, nearly back-to-back photons plus a soft third photon. Correspondly the high γγ mass solution will peak towards high energies, with a cut off due to the requirement that the third photon has to be detected in the apparatus ($E_\gamma \gtrsim 50$ MeV). The Dalitz plot shows an accumulation of events along the η mass band. In the low mass projection in Fig. 5 a pronounced η signal is observed. The peak occurs at the correct mass and has a width in agreement with the experimental γγ mass resolution. The ηγ events provide a good check of the analysis procedure. The background can be quantitatively accounted for by QED and events with a high γγ mass in the region of the X(2.8). There might be a few events at the η' mass. From these data we obtain

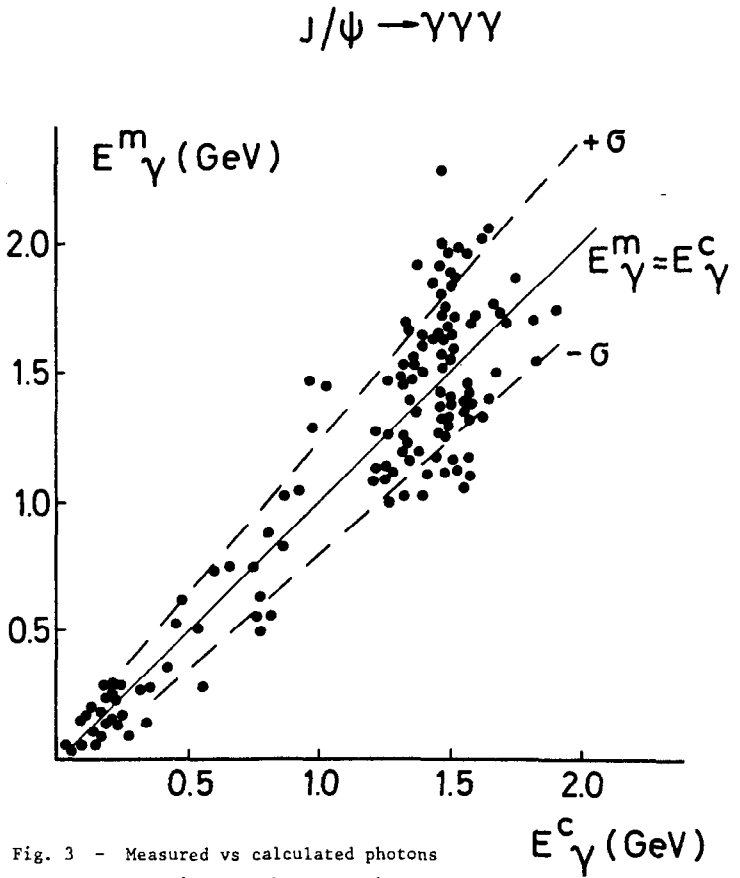

Fig. 3 - Measured vs calculated photons energies for the three-photon events at 3.1 GeV. The dotted lines indicate the resolution of the shower counter (± 1σ).

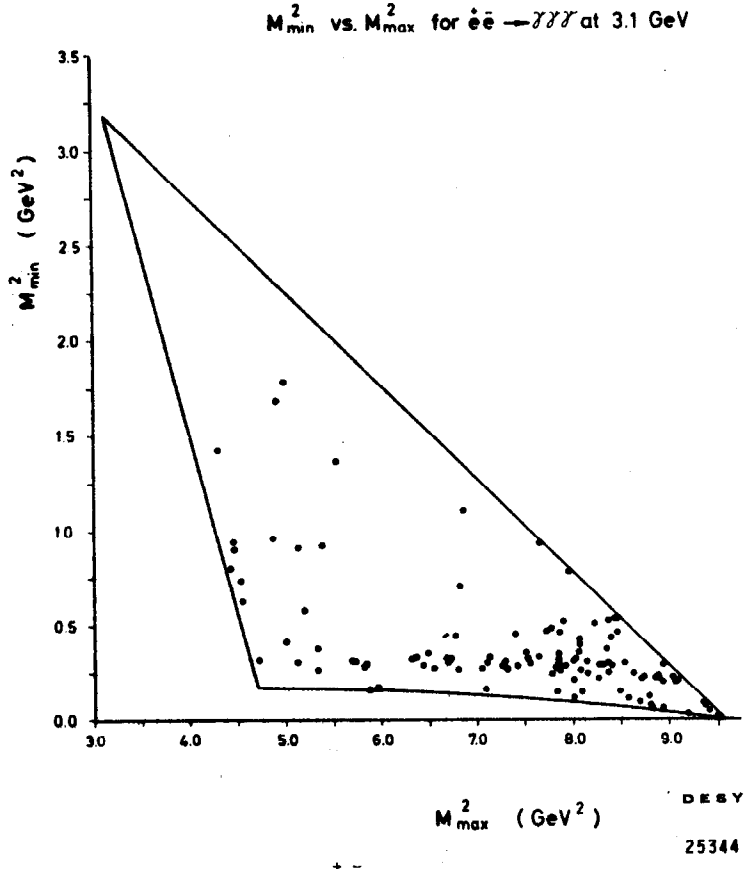

Fig. 4 - Dalitz plot for $e^+e^- \to \gamma\gamma\gamma$ at 3.1 GeV. The low mass boundary results from demanding an opening angle larger than 30^0 between any two photons.

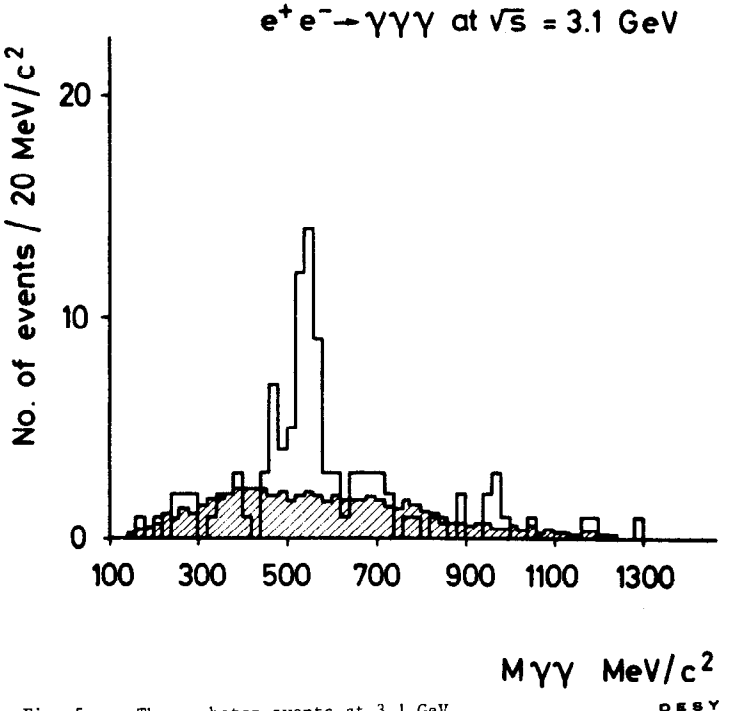

Fig. 5 - Three-photon events at 3.1 GeV plotted as a function of the lowest two-photon mass. Shaded area: QED events and events with high $\gamma\gamma$ mass in the X(2.8) region.

$$BR\ (J/\psi \to \eta\gamma) = (1.0 \pm 0.2) \cdot 10^{-3}$$

$$BR\ (J/\psi \to \eta'\gamma) < 4.4 \cdot 10^{-3} \quad (90\%\ C.L.)$$

The high mass projection is shown in Fig. 6a. Superimposed on a smoothly rising background, a narrow peak is observed in the mass range 2.8 - 2.9 GeV. The width is compatible with the experimental two-photon mass resolution ($\sigma_M \sim 40$ MeV at 2.8 GeV). The solid line is an absolute prediction of the background from the QED process and the kinematic reflection of the $\eta\gamma$ and $\eta'\gamma$ events. This is explained in more detail in Fig. 6b. The QED diagrams for $e^+e^- \to \gamma\gamma\gamma$ were computed and a Monte Carlo method was used to calculate the detection efficiency for these events. For an integrated luminosity of 421 nb^{-1}, 55 events are expected. Their high $\gamma\gamma$ mass distribution is shown in Fig. 6b. As expected, it is rising towards high mass values with a cutoff around 3.05 GeV. The narrow peak between 2.8 and 2.9 GeV, however, cannot be explained by multiplying the rising QED cross section with the decreasing mass acceptance. The kinematic reflection of the $\eta\gamma$ and $\eta'\gamma$ events into the high mass solution was also calculated via Monte Carlo and then normalized to the number of observed events in the η and η' mass region (36 and 3). These channels produce an almost flat spectrum in the high mass solution.

29 events are observed between 2.8 and 2.9 GeV. QED and the kinematic reflection of $\eta\gamma$, $\eta'\gamma$ can account for only 14 events. Fitting the narrow peak with a Gaussian leads to a 3.5 standard deviation signal for the existence of a particle X with a mass $M_X = (2.83 \pm 0.05)$ GeV and a branching ratio $BR(J/\psi \to X\gamma) \cdot BR(X \to \gamma\gamma) = (1.5 \pm 0.4) \cdot 10^{-4}$.

The three-photon data at 3.7 GeV are quite different. The number of events is clearly smaller. No $\eta\gamma$ or $\eta'\gamma$ have been seen. The high $\gamma\gamma$

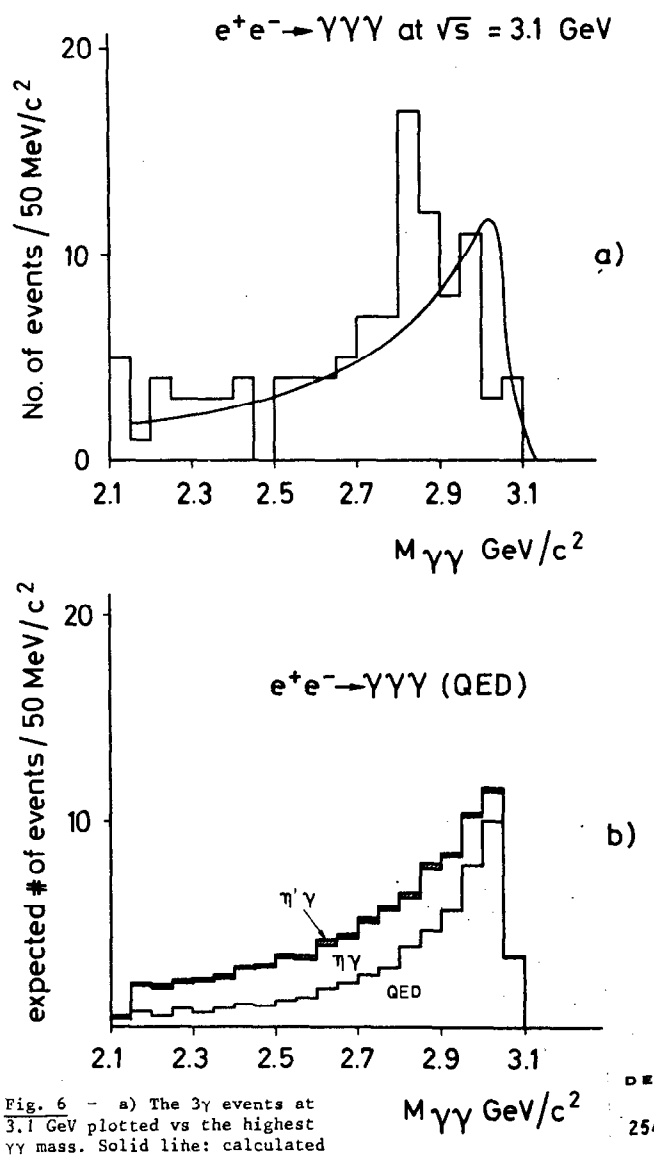

Fig. 6 - a) The 3γ events at 3.1 GeV plotted vs the highest $\gamma\gamma$ mass. Solid line: calculated background from Fig. 6b.
b) Calculated QED, $\eta\gamma$ and $\eta'\gamma$ contributions to the high mass solution.

mass solution is plotted in Fig. 7 together with the QED contribution. All $\gamma\gamma\gamma$ events at the $\psi'(3.7)$ are consistent with QED. Between 2.5 and 3.7 GeV there are 34 events; the QED calculation predicts 30 events. Between 2.7 and 2.9 GeV there are 5 events with a background of 1.3 events. The 4 events above background are compatible with a branching ratio of ψ' into $X\gamma$ of about the same size as that of J/ψ. We quote an upper limit

$$BR(\psi' \to X\gamma) \cdot BR(X \to \gamma\gamma) < 3.7 \cdot 10^{-4}.$$

Table 1 summarizes the branching ratios for radiative decays. Included are also results on $J/\psi \to \pi^0\gamma$ which were obtained by removing the 30° cut on the opening angle, and on $J/\psi \to \eta'\gamma$. The $\eta'\gamma$ final state has been studied by the DESY-Heidelberg group[4] and the DASP group using the $\eta' \to \rho\gamma \to \pi^+\pi^-\gamma$ decay mode.

Table 1

Branching ratios for J/ψ and ψ' radiative decays (preliminary). The upper limits are given for 90% confidence level.

Mode	J/ψ	ψ'
$\eta\,\gamma$	$(1.0\pm0.2)\cdot10^{-3}$	$< 1.3\cdot10^{-3}$
$\eta'\gamma$ $(\eta'\to\gamma\gamma)$	$< 4.4\cdot10^{-3}$	$< 1.4\cdot10^{-2}$
$\eta'\gamma$ $(\eta'\to\rho\gamma)$	$(2.5\pm1.0)\cdot10^{-3}$ $(2.4\pm0.7)\cdot10^{-3}$ (Ref.4)	$< 1.1\cdot10^{-3}$ (Ref.4)
$BR(J/\psi\to X\gamma)\cdot BR(X\to\gamma\gamma)$	$(1.5\pm0.4)\cdot10^{-4}$ $2.8<M_X<2.9$ GeV	$< 3.7\cdot10^{-4}$ $2.7<M_X<2.9$ GeV
$\pi^0\gamma$	$< 1.6\cdot10^{-4}$	

If the X(2.8) is the charmonium 1^1S_0 state (η_c) it is rather surprising that its mass is so far below the 1^3S_1 state $J/\psi(3.1)$. Another puzz-

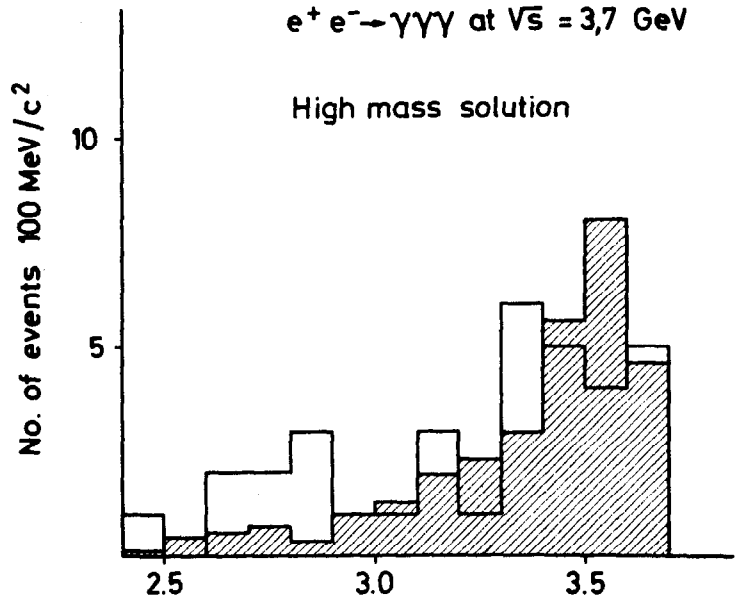

Fig. 7 – The three-photon events at 3.7 GeV, plotted vs the highest $\gamma\gamma$ mass. Shaded area: QED contribution.

ling feature is that until now no hadronic decays of the X have been observed. There are a few events of the type $J/\psi \to p\bar{p}\gamma$ with $M_{p\bar{p}}$ close to 2.9 GeV, but the $M_{p\bar{p}}$ distribution does not show a peak. We quote an upper limit $BR(J/\psi \to X\gamma)\cdot BR(X \to p\bar{p}) < 2\cdot 10^{-4}$.

The branching ratios of J/ψ into $\pi^0\gamma$, $\eta\gamma$, $\eta'\gamma$ cannot be explained in terms of usual quark diagrams

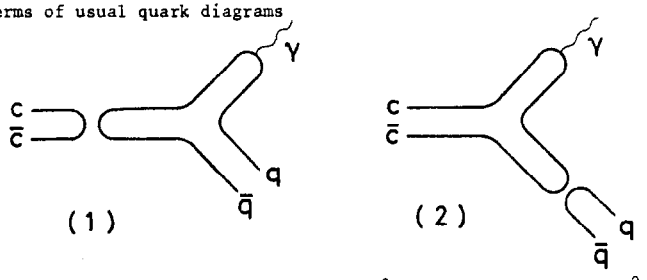

Diagram (1) predicts $BR(\eta\gamma) = 1/3\ BR(\pi^0\gamma)$, $BR(\eta'\gamma) \approx 0.01\ BR(\pi^0\gamma)$ in gross disagreement with the data.

From diagram (2) we get $BR(\pi^0\gamma) = 0$ and $BR(\eta'\gamma) \gg BR(\eta\gamma)$ (roughly a factor of 25-30) since η' is an almost pure SU_3 singulet. Again this is not in agreement with the data. A second problem is that the absolute rates of $J/\psi \to \eta\gamma$, $\eta'\gamma$ are rather high for radiative decays, namely of the same size as for hadronic decays like $J/\psi \to \pi^0\rho^0$. Putting in a factor of $1/\alpha$ to compare to hadronic channels we arrive at branching ratios which are much bigger than those for any specific twobody decay. A small $c\bar{c}$ admixture in the η' and η mesons is probably needed to explain the radiative branching ratios.

Measurement of electron-hadron final states above 4 GeV cms

The DASP detector has been used to search for the production of electron-hadron final states in e^+e^- collisions above 4 GeV cms. Provided the electrons are "direct" and not from trivial sources like Dalitz or π, K decays etc, such lepton-hadron final states might arise from the production and decay of a pair of heavy leptons $L\bar{L}$ with one of the particles decaying into leptons only, the other into hadrons plus a neutrino. For such events we expect low charged particle and photon multiplicity and only a small fraction of strange particles. An alternate source of electron hadron final states is the production of hadrons with a new quantum number like charm which inhibits strong and electromagnetic decays. Such hadrons would have to be produced in pairs and the observed electron would come from the leptonic or semileptonic decay of one of the new hadrons. Assuming the new quantum number to be charm, we expect fairly high charged particle and photon multiplicity and a sizeable fraction of strange particles.

For the present experiment, excellent electron identification was achieved by installing threshold Cerenkov counters on both sides of the beam tube (see Fig. 8). These counters, which covered the geometric acceptance of the magnets, were filled with Freon 114 at atmospheric pressure (n = 1.0014). The detection efficiency for electrons was better than 98%. Since they were close to the interaction point, the background from $K^\pm \to e\pi\nu$ and $K^0 \to e\pi\nu$ decays was small. Pulse-height measurements in two scintillation counters S_0 and S_M before and after the Cerenkov counter were used to distinguish between single and double tracks of minimum ionizing particles; by this method a large fraction of photon pair conversions and π^0 and η Dalitz decays was rejected.

The detector was triggered on a single charged particle traversing a spectrometer arm, firing the S_0 and S_M counters, and one of the

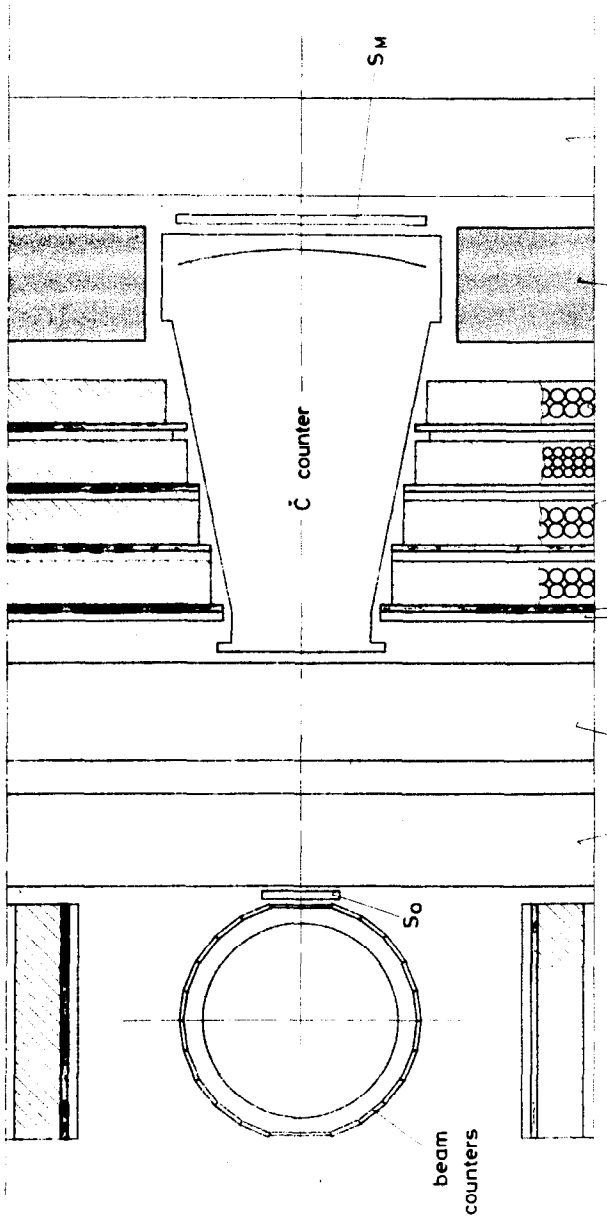

Fig. 8 – Part of the inner detector in front of one of the magnet apertures. Shown are the electron Cerenkov counter and the two scintillation counters S_o and S_M which are used to distinguish between single electrons and e^+e^- pairs via pulseheight measurements.

time of flight and shower counters located at the rear. For most of the experiment the magnet was powered at 1/3 full excitation corresponding to a cut off momentum of 200 MeV/c. Data were collected at cms energies between 4.0 and 4.2 GeV for a total integrated luminosity of 670 nb^{-1}. In addition data were taken at 3.60 – 3.68 GeV (266 nb^{-1}) and on the $\psi'(3.7)$ resonance (54 nb^{-1}).

Events with electrons were selected by requiring a signal in the appropriate Cerenkov counter. 4500 events were found. Among these were about 1500 Bhabha events. The cross section for $e^+e^- \to e^+e^-$, determined from this data sample, agreed well with QED. The Bhabha events were used to study the performance of the Cerenkov counters. 1900 events were found with a single electron and no additional track in the detector. They are from the reaction $e^+e^- \to e^+e^-\gamma$ where one of the electrons and the photon remain inside the beam pipe and the other electron is scattered at large angles. The momentum spectrum of these single electrons is shown in Fig. 9. Since these events are easily recognized they have been used to study the response of the detector to low momentum electrons.

Electron-hadron final states were selected by requiring in addition to the electron at least one non-showering charged particle track in the inner detector. A nonshowering track was defined by the following criteria: the particle traverses at least 5 of the 9 (or 12) tube chamber layers and the average number of tubes fired per layer is less than 1.5. A minimum ionizing particle fires on the average between 1 and 1.2 tubes per layer. The above criterion, applied to a sample of $\rho^0\pi^0$ ($\pi^+\pi^-\gamma\gamma$) events at the J/ψ, identified 85% of the pions correctly as "non-showering" and more than 90% of the photons as "showering" (E_γ > 200 MeV). The recognition of a showering particle

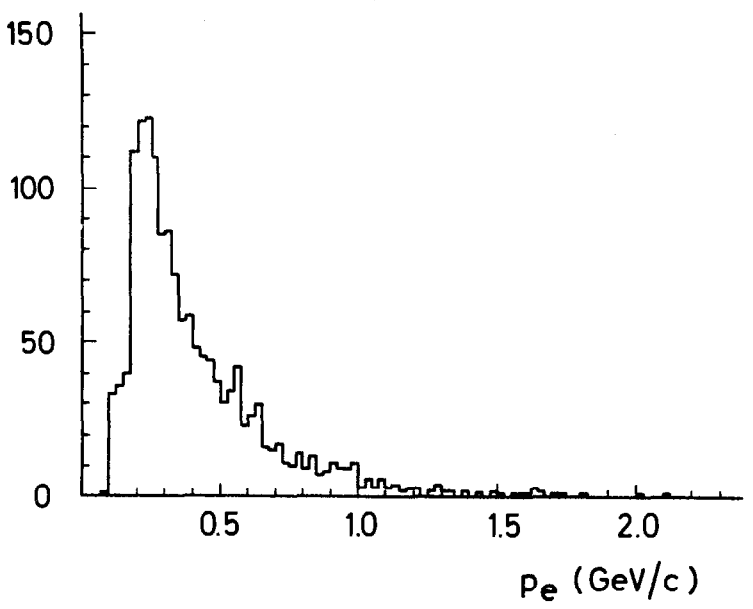

Fig. 9 – Momentum spectrum of "single electron" events from the reaction $e^+e^- \to e^\pm(e^\mp\gamma)$. The cutoff at 200 MeV/c is due to the magnetic field.

improves with energy. 97% of the Bhabha electrons are correctly identified.

84 events remained after requiring at least one nonshowering charged track in the inner detector. This requirement eliminated most of the events of electromagnetic origin like $e^+e^- \to e^+e^-$, $e^+e^-\gamma$, $e^+e^-\gamma\gamma$.

A number of further cuts can be applied to remove background events. In the following I want to discuss the possible background sources giving rise to electron-hadron final states and the experimental handles one has to remove the background.

1) Pair conversion of photons in the material in front of the Cerenkov counter and Dalitz decays of π^o (and η).
Since there is no magnetic field in the DASP inner detector, in most cases the electron and the positron from a pair conversion will both traverse the S_o and S_M counters and produce a large pulseheight in these counters. The same is true for more than 80% of the π^o Dalitz decays. Most of these events can therefore be excluded by a pulseheight cut in the S_o and S_M counters of less than twice the pulseheight of minimum ionizing particle.

The correlated pulseheight of S_o vs S_M for the 87 events is shown in Fig. 10. A distinct clustering is seen at a pulseheight of about 110, corresponding to single tracks of minimum ionizing particles. No such clustering is observed at twice this pulseheight. Since for more than 80% of the pair conversions and Dalitz decays both e^+ and e^- penetrate the S_o and S_M counters we can conclude that most of the e-hadron events are not due to this background. A careful analysis revealed that in the final event sample the number of Dalitz type

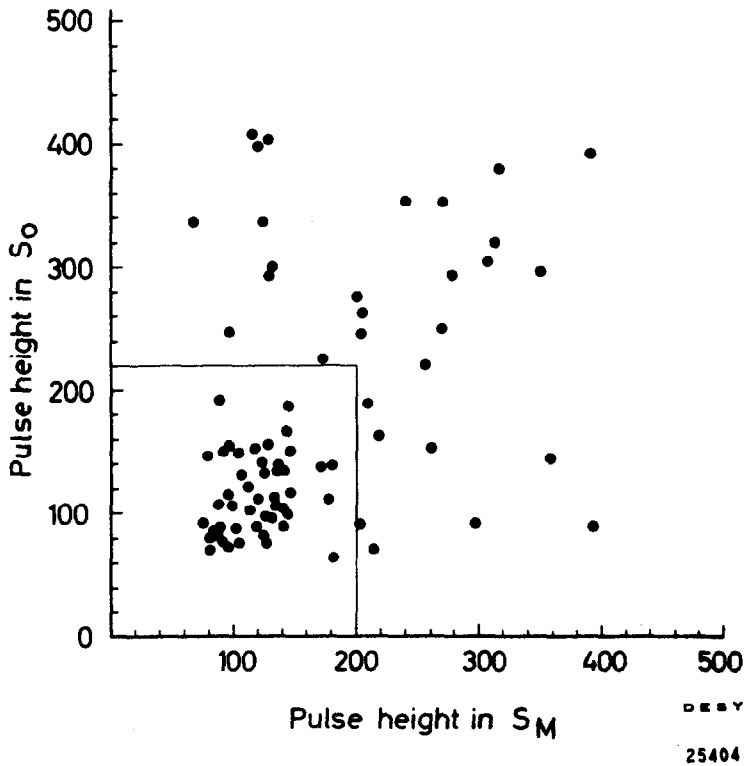

Fig. 10 - Pulseheight distribution in the S_o and S_M scintillation counters for events having an electron and at least one non-showering track. Cuts are indicated by solid lines.

events is less than 2. Pulseheight cuts as indicated by the solid lines have been applied. 47 events are left. The control sample of single electron events was reduced by 20% to this cut. Beam-gas interactions were removed rather effectively by the pulseheight cut; only 30% of them survived.

2) Misidentification of hadrons as electrons in the Cerenkov counter.

A pion has to have a momentum of more than 450 - 500 MeV/c to produce a δ ray electron with sufficient energy to be seen in the Cerenkov counter. The probability that a $\pi^{\pm}$ of momentum above 500 MeV/c is detected in the Cerenkov counter is of the order of $5 \cdot 10^{-3}$. By taking the inclusive $\pi^{\pm}$ yield measured in the same experiment we expect 2 - 3 events where a $\pi^{\pm}$ fakes an electron. However, these pions (with momenta $\gtrsim$ 500 MeV/c) will have a small pulseheight in the shower counter of the outer detector. Figure 11 shows a twodimensional plot of shower counter pulseheight vs momentum for the 47 e-hadron events. There are 4 events with momenta above 500 MeV/c, having the pulseheight of a minimum ionizing particle. These are probably due to pions which have produced a knock-on electron. Most of them were removed by the shower pulseheight cut shown as a dotted line.

In the following analysis only particles with momenta above 200 MeV/c were used.

3) Inelastic electron scattering from the gas in the storage ring.

The distribution of the vertex position along the beam axis (Fig.12) shows a very distinct peak near the interaction region. Beam gas interactions are uniformy distributed over the whole range. Applying

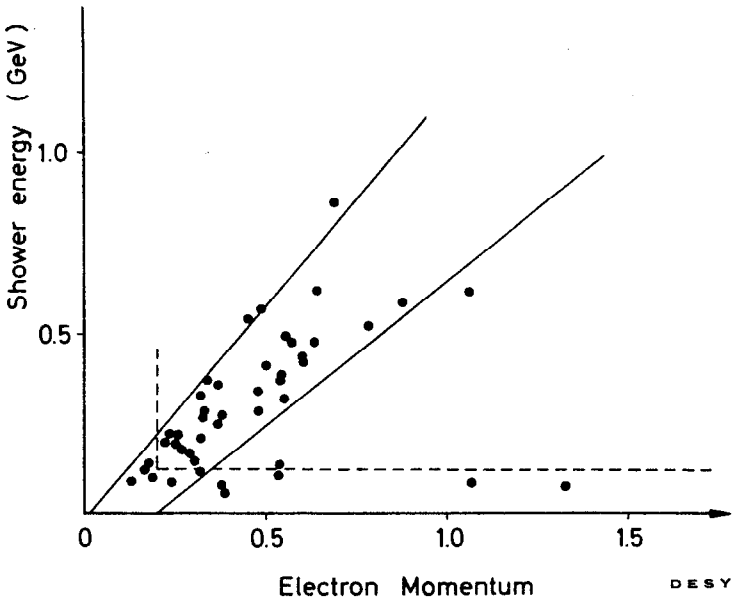

Fig. 11 - Measured shower energy plotted vs electron momentum. Solid lines indicate the shower counter resolution. Dotted lines show the cuts which were applied.

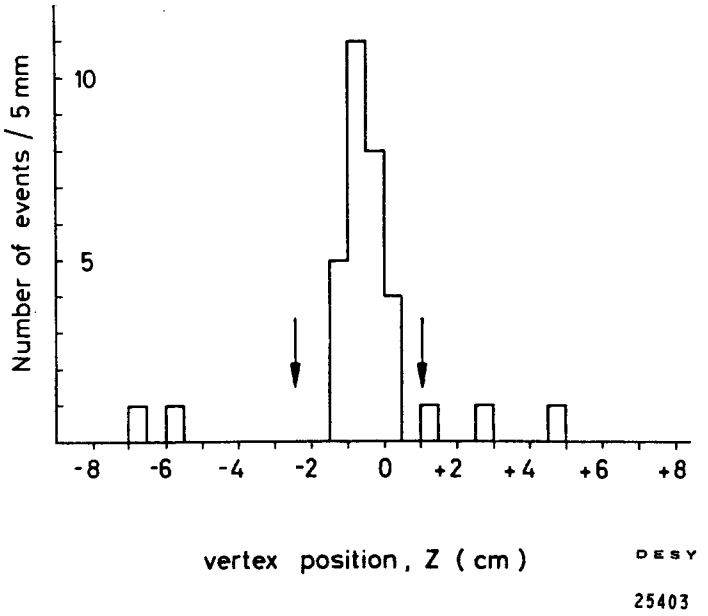

Fig. 12 - Distribution of the event vertex along the beam direction. Arrows indicate the accepted region.

the vertex cut indicated by the arrows, there remain 28 events with an estimated beam-gas background of 0.9 events.

4) Compton scattering in the material in front of the Cerenkov counter

Among the remaining events, 17 have positrons and 11 have electrons, so Compton backscattering cannot play an important role.

5) Kaon decay into electrons

A $K^{\pm} \to e^{\pm} \pi \nu$ decay can contribute only if the kaon decays before reaching the middle of the Cerenkov counter. The flight path is less than 70 cm. From the measured $K^{\pm}$ yield we expect less than 1.2 events of this type not taking into account the fact that the track of the decay electron will often extrapolate to a vertex outside the nominal interaction region. For a $K^{o} \to e\pi\nu$ to contribute it must decay before the S_o counter in order to satisfy the trigger requirement (flight path $\lesssim$ 15 cm). Less than 0.4 events are expected.

6) $e^+e^- \to e^+e^-$ + hadrons from two-photon scattering

This contribution was calculated by T.F.Walsh[5] for the DASP geometry. Less than 1 event is expected. Furthermore, the angular distribution from the $\gamma\gamma$ process is sharply peak forward, whereas the angular distribution of the 28 events is rather flat with no forward peaking (see Fig. 13). The QED type single electron events, on the other hand, show a pronounced forward peaking.

7) Leptonic decays of vector mesons

Cascade decays like $e^+e^- \to J/\psi$ + hadrons $\to e^+e^-$ + hadrons are easily

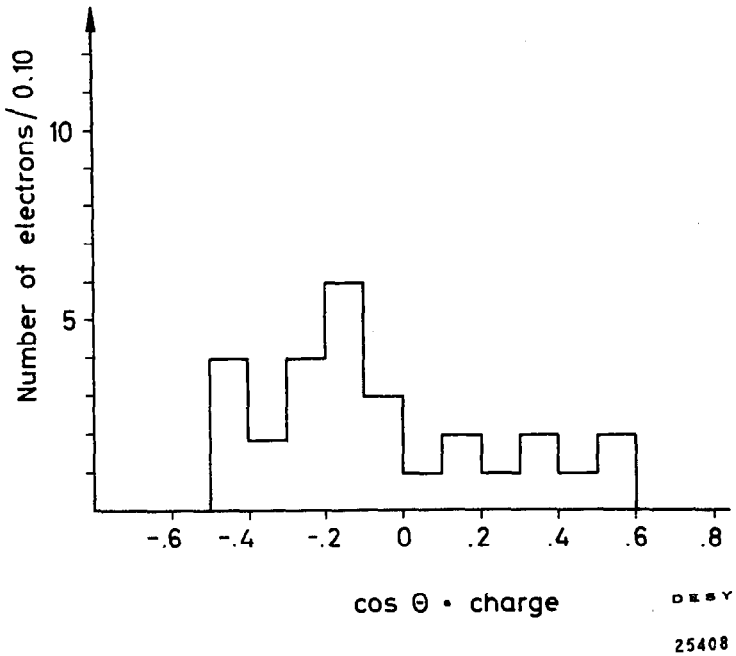

Fig. 13 – The production angular distribution. The abscissa defines the cosine of the production angle with respect to the lepton of the same sign ($\cos\Theta \cdot$ charge > 0 means forward hemisphere)

recognized since they contain two energetic electrons. No such events were found; the observed electrons all have momenta below 900 MeV/c. The vector mesons ρ^o, ω and ϕ have leptonic branching ratios which are too small by several orders of magnitude to explain the observed number of events. For instance, if we assume that all inclusive $\pi^{\pm}$ are from ρ^o decay we compute less than 0.05 events due to $\rho^o \to e^+e^-$.

The discussion of background contributions shows that most of the 28 events are associated with "direct electrons". An independent and probably more convincing proof is obtained by taking data at lower energies and demonstrating the existence of a threshold energy. Data were collected at cms energies of 3.60, 3.62 and 3.68 GeV (266 nb^{-1}) and around the $\psi'(3.7)$ resonance (54 nb^{-1}). In the 3.6 - 3.68 GeV data three events were found, two of which have only one track in addition to the electron. If the yield observed at 4 - 4.2 GeV would be entirely due to QED, we would expect 13 events at 3.6 - 3.68 GeV, most of them with more than two tracks. The contamination through multihadron events was checked by the data at the ψ'. Here 1.1 times as many hadronic events were recorded as in the data above 4 GeV. Applying the same analysis as above we obtained 9 events. Four of these were identified as cascade decays through the J/ψ (3.1) resonance. The remaining 5 events are consistent with the background estimates given above.

After all cuts 28 events remain having an electron and at least one non-showering track. Most of the events have high multiplicity (Fig.14). The charged tracks are in general non-showering; we conclude that they are due to hadrons. Conventional background sources, including the $\gamma\gamma$

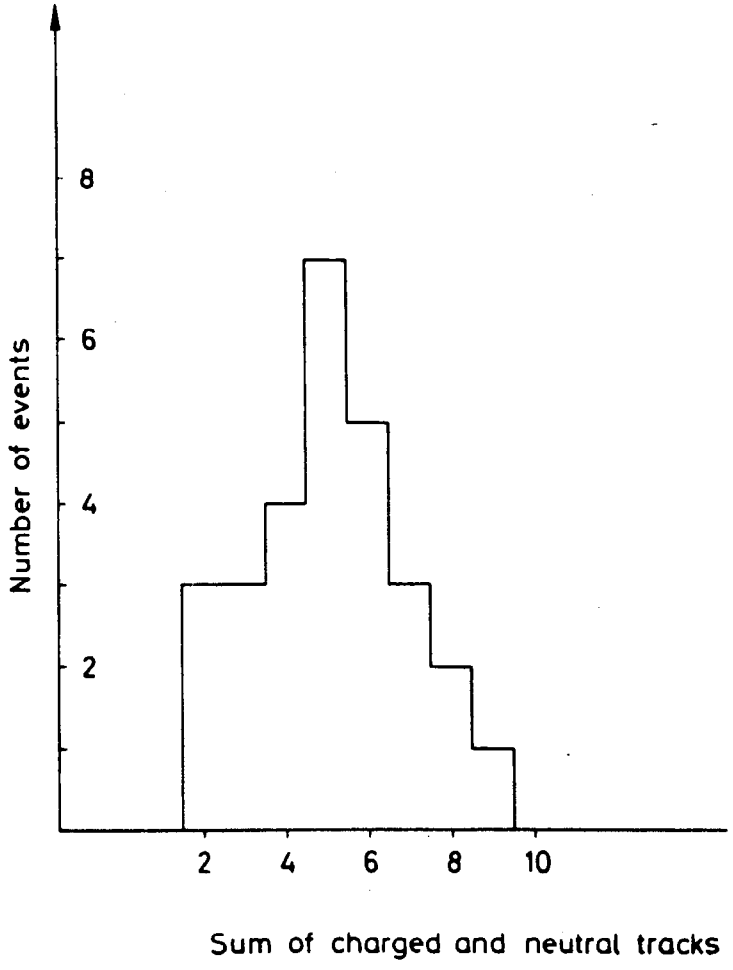

Fig. 14 - Observed number of tracks per event, including the electron.

process, could produce $\lesssim$ 7 events. Therefore we conclude that we have observed the production of a new particle which can only decay via the weak interaction. The observed threshold behaviour restricts the mass of the particle to the range 1.8 - 2.0 GeV.

Most of the events cannot be explained in terms of sequential heavy lepton production. The multiplicities for $e^+e^- \to L\bar{L} \to e$ + hadrons + neutrinos are expected to be low; about 80% of the events should have only two or three tracks, including the electron. Experimentally, there are only 6 events with 2 or 3 tracks, some of which might be background. Furthermore, the momentum distribution of the electrons does not agree with the expectation for a heavy lepton decay. Fig.15 shows that most of the electrons have low momenta. The dotted curve is the calculated momentum spectrum for the decay $L \to e\,\bar{\nu}_e\nu_L$, assuming M_L = 1.9 GeV, M_{ν_L} = 0 and (V-A) coupling. The curve is inconsistent with the data. If it is normalized to fit the data at low momenta it predicts 28 events above 700 MeV/c but none are seen. A neutrino mass M_{ν_L} as high as 1 GeV would be required to get better agreement, but this cannot be reconciled with the observed high multiplicities.

The six low multiplicity events have slightly higher momenta than the other events. They can be accounted for by background and the tail from the high multiplicity distribution.

The production of charmed mesons like $e^+e^- \to D^oD^{o*}$, $D^{o*}D^{o*}$ as seen at SPEAR[6] can well account for the bulk of the data. The low electron momenta suggest that the electrons come from semileptonic and not from purely leptonic decays of charmed mesons. Then fairly high mul-

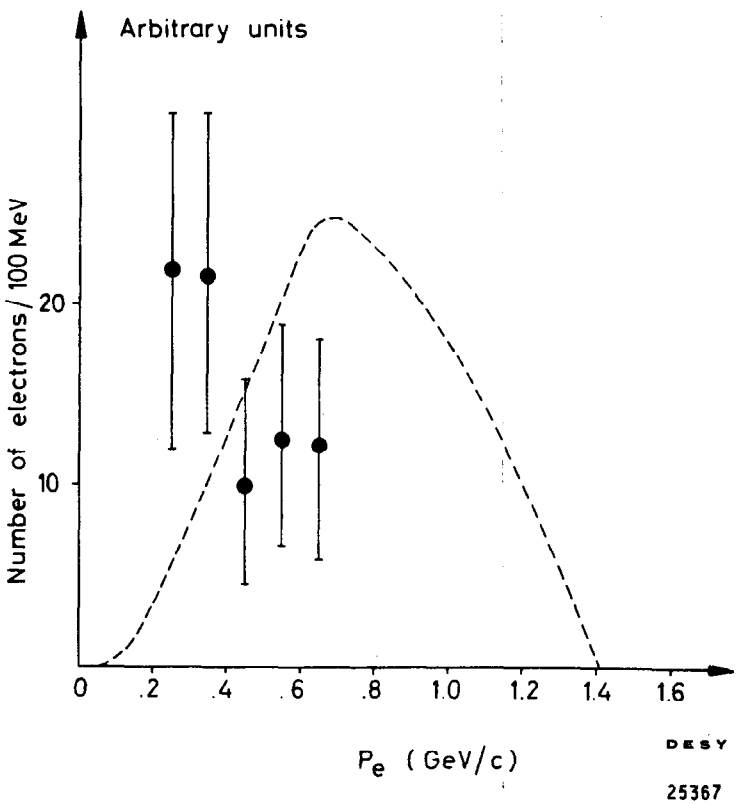

Fig. 15 - Acceptance corrected momentum spectrum for events with more than 3 tracks. The dotted curve was calculated for a heavy lepton of mass 1.9 GeV, decaying into electron plus two massless neutrinos. It has been normalized to fit the observed yield below 700 MeV/c.

tiplicities are expected. The observed momentum spectrum is in qualitative agreement with calculations by Ali and Yang[7], based on $D \to Ke\nu$ and $K\pi e\nu$ decays (Fig. 16).

Assuming an isotropic angular distribution we calculate a lower limit for inclusive electron production

$$\sigma(e^+e^- \to e + \text{hadrons}) \geq 1 \text{ nb}.$$

The DASP detector has also been used to search for correlations between electrons and $\pi^\pm$ or $K^\pm$ mesons. Pions and kaons were identified in the magnetic detector arms. Electrons were defined as showering charged particles in the inner detector. Due to a rather tight cut ($\geq$ 1.6 hits per tube chamber layer required) only very few hadrons were mislabelled as "electrons". The misidentification probability was determined by studying inclusive pion or kaon production at cms energies below 3.8 GeV. 600 $\pi^\pm$ mesons were observed in the magnetic detector, but only 19 ($\triangleq$ 3%) were accompanied by a track labelled as "electron". Among 73 kaons, only 1 kaon-"electron" candidate was found. In the 4.0 - 4.2 GeV range the percentage of pion-"electron" candidates remained about the same, but a clear enhancement was observed in the kaon-"electron" yield (11 K·e out of 106 $K^\pm$). This is shown in Fig. 17. Such a K-e correlation is predicted by the charm model, but at present the statistics is too poor to draw quantitative conclusions.

I want to thank my colleagues from the DASP collaboration for their help in preparing this talk.

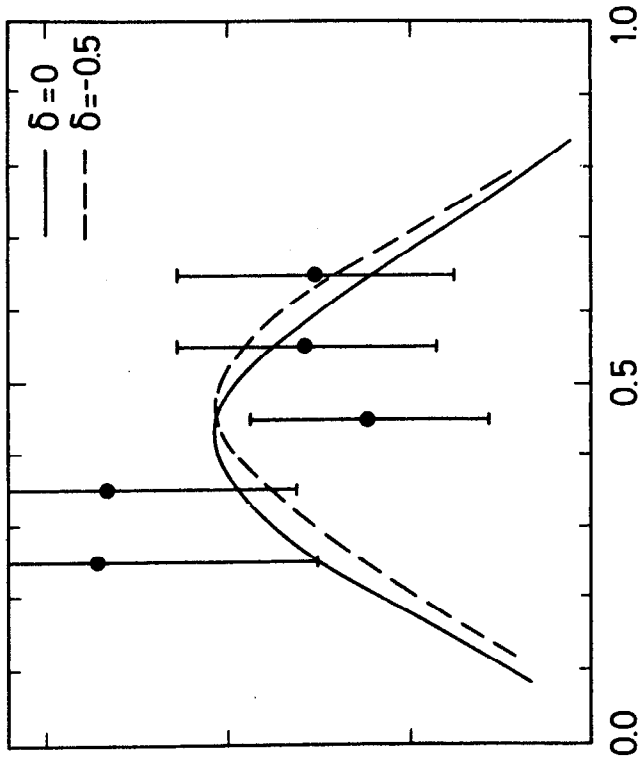

Fig. 16 - The energy spectrum of electrons from D meson decay, summed over $D \to Ke\nu$ and $D \to K\pi e\nu$. δ is a parameter used to describe the form factors for the couplings between the D meson and the K, K^* mesons (see Ref. 7).

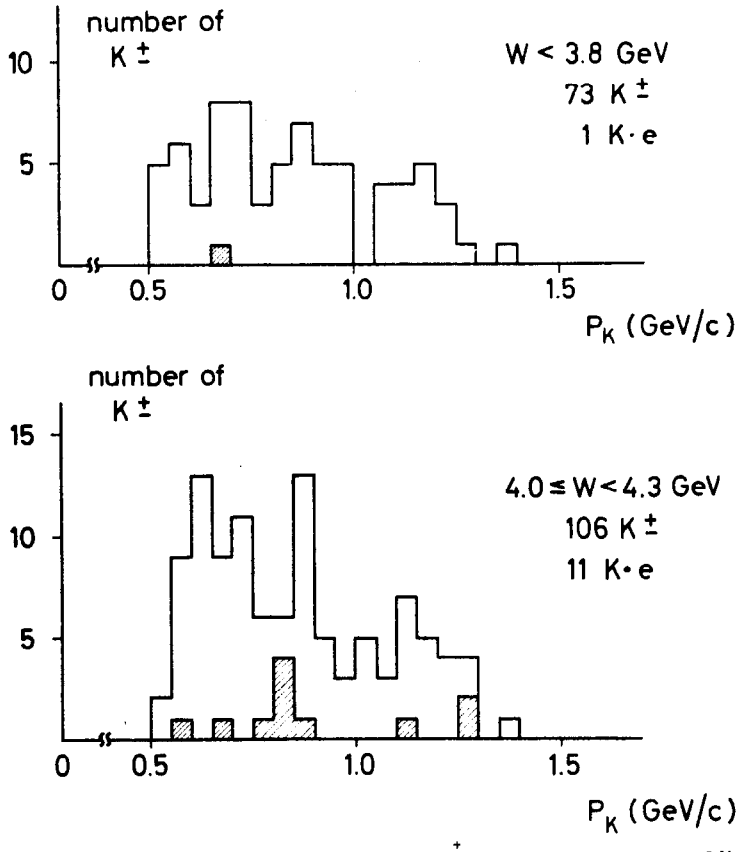

Fig. 17 – Momentum distribution of $K^{\pm}$ mesons observed in the magnetic detector arms. Shaded area: kaons associated with a track in the inner detector labelled as "electron". (Preliminary).

DESY

25409

References:

1) DASP-Collaboration
W.Braunschweig, H.-U.Martyn, H.G.Sander, D.Schmitz, W.Sturm, and W.Wallraff
I.Physikalisches Institut der RWTH Aachen

D.Cords, R.Felst, R.Fries, E.Gadermann, B.Gittelman, H.Hultschig, P.Joos, W.Koch, U.Kötz, H.Krehbiel, D.Kreinick, W.A.McNeely, K.C.Moffeit, A.Petersen, O.Römer, R.Rüsch, B.H.Wiik, and G.Wolf
Deutsches Elektronen-Synchrotron DESY, Hamburg,

G.Grindhammer, J.Ludwig, K.H.Mess, G.Poelz, J.Ringel, K.Sauerberg, and P.Schmüser
II. Institut für Experimentalphysik der Universität Hamburg,

W.deBoer, G.Buschhorn, B.Gunderson, R.Kotthaus, H.Lierl, H.Oberlack, and M.Schliwa
Max-Planck-Institut für Physik und Astrophysik, München,

S.Orito, T.Suda, Y.Totsuka, and S.Yamada
University of Tokyo

2) B.H.Wiik
Invited talk at the 1975 International Symposium on Lepton and Photon Interactions at High Energies; Stanford University, Stanford, California, Aug. 21-27, 1975

3) E.Pelaquier, F.M.Renard, Nuovo Cim. 32A, 421 (1976)

4) DESY-Heidelberg Collaboration, W.Bartel et al., DESY Report 76/40 (1976)

5) T.F.Walsh, private communication

6) G.Goldhaber et al., Phys.Rev.Lett. 37, 255 (1976)
G.Goldhaber, Invited Talk, this Conference

7) A.Ali, T.C.Yang, DESY Report 76/39 (1976)

RECENT PLUTO RESULTS FROM DORIS

H. Meyer

Gesamthochschule Wuppertal

The data reported have been obtained using the magnetic detector, PLUTO*, at the e^+e^- storage ring, DORIS. The detector will be described briefly and results will be given on final states with muons and on the observation of a correlated signal of electrons and K^o_s.

---

* Members of the PLUTO-collaboration:

J. Burmester, L. Criegee, H. C. Dehne, K. Derikum,

R. Devenish, J. D. Fox, G. Franke, G. Flügge, Ch. Gerke,

G. Horlitz, Th. Kahl, G. Knies, M. Rößler, S. Wolff, R. Schmitz,

T. N. Ranga Swamy, U. Timm, H. Wahl, P. Waloschek,

G. G. Winter and W. Zimmermann

Deutsches Elektronen Synchrotron
DESY, Hamburg

V. Blobel, H. Jensing, B. Koppitz, E. Lohrmann

II. Institut für Experimentalphysik der Universität
Hamburg

A. Bäcker, J. Bürger, C. Grupen, M. Rost

Gesamthochschule Siegen

H. Meyer, K. Wacker

Gesamthochschule Wuppertal

I. Detector

Fig. 1 shows a cross section of the detector. It has 14 cylindrical proportional wire chambers. The superconducting coil produces a 2 T magnetic field parallel to the beam axis. The usable magnetic volume is 1.4 m diameter x 1.05 m length. The detector contains two cylindrical lead converters, whose radii and thicknesses are 37.5 cm, 0.4 R.L. and 59.4 cm, 1.7 R.L. respectively. Wire chambers behind these converters allow the identification of electrons and photons. The detector is triggered by a logic combination of signals from the proportional wire chambers. This is done in two steps of hardware logic in which track elements are recognized both before the lead converters and behind them. Events are accepted if they satisfy one of the following conditions: (i) at least two tracks before the lead, with their azimuth angles not belonging to two adjacent 45° sectors, (ii) at least three track elements after one of the lead converters, (iii) two track elements after the second lead converter, if they are coplanar within $\pm$ 13.5^o. The momentum cut-off for tracks recognized by the trigger is 240 MeV/c. The solid angle for track recognition and for the trigger is 86% of 4π. The luminosity is monitored by small angle (130 mrad) e^+e^- scattering. More details on the detector can be found in Ref. 1

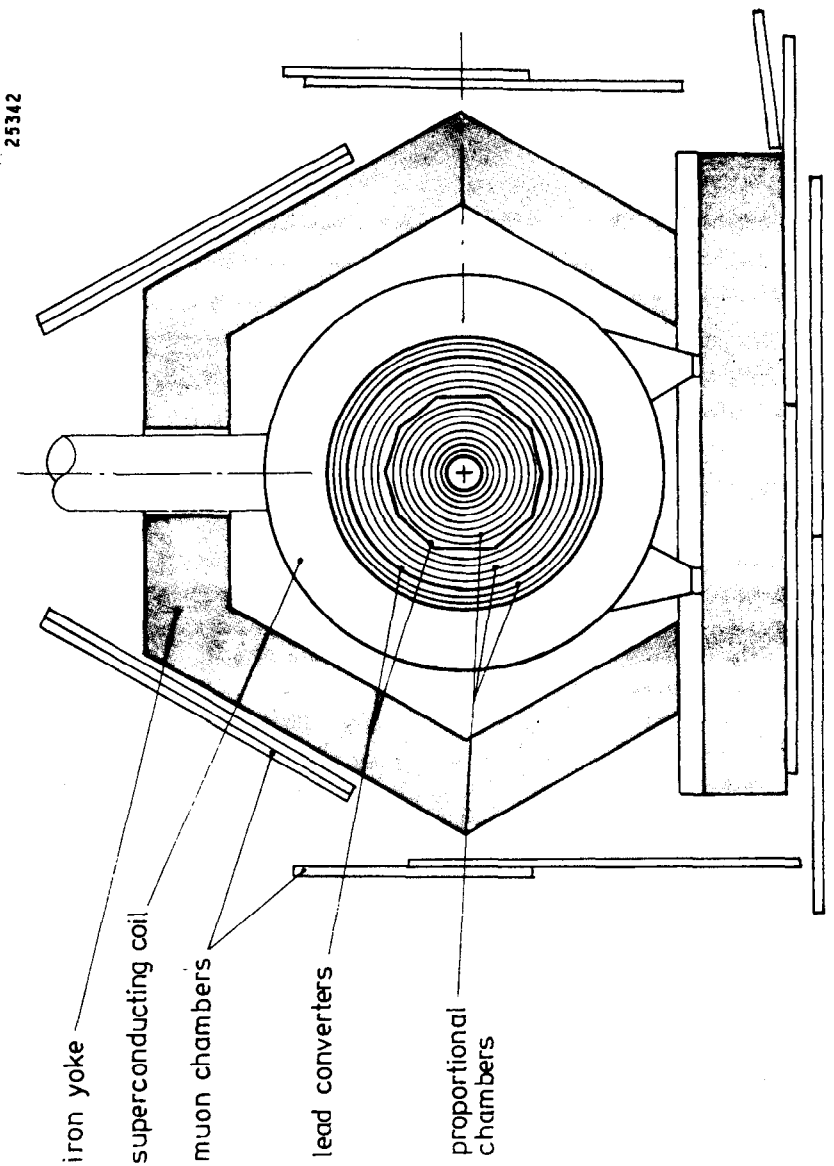

Fig. 1 Detector PLUTO viewed along the beam.

Muons were identified as particle tracks penetrating the flux return iron. Proportional tube chambers are used to detect the muons. The iron thickness of ≥ 65 cm requires a minimum muon momentum of 1 GeV/c. Measurements at the 3.1 resonance show that hadrons in the momentum range 1 - 1.5 GeV are misidentified as muons with a probability of $3.5 \pm 0.5\%$. The geometrical acceptance of the muon chamber is about 50% of 4π.

Electrons were identified by counting wire signals in the two proportional chambers following the thick (1.7 R.L.) lead converter of the detector. To be considered an electron candidate a track must (i) come from the interaction point and hit the converter ($|\cos\theta| \leq .55$) and (ii) have a momentum greater than 300 MeV/c. A candidate is counted as an electron, if it produces more than 10 wire signals inside a certain fiducial volume centered around the interaction of the track with the chambers, otherwise it is considered a hadron. If a second track produces signals inside the fiducial volume, the electron candidate is rejected. The efficiency for electrons to produce more than 10 wire signals was measured with the help of electrons from converted photons. It depends slightly on electron momentum, and averages 50% for electron momenta between 300 MeV/c and 1 GeV/c. The probability that a hadron simulates the signature of an electron was measured using multihadron decays of the 3.1 resonance and found to be about 3.5%.

Fig. 2 shows a typical multihadron event, viewed along the beam direction. Fig. 3 is an example of a radiative muon pair event, with the photon converted in the detector and Fig. 4 shows a typical large angle Bhaba event.

ıe combined efficiency to trigger and reconstruct events in PLUTO has een checked by a Monte Carlo program using as input a phase space model ith only pions. The result for the efficiency is $\sim 75\%$, almost independent of energy. Total crossections on the 3.1 and 3.7 resonances have been evaluated as a further overall check of our understanding of the detector. The excitation curves are shown in Figs. 5 and 6. This data has been integrated to obtain the resonance crossection allowing for radiative corrections[2]. The results are

$$= \begin{matrix} 9700 \pm 1200 \text{ nbMeV at } 3.1 \\ 3060 \pm 340 \text{ nbMeV at } 3.7 \end{matrix}$$

in reasonable agreement with published values[3].

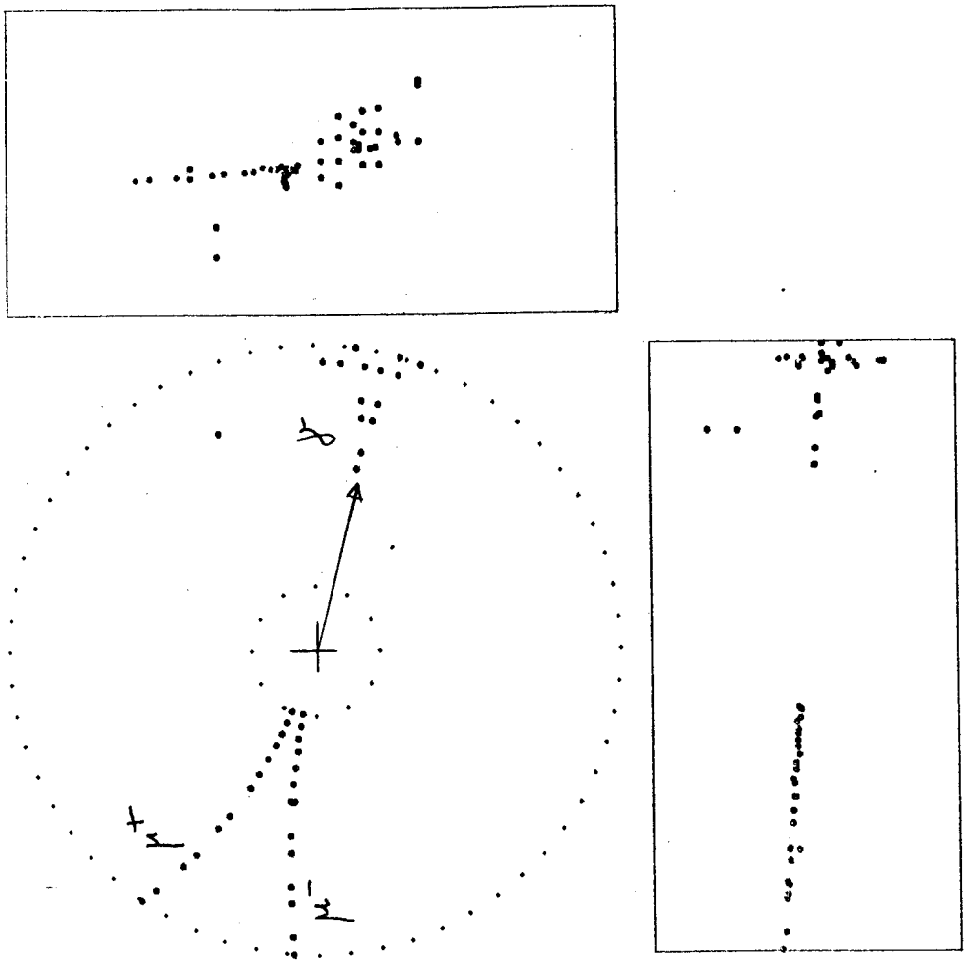

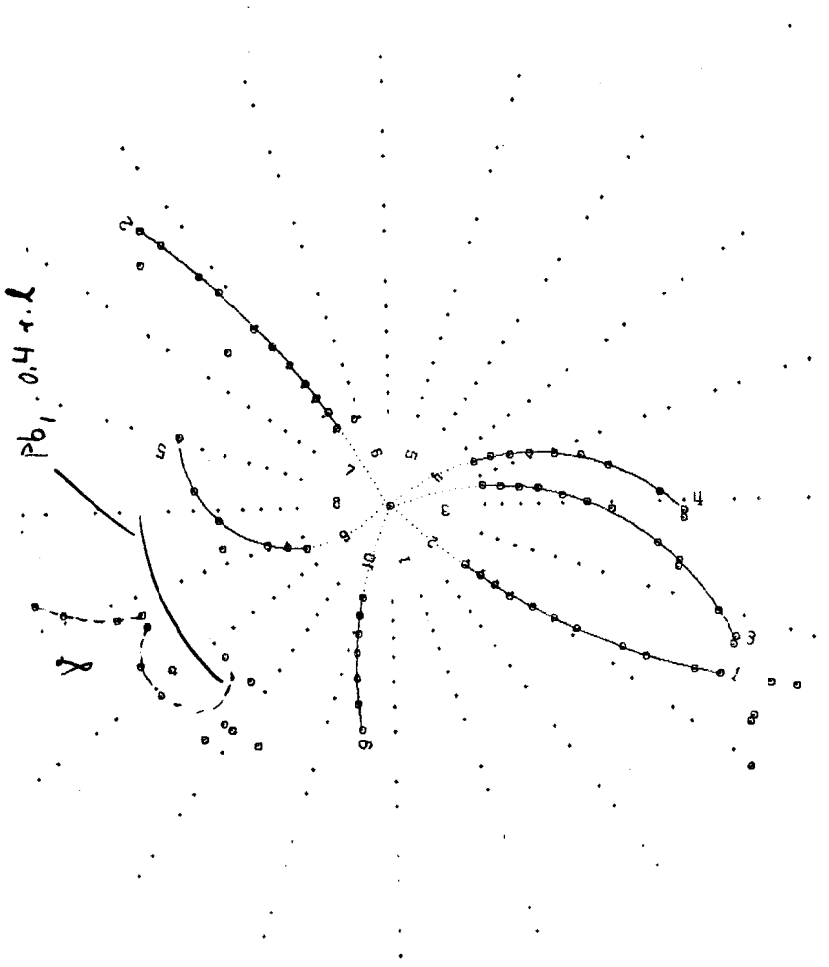

Fig. 3 Radiative muon pair production event.

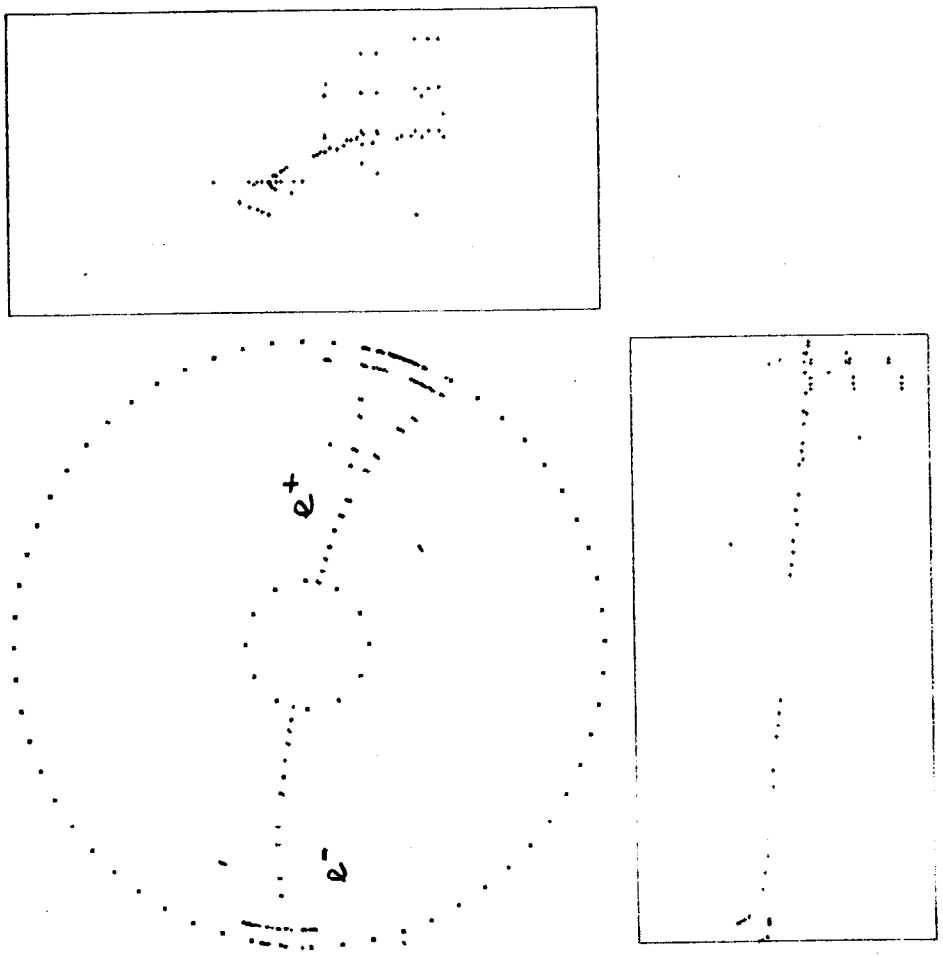

Fig. 4 Example of Bhabha scattering.

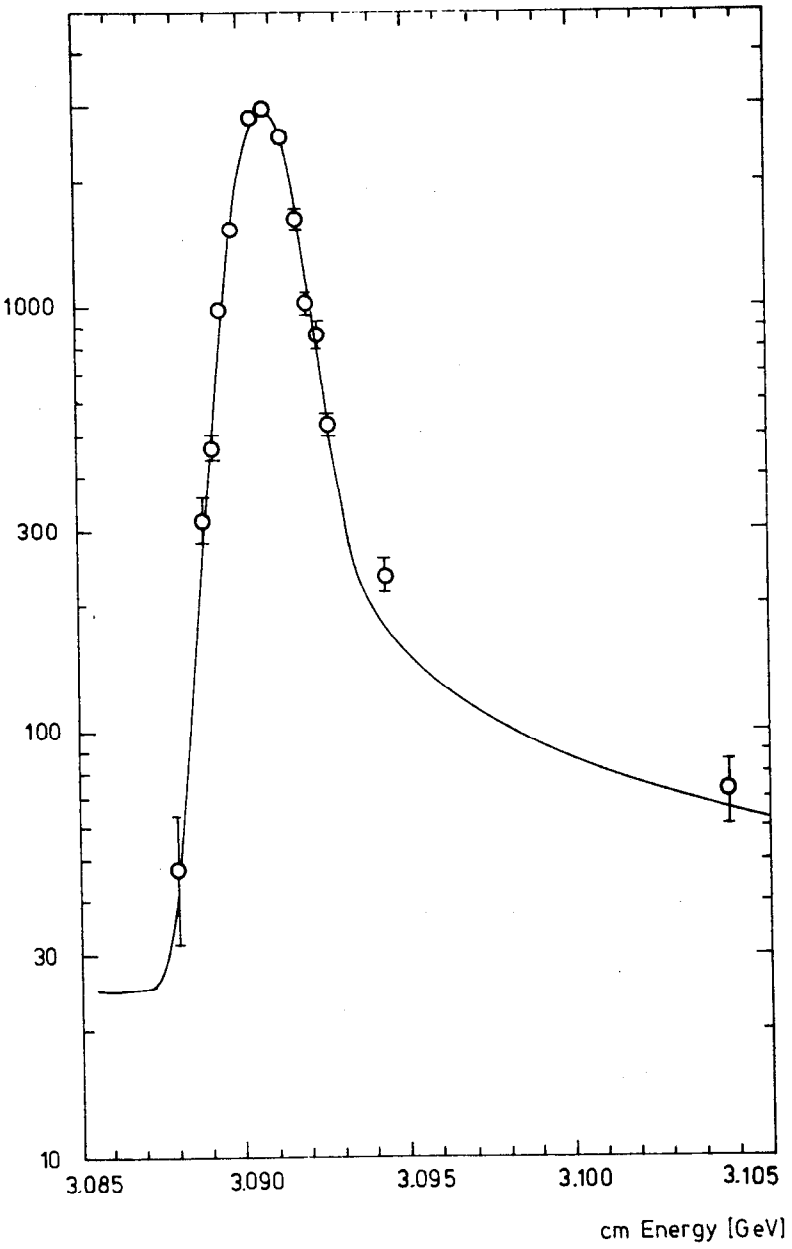

Fig. 5 Excitation curve for 3.1 resonance.

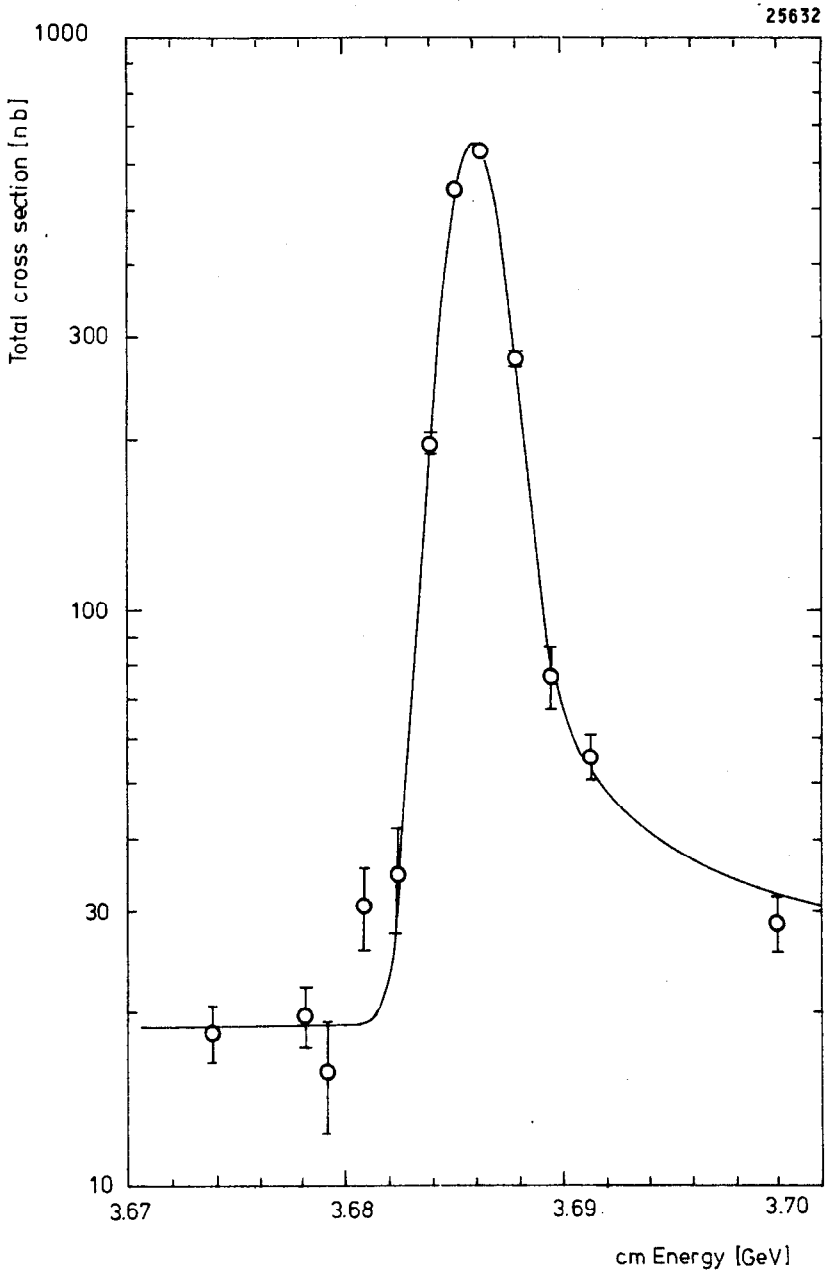

Fig. 6 Same as Fig. 5 for the 3.7 resonance.

II. Muon events

Events with muon candidates have been selected according to the following criteria:

1) At least two tracks with $|\cos\theta| \leq 0.87$

2) One track with momentum > 1 GeV and pointing to one of the muon detectors behind the iron.

3) The candidate track hits the muon chamber within $\pm$ 12.5 cm.

The events have been divided according to the multiplicity into two prongs and multiprongs ($n_{ch} \geq 3$).

The data analysed so far come mostly from the 4.0 - 4.2 GeV region ($\sim$75%), the rest near 4.4 GeV. The total integrated laminosity is $957\,nb^{-1}$.

We find 43 multiprong events with a muon candidate satisfying criteria 1 - 3 above. Using a muon misidentification probability of 3.5% we can account for 29 events. Seven events are due to the radiative process

$$e^+e^- \to \gamma\, 3.7$$
$$\downarrow$$
$$\pi^+\pi^-\, 3.1 \hookrightarrow \mu^+\mu^-$$

with the γ radiated along the beam direction and one decay muon of the 3.1 detected. These events were identified by reconstructing the above decay chain.

The final muon signal in the multiprongs is 7 ($\pm$ 7) events. Taking into account the detection efficiencies and the luminosity we can quote a 2 s.d. upper limit of 70 pb for the process (at p (μ) > 1.0 GeV)

$$e^+e^- \to \mu^\pm + \geq 2 \text{ hadrons}$$

Two prong events do have a large muon signal, as expected from QED reactions. In order to suppress QED events a cut in the coplanarity anlge of the two tracks of $>18^{\circ}$ is required. With this additional cut 98 two prong events with at least one muon are found. Only 12 events can be accounted for by hadron penetration. Of the remaining events 75 have been identified as due to

$$e^+e^- \rightarrow \mu^+\mu^-\gamma$$

To be identified as a radiative muon pair we take a cut in the missing mass squared to the two charged particles of 1.75 GeV^2.

In 67% of the 75 events we observe the radiated photon at the proper position to conserve transverse momentum. Furthermore, agreement is found with the predicted number of radiative muon pairs from QED calculations[4]. The final result for inclusive muon production in the two prong class is from 11 ± 6 events remaining is 96 pb (2 s.d. upper limit) for the reaction

$$e^+e^- \rightarrow \mu^{\pm} + 1 \text{ charged particle}$$

To be compatible with the evidence reported for the production of heavy leptons[5] a minimum mass of 1.95 GeV for the heavy lepton is required, pair produced with point crossection and a branching ratio of 17% into a muon and two neutrinos[6].

III. Electron-K^0_s Events

Since we can identify electrons in our detector we have searched for events that contain directly produced electrons. Specifically we were interested in events having K^0_s and electrons in correlation. This could signify the production and weak decay of charmed particles[7].

In order to obtain a sample enriched with K^0_s mesons we selected events which satisfy the following criteria: (i) Two tracks of opposite charge have a minimum distance (geometrical average) of 5 mm from the beam-beam interaction point, (ii) the reconstructed flight path of the parent particle meets the interaction point within certain bounds, (iii) there is at least one additional track.

The invariant two-particle mass of all events satisfying these criteria is shown in Figs. 7a - c. A clear signal from the decay $K^0_s \rightarrow \pi^+ + \pi^-$ is seen at all three energies. Because of the short decay length of the K^0_s there is a considerable background of normal hadronic events which accidentally meet the above criteria due to the finite resolution of the track reconstruction. The K^0_s detection efficiency in the $\pi^+ \pi^-$ decay mode as determined by Monte Carlo calculations rises slowly with momentum, and averages 20% for the observed events. The numbers of K^0_s events indicate that the crossection for K^0_s production increases with CMS energy between 3.6 and 4.4.GeV.

The result of a search for a correlated electron K^0_s signal is given by the number of identified electrons divided by the number of hadron tracks inside the electron acceptance ((i)-(ii) above). Fig. 7(d-f) shows this e/hadron ratio as a function of the invariant mass of the associated two pion system for the energy region 4.0 - 4.3 GeV. There is an enhancement at the K^0 mass, indicating a strong K^0_s-electron correlation, over a rather uniform background outside.

Such a background can be produced by the following sources:
(i) hadrons interacting in the lead converter, (ii) accidental overlap between a hadron track and a photon shower, (iii) electrons coming from very asymmetric Dalitz pairs or e^+e^- pairs originating in the beam pipe,

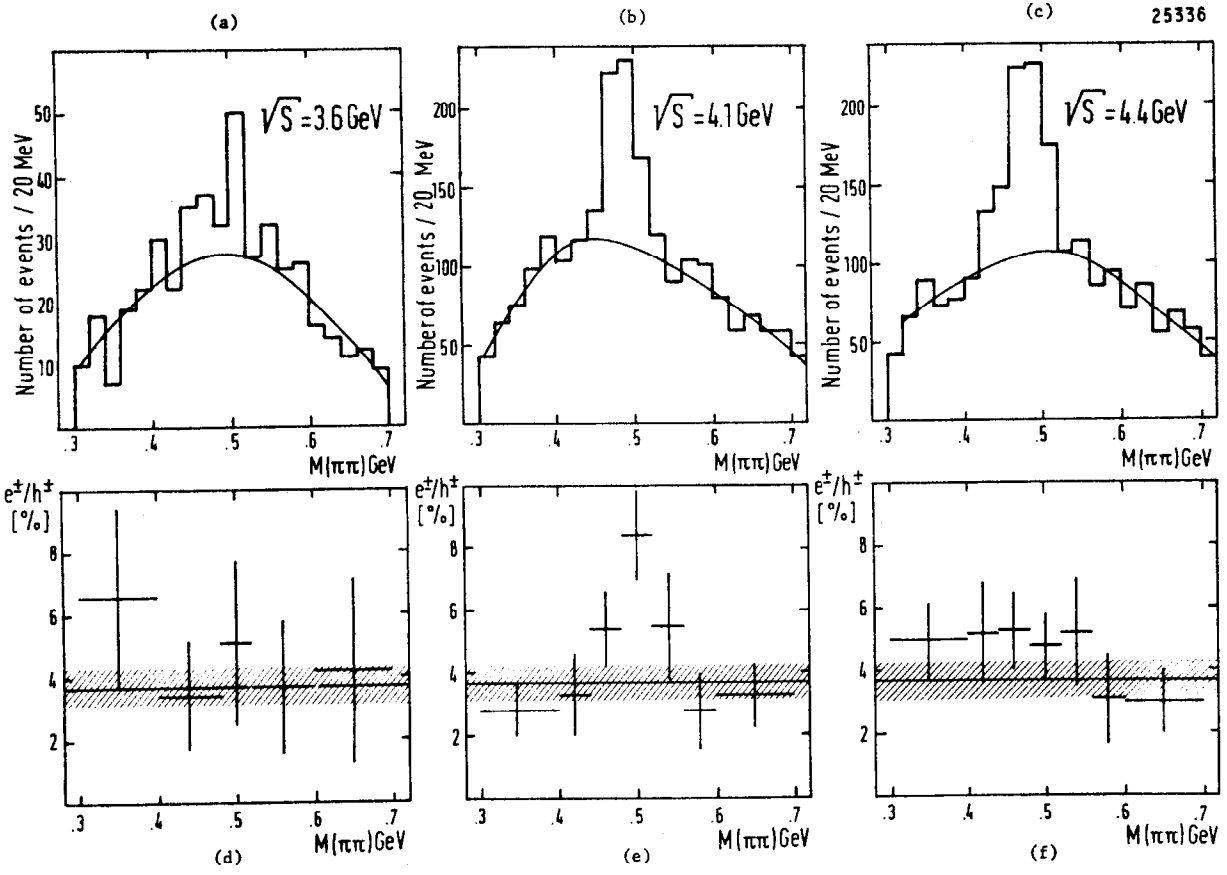

Fig. 7 Upper histograms: Invariant mass plots of selected $\overline{\pi}\pi$ pairs for three different CMS energies with hand-drawn background curves. Lower histograms: e/hadron ratio associated with the $\overline{\pi}\pi$ pairs plotted above. Shaded area: e/hadron ratio of a random sample of multiprong events.

(iv) photons producing Compton electrons, and (v) radiative processes leading to a $3.1 + \pi^+\pi^-$ final state with the subsequent decay $(3.1) \to e^+e^-$. Type (v) events were eliminated by visual inspection. The contribution of all other background sources was checked by measuring the electron/hadron ratio in a random sample of multihadron events (≥ 3 tracks). For events taken between 4.0 and 4.3 GeV we obtain the ratio $3.7 \pm 0.6\%$, indicated by the shaded area in Figs. 7d - 7f. Within errors this value is consistent with the ratio outside the K^0_S mass band at all three energies. We have checked the possibility that the $K^0_S\, e^\pm$ events are simulated by a correlated K^0_S $(K^0_S \bar{n}^0)$ production via background mechanism (iii) by searching for photons converted into fully detectable pairs. The contribution is negligible, < 0.7 events at 90% C.L. The e^+/e^- ratio at the K^0 peak is consistent with one.

In contrast to the energy region 4.0 - 4.3 GeV, the measurements at 3.6 and around 4.4 GeV show no significant K^0_S-electron correlation (Fig. 7d, 7f). Fig. 8 shows the energy dependence of the visible crossection for K^0_S e production (with decay $\pi^+\pi^-$), calculated by using all events from the mass bin $0.46 < m_{\pi\pi} < 0.54$ GeV/c^2. The cross section peaks markedly around $\sqrt{s} = 4.05$ GeV. Subtracting background and accounting for acceptance, branching ratio, and unobserved K^0_L mesons, we estimate the inclusive crossection at the peak as

$$(e^+e^- \to e^+K^0 + \text{anything}) = 3 \text{ nb}.$$

Systematic uncertainties of this estimate may well amount to a factor of two. We observe a multiplicity of 2.5 extra charged particles associated with the K^0_S events. The raw electron spectrum contains mainly small momenta (< 700 MeV/c), in qualitative agreement with semi-inclusive electron measurements of the DASP group at DORIS[8]. The observation of a correlated $e^\pm K^0_S$ signal can be considered as strong evidence for the production and weak decay of charmed particles. The energy dependence of the crossection argues against the possibility that the $K^0_S\, e^\pm$ events originate from the decays of heavy leptons. In addition, the observed charged multiplicity is inconsistent with the low value expected for heavy lepton decays[6].

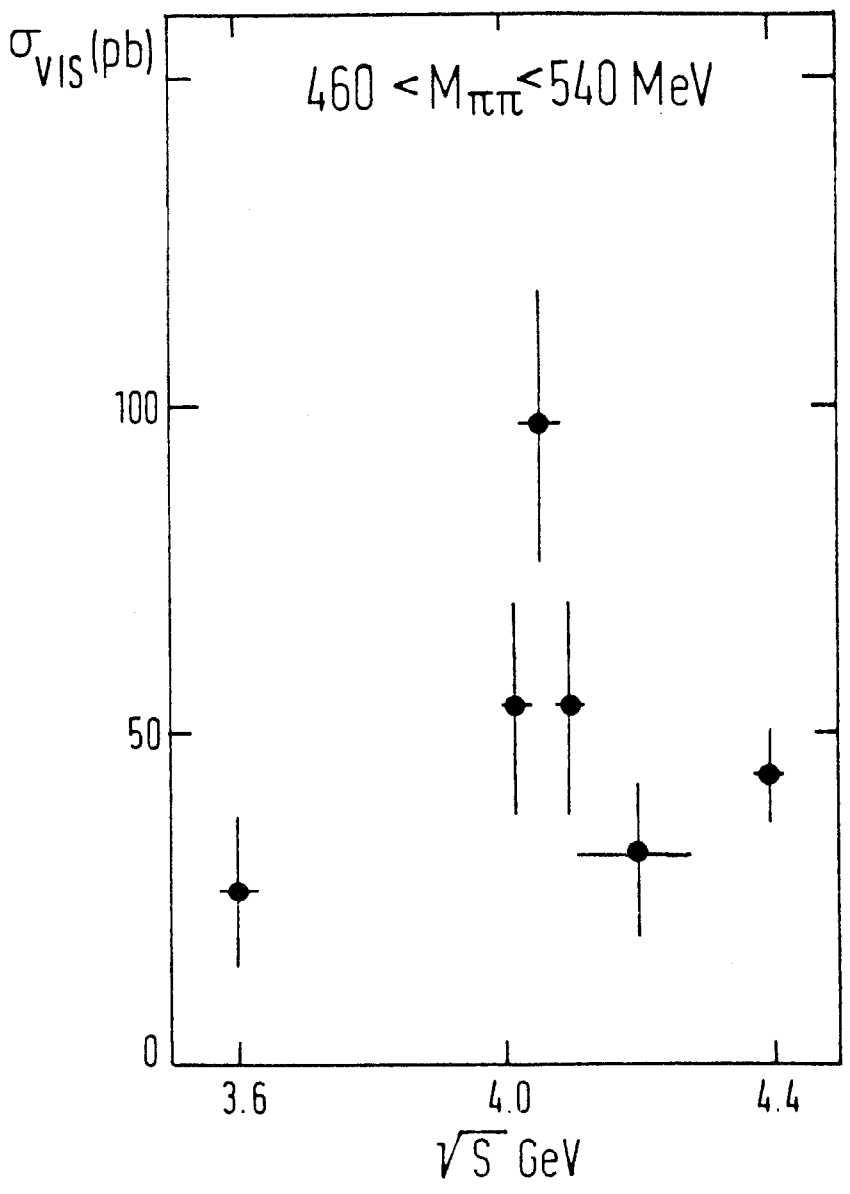

Fig. 8 Visible crossection for associated K^0_s e production versus CMS energy. Background is included.

Acknowledgements

I want to thank F. Gilman and D. W. G. S. Leith for the hospitality during the conference. Also my thanks to Peter Schmüser for very useful discussions.

References

1 L. Criegee et al.; Proc. 1973 Conf. on Instrumentation for High Energy Physics, 707 (1973)
E. Lohrmann; Journal de Physique 37, Coll. C-2 (1976) 15

2 G. Bonneau and F. Martin; Nucl. Phys. B27, 381 (1971)
D. R. Yennie; Phys. Rev. Letters 34, 239 (1975)
J. D. Jackson and D. L. Scharre; Nucl. Instr. & Methods 128, 13 (1975)

3 SLAC-PUB-1599 presented by V. Lüth at the International Conference on High Energy Physics Palermo (1975)

4 F. A. Berends, K. J. F. Gaemers and R. Gastmans; Nucl. Phys. B68, 541 (1974)

5 M. L. Perl et al., Phys. Rev. Lett. 35 (1975) 1489
M. L. Perl et al., Phys. Lett. 63B, 466 (1976)

6 Y. S. Tsai; Phys. Rev. D4, 2821 (1971)

7 S. L. Glashow, J. Iliopoulos, and L. Maiani; Phys. Rev. D2, (1970) 1285
M. K. Gaillard, B. W. Lee, and J. L. Rosner; Rev. Mod. Phys. 47 (1975) 277

8 W. Braunschweig et al., DESY 76/37, to be publ. in Phys. Letters

STUDY OF INTERMEDIATE STATES PRODUCED BY RADIATIVE DECAYS OF ψ'

George H. Trilling

Department of Physics and Lawrence Berkeley Laboratory
University of California, Berkeley, California 94720

I. INTRODUCTION

I shall, in this report, discuss recent experimental information on narrow states, intermediate in mass between the ψ and the ψ', which are produced by radiative decays of the ψ'. The data on which this information is based consists of about 350,000 ψ' decays detected by the SLAC/LBL magnetic detector operating at SPEAR. This detector has been described elsewhere,[1] and I shall not go into its details here.

In the present conventional interpretation of the ψ and ψ' particles as bound states of a charmed quark and charmed antiquark ($c\bar{c}$), the predicted properties of those $c\bar{c}$ states which might be expected to be lower in mass than the ψ' are given in Table I. The ψ and ψ' correspond to the $J^{PC} = 1^{--}$ state (with the ψ' presumably a radial excitation). Those states with charge parity $C = +1$ are all possible decay products (X) in the process

$$\psi' \rightarrow \gamma X \quad . \tag{1}$$

If we restrict the symbol X to those states intermediate in mass between the ψ' and the ψ, we might expect these to consist of the 2^1S_0 and the 1^3P_0, 1^3P_1, 1^3P_2 states. (We assume here that the 1^1S_0 state lies below the ψ.) Thus one may expect to find four X states with the properties $J^{PC} = 0^{-+}$, 0^{++}, 1^{++}, 2^{++}. Presumably the same dynamical effects which lead to the narrow ψ and ψ' widths also apply to the X's; hence their observed widths are expected to be determined purely by the resolution of the detector.

The methods which have been used in the magnetic detector at SPEAR to study X states are the following:

Table I. Expected $c\bar{c}$ states.

State	J^{PC}	Reaction (1) Possible?
$1\ ^1S_0$	0^{-+}	yes
$1\ ^3S_1$ (ψ)	1^{--}	no
$1\ P_1$	1^{+-}	no
$1\ ^3P_0$	0^{++}	yes
$1\ ^3P_1$	1^{++}	yes
$1\ ^3P_2$	2^{++}	yes
$2\ ^1S_0$	0^{-+}	yes
$2\ ^3S_1$ (ψ')	1^{--}	no

(1) Study of inclusive photon spectra with good resolution to search for monoenergetic photon lines.

(2) Study of the cascade processes,

$$\psi' \to \gamma_1 X \quad \big|\to \gamma_2 \psi \quad \big|\to e^+e^- \text{ or } \mu^+\mu^- . \qquad (2)$$

(3) Study of hadronic decays of X states,

$$\psi' \to \gamma X \quad \big|\to \text{hadrons} . \qquad (3)$$

In the subsequent sections, the results of these approaches are discussed in some detail.

II. INCLUSIVE PHOTON SPECTRA

The detection of monoenergetic photons emitted in ψ' decays is a conceptually simple and natural method to search for narrow intermediate states. The anticipated results of such a study would be the identification of various X states, and the determination of ψ' branching ratios for decay into each X state detected. The principal experimental difficulty arises from the enormous background of photons from π^0 decay, especially at the low energies where one expects to find the desired monoenergetic photons.

For such a study, the magnetic detector was used as a pair spectrometer,[2] the beam pipe wall and scintillation counter surrounding that wall serving as the thin converters, and the cylindrical spark chambers being used to measure the momenta of the outgoing electron and positron. The efficiency for detecting photons in this manner rises rapidly from zero below 120 MeV to $\sim 1\%$ at 200 MeV and thence slowly to about 2% at the highest photon energies. The resolution σ is about 4 MeV at 200 MeV. The results for both ψ and ψ' photon spectra are shown in Fig. 1. The general shapes of both spectra are the same (as might be expected from the fact that most ψ' decays lead to a ψ), but the ψ' spectrum exhibits

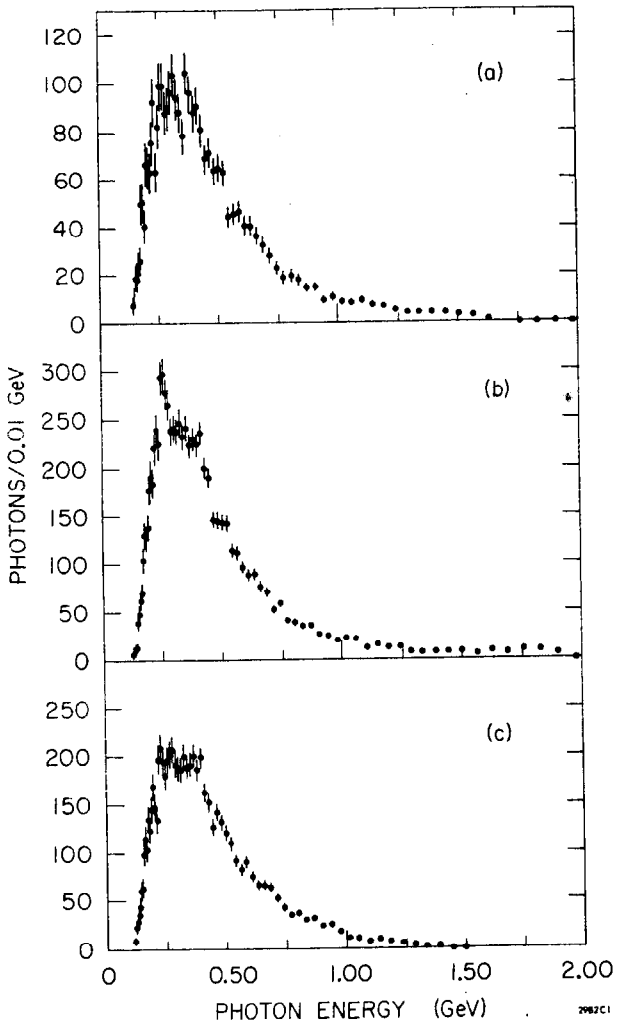

Fig. 1. Inclusive photon energy spectrum from (a) ψ decays, (b) ψ' decays, (c) Monte-Carlo calculation for ψ decays.

a clear spike at $E_\gamma = 261 \pm 10$ MeV (corresponding to $M_\chi = 3413 \pm 11$ MeV) with a width consistent with the resolution.[3] The sharp drop-off below 250 MeV is due to the loss of efficiency; and indeed this experiment is incapable, from the inclusive spectrum, to make any useful statement about monoenergetic photons of significantly lower energy. The ψ' branching ratio corresponding to this signal[4] is 0.075 ± 0.026, where the quoted error arises principally from systematic uncertainties in the background subtraction and in the evaluation of the relevant efficiencies.

It may be noted that the experiment of Badtke et al.,[5] in the other experimental area of SPEAR, using NaI crystals to detect photons, has a much lower energy threshold. Thus this group has reported monoenergetic lines at $E_\gamma = 256$, 168 and 121 MeV, all with an uncertainty of ± 7 MeV (corresponding to $M_\chi = 3418$, 3512 and 3561 MeV). The corresponding branching ratios are 0.1 ± 0.04, 0.09 ± 0.03, 0.08 ± 0.03 respectively.[4] The first of these is, within the substantial uncertainties of both measurements, compatible with the above magnetic-detector value. As will be seen below, the other two states have also been observed by the other methods in which the magnetic detector has been used to study X states.

III. CASCADE DECAY OF ψ'

The processes (2) were precisely those from which the first evidence for intermediate states was obtained by the DESY-DASP group.[6] In addition to providing a very clean way to identify those X states which have significant branching ratios for the decays $X \to \gamma\psi$, these processes can potentially yield the most powerful data for determinations of the spins of these same X states.[7] The main difficulty of such a study is the removal of background from the processes

$$\psi' \to \pi^o\pi^o\psi \to \gamma\gamma\gamma\gamma\psi \ ,$$

$$\psi' \to \eta\psi \to \gamma\gamma\psi \ .$$

The recent results[2] from the SLAC/LBL magnetic detector are obtained from

a study of events in which either γ_1 or γ_2 in (2) are converted into an e^+e^- pair in the manner already described in Section II, and the momentum of the unconverted photon is then determined by momentum-energy balance. To sharpen the resolution, a kinematic fit is made in which the dilepton pair is constrained to the ψ mass. Details concerning the removal of the above-mentioned backgrounds are given in Ref. 2; in the subsequent discussion we assume that such backgrounds have been removed. The remaining sample consists of 21 events.

For each event in the sample, there are two possible X masses depending upon which photon is assumed to arise from the ψ' decay and which from the X decay. The correct choice can in principle be made with adequate data from the requirement of small X widths. The scatter plot of the low $\psi\gamma$ mass versus the high $\psi\gamma$ mass for the 21-event sample is shown in Fig. 2, with the projections on both axes also exhibited. There are clear peaks at 3504 ± 10 MeV and 3543 ± 10 MeV with branching ratio products $B(\psi' \to \gamma X)B(X \to \gamma\psi)$ of 0.024 ± 0.008 and 0.01 ± 0.006 respectively, accounting for 16 of the 21 events. For both of these states, the required small width provides a unique resolution of the $\psi\gamma$ mass ambiguity in favor of the high mass solution. This choice also agrees well with the data of Badtke et al.[5] and with the results from studies of X hadronic modes discussed in Section IV. Of the remaining events, one lies at 3413 MeV (high $\psi\gamma$-mass solution) which, as discussed earlier, corresponds to a known X state (although a single event could just be background) and corresponds to a branching ratio product of 0.002 ± 0.002. Finally the remaining four events are all consistent with a single mass of 3455 ± 10 MeV (high $\psi\gamma$ solution) and a branching ratio product of 0.008 ± 0.004. It is also possible to throw out one of these four events as background and retain the other three at a common mass value of 3340 ± 10 MeV (low $\psi\gamma$-mass solution). Although this 3455 MeV (or 3340 MeV) signal looks reasonably solid in Fig. 2, it differs from the other signals in one important respect: as will be discussed later, there is no indication

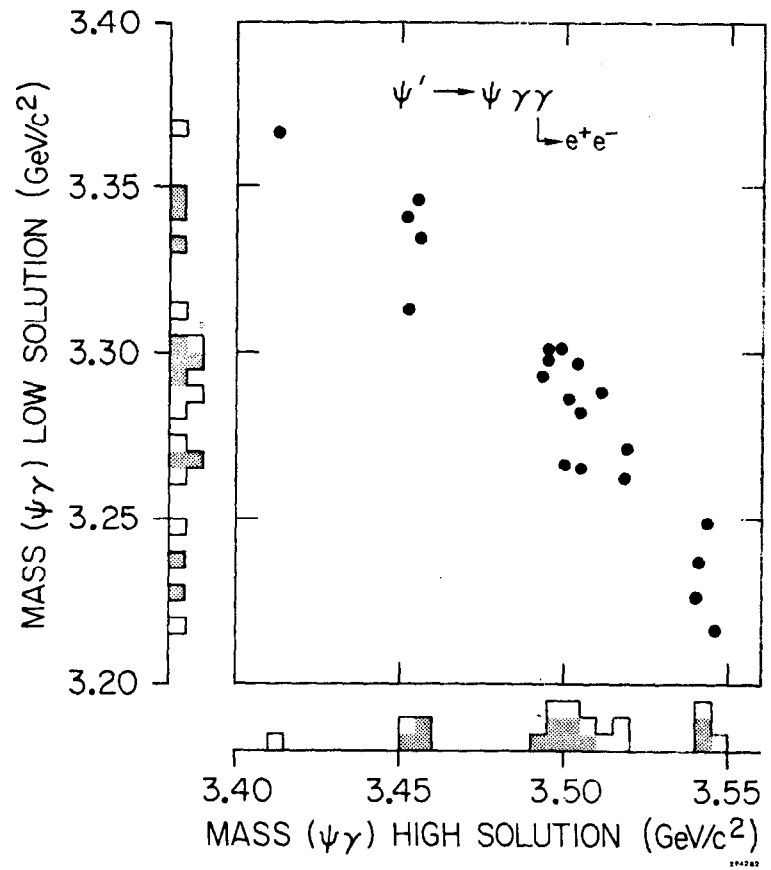

Fig. 2. Scatter plot of the two $\psi\gamma$ mass combinations from the process $\psi' \to \gamma\gamma\psi$.

for any observable hadronic mode at either of these masses, nor is there any clear evidence for this mode in the inclusive photon spectra in which the other X states show up. Thus this state clearly requires confirmation before it can be considered as established.

IV. HADRONIC DECAYS OF X

A. General Features

Hadronic decays of X states can be identified for those decay modes consisting only of charged outgoing particles all of which are detected in the apparatus. The specific decay modes studied are the following:

$$X \to \pi^+\pi^-\pi^+\pi^- \quad (4a)$$
$$\to \pi^+\pi^- K^+K^- \quad (4b)$$
$$\to \pi^+\pi^-\pi^+\pi^-\pi^+\pi^- \quad (4c)$$
$$\to \pi^+\pi^- \quad (4d)$$
$$\to K^+K^- \quad (4e)$$
$$\to \pi^+\pi^- p\bar{p}\,. \quad (4f)$$

Identification of reaction (3) is achieved, without detecting the photon, through energy and momentum balance. The major problem in the application of this procedure is the separation of $\psi' \to \gamma X$ from $\psi' \to \pi^0 X$ where X is a final state consisting of one of the groups of hadrons listed in (4). Fortunately this separation is reasonably straightforward for three reasons: (a) Decay modes of the form $\psi' \to \pi^0$ + all charged particles have relatively small branching ratios; (b) such decay modes have a π^0 spectrum spread over a wide range of energies whereas the photons in (3) are monoenergetic with relatively small energy; (c) the measurement of missing-mass-squared by which one distinguishes a missing photon from a missing pion is most precise when the energy taken up by the missing or neutral system is small -- this is just the case in reaction (3). These points have already been discussed in the paper of Feldman et al.,[3] and the recent work based on the much larger statistics now available confirms the validity of the γ-π^0 separation.

We do not here go into great detail on the fine points of the analysis, but do mention the following relevant elements:

(i) The X masses are determined from a one-constraint kinematic fit to reactions (3) and (4) using the bubble-chamber program SQUAW.

(ii) Care is used to remove certain prominent backgrounds:

(a) $\psi' \to \gamma X \to \gamma\pi^+\pi^-\pi^+\pi^-$, $\gamma\pi^+\pi^- K^+K^-$

Background: $\psi' \to \pi^+\pi^-\psi \to \pi^+\pi^-\mu^+\mu^-$, $\pi^+\pi^- e^+e^-$

(b) $\psi' \to \gamma X \to \gamma\pi^+\pi^-\pi^+\pi^-\pi^+\pi^-$

Background: $\psi' \to \pi^+\pi^-\psi \to \pi^+\pi^-\pi^+\pi^-\pi^+\pi^-$, $\pi^+\pi^-\pi^+\pi^-\pi^+\pi^-\pi^0$

(c) $\psi' \to \gamma X \to \gamma\pi^+\pi^-$, γK^+K^-

Background: $\psi' \to e^+e^-$, $\mu^+\mu^-$, γe^+e^-, $\gamma\mu^+\mu^-$

(iii) Time-of-flight information plus the kinematic fit are used to identify the X decay modes $\pi^+\pi^- K^+K^-$ and $\pi^+\pi^- p\bar{p}$. The kinematic fit alone is usually adequate to separate $X \to \pi^+\pi^-$ from $X \to K^+K^-$.

(iv) In the calculation of branching ratios corrections have been made for the effects of the various cuts used.

The mass spectra corresponding to the various final states (4) are shown in Figs. 3 and 4. On the basis of these spectra one can make the following remarks:

(1) All the mass spectra show a prominent peak at $M_X = 3415 \pm 10$ MeV.

(2) The 4π and $\pi\pi KK$ spectra also show clear peaks at $M_X = 3500 \pm 10$ MeV and 3550 ± 10 MeV. These three mass values are in good agreement with those observed by the other techniques previously discussed.

(3) The 6π spectrum above the 3415 MeV peak is compatible with populations from the above two states, although they are not clearly resolved.

(4) The combined $\pi^+\pi^-$ and K^+K^- spectra show a fairly clear peak at 3550 MeV but no significant signal at 3500 MeV.

(5) There is no evidence for any signal at 3450 MeV, the state suggested by the cascade decay data of Fig. 2.

(6) The peaks at the upper end of the 4π, $\pi\pi K\bar{K}$ and $\pi\pi p\bar{p}$ spectra do not

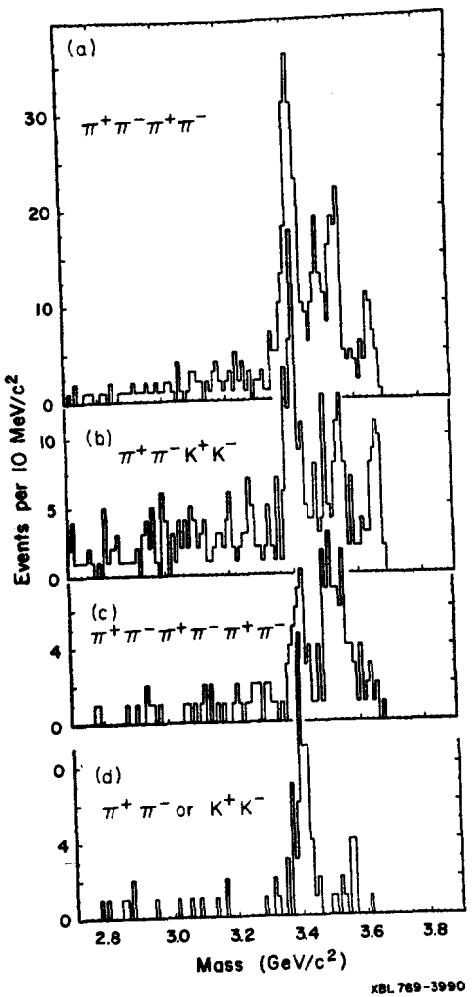

Fig. 3. Mass spectrum for multihadron states X fit to the reaction $\psi' \to \gamma X$ with X being (a) $\pi^+\pi^-\pi^+\pi^-$, (b) $\pi^+\pi^-K^+K^-$, (c) $\pi^+\pi^-\pi^+\pi^-\pi^+\pi^-$, (d) $\pi^+\pi^-$ or K^+K^-.

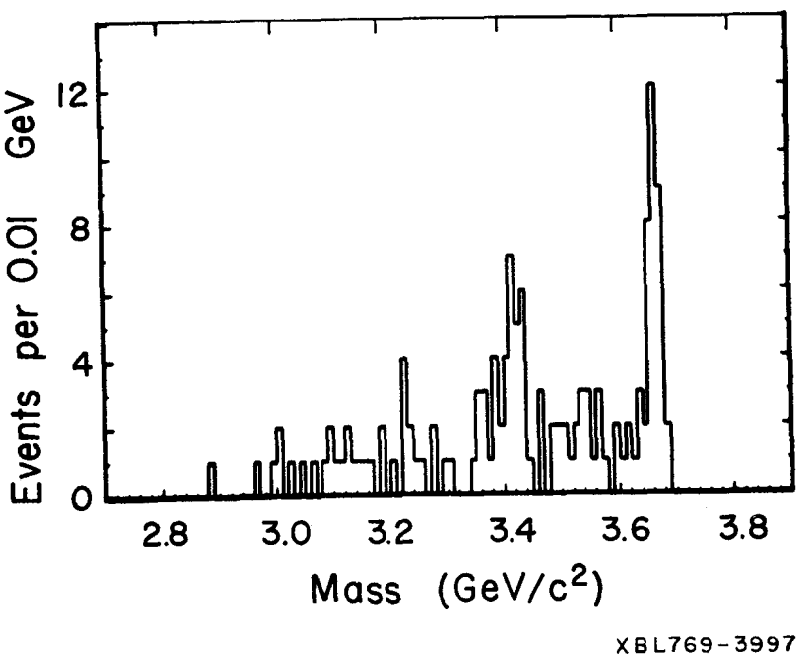

Fig. 4. Mass spectrum of $\pi^+\pi^-p\bar{p}$ for events fit to the reaction $\psi' \to \gamma\pi^+\pi^-p\bar{p}$.

come from X states, but rather correspond to the direct decay modes $\psi' \to 4\pi$, $\pi\pi K\bar{K}$, $\pi\pi p\bar{p}$. There is also a small but finite contribution from $\psi' \to 6\pi$ at the upper end of the 6π spectrum. The absence of such population at the upper end of the $\pi^+\pi^-$, K^+K^- spectrum is not in itself proof of the absence of the direct modes $\psi' \to \pi^+\pi^-$, K^+K^-, because cuts used to remove $\psi' \to e^+e^-$, $\mu^+\mu^-$ background also remove $\psi' \to \pi^+\pi^-$, K^+K^-.

B. Study of the X(3415) Decays

Table II shows preliminary values of branching ratios for the various identified decay modes. To obtain the X branching ratios, I have divided the branching ratio products by the total $\psi' \to \gamma X(3415)$ branching ratio of 0.075 ± 0.026 discussed in Section II.

Figure 5 shows the $\pi^+\pi^-$ and $K^\pm\pi^\mp$ spectra from the $\pi^+\pi^-\pi^+\pi^-$ and $\pi^+\pi^-K^+K^-$ decay modes, from which it is clear that the ρ and $K^*(891)$ are the only prominent resonances. Remarkably (since there are no obvious selection rules which forbid these processes), there is no significant $\rho\rho$ or $K^*(891)\overline{K^*}(891)$ signal: the ρ and K^* almost always seem accompanied by nonresonant meson pairs.

Other interesting properties can be summarized as follows:

(1) The G parity is even and charge parity is even; hence the isospin must be even. The K^+K^- decay mode thus requires that $I = 0$.

(2) The observed equality of $\pi^+\pi^-$ and K^+K^- branching ratios agrees with expectations for an SU(3) singlet assignment for the X(3415).

(3) The observed ratio of $\dfrac{X \to \rho\pi^+\pi^- \to \pi^+\pi^-\pi^+\pi^-}{X \to K^*(891)K\pi \to K^+\pi^-K^-\pi^+}$ decay rates, namely 1.12 ± 0.55, is also in agreement with the SU(3) singlet prediction of 9/8.

(4) The branching ratios for X(3415) to $\pi^+\pi^-$, $\pi^+\pi^-\pi^+\pi^-$ and $\pi^+\pi^-\pi^+\pi^-\pi^+\pi^-$ are very similar to the corresponding values observed for ψ decay to $\pi^+\pi^-\pi^0$, $\pi^+\pi^-\pi^+\pi^-\pi^0$, $\pi^+\pi^-\pi^+\pi^-\pi^+\pi^-\pi^0$ respectively.[8] (In making this comparison a π^0 is added to go from X to corresponding ψ decay modes to take account of the opposite G parities.)

Table II. X(3415) branching ratios.

Final state	$B(\gamma X) \times B(X \to \text{final state})$	$B(X \to \text{final state})$[a]
$\pi^+\pi^-\pi^+\pi^-$	$(3.2 \pm 0.6) \times 10^{-3}$	$(4.3 \pm 1.7)\%$
$\pi^+\pi^-K^+K^-$	$(2.7 \pm 0.7) \times 10^{-3}$	$(3.6 \pm 1.5)\%$
$\pi^+\pi^-\pi^+\pi^-\pi^+\pi^-$	$(1.4 \pm 0.5) \times 10^{-3}$	$(2 \pm 1)\%$
$\pi^+\pi^-$	$(0.7 \pm 0.2) \times 10^{-3}$	$(1 \pm 0.5)\%$
K^+K^-	$(0.7 \pm 0.2) \times 10^{-3}$	$(1 \pm 0.5)\%$
$\pi^+\pi^-p\bar{p}$	$(0.4 \pm 0.13) \times 10^{-3}$	$(0.5 \pm 0.2)\%$
$\psi\gamma$	$(2 \pm 2) \times 10^{-3}$	$(3 \pm 3)\%$

Resonance Production:

$$\frac{B(X \to \rho^0\pi^+\pi^-)}{B(X \to \pi^+\pi^-\pi^+\pi^-)} = 0.39 \pm 0.12$$

$$\frac{B(X \to K^*(891)K^\pm\pi^\mp)}{B(X \to \pi^+\pi^-K^+K^-)} = 0.41 \pm 0.10$$

a. Calculated using $B(\psi' \to \gamma X(3415)) = 0.075 \pm 0.026$.

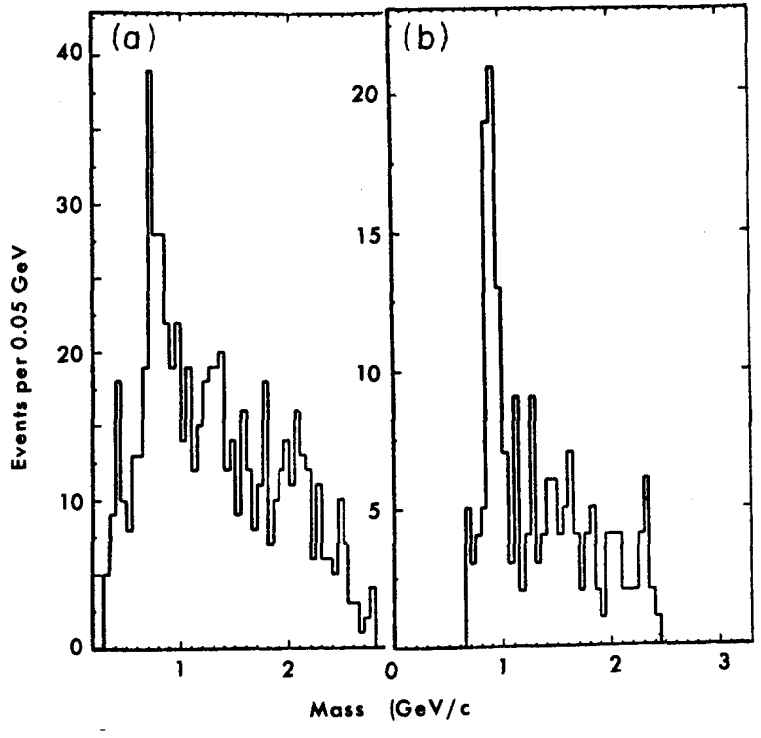

Fig. 5. (a) $\pi^+\pi^-$ mass spectrum from $\chi(3415) \rightarrow \pi^+\pi^-\pi^+\pi^-$ (four combinations per event); (b) $K^\pm\pi^\mp$ mass spectrum from $\chi(3415) \rightarrow \pi^+\pi^-K^+K^-$ (two combinations per event).

C. The $\chi(3500)$ and $\chi(3550)$ Decays

Tables III and IV show branching ratio products for $\chi(3500)$ and $\chi(3550)$. Estimates of the χ branching ratios, obtained by using the ψ' branching ratio results of Badtke et al.[5] are also given in Tables III and IV. The prominence of the radiative mode $\gamma\psi$ is evident for both χ states. The importance of this mode relative to the normal hadronic modes is very reminiscent of the prominence of the decay modes $\psi' \rightarrow \psi$ + anything relative to the standard ψ' hadronic modes. Although ρ and $K^*(891)$ production are significant pieces of the $\pi^+\pi^-\pi^+\pi^-$ and $\pi^+\pi^-K^+K^-$ modes for both $\chi(3500)$ and $\chi(3550)$ it is again true that both $\rho\rho$ and $K^*\bar{K}^*$ seem absent. The ratios of $\rho\pi\pi$ to $K^*K\pi$ again satisfy, to within the rather large statistical uncertainties, the SU(3) singlet predictions.

V. SPIN INFORMATION

For the hadronic modes, one can measure the distribution of θ, the angle between the beam direction and the outgoing photon. The general form is,[7]

$$W(\theta)d\cos\theta = 1 + A\cos^2\theta \qquad (5)$$

where $|A| \leq 1$.

The value of A can be unambiguously predicted only for spin $J = 0$, namely $A = 1$. For spins 1 and 2, there can be several multipoles in the amplitude and the predictions are ambiguous. However if one assumes that only the electric dipole contributes significantly, one obtains,

$$A = -1/3 \qquad J = 1$$

$$A = 1/13 \qquad J = 2$$

The actual experimental results, based on using all the observed hadronic decay modes are as follows[8]:

$$\chi(3415) \qquad A = 1.4 \pm 0.4$$

$$\chi(3500) \qquad A = 0.1 \pm 0.4$$

$$\chi(3550) \qquad A = 0.3 \pm 0.4$$

Figure 6b and Fig. 7 show the distributions of $|\cos\theta|$ from which

Table III. $\chi(3500)$ branching ratios.

Final state	$B(\gamma\chi) \times B(\chi \to \text{final state})$	$B(\chi \to \text{final state})$[a]
$\pi^+\pi^-\pi^+\pi^-$	$(1.1 \pm 0.4) \times 10^{-3}$	1.2%
$\pi^+\pi^- K^+K^-$	$(0.6 \pm 0.3) \times 10^{-3}$	0.7%
$\pi^+\pi^-\pi^+\pi^-\pi^+\pi^-$	$(1.7 \pm 0.6) \times 10^{-3}$	1.9%
$\pi^+\pi^-$ and K^+K^-	$< 0.15 \times 10^{-3}$	< 0.2%
$\pi^+\pi^-\bar{p}p$	$(0.1 \pm 0.08) \times 10^{-3}$	0.1%
$\psi\gamma$	$(24 \pm 8) \times 10^{-3}$	26%

Resonance Production:

$$\frac{B(\chi \to \rho^o\pi^+\pi^-)}{B(\chi \to \pi^+\pi^-\pi^+\pi^-)} = 0.24 \pm 0.20$$

$$\frac{B(\chi \to K^*(891)K^\pm\pi^\mp)}{B(\chi \to \pi^+\pi^- K^+K^-)} = 0.35 \pm 0.18$$

a. Calculated using $B(\psi' \to \gamma\chi(3500)) = 0.09$ from Ref. 5. The sum of all uncertainties being rather large, these figures are to be considered estimates and no errors are quoted.

Table IV. $\chi(3550)$ branching ratios.

Final state	$B(\gamma\chi) \times B(\chi \to \text{final state})$	$B(\chi \to \text{final state})$[a]
$\pi^+\pi^-\pi^+\pi^-$	$(1.6 \pm 0.4) \times 10^{-3}$	2%
$\pi^+\pi^- K^+K^-$	$(1.4 \pm 0.4) \times 10^{-3}$	1.8%
$\pi^+\pi^-\pi^+\pi^-\pi^+\pi^-$	$(0.8 \pm 0.5) \times 10^{-3}$	1%
$\pi^+\pi^-$ and K^+K^-	$(0.2 \pm 0.1) \times 10^{-3}$	0.2%
$\pi^+\pi^-\bar{p}p$	$(0.2 \pm 0.1) \times 10^{-3}$	0.2%
$\psi\gamma$	$(10 \pm 6) \times 10^{-3}$	12%

Resonance Production:

$$\frac{B(\chi \to \rho^o\pi^+\pi^-)}{B(\chi \to \pi^+\pi^-\pi^+\pi^-)} = 0.31 \pm 0.17$$

$$\frac{B(\chi \to K^*(891)K^\pm\pi^\mp)}{B(\chi \to \pi^+\pi^- K^+K^-)} = 0.25 \pm 0.13$$

a. Calculated using $B(\psi' \to \gamma\chi(3550) = 0.08$ from Ref. 5. The comment about errors given in Table III also applies here.

the above values of A are derived. Figure 6a, which applies only to the $\chi(3415) \to \pi^+\pi^-$ or K^+K^- mode shows the distribution of $|\cos\theta'|$ where θ' is the angle between dimeson line and the photon. This distribution is expected to be isotropic for $J = 0$, and would normally contain terms in $\cos^2\theta'$ and $\cos^4\theta'$ if $J = 2$ (the next lowest allowed spin for state with a $\pi^+\pi^-$ or K^+K^- decay mode). Unfortunately the statistics are small, but there is no obvious deviation from isotropy.

The main conclusion from these results is that only the $\chi(3415)$ gives a good fit to spin zero. For the $\chi(3500)$, the radiative cascade decay process with its additional useful variables can potentially provide much more conclusive information on the spin.[7] Preliminary analysis of events in which the photons are detected in the shower counters of the magnetic detector (a much larger sample than that discussed in Section III, where one photon is required to convert into an e^+e^- pair prior to reaching the first spark chamber) appears to rule out spin zero and thus confirms the tentative conclusion based on the γ angular distribution in the hadron decays.

Guided by the predictions of the charm model (see Table I), the fact that $\pi^+\pi^-$, K^+K^- decay modes imply $J^P = 0^+, 2^+, \ldots$, and the previous discussions of angular distributions, one is led to a favored assignment:

$$\chi(3415) \qquad J^{PC} = 0^{++}$$

$$\chi(3500) \qquad J^{PC} = 1^{++}$$

$$\chi(3550) \qquad J^{PC} = 2^{++} \ .$$

Complete experimental confirmation of these assignments is obviously desirable, but will not come easily with the present detectors.

VI. CONCLUDING REMARKS

From the totality of the information given we can come to the following conclusions:

1. There are three clearly-established states between the ψ' and the ψ at masses of 3415, 3500 and 3550 MeV (an actual average of all data done

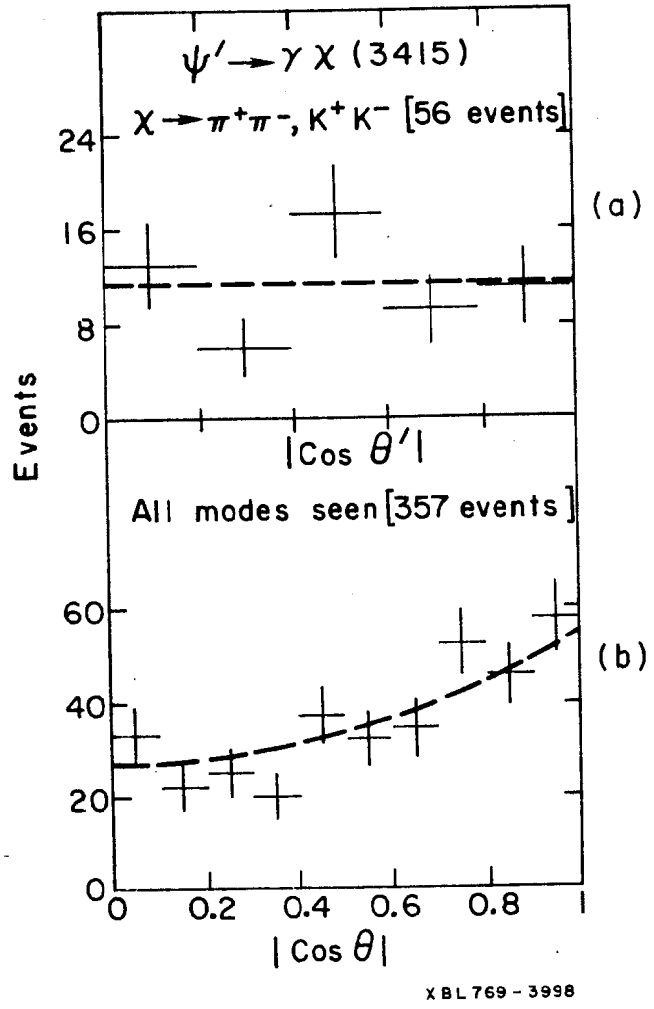

Fig. 6. Decay angular distributions for X(3415). Angles are defined in text and dashed lines represent prediction for J = 0.

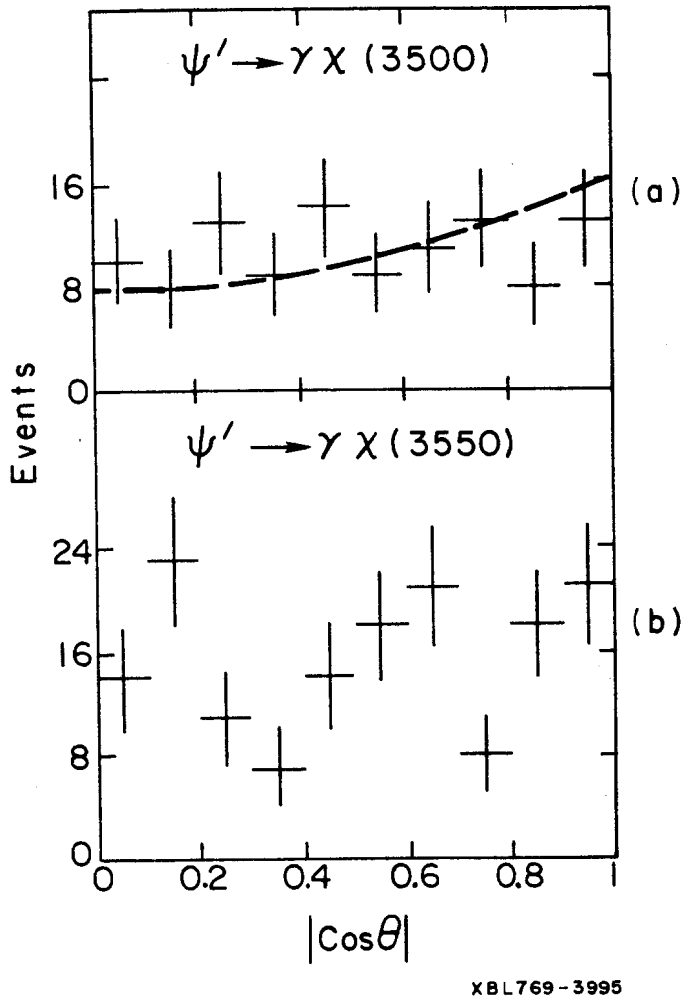

Fig. 7. Angular distributions for (a) X(3500) and (b) X(3550). Dashed line represents prediction for J = 0.

by G. Feldman[10] gives values of 3414, 3508 and 3552 MeV for the masses). Thus the ambiguity between 3270 and 3500 MeV as the mass of the first state seen in the cascade decay mode[6] is removed.

2. The three above states all show significant hadronic decay modes. The radiative mode $X \to \gamma\psi$ seems the dominant one for the X(3500), very substantial for the X(3550), and, at most, of the same order as individual hadronic modes for the X(3415).

3. The limited information on isospin and SU(3) supports for the X states the $I = 0$ and SU(3) singlet properties predicted by the $c\bar{c}$ model.

4. The cascade process suggests the existence of another X state at a mass of 3455 or perhaps 3550 MeV. There is no evidence for hadronic decay modes of such a state.

5. There is a preferred but not conclusively established set of spin assignments, namely $J^P = 0^+$, 1^+ and 2^+ for the X(3415), X(3500) and X(3550) respectively. Thus of the states expected from the $c\bar{c}$ model the pseudoscalar is missing. Perhaps the 3455 MeV state seen in the cascade process is in fact this pseudoscalar, but there are no experimental data to support this hypothesis.

6. In my view, further substantial progress in this area can only come from coupling a much superior neutrals detector to a charged-particle detector at least as good as the present SLAC/LBL instrument.

The results presented in this paper come from the work of the SLAC/LBL collaboration, whose membership is: G. S. Abrams, M. S. Alam, A. M. Boyarski, M. Breidenbach, W. C. Carithers, W. Chinowsky, S. C. Cooper, R. G. DeVoe, J. M. Dorfan, G. J. Feldman, C. E. Friedberg, D. Fryberger, G. Goldhaber, G. Hanson, J. Jaros, A. D. Johnson, J. A. Kadyk, R. R. Larsen, D. Lüke, V. Lüth, H. L. Lynch, R. J. Madaras, C. C. Morehouse, H. K. Nguyen, J. M. Paterson, M. L. Perl, I. Peruzzi, M. Piccolo, F. M. Pierre, T. P. Pun, P. Rapidis, B. Richter, B. Sadoulet, R. H. Schindler, R. F. Schwitters, J. Siegrist, W. Tanenbaum, F. Vannucci, J. S. Whitaker, and J. E. Wiss. I am particularly indebted to J. S. Whitaker, W. Tanenbaum, B. Sadoulet and A. D. Johnson for valuable discussions.

FOOTNOTES AND REFERENCES

1. J.-E. Augustin et al., Phys. Rev. Lett. 34, 764 (1975).
2. J. S. Whitaker et al., LBL-5382, submitted to Phys. Rev. Lett.
3. Evidence for this state was first reported by G. J. Feldman et al., Phys. Rev. Lett. 35, 821 (1975).
4. For efficiency determinations, the angular distribution relative to the beam has been assumed to be $(1 + \cos^2\theta)$ for the 260 MeV photon and isotropic for the others, in accordance with the results discussed in Section V.
5. D. H. Badtke et al., paper submitted to the XVIIIth International Conference on High Energy Physics, Tbilisi, USSR (1976).
6. W. Braunschweig et al., Phys. Letters 57B, 407 (1975); also W. Tanenbaum et al., Phys. Rev. Lett. 35, 1323 (1975).
7. G. Karl, S. Meshkov and J. L. Rosner, Phys. Rev. D13, 1203 (1976); L. S. Brown and R. N. Cahn, Phys. Rev. D13, 1195 (1976).
8. B. Jean-Marie et al., Phys. Rev. Lett. 36, 291 (1976).
9. The coefficients of $\cos^2\theta$ here differ slightly from values quoted earlier because we have used a slightly different and larger event sample to reduce as much as possible the statistical errors.
10. G. Feldman, Lectures at the SLAC Summer Institute (1976).

Production of Muons in Hadron-Nucleus Collisions*

A. J. S. Smith

Department of Physics, Princeton University
P. O. Box 708, Princeton, New Jersey 08540
USA

INTRODUCTION

In this lecture I shall describe an experiment in progress[1] at the Fermi National Accelerator Laboratory (FNAL) to study the production of $\mu^+\mu^-$ pairs in hadron-hadron collisions. So far, we have used beams of 225 - GeV π^+, π^- and protons incident on carbon and tin targets for most of the data. In an earlier run, a 150 GeV positive beam was used with a beryllium target. The results I report of the 150 GeV run are final; those at 225 GeV are preliminary.

The goal of this experiment is to carry out, as completely as possible, a measurement of μ-pair production over a wide range of kinematic variables and particle types, using a spectrometer with good resolution and very large acceptance. Only such a comprehensive experiment can measure differential cross sections without resorting to model-dependent assumptions. There are many interesting aspects of these measurements: Among them are the study of the production mechanism of the new particles[2] J/ψ and ψ', as well as a search for other states decaying to μ-pairs. I shall discuss in detail the features of J/ψ production by π^+, π^-, and protons, and compare them with the production of the more common vector mesons ρ°, ω, φ, and with non-resonant μ-pairs in neighboring mass regions. The non-resonant pairs are also of great interest; for example, in 1970 Drell and Yan[3] proposed parton-antiparton ($q\bar{q}$) annihilations as their source, and since then many predictions of yields have been made by numerous authors. Virtual bremsstrahling has been put forth as another possible source of non-resonant pairs.[4]

To produce μ-pairs with proton beams by quark-antiquark annihilation all antiquarks must come from the sea. On the other hand, pion beams contain valence antiquarks and hence present a more straightforward probe with which to test these models. Also, because the valence antiquarks of π^+ and π^- have charge $\frac{1}{3}$ and $-\frac{2}{3}$ respectively, a cross-section ratio of $\frac{1}{4}$ is predicted for μ-pairs produced by π^+ mesons

versus π^- on an isospin symmetric target. Thus by using π^+ and π^- beams of the same momentum incident on a carbon target, our experiment can test the Drell-Yan mechanism in a way not too dependent upon details of a particular model.

The experiment is also sensitive to processes resulting in "multi-muon" final states (states having more than two muons). Such events could originate in associated production of J/ψ pairs, or of a J/ψ along with a charmed particle decaying promptly into a muonic final state. We have searched for multimuon events, finding none above background, as explained in what follows. This negative result puts quite stringent upper limits on associated production processes.

Finally, one of the most compelling motivations for this experiment was to ascertain the source of the single prompt leptons, first observed in high-energy p-nucleus collisions at Serpukhov[5] and FNAL[6]. (Prompt leptons are those not attributable to π or K decays.) These measurements were all made at high transverse momenta and near 90° in the center-of-mass system. Since then other experiments[7] have detected prompt leptons over a wide range of kinematic variables, and have found the ratio of the yields to be approximately $\mu/\pi \approx 10^{-4}$, and quite insensitive to the kinematic region of the experiment.

Our goal is to see if these single leptons can be accounted for by lepton pairs. (We actually study only muons -- there could be different sources of electrons.) We obtain the pair contribution to the inclusive single-muon yield by measuring the differential cross-sections for all μ-pairs, and then integrating over one muon in the pair. The conclusion, as described below, is that our measured μ-pairs at 150 GeV are sufficient to explain the prompt single muon measurements in the kinematic range of our experiment. When our 225 GeV data have been completely analyzed, they should give an even more comprehensive measurement of the pair contribution to the single-μ yield, because of greater statistical power and because of the wider range of acceptance for the higher momentum beam.

Before discussing the experiment in detail, it seems appropriate to define the variables of μ-pair production. Table I shows the variables we use, as well as the range of each accepted by the spectrometer. It is seen that we have virtually complete coverage for all μ-pairs produced in the forward hemisphere in the center of mass system.

Table I

Variables to Describe the Production of μ-Pairs

Variable	Acceptance
$M^2_{\mu\mu} \equiv (p_+ + p_-)^2$	.211 GeV < $M_{\mu\mu} \lesssim$ 12 GeV
$x_F \equiv p^*_{/\!/}/p^*_{/\!/\,MAX} \approx 2p^*_{/\!/}/\sqrt{s}$	$0 < x_F < 1$
$p_\perp \equiv$ Transverse momentum of pair	$0 < p_\perp \lesssim 4$ GeV/c
$\theta^* \equiv$ Helicity angle of μ's from decaying state	$0 < \lvert\cos\theta^*\rvert < 0.8$

EXPERIMENTAL CONSIDERATIONS

To obtain a large acceptance detector for our experiment, we have modified the Chicago-Cyclotron spectrometer, constructed for μ-p scattering experiments by a Chicago-Harvard-Oxford group, whom we specially acknowledge. This detector, located in the muon laboratory at Fermi National Accelerator Laboratory, is fed by a secondary beam from the "neutrino" target. The beam is very long ($\sim$ 1 KM), a good feature for μ-p scattering, but less than optimal for hadron experiments, in that even at 225 GeV/c about 43% of the kaon flux is lost by decays.

For this experiment the highest possible beam momentum is desirable; not only is there more energy available to produce new objects, but the folding forward in the laboratory of the reaction products gives one

a larger detection efficiency for a given magnet aperture. Unfortunately, the pion flux decreases drastically once the beam momentum exceeds roughly half the momentum of the primary protons. This fact determines the maximum useful beam momentum. For our first run, the accelerator operated at 300 GeV, so we chose p_{beam} = 150 GeV, obtaining a π^+/p ratio of $\sim \frac{1}{3}$. Last winter in our second run, when the primary energy was 400 GeV, we put p_{beam} = 225, at which $\pi^+/p \sim \frac{1}{5}$. So far we have used beryllium, carbon, and tin targets, with beams of π^+, π^-, and protons, the intensities being $\lesssim 2 \times 10^6$/burst for protons, $\lesssim 5 \times 10^5$ burst for π^+ and π^-.

The beam was defined by three scintillation counters upstream of the detector, two of which were separated by a dipole magnet to sweep out debris from interactions along the beam. To identify pions and protons individually, three threshold gas Cerenkov counters averaging about 70 meters in length were placed in the beam. The construction was very simple: the existing beam pipes between transport elements were filled with helium gas to a pressure just below the threshold for Cerenkov radiation from protons. (The operating pressure was about .2 atmospheres absolute at 225 GeV/c.) In each counter, light from pions was focussed by a spherical mirror through a quartz window onto an RCA 31000-M phototube, which has excellent ultra-violet sensitivity. Information from the Cerenkov counters was recorded for each event, allowing us to accumulate π^+ and proton data simultaneously. This feature is very desirable in that many systematic effects, such as changes in magnet currents, beam intensity, detector efficiencies, to name a few, cancel out in a comparison of proton-induced and π^+-induced events.

The spectrometer is shown in Fig. 1. Interactions took place when the beam, typically 3cm x 3cm wide, struck the target, usually $\sim$ .25 interaction lengths thick. (The last beam-defining counter is shown as T_3 in the figure.) To detect the rare μ-pair events in the presence of overwhelming hadronic processes, we absorbed the hadrons

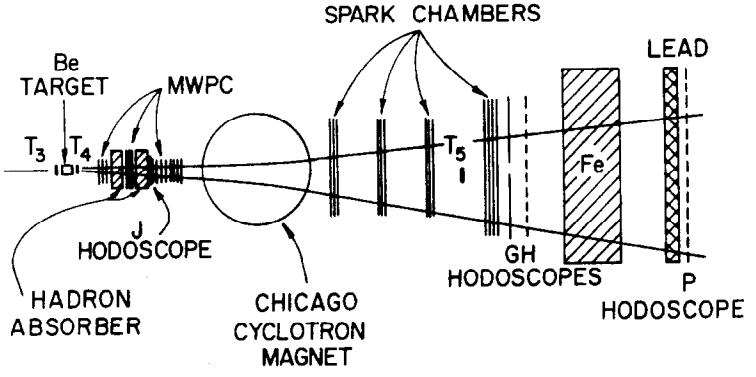

Fig. 1 - The Spectrometer.

before a substantial fraction could decay by placing a 2.2 meter thick steel hadron absorber 1.3 meters downstream from the target. Thus only muons emerged into a large cylindrical magnet (the former Chicago Cyclotron), 2.2 meters in radius and 1.27 meters in gap height. Downstream from the magnet, the muons had to penetrate an additional 2.5 meters of iron, after which they were detected by a large scintillation-counter hodoscope (shown as P in Fig. 1). The apparatus is charge symmetric - hence π^- - induced pairs were measured simply by reversing the polarity of all beam magnets.

The trigger requirements were as follows: 1) One and only one beam particle and no "halo" particles within a time interval of $\sim$ 100 nsec. 2) $\geq$ 2 particles leaving the target, as determined by pulse-height in counter T_4 situated just downstream of the target. 3) $\geq$ 1 particle in the G hodoscope. 4) $\geq$ 2 hits in the P hodoscope. (To reject single μ's accompanied by low-energy electromagnetic showers, the P hodoscope was mounted flush against the downstream side of a 20cm-thick Pb wall. Additional rejection was accomplished by requiring the muon pulses to be in non-adjacent counters.) 5) No count in T_5, a 7.5cm-square counter downstream of the magnet to veto beam muons. 6) For most of the 225-GeV/c running, we also required two non-adjacent hits, either vertically or horizontally, in a hodoscope (shown as J in Fig. 1) placed at the downstream edge of the hadron absorber. This requirement, while reducing the trigger rate from background and low-mass pairs, had a completely negligible effect on the detection efficiency of pairs with masses > 1 GeV.

Approximately 70% of all triggers were clean μ-pair events. The rest, mainly single muons showering into the P hodoscope, were easily eliminated by the analysis. The trigger rate was about 1 in 10^5 beam particles.

The particle trajectories were measured by multi-wire proportional chambers (MWPC) upstream of the magnet, and by wire spark chambers downstream, where instantaneous rates were always lower than 10^5/sec. The MWPC configuration is shown in Fig. 2. The unique feature of our experiment is the chambers in front of the absorber, which were used to measure the directions of the μ's before any significant multiple scattering occurred. These chambers enabled us to obtain good mass resolution, reconstruction efficiency, and background rejection even at the lowest μ-pair masses. For the data reported here, a 4-plane module 55cm x 55cm in area was used, consisting of an X- and a Y-measuring plane, and also a U and a V plane at 45° to X, Y. For data we are still analysing, an additional module with 2X and 2Y planes was used to determine more precisely the vertex in the target. To follow the μ's as they scattered through the absorber, another MWPC module (XYUV) was placed half way through the steel, where the hadron showers had subsided to an extent that the average hit multiplicity was about 4.

To eliminate the effect of the multiple scattering in the absorber from the momentum determination, we remeasured the muon trajectories before they entered the cyclotron magnet. Eight MWPC planes (4X, 4Y), each 1m by 1m in area, were used. To complete the momentum analysis, we measured the trajectories, after they had been deflected by the magnet, with 12 planes of capacitive read-out wire spark chambers 2m by 4m in area, and 8 even larger magnetostrictive planes 2m by 6m. The planes alternated U X X V, with U and V tilted $\pm 15^\circ$ with respect to X, to provide narrow-angle stero "views".

Event reconstruction downstream of the absorber was straightforward, since all the chambers had in general better than 90% efficiency, and only about 10 percent of the events had an extra track, (usually an accidental) through the spectrometer. A typical mass resolution $\frac{\Delta M}{M}$ of $\sim$ 1.6% (standard deviation) was obtained. Accidental

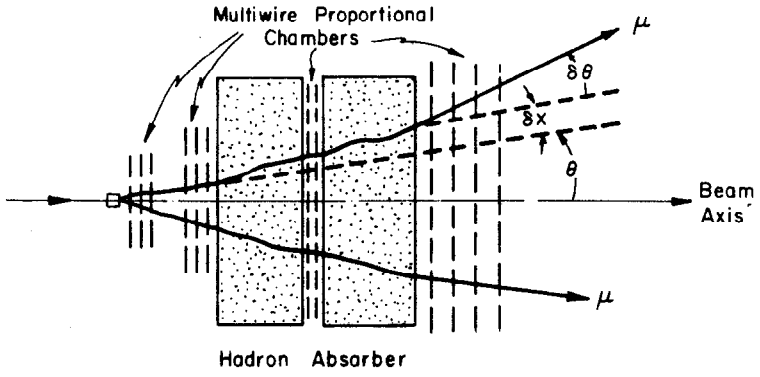

Fig. 2 - Details of the upstream configuration of the detector. Variables are defined in the text.

tracks, as well as any hadrons penetrating the absorber, were eliminated by requiring all μ tracks to point within resolution to struck counters in the P hodoscope. A small contamination from beam muons was eliminated, with no loss of good events, by rejecting any event in which the laboratory momentum of either muon exceeded 88% of the beam momentum.

The most difficult part of the analysis was reconstructing the events upstream of the hadron absorber. The procedure by which the tracks emanating from the target were matched to those downstream of the absorber was tested by a Monte Carlo simulation. Clean μ-pairs were generated and transported through the spectrometer. Hadron tracks and extra hits from real data were superimposed, and the reconstruction program then was asked to find the μ-tracks. For masses above 500 MeV a large and uniform efficiency was obtained for a typical x_F of 0.3. For a mass of 325 MeV the efficiency had only dropped by a factor of 2. The rejection of background from muons produced in the absorber was measured in a similar manner, this time the μ-pairs being generated within the first interaction length of the absorber. We found the rejection power to be greater than 15 at a mass of 300 MeV and to rise sharply with increasing pair mass to at least 100 by 1 GeV. (This factor is independent of the factor of 50 or more against primary interactions in the absorber obtained by demanding at least two particles in the counter T_4 in order to trigger.)

Dead-time in the readout electronics of the MWPC's upstream of the absorber limited their use to maximum incident beam fluxes of $\sim 10^6$/pulse. To study μ-pairs with masses $\gtrsim$ 1 GeV, we were able to turn these chambers off and run with fluxes as high as 3×10^6/burst. This was possible because the MWPC's downstream of the absorber provided good enough direction measurements to separate background μ-pairs produced in the absorber from pairs of 1 GeV mass or more produced in the target. As shown in Fig. 2, because of multiple scattering the trajectory measured by these MWPC's alone differs from the true trajectory by

an angle $\delta\Theta$ and a displacement δx. (A similar situation pertains to the y-coordinate.) Muon pairs produced in the target were separated from those produced in the steel absorber by a χ^2 procedure. Specifically, $\delta\Theta_x$, δx, $\delta\Theta_y$ and δy were varied to minimize the χ^2 of each of the two muon tracks for two assumptions: First, that the μ came from the center of the target; second, that it came from a point 1 interaction length into the absorber. Excellent separation was obtained even for masses below 1 GeV. In the expression for χ^2, the uncertainties in and correlations between $\delta\Theta_x$ and δx, $\delta\Theta_y$ and δy were calculated for the multiple scattering of the absorber, from well-known formulae in Rossi's book.[8] The mass resolution obtained by this method was typically $\frac{\Delta M}{M} \approx .04$, mainly due to the uncertainty in opening angle from multiple scattering. This is perfectly adequate to study the interesting features of both continuum and resonant μ-pairs.

FINAL RESULTS OF μ-PAIR PRODUCTION BY 150-GeV/c π^+ AND PROTONS

In this run, a beryllium target was used with positive beam to study the reactions $(\pi^+_p) + Be \rightarrow \mu^+\mu^- + X$. Figure 3 shows the mass spectra of all μ-pairs with $x_F \geq 0.15$, after correction has been made for the efficiency of the spectrometer. The acceptance calculation assumed a uniform angular distribution in $\cos\Theta^*$ for muons from the decaying pair. For the ρ-ω mass region, our analysis gives a distribution $dN/d(\cos\Theta^*) = 1 - (0.07 \pm 0.24)\cos^2\Theta^*$, consistent with the assumption used in the acceptance. In any case, the only effect of a 1 - standard deviation decay asymmetry would be to produce a uniform 5% change in the over-all acceptance. The measured width of the ρ-ω peak is 100 MeV, narrow enough to indicate a substantial ω contribution.[9]

A striking feature of both pion-induced and proton-induced spectra is the prominent continuum present at very low masses, falling steeply by about 500 MeV. The observation of this continuum has impor-

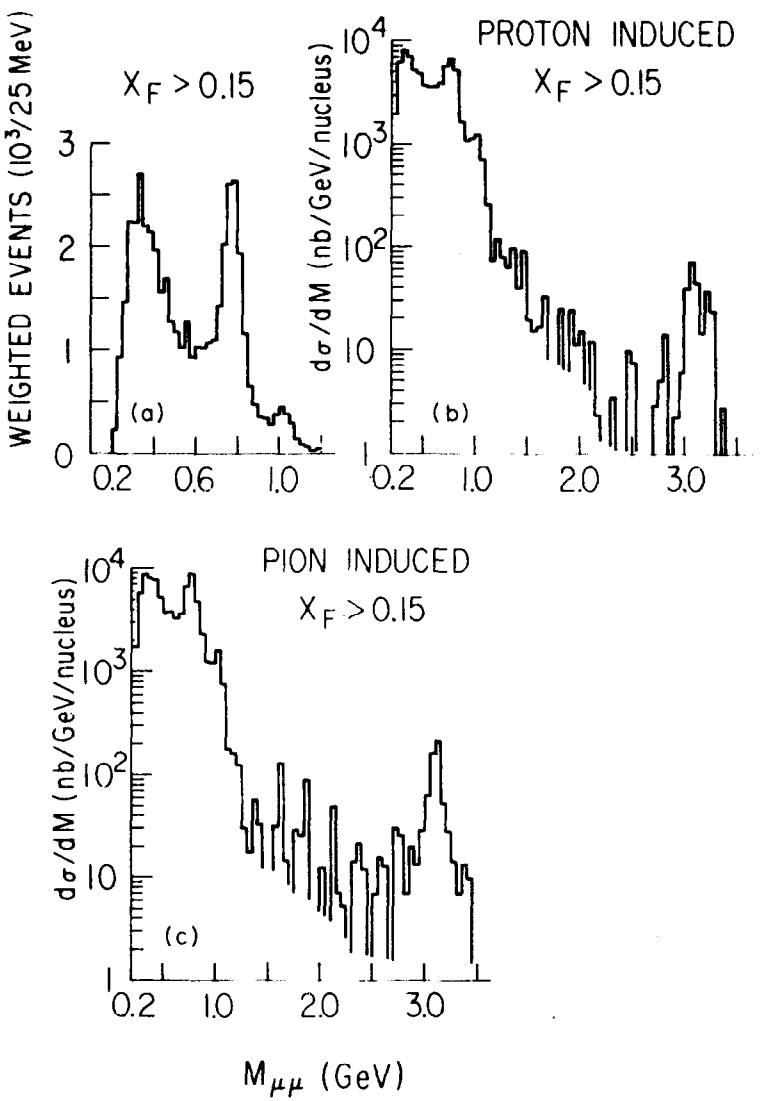

Fig. 3 - Effective Mass Distributions, 150 GeV beam, corrected for detector efficiency, for $x_F > 0.15$. a) Combined π^+ and p induced events with $M_{\mu\mu} < 1.2$ GeV/c^2. b) Proton induced events, logarithmic scale. c) pion-induced events, logarithmic scale.

tant implications for the single direct lepton question, so it is important to be sure that is not caused by background of one form or another. The most obvious source of background, the decays of uncorrelated π's or K's, is eliminated because 99% of the observed pairs have muons of opposite charge ($\mu^+\mu^-$). Secondary processes in the shield are negligible because of trigger and reconstruction rejections. Other sources which have been estimated quantitatively include photoproduction of μ-pairs in target and absorber, secondary ρ-ω production and decay in the absorber, and even the associated production and subsequent decay of $K^+ K^-$ pairs. All background sources combined produce less than 10% of the observed low-mass pairs, so we conclude the signal is real.

There are some very plausible sources of this prompt low-mass continuum. The two most obvious are the Dalitz decays of η and ω, which although they have not been observed experimentally, have reliably calculated branching ratios:[10] $\Gamma(\eta \to \mu^+\mu^- \gamma)/\Gamma(\eta \to \gamma\gamma) = 7.5 \times 10^{-4}$; $\Gamma(\omega \to \pi^o \mu^+\mu^-)/\Gamma(\omega \to \pi^o \gamma) = 5.5 \times 10^{-4}$. If we assumed all the low-mass continuum were due to η decay, the inclusive η production cross-section required would be 11 mb/nucleon, or about 10% of the π inclusive cross-section. This is entirely reasonable - although no measurements have been made at low $p_\perp$ at high $p_\perp$ the ratio of inclusive cross-sections[11] of η and π is $\frac{\eta}{\pi} \sim 0.5$. If we assumed that ρ_o and ω production are equal ($\sigma_{\rho_o} = \sigma_\omega$), then the process $\omega \to \mu^+\mu^-\gamma$ would explain 13% of the continuum.

The dependence of μ-pair production upon the kinematic variables of Table I was studied by first dividing the data into 6 mass intervals. (The dependence upon particle type, π^+ or p, is studied as well.) In Fig. 4 is shown the dependence upon longitudinal momentum, where $Ed\sigma/dx_F$ is plotted vs. x_F. In each mass interval π^+ mesons produce more μ-pairs at large x_F. It appears that the differential cross sections for π^+ and p approach equality at $x_F = 0$. Also, in Fig. 5 is shown the dependence of the differential cross sections upon $p_\perp$, in the form $p_\perp^{-1}\, d\sigma/dp_\perp$.

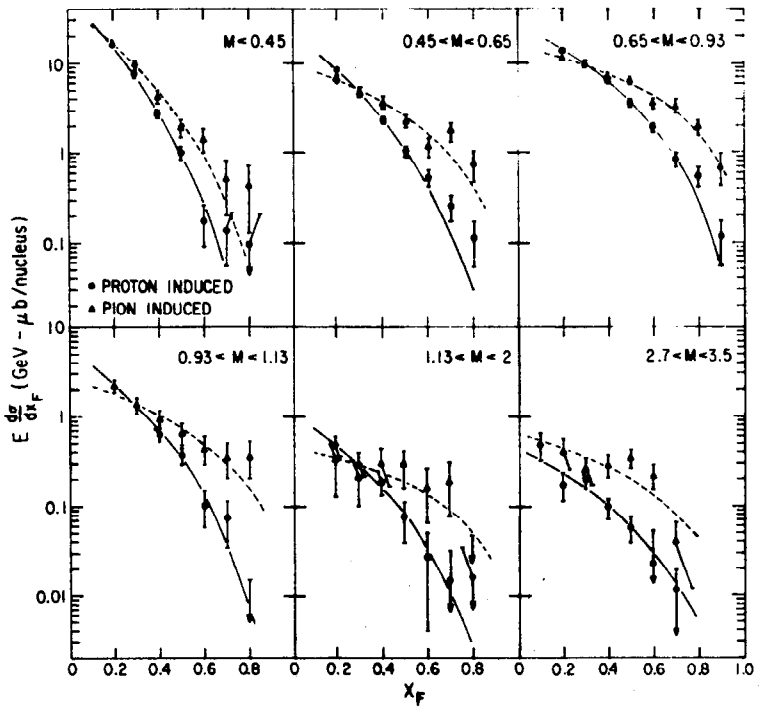

Fig. 4 - Invariant cross-sections vs. Feynman X. The curves are the fits of Table II.

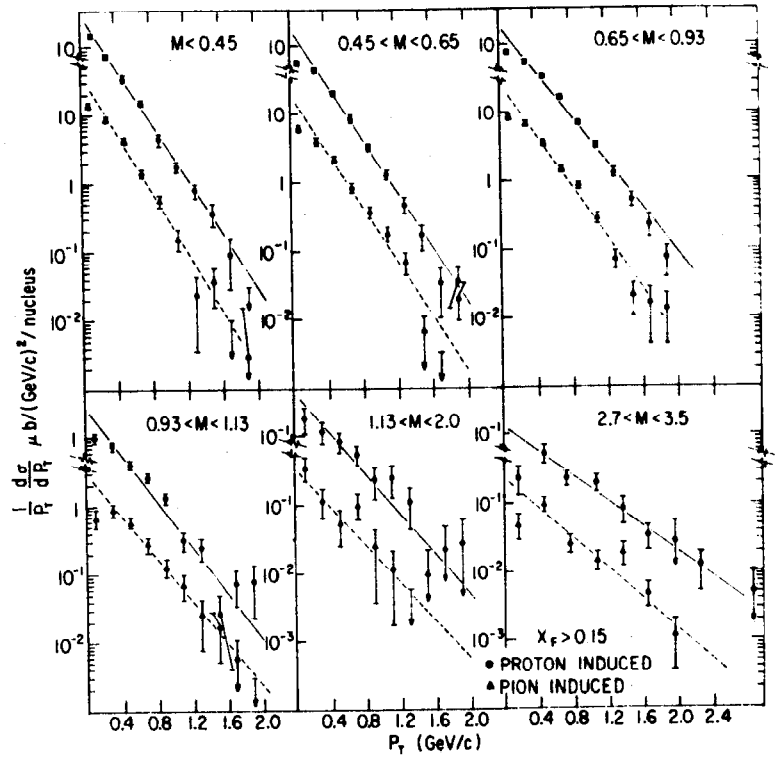

Fig. 5 - Differential cross-section $d\sigma/dp_\perp/p_\perp$ vs. $p_\perp$. The curves are the fits of Table II.

Here no significant differences appear between π^+- and p-induced spectra. The data of Fig. 4 have been fitted to the forms $Ed\sigma/dx_F \propto (1-x)^c$ and $p_\perp^{-1}\, d\sigma/dp_\perp \propto e^{-bp_\perp}$ respectively. The lowest $p_\perp$ bin in Fig. 5 has not been included in the fit. The results of the fits are given in Table II, along with the normalization constant obtained from the parametrization $E\, d^3\sigma/d^3p = A(1 - x_F)e^{-bp_\perp}$. As described in the previous section, the high-mass data, mainly J/ψ production, were obtained without the front MWPC's. We verified that the normalization of this data and the rest, where the MWPC's were used, agreed to within 10%. Other results listed in the table include the cross-sections per nucleon obtained by using the dependence upon the atomic mass number A reported by Binkley et al.:[12] $\sigma(A) \propto A^{0.67}$ for $M_{\mu\mu} < 1.13$ GeV, $\propto A^{0.85}$ for $1.13 < M_{\mu\mu} < 2$, and $\propto A^1$ for $M_{\mu\mu} > 2$ GeV. As will be discussed below, we have confirmed in our 225 GeV experiment the linear A-dependence for high-mass μ-pairs. Finally we give total cross-sections for $x_F > 0$ for the various mass regions. Note that we cannot resolve ρ^0 and ω, so have assumed their production to be equal, as suggested by the width of the peak.

AN APPARENT SOLUTION OF THE SINGLE LEPTON PUZZLE

As mentioned in the introduction to this lecture, an important goal of our experimental program was to find out whether or not μ-pair production can account for the anomalous direct muons observed by numerous authors in p-nucleus collisions. In none of these previous experiments, however, was there a significant acceptance for detecting a second muon, should it have been there. By gathering up all the pairs, then, we can simply see how much they contribute to the yield of single μ's. It has already been estimated by several authors[13] that μ-pairs from the known resonances ρ^0, ω, φ, and J/ψ were insufficient, explain-

Table II - Results of fitting the Lorentz invariant cross-section per Be nucleus to the form $Ed^3\sigma/d^3p = A(1-x_F)^c \exp(-bP_T)$ for different mass regions. The x_F and P_T projections of the data were fit independently. Calculation of the integrated cross-sections is described in the text.

Region	Mass GeV	Source	A nb/GeV^2/c^3	b (GeV/c)$^{-1}$	c	Cross Section /Nucleus $x_F > 0.15$ nb	Cross Section/Nucleon $x_F > 0.15$ nb	$x_F > 0$ nb
			Proton Production					
I	0.21 - 0.45	Continuum	$2.67\pm.63 \times 10^4$	4.63±.15	6.03±.22	1470±300	340±70	1550±620
II	0.45 - 0.65	Continuum	$9.03\pm1.8 \times 10^3$	4.58±.14	4.34±.21	800±160	185±37	620±220
III	0.65 - 0.93	ρ-ω	$4.69\pm.95 \times 10^3$	3.79±.09	2.79±.12	960±190	220±44	510±150
		Continuum	$1.83\pm.40 \times 10^3$			372±75	86±17	200±60
IV	0.93 - 1.13	φ	$1.06\pm.21 \times 10^3$	3.93±.28	4.06±.40	127±38	29±9	83±25
		Continuum	$.55\pm.11 \times 10^3$			66±20	15±5	43±13
V	1.13 - 2.0	Continuum	250±100	3.41±.85	3.78±.80	39±16	6.0±2.5	16±7
VI	2.7 - 3.5	J	36±12	2.08±.26	2.94±.32	14±5	1.6±.6	3.3±1.1
			Pion Production					
I	0.21 - 0.45	Continuum	$2.20\pm.44 \times 10^4$	5.07±.25	4.30±.33	1660±330	383±76	1250±500
II	0.45 - 0.65	Continuum	$4.02\pm.80 \times 10^3$	4.64±.24	1.92±.25	780±160	180±37	370±130
III	0.65 - 0.93	ρ-ω	$3.41\pm.70 \times 10^3$	4.31±.16	1.34±.14	960±190	220±44	370±110
		Continuum	$1.46\pm.30 \times 10^3$			410±82	94±20	160±50
IV	0.93 - 1.13	φ	$4.90\pm1.5 \times 10^2$	3.61±.40	1.73±.44	160±48	37±11	70±21
		Continuum	$1.47\pm.44 \times 10^2$			48±14	11±3	21±6.4
V	1.13 - 2.0	Continuum	89±53	3.2±2.4	1.33±1.0	40±24	6.2±3.7	10±6
VI	2.7 - 3.5	J	81±27	2.57±.36	1.72±.38	35±12	3.9±1.3	6.5±2.2

ing at most about 30% of the single μ's. These estimates were made difficult by the fact that the data was obtained by various experiments differing vastly in almost every respect. By contrast, in our experiment we calculate the single μ yield from all pairs over our large kinematic region, and compare with single-μ measurements from the same target, beryllium. In this way many systematic uncertainties are made negligible.[14]

To include all significant μ-pairs in our calculation, we had to extrapolate our cross-sections down to $x_F = 0$ using a parametrization of the measured data for $x_F \geq 0.15$. First, we assumed the cross-section $Ed\sigma/dx_F \approx d\sigma/dy$ to be flat in the region $0 < x_F < 0.15$. Second, we parametrized the data to the form $d\sigma/dx_F = A(1 - x_F)^c$ and then extrapolated to $x_F = 0$. These two methods agreed to within 10%. If one used the (probably wrong) extrapolation $Ed\sigma/dx_F = A(1 - x_F)^c$ down to $x_F = 0$ one obtains larger cross-sections because the rapidity plateau has been ignored. The parameters used in these fits are given in a recent publication,[15] and are omitted here. The contribution for each of the sources in Table II was calculated separately. The mass dependence of the continuum was parametrized as $\exp(-5M_{\mu\mu})$ within each mass interval. Two independent calculations, one by Monte Carlo techniques, the other by a numerical integration, agreed perfectly.

The sensitivity of our calculation to the $p_\perp$-dependence of the pair spectra was studied also. Because our pair measurements extended out past $p_\perp$ of 2 GeV/c, and virtually all single μ's of $p_\perp \leq 2$ GeV were found to come from pairs within this $p_\perp$ region, we therefore do not depend on extrapolations.

Figure 6a shows our calculated single-μ yield at $x_F = 0$ as a function of $p_\perp$, indicating separately the contributions from vector mesons and the continuum. The π^- cross-section on beryllium,[16] multiplied by 10^{-4}, is shown for reference. It is seen that vector mesons

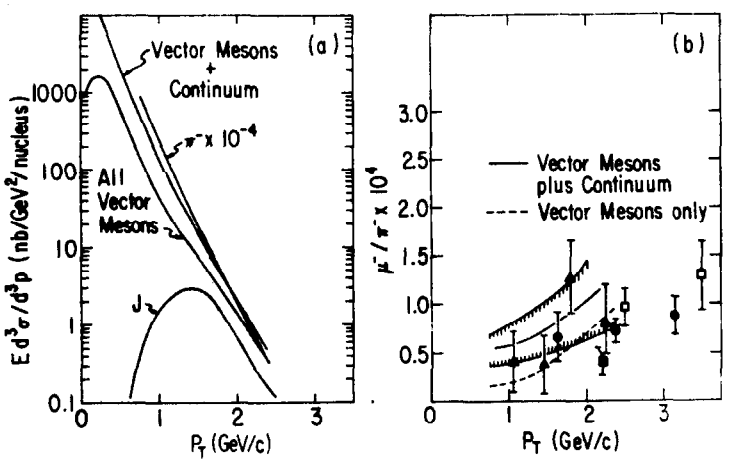

Fig. 6 - a) Invariant cross-sections vs. $p_\perp$ for single μ's produced at $x_F = 0$ by the μ-pairs measured in 150 GeV $\bar{p}$-Be collisions. The π^- cross-section is also shown, scaled by 10^{-4}. b) Comparison of existing single μ data with the μ^-/π^- ratio calculated from our pair measurements. (■ Denotes Ref. 5; ● and □, Ref. 6; ▲, Bintinger et al., Ref. 7).

cannot account for the observed single μ yield (which follows $\pi^- \times 10^{-4}$), especially as $p_\perp$ goes below 2 GeV/c. However, with the addition of the continuum, quite good agreement is seen. Figure 6b shows a comparison of our calculated single μ's from pairs with other experimental measurements of μ^+/π^+ and μ^-/π^-. The agreement is good, indicating that pairs can account for the observed single μ yields. The hatch marks show the uncertainties in the calculation of μ^-/π^-, which are mainly due to the extrapolation of our pair cross-sections to $x_F = 0$. (In our 225 GeV data, the extrapolation, and hence the systematic uncertainty, will be significantly smaller.) The dashed curve in Fig. 6b shows the single-μ contribution from vector mesons alone.

There have also been several measurements of single μ's in the forward direction.[17,18] In these experiments, all μ's are accepted which have $p_\perp \lesssim 600$ MeV/c because of multiple scattering. To compare with them, we have summed, at a given value of x_F, all single μ's with $p_\perp < 600$ MeV/c coming from pairs. The results are shown in Fig. 7. In particular, Fig. 7(b) shows once again that pairs can account for most of the single μ's and that for small values of x_F of the single μ, the continuum becomes the dominant source. An experiment by Kasha et al.[17] has also found that single μ's in the forward direction arise mainly from pairs, but proposes a strong source of μ pairs (in addition to ρ^0, ω decays) with a mass of about 900 MeV. We definitely do not see such a source.

The basic conclusion from our measurements is, then, that μ-pairs can account for the yield of single μ's for $p_\perp \lesssim 2$ GeV at $x_F = 0$, and also in the forward direction. Particularly in the forward direction, the continuum pairs are a significant source of single μ's.

It should be mentioned that there are no single-μ measurements, because of experimental difficulties, in the kinematic region ($x \tilde{<} 0$,

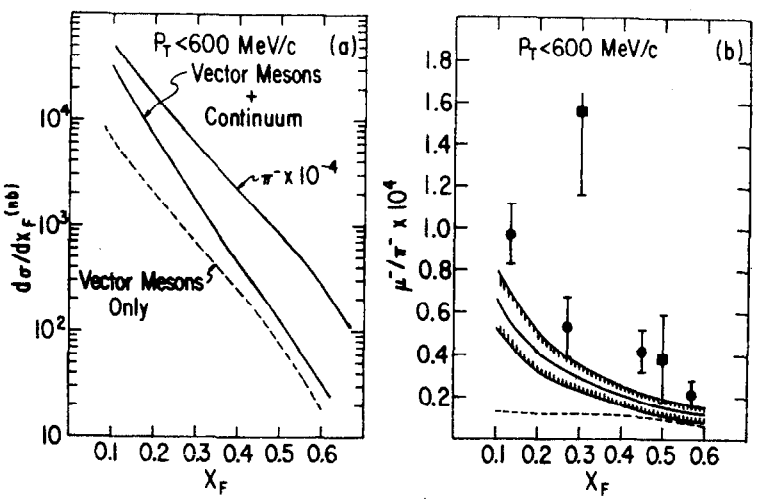

Fig. 7 - a) Single-μ differential cross-section vs x_F in the forward direction (integrated over all $p_\perp$ < 600 MeV/c). b) Comparison of the μ/π ratio measured in Ref. 17 (●) and Ref. 18 (■) with the yield calculated from μ pairs. The solid line and hatch marks show the yield from μ-pairs of all sources. The dashed line is the yield from vector mesons only.

$P_\perp \lesssim 1$ GeV/c) where the largest contribution from decays of charmed particles is expected. Therefore it is still possible that a substantial contribution from the decays $D_o \to K\mu\nu$ exists.[19]

PRELIMINARY RESULTS: μ-PAIR PRODUCTION AT 225 GeV/c

At the higher beam momentum of 225 GeV we have a usefully large acceptance for all pairs produced in the foward hemisphere, and in our second run, which ended this April, we have collected about 20 times as much data as in the 150 GeV sample just described. In addition, we were able to use both positive and negative beams, which allows us to compare π^+ and π^- produced pairs. Except for a one-week run with a tin target to measure the A-dependence, we used exclusively a carbon target to exploit its isoscalar nature in interpreting the comparison of pairs produced by π^+ and π^- mesons. In all the results I shall now present, only the MWPC's downstream of the hadron absorber have been used in the analysis. Therefore I shall discuss only those pairs with masses > 1.5 GeV, where as explained above the upstream MWPC's are not needed. The complete analysis is in progress and will be reported within the next few months.

The general features of the high-mass μ-pair spectra are apparent from Fig. 8, in which all the data analyzed so far, about 85% of our exposure, are shown. We observe a sharply falling continuum out to about 2.7 GeV, where the large peak from the J/ψ sets in. The width of this peak shows the mass resolution of the spectrometer. A shoulder is seen around 3.7 GeV, the mass of the ψ'. In what follows, we shall discuss the properties of these events in detail, comparing and contrasting the resonant and non-resonant μ-pairs. Finally, the results of a search for events having 3 or more μ's will be given.

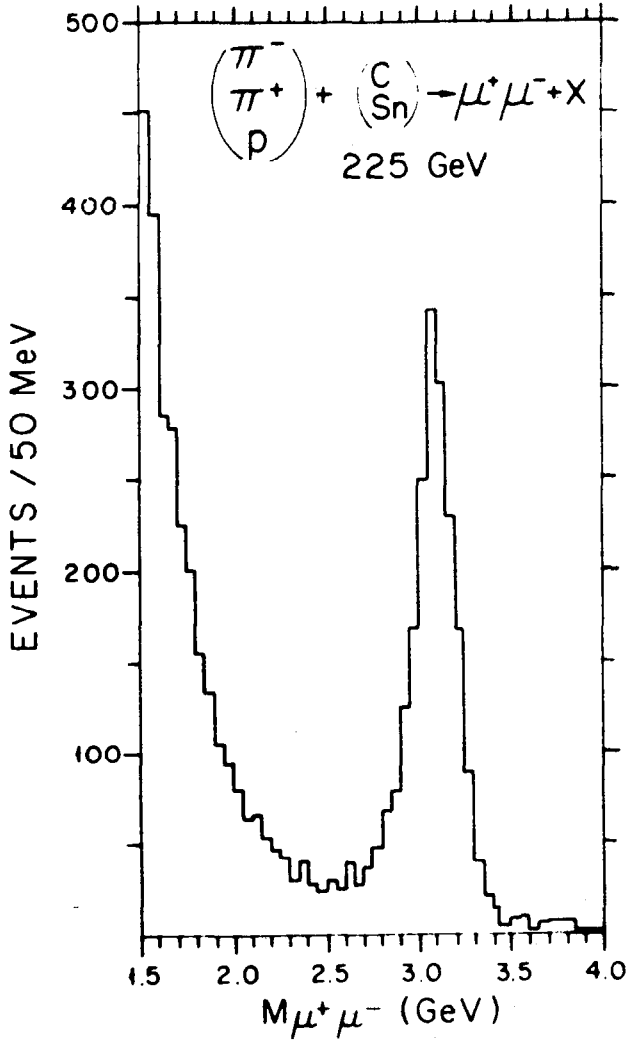

Fig. 8 - Mass spectrum of all $\pi^{\pm}$ and p induced events at 225 GeV, uncorrected for acceptance.

PRODUCTION OF THE J/ψ AND ψ'

The sample of J/ψ events obtained in our 225 - GeV run is the most comprehensive of any experiment to date. The more than 2000 events give adequate statistical power to determine precisely the dependence upon kinematical variables of the differential cross section for J/ψ production, over the wide range of spectrometer acceptance. The use of π^+, π^-, and proton beams gives additional insight into the production dynamics.

The raw data for $M_{\mu\mu} > 2$ GeV are shown in Fig. 9. Part a) shows all p-induced events, part b) all $\pi^{\pm}$-induced events. In the inserts the scale is expanded for $M_{\mu\mu} \geq 3.35$ GeV, and in part c) of the figure all events from $\pi^{\pm}$ and p with masses $M_{\mu\mu} > 3.35$ GeV have been combined. An apparent enhancement appears in all cases at M = 3.7 GeV, which we interpret as ψ' production. Although there are only a small number of ψ' candidates, they can be used effectively to get the approximate level of ψ' production relative to that of the J/ψ. To get as large a sample as possible we have combined carbon and tin data, assuming that J/ψ and ψ' production have the same dependence on A. We have performed a very simple background subtraction assuming a straight-line continuum, obtaining 6 π-induced events, and 4 p-induced events. Using the same x_F- and $p_\perp$-dependence for ψ' as for J/ψ we calculate the average detection efficiency and estimate roughly the ratio of ψ' to J/ψ production, finding:

$$\text{Proton-Induced:} \quad \frac{B\sigma(\psi')}{B\sigma(J/\psi)} \approx 3 \times 10^{-3}$$

$$\text{Pion-Induced:} \quad \frac{B\sigma(\psi')}{B\sigma(J/\psi)} \approx 7 \times 10^{-3}.$$

These values are lower than those reported by Snyder et.al.,[20] who

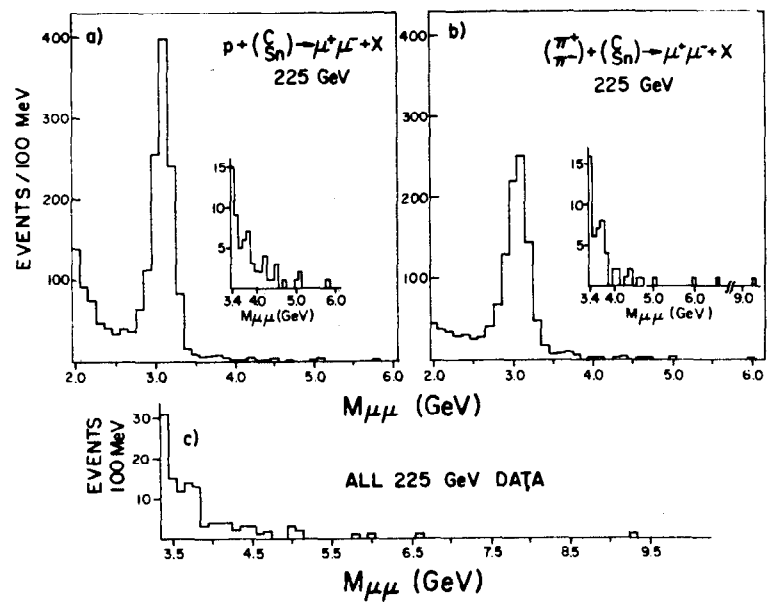

Fig. 9 - Mass distributions uncorrected for efficiency. a) p-induced events, b) π^+ and π^- events combined, c) All events above 3.35 GeV. The inserts in a) and b) magnify the ψ' region.

quote, at $y = 0$ (or $x_F = 0$), for protons on beryllium, at 400 GeV, $\frac{B\frac{d\sigma}{dy}(\psi')}{B\frac{d\sigma}{dy}(J/\psi)} \simeq 0.02$. This suggests that the ψ' cross section is increasing faster with energy than that of J/ψ in the range $20 < \sqrt{s} < 27$ GeV, although more work is needed to settle this issue.

Figure 9(c) shows that only a few events were observed in the mass range from 4 to 10 GeV, where the average detection efficiency was $\gtrsim 12\%$. There is thus no evidence for resonances to the level of this exposure, where each event corresponds to $\sim 10^{-35}$ cm^2/nucleon.

To obtain differential cross sections for J/ψ production, the events in the mass range $2.7 < M_{\mu\mu} < 3.5$ GeV were binned in x_F, $p_\perp$, and $\cos\Theta^*$, and then corrected for the spectrometer acceptance. This efficiency was calculated by a Monte Carlo simulation, which included effects of energy loss, multiple scattering and bremsstahlung, as well as the transport of the particles through the spectrometer to the final hodoscope. To obtain absolute cross-sections we divided by the effective luminosity, corrected for absorption of the beam in the somewhat thick targets. We collected approximately half of the positive-beam carbon data with a 7.5 cm thick target, the other half with a 12.5 cm target. No evidence, either in absolute rate or in energy distribution of the events, was seen of secondary production, so we have combined the data from the two targets in what follows.

The differential cross-sections are shown in Fig. 10 as a function of x_F, in Fig. 11 of $p_\perp^2$, and in Fig. 12, of $\cos\Theta^*$. The cross-sections are expressed as nanobarns/nucleon, using a linear dependence upon the atomic mass number A, as observed by Binkley et. al.[12] in neutron-nucleus interactions. (The result of our own measurement of the A-dependence of total cross-sections is given below.)

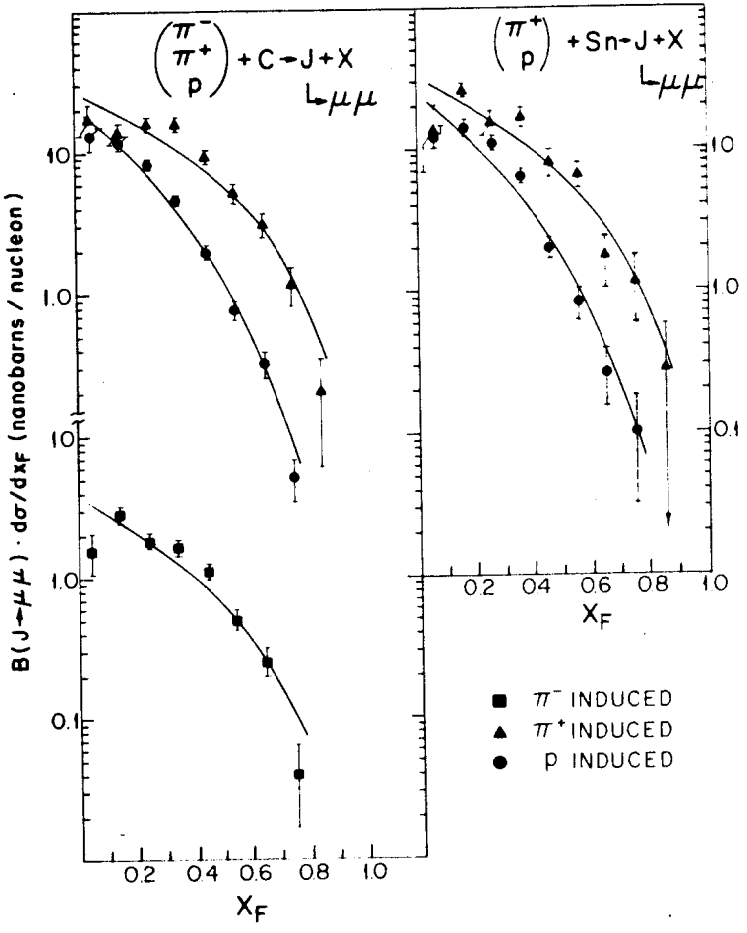

Fig. 10 - Differential cross-sections $B(J\to\mu\mu)\cdot d\sigma/dx_F$ for J production. Fits have been made to the form $(1-x)^b$.

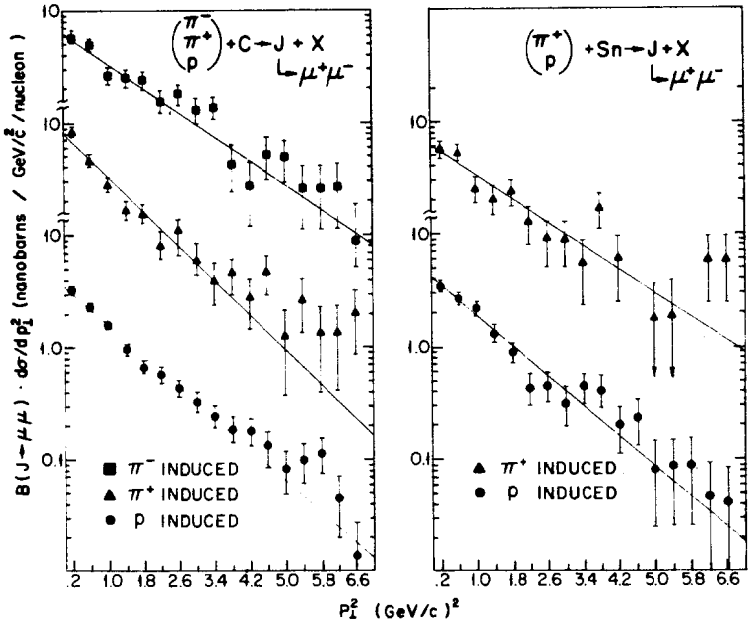

Fig. 11 - Differential cross-sections $B(J\to\mu\mu)\cdot d\sigma/dp_\perp^2$ for J production as a function of $p_\perp^2$. The lines shown are fits to the form $Fe^{-gp_\perp^2}$.

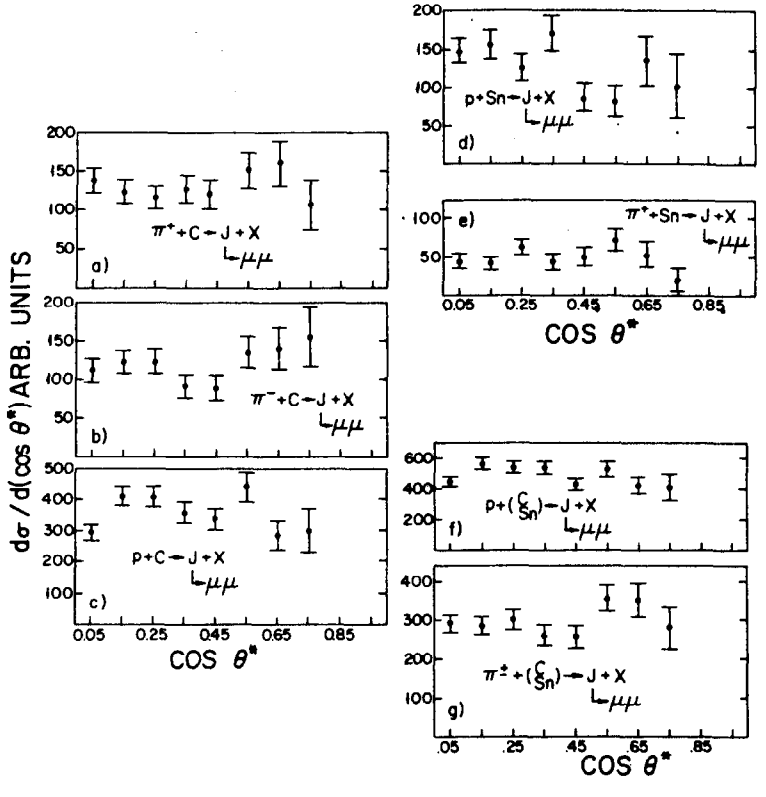

Fig. 12 - Relative differential cross-sections $d\sigma/d(\cos\theta^*)$ for J production.

The x_F-dependence of the cross-section is, qualitatively, independent of target type, and much broader for π-induced events than for those induced by protons. The data have been fitted to the form $\frac{d\sigma}{dx_F} = A(1-x)^b$, as suggested by parton models; the results of the fitting procedure are given in Table IIIa. The fit to the π^--C data is not good, being dominated by one high bin, but aside from that, the fits give a reasonable description. The values for π^+ and p induced events are in good agreement with our earlier results at 150 GeV/c.

Next, the distributions in $p_\perp^2$ were fitted to linear and quadratic forms, respectively:

$$B(J/\psi\to\mu\mu)\cdot\frac{d\sigma}{dp_\perp^2} = Ce^{-dp_\perp} \text{ and } B(J/\psi_{\mu\mu})\cdot\frac{d\sigma}{dp_\perp^2} = Fe^{-gp_\perp^2}.$$

As seen from the table, either parametrization is adequate, and there are no striking differences among the various reactions.

In Table IIIc are given the results of fitting the relative distributions in $\cos\theta^*$ of Fig. 12 to the form

$$\frac{d\sigma}{d(\cos\theta^*)} = A(1+\alpha\cos^2\theta^*).$$

In no case is there compelling evidence of any significant polarization of the J/ψ.

To find more precise values of α, we have therefore combined all proton data (Fig. 12f) and all $\pi^\pm$ data (Fig. 12g), obtaining $\alpha_p = -0.26 \pm 0.19$ and $\alpha_\pi = 0.26 \pm .25$, respectively. Further study is required to see if the small polarization in the proton events is significant.

Values of the total cross-sections (times branching ratio) for J/ψ production are given in Table IV for the range $0 \le x_F \le 1$. The errors have been inflated somewhat arbitrarily because of the preliminary nature of the data, and should be about twice as small in the final analysis. To obtain the cross-section per nucleon, one must know

Table III - Properties of the Differential Cross-section for J/ψ production at 225 GeV.

Note: To obtain cross-sections per nucleon, we have used a linear dependence on atomic mass number.

a) Dependence on x_F: $B \cdot \frac{d\sigma}{dx_F} = A(1-x)^b$ nanobarns/nucleon.

Beam	Target	A	b	χ^2/dof
p	C	22.3±1.8	3.98±0.20	3.6
π^+	C	27.7±3.3	2.62±0.22	3.5
π^-	C	39.1±5.0	2.15±0.16	5.2
p	Sn	25.8±3.4	3.94±0.30	4.1
π^+	Sn	32.2±6.7	2.33±0.32	1.7

b) Dependence on $p_\perp$: (units of $\frac{d\sigma}{dp^2}$ are nanobarns/nucleon/$(GeV/c)^2$)

		LINEAR $B \cdot d\sigma/dp_\perp^2 = Ce^{-dp_\perp}$			QUADRATIC $B \cdot d\sigma/dp_\perp^2 = Fe^{-gp_\perp^2}$		
Beam	Target	C	d	χ^2/dof	F	g	χ^2/dof
p	C	9.1±0.9	1.97±.08	1.8	3.5±0.3	0.80±0.06	1.2
π^+	C	20.9±3.3	2.03±.15	.5	7.9±1.2	0.88±0.12	1.6
π^-	C	13.9±2.2	1.58±.13	1.5	6.2±0.8	0.59±0.06	1.0
p	Sn	9.8±1.5	1.86±.14	1.3	4.1±0.6	0.78±0.09	0.95
π^+	Sn	13.2±4.5	1.56±.25	0.95	6.2±1.4	0.64±0.14	1.0

c) Dependence on $\cos\theta^*_{\mu\mu}$: we have fitted the form $d\sigma/d(\cos\theta^*) \propto (1+\alpha\cos^2\theta^*)$

Beam	Target	α	χ^2/dof
p	C	-0.068±.24	3.14
π^+	C	0.181±.37	0.64
π^-	C	0.36 ±.44	1.3
p	Sn	-0.947±.31	2.0
π^+	Sn	-0.35 ±.45	1.45
p	C+Sn	-0.267±0.19	2.2
π^+,π^-	C+Sn	0.26 ±.25	1.34

Table IV

Total Cross-Sections for J/ψ Production, 225 GeV Beam

Beam	Target	No. of Events	$\sigma(x_F>0)$ nb/nucleon
p	C	868	4.13±0.37
π^+	C	390	8.1 ±1.2
π^-	C	350	9.8 ±1.4
p	Sn	331	4.85±0.7
π^+	Sn	150	9.50±1.4

Note: A linear dependence on atomic mass number has been used

the dependence on atomic mass number A, which is found by comparing the actually measured cross-sections per nucleus for carbon and tin. Assuming the form $\sigma(A) \propto A^{\alpha}$ we find $\sigma_{\pi} \propto A^{1.08 \pm 0.10}$ $\sigma_{p} \propto A^{1.03 \pm 0.15}$. This is consistent with a linear dependence, which we have therefore used in obtaining Table IV.

The dependence of the cross section for J/ψ production on beam energy is quite interesting, as seen in Fig. 13, where $\left.\frac{d\sigma}{dx_F}\right|_{x_F=0}$ and $\left.\frac{d\sigma}{dy}\right|_{y=0}$ for proton-induced events are plotted versus $\sqrt{s} \simeq \sqrt{2M_p E_{Lab}}$. It would be better to plot the total cross-section σ vs $\sqrt{s}$, but most experiments[21] so far have only been sensitive near $x_F = 0$, where there is the simple relationship between x_F and the center-of-mass rapidity y: $\left.d\sigma/dy\right|_{\theta} \simeq (2M_J/\sqrt{s})\left.(d\sigma/dx_F)\right|_{\theta}$. One sees a large increase from threshold up to $\sqrt{s}$ = 16.8 GeV (E_{Lab} = 150 GeV) and then a virtual constancy of $\frac{d\sigma}{dy}$ for $\sqrt{s}$ > 20 GeV. One infers from this a similar behaviour of the total cross section.

The results of Table IV provide a test of charge symmetry in inclusive J/ψ production by π^+ and π^-, and also a measure of the relative effectiveness of π and p in producing J/ψ's. First, we find that the ratio of the π^+/π^- cross-sections is consistent with unity:

$$\frac{\sigma^+(x>0)}{\sigma^-(x>0)} = 0.83 \pm .16.$$

In our final analysis, the error should be about half that given here, because in principle there are only very small systematic errors in this comparison. Also, as will be discussed below, the continuum is smaller for π^+ events than for π^-, an effect which will push the above ratio closer to one. The analysis of this correction is not as yet complete. Secondly, the proton-induced events: averaging π^+ and π^- results, we have, for carbon,

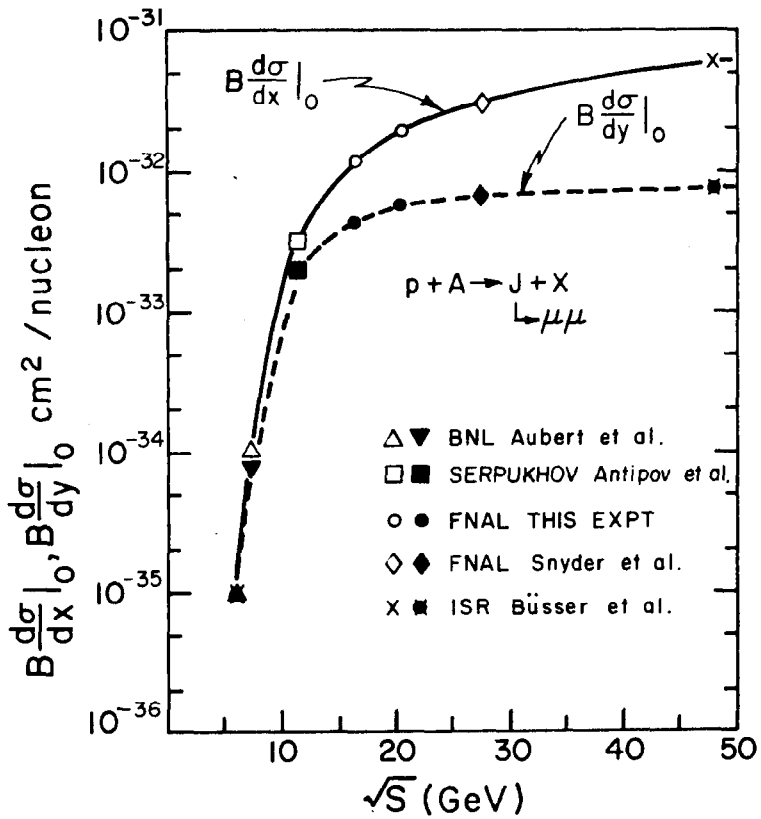

Fig. 13 - Energy dependence of J production cross-sections at $x_F = 0$. The open points show $(d\sigma/dx_F)_0$, the solid points show $(d\sigma/dy)_0$, where y is the center-of-mass rapidity. For experiments using nuclear targets, a linear A dependence has been used to obtain cross-sections/nucleon.

$$\frac{\sigma_p(x>0)}{\sigma_\pi(x>0)} = \frac{4.13 \pm .37}{8.97 \pm .92} = 0.46 \pm .063.$$

Again, this error will be reduced somewhat in the final analysis.

To conclude the discussion of J/ψ production by hadrons, I summarize the most important qualitative features which have emerged:

A dependence	-	linear for both π^+ and p.
x_F dependence	-	independent of target material, much broader for π beams than proton beam.
$p_\perp$ dependence	-	independent of both beam and target material. Much broader than that of lower mass vector mesons.
Beam energy dependence	-	$d\sigma/dy\big\|_{y=0}$ increases sharply from threshold, becoming virtually constant for $\sqrt{s} \gtrsim 20$ GeV. Dependence of total cross section has not been measured, except at Fermilab energy, and must be inferred.
Cross-section ratios	-	For x>0, π^+/π^- consistent with unity, π's give twice as large a cross section as protons.

STUDY OF NON-RESONANT μ-PAIRS

It is very important to learn about the process by which non-resonant, or continuum μ-pairs are produced. For example, the parton models make quantitative predictions for the cross sections, but say little about the transverse momenta expected for the pairs. So far, all previous experiments have used neutron or proton beams, so all the antiquarks are provided by the sea, leading to rather model-dependent predictions for the features of the resulting spectrum. This is the first experiment to use π^+ and π^- beams on an isoscalar target, a particularly attractive experimental situation, in that valence antiquarks are present in the beam. Annihilations of fractionally charged valence quarks in the target with the antiquark in the projectile should then show a charge asymmetry

$$\frac{\sigma(\pi^+C)}{\sigma(\pi^-C)} = 1/4,$$

independent of details of the model. Unfortunately this large asymmetry is diluted by the presence of the isospin-symmetric quark-pairs in the sea. Using recent measurements of structure functions, Altarelli, Brandt, and Cabibbo, [22] and Farrar[23] have estimated the effect of the sea, finding the charge ratio to be close to 1 at low pair masses, and then to decrease slowly to the value 1/4 as M^2/s increases. For example, at $M_{\mu\mu} \simeq 2.5$ GeV the ratio is predicted to be ~ 0.6.

In four mass intervals below the J/ψ and two at higher masses, we compare the production of dimuons by π^+ and p and by π^+ and π^- on carbon. Figures 14a and 14b show these cross-section ratios and equivalent ratios for the J/ψ mass region. Of particular interest is the π^+/π^- ratio, which appears to change from approximately unity at low mass to about .25 at the highest masses, except for the J/ψ mass region, where it returns, within errors, to unity. Within the limited statistics, this behaviour is in agreement with the prediction of Ref. 22.

When π^+ and proton induced pairs are compared, on the other hand (Fig. 14a), the J/ψ and neighboring continuum regions do not show any significant difference. In both Figs. 14a and 14b the ρ_o-ω and φ mass regions are also shown, where a charge ratio of 1 is expected from isospin conservation.

Other features of the data have been studied in a preliminary manner by selecting three mass regions having significant numbers of events, in a region relatively free of resonance signal. The regions

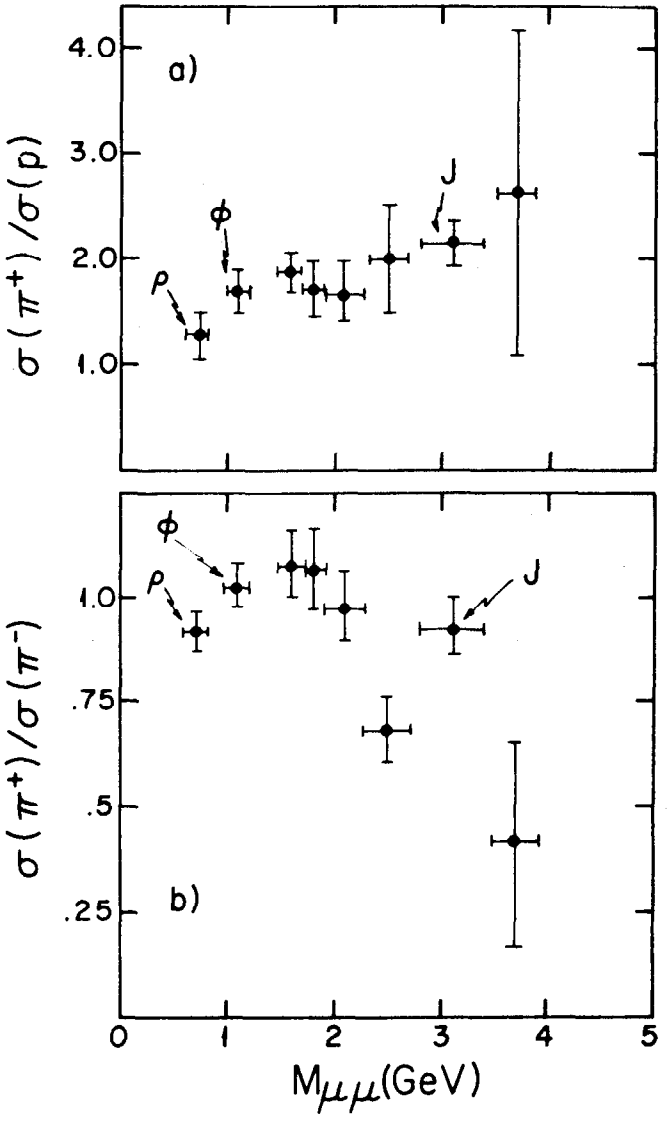

Fig. 14 - Ratios of total cross-sections for $x_F > 0$ vs. pair mass.

are: 1.5-1.9 GeV/c^2, 1.9-2.3 GeV/c^2, and 2.3-2.7 GeV/c^2.

Figure 15 shows the dependence of the cross-section in these bins on the variable $x_F \simeq \frac{2p_{//}^*}{\sqrt{s}}$, for p, π^+, and π^- incident on carbon. The basic feature of all these distributions, that the π-induced events have a slower fall-off with increasing x_F than those of p-induced events, is very similar to what we have observed in production of the resonances ρ, ω, φ, and J/ψ. The data have been fitted to the form $B \cdot d\sigma/dx_F = A(1 - x_F)^b$; the best fits, of somewhat limited statistical significance, are summarized in Table Va.

Figure 16 illustrates the dependence of the differential cross-sections $d\sigma/dp_\perp^2$ upon the transverse momentum $p_\perp$ of the dimuon. Exponentials both linear and quadratic in $p_\perp^2$ have been fit to these spectra, the results appearing in Table Vb. The quadratic fits are shown in the figure, although either hypothesis gives an adequate fit.

Figure 17 shows an interesting feature of μ-pair production. We have plotted the average transverse momentum $\langle p_\perp \rangle$ as a function of the dimuon mass, for π^+ and p-induced events. (The analysis of the π^- sample is not yet completed.) No discontinuity at all is apparent between $\langle p_\perp \rangle$ of resonant and non-resonant dimuons. Instead, one sees a slow, smooth increase of $\langle p_\perp \rangle$ with increasing dimuon mass. As described in Professor Lederman's talk, within rather large uncertainties this smooth increase continues out to μ-pair masses of 10 GeV.

We have also studied the differential cross-section as a functions of $\cos\theta^*$; a hint of polarization of the form $1 + \cos^2\theta^*$ is suggested by the data, but the statistics are insufficient for a firm conclusion to be reached.

In an upcoming experiment to run at Fermilab in Spring '77, we shall measure these cross-sections to a level of 10^{-37} cm^2/event, approximately 100 times more sensitively than the present exposure. Be-

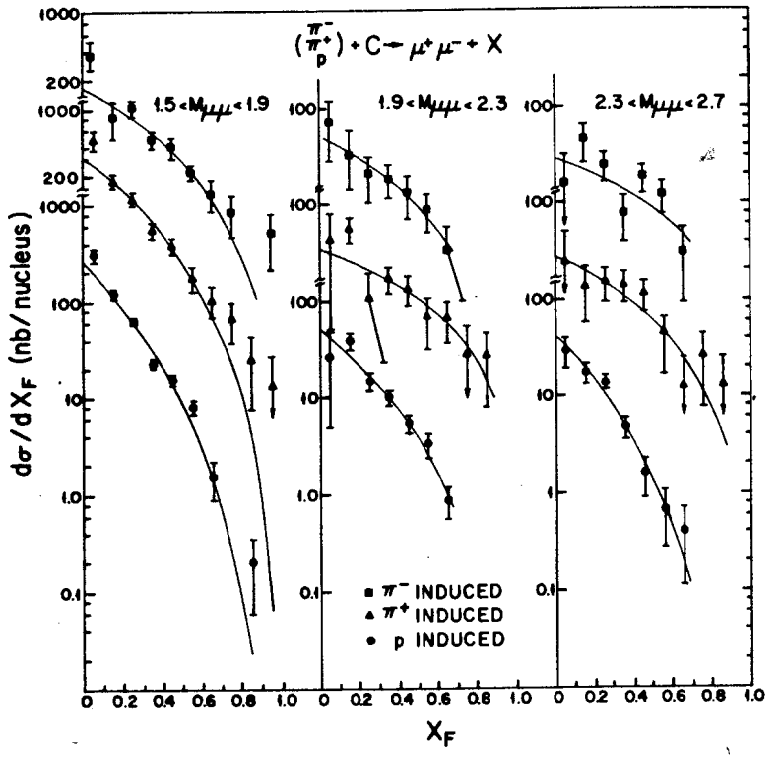

Fig. 15 - Dependence of pair cross-sections on x_F for various intervals of pair mass.

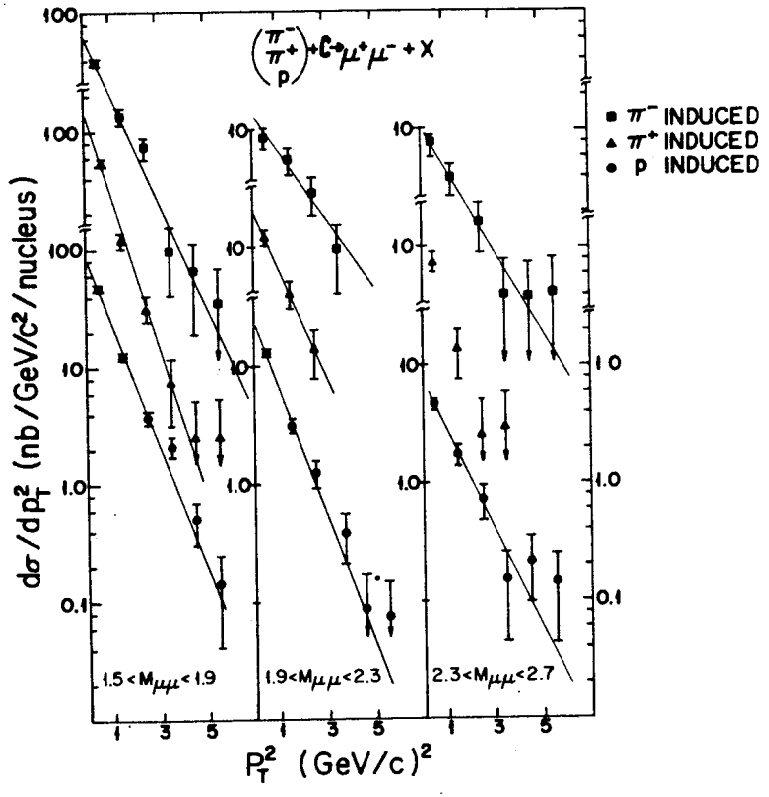

Fig. 16 - Differential cross-section vs. $p_\perp^2$ for various intervals of pair mass.

Table V - Fits of Differential Cross-sections of continuum μ-pairs.

$$\begin{pmatrix} p \\ \pi^+ \\ \pi^- \end{pmatrix} + C \rightarrow \mu^+\mu^- + X$$

Note: All cross-sections are per Carbon Nucleus.

a) Dependence on x_F: $B \cdot \frac{d\sigma}{dx_F} = A(1-x)^b$ nanobarns/nucleon

Beam	Mass Region	A	b	χ^2/dof
p	1.5-1.9	260±32	4.9±.3	3.4
	1.9-2.3	51±21	3.8±.7	.82
	2.3-2.7	45±11	5.2±.6	.86
π^+	1.5-1.9	321±92	3.5±.6	1.4
	1.9 2.3	34±18	1.7±.8	.88
	2.3-2.7	28±29	2.3±1.6	.63
π^-	1.5-1.9	170±78	2.5±.7	1.5
	1.9-2.3	52±23	2.4±.8	.16
	2.3 2.7	29±11	1.7±.7	1.7

b) Dependence on p_T: (units of $\frac{Bd\sigma}{dp_T^2}$ are nanobarns/(GeV/c^2)/nucleus)

		Linear $B\cdot d\sigma/dp_T^2 = Ce^{-dp_T}$			Quadratic $B\cdot d\sigma/dp_T = Fe^{-gp_T^2}$		
Beam	Mass Region	C	d	χ^2/dof	F	g	χ^2/dof
p	1.5-1.9	381±30	2.9±.1	3.9	84±4	1.2±.05	1.9
	1.9-2.3	110±33	3±.3	.75	24±3	1.3±.1	.55
	2.3-2.7	25±14	2.4±.5	.85	7.5±1.2	.98±.12	.75
π^+	1.5-1.9	586±106	3.3±.2	.88	110±11	1.4±.1	.3
	1.9-2.3	66±30	2.4±.5	.3	21±6	1.1±.25	.001
	2.3-2.7	89±60	3.5±.8	.44	17±6	1.7±.4	.5
π^-	1.5-1.9	269±60	2.7±.2	2.7	67±7	1.1±.1	1.1
	1.9-2.3	28±12	1.6±.4	1.2	13±3	.65±.15	.5
	2.3-2.7	32±18	2.0±.5	.5	11±3	.81±.18	.3

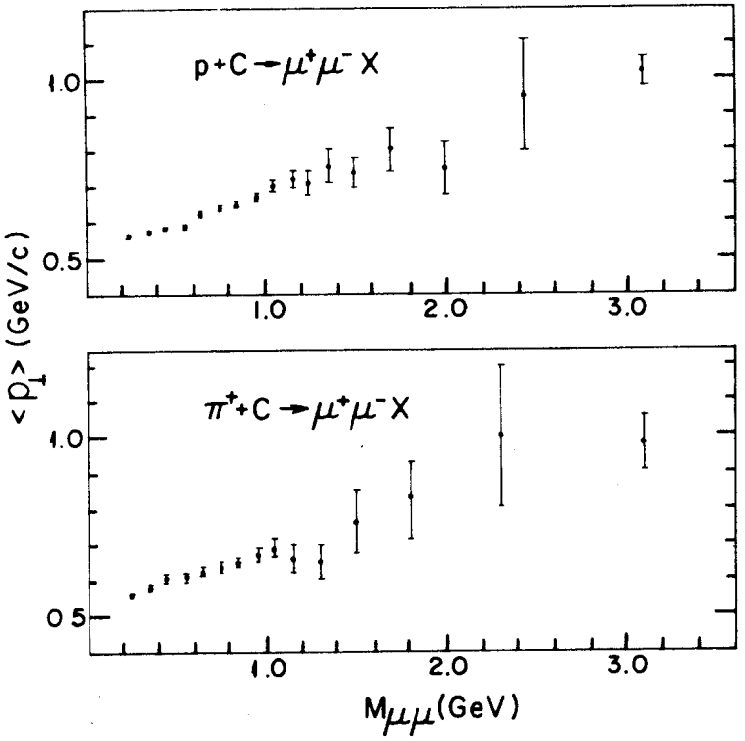

Fig. 17 - Average $p_\perp$ of muon pairs vs. pair mass, uncorrected for efficiency.

cause the results of our experiment and others are so far very suggestive of quark-antiquark annihilation, one should perhaps take seriously another prediction, that the π^-/p cross-section ratio for $\mu\mu$ production rises sharply with increasing M^2/s, reaching a value > 100 for $M_{\mu\mu} = 10$ GeV. Our new run will test this prediction conclusively.

SEARCH FOR MULTIMUON EVENTS

The efficiency of the spectrometer for the detection of an extra muon accompanying a μ-pair is very large. Such extra muons are expected if, for example, the J/ψ is produced in pairs, or in association with charmed mesons, as is required by the Okubo-Zweig-Iizuka rule.[24] We have searched all our data - about 850,000 μ-pair events in all - and 2100 J/ψ events for any having extra muons. After performing cuts on the data to reduce to a negligible level the backgrounds from secondary interactions and muons in the halo around the beam, we were left with 1229 three-muon events, and one event with 4 muons, the latter being a double $\rho \to \mu\mu$ event. Only 2 of the 2100 J/ψ events had an extra μ. This level of extra muons is completely consistent with the contamination expected from pi decay, namely $\simeq 2 \times 10^{-3}$. We thus conclude there is no evidence at this level for extra muons accompanying either high or low mass pairs.

The computation of cross section limits is made simple by the fact that the major losses of single muons in the forward hemisphere are due to the 8 GeV range requirement imposed by the iron muon identifiers, to the geometrical aperture of the proportional chambers, and to a halo-suppressing requirement in the analysis that all muon laboratory momenta must be less than 100 GeV/c. The first eliminates an elliptical segment in the $x_F - p_\perp$ plane with intercepts at Feynman $x_F = .035$ and $p_\perp = 740$ MeV/c. The last eliminates muons with $x_F > .43$. Within these boundaries our acceptance is more than 50%. The cross section limit for J/ψ events accompanied by an extra muon is $\frac{\sigma(J + \mu)}{\sigma(J)} < 2.5 \times 10^{-3}$ with 90% confidence. This result rules out, for example, pair production of J/ψ's to a limit of 3.5%, within the virtually complete acceptance for detecting at least one of the 2 muons from the second J/ψ. The limits on associated production of charmed particles are of course dependent on the branching ratio assumed for their muonic decays, as well as the model of production. Eventually we shall calculate limits for the popular models, but for now I simply state that the limit for a charmed particle accompanying a J/ψ is $\lesssim \frac{5 \times 10^{-3}}{BR(\text{meson} \to \mu)}$, which for the usual assumption of about 0.1 for the branching ratio, says that $\lesssim 5\%$ of J/ψ's are produced in association with charm. Similar limits over a somewhat more restricted acceptance have been reported for neutron-nucleus collisions at Fermilab.[25]

CONCLUSION AND ACKNOWLEDGEMENT

The experimental results on dimuon physics are becoming quite precise. They are generally in agreement with the parton model, but there is a disturbing feature in that the high average transverse momenta are not easily explained. It is also puzzling that the differential cross sections of resonances and continuum are so similar in their dependence on the kinematic variables. Finally, we all wish to know why there is no evidence of muonic decays of charmed particles, either as evidenced in copious yields of single μ's or in extra muons accompanying J/ψ events.

I wish to thank Professors Gilman and Leith for their kind invitation and hospitality. It is also a pleasure to acknowledge the staff of Fermilab and particularly the members of the Chicago-Harvard-Oxford Illinois μ-scattering group who have provided the spectrometer for our work.

REFERENCES

* This research was performed at Fermilab and supported in part by the NSF and ERDA.

1 The authors of this work are members of the Chicago-Princeton (II) collaboration: K.J. Anderson, G.G. Henry, J.E. Pilcher, E.I. Rosenberg, J.G. Branson, K.T. McDonald, G.H. Sanders, A.J.S. Smith, and J.J. Thaler. In addition G.E. Hogan and C. Newman participated in the analysis of the 225 GeV data. Preliminary results were reported in K.J. Anderson et al., Phys. Rev. Lett. 36, 237 (1976).

2 J.J. Aubert et al., Phys. Rev. Lett. 33, 1404 (1974); J.F. Augustine et al., op cit, p. 1406.

3 S.D. Drell and T.M. Yan, Phys. Rev. Lett. 25, 316 (1970).

4 G.R. Farrar and S.C. Frautschi, Phys. Rev. Lett. 36, 1017 (1976).

5 V.V. Abramov et al., reported in the Proceedings of the 17th Int. Conf. on High Energy Physics, London, 1974, p. V-53.

6 J.P. Boymond, et al., Phys. Rev. Lett. 33, 112 (1974); J.A. Appel et al., Phys. Rev. Lett. 33, 722 (1974).

7 F.W. Büsser et al., Phys. Letters 53B, 212 (1974), D. Bintinger et al, Phys. Rev. Lett. 35, 72 (1975).

8 B. Rossi, High Energy Particles, Prentice Hall, 1956.

9 The ρ_o-width observed in $\rho \to \mu\mu$ decay is narrower than in $\rho \to \pi\pi$ decay because of the photon propagator in the former decay.

10 C. Jarlskog and J. Pilkuhn, Nucl. Phys. B1, 264 (1967); C. Quigg and J.D. Jackson, LBL Report UCRL-18487; C.H. Lai and C. Quigg, FNAL Preprint FN-296 (1976).

11 F.W. Büsser et al., Phys. Letters 55B, 232 (1975).

12 M. Binkley et al., Phys. Rev. Lett. 37, 574 (1976).

13 M. Bourquin and J.M. Gaillard, Phys. Letters, 59B, 191 (1975); J.W. Cronin, in Proceedings of the International School of Subnuclear Physics, Erice, 1975.

14 For example, the effects of the peculiar A-dependence of high p_t processes reported by Cronin et al., Phys. Rev. D11, 3105 (1975) are avoided.

15 K.J. Anderson et al., Phys. Rev. Lett. 37, 803 (1976); K.J. Anderson et al., Phys. Rev. Lett. 37, 799 (1976).

16 T. Eichten et al., Nucl. Phys. B44, 333 (1972); W.F. Baker et al., Phys. Letters 51B, 303 (1974).

17 L.B. Leipuner et al., Phys. Rev. Lett. 35, 1613 (1975); H. Kasha et al., Phys. Rev. Lett. 36, 1007 (1976).

18 D. Buchholz et al., Phys. Rev. Lett. 36, 932 (1976).

19 This was emphasized by P.A. Piroué, Division of Particles and Fields Meeting, Upton, L.I., October 1976.

20 H.D. Snyder et al., Phys. Rev. Lett. 36, 1415 (1976).

21 F.W. Büsser et al., Phys. Letters, 56B, 482 (1975); Y.M. Antipov et al., Phys. Letters 60B, 309 (1976); also References 2 (Aubert et al.) and 20.

22 G. Altarelli et al., Nucl. Phys. B92, 413 (1975).

23 G.R. Farrar, Nucl. Phys. B77, 426 (1974).

24 A. Okubo, Phys. Letters, 5, 165 (1963); G. Zweig, CERN Report TH-412 (1964); I. Iizuka, Prog. Theor. Phys., Suppl. No. 37-38, 21 (1966); D. Givers, Phys. Rev. D11, 3253 (1975); R.M. Barnett and D. Silverman, Phys. Rev. D12, 2037 (1975).

25 M. Binkley et al., Phys. Rev. Lett. 37, 578 (1976).

CONVERGENCES

Sheldon L. Glashow*

Lyman Laboratory of Physics

Harvard University

Cambridge, Massachusetts 02138

These are scattered remarks concerning what is happening *to* (not, *in*) elementary particle physics. New developments are unfolding with unprecedented speed, so that we do not even attempt to give a comprehensive review at this time. I shall talk mostly about charm, both its phenomenology and its impact on our belief in quarks, chromodynamics, and unified theories. Beneath the newsworthy experimental discoveries of the last two years lies a quieter and more profound theoretical development: the emergence of a theory of particle physics. My closer collaborators in what I shall discuss include:

B. J. Bjørken	DORIS	L. Maiani
BNL	FNAL	H. D. Politzer
CERN	H. Georgi	SPEAR
A. De Rújula	J. Iliopoulos	S. Weinberg

*Research supported in part by the National Science Foundation under Grant No. MPS75-20427.

I. POETIC INTRODUCTION

Hark, Hark the Quark

by Judith R. Goldsmith

A revolution's brewing,
But there's no cause for alarm,
It's happening in the microworld
And simply fraught with *charm*.

The charm's the fourth quark
At the heart of the matter,
The quark is very basic to the
Structure of the latter.

Up quarks, down quarks,
Strange quarks, antiquarks:
They have yet to see one,
Which doesn't mean, of course,
That there cannot be one.

The quest for the quark
Poses questions galore:
But I find it quite disarming,
If not positively *charming*
It's revolution - happily not war!

Anti-Nuclear Article

by Allen Herzog

I deplore articles
On nuclear particles.

I see no reason
To extol the meson.
Colored or albino,
I dislike the neutrino.

I never carry on
With the bare baryon,
Nor can *I have it on*
With the glum graviton.

I remain in the dark
On the charms of the quark,
Nor am I adept on
The loves of the lepton.

Strangeness and charm
Cause me alarm.
I deplore articles
Pro- or anti-particles.

Author's Reply

Don't pick on small particles
You find in my articles.
My next theory, if true,
Has some bigger than you!

II. A SIMPLE AND ELEGANT THEORY OF ELEMENTARY PARTICLE PHYSICS IS EMERGING

It is now recognized by many that the fundamental interactions - weak, strong and electromagnetic - arise from local symmetry of the underlying Lagrangian. All these interactions are simply generalizations of quantum electrodynamics in the direction first pointed out by Yang and Mills. Strong interactions result from an exact color SU(3) symmetry; the others from a local symmetry group which is spontaneously broken by the Higgs mechanism. The resulting system is renormalizable, and lies within the framework of relativistic quantum mechanics established for us by the masters of the last generation.

The local symmetry group of strong interactions is SU(3), and the dynamical variable relevant to it is called *color*. Fundamental fermions are of two kinds: color triplets called *quarks*, which are the constituents of all hadrons; and color singlets called *leptons*, which are immune to strong interactions.

Exact color SU(3) symmetry - also known as *quantum chromodynamics* - is expected to display the complementary attributes of *infrared slavery* and *ultraviolet freedom*. According to the former, the force between quarks does not decrease with distance, so that constituent quarks cannot be isolated from hadrons of which they are part. Indeed, no color-bearing system, neither gluons, nor diquarks, etc., is isolable. Truth to tell, the irrevocable confinement of quarks by QCD has not yet been proven beyond reasonable doubt. But, we feel that this will be shown. Time, and the hard work of my friends, will tell.

Assuming confinement, we can milk QCD for quite a lot. The remarkable successes of non-relativistic SU(6) in describing the systematics of hadron spectroscopy are now comprehensible. Color, of course, solves the statistics problem, and QCD explains the absence of colored hadron states. Moreover, it seems that the quark confining force is necessarily dominantly spin-independent, and independent of the identity of constituent quarks as well. Because the three commonly found quarks are crudely degenerate in mass, we obtain an approximate SU(6) symmetry. One minor triumph of the model is the explanation of the $\Sigma\Lambda$ mass splitting, and we shall describe it anon.

On the other hand, in the limit of short distances or high energy, the strong interactions become weak. Thus may we understand the scaling behavior observed in deep-inelastic lepton scattering at not such asymptotic energies. Recent work by De Rújula, Georgi, and Politzer demonstrates the power of QCD. They now understand the local duality of Bloom and Gilman, the precocious onset of scaling, and the anticipated departures from exact scaling. Paraphrasing Leon Lederman, the proton really does appear to be like three free pointlike jewels threaded on an immaterial yet unbreakable string.

Color is not the dynamical variable seen by weak and electromagnetic interactions; it is rather quark and lepton identity. (Quark identity is often called *flavor*. Were it odor, unified weak and electromagnetic interactions could be known as the Osmic Force.)

The local symmetry group of weak and electromagnetic

forces is known to be *at least* SU(2) × U(1). Whatever the group, it is spontaneously broken down so that only a U(1) subgroup is left unbroken. The gauge field corresponding to this U(1) subgroup is the massless photon. The others - at least three in number - are the massive intermediaries of weak interactions. Neither the $W^{\pm}$ nor the predicted Z^0 have yet been seen. But, the effects of the latter (neutral currents) have become, over the past two years, almost as familiar as those of the former.

Our gauge theory of elementary particle interactions must give sensible predictions, and this seems to require that it is renormalizable. A necessary requirement for this is that the weak and strong interactions do not get into one another's way. This is neatly satisfied by the fact that the two interactions, metachromatic and isochromatic if you will, act on totally distinct dynamical variables. Another triumph of QCD, aside from its phenomenological successes, is that it satisfies this rather unusual constraint. (Compare, for example, Sakurai's antique, outmoded but prescient vector meson theory. He also believed in a local SU(3) symmetry but where ρ, ω and K^* were the gauge fields. His strong local symmetry was *flavor* SU(3), and it would simply leave no room for renormalizable weak interactions.)

Another necessary condition for the theory to be renormalizable is that the currents coupled to gauge fields be free of triangle anomalies. In the conventional context, this means that the number of weak pairs of quark flavors (like u,d) must equal the number of lepton pairs (like ν,e). Thus, the existence of muons and muon-neutrinos compels the existence of strangeness and charm: the quark pair (c,s). Charm, strangeness, and muons are parts to the same puzzle.

The GIM arguments for charm provide independent arguments for the existence of a fourth quark with specified weak and electromagnetic couplings. This line of thought is more phenomenological: charm is needed to ensure that the weak neutral current as well as order α radiative corrections to it conserves strangeness. Observed $\Delta S = 0$ neutral currents are a common meeting ground for both theories of charm and of Z^0. Even before the discovery of the J/ψ, it was clear that theorists were on the correct track. Elaborate theories that could do without charm could be constructed (Georgi suggested one), but they were ugly as sin. Their very existence served as a foil to make one believe even more strongly in the simplicity of charm.

I have sketched the simple model of elementary particle physics that has quietly emerged in recent years and now dominates our discipline. Of course, there is and there will remain much to be done. There is the formidable problem of hadron-hadron scattering, perhaps only somewhat more fundamental than the problem of scattering of two lithium atoms. There are connections to be made with Regge, with duality, with bag theories, etc. But, at last, most theorists can agree that they are attacking the same problems with the same fundamental theory: they differ only in method. Hadron physicists (or, quark chemists) can now find themselves in a position analogous to biologists, where the problem is life and the theory is quantum chemistry. There is room for immense technical variety only in what goes between.

At a more fundamental level, the theory is wide open: why are there only color singlets and triplets? How many are there of each? Can we understand their masses, or compute the Cabibbo angle? How do we account for CP violation and gravity? But, these questions all relate to a more basic discipline than what has been called elementary-particle physics in recent decades. Hadron physics is no more ultimate than its predecessor, nuclear physics; but a new frontier is now revealed.

III. CURRENT EVENTS

1. *The Charge of Charm*

a. *For the GIM mechanism to succeed* to order G, Q(c) = 2/3 or Q(c) = -4/3. For it to work to order αG, only Q(c) = 2/3 is acceptable.

b. *The electromagnetic decay width of J/ψ* comes out just about right with Q(c) = 2/3. For other *a priori* acceptable possibilities: -1/3, 5/3, -4/3, it comes out wrong by at least a factor of four.

c. *The jump in R* = σ(hadrons/σ(muons) between 2 - 3 GeV and 4 - 5 GeV is about ΔR = 2.5. Here is what we would expect theoretically:

Q(c)	Heavy Lepton?	ΔR
-1/3	no	0.3
-1/3	yes	1.3
2/3	no	1.3
2/3	yes	2.3
-4/3	no	5.3
-4/3	yes	6.3
5/3	no	8.3
5/3	yes	9.3

Evidently, we would like to believe in charm with Q(c) = 2/3, and in Perl's heavy lepton too.

d. *Charges of charmed mesons.* Let $D^+ = c\bar{d}$ and $D^0 = c\bar{u}$ denote charm = 1 mesons with favored decays into strangeness = -1 states. We find

Q(c) =	5/3	2/3	-1/3	-4/3
$Q(D^+)$ =	2	1	0	-1
$Q(D^0)$ =	1	0	-1	-2

Experiment reveals $Q(D^+) = 1$ and hence Q(c) = 2/3.

e. *Charges of charmed baryons.* Let Σ_c, Λ_c denote I = 1,0 baryons containing just one charmed quark. We find

Q(c) =	5/3	2/3	-1/3	-4/3
$Q(\Lambda_c)$ =	2	1	0	-1
$Q(\Sigma_c)$ =	3,2,1	2,1,0	1,0,-1	0,-1,-2

Again, experiment compels the conventional assignment of Q(c).

f. *We conclude categorically that Q(c) = 2/3.*

2. *Hyperfine Mass Splittings*

Chromodynamics suggests an origin to a spin-independent, flavor-independent quark-confining force. A residual spin-dependent force is produced by the spin-spin Fermi coupling of the quarks, $\mathcal{H} \sim \Sigma \sigma_i \cdot \sigma_j (m_i m_j)^{-1}$. Let us review how successful this picture is:

a. *States with no charmed quarks.* We deduce immediately that $m(\rho) - m(\pi) > 0$. Moreover, we find

$$\frac{m(K^*) - m(K)}{m(\rho) - m(\pi)} = \frac{m_u}{m_s} \approx 2/3.$$

This estimate of m_u/m_s concurs with that deduced from baryon magnetic moments *and moreover* with that deduced from mass splittings between corresponding strange and nonstrange particles. For baryons, we now deduce

$$m(\Delta) - m(N) \sim 3m_u^{-2} \sim 3\ m_u^{-2}$$

$$m(\Sigma^*) - m(\Sigma) \sim 3(m_u m_s)^{-1} \sim 2\ m_u^{-2}$$

$$m(\Xi^*) - m(\Xi) \sim 3(m_u m_s)^{-1} \sim 2\ m_u^{-2}$$

$$m(\Sigma) - m(\Lambda) \sim 2[m_u^{-2} - (m_u m_s)^{-1}] \sim 2/3\ m_u^{-2}\ ,$$

which are in *excellent agreement* with the experimentally measured hyperfine splittings.

b. *Mesons with one charmed quark.* We deduce $m_c/m_u \approx 5$ from the observed mass of J/ψ. Thence:

$$m(\Sigma_c^*) - m(\Sigma_c) \sim 3(m_u m_c)^{-1} \sim 3/5\ m_u^{-2}$$

$$m(\Sigma_c) - m(\Lambda_c) \sim 2[m_u^{-2} - (m_u m_c)^{-1}] \sim 8/5\ m_u^{-2}.$$

Comparison with the observed uncharmed baryon spectrum gives

$$m(\Sigma_c^*) - m(\Sigma_c) \sim 60\ \text{MeV}$$

$$m(\Sigma_c) - m(\Lambda_c) \sim 160\ \text{MeV}.$$

Similar arguments predict

$$m(D^*) - m(D) \approx 3/10\ [m(K^*) - m(K)] = 120\ \text{MeV}$$

$$m(F^*) - m(F) \approx 1/5\ [m(K^*) - m(K)] = 80\ \text{MeV}.$$

The observed D^*-D mass splitting is only slightly larger than this crude prediction. F and F^* still await discovery.

c. *States with two charmed quarks.* Following our noses, we predict for the splitting between J/ψ and its paracharmonium partner

$$m(1^-) - m(0^-) \approx \frac{9}{100}[m(K^*) - m(K)] \approx 36\ \text{MeV},$$

and similarly for ψ' and its corresponding parastate. In both cases, this prediction seems to be wrong by a factor of about five.

States made of two heavy quarks seem to behave differently from states with just one. Perhaps this is not so surprising, since protonium ($\bar{p}p$) is certainly a different kettle of fish than positronium or the hydrogen atom. Schnitzer's way of dealing with the charmonium levels, for example, does not successfully describe ordinary or singly-charmed hadrons. The eventual discovery of doubly-charmed baryons will be useful in this connection. Our naive prediction is

$$m(ccu; j = 3/2) - m(ccu; j = 1/2) \approx 3\ m_u^{-1} m_c^{-1} \approx 3/5\ m_u^{-2} \approx 60\ \text{MeV}$$

Will this prove to be correct, or an underestimate by a factor of about five?

3. *Charm Spectroscopy*

a. *Charmed S-wave mesons.* The lightest weakly-decaying pseudoscalar states are known as $D^+ = (c\bar{d})$, $D^0 = (c\bar{u})$ and $F^+ = (c\bar{s})$. Both D's have been observed near 1.87 GeV, with D^+ apparently somewhat heavier than D^0. All this is in accordance with theoretical anticipation. The predicted mass of F is about 1.98 GeV, and its preferred weak decay modes must involve two strange particles or an η or η'.

Charmed pseudoscalar mesons must have heavier vector partners. D^* was predicted to lie about m_π heavier than D. Observed recoil mass spectra strongly suggest the existence

of such states slightly above 2 GeV. The value of the hyperfine mass splitting makes electromagnetic mass splittings very relevant in the determination of the D^* decay scheme, whether by charged or neutral pion emission or by electromagnetic decay. Because of this, D^* decay is expected preferentially to yield neutral rather than charged D's.

The F^*-F mass splitting is predicted to be considerably smaller than m_π. Thus, all F^*'s are expected to decay into F and a photon. No evidence for F or F^* is yet reported.

b. *Charmed p-wave mesons.* In this case, there is one unit of orbital angular momentum ℓ between the constituent quarks. Because the charmed quark is heavy, we expect the sum of the light quark spin σ and the orbital momentum to be approximately a good quantum number: $j = |\ell + \sigma| = 1/2$ or $3/2$. Our predictions for the masses (in GeV) of these states follow:

J^P	j	D^{**}	F^{**}
0^+	1/2	2.24	2.46
1^+	1/2	2.25	2.47
1^+	3/2	2.33	2.51
2^+	3/2	2.36	2.53

Somewhat larger predicted masses are obtained by the Cornell group.

All of the D^{**}'s are expected to decay strongly by pion emission: the even-J states to ground state D's, the J = 1 states to D^*'s.

The even-J F^{**}'s should decay by kaon emission to ground-state D's. The J = 1 F^{**}'s are permitted only Zweig-forbidden two-pion decays to F or F^*.

c. *Singly-charmed s-wave baryons.* Predicted masses for the non-strange states, adapted to the single observed bubble chamber event of Cazzoli *et al.*, are in excellent agreement with recent observations reported by W. Y. Lee:

$$\Lambda_c(J^P = 1/2^+, I = 0) \text{ -- } 2.26 \text{ GeV}$$

$$\Sigma_c(J^P = 1/2^+, I = 1) \text{ -- } 2.42 \text{ GeV}$$

$$Y_c(J^P = 3/2^+, I = 1) \text{ -- } 2.48 \text{ GeV}$$

For completeness, we give predictions for the strange states:

$$(J^P = 1/2^+, S = -1) \text{ -- } 2.42 \text{ GeV}$$

$$(J^P = 1/2^+, S = -1) \text{ -- } 2.51 \text{ GeV}$$

$$(J^P = 3/2^+, S = -1) \text{ -- } 2.56 \text{ GeV}$$

$$(J^P = 1/2^+, S = -2) \text{ -- } 2.68 \text{ GeV}$$

$$(J^P = 3/2^+, S = -2) \text{ -- } 2.72 \text{ GeV}.$$

The production of these states would be signalled by an observable yield of Ξ and $\bar{\Xi}$. One should be on the lookout for an anomalous yield of these particles.

4. *Production of Charmed Pairs by "Photons"*

a. *Ranges of s.* Electron-positron annihilation at $\sqrt{s} \sim 4.03$ GeV is proven to be a fruitful source of D and D^*. Much of the charm production cross section (an *a priori* 1.3 units of R) is consumed by quasi-two-body production of $D^*\bar{D} + \bar{D}^*D + \bar{D}^*D^*$. Nearby, at $\sqrt{s} = 4.2$ GeV, this seems no longer to be the case. Can we expect a significant quasi-two-body yield of charmed hadrons just beyond each new threshold? If so, electron-positron annihilation can provide a series of

windows through which we may study different aspects of charm spectroscopy:

4.0 - 4.1 GeV	D and D^*
4.2 - 4.3 GeV	F and F^*
4.3 - 4.4 GeV	D^{**}
4.5 - 4.6 GeV	F^{**}
5.0 - 5.5 GeV	S = 0 charmed baryons
5.2 - 5.7 GeV	S = 1 charmed baryons
5.4 - 5.9 GeV	S = 2 charmed baryons

If this is somewhat the way things will turn out - and I think they will - then there is need of a properly instrumental e^+e^- annihilation facility like SPEAR capable of running from 4 - 6 GeV for many years to come.

b. *Spinology*. Amusing new arguments let us estimate the relative yield of different hyperfine states in quasi-elastic two-body charm production by photons (either in e^+e^- annihilation or by production and dissociation of virtual ψ's by photons.)

In these processes, a virtual photon produces an s-wave pair of charmed quarks. One or two pairs of light quarks are produced by the strong interactions and the resulting system reconstitutes itself into two charmed mesons or a charmed baryon and antibaryon. Chromodynamics says that the process does not take place the other way around: if the photon produces a pair of light quarks, the strong interactions are most reluctant to produce a pair of charmed quarks: this is merely another aspect of the Zweig-Iizuka rule, now comprehended as asymptotic freedom. Physics chooses a road quite opposite to what naive SU(4) would suggest.

The production of the light quarks is insensitive to the spins of the charmed quarks. We might expect non-relativistic spin x isospin symmetry to describe the light quark system. Let us apply these ideas to various quasi-two-body processes:

$\gamma \to (D \text{ or } D^*) + (\bar{D} \text{ or } \bar{D}^*)$: Let S, $\bar{S}$, s, $\bar{s}$, ℓ denote spins of the heavy quark and antiquark, light quark and antiquark, and the orbital angular momentum of $(s\bar{s})$ relative to $(\bar{S}s)$. Other orbital momenta are zero. Let P(i,j) denote the probability that the final D has 2J = i while the final $\bar{D}$ has 2J = j. Evidently

$$P(0,2) = P(2,0), \quad P(0,0) + 2P(0,2) + P(2,2) = 1 .$$

Consider the operator $(S + \bar{s})^2 = 3/2 + 2S\cdot\bar{s}$. Taking its mean value, noting that $\langle S\cdot\bar{s}\rangle = 0$, we obtain

$$2[P(2,0) + P(2,2)] = 3/2 .$$

Now take the mean value of $(S + \bar{s})^2 (\bar{S} + s)^2$:

$$4P(2,2) = 9/4 + 4\langle (S\cdot\bar{s})(s\cdot\bar{S})\rangle .$$

The decoupling of light and heavy spins implies $s + \bar{s} + \ell = 0$. Thus $(s + \bar{s})^2 = 2$, and with a little thought $\langle (S\cdot\bar{s})(s\cdot S)\rangle = 1/6$. Putting it all together: P(2,2) = 7/12, P(2,0) = P(0,2) = 2/12, P(0,0) = 1/12. Thus we see the suppression of $D\bar{D}$ production.

$\gamma \to (D^{**}) + (\bar{D} \text{ or } \bar{D}^*)$: Spins are defined as before but ℓ is the relative orbital momentum of S and $\bar{s}$. Once again, $\ell + s + \bar{s} = 0$. This means $s^2 = (\ell + \bar{s})^2 = 3/4$, so that only two of the four D^{**} may be produced in this fashion: the 0^+ and 1^+ states with j = 1/2. P(i,j) is defined as before, with

i being twice the spin of the D^{**}, and

$$P(0,0) + P(2,0) + P(0,2) + P(2,2) = 1 .$$

From the mean value of $(\bar{S} + s)^2$ we obtain

$$P(0,2) + P(2,2) = 3/4 ,$$

and from the mean value of $(S + \bar{s} + \ell)^2$ we obtain

$$P(2,0) + P(2,2) = 3/4 .$$

Taking the mean value of $(S + \bar{s} + \ell)^2 (\bar{S} + s)^2$ we find

$$4P(2,2) = 9/4 + 4\langle (s \cdot S)(s \cdot \bar{S}) \rangle ,$$

hence

$$P(2,2) = 1/2, \quad P(0,2) = P(2,0) = 1/4 .$$

The Λ_c, Σ_c, Y_c System. S, s, t denote heavy and light quark spins; $\bar{S}, \bar{s}, \bar{t}$ corresponding antiquark spins. Consider first the production of I = 1 particles Σ_c and Y_c only, with P(i,j) defined as before:

$$P(1,3) = P(3,1), \quad P(1,1) + 2P(1,3) + P(3,3) = 1 .$$

Taking the mean value of $(S + s + t)^2$, and using the fact that $(s + t)^2 = 2$ in an I = 1 state, we find

$$11 = 3P(1,1) + 18P(1,3) + 15P(3,3) .$$

From $(S + s + t)^4$ we find

$$\frac{121}{16} + 4\langle [(s+t) \cdot S]^2 \rangle = \frac{9}{16}[P(1,1) + P(1,3)] + \frac{225}{16}[P(3,1) + P(3,3)] .$$

Since heavy and light spins are uncorrelated, we know $\langle S_i S_j \rangle = 1/4\ \delta_{ij}$, and, $\langle (s + t)_i (s + t)_j \rangle = 2/3\ \delta_{ij}$,

so that

$$153 = 9P(1,1) + 234P(1,3) + 225P(3,3) .$$

From these equations, we find P(1,1) = 1/27, P(1,3) = P(3,1) = 8/27 and P(3,3) = 10/27.

Finally, we relax the constraint to I = 1 baryons, and make use of spin-isospin SU(4) for light quarks. The final state is a singlet made up of baryon and antibaryon, each a symmetric combination involving two light quarks. The baryon is an SU(4)-10, the antibaryon a $\overline{10}$. The SU(2) × SU(2) content of a 10 is (0,0) + (1,1), so that the singlet in $10 \times \overline{10}$ is exactly 10% composed of isosinglets. We thereby obtain 3:1:8:8:10 for the relative production of $\bar{\Lambda}_c \Lambda_c$, $\bar{\Sigma}_c \Sigma_c$, $\bar{\Sigma}_c Y_c$, $\bar{Y}_c \Sigma_c$ and $\bar{Y}_c Y_c$.

In brief summary, when a Λ_c is produced via a heavy photon, it was produced directly 10% of the time, it is the decay product of Σ_c 30% of the time, and of Y_c 60% of the time. It is not so surprising that the alleged $\bar{\Lambda}_c$'s from FNAL seem to result frequently from cascade decays from heavier states.

IV. SOME OPEN QUESTIONS

1. *Does the GIM Mechanism Work for Charm?*

The main *raison d'etre* for charm is to suppress strangeness-changing neutral currents. In the simplest models, the same mechanism also suppresses charm-changing neutral currents. Steven Weinberg and I recently stressed the possibility of constructing models which treat strangeness and charm differently. In these models, there are no observable strangeness-changing neutral current effects, but there are such charm-changing effects.

The most sensitive test for strangeness-changing neutral current effects is in the K_0 system. If GIM works, we expect the K_1-K_2 mass difference to be second-order weak, so that

$$\Delta M \sim \Gamma(K_1) \ .$$

Should GIM fail for strangeness, we should expect

$$\Delta M_K >> \Gamma(K_1) \ .$$

The former result is true, and we know that GIM is needed for strangeness.

If GIM is true for charm, the D_1-D_2 mass difference is expected not only to be second-order weak but to be Cabibbo suppressed. (This is because the principal decays of D are Cabibbo allowed.):

$$\Delta M_D \sim \sin^2\theta\, \Gamma(D) \ .$$

On the other hand, should GIM fail for charm (either to order G or to order αG), we should expect

$$\Delta M_D >> \Gamma(D) \ .$$

In the former case, the decays of D will be principally into $S = -1$ states, with $S = 0$ states suppressed by $\sin^2\theta$ and $S = +1$ states suppressed by $\sin^4\theta$. If a pair of oppositely charmed neutral D's is produced and allowed to decay, the final state will display $|S| = 2$ less than 1% of the time.

On the other hand, should GIM fail for charm, D and $\bar{D}$ will mix thoroughly with each other before decaying. A produced D will decay equally into channels appropriate to D or $\bar{D}$.

The following tests will soon be carried out. First, a set of e^+e^- annihilation events is collected which displays a clear $K^-\pi^+$ enhancement. The strangeness of the remaining particles is measured, or at least, an estimate is made for the frequency of K^- relative to K^+. If GIM applies, we expect a very small K^-/K^+ ratio. Otherwise, $K^-/K^+ \sim 1$. Among the same events, a similar test devolves upon the semi-leptonic decay modes. Detect charged leptons produced in association with the $K^-\pi^+$ enhancement. If GIM applies, we expect to see an associated ℓ^- frequently, and very rarely an associated ℓ^+. Otherwise $\ell^-/\ell^+ \sim 1$.

Present theory does not require that GIM apply to charm, even though it is the case in the simpler models we can build. Fortunately, theory does suggest that the problem is a yes or no affair: either there is almost total $D\bar{D}$ mixing before decay, or practically none. This is the kind of question that we can demand an experimental answer to soon. And, the answer is of utmost importance to the model builders.

2. *How Many Quarks? How Many Leptons?*

Once upon a time, there were only three kinds of quarks, four kinds of leptons, and only charged-current weak interactions. Now we have conclusive evidence for a fourth kind of quark, and for neutral-current weak interactions. And, there is no obvious reason that we are done finding such novelties.

There seems to be a fifth lepton. Evidence reported at this meeting seems to me to confirm the existence of Perl's lepton with a mass near 2 GeV. Granting it its own neutrino, this makes six leptons. Arguments based on lepton-quark symmetry or upon anomaly cancellation suggest that there should be more quarks as well. What does experiment say?

First of all, there are no bumps in e^+e^- annihilation that may not be attributed to the "observed" four quarks. More precisely, if there is a fifth quark, its "-onium" state must be heavier than 7.8 GeV. New hadrons containing just one new quark must therefore be heavier than 4.2 GeV. But, these energies are accessible to present-day neutrino experiments.

Within the context of the $SU(2) \times U(1)$ weak-interaction model, there can be little or no coupling between left-handed u and d quarks and other quarks. If valence quarks can be converted into new quarks by weak couplings, it is only the right-handed u and d that matter. This is what we defined as *fancy*, years ago. Fancy can lead to $(1-y)^2$ contributions to charged-current neutrino cross sections, and to y-independent contributions to antineutrino cross sections. But, these effects must of course involve an energy threshold. Evidently, antineutrino cross sections are more vulnerable to fancy than are neutrino cross sections.

Fancy anticipates a rise in $\sigma(\bar{\nu})/\sigma(\nu)$ and in $\langle y \rangle$ for $\bar{\nu}$ scattering at energies well beyond threshold and for invariant mass $W > 4$ GeV. This is more or less what has been seen under the rubric "high-y anomaly". There is at present some disagreement between counter groups and bubble chamber people. Definitive results are needed.

The atomic physics experiments, recently reported, which purport to measure the parity-violating coupling of electrons to hadrons are also relevant to this question. Although parity violation seems to have been seen (if true, ruling out the popular purely-vector theories), the magnitude of the observed effect seems to be considerably smaller than what is predicted in fancy-free models. Again, this can be taken as a vague indication of the possible existence of more than four quarks.

The real test for the existence of new quarks will be done in e^+e^- annihilation at higher energies. Pep and Petra will be ideal quark spectrometers. A jump in R preceded by one or more sharp bumps is a tried and true signal for a new quark. What worked for charm should work for truth and beauty as well. However, instrumentation must be sensitive enough to detect $Q = -1/3$ as well as $Q = 2/3$ quarks. One thing should make the search for hadrons with just one new heavy quark (sons of charm) easier. At high energies ($s = 100 - 1000$), conventional hadronic events, even those involving c quarks, should be pretty much jet-like. However, just above a new two-body threshold, the new physics will be rather isotropic and not jet-like at all. Those events displaying high sphericity will be the place to look for new hadrons. Indeed, this technique might even aid in the search for charmed hadrons at $\sqrt{s} = 6 - 8$ GeV, where conventional (u,d,s) events are already distinctly jet-like.

Betting on the existence of charm is now closed. But, there seems to be no agreement among theorists on what the correct number of quarks should be. I have seen arguments for 4, 5, 6, 7, 8, and even an infinite number. I suggest that we organize a ship's lottery. Having no prejudices myself, I offer to be the bank.

The four flavors × three colors of "known" quarks.

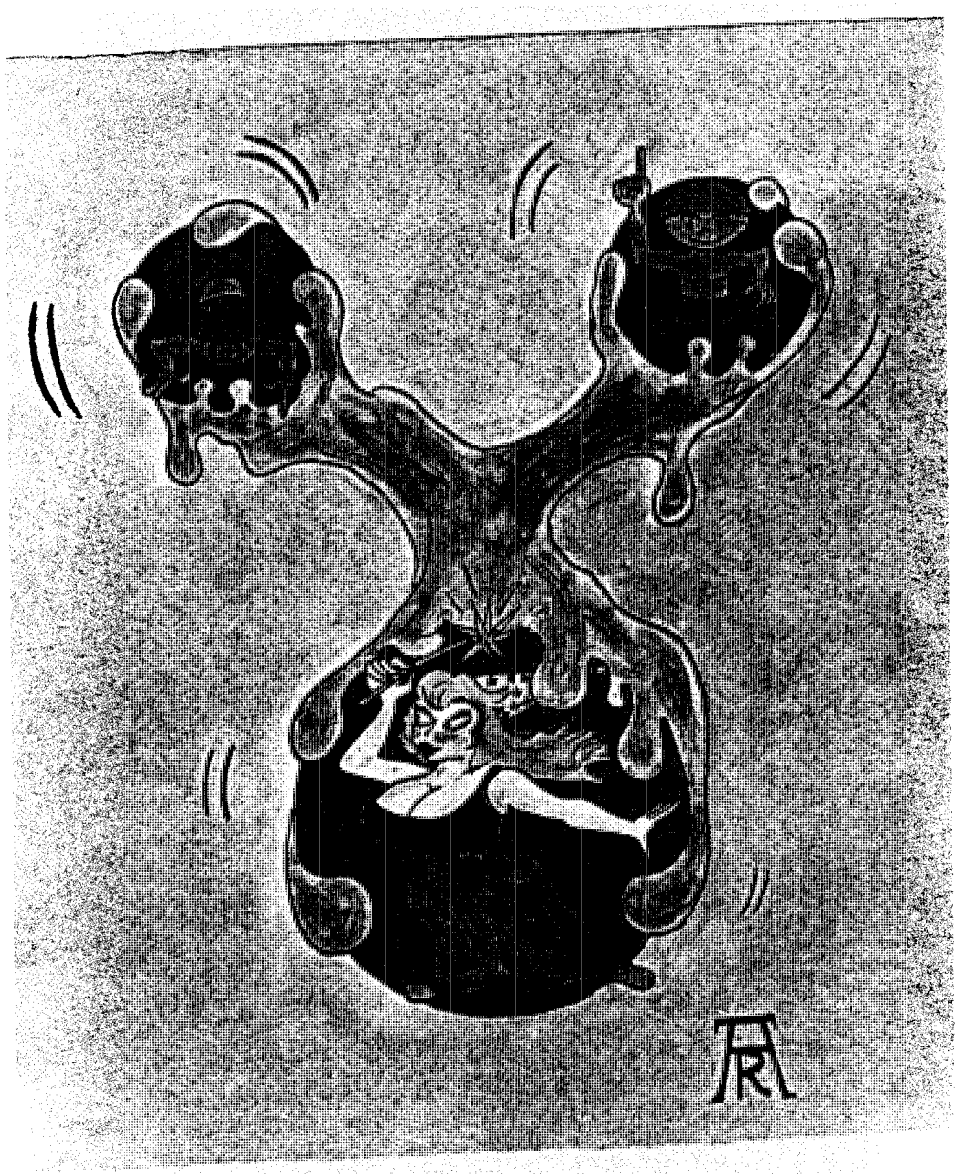

Charmed Baryon

Both drawings courtesy of A. De Rujula

PARTICIPANTS

A

Ronald Adler
Dept. de Fisica
Universidade Federal
Cidade Universitaria
50.000-Recife-Pe., Brazil

Moshe Aelion
SLAC - Bin 81

Saj Alam
SLAC - Bin 95

Robert L. Anderson
SLAC - Bin 94

Sarah C. B. Andrade
Dept. de Fisica
Pontificia Universidade Catolica
Rua Marques de S. Vicente 209
Gavea - CEP 20.000
Rio de Janeiro Z.C. 19, Brazil

Raymond G. Arnold
SLAC - Bin 12

William B. Atwood
SLAC - Bin 96

B

Craig Ballagh
c/o Fretter-Bingham Group
Department of Physics
University of California
Berkeley, California 94726

Varouzhan Baluni
Mass. Institute of Technology
Department of Mathematics
Cambridge, Mass. 02139

Vera Baltar
University of California
Department of Physics
Santa Barbara, California 93106

James Bjorken
SLAC - Bin 81

Stephen Blaha
Williams College
Department of Physics
Williamstown, Mass. 01267

Richard Blankenbecler
SLAC - Bin 81

Elliott Bloom
SLAC - Bin 98

Arno Bohm
University of Texas
Physics Department
Austin, Texas 78712

Henrik G. Bohr
Niels Bohr Institute
17, Bldgdamsvej
DK-2100
Copenhagan Ø, Denmark

M. Borghini
SLAC - Bin 78

Bennett Bradson
Indiana University
Department of Physics
Bloomington, Indiana 47401

David Brayshaw
SLAC - Bin 81

Martin Breidenbach
SLAC - Bin 95

Stanley Brodsky
SLAC - Bin 81

John L. Brown
SLAC - Bin 71

Karl Brown
SLAC - Bin 94

Robert Budny
Rockefeller University
1230 York Avenue
New York, New York 10021

Fatin Bulos
SLAC - Bin 98

Ray A. Burnstein
Illinois Institute of Technology
Department of Physics
Chicago, Illinois 60616

C

B. A. Campbell
McGill University
Department of Physics
P.O. Box 6070, Station A
Montreal, Quebec, Canada H3C 3G1

Richard Capps
Purdue University
Department of Physics
Lafayette, Indiana 47907

Terry Carrol
SLAC - Bin 78

William Caswell
SLAC - Bin 81

George B. Chadwick
SLAC - Bin 78

Vladimir Chaloupka
SLAC - Bin 78

Michael Chanowitz
Lawrence Berkeley Laboratory
Building 50
University of California
Berkeley, California 94720

Chih Kwan Chen
Argonne National Laboratory
High Energy Physics Division
Bldg. 362
9700 S. Cass Avenue
Argonne, Illinois 60439

P. Chen
Calif. Institute of Technology
Department of Physics
Pasadena, California 91109

Byung Ha Cho
Korea Advanced Institute of Science
P. O. Box Chongyangni
Seoul, Korea

Gilbert Chu
Harvard-MIT Program in
Health Science and Technology
Cambridge, Mass. 02139

Robert Clark
Texas A & M
Department of Physics
College Station, Texas 77843

E. W. Colglazier
144 Morningside Drive
San Antonio, Texas 78209

John Collins
Princeton University
Physics Department
Princeton, N. J. 08540

Susan Cooper
Lawrence Berkeley Laboratory
University of California
Berkeley, California 94207

Jose Cortez
Lawrence Livermore Laboratory
Department of Physics
Livermore, California 94550

R. L. Cottrell
SLAC - Bin 96

Paul Cowell
SLAC - Bin 63

George Cozzika
CERN Lab I-EP Div.
1211 Geneva 23
Switzerland

Gerarolo Cristofano
University of California
Department of Physics
Santa Cruz, California 95050

D

Thomas Degrand
SLAC - Bin 81

Emanuel Derman
Dept. of Theoretical Physics
12 Parks Road
Oxford OX1 3PQ
England

H. DeStaebler
SLAC - Bin 96

Alain Diamant-Berger
SLAC - Bin 63

Peter Dobson
University of Hawaii
Dept. of Physics
Honolulu, Hawaii 96822

Jonathan Dorfan
SLAC - Bin 61

Sidney Drell
SLAC - Bin 80

Robert Dulude
Dept. of Physics
Brown University
Providence, R. I. 02906

M. Duong-Van
SLAC - Bin 65

William Dunwoodie
SLAC - Bin 62

Stanley Durkin
SLAC - Bin 62

E

John Edighoffer
HEPL - Room 122
Stanford University
Stanford, California 94305

Bonnie Jean Edwards
Dept. of Physics
University of Alberta
Edmonton, Canada

Estia J. Eichten
Cornell University
Dept. of Physics
Ithaca, N. Y. 14850

Yoav Eylon
Lawrence Berkeley Laboratory
Bldg. 50A, Room 3115
University of California
Berkeley, California 94720

F

Dara Faroughy
University of California
Department of Physics
Irvine, California 92717

F. L. Feinberg
Physics Department
University of California
Los Angeles, California 90024

Gary Feldman
SLAC - Bin 61

Erasmo Ferreira
SLAC - Bin 81

Max Ferro-Luzzi
SLAC - Bin 62

Martin Fessler
SLAC - Bin 63

Clive Field
SLAC - Bin 78

David Finkelstein
Yeshiva University
Belfer School of Science
Dept. of Physics
New York, N. Y. 10033

Neil Fleishon
Lawrence Berkeley Laboratory
University of California
Berkeley, California 94720

Deiter Freytag
SLAC - Bin 78

W. F. Fry
University of Wisconsin
Department of Physics
Madison, Wisconsin 53706

David Fryberger
SLAC - Bin 20

Jose Fulco
SLAC - Bin 81

G

Angela Galtieri
Lawrence Berkeley Laboratory
University of California
Berkeley, California 94720

Murdock Gilchriese
SLAC - Bin 62

Frederick J. Gilman
SLAC - Bin 81

Sheldon L. Glashow
Harvard University
Department of Physics
Cambridge, Mass. 02138

Gary Godfrey
SLAC - Bin 98

Gerson Goldhaber
University of California
Lawrence Berkeley Laboratory
Berkeley, California 94207

John Gunion
University of California
Department of Physics
Davis, California 95616

David B. Gustavson
SLAC - Bin 94

Alan H. Guth
Columbia University
Department of Physics
538 W. 120th St.
New York, N. Y. 10027

H

Teruhiko Hagiwara
Rockerfeller University
Department of Physics
New York, N. Y. 10021

Geoff Hall
SLAC - Bin 78

Gail Hanson
SLAC - Bin 61

Everett Harvey
University of Wisconsin
Department of Physics
Madison, Wisconsin 53706

Frank Heile
SLAC - Bin 61

David Hitlin
SLAC - Bin 63

Alan Honma
SLAC Bin 62

David Horn
Calif. Institute of Technology
Dept. of Physics 452-48
Pasadena, California 91125

Benedikt Humpert
SLAC - Bin 81

David Hutchinson
SLAC - Bin 62

Rudolph C. Hwa
University of Oregon
Inst. of Theoretical Science
Eugene, Oregon 97403

Woei-Yann Pauchy Hwang
2E5, DRL - Dept. of Physics
University of Pennslyvania
Philadelphia, Pa. 19174

J

J. D. Jackson
Lawrence Berkeley Laboratory
Bldg. 50
University of California
Berkeley, California 94720

Shirley A. Jackson
Fermi National Accelerator Laboratory
P. O. Box 500
Batavia, Illinois 60510

Robert Jaffe
Massachusetts Institite of Technology
Dept. of Physics 6-316
Cambridge, Mass. 02139

John Jaros
SLAC - Bin 61

S. D. Joglekar
Institute for Advanced Study
Princeton, New Jersey 08540

William B. Johnson
SLAC - Bin 62

Lewis H. Jones
University of Maryland
Dept. of Physics
College Park, Maryland 20742

Stanley T. Jones
University of Alabama
Dept. of Physics & Astronomy
P.O. Box 1921
University, Alabama 35486

Nikola Jurisic
University of Central Venezuela
Facultad de Ciencias
Caracas, Venezuela

K

Kimiyo Kanai
Tokyo Metropolitan University
Department of Physics
Setagaya-Ku
Tokyo, Japan

J. S. Kang
University of Maryland
Department of Physics
College Park, Maryland 20742

Sinan Kaptanoglu
SLAC - Bin 81

Inga Karliner
Physics Department
University of Illinoia
Urbana, Illinois 61801

Lewis P. Keller
SLAC - Bin 20

Christian Kiesling
SLAC - Bin 98

D. Y. Kim
University of Regina
Dept. of Physics & Astronomy
Regina, Saskatchewan, Canada S4S 0A2

Jasper Kirby
SLAC - Bin 63

Leslie Klein
SLAC - Bin 61

Claude Kochowski
Fermi National Accelerator Laboratory
P. O. Box 500
Batavia, Illinois 60510

L. Kogan
SLAC - Bin 65

W. Kozanecki
Harvard University
Department of Physics
42 Oxford St.
Cambridge, Mass. 02138

Paul Kunz
SLAC - Bin 62

Betty Kwan
SLAC - Bin 61

L

Robert Lacy
201 Greenway
Lake Charles, La. 70601

Kenneth Lane
SLAC - Bin 81

Rudy R. Larsen
SLAC - Bin 95

Tom Lasinski
SLAC - Bin 62

Vicente Llamas
Physics Department
New Mexico Highlands University
Las Vegas, New Mexico 87701

Leon Lederman
Columbia University
Department of Physics
New York, N. Y. 10027

W. Y. Lee
Columbia University
Department of Physics
New York, N. Y. 10027

David W. G. S. Leith
SLAC - Bin 62

Peter Lepage
SLAC - Bin 81

Ling-Fong Li
Carnegie Mellon University
Department of Physics
Pittsburg, Pa. 15213

Art Liberman
Hanson Laboratory
Stanford University
Dept. of Physics
Stanford, California 94305

John Liu
SLAC - Bin 63

Richard J. Loveless
University of Wisconsin
Department of Physics
Madison, Wisconsin 53706

Dieter Luke
SLAC - Bin 61

Vera Luth
SLAC - Bin 95

M

Rabinder Madan
No. Carolina A&T State Univ.
Department of Physics
Greensboro, N. Carolina 27411

Leon Madansky
Johns Hopkins University
Department of Physics
Baltimore, Maryland 21218

Francois Martin
SLAC - Bin 81

John Malos
SLAC - Bin 62

Evandelos Manesis
Univ. of Ivannina
Dept. of Physics
Ivannina, Greece

Phillip D. Mannheim
SLAC - Bin 81

Jim Martin
SLAC - Bin 61

Max Marshall
SLAC - Bin 62

Stephen McGuire
Dept. of Physics
Cornell University
Ithaca, N. Y. 14850

Mac D. Mestayer
SLAC - Bin 96

D. I. Meyer
University of Michigan
Dept. of Physics
Ann Arbor, Michigan 48104

Heinrich Meyer
DESY
Notkestieg 1
2000 Hamburg 52
West Germany

W. T. Meyer
SLAC - Bin 62

Hannu Miettinen
SLAC - Bin 81

Karnig O. Mikaelian
Physics Department
Northwestern University
Evanston, Illinois 60201

Jaime Millan
937 Riley Drive Bldg. #91
Albany, California 94706

David Miller
SLAC - Bin 95

Michiko Miyamoto
1-11-2 Yamate, Nakasuji
Takarazuka, Hyogo-Ken
Japan

Jim Moore
SLAC - Bin 61

Matias Moreno
Instituto de Fisica
Dept. de Fisica Teorica
Apartado Postal 20-364
Mexico 20, D.F.

Harry Morrison
Dept. of Physics
Massachusetts Institute of Technology
Cambridge, Massachusetts 02139

P. Musset
CERN
1211 Geneva 23
Switzerland

N

Nobuya Nakazawa
Kogakuin University
24-2, Nishishinjuku-1 Chome
Shinjuku-ku
Tokyo 160, Japan

Frank Nezrick
Fermi National Accelerator Laboratory
P. O. Box 500
Batavia, Illinois 60510

Jack Ng
SLAC - Bin 81

Wei-Tou Ni
California Institute of Technology
Kellogg Radiation Lab 106-38
Pasadena, California 91125

H. Pierre Noyes
SLAC - Bin 81

O

Robert J. Oakes
Northwestern University
Department of Physics
Evanston, Illinois 60201

Al Odian
SLAC - Bin 65

Harry Orbach
SLAC - Bin 81

Mark Oreglia
SLAC - Bin 81

John L. Orthel
University of California
Department of Physics
Berkeley, California 94805

P

C. Y. Pang
Columbia University
Department of Physics
New York, N. Y. 10027

W. K. H. Panofsky
SLAC - Bin 80

Robert Panvini
Vanderbilt University
Department of Physics
Nashville, Tennessee 37235

Sherwood Parker
Department of Physics
University of Hawaii
Honolulu, Hawaii 96822

R. Partridge
California Institute of Technology
Department of Physics
Pasadena, California 91109

Ewan Paterson
SLAC - Bin 95

Martin Perl
SLAC - Bin 61

Ida Peruzzi
SLAC - Bin 95

H. Pessard
SLAC - Bin 96

So Young Pi
Rockefeller University
Department of Physics
New York, N. Y. 10021

Marcello Piccolo
SLAC - Bin 95

Bernard Pire
SLAC - Bin 81

Frank Porter
University of California
Department of Physics
Berkeley, California 94805

Richard Prepost
University of Wisconsin
Department of Physics
Madison, Wisconsin

C. Y. Prescott
SLAC - Bin 96

Ting Pun
SLAC - Bin 61

Q

Helen Quinn
Stanford University
Department of Physics
Stanford, California 94305

R

Petros Rapidis
SLAC - Bin 61

Blair Ratcliff
SLAC - Bin 62

Tillmann Reichelt
SLAC - Bin 94

Leo Resvanis
University of Pennsylvania
Department of Physics
Philadelphia, Pa. 19174

David M. Ritson
SLAC - Bin 94

Leon Rochester
SLAC - Bin 96

S

Chris Sachrajda
CERN - Th. Div.
1211 Geneva 23
Switzerland

T. Sato
SLAC - Bin 96

Peter Schacht
SLAC - Bin 62

John Scheid
Calif. Institute of Technology
SLAC - Bin 62

Rafe Schindler
SLAC - Bin 95

Ivan Schmidt
SLAC - Bin 81

Peter Schmuser
University of Hamburg
DESY
Notkestieg 1
2000 Hamburg 52
West Germany

David Martin Scott
Rutherford Laboratory
Chilton, Didcot, Oxfordshire
OX110QX
Oxford, England

Brian Serot
SLAC - Bin 61

L. M. Sehgal
III. Physikalisches Institut
Jagerstrasse 51
Aachen, Germany

Michael Shaevitz
Fermi National Accelerator Laboratory
Lab B - Exp. 21
P.O. Box 500
Batavia, Illinois 60510

Steve Shapiro
SLAC - Bin 62

Gordon Shaw
Physics Department
University of California
Irvine, California 92717

Sun-Shing Shei
Institute for Advanced Study
Princeton, New Jersey 08540

Ronald C. Shellard
Department of Physics - TED
University of California
Los Angeles, California 90024

James Siegrist
SLAC - Bin 95

A. J. Stewart Smith
Princeton University
Department of Physics
Princeton, New Jersey 08540

Kwang Sup Soh
70-10 Shinkyo
Chongno
Seoul, Korea

Michael Sokoloff
University of California
Department of Physics
Berkeley, California 94805

Hi Sung Song
Department of Physics
Seoul National University
College of Natural Sciences
Seoul 151, Korea

Cherrill Spencer
University of Wisconsin
SLAC - Bin 98

Andrew J. Spiessbach
Institute of Theoretical Science
University of Oregon
Eugene, Oregon 97403

R. Suaya
McGill University
High Energy Physics Group
P.O. Box 6070
Montreal, Quebec, Canada H3C 3G1

Robin Staffin
SLAC - Bin 81

M. Lynn Stevenson
Lawrence Berkeley Laboratory
Building 50
University of California
Berkeley, California 94720

Karl Strauch
Harvard University
Department of Physics
Cambridge, Massachusetts 02138

Ryszard Stroynowski
SLAC - Bin 62

Linda Stutte
California Institute of Technology
Department of Physics
Pasadena, California 91109

Kurt Sundermeyer
Massachusetts Institute of Technology
Department of Physics
Cambridge, Massachusetts 02139

D. L. Swanson
Department of Physics - TEP
University of California
Los Angeles, California 90024

T

Eiichi Takasugi
Ohio State University
Department of Physics
174 W. 18th Ave.
Columbus, Ohio 43210

W. Tanenbaum
SLAC - Bin 95

Richard E. Taylor
SLAC - Bin 96

Michael J. Teper
University of Oregon
Department of Physics
Eugene, Oregon 97403

John Townsend
Physics Department
Harvey Mudd College
Claremont, California 91711

George Trilling
University of California
Lawrence Berkeley Laboratory - Bldg. 50
Berkeley, California 94720

T. Trippe
University of California
Lawrence Berkeley Laboratory
Berkeley, California 94720

Y. S. Tsai
SLAC - Bin 81

John Tsai
Stanford University
Department of Physics
Stanford, California 94305

Peter Turner
SLAC - Bin 81

Henry Tye
SLAC - Bin 81

Chia Tze
SLAC - Bin 81

U

Luis Urrutia
Department of Physics - TEP
University of California
Los Angeles, California 90024

V

Francois Vannucci
SLAC - Bin 95

K. V. Vasavada
Indiana-Purdue University
Department of Physics
Indianapolis, Indiana 46205

Wayne Vernon
University of California
Physics Department B019
La Jolla, California 92093

F. Villa
SLAC - Bin 65

W

Walter Wada
Department of Physics
Ohio State University
174 West 18th Avenue
Columbus, Ohio 43210

Marvin Weinstein
SLAC - Bin 81

Jeff Weiss
Fermi National Accelerator Laboratory
P. O. Box 500
Batavia, Illinois 60510

W. A. Wenzel
Lawrence Berkeley Laboratory
Building 50 - 149
Berkeley, California 94720

H. H. Williams
University of Pennsylvania
Department of Physics
Philadelphia, Pa. 19174

Steve Williams
SLAC - Bin 62

Stanley Wojcicki
Stanford University
SLAC - Bin 63

Lincoln Wolfenstein
Carnegie-Mellon University
Department of Physics
Pittsburgh, Penn. 15213

Gordon Woo
Massachusetts Institute of Technology
Department of Physics
Cambridge, Massachusetts 02139

Craig Woody
Johns Hopkins University
SLAC - Bin 62

Y

T. C. Yang
DESY
Notkestieg 1
D-2, 52 Hamburg
West Germany

Shimon Yankielowicz
SLAC - Bin 81

George P. Yost
University of California
Department of Physics
Berkeley, California 94805

James E. Young
Massachusetts Institute of Technology
Department of Physics
Cambridge, Massachusetts 02139